**Carlos**

**Rodríguez García**

PhD Thesis

# Multicomponent Strategies for GPCR Targeting: Allosteric Modulation of Dopamine Receptor $D_2$ and Development of Potent and Selective $CB_2R$ Agonists

Santiago de Compostela, 2024

PHD PROGRAMME IN DRUG RESEARCH AND DEVELOPMENT

DOCTORAL THESIS

# Multicomponent Strategies for GPCR Targeting: Allosteric Modulation of Dopamine Receptor $D_2$ and Development of Potent and Selective $CB_2R$ agonists

Carlos Rodríguez García

Director: Eddy Sotelo

Tutor: Eddy Sotelo

**PHD PROGRAMME IN DRUG RESEARCH AND DEVELOPMENT**

SANTIAGO DE COMPOSTELA, 2024

## Acknowledgments

En primer lugar, deseo expresar mi profunda gratitud hacia mi tutor y director de Tesis Doctoral, **Eddy Sotelo**, cuyo apoyo y guía han sido fundamentales a lo largo de estos años. Gracias por acogerme en la familia ComBioMed, y por la incansable dedicación demostrada en el desarrollo de este trabajo.

A **Jhonny Azuaje**, por su constante paciencia desde el inicio, tanto en mi introducción al entorno del laboratorio y las primeras lecciones de trabajo, como en responder a todas las dudas y preguntas que me han surgido desde entonces.

A **Rodrigo Bernárdez**, por su inigualable guía y apoyo a lo largo de nuestro tiempo juntos en la industria, que ha continuado hasta el último día de trabajo en esta Tesis. Su disposición a compartir sus conocimientos y experiencia han tenido un valor incalculable en mi proceso de aprendizaje.

A **María Majellaro**, por su contagiosa alegría y su siempre entusiasta disposición a la hora de resolver todas mis dudas en el laboratorio.

A todos los colaboradores de esta Tesis Doctoral, que han participado en aumentar su calidad y valor científico: **Rita Paleo** y **Xerardo García-Mera**, del departamento de Química Orgánica de la Universidad de Santiago de Compostela, **María Isabel Loza** y **José Brea**, del laboratorio de farmacología de la Universidad de Santiago de Compostela, **Gemma Navarro Brugal**, del laboratorio de farmacología de la Universidad de Barcelona, **Miguel Abad** y **Jorge Barbazán**, del Instituto de Investigación Sanitaria de Santiago de Compostela.

Al personal técnico y administrativo de la Universidad de Santiago de Compostela, en especial a **Xosé González**, técnico del Laboratorio de Química Orgánica de la Facultad de Farmacia por facilitarnos el trabajo del día a día, y a los técnicos de **Unidad de Rayos X**, **Espectrometría** y **Resonancia Magnética Nuclear**.

Me gustaría expresar un agradecimiento especial a **Claudia Gioè** y **Rubén Prieto**, quienes han sido mis compañeros desde el inicio de la tesis. Ha sido increíble contar con su compañía durante todo este tiempo. Quisiera agradecerles por todos sus consejos y apoyo en la redacción del manuscrito, así como toda la ayuda prestada a lo largo de los años a la hora de realizar cualquier trámite.

USC
DE COMPOSTELA

A **Hugo Fojo**, **Aitor García**, **Lucía Campos**, **Darío Miranda**, **Sandra Ortigueira** y **David Reza**, por haber contribuido con sus comentarios y correcciones a la revisión de esta Tesis Doctoral, y por su inestimable compañía tanto dentro como fuera del laboratorio durante estos años.

Al resto de compañeros de ComBioMed: **Martina Migliavacca**, **Ana Mallo**, **Antonio Andújar**, **Lucía González**, **Iván Rodríguez** y **Carla Lorenzo**.

Finalmente, un agradecimiento especial a **Eddy Sotelo** y al grupo **ComBioMed** por haber financiado mi tesis de doctorado durante este tiempo.

USC
UNIVERSIDADE DE SANTIAGO DE COMPOSTELA

# INDEX

**GLOSSARY** ..... **I**

**RESUMO** ..... **VIII**

**1 INTRODUCTION** ..... **1**

1.1 Evolution of GPCRs study ..... 1

1.2 Rhodopsin receptor family ..... 3

1.3 Dopamine and dopamine receptor (DR) ..... 4

1.4 Dopamine $D_2$ receptor ($D_2R$) ..... 6

1.4.1 Structure, function, and localization ..... 6

1.4.2 Signaling ..... 10

1.4.3 Parkinson's disease (PD) ..... 12

1.4.4 Pathophysiology of PD ..... 13

1.4.5 Treatments of PD ..... 14

1.4.6 Schizophrenia ..... 16

1.4.7 Pathophysiology of schizophrenia ..... 16

1.4.8 Treatments of schizophrenia ..... 17

1.4.9 Allosterism ..... 19

1.4.10 Allosteric modulation of the $D_2R$ ..... 24

1.4.11 Melanostatin ..... 25

1.5 Endocannabinoid system ..... 31

1.6 $CB_2$ receptor ($CB_2R$) ..... 33

1.6.1 Structure, function, and localization ..... 34

1.6.2 Signaling ..... 36

1.6.3 Therapeutic potential of $CB_2R$ ..... 39

1.6.4 $CB_2R$ as a therapeutic target in cancer ..... 42

USC UNIVERSIDADE DE SANTIAGO DE COMPOSTELA

1.6.5 $CB_2R$ ligands in clinical trials ..... 48
1.6.6 Synthetic cannabinoid receptor agonists (SCRAs) ..... 50
1.7 MCRs ..... 57
1.7.1 Isocyanide-based multicomponent reactions. ..... 58
1.7.2 Ugi four component reaction (U-4CR). ..... 59
1.7.3 Passerini reaction and PADAM synthetic route ..... 63
**2 OBJECTIVES ..... 68**
**3 RESULTS AND DISCUSSION ..... 72**
3.1 CHAPTER I ..... 72
3.1.1 Design ..... 74
3.1.2 Chemistry ..... 78
3.1.3 Biological evaluation ..... 94
3.1.4 Structure-Activity Relationships ..... 102
3.2 CHAPTER II ..... 133
3.2.1 Design ..... 137
3.2.2 Chemistry ..... 141
3.2.3 Biological evaluation ..... 150
3.2.4 Structure-Activity Relationship ..... 167
3.2.5 Molecular docking simulations ..... 230
3.2.6 Functional assays ..... 235
3.2.7 Biological assays: antiproliferative effect in the U87 glioblastoma cell line 246
**4 CONCLUSIONS ..... 248**
**5 EXPERIMENTAL SECTION ..... 252**
5.1 GENERAL CONSIDERATIONS ..... 252
5.1.1 Synthesis and purification ..... 252

USC UNIVERSIDADE DE SANTIAGO DE COMPOSTELA

5.1.2 Structural characterization ..... 252
5.1.3 Pharmacological evaluation ..... 254
5.2 CHAPTER I ..... 257
5.2.1 Synthesis of melanostatin derivatives ..... 257
5.2.2 Spectroscopic and analytical data for all compounds described ..... 261
5.2.3 Statistical analysis: One sample t-test for all compounds described ..... 287
5.2.4 Circular dichroism (CD) of Series I, II and III ..... 297
5.2.5 Chiral HPLC separation of enantiomers and characterization of 34b ..... 306
5.3 CHAPTER II ..... 308
5.3.1 Synthesis of SCRAs analogues ..... 308
5.3.2 Spectroscopic and analytical data for all compounds described ..... 315
5.3.3 X-ray crystallography of (2*S*)-188 ..... 363
**6 REFERENCES ..... 365**
**7 APPENDICES ..... 377**
7.1 Appendix 1. Conflict of Interest ..... 377
7.2 Appendix 2. Permission to publish images and figures ..... 378

USC UNIVERSIDADE DE SANTIAGO DE COMPOSTELA

USC
UNIVERSIDADE
DE SANTIAGO
DE COMPOSTELA

# GLOSSARY

| | |
|---|---|
| **2-AG** | 2-Arachidonoylglycerol |
| **5-HT** | Serotonin |
| **5-HT$_{2A}$R** | Serotonin 2A Receptor |
| **5-HT$_{2B}$R** | Serotonin 2B Receptor |
| **7TM** | 7 Transmembrane |
| **A$_1$AR** | A$_1$ Adenosine Receptor |
| **A$_{2A}$AR** | A$_{2A}$ Adenosine Receptor |
| **A$_{2B}$AR** | A$_{2B}$ Adenosine Receptor |
| **A$_3$AR** | A$_3$ Adenosine Receptor |
| **AADC** | L-Amino Acid Decarboxylase |
| **AC** | Adenylyl Cyclase |
| **AcOEt** | Ethyl Acetate |
| **AEA** | Anandaminde (N-arachidonoylethanolamide) |
| **ADP** | Adenosine Diphosphate |
| **ADTN** | 2-amino-6,7-dihydroxy-3,4-tetrahydronapthtalene |
| **Akt** | Ak strain transforming (Protein Kinase B or PKB) |
| **Ang1** | Angiopoietin 1 |
| **Ang2** | Angiopoietin 2 |
| **ApoE** | Apolipoprotein E |
| **ATF** | Activating Transcription Factor |
| **BCP** | B-carophyllene |
| **Bn** | Benzyl |
| **Boc** | *Tert*-butoxy carbonyl |
| **cAMP** | Cyclic Adenosine Monophosphate |
| **CB$_1$R** | Cannabinoid Receptor 1 |
| **CB$_2$R** | Cannabinoid Receptor 2 |
| **CBD** | Cannabidiol |

USC UNIVERSIDADE DE SANTIAGO DE COMPOSTELA

| | |
|---|---|
| **CCR5** | C-C Chemokine Receptor type 5 |
| **CD** | Circular Dichroism |
| **CHO** | Chinese Hamster Ovary |
| **CI** | Chemical Ionization |
| **CKD** | Chronic Kidney Disease |
| **CNS** | Central Nervous System |
| **COMT** | Catechol-O-Methyltransferase |
| **CpG** | Cytosine-Guanine Motifs |
| **CRC** | Colorectal Cancer |
| **CREB** | cAMP Response Element-Binding Protein |
| **CXCR4** | C-X-C Chemokine Receptor type 4 |
| **Cy** | Cyclohexyl |
| **$D_1R$** | Dopamine Receptor 1 |
| **$D_2R$** | Dopamine Receptor 2 |
| **$D_2R_{Spi}$** | Dopamine Receptor 2 Spiperone complex |
| **$D_{2L}R$** | Dopamine Receptor 2 Long |
| **$D_{2S}R$** | Dopamine Receptor 2 Short |
| **$D_3R$** | Dopamine Receptor 3 |
| **$D_4R$** | Dopamine Receptor 4 |
| **$D_5R$** | Dopamine Receptor 5 |
| **DAG** | Diacylglycerol |
| **DCM** | Dichloromethane |
| **DEA** | Drug Enforcement Administration |
| **DIEA** | *N*,*N*-Diisopropylethylamine |
| **DMF** | Dimethylformamide |
| **DMSO** | Dimethyl Sulfoxide |
| **DPPA** | Diphenylphosphoryl Azide |
| **DR** | Dopamine Receptor |
| **EBP** | Extended Binding Pocket |

USC UNIVERSIDADE DE SANTIAGO DE COMPOSTELA

| | |
|---|---|
| **$EC_{50}$** | Half Maximal Effective Concentration |
| **eCB** | Endocannabinoid |
| **ECL** | Extracellular Loop |
| **ECS** | Endocannabinoid System |
| **EDC** | 1-Ethyl-3-(3-dimethylaminopropyl)carbodiimide |
| **EGF** | Epithelial Growth Factor |
| **$E_{max}$** | Maximum Effect |
| **EMCDDA** | European Monitoring Center for Drugs and Drug Addiction |
| **ERK** | Extracellular Signal-Regulated Kinase |
| **ESI** | Electrospray Ionization |
| **Et** | Ethyl |
| **FAAH** | Fatty Acid Amide Hydrolase |
| **Fab** | Fragment Antigen Binding |
| **FDA** | Food and Drug Administration |
| **FGA** | First Generation Antipsychotic |
| **GABA** | Gamma-Aminobutyric Acid |
| **GBM** | Glioblastoma |
| **Gi** | Inhibitory G-Protein |
| **GIRK** | G-Protein Inwardly Rectifying Potassium Channel |
| **GPCR** | G-Protein-Coupled Receptor |
| **GPR55** | G-Protein-Coupled Receptor 55 |
| **GRK** | G-Protein Receptor Kinase |
| **Gs** | Stimulatory G-Protein |
| **GTP** | Guanosine Triphosphate |
| **HBA** | Hydrogen Bond Acceptor |
| **HBD** | Hydrogen Bond Donor |
| **HEK** | Human Embryonic Kidney |
| **HER1** | Human Epidermal Growth Factor Receptor 1 |
| **HER2** | Human Epidermal Growth Factor Receptor 2 |

USC UNIVERSIDADE DE SANTIAGO DE COMPOSTELA

| | |
|---|---|
| **HER3** | Human Epidermal Growth Factor Receptor 3 |
| **HER4** | Human Epidermal Growth Factor Receptor 4 |
| **Het** | Heterocycle |
| **Hex** | Hexane |
| **HIV** | Human Immunodeficiency Virus |
| **HOAt** | 1-Hydroxy-7-azabenzotriazole |
| **HOBt** | 1-Hydroxybenzotriazole |
| **Homopro** | Homoproline |
| **HPLC** | High-Performance Liquid Chromatography |
| **HPT** | Hyperparathyroidism |
| **HRMS** | High-Resolution Mass Spectrometry |
| **HTRF** | Homogeneous Time-Resolved Fluorescence |
| ***i-Bu*** | Isobutyl |
| ***i-Pr*** | Isopropyl |
| **IBMX** | 3-Isobutyl-1-methylxanthine |
| **$IC_{50}$** | Half-Maximal Inhibitory Concentration |
| **ICAM** | Intercellular Adhesion Molecule 1 |
| **IDIS** | Institute of Health Research of Santiago |
| **IFN** | Interferon |
| **IL-10** | Interleukin-10 |
| **IL-1β** | Interleukin-1 beta |
| **IMCR** | Isocyanide-based Multicomponent Reaction |
| **IPA** | Isopropyl Alcohol |
| **IRF7** | Interferon Regulatory Factor 7 |
| **IKKγ** | IκB Kinase Gamma |
| **JAK** | Janus Kinase |
| **JNK** | c-Jun N-terminal Kinase |
| **$K_i$** | Inhibition Constant |
| **L-DOPA** | Levodopa |

USC UNIVERSIDADE DE SANTIAGO DE COMPOSTELA

| | |
|---|---|
| **LRMS** | Low Resolution Mass Spectrometry |
| **LPS** | Lipopolysaccharide |
| **MAGL** | Monoacylglycerol Lipase |
| **MAO** | Monoamine Oxidase |
| **MAP** | Mitogen-Activated Protein |
| **MAPK** | Mitogen-Activated Protein Kinase |
| **mbIIG** | Loop Modified Cytochrome $b_{562}$ IIG |
| **MCR** | Multicomponent Reaction |
| **Me** | Methyl |
| **MEK** | Mitogen-Activated Protein Kinase |
| **MeOH** | Methanol |
| **MMP-2** | Matrix Metalloproteinase 2 |
| **Mp** | Melting Point |
| **MS** | Mass Spectrometry |
| **NAM** | Negative Allosteric Modulator |
| **NAPE** | N-Acyl-Phosphatidylethanolamine |
| **NAPE-PLD** | NAPE-Specific Phospholipase D |
| **NB** | Neuroblastoma |
| **NF-κβ** | Nuclear Factor kappa B |
| **NMDA** | N-Methyl-D-Aspartate |
| **NMR** | Nuclear Magnetic Resonance |
| **NPA** | N-Propylnorapomorphine |
| **NPS** | New Psychoactive Substances |
| **PADAM** | Passerini reaction-Amine Deprotection-Acyl Migration |
| **PAM** | Positive Allosteric Modulator |
| **PD** | Parkinson's Disease |
| **pDC** | Plasmacytoid Dendritic Cells |
| **PEP** | Protease Prolyl Endopeptidase |
| **PI3K** | Phosphoinositide-3 Kinase |

USC UNIVERSIDADE DE SANTIAGO DE COMPOSTELA

| | |
|---|---|
| **PKA** | Protein Kinase A |
| **PLG** | L-Prolyl L-Leucylglycinamide |
| **Pro** | Proline |
| **REM** | Rapid Eye Movement |
| **$R_H$** | Receptor High Affinity State |
| **$R_L$** | Receptor Low Affinity State |
| **RT** | Room Temperature |
| **RUNX2** | Runt-Related Transcription Factor 2 |
| **SAM** | Silent Allosteric Modulator |
| **SAPK** | Stress-Activated Protein Kinases |
| **SAR** | Structure-Activity Relationship |
| **SCRA** | Synthetic Cannabinoid Receptor Agonist |
| **SD** | Standard Deviation |
| **SEM** | Standard Error of the Mean |
| **SGA** | Second Generation Antipsychotic |
| **SI** | Selectivity Index |
| **SSR** | Structure-Selectivity Relationship |
| **SSTR5** | Somatostatin Receptor 5 |
| **STAT1** | Signal Transducer and Activator of Transcription 1 |
| ***t-Bu*** | Tertbutyl |
| **TBK1** | Tank-Binding Kinase 1 |
| **TGA** | Third Generation Antipsychotic |
| **TH** | Tyrosine Hydroxylase |
| **THC** | Tetrahydrocannabinol |
| **TIMP-2** | Tissue Inhibitor of Metalloproteinases 2 |
| **TFA** | Trifluoroacetic Acid |
| **TLC** | Thin-Layer Chromatography |
| **TNF** | Tumor Necrosis Factor |
| **TRPV1** | Transient Receptor Potential Cation Channel Subfamily V Member 1 |

USC UNIVERSIDADE DE SANTIAGO DE COMPOSTELA

| | |
|---|---|
| **U-3CR** | Ugi-3-Component Reaction |
| **U-4CR** | Ugi-4-Component Reaction |
| **UV** | Ultraviolet |
| **VCAM-1** | Vascular Cell Adhesion Molecule 1 |
| **VEGF** | Vascular Endothelial Growth Factor |
| **VEGFR** | Vascular Endothelial Growth Factor Receptor |
| **VGCC** | Voltage-Gated Calcium Channel |

USC
UNIVERSIDADE DE SANTIAGO DE COMPOSTELA

# RESUMO

Os receptores acoplados a proteínas G (GPCRs) teñen unha importancia significativa como dianas terapéuticas, sendo o obxectivo de aproximadamente o 35% dos medicamentos dispoñibles no mercado. Os GPCRs son receptores transmembrana de sete dominios que regulan diversas fervenzas de sinalización intracelular en resposta a hormonas, neurotransmisores, ións, fotóns e outros estímulos extracelulares. Esta transdución de sinais mediado por GPCRs é fundamental para a maioría dos procesos fisiolóxicos, como a visión, o olfacto e o tacto, ou funcións cardiovasculares, endocrinas e reprodutivas. Por iso, os programas de descubrimento de fármacos actuais están orientados a mellorar a terapia de máis de cincuenta dianas GPCR e aumentar a lista de posibles GPCR obxectivo. A presente Tese Doutoral centra o seu traballo nos receptores acoplados a proteínas G de dopamina $D_2$ e de cannabinoides $CB_2$.

A dopamina é un neurotransmisor catecolamina involucrado en numerosos procesos fisiolóxicos, como a motivación, o pracer, a memoria, a aprendizaxe, ou a modulación da sinalización endocrina, entre outros, no sistema nervioso central (SNC). A dopamina leva a cabo a maioría das súas accións fisiolóxicas a través de cinco GPCRs diferentes, pero estreitamente relacionados, que se dividen en dous grupos principais: receptores de tipo $D_1$ ($D_1R$ e $D_5R$) e receptores de tipo $D_2$ ($D_2R$, $D_3R$ e $D_4R$). $D_2R$ está expresado principalmente no corpo estriado, o núcleo accumbens e o tubérculo olfatorio, pero tamén se atopa na substancia negra, a área tegmental ventral, o hipotálamo, a cortiza cerebral e o hipocampo. Este receptor está relacionado co comportamento adictivo e compulsivo debido á súa implicación no sistema de recompensa, a motivación e funcións de aprendizaxe.

O receptor de dopamina $D_2$ xoga un papel significativo no desenvolvemento e manexo de enfermidades como a esquizofrenia e a enfermidade de Parkinson debido ao seu papel central no sistema dopaminérgico do cerebro. A teoría da dopamina na esquizofrenia postula que esta condición asóciase cunha actividade aumentada dos sistemas dopaminérxicos en certas áreas do cerebro. Os receptores $D_2$ son particularmente relevantes aquí, xa que están involucrados na mediación de moitos efectos da dopamina relacionados coa cognición, o comportamento e a percepción. Os antipsicóticos tradicionais, utilizados para tratar a esquizofrenia, adoitan ser antagonistas do $D_2R$, o que significa que bloquean a actividade deste receptor. Isto axuda a reducir os síntomas psicóticos, con todo, ten efectos secundarios asociados como parkinsonismo, hiperprolactinemia, distonía, acatisia e discinesia tardía.

A enfermidade de Parkinson está caracterizada pola morte de neuronas produtoras de dopamina na substancia negra do cerebro. Isto leva a unha diminución nos niveis de dopamina e afecta o funcionamento dos receptores $D_2$. A activación do $D_2R$ mediante agonistas foi considerada como unha estratexia viable no tratamento do Parkinson. A levodopa, un precursor da dopamina, continúa sendo o tratamento sintomático máis efectivo para esta enfermidade, con todo, presenta unha baixa biodisponibilidad e unha vida media extremadamente corta no plasma. Os agonistas de $D_2R$ evitan a necesidade da síntese presináptica de dopamina e presentan unha biodispoñibilidade moito maior. A pesar diso, esta solución non foi suficiente para tratar efectivamente o Párkinson, polo que a comunidade médica necesita novas estratexias que poidan superar estas dificultades. No primeiro capítulo desta tese, exploraremos unha destas estratexias mediante a síntese de ligandos alostéricos do $D_2R$.

Os moduladores alostéricos son compostos que interaccionan con sitios de unión topolóxicamente distintos do sitio ortostérico. Mostran vantaxes específicas respecto aos ligandos tradicionais, como unha maior selectividade polos subtipos de GPCRs e o potencial de preservar a dependencia espacial e temporal da actividade, característico dos ligandos fisiolóxicos endóxenos. Os moduladores alostéricos do $D_2R$ amosaron potencial clínico como medicamentos máis seguros e eficientes no tratamento de enfermidades do SNC, como o Párkinson e a esquizofrenia. Dende o punto de vista farmacolóxico, os moduladores alostéricos poden clasificarse en tres categorías: moduladores alostéricos positivos (PAMs) se o modulador aumenta o efecto (potencia e eficacia) do agonista; moduladores alostéricos negativos (NAMs) se o modulador diminúe o efecto do ligando endóxeno; e moduladores alostéricos silentes (SAMs) se o modulador se une ao sitio alostérico e non ten efecto no ligando endóxeno. Considerando que PAMs e NAMs poden afectar tanto á potencia como á eficacia do ligando endóxeno, as opcións de estratexias terapéuticas expándense a agonistas PAM, antagonistas PAM, agonistas NAM, e agonistas inversos NAM.

A melanostatina ou PLG (L-prolyl-L-leucyglycinamide) é un dos poucos exemplos de neuropéptido que actúa como PAM no $D_2R$, aumentando o efecto da dopamina e dos seus agonistas sintéticos. A melanostatina favorece a unión destes ligandos aos subtipos de receptor $D_2R$ e $D_4R$, pero non aos subtipos $D_1R$ e $D_4R$. O mecanismo de acción deste neuropéptido consiste na transformación do $D_2R$ dende o seu estado de baixa afinidade ao seu estado de alta afinidade, facéndoo máis selectivo á acción de agonistas. Debido ao seu

USC
DE SANTIAGO
DE COMPOSTELA

importante rol na modulación do $D_2R$, a melanostatina foi obxecto de múltiples estudos centrados no desenvolvemento de futuros tratamentos de enfermidades neurodexenerativas como a esquizofrenia ou a enfermidade de Párkinson, para as que a actividade terapéutica da melanostatina foi confirmada por varios estudos. Con todo, a pesar do seu gran potencial, este neuropéptido leva asociados certos problemas farmacocinéticos (pouca absorción gastrointestinal e labilidade fronte a proteasas do SNC) que entorpecen a progresión dos ensaios clínicos e o seu uso no Parkinson. Por iso, e grazas aos positivos resultados terapéuticos iniciais, múltiples grupos de investigación intensificaron a exploración e o desenvolvemento da melanostatina como ligando alostérico do $D_2R$, culminando na creación de varias coleccións de análogos deste neuropéptido. Estes esforzos foron liderados polo grupo do profesor Sampaio-Dias, da universidade do Porto, cuxo programa de investigación constitúe o proxecto orientado á obtención de análogos da melanostatina máis exhaustivo. Entre os seus resultados inclúense varios compostos máis lipofílicos e con mellor actividade PAM que a melanostatina, ademais de demostrar a capacidade do sitio alostérico do $D_2R$ de acomodar aneis heteroaromáticos na posición N-terminal da melanostatina, e a tolerabilidade do éster metílico en lugar da habitual amida terminal.

Inspirado polo éxito do grupo do profesor Sampaio-Dias, e empregando a estrutura da melanostatina como modelo, o primeiro capítulo desta Tese Doutoral describe o deseño, síntese e optimización de análogos da melanostatina como moduladores alostéricos do $D_2R$. Os resultados aquí descritos forman parte dun proxecto metodolóxico que demostra as vantaxes competitivas das reaccións multicomponente en Química Médica. Neste contexto, deseñamos a síntese de tres sets de peptidomiméticos, cada un dos cales se centra nunha modificación estrutural diferente (Figura I).

O primeiro set consistiu nunha proba de concepto que validou o uso da reacción de Ugi como estratexia sintética multicompoñente no desenvolvemento de análogos da melanostatina. Para iso deseñouse a síntese de trinta e dous peptidomiméticos mediante as seguintes exploracións estruturais: substitución do residuo de prolina por homoprolina, metilación do nitróxeno da amida secundaria, substitución do residuo de isobutilo por isopropilo e substitución da amida terminal por éster metílico. Esta aproximación aproveita a similitude entre a estrutura da melanostatina e o aducto de Ugi (acilamino amida), e permite explorar de forma eficiente as características máis significativas da relación estrutura-actividade (SAR) dentro destas series, todo iso nunha soa etapa de reacción. A reacción de

USC
UNIVERSIDADE DE SANTIAGO DE COMPOSTELA

Ugi conleva a formación dun estereocentro, que se resolveu mediante purificación en columna cromatográfica. A asignación de cada diastereoisómero foi realizada mediante unha combinación de resonancia magnética nuclear de protón ($^1$H RMN) e dicroísmo circular (CD).

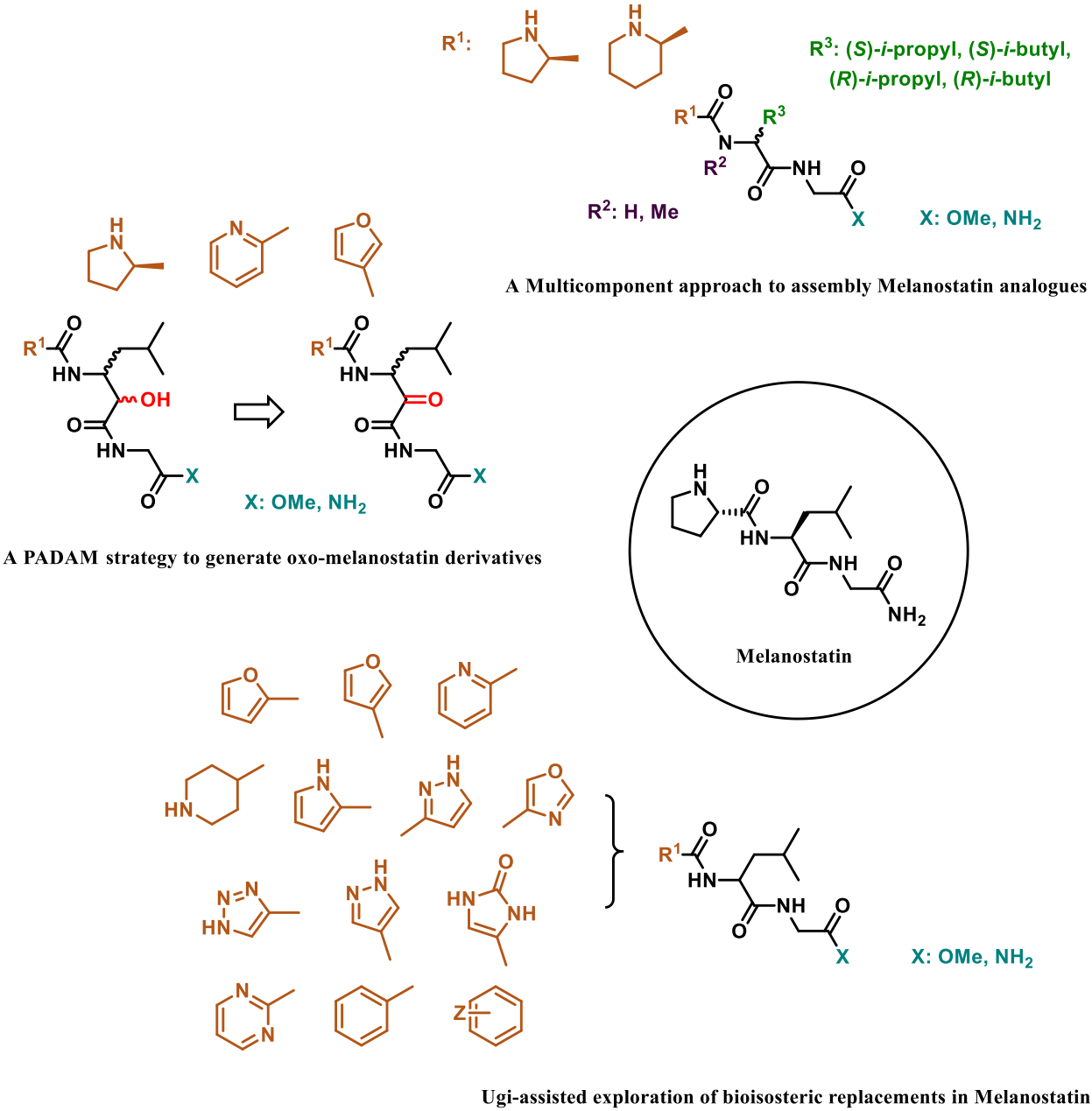



Figura I. Estratexia de deseño e elementos de diversidade estudados durante o primeiro capítulo da tese.

USC
UNIVERSIDADE DE SANTIAGO DE COMPOSTELA

O segundo set está centrado na substitución da prolina por vinte e tres heterociclos, tanto aromáticos como non aromáticos. Estes derivados foron sintetizados na súa forma de éster metílicos e na súa forma de amida. Do mesmo xeito que no primeiro set, os compostos descritos nesta serie son resultado da reacción de Ugi e, polo tanto, presentan un carbono asimétrico. Neste caso, este estereocentro permaneceu sen resolver e os compostos deste set foron avaliados como mestura racémica, salvo no caso dun dos compostos máis atractivos. Esta molécula foi empregada para realizar modificacións adicionais, como a separación dos seus enantiómeros por cromatografía líquida de alta resolución (HPLC) ou a metilación do nitróxeno da amida secundaria.

Para a obtención do terceiro e último set empregamos unha estratexia multicompoñente alternativa á reacción de Ugi. Mediante unha post-transformación da reacción de Passerini, coñecida como a ruta sintética PADAM (Passerini reaction, amine deprotection, acyl migration) obtivemos vinte e catro novos análogos que introducen un carbono adicional na estrutura da melanostatina. Ademais, como resultado da PADAM, este carbono ten unido un grupo hidroxilo, que pode ser oxidado ao grupo carbonilo correspondente, engadindo un novo punto de derivatización.

A análise dos datos farmacolóxicos demostra a efectividade das estratexias multicomponente na obtención de moduladores alostéricos do $D_2R$. Dos 110 análogos da melanostatina sintetizados, corenta e seis demostran unha efectividade similar ou superior (incremento do efecto de 0.1 µM de dopamina 10-40.02%) á melanostatina en polo menos unha das dúas concentracións avaliadas (0.01 nM e 1 nM). Ademais, trinta e seis compostos exhiben unha efectividade similar ou superior pero de sentido inverso (diminución do efecto de 0.1 µM de dopamina 10.31-54.18%) á melanostatina, é dicir, diminúen o efecto da dopamina, en polo menos unha das dúas concentracións avaliadas (0.01 nM e 1 nM).

O sistema endocannabinoide (ECS) está formado polos receptores de cannabinoides 1 e 2 ($CB_1R$ e $CB_2R$), os seus ligandos endóxenos (endocannabinoides, eCBs), e as encimas involucradas na síntese, metabolismo e transporte dos eCBs. $CB_1R$ está principalmente expresado no SNC, mentres que $CB_2R$ atópase fundamentalmente na periferia e células do sistema inmune, o que converte a este último nunha posible diana terapéutica para o tratamento de enfermidades autoinmunes e do cancro. A activación de $CB_2R$ recibiu atención polos seus efectos farmacolóxicos como antioxidante, antinflamatorio, inmunomodulador e anti apoptótico, que pode exercer sen causar os efectos psicotrópicos derivados da activación

USC
DE SANTIAGO
DE COMPOSTELA

de $CB_1R$. Ademais, $CB_2R$ demostrou potencial terapéutico en enfermidades onde existe activación da microglía e neuro inflamación, como a dor neuropática ou a enfermidade de Alzheimer.

O papel do ECS no contexto do cancro foi investigado en profundidade recentemente e varios estudos demostraron os efectos antitumorais dos agonistas do $CB_2R$ en diferentes tipos de cancro. A activación selectiva do receptores $CB_2R$ mediante agonistas demostrou ser prometedora en varios aspectos do tratamento contra o cancro. Un beneficio notable é a súa habilidade para provocar a morte celular programada, coñecida como apoptosis, nas células cancerígenas. Descubriuse que estes agonistas de $CB_2R$ inician procesos de sinalización que fomentan a apoptosis especificamente en células tumorais, protexendo ao mesmo tempo as células normais, o que resulta na diminución do tamaño do tumor. Este método dirixido reduce os efectos secundarios típicos da quimioterapia tradicional, que xeralmente impacta tanto ás células cancerosas como ás sas. Adicionalmente, os agonistas de $CB_2R$ presentan efectos anti-proliferativos, impedindo o crecemento e a división das células tumorais. Estes poden alterar os mecanismos de sinalización que controlan a proliferación celular, diminuíndo desta maneira o desenvolvemento e avance do tumor.

Pese ao considerable potencial preclínico que presenta a activación do $CB_2R$, moi poucos ligandos que teñen como diana este receptor foron probados en ensaios clínicos, e ningún alcanzou aínda o mercado. A dificultade de dispoñer de agonistas potentes e altamente selectivos polo $CB_2R$, que carezan dos efectos adversos producidos pola activación do $CB_1R$, limita a aplicación completa do potencial terapéutico deste receptor.

O segundo capítulo da presente Tese Doutoral describe o deseño, síntese e optimización dunha serie de novos e potentes ligandos selectivos de $CB_2R$ mediante a estratexia sintética PADAM. Do mesmo xeito que no primeiro capítulo, os resultados aquí descritos forman parte dun proxecto metodolóxico que demostra as vantaxes competitivas das reaccións multicompoñente en Química Médica.

Estes ligandos foron deseñados por analoxía coa estrutura dos agonistas sintéticos dos receptores cannabinoide (SCRAs). Durante a última década, os SCRAs xurdiron como o grupo máis grande e desafiante de novas substancias psicoactivas (NPS). Inicialmente concibidos no contexto de programas de descubrimento de fármacos, os SCRAs evolucionaron, converténdose nun problema de saúde pública debido aos seus efectos adversos, a súa dosaxe non regulada e o uso variable, que aumentan a probabilidade de

USC
UNIVERSIDADE DE SANTIAGO DE COMPOSTELA

intoxicación, sobredose e toxicidade grave. A maioría deles están pensados para activar $CB_1R$, pero moitos actúan tamén como agonistas de $CB_2R$. O grupo ComBioMed desenvolveu recentemente unha ampla colección de análogos dos SCRAs mediante unha aproximación multicompoñente que empregou a reacción de Ugi como metodoloxía sintética. Este procedemento aproveita a semellanza estrutural entre o farmacóforo de SCRA e a estrutura química dos aductos de Ugi (acilamino amida) e permitiu a identificación de corenta e sete compostos que destacan pola súa excelente afinidade (valores de $K_i$ $CB_2R$ entre 34.8 – 307 nM) e perfil de selectividade (>100 veces sobre o $CB_1R$). De forma análoga, o obxectivo do segundo capítulo desta Tese Doutoral foi a exploración dos espazos de diversidade optimizados no traballo da Dra. Gioè dentro da nova estrutura resultante da PADAM. Este estudo inspirouse no modelo farmacofórico da familia de SCRAs (Figura II) e nas tendencias SAR observadas nos traballos previos do grupo ComBioMed.

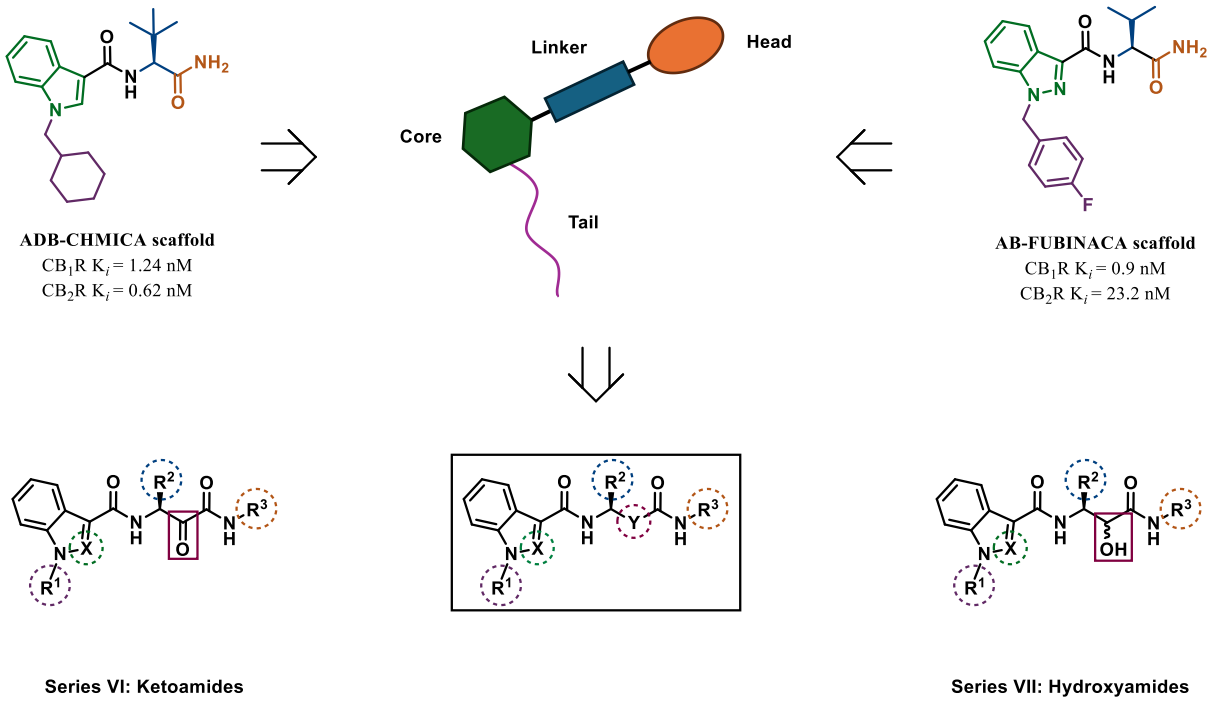



Figura II. Estratexia de deseño e os puntos de diversidade estudados durante o segundo capítulo desta tese.

Esta aproximación permite a síntese converxente e de alto rendemento de hidroxiamidas e cetoamidas, facilitando a exploración eficiente deste farmacóforo para identificar ligandos selectivos polo $CB_2R$, á vez que introduce un novo punto de diversidade en forma dun carbono adicional. Ademais, fixemos fincapé en explorar as características máis significativas

USC
UNIVERSIDADE DE SANTIAGO DE COMPOSTELA

da relación estrutura-actividade (SAR) e a relación estrutura-selectividade (SSR) dentro destas series.

Dende un punto de vista estrutural, a ruta sintética PADAM mantén os elementos farmacofóricos da estrutura dos SCRAs, co linker situado entre o núcleo heterocíclico e a cabeza do modelo farmacofórico. Isto permite a modificación e exploración en cinco posicións diferentes (Figura II). Previuse que o uso de ácidos N-substituidos-indol (ou indazol)-3-carboxílicos ($R^1$), α-boc-amino aldehídos ($R^2$) e isonitrilos ($R^3$) xerarían aductos de Passerini que, tras ser tratados con ácido trifluoroacético (TFA), axústanse perfectamente á estrutura do compostos obxectivo, coa incorporación dun carbono adicional. Explotando a versatilidade desta estratexia multicomponente, decidimos introducir diferentes grupos en $R^2$, para avaliar o impacto do volume estérico nesta posición, e en $R^3$, para avaliar o impacto da introdución de grupos na amida terminal.

Unha análise exhaustiva dos datos de afinidade obtidos para os 158 novos derivados (hidroxiamidas e cetoamidas) demostra a efectividade do proceso de farmacomodulación. A partir dun prototipo dual $CB_1R$-$CB_2R$, logramos disociar por completo o perfil de afinidade/selectividade destes receptores e descubrir novos e potentes ligandos que recoñecen especificamente o $CB_2R$. Oitenta e seis compostos descubertos neste capítulo destacan pola súa excelente afinidade (valores de $K_i$ $CB_2R$ entre 5.70 – 288 nM) e perfil de selectividade (>100 veces sobre o $CB_1R$). É importante destacar que a ruta sintética PADAM ten como resultado a formación dun carbono asimétrico no novo átomo de carbono unido ao hidroxilo. Co obxectivo de identificar o eutómero na parella de diastereisómeros, nove ligandos foron seleccionados para resolver este estereocentro e poder avaliar o impacto que a configuración deste carbono ten na afinidade e selectividade. A análise dos seus perfís de unión a $CB_1R$ e $CB_2R$ revelou a superioridade do perfil farmacolóxico da conformación (*R*), que en todos os casos correspondeu co produto maioritario da PADAM. Isto permitiu a purificación exclusiva do eutómero ao longo de toda a serie de hydroxiamidas, e polo tanto, os compostos pertencentes a esta serie son diastereoisómeros puros e non mesturas racémicas.

Por último, realizouse unha avaliación farmacolóxica avanzada e estudos *in vitro* dos ligandos seleccionados para o $CB_2R$. Este apartado está dedicado a unha caracterización máis profunda da farmacoloxía e á avaliación preliminar dalgunhas das aplicacións terapéuticas dos mellores compostos identificados nesta Tese Doutoral. Inicialmente, corroborouse o comportamento agonista dos compostos seleccionados a través de experimentos funcionais de

USC
DE SANTIAGO
DE COMPOSTELA

AMPc, logo realizouse un estudo detallado das súas vías de sinalización (nesgadas ou non nesgadas). Os ligandos seleccionados (**(2*R*)-178**, **(2*R*)-182**, **(2*R*)-183**, **(2*R*)-188**, **(2*R*)-193**) agrupáronse segundo o seu comportamento funcional como ligandos nesgados pola vía da proteína G. O fenómeno polo cal os ligandos dos GPCR modulan selectivamente a vía da proteína G e/o da β-arrestina para mediar rutas específicas de transdución de sinais coñécese como "selectividade funcional" ou "agonismo nesgado". O concepto de agonismo nesgado transformou significativamente a nosa comprensión da sinalización dos GPCR e revolucionou o campo do descubrimento de fármacos. Con todo, os mecanismos moleculares que subxacen ao nesgo na sinalización aínda son en gran medida descoñecidos, e investigar as contribucións funcionais das vías de sinalización da proteína G e a β-arrestina para os ligandos endóxenos e exógenos segue sendo unha tarefa desafiante. Tras a activación dos receptores de membrana (GPCRs), poden coexistir diversas vías de sinalización e efectores celulares. Ademais das proteínas G, os GPCR poden interactuar con múltiples moléculas de sinalización intracelular, incluíndo β-arrestinas, proteínas de andamiaxe e outras moléculas de sinalización. Estas moléculas desempeñan un papel na sinalización dos GPCR ao involucrar vías alternativas, o que resulta na activación de diversos efectores celulares e respostas. A natureza complexa da sinalización dos GPCRs, coa participación de múltiples vías, expón desafíos para identificar ligandos que exhiban sinalización nesgada. Comprender os perfís de sinalización nesgada de novos agonistas selectivos do $CB_2R$ é esencial para o desenvolvemento de fármacos cunha eficacia e perfís de seguridade mellorados. Esta comprensión pode axudar a identificar compostos con perfís de sinalización favorables, activando selectivamente vías específicas mentres se evitan outras. Estes avances poden contribuír ao desenvolvemento de fármacos máis selectivos e con menores efectos secundarios.

Finalmente, dous dos ligandos máis potentes e selectivos (**87** e **(2*R*)-178**) foron seleccionados para levar a cabo ensaios *in vitro* nos que avaliar a súa eficacia na redución da proliferación dun cancro altamente agresivo (glioblastoma). Debido á potencial aplicación dos agonistas do $CB_2R$ no tratamento do cancro, o noso obxectivo foi investigar a actividade proliferativa dos nosos compostos máis prometedores nunha liña celular modelo. Baseándonos en estudos previos que demostraron a efectividade *in vitro* de dous fitocannabinoides, o $\Delta^9$-THC e o CBD (un fitocannabinoide non psicoactivo), nunha liña celular de glioblastoma (U87), seleccionamos esta liña como o noso modelo. O glioblastoma é un tumor altamente agresivo do sistema nervioso central caracterizado por unha reducida

USC
UNIVERSIDADE DE SANTIAGO DE COMPOSTELA

supervivencia dos pacientes e unha demanda urxente de novas opcións de tratamento. Observamos que os compostos seleccionados reduciron significativamente a proliferación celular da liña celular de glioblastoma U87 de maneira dependente da dose, con reducións que oscilaron entre aproximadamente o 30% e o 60%. En particular, o composto **(2*R*)-178** amosou unha notable redución (58%) na proliferación do glioblastoma a unha concentración de 20 μM. Aínda que estes achados son preliminares, a inhibición observada da proliferación celular *in vitro* resalta o potencial dos agonistas seleccionados do $CB_2R$ como candidatos prometedores para unha maior exploración e inclusión en programas de desenvolvemento de fármacos. Ademais, estes resultados validan o papel do agonismo do $CB_2R$ na inhibición da proliferación celular en modelos de cancro *in vitro*, subliñando a importancia da modulación do sistema endocannabinoide (ECS) no tratamento do cancro.

USC
UNIVERSIDADE DE SANTIAGO DE COMPOSTELA

USC
UNIVERSIDADE
DE SANTIAGO
DE COMPOSTELA

# 1 INTRODUCTION

G protein-coupled receptors (GPCRs) hold significant prominence as drug targets, with a minimum of 134 GPCRs being the focus of drugs approved in the United States or European Union. Additionally, about 35% of the drugs available in the market aim at GPCRs.[1] In the year 2019, five out of the twenty first-in-class therapeutic agents that gained approval targeted GPCRs, contributing to annual sales of GPCR-targeting medications surpassing $114 billion USD in 2018.[2] Furthermore, GPCRs are currently the most intensively investigated drug targets in the pharmaceutical industry as they are targeted by about 50% of recently launched drugs.[3]

GPCRs are seven-transmembrane domain proteins that regulate a diverse array of intracellular signaling cascades in response to hormones, neurotransmitters, ions, photons, odorants, and other extracellular stimuli. As such, they play an essential role in physiology and disease.[4] The variety of the extracellular ligands is reflected in the structural diversity of more than 800 humans GPCRs, which can be grouped into five major families and numerous subfamilies (depending on their amino acid sequences).[5] Signal transduction by GPCR is fundamental for most physiological processes, from vision, smell, and taste to neurological, cardiovascular, endocrine, and reproductive functions; thus, the GPCR superfamily is a major target for therapeutic intervention.[6] Current drug discovery efforts aim to improve therapies for more than 50 established GPCR targets and expand the list of targeted GPCRs. In addition to activating GPCR signals with agonists and inhibiting GPCRs with antagonists and inverse agonists, trends in modern pharmacology include discovery of allosteric and/or functionally selective modulators that bias downstream signaling toward specific G protein-activated or β-arrestin-activated pathways.[6]

## 1.1 EVOLUTION OF GPCRS STUDY

In 1983, the primary structure of rhodopsin, the first identified and model GPCR, was published.[7] It was shown that this protein is a membrane-spanning protein that converts the energy from light into intracellular signaling cascades, which enables us to see. Significant technical advances have been made through the development of methods for radioligand

USC UNIVERSIDADE DE SANTIAGO

binding, solubilization, and purification of monoamine-binding GPCRs, which have further developed the concept of the GPCR superfamily.[8] The number of known GPCRs has grown rapidly, and it has become evident that this family of proteins can bind to a broad range of ligands, including small organic compounds, eicosanoids, peptides, and proteins. The classification of this superfamily was first developed attending to the differences in the primary structure of its members, resulting in the phylogenetic classification.[9] This was the first attempt by Attwood and Findlay in 1993 when they developed sequence-based fingerprints of the seven characteristic GPCR hydrophobic domains.[10] These were subsequently used as diagnostic tools for identifying sequences belonging to the GPCR superfamily, which led to an increase in their dataset from 240 to 393 rhodopsin-like GPCRs from different species.[10,11]

One year later, Kolakowski presented an important overview of the GPCR superfamily and the A-F classification system.[5] Kolakowski included all receptor proteins that were proven to bind G-proteins, while the remaining seven transmembrane-spanning proteins were assigned to the O (Other) family. Nockaert and Pin introduced a similar but extended nomenclature system for classifying GPCRs in 1999, in which the GPCRs were divided into family 1-5 on the basis of structural and ligand-binding criteria.[5]

When the first draft of the human genome came out in 2001, it facilitated a more comprehensive view of the human GPCR repertoire.[5] Many full-length GPCR sequences were collected, while simultaneously and independently, Frediksson and colleagues divided 802 (known and predicted) human GPCRs into families on the basis of phylogenetic criteria.[12] This divided most human GPCRs into five families (Figure 1.1): Glutamate (class C), Rhodopsin (class A), Adhesion, Frizzled/Taste2 and Secretin (class B).[12]

The total number of known and verified human GPCRs has continued to grow and now consists of at least 799 unique full-length members to which several new GPCRs with highly complex genomic structures have recently been added.[5]

USC
UNIVERSIDADE DE SANTIAGO DE COMPOSTELA

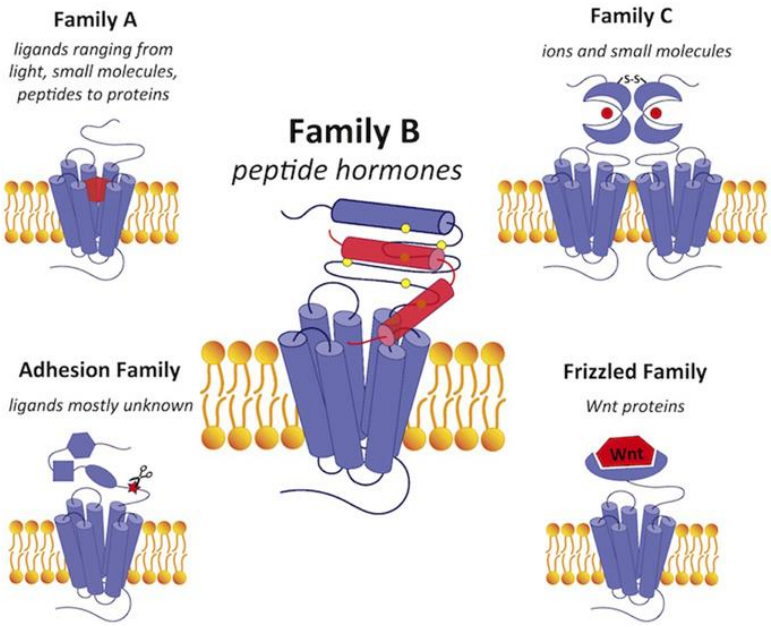



Figure 1.1. Classification of the GPCR superfamily based on their phylogenetic relationship (Figure from Culhane, K.; Liu, Y.; Yingying, C.; Yan, E. Transmembrane Signal Transduction by Peptide Hormones via Family B G Protein-Coupled Receptors. Frontiers in Pharmacology 2015, 6. https://doi.org/10.3389/fphar.2015.00264. Licensed under CC BY).[13]

## 1.2 RHODOPSIN RECEPTOR FAMILY

The Rhodopsin receptor family is the largest family of GPCRs, contains approximately 670 full-length human receptor proteins, and can be further divided into four groups: α, β, γ, and δ.[5] Considering their primary structure and ligand preference, the Rhodopsin family of GPCRs is highly heterogeneous. The diversity is not found in their N-termini, where most receptors have only a short stretch of amino acids, but within the transmembrane regions, although most Rhodopsin family receptors do share specific sequence motifs within the 7TM regions.[5]

Rhodopsin members bind to a vast variety of ligands, such as peptides, amines, and purines, and the family also contains the largest number of receptors targeted by clinically used drugs.[5]

The α-group contains at least 19 important drug targets: the histamine receptors 1 and 2; the dopamine receptors 1 and 2; the serotonin receptors 1A, 1D and 2A; the adrenoceptors 1A, 2A, B1 and B2; the muscarinic receptor 3; the prostanoid receptors TP, EP1, EP3, IP1 and FP; and the cannabinoids receptor 1 and 2.[5,14] In this Doctoral Thesis we will focus on the dopamine receptor 2 ($D_2R$) and the cannabinoid receptor 2 ($CB_2R$).

USC UNIVERSIDADE DE SANTIAGO DE COMPOSTELA

### 1.3 DOPAMINE AND DOPAMINE RECEPTOR (DR)

Dopamine is a catecholamine neurotransmitter involved in numerous physiological processes, such as motivation, pleasure, cognition, memory, learning, and endocrine signaling modulation, among others, in the central nervous system (CNS).[15] It contains a nucleus of catechol (benzene ring with two adjacent hydroxyl groups) and a side chain of ethylamine or one of its derivatives. Dopamine is synthesized from the amino acid tyrosine via a two-step enzymatic process (Figure 1.2).

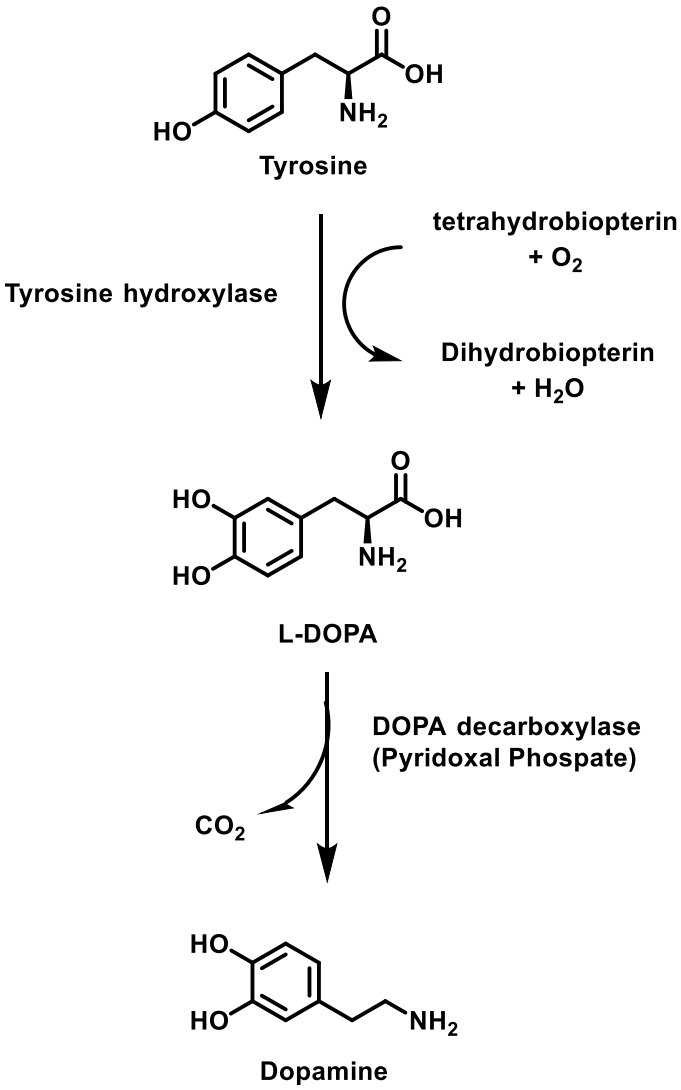



Figure 1.2. Biosynthesis of dopamine.

The first rate-limiting reaction involves the conversion of tyrosine into L-3,4-dihydroxyphenylalanine (L-DOPA or levodopa) catalyzed by tyrosine hydroxylase (TH). The

USC UNIVERSIDADE DE SANTIAGO DE COMPOSTELA

second step is carried out by aromatic L-amino acid decarboxylase (AADC), which produces dopamine by decarboxylation of DOPA.[16]

Dopamine, like other monoamine neurotransmitters, typically modulates neuronal circuitry through a relatively slow alteration of rapid neurotransmission, which is primarily mediated by neurotransmitters like glutamate and GABA.[17] Four major dopaminergic pathways have been identified in the mammalian brain; the nigrostriatal, mesolimbic, mesocortical and tuberoinfundibular systems that originate from the A9 (nigrostriatal), A10 (mesolimbic and mesocortical, often collectively termed the mesocorticolimbic pathway), and A8 (tuberoinfundibular) groups of dopamine-containing cells.[18]

The dopaminergic systems have been the focus of much research over the past 50 years, mainly because deregulation of the dopamine signaling is implicated in the physiopathology of neuropsychiatric diseases of high prevalence, such as Parkinson's disease, schizophrenia, Tourette's syndrome, and hyperprolactinemia.[15] A simple search of the terms "dopamine receptor" in the PubMed database result in more than 67,000 entries, and the number of articles addressing dopamine receptor physiology is growing on a daily basis.[19]

Most of the physiological actions of dopamine are mediated by five distinct but closely related GPCRs, which are divided into two major groups: $D_1$ and $D_2$ classes of dopamine receptors.[20] This classification is generally based on original biochemical observations showing that dopamine is able to modulate adenylyl cyclase (AC) activity, to which $D_1R$ is positively coupled, while $D_2R$ decreases AC activity. Thus, the separation was based mostly on their ability to modulate cAMP production and the differences in their transduction pathways, genetic organizations, structure, sequence alignment, and function.[18,21] A later characterization of the dopamine receptor families using genetic cloning approaches revealed that multiple receptor subtypes can be activated by dopamine. On the basis of their structural, pharmacological, and biochemical properties, these receptors were classified as either $D_1$-class dopamine receptors ($D_1R$ and $D_5R$) or $D_2$-class dopamine receptors ($D_2R$, $D_3R$, and $D_4R$).[18] The first ones share 80% amino acid sequence homology within the transmembrane regions, coupled with the stimulatory G-protein ($G_S$) to stimulate the activity of adenylyl cyclase. Similarly, $D_2R$ shares 75% homology with the $D_3R$ transmembrane region and 53% homology with the $D_4R$ transmembrane regions, respectively. Additionally, these receptors couple with the inhibitory G-protein ($G_i$) to inhibit the activity of adenylyl cyclase.[21]

USC UNIVERSIDADE DE SANTIAGO DE COMPOSTELA

## 1.4 DOPAMINE $D_2$ RECEPTOR ($D_2R$)

### 1.4.1 Structure, function, and localization

GPCR structures have been effectively employed in guiding the discovery of new ligands.[22] In the case of $D_2$-class receptors, structures of $D_3R$ and $D_4R$ have been elucidated in complex with the benzamide antipsychotics eticlopride and nemonapride, respectively.[22] However, despite the fact that $D_2R$ was cloned nearly 30 years ago and has been the subject of extensive pharmacological, mutagenesis, and molecular-modelling studies, there remains a notable absence of high-resolution structures of $D_2R$ in complex with ligands, which limits our molecular understanding of its function.[23] Inactive conformations of $D_2R$ have been described in complexes with risperidone,[23] haloperidol,[24] and spiperone.[22] Figure 1.3 shows the structure of $D_2R$ in complex with spiperone ($D_2R_{spi}$).

Crystallization was accomplished using a stable construct of the $D_2R$, which includes mbIIG (loop-modified cytochrome $b_{562}$IIG), since the wild-type $D_2R$ was not expressed in the insect cells utilized in the study.[22] Additionally, an antibody recognizing the $D_2R$ structure (IgG3089) was generated and a novel Fab (Fragment, antigen binding) fragment of IgG3089 was prepared.[22] With the stabilized construct and Fab3089, crystals of $D_2R$ were successfully obtained. The structure of $D_2R$ was determined in complex with spiperone at a resolution of 3.1 Å using an X-ray free-electron laser.[22] $D_2R_{spi}$ displayed the canonical GPCR fold, featuring seven transmembrane helices (TM1-7) and an intracellular amphipathic helix 8 (H8). The stabilized conformation demonstrated to be the inactive state conformation. Similar to other class A GPCRs, the ligand-binding pocket was covered by the C-terminal segment of the extracellular loop (ECL) 2, which is stabilized by a disulfide bond between Cys107$^{3.25}$ on TM3 and Cys182$^{45.50}$ on ECL2.[22] The ligand-binding pocket of $D_2R_{spi}$ is depicted in Figure 1.4.

USC UNIVERSIDADE DE SANTIAGO DE COMPOSTELA

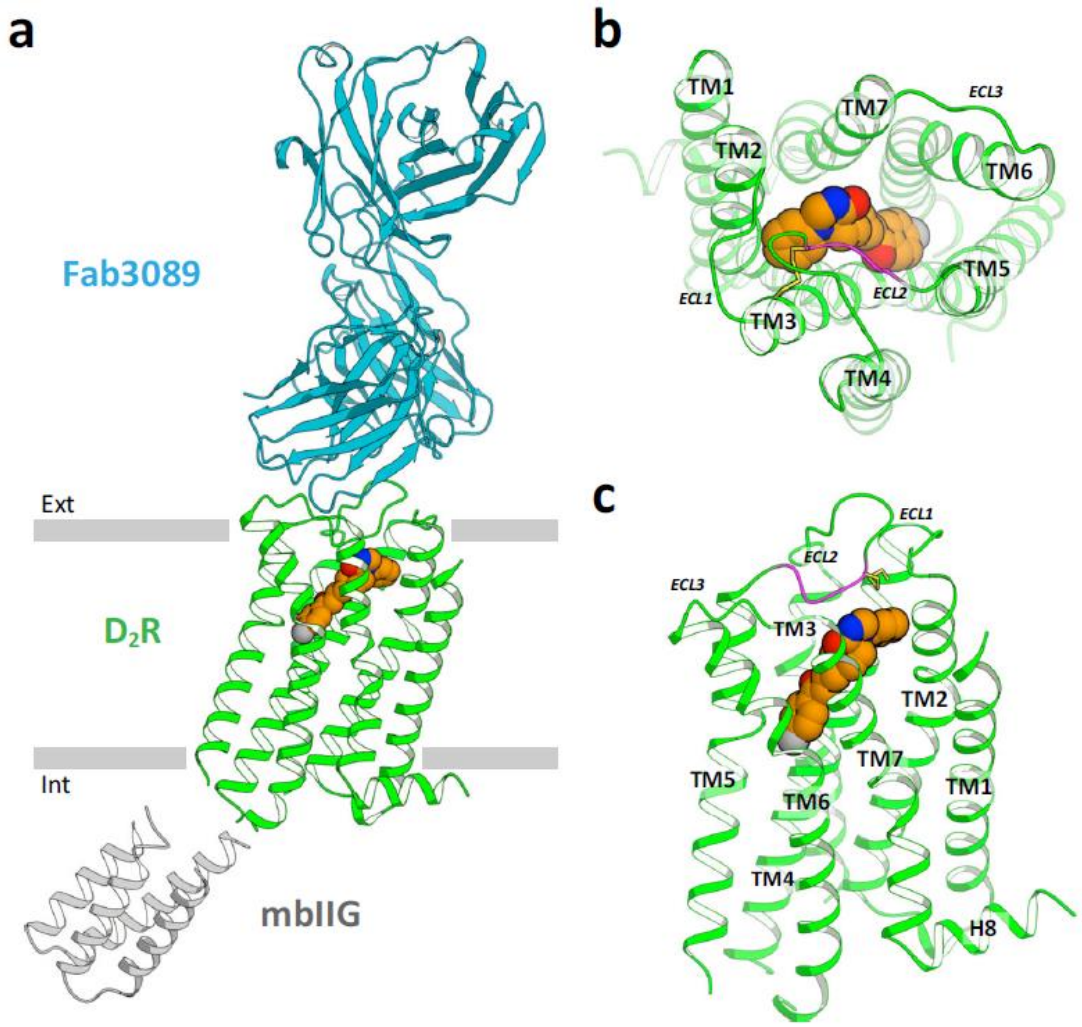



Figure 1.3. Structure of $D_2R$ in complex with spiperone. a) Overall structure of $D_2R_{spi}$-Fab 3089 complex. Extracellular (b) and side (c) views of $D_2R_{spi}$. Spiperone, $D_2R$, Fab3089, and mbIIG are indicated in orange, green, cyan, and gray, respectively. The disulfide bond and the C-terminal segment of ECL2 are shown in yellow and magenta, respectively, in (b) and (c). Ext, extracellular; Int, intracellular (Figure from Im, D.; Inoue, A.; Fujiwara, T.; Nakane, T.; Yamanaka, Y.; Uemura, T.; Mori, C.; Shiimura, Y.; Kimura, K. T.; Asada, H.; Nomura, N.; Tanaka, T.; Yamashita, A.; Nango, E.; Tono, K.; Kadji, F. M. N.; Aoki, J.; Iwata, S.; Shimamura, T. Structure of the Dopamine $D_2$ Receptor in Complex with the Antipsychotic Drug Spiperone. Nat Commun 2020, 11, 6442. https://doi.org/10.1038/s41467-020-20221-0. Licensed under CC BY).[22]

USC UNIVERSIDADE DE SANTIAGO DE COMPOSTELA

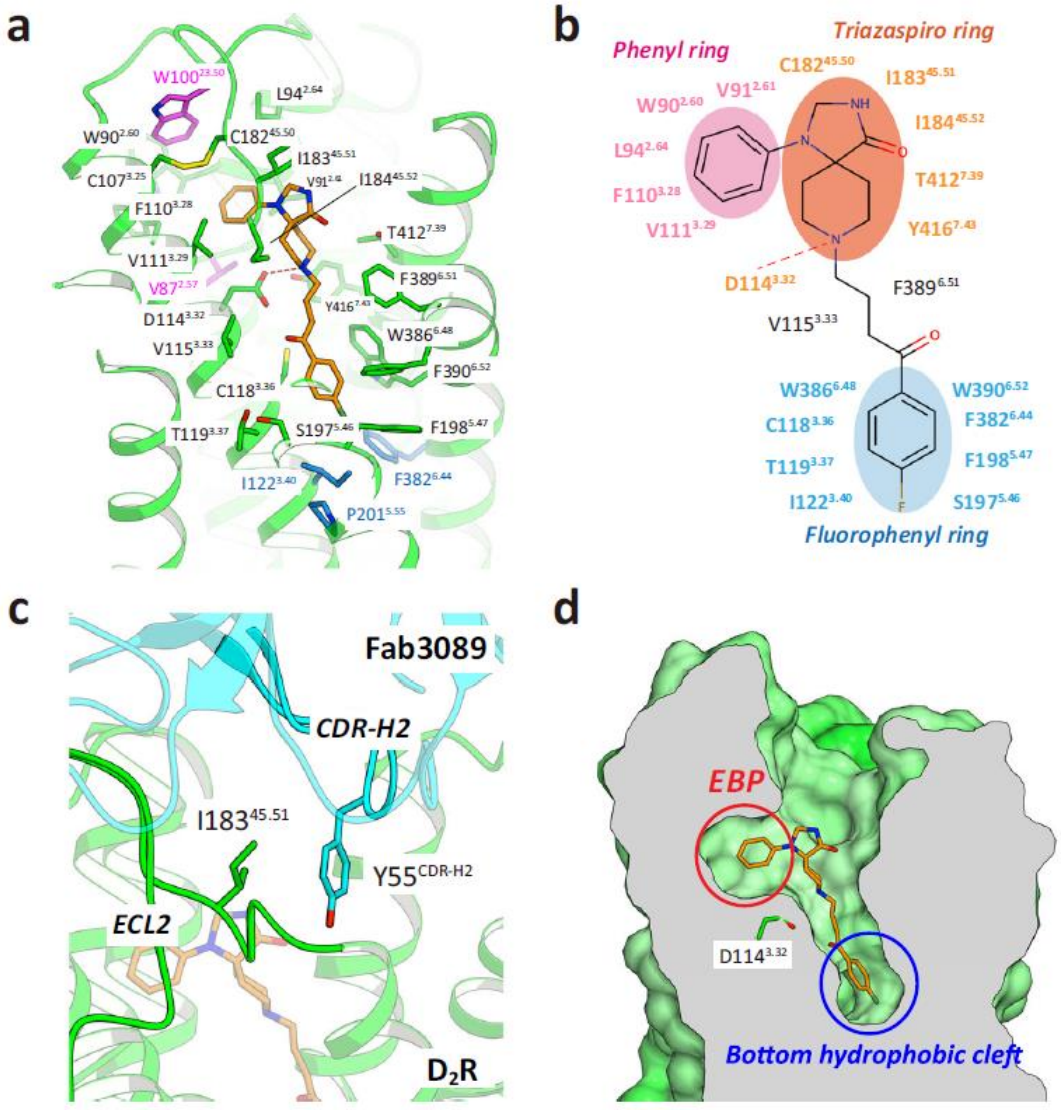



Figure 1.4. The ligand-binding pocket of $D_2R_{spi}$. a) Close-up view of the ligand-binding pocket of $D_2R_{spi}$. Spiperone and $D_2R$ are indicated in orange and green, respectively. The side chains of the contact residues within 4.5 Å of spiperone are shown as green sticks. b) Diagram of the interactions between $D_2R$ and spiperone. c) Fab3089 binding site. The side chains of $I183^{45.51}$ of $D_2R_{spi}$ and Y55 of Fab3089 are shown as green and cyan sticks, respectively. d) Vertical cross section of (a). Red and blue circles indicate the EBP and the bottom hydrophobic cleft, respectively (Figure from Im, D.; Inoue, A.; Fujiwara, T.; Nakane, T.; Yamanaka, Y.; Uemura, T.; Mori, C.; Shiimura, Y.; Kimura, K. T.; Asada, H.; Nomura, N.; Tanaka, T.; Yamashita, A.; Nango, E.; Tono, K.; Kadji, F. M. N.; Aoki, J.; Iwata, S.; Shimamura, T. Structure of the Dopamine $D_2$ Receptor in Complex with the Antipsychotic Drug Spiperone. Nat Commun 2020, 11, 6442. https://doi.org/10.1038/s41467-020-20221-0. Licensed under CC BY).[22]

In $D_2R_{spi}$, spiperone is surrounded by residues from TM2, 3, 5, 6, and 7 as well as ECL2.[22] The tertiary amine in the triazaspiro ring forms a salt bridge with $Asp114^{3.32}$, a feature strictly conserved in aminergic receptor structures. On the opposite side of spiperone

from Asp114$^{3.32}$, there are hydrophobic interactions between spiperone and Phe389$^{6.51}$, which are crucial for spiperone binding.[22] Furthermore, there are interactions between the triazaspiro ring and Ile183$^{45.51}$, Ile184$^{45.52}$, and Cys182$^{45.50}$ on ECL2.

On the extracellular side of the salt bridge, the phenyl ring of spiperone is situated in an extended binding pocket (EBP) between TM2 and TM3.[22] This EBP is formed by residues Val87$^{2.57}$, Trp90$^{2.60}$, Val91$^{2.61}$, Leu94$^{2.64}$, Trp100$^{23.50}$, Phe110$^{3.28}$, Val111$^{3.29}$, and Cys182$^{45.50}$, and is likely essential for spiperone binding. Within the EBP spiperone's phenyl ring engages in hydrophobic interactions with Trp90$^{2.60}$, Val91$^{2.61}$, Leu94$^{2.64}$, Phe110$^{3.28}$, and Val111$^{3.29}$.[22]

Finally, on the intracellular side of the salt bridge, the fluorophenyl ring of spiperone deeply penetrates the ligand-binding pocket, binding within the bottom hydrophobic cleft.[22] In this cleft, the fluorophenyl ring forms a CH–π interaction with Cys118$^{3.36}$, hydrophobic interactions with Thr119$^{3.37}$, Ile122$^{3.40}$, Ser197$^{5.46}$, Phe198$^{5.47}$, and Phe382$^{6.44}$, and edge-to-face π interactions with Trp386$^{6.48}$ and Phe390$^{6.52}$. The interaction with Phe390$^{6.52}$ is essential for spiperone binding, while contact with Phe198$^{5.47}$ is not necessary.[22]

The $D_2R$ presents two isoforms $D_{2S}R$ (short) and $D_{2L}R$ (long) that differ because of a 29 amino acid insertion in the third intracellular loop on $D_{2L}R$.[25] Because this loop seems to play a central role in receptor coupling, the existence of a splicing mechanism at this level could imply functional diversity. However, no obvious differences have been reported between the two $D_2R$ isoforms.[15] Both of them can inhibit intracellular cAMP via Gi,[25] and they revealed the same pharmacological profile, even though a marginal difference in affinity has been reported. $D_{2S}R$ primarily function as autoreceptors on the presynaptic membrane, while $D_{2L}R$ acts as a postsynaptic receptor.[21]

$D_2R$ are mainly expressed in the striatum, the nucleus accumbens and the olfactory tubercle, but they are also expressed at substantia nigra, ventral tegmental area, hypothalamus, cortical areas, septum, amygdala and hippocampus.[18] The $D_2R$ has a variety of physiological functions:[18] activation of the $D_{2S}$ autoreceptors results in decreased dopamine release, which leads to a decrease in locomotor activity, whereas $D_{2L}R$ activation leads to increases in locomotion. Because these $D_2$-class autoreceptors are generally activated by a lower concentration of dopamine agonists than necessary to activate postsynaptic receptors, the same dopamine agonists can induce a biphasic effect, leading to decreased activity at low doses and behavioral activation at high doses.[18] This receptor is related to addictive and compulsive behaviors due to its implication in reward, motivation and learning functions.[26]

USC DE SANTIAGO DE COMPOSTELA

Additionally, it mediates memory functions (working memory) within hippocampal regions, as well as executive functions (attention, planning).[21]

### 1.4.2 Signaling

All dopamine receptors are GPCRs, and so their signaling is mediated by the interaction with and activation of heterotrimeric GTP-binding proteins (G proteins).[27] Specifically, $D_2$-like receptor signaling is mediated by activation of $G\alpha_{i/o}$ (Figure 1.5), a class of proteins inactivated by pertussis toxin-catalyzed ADP-ribosylation. For $D_2R$, there is debate regarding which G protein interacts with $D_{2S}R$ and $D_{2L}R$, as it seems likely that both isoforms can activate multiple $G\alpha_{i/o}$ subtypes. However, accumulating evidence from a variety of approaches has identified $G\alpha_o$ as the $G\alpha_{i/o}$ subtype that is most robustly activated by $D_{2L}R$ and by $D_{2S}R$, and, furthermore, the G protein subtype that is predominantly coupled to $D_2$-like receptors in mouse brain.[27]

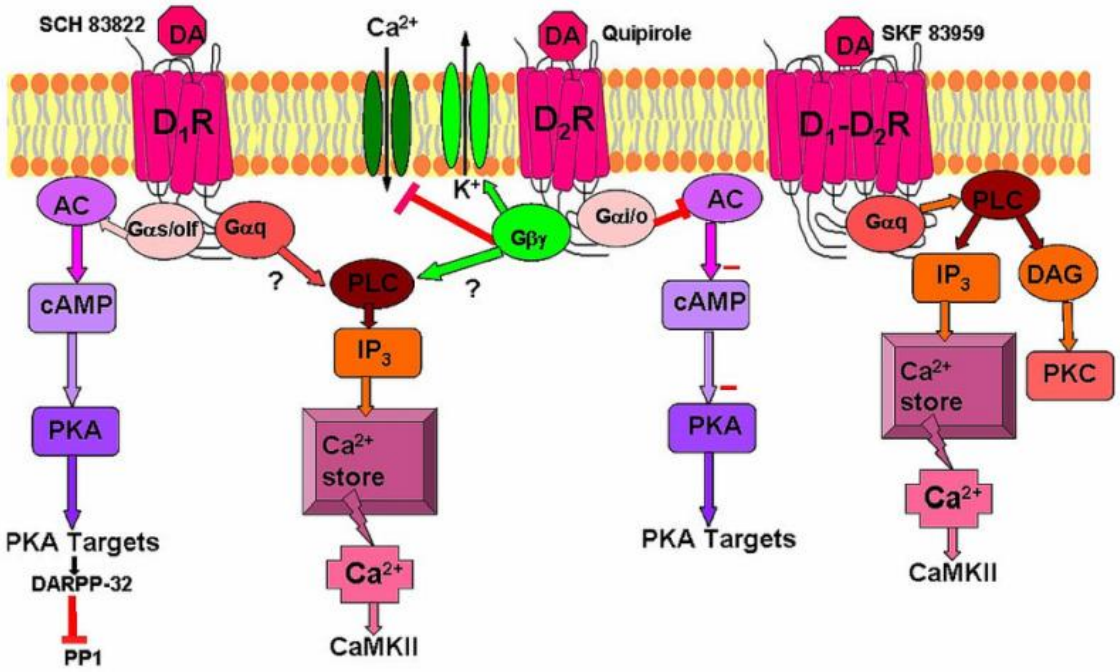



Figure 1.5. Signaling pathways though dopamine homomeric $D_1R$ and $D_2R$ and heteromeric $D_1$-$D_2$ receptors. The respective agonists of the different receptor types are shown above the receptors (Figure from Popova, E. Role of Dopamine in Retinal Function. In Webvision: The Organization of the Retina and Visual System [Internet]; University of Utah Health Sciences Center, 2020. https://www.ncbi.nlm.nih.gov/books/NBK561740/. Licensed under CC BY-NC).[28]

USC UNIVERSIDADE DE SANTIAGO DE COMPOSTELA

The inhibitory effect of the AC that the $D_2R$ presents in the pituitary and in the CNS was shown early in the 1980s.[15] This causes an overall decrease in the levels of cAMP, and subsequently, decreases protein kinase A (PKA) activity (Figure 1.5).[21]

$D_2$-like receptors also mediate changes in intracellular calcium levels, with opposing effects depending on the cell type.[15] $D_2R$ in neostriatal large aspiny (cholinergic) interneurons inhibit N-type $Ca^{2+}$ channels via a membrane-delimited pathway that probably involves $G_{\beta\gamma}$ subunits (Figure 1.5).[27] The $G_{\beta\gamma}$ subunits target the I-II transmembrane domain linker region and/or the COOH terminus of the α-subunit of these $Ca^{2+}$ channels, decreasing the amount of current carried. $D_2R$ in striatal medium spiny neurons decrease L-type $Ca^{2+}$ currents. This response is also mediated by $G_{\beta\gamma}$ subunits, although rather than being membrane delimited, the pathway involves $G_{\beta\gamma}$ stimulation of cytosolic phospholipase C, mobilization of $Ca^{2+}$, and activation of calcineurin.[27] The functional effects of this modulation may possibly regulate neurotransmitter release when the N-type $Ca^{2+}$ channels are targeted; thus, $D_2R$ activation of neostriatal interneurons inhibits the release of acetylcholine, and $D_2$-like receptor stimulation decreases glutamate release in the striatum, presumably via effects on N-type $Ca^{2+}$ channels.[27] Inhibition of glutamate release may implicate tonic $D_2R$ activity in the prevention of excessive glutamate release; together with $D_2R$ inhibition of L-type channels in neostriatal medium spiny neurons, this would be expected to promote the downstate in neostriatal projection neurons.[27]

Finally, $D_2$-like receptor activation increases outward potassium currents (Figure 1.5), leading to cell hyperpolarization, whose functional significance seems to be the inhibition of dopamine release by autoreceptors in the brain and of prolactin secretion in the pituitary.[15]

The above signaling pathways belong to the called canonical pathways,[21] meaning that they are G-protein dependent. However, the $D_2R$ can exert its activity in different ways, independent of the G-protein, which are called non-canonical pathways. One of the most studied pathways of this kind occurs via the molecule β-arrestin-2 or arrestin-3.[21] Activation of GPCRs by ligand binding leads to the formation of signaling scaffolds mediated by arrestin-3, which bring elements of specific signaling pathways into closer proximity. These scaffolds regulate an increasing number of signaling molecules, including mitogen activated protein kinase (MAPK), extracellular receptor kinase (ERK), c-JUN N-terminal kinase (JNK), Akt or phosphoinositide-3 kinase (PI3K), among others.[21]

USC UNIVERSIDADE DE SANTIAGO DE COMPOSTELA

One more level of complexity is added to the $D_2R$ signaling process when considering the possible homo and heteromerization that can occur.[27] The $D_2R$ can participate in heteromers with other GPCRs, including the somatostatin receptor subtype SSTR5, the serotonin receptors 5-$HT_{1A}$ and 5-$HT_{2A}$[29,30] and the adenosine $A_{2A}$ receptor. Intermembrane interactions of the $D_2R$ with neurotensin and metabotropic glutamate receptors are also potentially mediated by direct receptor-receptor interactions.[27] The formation of heteromers can be constitutive, or stimulated by the binding of ligands, particularly agonists, and may underlie mutually inhibitory or stimulatory interactions.[27] There is considerable behavioral and functional evidence for interactions between brain dopamine and adenosine systems and between dopamine and somatostatin, and receptor heteromerization is likely to be a molecular mechanism of these interactions.[27]

$D_2R$ signal transduction pathways are complex, as it is implicated in several human physiological functions, and a better comprehension of them would result in improved treatment methods for $D_2R$-related pathologies.

### 1.4.3 Parkinson's disease (PD)

Since 1915, over 85,000 papers have been published on the at present second most important neurodegenerative disorder in the elderly population, Parkinson's disease (PD), only behind Alzheimer's disease.[31] To put into perspective the relevance of this condition nowadays:

- Nearly one million people in the U.S. are living with PD. This number is expected to rise to 1.2 million by 2030.
- Nearly 90,000 people in the U.S. are diagnosed with PD each year.
- More than 10 million people worldwide are living with PD.
- The incidence of Parkinson's disease increases with age, but an estimated 4% of people with PD are diagnosed before age 50.

The combined direct and indirect cost of Parkinson's, including treatment, social security payments and lost income, is estimated to be nearly $52 billion per year in the U.S. alone.[32] Furthermore, medications alone cost an average of $2,500 a year and the therapeutic surgery can cost up to $100,000 per person.[32] The personal effect of PD is enormous. Unique to a degenerative disease, its duration can span decades. The typical presentation includes a slow progression with accumulating disability for affected individuals. Parkinson's disease also has

USC UNIVERSIDADE DE SANTIAGO DE COMPOSTELA

profound consequences for caregivers, most experiencing excessive strain. Altogether, PD conveys a mounting socioeconomic burden for society.[33]

The symptoms can be divided into motor features, including bradykinesia, gait disturbance, tremor, rigidity, and speech deficits,[34] which are hard to miss, and non-motor symptoms, such as depression, hyposmia, cognitive impairment, sleep disorders and constipation, which are much less visible components of PD.[33,35] Except for genetic testing in selected cases, a definitive diagnosis can only be established on the basis of post-mortem identification of hallmark neuropathological changes in the brain.[35]

### 1.4.4 Pathophysiology of PD

Pathologically, the motor symptoms of PD are attributed to dopaminergic cell loss within the substantia nigra pars compacta, and ultimately leads to dysfunction of the basal ganglia (a group of deep nuclei involved in the initiation and execution of movement).[36] Parkinson's disease is also defined by the accumulation of α-synuclein in Lewy bodies and Lewy neurites.[37] This Lewy pathology is characterized by a crowded environment of membranes, including vesicular structures and dysmorphic organelles, such as dysmorphic mitochondria, and high lipid content. A new insight is that even in early disease stages, similar pathological changes can occur in multiple organs, including the skin, colon, and salivary glands, suggesting that PD is a multisystem disease. This recognition might ultimately yield new diagnostic avenues, because these systemic tissues are better accessible than tissue from the brain when a person is alive.[33]

The most well-known and cited hypothesis for PD progression is proposed by Braak's group.[38] According to this model, PD begins in stages 1 and 2. During stage 1, α-synuclein pathology is found in the olfactory bulb, together with enteric system disfunction and hyposmia. In stage 2, the pathology is present in the medulla, and patients typically show depression. Pathology progresses to the substantia nigra during stage 3, also called a pre-symptomatic phase. REM sleep behavior is considered the main symptom during this phase and afterwards, patients begin to manifest motor symptoms. In stage 4, most patients are diagnosed when cortical involvement expands to the temporal mesocortex. Stages 5 and 6 mark advanced PD, which involves the entire cerebral cortex and can lead to impaired cognition and hallucinations in patients.[35]

USC UNIVERSIDADE DE SANTIAGO DE COMPOSTELA

### 1.4.5 Treatments of PD

From a therapeutic perspective, the introduction of levodopa (L-DOPA) in the 1960s represented a breakthrough in the treatment of PD, and it continues to be the most effective symptomatic therapy in the Parkinsonian disorders.[31] In addition to dopamine precursors, other symptomatic treatments for PD include dopamine agonists, monoamine oxidase (MAO) inhibitors and catechol-O-methyltransferase (COMT) inhibitors.[39] Since Parkinsonism occurs due to death and depletion of dopamine-generating cells in the substantia nigra, all of these drugs have a common goal: to restore the equilibrium of dopamine in those regions of the brain where such balance is compromised due to dopaminergic cell loss.[39]

Side effects are commonly associated with antiparkinsonian pharmacological therapy and can significantly reduce the quality of life of patients suffering from PD.[39] The most common among them are dyskinesia, akinesia, nausea, hypotension, muscular rigidity and psychosis (related to L-DOPA treatment), and sleep disturbances, anxiety, nausea, stomatitis, orthostatic hypotension and hallucinations (related to MAO inhibitors).[39] To address L-DOPA related side effects, it is typically combined with carbidopa, an inhibitor of the enzyme aromatic L-amino acid decarboxylase (also known as DOPA decarboxylase) outside the central nervous system.[40] This enzyme is responsible for converting L-DOPA into dopamine, which causes nausea and vomiting when it occurs in the bloodstream.

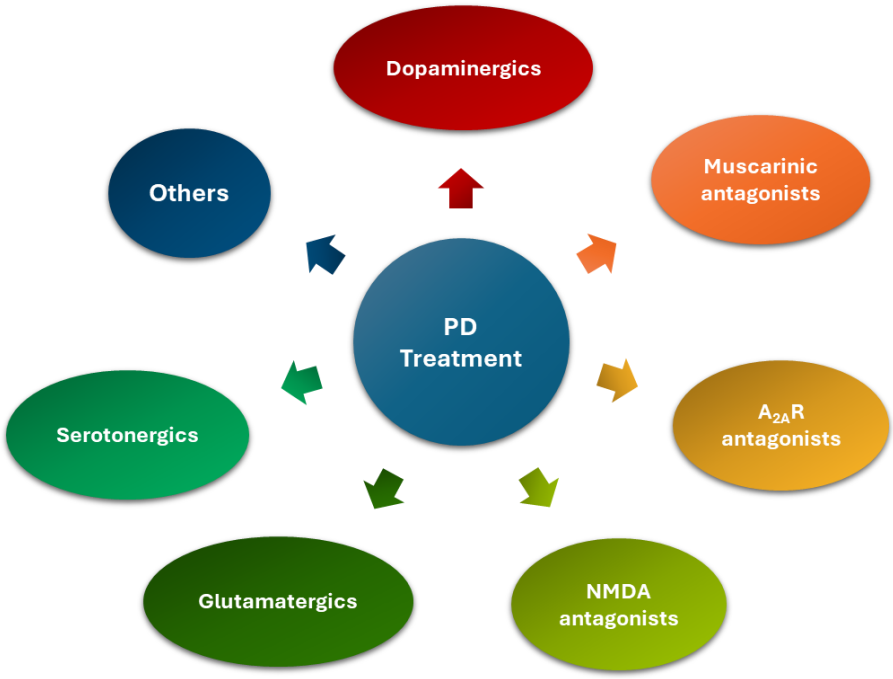



Figure 1.6. Schematic of various strategies for PD treatment.

Diverse dopaminergic and non-dopaminergic pharmacological approaches have been developed to manage such complications (Figure 1.6), including novel L-DOPA formulations, COMT inhibitors, dopamine agonists, muscarinic, N-methyl-D-aspartate (NMDA) receptor and adenosine $A_{2A}R$ antagonists, serotonergic and glutamatergic agents, and metabotropic glutamate receptor 5 modulators, with controversial results (Figure 1.6).[31,41] These approaches can improve the quality of life of PD patients for many years, as they address the clinical symptoms of PD, including motor and non-motor features.[41] However, PD is still incurable, as no treatment can stop or even slow down the progression of the disease.

Given the poor bioavailability and extremely short plasma half-life of L-DOPA, $D_2R$ agonists were viewed as a viable alternative since they could stimulate the $D_2R$ directly, bypassing the need for presynaptic dopamine synthesis. Although these compounds have lower efficacy compared with L-DOPA, $D_2R$ agonists are longer-lasting and have greatly improved bioavailability.[36] Figure 1.7 shows some examples of $D_2R$ agonist drugs in clinic.

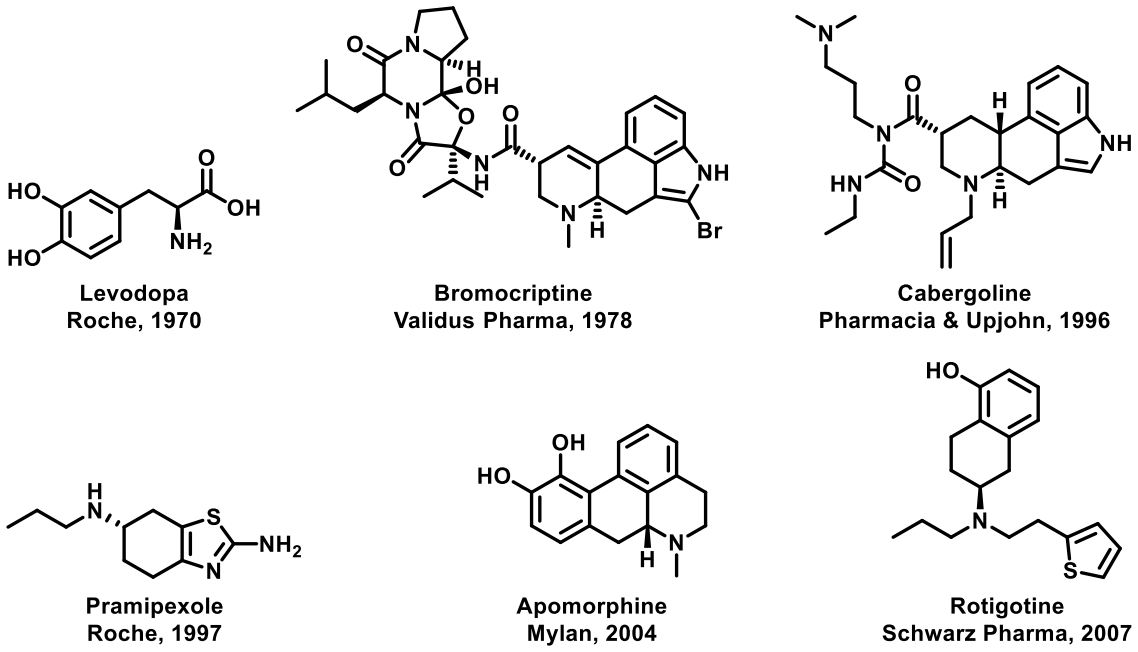



Figure 1.7. Dopamine receptor agonist anti-PD drugs in clinic.[42]

However, all these solutions have fallen short so far on its way to effectively treat PD, so the medical community is in need of new strategies that can overcome these difficulties. In the first chapter of this Doctoral Thesis, we will explore one of these strategies, focusing our attention on allosteric ligands for the $D_2R$.

USC DE SANTIAGO DE COMPOSTELA

### 1.4.6 Schizophrenia

Schizophrenia is a complex pathology of unknown etiology with a heterogeneous combination of symptoms.[43] Characteristic (but not exclusive) symptoms of the illness can be divided into "positive", "negative", and "cognitive" categories.[43] First ones are behaviors and thoughts unusually present in a healthy person, such as recurrent psychosis ("loss of contact with reality" consisting of delusions), hallucinations and disorganized speech and behavior. Negative symptoms are defined by the amotivational syndrome, which includes social withdrawal, affective flattening, anhedonia (inability to feel pleasure) and diminished initiative and energy. Finally, cognitive symptoms are expressed as a broad set of cognitive dysfunctions.[43]

Schizophrenia is a major therapeutic challenge of modern medicine, with a lifetime prevalence of about 1%.[44,45] Patients with schizophrenia generally experience serious impairments in multiple domains of everyday life, including the ability to maintain social relationships, sustain employment and live independently. These deficits typically persist after patients achieve remission from psychotic symptoms.[43] This disease accounts for a huge health care burden, with annual associated costs in the U.S. estimated to be more than $150 billion.[45] Such a huge cost for a disorder affecting 1% of the population is attributable to the fact that typical onset takes place in early adulthood, and the long-term limitations in social and occupational function mentioned before.[45]

Patients with schizophrenia also see their life expectancy cut about 15 years shorter than the general population, and they have a 5% to 10% life-time risk of death by suicide.[45] The high rate of cigarette smoking among people with schizophrenia, the increased likelihood they will have an unhealthy lifestyle and the obesity-promoting effects of antipsychotic drugs contribute to metabolic syndrome, diabetes and excess cardiovascular and respiratory deaths among these patients, explaining their high mortality ratio.[43]

### 1.4.7 Pathophysiology of schizophrenia

Schizophrenia typically develops in early adulthood, and it is rare before age 16; although cognitive deficits and negative symptoms may attract less clinical attention than the positive symptoms, they typically begin before the onset of the first psychotic episode, with people at risk of developing schizophrenia having their cognitive function considerably lowered.[45]

A long-standing hypothesis proposes that schizophrenia disrupts the process of neurodevelopment.[45] This process starts in the childhood with the production of synaptic

connections before a switch in adolescence to synaptic pruning, such that the number of synapses in an adult is about half of a young child. Therefore, a reduction in the gray matter over adolescence and early adulthood and the concomitant reorganization of both structural and functional brain networks is observed. Schizophrenia leads to widespread impairments in neural communication and the development of cognitive deficits in individuals with the disorder.[45]

### 1.4.8 Treatments of schizophrenia

More than 60 years have passed since the discovery of chlorpromazine and antipsychotics still remain as the main treatment for schizophrenia.[43] Although all antipsychotics act to block reception of the dopamine pathway, they have been classified into "typical" or first-generation antipsychotics (FGAs, Figure 1.8), and atypical or second-generation antipsychotics (SGAs, Figure 1.8).[46] However, this classification is controversial, as all antipsychotics are believed to act via reducing dopaminergic tone, and because both classes are heterogeneous in molecular structure, extra-dopaminergic targets, and adverse effects. Extrapyramidal adverse effects, such as Parkinsonism, had been believed to be the unavoidable result of antipsychotic efficacy conferred by $D_2R$ blockade.[43] Along with Parkinsonism, these side effects include hyperprolactinemia, dystonia, akathisia, and tardive dyskinesia.

SGAs block serotonin receptors at lower concentration than they block dopamine receptors and/or might block subcortical $D_2R$ more than striatal $D_2R$.[43] These drugs are associated with less Parkinsonism, akathisia, and tardive dyskinesia than FGAs at therapeutic dose. However, no SGA is entirely free of associated Parkinsonism, and all currently available antipsychotics are believed to work predominantly via $D_2R$ blockade. Moreover, most SGAs are associated with other adverse effects, such as weight gain, diabetes and, consequently, increased risk of cardiovascular complications.[43]

After the identification of aripiprazole and the subsequent introduction of cariprazine, a novel category of antipsychotics has surfaced, known as third-generation antipsychotics (TGAs, Figure 1.8).[46] Aripiprazole, recognized by its distinctive pharmacological profile, serves as a potent partial agonist at both presynaptic and postsynaptic $D_2R$, and it also functions as a partial agonist at the serotonin 5-$HT_{1A}$ receptor. Notably, this medication demonstrates a reduced likelihood of inducing motor side effects.[46]

USC UNIVERSIDADE DE SANTIAGO DE COMPOSTELA

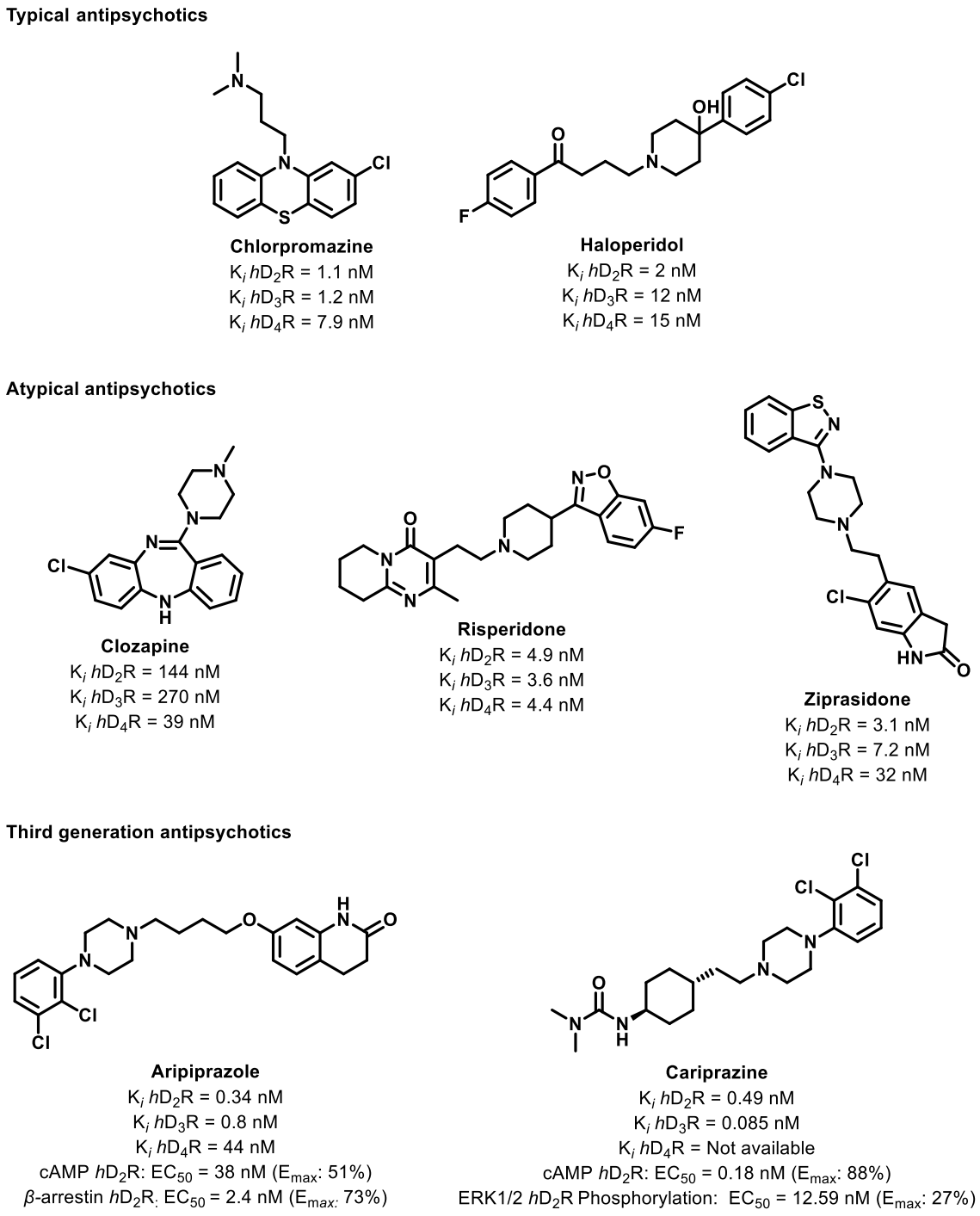



Figure 1.8. Examples of commercial antipsychotic drugs.[47-51]

Finally, although positive symptoms improve with antipsychotic treatment, there is little evidence that negative and cognitive symptoms react the same way other than in situations in which these are secondary to the former.[45]

USC UNIVERSIDADE DE SANTIAGO DE COMPOSTELA

### 1.4.9 Allosterism

Traditionally, drug discovery programs aimed to target GPCRs have been directed to develop ligands (agonists, antagonists, and inverse agonists) that bind to the orthosteric site (i.e., the binding site of endogenous agonists). However, in recent years, advances in the search of allosteric modulators of GPCRs have emerged as promising new approaches for developing therapeutic agents that may be useful for the treatment of several disorders.[52] Allosteric modulators are compounds that interact with binding sites topographically distinct from the orthosteric site. They show specific advantages, such as the increased selectivity for GPCR subunits and the potential to preserve activity dependence and both spatial and temporal characteristics of endogenous physiological ligands.[53] Allosteric modulators of dopamine $D_2R$ have shown clinical potential as more efficient and safer drugs for a number of CNS disorders, including PD and schizophrenia.[3]

From the pharmacological standpoint, the simplest classification of the allosteric modulators comprises three types of compounds:[53] positive allosteric modulators (PAMs) if the modulator potentiates the effect (potency and efficacy) of the agonist; negative allosteric modulators (NAMs) if the modulator decreases the effect of the endogenous ligand; and silent allosteric modulators (SAMs) if the modulator binds to the allosteric site and have no effect on the endogenous ligand. The latter does not have an effect per se, but prevents PAM and NAM to bind to the allosteric site; as an example, flumazenil is a neutral allosteric modulator of gamma-aminobutyric acid $(GABA)_A$ receptor and is used as an antidote to benzodiazepine overdose.[53] The scenario becomes more complicated considering that allosteric compounds can also directly stimulate or inhibit the receptor by themselves, with or without modulating the response of an orthosteric agonist. Thus, PAMs and NAMs can influence both the affinity and efficacy of the orthosteric agonist, expanding the options of allosteric therapeutic strategies to PAM agonists, PAM antagonists, NAM agonists and NAM inverse agonists.[53]

Another level of complexity is added by the influence of allosteric ligands on dopamine receptors homo- and heterodimerization. Specifically, $D_2R$ forms diverse heteromeric complexes (e.g. $D_1R$-$D_2R$ and $D_2R$-$D_3R$) with different signaling properties compared to the respective monomers in functional assays. Furthermore, the binding of an agonist or antagonist to one of the individual receptors on the dimer can alter the binding and the functional properties of agonist or antagonist interaction with the other half, suggesting an allosteric type of interaction between the two protomers.[53]

USC UNIVERSIDADE DE SANTIAGO DE COMPOSTELA

Despite the complex pharmacological profile of allosteric modulators, they have received great attention in the last years because of the several advantages they present with respect to orthosteric ligands:[53]

- Receptor selectivity: allosteric binding sites are generally less conservated through receptor subspecies than the orthosteric site, allowing the development of highly selective allosteric modulators.
- Maintenance of temporal and spatial fidelity: PAMs will only have an effect when the endogenous ligand is released, contrary to the orthosteric ligands that modulate the receptor indiscriminately, thus maintaining its temporal and spatial fidelity (Figure 1.9).

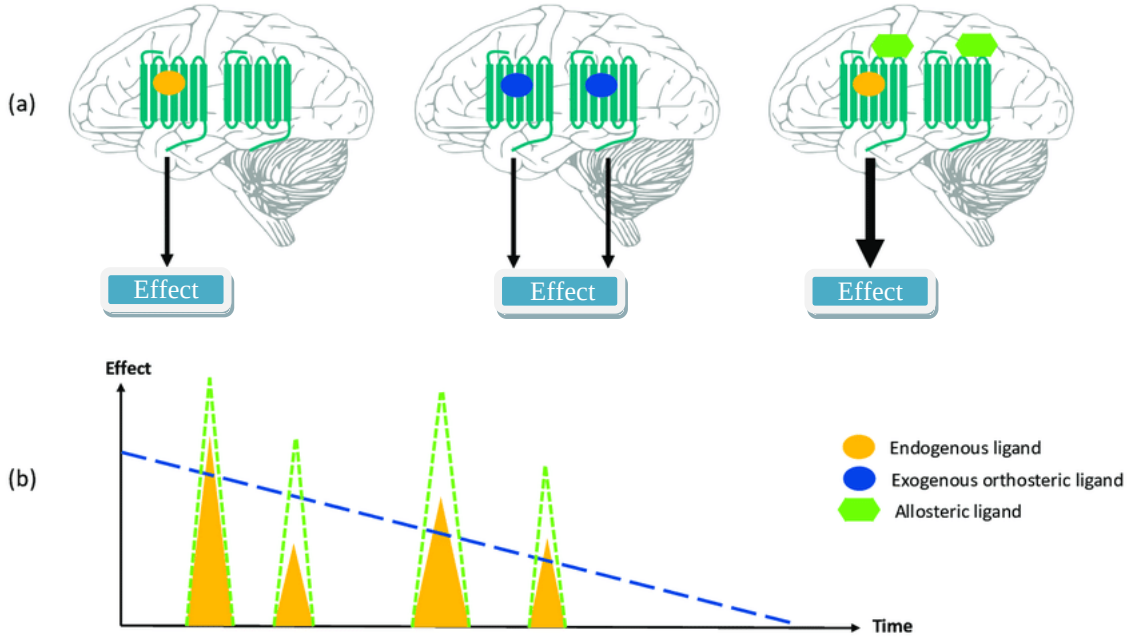



Figure 1.9. Spatial (a) and temporal (b) fidelity of positive allosteric modulation of the endogenous ligand (Figure from Fasciani, I.; Petragnano, F.; Aloisi, G.; Marampon, F.; Carli, M.; Scarselli, M.; Maggio, R.; Rossi, M. Allosteric Modulators of G Protein-Coupled Dopamine and Serotonin Receptors: A New Class of Atypical Antipsychotics. Pharmaceuticals 2020, 13, 388. https://doi.org/10.3390/ph13110388. Licensed under CC BY).[53]

- Ceiling effect: the allosteric ligands set a limit to the effect of the orthosteric ligand, reached when all the available allosteric binding sites are occupied. This may reduce toxicity or overdose for those allosteric modulators with a defined fold shift of agonist potency. As an example, first generation antipsychotics presents trouble when used to treat schizophrenia, as they present extrapyramidal side

USC UNIVERSIDADE DE SANTIAGO DE COMPOSTELA

effects when more than 80% of the dopamine receptors in the striatum are occupied by the antagonist. Keeping the drug dosage under the required levels is often difficult with orthosteric drugs, but feasible with allosteric drugs.

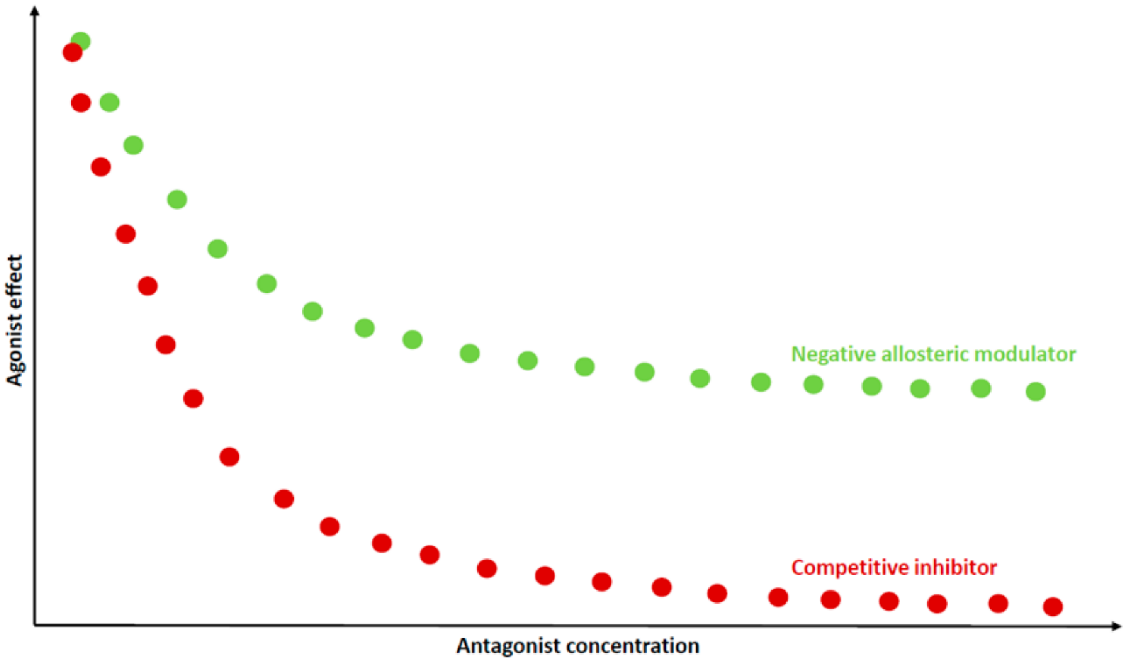



Figure 1.10. Ceiling effect of negative allosteric modulator. Elevating the concentration of the competitive antagonist suppresses the impact of the endogenous agonist until the signaling is completely subdued (depicted by red dots). Conversely, increasing the concentration of the negative allosteric modulator attenuates the signal but does not fully extinguish it (illustrated by green dots) (Figure from Fasciani, I.; Petragnano, F.; Aloisi, G.; Marampon, F.; Carli, M.; Scarselli, M.; Maggio, R.; Rossi, M. Allosteric Modulators of G Protein-Coupled Dopamine and Serotonin Receptors: A New Class of Atypical Antipsychotics. Pharmaceuticals 2020, 13, 388. https://doi.org/10.3390/ph13110388. Licensed under CC BY).[53]

- Probe dependence: the effects of the allosteric modulator depend on the orthosteric ligand and on the receptor signaling under examination. This has clinical implications when allosteric modulators act on receptors with more than one endogenous agonist.
- Improved chemical tractability: Orthosteric sites often impose stringent limits to the ligand conformation required for binding, while this requirement is less stringent for allosteric sites.[53]

To comprehend the influence of allosteric modulators on receptor function, their effects are quantified using a dose-response curve. This curve is a graphical representation that illustrates the relationship between the concentration of a modulator (allosteric ligand) and the

USC UNIVERSIDADE DE SANTIAGO

biological response of a target protein or receptor.[54] Two key pharmacological parameters are derived from this curve: the maximum effect ($E_{max}$) and the half-maximal effective concentration ($EC_{50}$). $E_{max}$ is the highest response attainable with an agonist, defining the upper limit of the curve and reflecting the full response capacity of the receptor system.[55] $EC_{50}$ represents the agonist concentration necessary to achieve half of this maximal response, indicating the agonist's potency.[55]

Figure 1.11A illustrates the impact of an allosteric modulator on the affinity of both full and partial agonists.[56] An increased affinity results in a leftward shift of the dose-response curve, while a decreased affinity leads to a rightward shift. Figure 1.11B shows the effect of allosteric changes in the efficacy of full and partial agonists. In this scenario, an increased efficacy will shift the curve to the left for a full agonist, whereas for a partial agonist, it will result in an increase in the maximal response. Conversely, a decreased efficacy will shift the curve to the right and reduce the $E_{max}$.

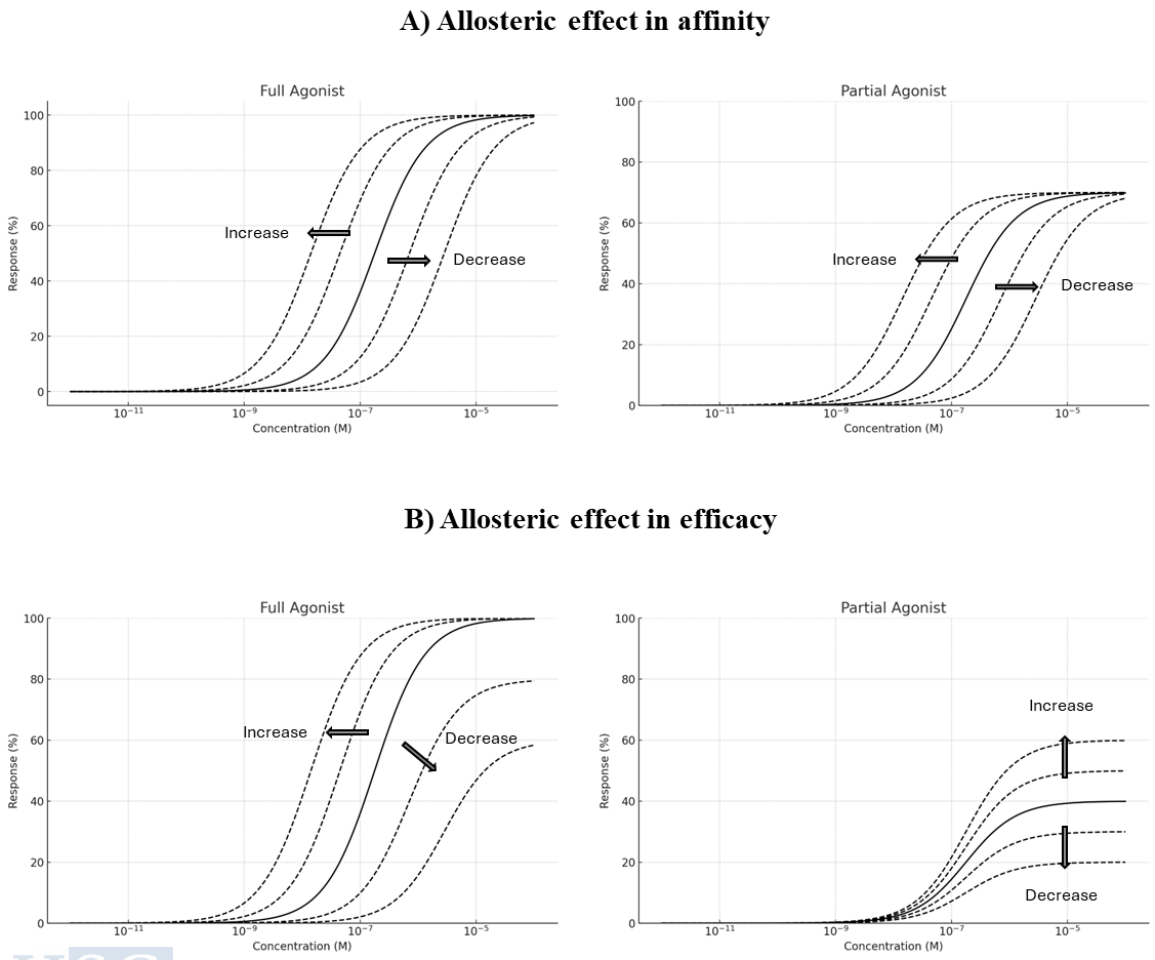



Figure 1.11. Possible effects of an allosteric modulator on the dose-response curve of an agonist.[56]

As an example, Figure 1.12 shows the dose-response curves at the serotonin receptors of serotonin (5-HT) and 5-HT in combination with 1 μM of a dual allosteric modulator of the 5-$HT_{2C}$ receptor and the 5-$HT_{2B}$ receptor.[57]

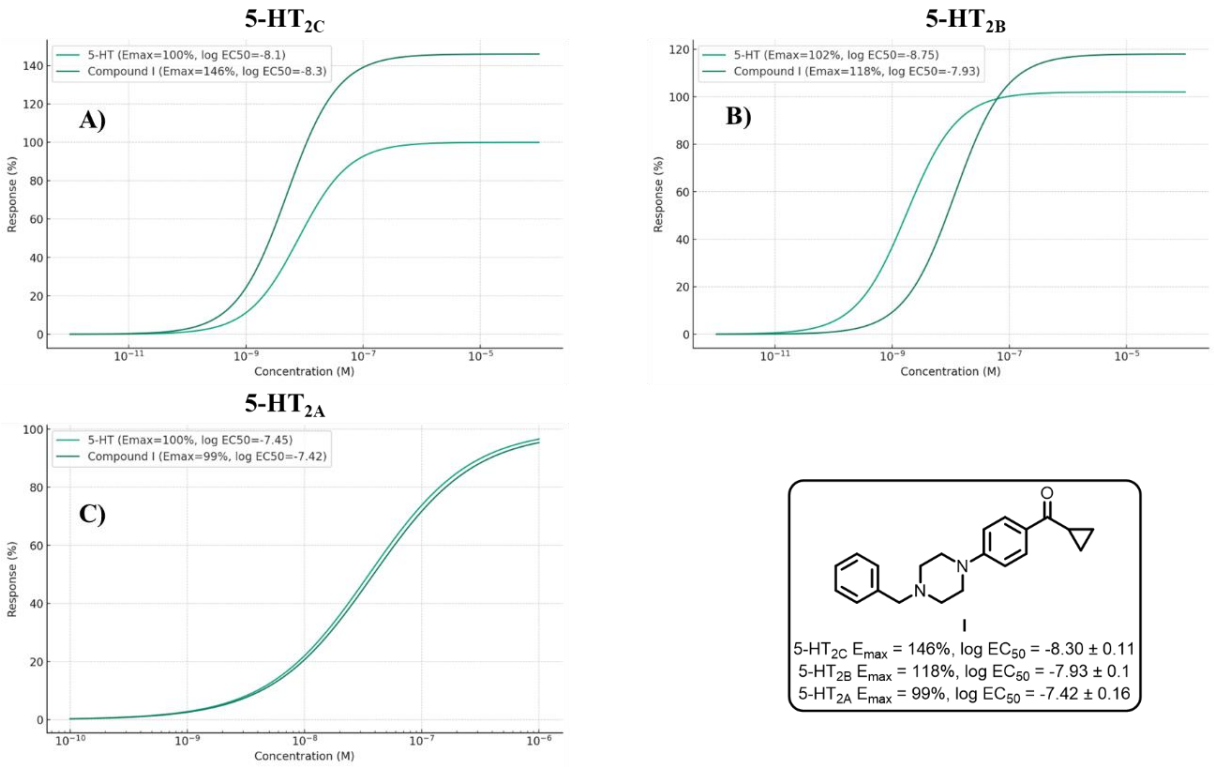



Figure 1.12. Representation of the dose-response curves of 5-HT and 5-HT + 0.1 μM compound **I** at the serotonin receptors 5-$HT_{2C}$ (A), 5-$HT_{2B}$ (B), and 5-$HT_{2A}$ (C).[57]

The results showed that compound **I** exhibited PAM activity at 5-$HT_{2C}$ receptor (Figure 1.12A), demonstrating an enhancement in the potency of 5-HT ($E_{max}$ increased from 100% to 146%) without affecting efficacy (similar $EC_{50}$). Conversely, compound **I** was found to exhibit NAM activity at the 5-$HT_{2B}$ receptor (Figure 1.12B), reducing the $EC_{50}$ of 5-HT by 10-fold. Finally, compound **I** showed no activity at the 5-$HT_{2A}$ receptor (Figure 1.12C).

Presently, only three allosteric modulators have received approval for commercial distribution, with several others undergoing clinical trials.[46] Among these, cinacalcet serves as a positive allosteric modulator (PAM), while maraviroc and plerixafor function as negative allosteric modulators (NAMs) (Figure 1.13). Cinacalcet, an orally bioavailable PAM targeting the calcium-sensing GPCR receptor, has been FDA-approved and available in the USA since 2004. It is prescribed for treating secondary hyperparathyroidism (HPT) in chronic kidney disease (CKD) patients undergoing dialysis and for managing hypercalcemia in individuals

USC DE SANTIAGO DE COMPOSTELA

with parathyroid carcinoma.[58] Maraviroc, a negatively allosteric modulator, gained FDA approval in 2007 as the first-in-class chemokine GPCR CCR5 receptor antagonist, primarily for use in HIV treatment-experienced patients.[59] Finally, plerixafor received FDA approval in 2008, used in combination with granulocyte colony-stimulating factor. These compounds function by mobilizing hematopoietic stem cells to peripheral blood, facilitating their collection for subsequent autologous transplantation in patients with multiple myeloma and non-Hodgkin's lymphoma.[60]

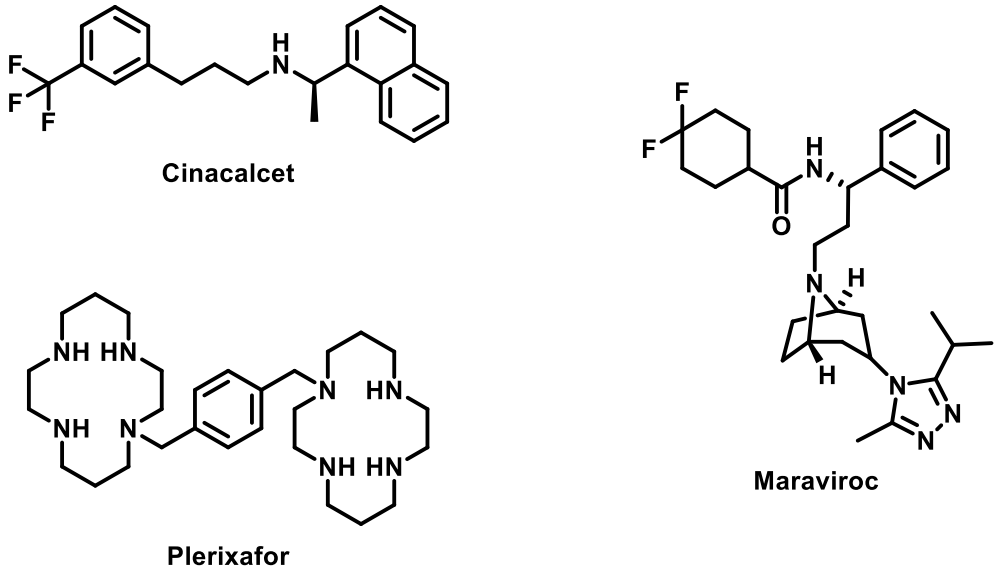



Figure 1.13. Allosteric modulators approved for clinical use.

### 1.4.10 Allosteric modulation of the $D_2R$

The best-known allosteric effect within the dopamine receptors is the ability of sodium ions to regulate the binding of agonists, converting the receptors from their high affinity state ($R_H$) to their low affinity state ($R_L$), which decreases agonist binding.[61] The molecular site of sodium interaction with dopamine receptors has been shown to rely upon a conserved aspartic acid residue at position 2.50, where hydrogen ions bind as well. Like sodium, low pH or conditions that increase the concentration of hydrogen ions weakens agonist binding.[61]

Additionally the $D_2R$ is modulated by zinc ions, which can also inhibit the binding of sodium-insensitive antagonists and occupy distinct allosteric sites from those of sodium ions.[61] Although the potential physiological relevance of zinc's modulation of $D_2R$-like antagonist binding is not clear, it may be therapeutically relevant in the case of antipsychotic drug treatments. Since zinc inhibits antagonistic binding to the $D_2R$, the presence of elevated

USC UNIVERSIDADE DE SANTIAGO DE COMPOSTELA

levels of synaptic zinc may explain the fact that 15-20% of schizophrenic patients do not respond to antipsychotic drug treatments.[61]

In addition to sodium and zinc ions, $D_2R$ can be allosterically modulated by amiloride (3,5-Diamino-N-(aminoiminomethyl)-6-chloropyrazinecarboxamide) and its derivatives methylisobutylamiloride and benzamil (Figure 1.14).[61] These modulators decrease radiolabeled spiperone ($^3$[H]spiperone) binding to cloned human $D_1$ and $D_2$-like dopamine receptors by accelerating $^3$[H]spiperone dissociation rates.

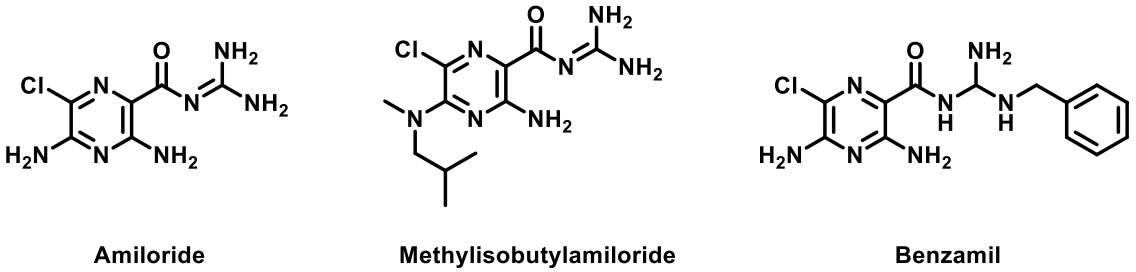



Figure 1.14 Allosteric modulators of the $D_2R$: amiloride, methylisobutylamiloride and benzamil.[61]

These allosteric modulators of the $D_2R$ have not shown any therapeutical effect. However, their mechanism of allosteric binding is useful to help in the design of ligands which can modulate effectively the $D_2R$.[21,61]

### 1.4.11 Melanostatin

Melanostatin, also called L-prolyl-L-leucyglycinamide (PLG) is one of the few examples of a neuropeptide acting as a $D_2R$ PAM, and was first isolated in 1971 from bovine hypothalamic tissue.[21] Melanostatin, formed by exocyclic cleavage of oxytocin hormone through the action of the enzyme exopeptidase (Figure 1.15), is found in the central nervous system, where it exhibits its biological function through the nigrostriatal pathway.[62–64] This neuropeptide interacts with $D_2R$ increasing the effect of dopamine and its synthetic agonists such as N-propylnorapomorphine (NPA), apomorphine and 2-amino-6,7-dihydroxy-3,4-tetrahydronapthtalene (ADTN). Studies using radiolabeled NPA and quinpirole show that it potentiates the binding of these ligands in a dose-dependent manner to $D_{2L}R$, $D_{2S}R$ and $D_4R$ subtypes to give a bell-shaped dose-response curve, without enhancing binding to $D_1R$ and $D_3R$. Mechanistically, melanostatin acts by promoting the conversion of $D_2R$ from their low affinity state to a higher affinity state, making them more selective to agonists (PAM behavior).[63]

USC UNIVERSIDADE DE SANTIAGO DE COMPOSTELA

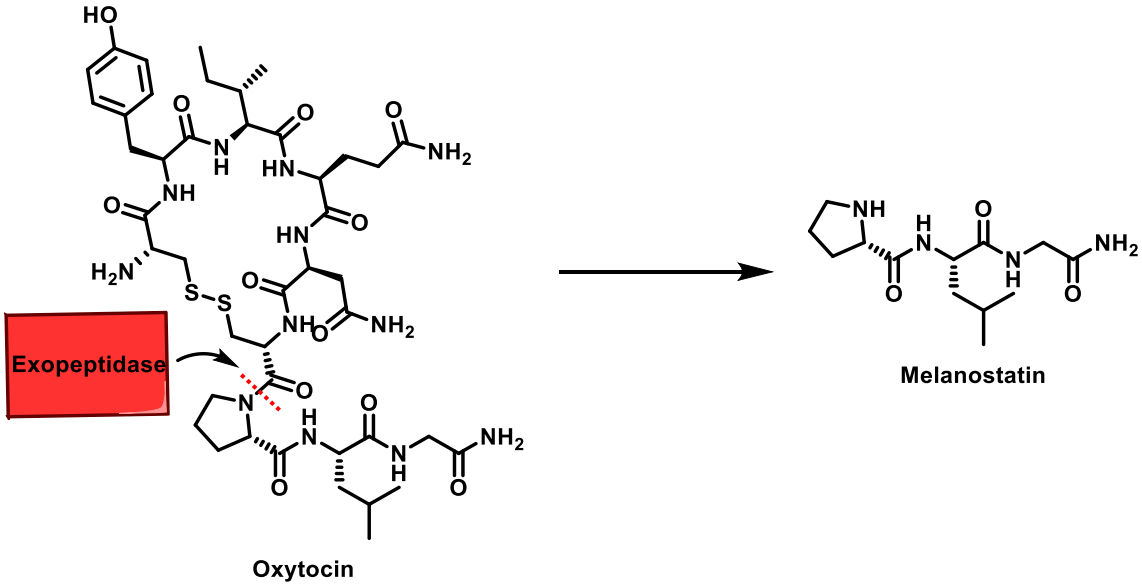



Figure 1.15. Biosynthesis of melanostatin.

X-ray crystallography and structure-activity relationship (SAR) studies using constrained peptidomimetics suggest that melanostatin adopts a type-II β turn formed by intramolecular hydrogen bonding between the carbonyl oxygen atom of the L-proline residue and the *trans* amide proton of the glycinamide residue (Figure 1.16).[63]

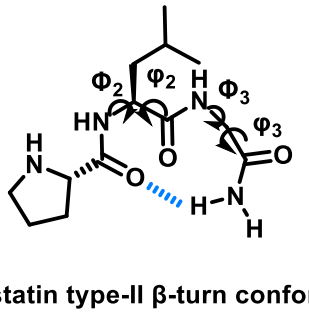



Figure 1.16. Bioactive conformation of melanostatin.[62]

However, some melanostatin derivatives display similar pharmacological activity despite the fact that they are unable to adopt such conformation, suggesting that this peptidomimetic may adopt other bioactive conformations besides the postulated type II β-turn motif.[64] Furthermore, the group of Sampaio-Dias et al. described a peptidomimetic derivative whose activity cannot be unequivocally attributed to the same binding mode that melanostatin does at the $D_2R$, and it might explore different allosteric pockets at this receptors or interact with other key-residues at the putative melanostatin binding site, inducing different conformational

USC UNIVERSIDADE DE SANTIAGO DE COMPOSTELA

changes at the orthosteric site that selectively discriminate different agonists by stabilizing specific active conformations of the receptor.[63]

Due to its important role in $D_2R$ modulation, melanostatin has been the focus of multiple studies for further development in the treatment of neurodegenerative diseases in which dopamine homeostasis is unbalanced, such as PD or schizophrenia. In fact, the therapeutical activity of melanostatin in PD treatment has been confirmed by several studies.[63] Moreover, this neuropeptide possesses the capacity to interact with other drugs, altering their effects. For instance, it can act as an antagonist, counteracting the dyskinesia induced by antipsychotic drugs and morphine-induced catalepsy.[64]

Additionally, clinical trials with human subjects unveiled the therapeutic potential of melanostatin as an antidepressant for individuals grappling with clinical mental depression.[21] Furthermore, it has shown potential in alleviating the motor symptoms of PD, potentiating the effect of levodopa when used in combination therapy, and reducing levodopa-induced dyskinesia.[65] Despite its great potential, pharmacokinetics issues associated with this neuropeptide (e.g., low gastrointestinal absorption and lability towards CNS proteases) hinder the progression of clinical assays and its use in PD.[65] Nevertheless, the positive initial therapeutic results inspired multiple research groups to intensify their exploration and development of melanostatin as an allosteric ligand for the $D_2R$, ultimately leading to the creation of various collections of melanostatin analogues.[21,62,63,65]

The group of Sampaio-Dias has recently led the search of novel melanostatin analogues. Their research program constitutes the most comprehensive project aimed to develop PLG peptidomimetics. Their exhaustive studies included: 1) the substitution of the proline residue, in the search for new and more active surrogates, 2) the modification of the leucine residue, and 3) the exploration of the terminal amide moiety present in the glycine.[62–65]

Through direct coupling chemistry, they were able to identify several lead compounds with enhanced overall lipophilicity and PAM activity compared to that of melanostatin (Figure 1.17),[65] paving the way for the discovery of suitable candidates to treat CNS-related diseases.

Aside from the excellent pharmacological results, their work also provided insights into the SAR of the allosteric binding to the dopamine $D_2R$. Compound **II** (Figure 1.17) exhibited statistically significant activity in radiolabeled NPA ([$^3$H]-NPA) binding, unlike the diastereomeric mixture obtained from a racemic 2-azanorbornane scaffold. This underscores

USC UNIVERSIDADE DE SANTIAGO DE COMPOSTELA

the crucial role of stereochemistry of such moiety in achieving significantly active modulators of the dopamine receptor.[66] Compounds **III-VI** corroborate that $D_2R$ allosteric site can accommodate heteroaromatic rings at N-terminal position of melanostatin, establishing furan and 2-picolinoyl as suitable heterocyclic scaffolds to be used as proline surrogates.[62,63] Moreover, the good pharmacological profile observed in derivatives characterized by the absence of the naturally occurring C-terminal carboxamide group (compounds **III** and **VI)** indicates that the ester group can be tolerated and they cannot adopt the suggested type-II β-turn bioconformation.[63,64] This finding suggests that heteroaromatic scaffolds at the prolyl position of melanostatin may have a significant impact on the folding of these tripeptidomimetics, inducing an extended conformation rather than a type-II β-turn.[63] Interestingly, while compound **V** exhibited a modulatory effect at 1 nM, its regioisomer was not able to potentiate the effect of 0.1 µM of dopamine within the range of 0.01-1 nM, proving that the orientation of the oxygen atom within the furoyl moiety is the determinant for potency.[64]

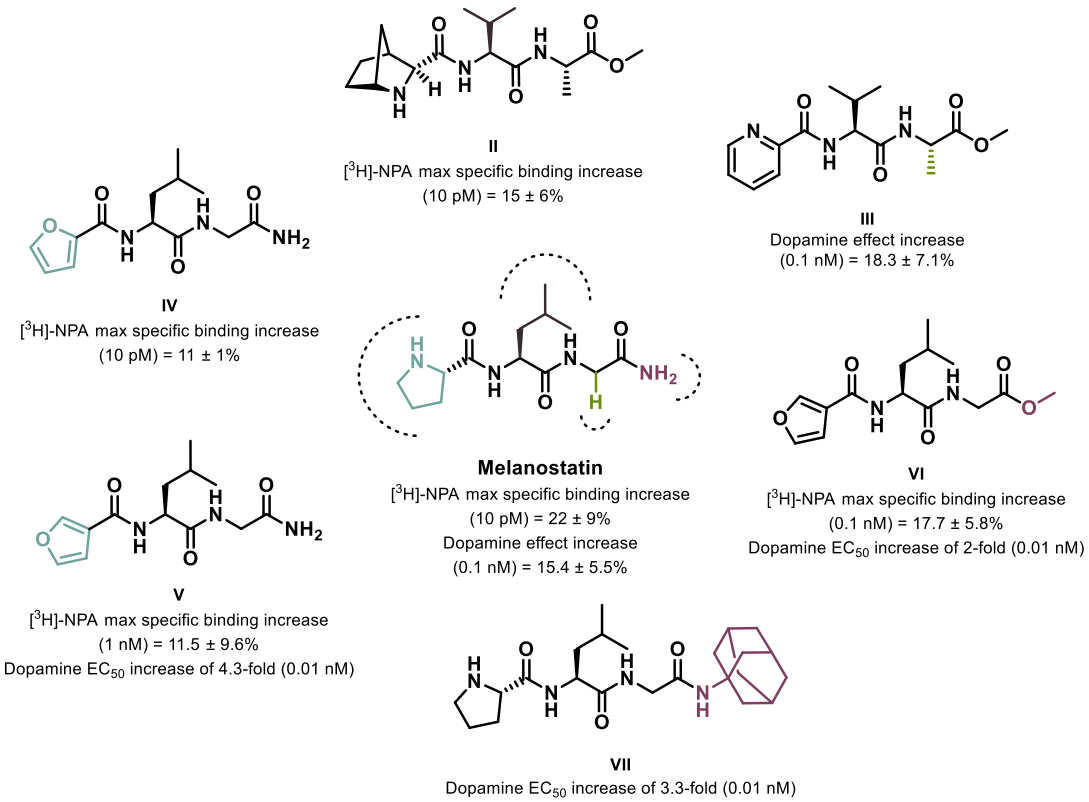



Figure 1.17. Structure and pharmacological data of melanostatin and remarkable analogues synthesized by Sampaio-Dias et al.[62-66]

USC UNIVERSIDADE DE SANTIAGO DE COMPOSTELA

More recently, the same group has developed novel melanostatin conjugates bearing amantadine residues at the terminal carboxamide group.[65] The conjugates displayed no intrinsic agonistic effect, while exhibiting biological data corroborating the PAM-based effects of the compounds. In this study, it was demonstrated, once again, that the C-terminal primary amide is not essential for the PAM activity, as its replacement with a hydrophobic secondary amide resulted in a 3.3-fold increase in dopamine potency at 0.01 nM, while the original neuropeptide was found inactive under these conditions. The potent PAM potency of **VII** and its very low neurotoxicity profile suggest a safe therapeutical window and support the exploration of substitutions in the terminal amide.[65]

In all these investigations, the synthetic approach remains consistent. Illustrated in Figure 1.18, the general scheme is based on classical direct coupling and amino acid chemistry, employing a linear synthesis that involves up to four reaction steps to attain certain final products.[62] While the yields are consistently excellent (79-100%), it is our conviction that adopting a multicomponent approach could streamline the process and enable the introduction of unexplored diversity within the melanostatin core, making it less time-consuming and more cost-effective. Acknowledging these potential benefits, the first chapter of this Doctoral Thesis will specifically concentrate on developing a diverse library of melanostatin analogs through the utilization of multicomponent strategies, that will be discussed later in the text. This approach aims to enhance efficiency and cost-effectiveness in comparison to traditional linear synthesis methods.

USC
UNIVERSIDADE DE SANTIAGO DE COMPOSTELA

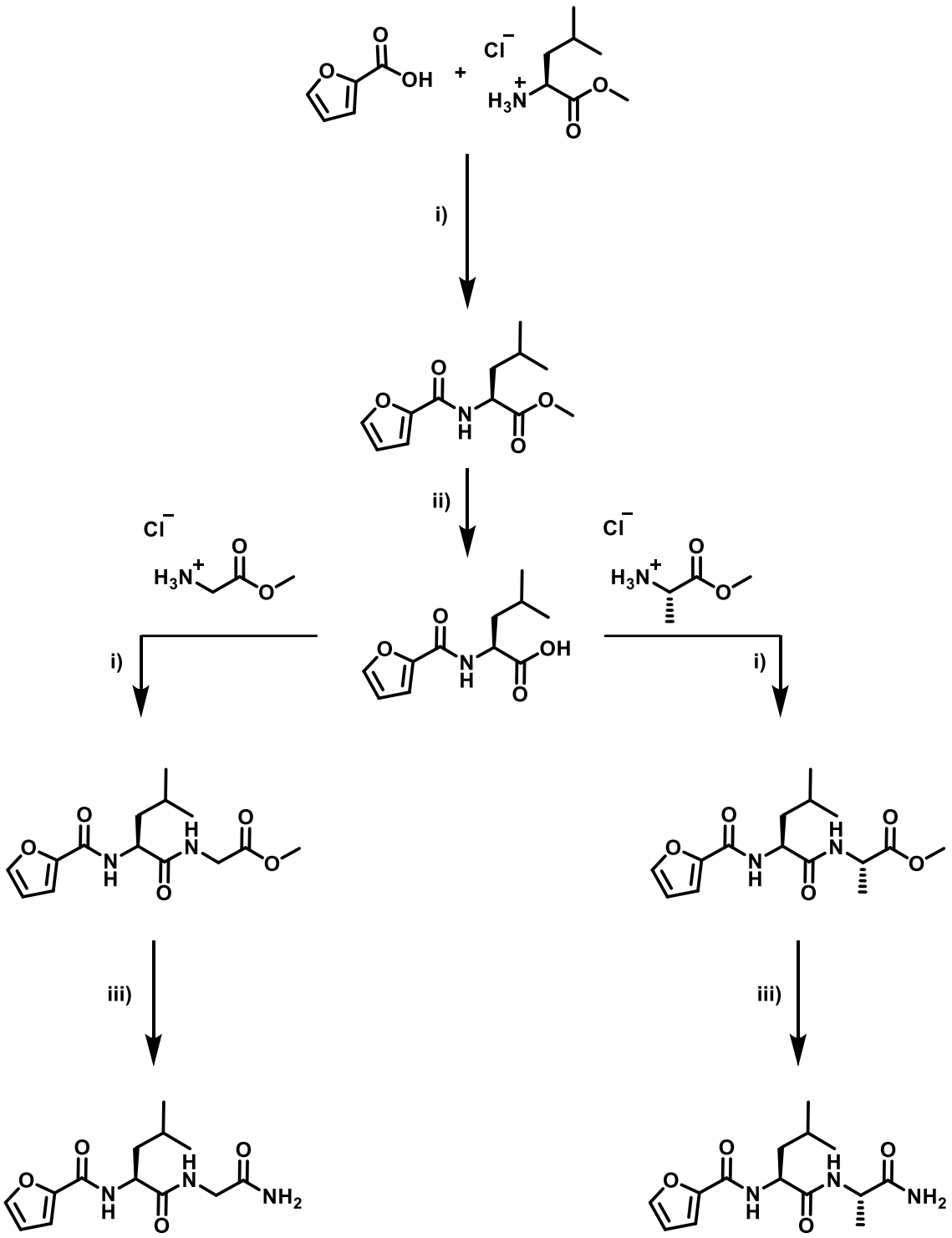



Figure 1.18. Synthetic scheme of melanostatin 2-furoic analogues. Reagents and conditions: (i) DIEA, TBTU, $CH_2Cl_2$; (ii) LiOH, MeOH/$H_2O$ followed by $H_2SO_4$ 1 M; (iii) $NH_3$ (g), MeOH.[62]

USC UNIVERSIDADE DE SANTIAGO DE COMPOSTELA

## 1.5 ENDOCANNABINOID SYSTEM

The effects of *Cannabis sativa*, commonly called Marijuana, have been long known and exploit throughout human history for both medicinal and recreational purposes,[67,68] but not until half a century ago, the structure of its major psychoactive principal, $\Delta^9$-tetrahydrocannabinol ($\Delta^9$-THC), was established.[67] The $CB_1$ cannabinoid receptor ($CB_1R$) was then discovered and subsequently cloned thanks to its responsiveness to THC, hence, the name "cannabinoid" receptor.[69] Not long after that, another cannabinoid receptor was identified and successfully cloned, later termed as the cannabinoid receptor 2 ($CB_2R$). These cannabinoid receptors, along with their ligands (endocannabinoids, eCBs), and the enzymes involved in the synthesis, metabolism and transport of eCBs, constitute the endocannabinoid system (ECS, Figure 1.19).[70]

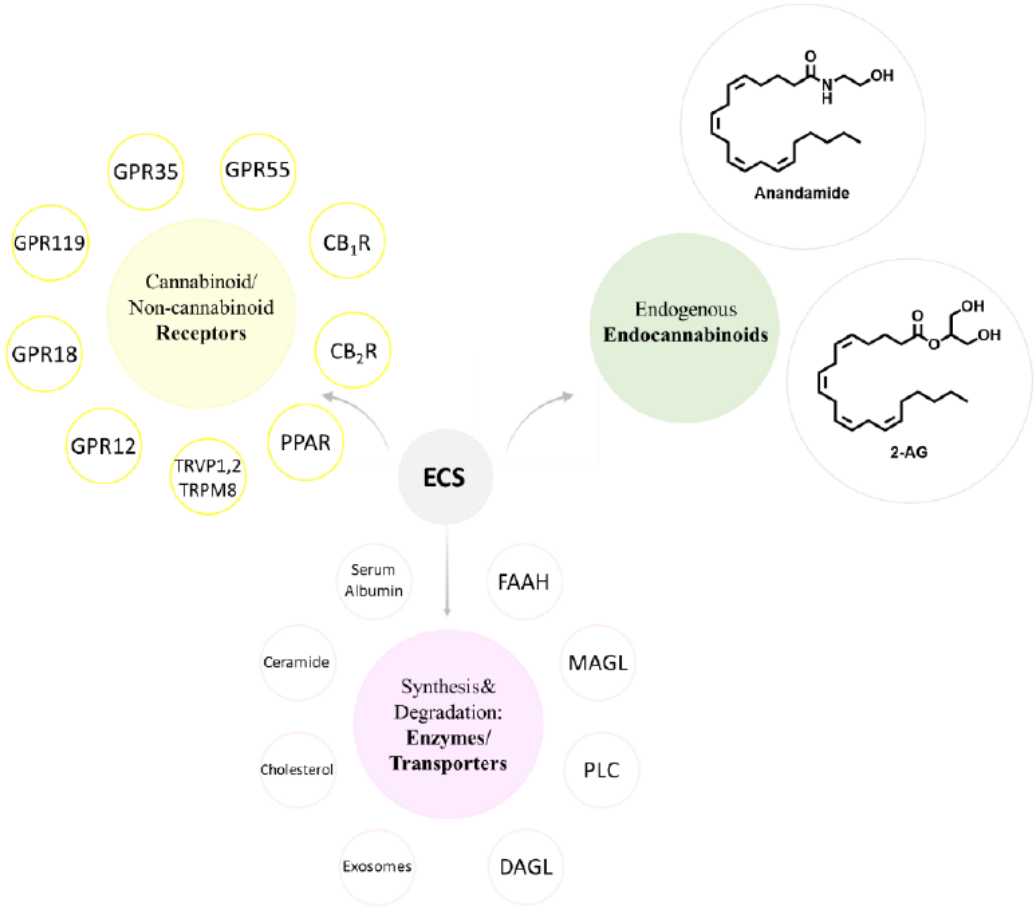



Figure 1.19. Representation of the endocannabinoid system (Figure from Gioé-Gallo, C. Discovery and Optimization of Selective $CB_2$ Receptor Agonists. PhD diss., University of Santiago de Compostela, Santiago de Compostela, 2023).[71]

USC UNIVERSIDADE DE SANTIAGO DE COMPOSTELA

Anandamide (N-arachidonoylethanolamide, AEA) and 2-AG (2-arachidonoylglycerol) were the first identified endogenous agonists of the CBRs, and remain the best studied endocannabinoids, both derivatives of arachidonic acid.[68,69]

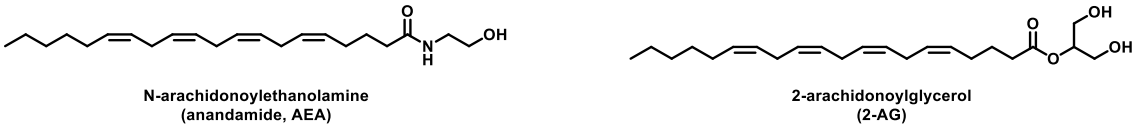



Figure 1.20. Structure of the most representative endocannabinoids.

These two compounds present different properties, being Anandamide a high-affinity partial agonist of $CB_1R$, with almost no effect on $CB_2R$, while 2-AG is a full agonist at both CBRs with moderate to low affinity.[68] Interestingly, both Anandamide and 2-AG have been reported to interact with other receptors, such as the transient receptor potential cation channel subfamily V member 1 (TRPV1), activated by Anandamide, while interactions between 2-AG and other receptors have only come out recently.[68] Both endocannabinoids are produced on demand in respond to increased intracellular $Ca^{2+}$ concentration, although they are synthesized, transported and inactivated in respective targets separately.[68] Anandamide is catalyzed from N-acyl-phosphatidylethanolamine (NAPE) by NAPE-specific phospholipase D (NAPE-PLD) or via other routes. On the other hand, 2-AG is produced from diacylglycerol (DAG) by either DAG lipase α or β (being DAGα the prominent one in the adult brain).[68] After release into the intracellular space, due to their uncharged hydrophobic nature, endocannabinoids are unable to diffuse freely like other neurotransmitters, and so several models haven been proposed to explain the transport of Anandamide: simple diffusion driven by concentration gradients generated from enzymatic degradations, endocytosis involving caveolae/lipid rafts, and through certain carrier proteins like fatty acid binding proteins and heat shock protein 70.[68] 2-AG may share the same transport system as Anandamide, but it is not well understood yet. Finally, once endocannabinoids are taken up by the cells, they can be degraded through hydrolysis and/or oxidation.[68]

$CB_1R$ and $CB_2R$ are membrane receptors that recognize cannabinoids, but several other receptors such as GPCRs, ion channels or nuclear receptors have been reported to interact with endocannabinoids and synthetic cannabinoids.[68] $CB_1R$ is primarily present in the CNS, whereas $CB_2R$ is prominently expressed in the periphery and in cells of the immune system, which makes $CB_2R$ a potential therapeutic target for the treatment of challenging autoimmune diseases, neuropathic pain, and cancer.[71] A graphical representation of the distribution and

USC UNIVERSIDADE DE SANTIAGO

functions of $CB_1R$ and $CB_2R$ all over the body is presented in Figure 1.21. Since the focus of the second part of this work is dedicated to $CB_2R$, we will briefly describe the most salient features of its structure, function, and medicinal chemistry.

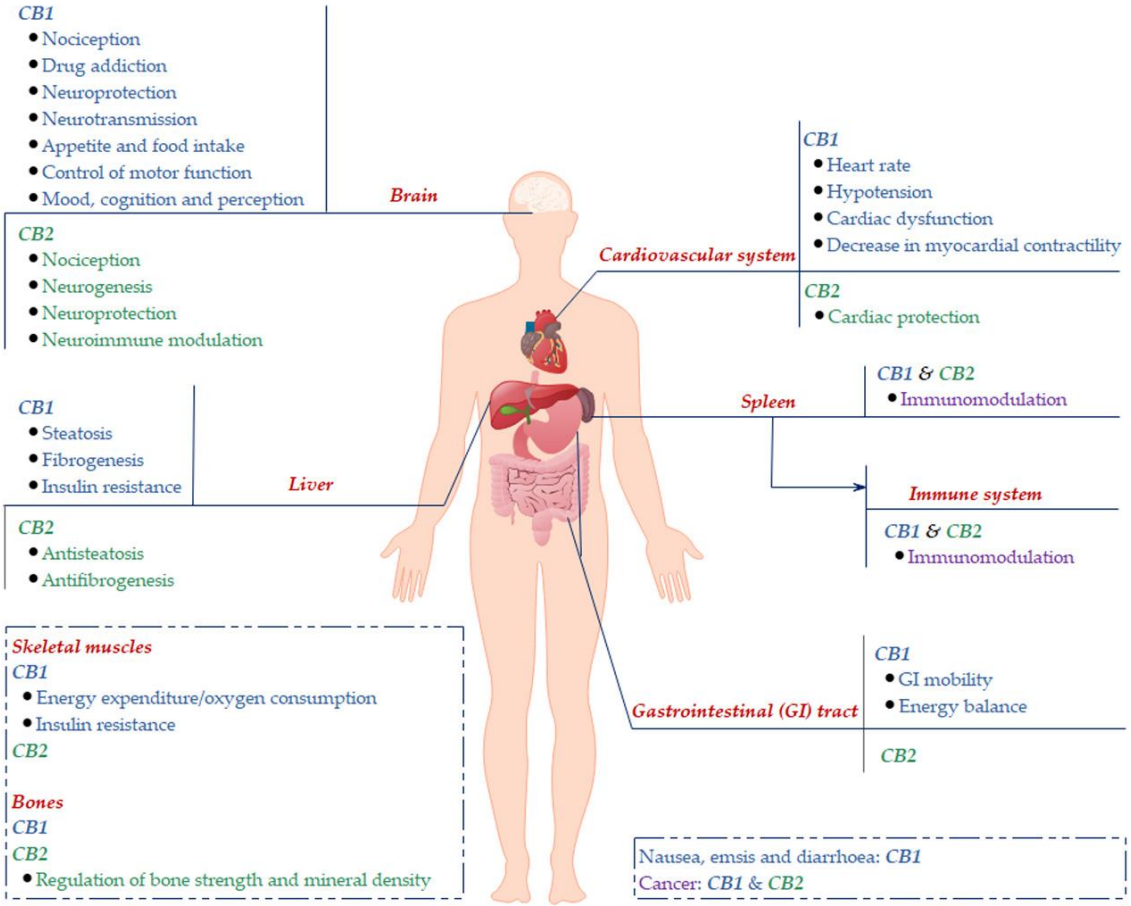



Figure 1.21. The functions and distribution of $CB_1R$ and $CB_2R$ throughout the body (Figure from An, D.; Peigneur, S.; Hendrickx, L. A.; Tytgat, J. Targeting Cannabinoid Receptors: Current Status and Prospects of Natural Products. IJMS 2020, 21, 5064. https://doi.org/10.3390/ijms21145064. Licensed under CC BY).[72]

## 1.6 $CB_2$ RECEPTOR ($CB_2R$)

A major limitation for the therapeutic development of compounds that activate $CB_1R$ is the presence of undesirable psychoactive side effects.[73] These $CB_1R$-mediated psychotropic actions produce both practical and administrative hurdles that has severely curtailed the development of direct-acting $CB_1R$ agonists. In contrast, activation of $CB_2R$ does not appear to produce these psychotropic effects.[73] Thus, the abundant peripheral expression of $CB_2R$, the increasing evidence of its therapeutic potential, and the observation that $CB_2R$ activation

USC UNIVERSIDADE DE SANTIAGO DE COMPOSTELA

produces desirable actions in a range of preclinical models attracted considerable interest and generated much activity in both academic groups and pharmaceutical companies.[73]

### 1.6.1 Structure, function, and localization

The $CB_2R$ is a member of the class A (rhodopsin-like) G protein-coupled receptor family, which consists of seven transmembrane domains connected by three extracellular loops and three intracellular loops.[74] The N-terminus of the receptor is located in the extracellular space, while the C-terminus is located intracellularly. The transmembrane domains form a central hydrophobic cavity that serves as the ligand-binding site for the receptor. While composed of 360 amino acid residues, the $CB_2R$ is highly homologous to the $CB_1R$, with approximately 44% sequence identity.[69]

The crystal structure of the human $CB_2R$ has been recently resolved at high resolution (2.8 Å) using X-ray crystallography (Figure 1.22).[75]

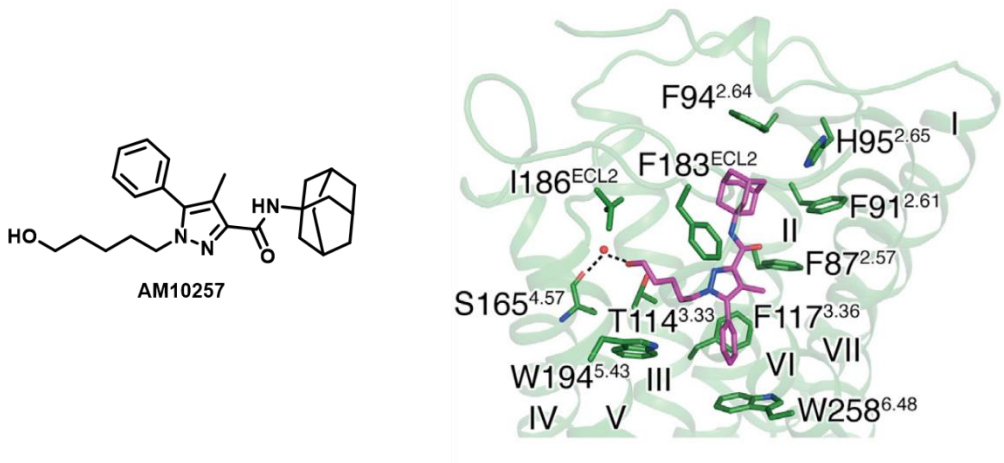



Figure 1.22. Structure of AM10257 and its binding to $CB_2R$ (Adapted from Li, X.; Hua, T.; Vemuri, K.; Ho, J.-H.; Wu, Y.; Wu, L.; Popov, P.; Benchama, O.; Zvonok, N.; Locke, K.; Qu, L.; Han, G. W.; Iyer, M. R.; Cinar, R.; Coffey, N. J.; Wang, J.; Wu, M.; Katritch, V.; Zhao, S.; Kunos, G.; Bohn, L. M.; Makriyannis, A.; Stevens, R. C.; Liu, Z.-J. Crystal Structure of the Human Cannabinoid Receptor CB2. Cell 2019, 176, 459-467.e13. https://doi.org/10.1016/j.cell.2018.12.011).[75]

The structure revealed that the $CB_2R$ has a pocket within the transmembrane domains that accommodates ligand binding. The pocket is lined by a series of hydrophobic amino acid residues, including Trp258$^{6.49}$, Val260$^{6.50}$, Ile263$^{6.53}$, Phe265$^{6.55}$, Phe282$^{7.35}$, and Phe289$^{7.42}$, which interact with the alkyl chain of ligands. Additionally, the $CB_2R$ has several polar amino acid residues that form hydrogen bonds with ligands, including Thr197$^{5.42}$, Ser201$^{5.46}$,

USC UNIVERSIDADE DE SANTIAGO DE COMPOSTELA

Ser204$^{5.49}$, and Ser207$^{5.52}$. The hydrophobic and polar interactions within the ligand-binding pocket are important for determining the affinity and selectivity of ligands for the $CB_2R$.[75]

In addition to the ligand-binding pocket, the $CB_2R$ has several other important structural features. The receptor has a highly conserved disulfide bond between Cys98$^{2.63}$ and Cys178$^{4.55}$, which is important for stabilizing the extracellular loop 2 of the receptor.[75] The intracellular loops are important for interacting with G proteins and other intracellular signaling molecules, and the C-terminus of the receptor contains phosphorylation sites that are important for regulating receptor activity.

The $CB_2R$ is primarily expressed in immune cells and peripheral tissues throughout the body.[76,77] Specifically, $CB_2R$ is found in high levels in cells of the immune system, such as T cells, B cells, and macrophages, as well as in other cell types including bone cells, liver cells, and skin cells.[76,77] $CB_2R$ has also been identified in the gastrointestinal tract, reproductive system, and nervous system.[77,78] . Initial studies suggested that $CB_2R$ was absent from the healthy brain, but subsequently studies have now shown $CB_2R$ expression in diseased brain cells, including astrocytomas, microglia and astrocytes in Alzheimer's disease, and T cells, microglia, and astrocytes in multiple sclerosis.[69]

Unlike $CB_1R$, which acts as the primary mediator of the psychoactive effects of cannabinoid ligands, $CB_2R$ activation does not induce psychoactivity and is primarily associated with suppression of inflammation via its expression in various components of the immune system,[79] suggesting that $CB_2R$ plays an important role in regulating the immune response. Additionally, the distribution of $CB_2R$ in peripheral tissues suggests that it may be involved in other physiological processes as well, such as bone remodeling and wound healing.[80]

$CB_2R$ activation has shown considerable preclinical promise in the treatment of autoimmune conditions and diseases with an inflammatory component (including stroke, cardiovascular disease, neurodegeneration, arthritis, inflammatory bowel disease, fibrosis, and some types of pain), as well as in osteoporosis, metabolic disorders, and cancer.[79] However, few $CB_2R$-targeted ligands have been clinically trialed and none have yet reached the market. A potential reason for this is poor target engagement of current $CB_2R$ ligands. Effective therapeutic exploitation of $CB_2R$-mediated functions will require ligands that have high affinity and selectivity for $CB_2R$ to avoid adverse off-targets effects, such as psychoactivity

USC UNIVERSIDADE DE SANTIAGO DE COMPOSTELA

via $CB_1R$, and that are optimized physicochemically for bioavailability and favorable pharmacokinetics.[79]

### 1.6.2 Signaling

The initial discovery of the $CB_1R$ was based on its function as a GPCR coupled to $G_{i/o}$ α proteins.[69] This coupling inhibits adenylyl cyclase, resulting in a decrease in cellular cAMP levels. The cellular signaling of the $CB_2R$ has also been characterized as $G_{i/o}$-coupled signaling,[69] however, the effectiveness of $G_{i/o}$ in inhibiting cAMP production varies depending on the experimental model and agonist used. In addition to $G_{i/o}$-mediated signaling, both $CB_1R$ and $CB_2R$ undergo phosphorylation by G protein receptor kinases (GRKs).[69] Subsequently, they associate with either β-arrestin1 or β-arrestin2. These β-arrestins can act as a scaffold for interacting with proteins that redirect signaling along β-arrestin-mediated pathways. Both $CB_1R$ and $CB_2R$ can stimulate extracellular signal-regulated kinase (ERK) 1 and 2 through interactions with either $G_{\beta\gamma}$ or β-arrestin.[69] Besides cAMP production modulation, $CB_2R$ coupling to $G_{i/o}$ proteins also activates a wide range of different signaling pathways: MAPK (p44/42 and p38), PI3K/AKT, JAK/STAT1, JNK, NFkB, CREB/ATF, sphingomyelinase, caspase, as well as some potassium and calcium ion channels.

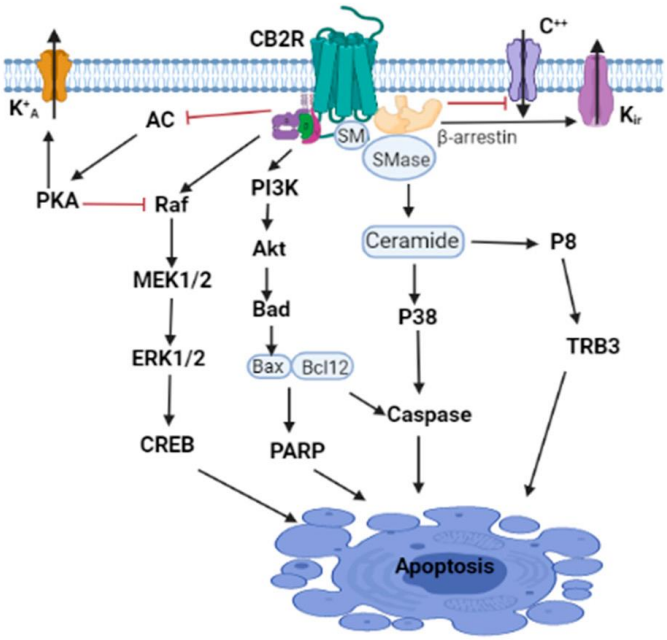



Figure 1.23. $CB_2R$ signaling pathways (Figure from Kibret, B. G.; Ishiguro, H.; Horiuchi, Y.; Onaivi, E. S. New Insights and Potential Therapeutic Targeting of CB2 Cannabinoid Receptors in CNS Disorders. IJMS 2022, 23, 975. https://doi.org/10.3390/ijms23020975. Licensed under CC BY).[81]

Among them, adenylyl cyclase and ERK1/2 modulation are the best studied, while other pathways such as those involving arrestin, Akt, ceramide and ion channel modulation are much less well-studied.[73] A visual representation of the various signaling pathways in which $CB_2R$ is involved is presented in Figure 1.23.

#### 1.6.2.1 Adenylyl cyclase (AC)

Stimulation of the $CB_2R$ leads to activation of pertussis toxin sensitive $G_{i/o}$ proteins, resulting in the inhibition of adenylyl cyclase and a decrease in cAMP levels. However, the expression levels and environment in which $CB_2R$ are expressed strongly influence their coupling to adenylyl cyclase and its inhibition.[73] For instance, when $CB_2R$ on human lymphocytes, which naturally express $CB_2R$, are stimulated, they poorly inhibit forskolin-stimulated adenylyl cyclase compared to $CB_2R$ expressed in HEK or CHO cells that have been transfected with $CB_2R$. Similarly, activation of $CB_2R$ in mouse spleen cells that endogenously express $CB_2R$ does not inhibit forskolin-stimulated adenylyl cyclase at physiologically relevant agonist concentrations.[73] However, when $CB_2R$ are activated in the BV2 microglial cell line, adenylyl cyclase is inhibited.

An interesting case is the natural product 4'-O-methylhonokiol, which exhibits inverse agonism for cAMP production and agonism for the release of intracellular calcium.[73]

#### 1.6.2.2 MAP kinase

MAP kinases are enzymes that play a crucial role in various signaling cascades involved in essential cellular processes such as cell proliferation, migration, transformation, and cell death.[73] The activation of ERK1/2 by $CB_2R$ agonists in CHO cells transfected with receptors was first reported by Bouaboula et al. (1996).[73] They observed that this activation is both time and dose dependent. Furthermore, they found that it is sensitive to pertussis toxin, indicating the involvement of $G_{i/o}$ proteins, but independent of adenylyl cyclase. Their study also demonstrated that the activation of this signaling cascade leads to the phosphorylation of the transcription factor krox-24, suggesting a potential role of $CB_2R$ in the control of gene transcription.

Unlike the inhibition of adenylyl cyclase, the activation of ERK1/2 is consistently observed in both recombinant and non-recombinant cells and systems.[73] Robust activation of ERK1/2 has been reported in immune cells, microglia, and macrophages, providing further evidence for the physiological relevance of this pathway.[73]

USC DE SANTIAGO DE COMPOSTELA

In addition, p38 MAPK activation by the non-selective $CB_2R$ agonist $\Delta^9$-THC was found to have a pro-apoptotic effect in the human leukemia Jurkat cell line and induce cytotoxicity in J774-1 macrophages.[73] These effects were exclusively mediated by $CB_2R$. Interestingly, Yamaori et al. also discovered in 2013 a JNK-mediated cytoprotective effect of $\Delta^9$-THC activation of $CB_2R$ in the same cells. Thus, the same ligand for $CB_2R$ can activate different MAPKs, resulting in diverse responses and outcomes.[73]

#### 1.6.2.3 Beta-arrestin signaling

Beta-arrestins are versatile proteins that can dampen G protein signaling by directly interacting with GPCRs. Additionally, they act as scaffolds, facilitating the recruitment of other signaling complexes to GPCRs.[73] The work of Atwood et al. and McGuinness et al. showed that the $CB_2R$ ligands tested recruited arrestin to the plasma membrane.[82,83]

#### 1.6.2.4 Ion channels

Although initial experiments did not observe functional coupling between $CB_2R$ and inwardly rectifying potassium channels (GIRK channels) and calcium channels, subsequent reports suggest that $CB_2R$ can indeed modulate the activity of these channels.[73] Atwood et al. demonstrated the $CB_2R$-mediated inhibition of voltage-gated calcium channels (VGCCs) in AtT20 cells. They found that CP55940 effectively inhibited VGCCs, while WIN55212-2 was inactive on its own but antagonized the inhibitory effect of CP55940.[82] Therefore, the lack of ion channel modulation observed in earlier studies is likely attributed to the functional selectivity of the ligands used at that time.[73]

#### 1.6.2.5 Internalization

Upon agonist binding, most G protein-coupled receptors (GPCRs) undergo internalization to some extent.[73] This internalization process plays a role in reducing the GPCR's signaling ability at the cell membrane. Furthermore, internalized GPCRs have the potential to activate novel signaling pathways that are not accessible to GPCRs residing on the cell surface membrane. Thus, the internalization of a GPCR in response to a ligand can be regarded as a form of signaling. The internalization of $CB_2R$ varies in response to agonists, with some agonists causing significant internalization and others being inactive.[73]

USC UNIVERSIDADE DE SANTIAGO DE COMPOSTELA

### 1.6.3 Therapeutic potential of $CB_2R$

Activation of $CB_2R$ has received attention for its pharmacological effects as antioxidant, anti-inflammatory, immunomodulatory and antiapoptotic that can be achieved without causing psychotropic adverse effects through $CB_1R$.[84] Additionally, $CB_2R$ has been shown to have potential as a therapeutic target in models of diseases where activation of the microglia and neuroinflammation are present, such as neuropathic pain or Alzheimer's disease (Figure 1.24).[85] Some of the most relevant features of $CB_2R$ as a therapeutic target are summarized below:

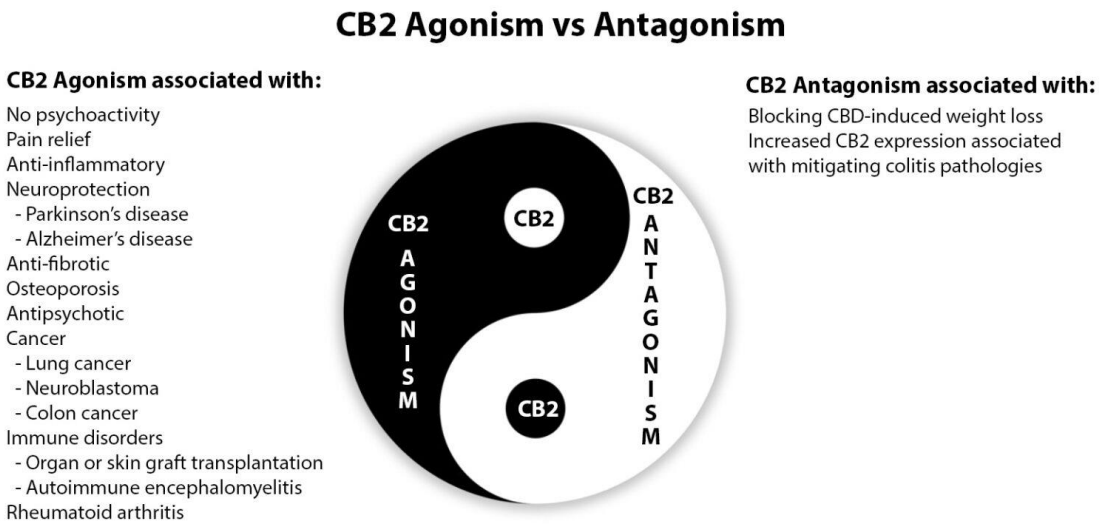



Figure 1.24. Pharmacological effects of $CB_2R$ activation (Figure from https://cannakeys.com/cb2-agonism/).[86]

#### 1.6.3.1 Inflammation

There is growing evidence indicating that stimulating $CB_2R$ has anti-inflammatory effects in different inflammatory diseases, since it hinders the production of inflammatory cytokines and chemokines while promoting the release of anti-inflammatory cytokines.[87] Notably, mice lacking $CB_2R$ exhibit an amplified inflammatory response.[87] Therefore, therapeutic strategies targeting the modulation of $CB_2R$ signaling show promise for treating inflammatory conditions.

Plasmacytoid dendritic cells (pDC) play a crucial role in initiating the body's immune response.[84] Autoimmune disorders like systemic lupus erythematosus and rheumatoid arthritis are characterized by heightened and persistent stimulation of pDC. In a study conducted by Henriquez et al.,[88] it was found that treating pDC with JWH133, a potent and selective $CB_2R$

agonist, resulted in the suppression of IFNα and TNFα responses stimulated by CpG (cytosine-guanine motifs). Moreover, JWH133 inhibited key indicators of pDC activation, including phosphorylated levels of IRF7, TBK1, NFκB, and IKKγ. The treatment with JWH133 also caused differential modifications in AKT phosphorylation at S473 and T308. Consequently, the activation of $CB_2R$ represents a potential therapeutic target for addressing inflammatory conditions caused by abnormal pDC activity.[87]

#### 1.6.3.2 Atherosclerosis

Atherosclerosis is a chronic inflammatory disease and the leading cause of cardiac disorders and stroke worldwide, and has been associated with the cannabinoid system.[87] The role of $CB_2R$ in atherosclerosis was initially demonstrated by Steffens et al. through an *in vivo* study.[89] They showed that low-dose oral THC significantly reduced both plaque size and the number of macrophages in $ApoE^{-/-}$ mice compared to untreated control mice. Additionally, when the $CB_2R$ selective inverse agonist SR144528 was co-administered, these effects were abolished. Another study by Netherland et al.[84] also confirmed that $CB_2R$ activation decreased macrophage infiltration, inflammation, and the progression of atheromatous plaques.

In a mouse model of atherosclerosis induced by a high-fat diet plus lipopolysaccharide (LPS) treatment, Zhang et al. reported that BCP (β-caryophyllene, a $CB_2R$ selective agonist) dose-dependently reduced the attachment of human monocytic cells to the surface of the aorta.[84] This finding further suggests the potential therapeutic impact of $CB_2R$ activation in reducing atherosclerosis-related processes.

Additional studies suggested the $CB_2R$-mediated regulation of atherosclerosis, as the use of JWH133 attenuated TNF-α- (tumoral necrosis factor alfa) and/or endotoxin-induced expression of ICAM-1 (intercellular adhesion molecule 1) and VCAM-1 (vascular cell adhesion molecule 1) in isolated aortas and prompted monocyte-aortic vascular endothelium adhesion.[87] This protective effect was abolished by $CB_2R$ blockers but not by $CB_1R$ blockers, thus, $CB_2R$ stimulation might alleviate endotoxin-driven vascular inflammation. Similarly, pretreatment of human coronary artery smooth muscle cells with the same $CB_2R$ agonist resulted in dose-dependent inhibition of proliferation and migration of vascular smooth muscle cells, which was also reversed by blockade of $CB_2R$.[87] Finally, $CB_2R$ agonism mitigated the TNF-α activation of Ras (rat sarcoma virus), MAPKs, stress-activated protein kinases (SAPK)/Jun amino-terminal kinases (JNK), and Akt. Once again, the use of a $CB_2R$

USC UNIVERSIDADE DE SANTIAGO DE COMPOSTELA

blocker inhibited these effects, indicating that $CB_2R$ activation counteracted TNF-α induced pathway.[87]

#### 1.6.3.3 Bone disorders

Compared to $CB_1R$, $CB_2R$ is expressed at higher levels in bone cells and plays a critical role in regulating the balance between bone resorption and osteogenesis.[87] During bone remodeling, the $CB_2R$ expression is increased, and its activation enhances osteoblast proliferation and function by promoting the expression of key osteogenic factors such as RUNX2, bone sialoprotein, osteopontin, alkaline phosphatase, and osteocalcin.[87]

Studies conducted on $CB_2R$-knockout mice have shown that they develop osteoporosis at 12 months, exhibit reduced osteoblast production and function, and exhibit increased osteoclast production.[87] In clinical studies involving postmenopausal women, it was observed that the gene encoding $CB_2R$ is associated with low bone mineral density.[87]

Therefore, targeting $CB_2R$ may hold promise as a translational approach for developing pharmacologic agents that can enhance bone health and address conditions such as osteoarthritis and osteoporosis, as shown in the work of Hashiesh et al., where systematic administration of JWH133 mitigated osteoarthritis pain induced by monosodium iodoacetate, decreased the expression of inflammatory cytokines (IL-1β and TNF-α), and increased the levels of anti-inflammatory IL-10.[87]

#### 1.6.3.4 Neuroprotection

In contrast to $CB_1R$, which is abundantly expressed in most brain regions, $CB_2R$ was previously considered to be restricted to peripheral tissues and predominantly expressed by immune cells. However, this receptor has been recently found to be strongly upregulated in the brain in CNS diseases characterized by neuroinflammatory processes and microglial cell activation,[90] such as neurological pain,[90] stroke,[90,91], Alzheimer's disease,[90,91], PD,[91] or multiple sclerosis.[90,91] The activation of $CB_2R$ decreases neuroinflammation, partly by mediating the transition of microglial phenotype from a predominantly neurotoxic M1 to a neuroprotective M2, suggesting an important role of $CB_2R$ in restoring homeostasis.[90] In addition, in the activated astrocytes and microglia, $CB_2R$ is involved in neuroprotection through the inhibition of chemokine production in astrocytes and the reduction of neurotoxic factors produced by microglia.[90] Therefore, due to $CB_2R$ inducible nature during

USC UNIVERSIDADE DE SANTIAGO DE COMPOSTELA

inflammation and neuroprotective properties, ligands that activate or inhibit their activity could be used for potential therapeutic purposes in various CNS disorders.

#### 1.6.3.5 Analgesic

Pain is a ubiquitously unpleasant feeling among humans frequently arising from both actual and potential tissue damage.[91] Some studies have demonstrated that $CB_2R$ is redistributed in many important portions of pain pathways, such as dorsal root ganglia (DRG) and afferent fibers in the dorsal horn of the spine, and may be upregulated under inflammatory and neuropathic pain conditions.[91] In addition, it is being increasingly recognized that $CB_2R$ is located in neuronal circuits in the brain relevant for pain control and dopamine-mediated reward.[91] Mice lacking the $CB_2R$ gene ($CB_2R^{-/-}$) displayed heightened hypersensitivity to pain (hyperalgesia) and an increased sensitivity to normally non-painful stimuli (allodynia) following sciatic nerve injury. Conversely, transgenic mice overexpressing $CB_2R$ exhibited a reduced manifestation of neuropathic pain. Furthermore, the deletion of $CB_2R$ contributed in the development of contralateral mirror image pain, which was associated with increased activation of microglial and astrocytic cells in the contralateral spinal horn.[91]

### 1.6.4 $CB_2R$ as a therapeutic target in cancer

The anticancer activity derived from $CB_2R$ agonism has been suggested in previous studies through the oral administration of $\Delta^9$-THC, $\Delta^8$-THC, and cannabinol, which prevented the proliferation of Lewis lung adenocarcinoma cell growth *in vitro* and *in vivo*.[92] Many other cannabinoids have since been demonstrated to inhibit proliferation, metastasis, angiogenesis and apoptosis in different cancer types. This anticancer activity is suggested to be due to their ability to modulate cellular signaling mechanisms controlling cell proliferation and survival.[87]

The abnormal expression of the endocannabinoid system is observed in various types of cancers, indicating its potential involvement in tumor cell progression.[93] Malignant cells exhibit higher levels of endocannabinoids compared to non-malignant cells.[93] For instance, meningiomas show elevated levels of 2-AG, while gliomas demonstrate increased levels of AEA. In colon cancer, anandamide levels are elevated by two to three times, and in prostate cancer, they are elevated by more than three times.[93] The involvement of endocannabinoid metabolizing enzymes, namely FAAH and MAGL, has also been examined.[93] In prostate adenocarcinoma, elevated levels of FAAH have been documented, which could be linked to a

USC
DE SANTIAGO
DE COMPOSTELA

negative cancer prognosis.[93] On the other hand, overexpression of MAGL in non-aggressive tumor cells leads to increased migration and invasion of the cells, potentially impacting cancer survival. Some studies on prostate tumor cells have indicated that inhibiting MAGL exhibits an anti-proliferative effect on cells treated with Epithelial Growth Factor (EGF).[93]

Compared to normal tissues, cannabinoid receptors are also highly expressed in many tumor cells, and this increased expression has been associated with tumor aggressiveness and disease outcome.[93] Specifically, breast cancer cells have exhibited an overexpression of $CB_2R$. While $CB_2R$ is not widely expressed in normal breast tissue, more than 90% of positive human epidermal growth factor receptor 2 (HER2+) breast tumors express $CB_2R$. This overexpression has been linked to the activation of HER2+ pro-oncogenic pathways as well as HER2- pro-oncogenic signaling. Additionally, there is a correlation between $CB_2R$ overexpression, histological tumor grade, and poor prognosis.[93]

$CB_1R$ and $CB_2R$ have been reported as Tamoxifen molecular targets in breast cancer,[93] and their concentration is increased in prostate cancer as well, where a high expression of $CB_1R$ has been linked to a poorer prognosis.[93] In colon carcinoma, $CB_2R$ is also overexpressed, similar to gliomas where $CB_1R$ has also been found.[94] The overexpression of $CB_2R$ in these cases has been associated with tumor grade and a worse disease prognosis. In pancreatic cancer, a higher expression of $CB_1R$ has also been correlated with an unfavorable cancer prognosis.[95] However, in hepatocarcinoma, elevated levels of both $CB_1R$ and $CB_2R$ are associated with an improvement in cancer outcome.[49] In squamous carcinoma cells of the tongue, an overexpression of both $CB_1R$ and $CB_2R$ has been reported and associated with disease prognosis.[96] Notably, the overexpression of $CB_1R$ serves as a better survival marker compared to the overexpression of $CB_2R$. Lastly, studies in ovarian cancer have revealed that invasive tumors exhibit higher expression of $CB_1R$ compared to benign tumors. This overexpression may be linked to the invasiveness of ovarian cancer.[93]

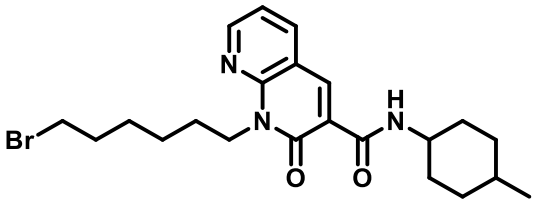
In recent studies involving breast and prostate cancer cell lines, it has been discovered that $CB_2R$ plays a role in regulating the metastasis of tumor cells.[93] Activation of $CB_2R$, either by external or internal means, leads to the formation of heterodimers with the chemokine receptor CXCR4. These heterodimers inhibit pathways that are involved in tumor progression. In a similar manner, $CB_2R$ and GPR55 form heteromers in cancer cells, and the modulation of these structures with unique signaling properties can modify the antitumoral activity of cannabinoids *in vivo*.[97] Finally, HER2-targeted therapies have dramatically

USC DE SANTIAGO DE COMPOSTELA

improved the clinical outcome of HER2-positive breast cancer patients, however, innate and acquired resistance remain an important clinical challenge, so a new target for antitumor treatments appears to be the heterodimer HER2-$CB_2R$, since the disruption of these complexes triggers the inactivation and degradation of HER2, promoting in turn antitumoral responses.[98]

#### 1.6.4.1 $CB_2R$ and neuroblastoma

Neuroblastoma (NB) is a prevalent type of solid extracranial tumor in children, and it is associated with high mortality rates.[99] It originates from underdeveloped nerve cells in the sympathetic nervous system and can manifest as a variety of clinical outcomes, ranging from spontaneous regression to incurable progression with limited treatment options and a grim prognosis. Hence, there is a crucial need to discover new compounds that can deliver effective and efficient outcomes in the treatment of neuroblastoma.[99] The work of Gado et al. showed $CB_2R$ agonists as promising anti-cancer agents through the arrest of cell viability in high-risk neuroblastoma.[99] The ERK/MAPK signaling pathway is known to play a role in NB, contributing to the progression towards a pro-tumor cell phenotype, and is also involved in resistance to chemotherapy. They observed that FG158a (a new $CB_2R$ agonist, Figure 1.25) was able to modulate ERK1/2 expression in SH-SY5Y cells, and that the effect is mediated by $CB_2R$, thus suggesting that the potential anti-cancer effect of this compound might involve this signaling pathway.[99]




**FG158a**
$CB_1R$ $K_i$ > 10,000 nM
$CB_2R$ $K_i$ = 21 nM
Reduction of cell viability of neuroblastoma cell lines SH-SY5Y
$IC_{50}$ = 11.8 μM

Figure 1.25. FG158a structure and pharmacological data.[99]

#### 1.6.4.2 $CB_2R$ and breast cancer

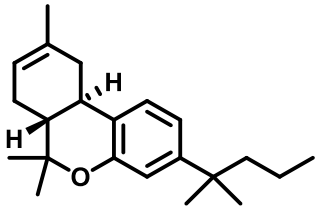
Breast cancer is a prevalent form of cancer among women globally and ranks as one of the primary causes of cancer-related deaths in the female population. According to the

World Health Organization, it accounts for approximately 16% of all cancers diagnosed in women. The incidence of breast cancer varies with age and is on the rise.[93]

15% to 20% of all breast tumors belong to a subtype that is characterized by overexpression of HER2, which promotes oncogenic signaling by modulating the expression and activity of proteins controlling cell proliferation, differentiation, death, migration, and angiogenesis.[98] HER2 activation occurs through the process of ligand- or overexpression-induced dimerization with other family members (HER1, HER3 and HER4). This dimerization leads to trans-phosphorylation and autophosphorylation of the HER homo/heterodimer constituents within their cytosolic kinase domains.[98] Trastuzumab, a recombinant humanized monoclonal anti-HER2 antibody, has significantly improved the outcome of these patients but, despite its efficacy in many HER2+ breast cancer cases, some patients do not respond to this treatment.[98] Since a new target for antitumor treatments is needed, the work of Blasco-Benito et al. describes a mechanism by which the modulation of the $CB_2R$ disrupts the heterodimer $CB_2R$-HER2 inactivating the latter and leading to an antitumoral activity.[98] In the absence of any pharmacological treatment, HER2+ breast cancer cells exhibit elevated levels of HER2, which leads to the upregulation of $CB_2R$ expression. Subsequently, HER2 and $CB_2R$ combine to form heteromers on the cell's outer membrane. This shields HER2 from degradation and promotes its typical oncogenic signaling, resulting in tumor-promoting responses. When THC is introduced (or other means such as $CB_2R$ agonists are employed to hinder the interaction between HER2 and $CB_2R$), the two receptors physically separate. Moreover, the disruption of HER2-$CB_2R$ interaction leads to the inactivation of HER2 (by disrupting HER2-HER2 homodimers) and enhances its susceptibility to degradation. Ultimately, this degradation of HER2 and activation of $CB_2R$ culminate in an anti-tumor response.[98]

The anticancer effect of $CB_2R$ agonism in this cancer type has also been studied by Qamri et al.,[100] whose work showed that JWH133 (Figure 1.26) provided a dose-dependent inhibition of the proliferation and migration of MDA-MB231 and MDA-MB468 cells, although the growth factor HER2 is not overexpressed in these cell lines. JWH133 resulted in a significant decrease in tumor growth and lung metastasis and markedly attenuated angiogenesis in mice. These effects were abolished by SR144528, proving this receptor implication in the anticancer activities.[87]

USC UNIVERSIDADE DE SANTIAGO DE COMPOSTELA

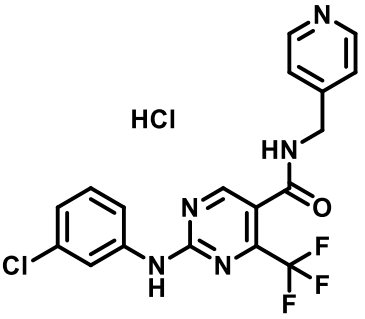


**JWH133**
$CB_1R$ $K_i$ = 677 nM
$CB_2R$ $K_i$ = 3.4 nM
Maximum inhibitory effect on MDA-MB231 cell line proliferation of 58% at 10 μM compared with control

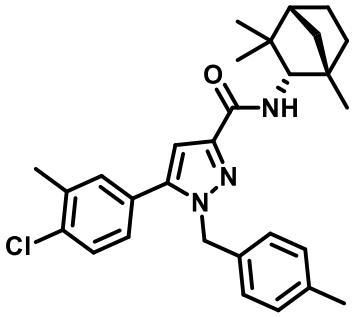
Figure 1.26. JWH133 structure and pharmacological data.

### 1.6.4.3 $CB_2R$ and colorectal cancer

Along with the lung and female breast, colorectal cancer (CRC) are the three most prevalent cancer types in both genders.[101] Frequently, CRC is described as a non-malignant tumor known as tubular adenoma and serrated polyp, which undergoes modifications leading to CRC over time.[101] Several factors, such as gene mutations, epigenetic changes, and inflammatory responses, play a significant role in the heterogeneous sequence from polyp to CRC.[101] The primary treatment for CRC mainly relies on the cancer stage and typically commences with surgery targeting the initial polyp form. Subsequently, adjuvant therapy utilizing chemotherapeutic agents is administered, and using cannabinoids for alleviation of cancer-induced pain, emesis, cachexia, or dysgeusia has been well documented.[101]



**GW833972A**
$CB_1R$ $K_i$ > 1000 nM
$CB_2R$ $K_i$ = 7.8 nM
Cytotoxic effect on HT-29 cell line
$IC_{50}$ = 24.92 ± 6.99 μM at 48 h



**SR144528**
$CB_1R$ $K_i$ = 400 nM
$CB_2R$ $K_i$ = 0.6 nM

Figure 1.27. GW833972A and SR144528 structure and pharmacological data.

UCC UNIVERSIDADE DE SANTIAGO DE COMPOSTELA

The work of Alenabi et al.[101] showed that $CB_2R$ agonism (GW833972A, Figure 1.27) exerts a concentration- and time-dependent cytotoxicity on HT-29 cells, that was reversed by the simultaneous use of SR144528. The apoptotic effect of this $CB_2R$ agonist was also tested in the same cell line, revealing that GW833972A increased the number of cells with early and late apoptotic situation, and at the highest given concentration even the rate of necrotic cells was remarkably elevated. In a similar way as the first case, the use of SR144528 clearly reduced the apoptotic and necrotic cells population, evidencing the role of the $CB_2R$ in the anticancer activity.[101]

#### 1.6.4.4 $CB_2R$ and malignant gliomas

Malignant gliomas are recognized as the most prevalent malignant brain tumors with a bleak prognosis.[87] Sánchez et al. investigated the antitumor effect of JWH133 and demonstrated that incubating rat glioma C6 cells with this $CB_2R$ agonist led to a significant decrease in cell viability by approximately 50%.[87] This effect was attributed to the activation of apoptotic cell death through ceramide synthesis and stimulation of ERK1/2. When JWH133 was administered directly into glioma tumors in a mouse model lacking the Rag-2 gene, it resulted in a remarkable reduction in tumor growth by around 71%.[87] Furthermore, JWH133 hindered the growth of highly malignant human astrocytoma in Rag-2 deficient mice. Overall, the activation of $CB_2R$ demonstrated antitumor activity by inducing apoptosis through ceramide synthesis and ERK1/2 activation.[87]

In a related study conducted by the same research group using the same mouse model, intratumoral treatment with JWH133 led to a significant downregulation of proangiogenic factors, specifically vascular endothelial growth factor (VEGF) and angiopoietin 2 (Ang 2). These results were further validated in glioma and astrocytoma xenografts, where JWH133 inhibited the expression of VEGF, Ang1, Ang2, MMP-2, and TIMP-2.[87]

#### 1.6.4.5 $CB_2R$ and glioblastoma

Glioblastoma (GBM), the most common form of primary brain tumor in adults, is characterized by its high aggressiveness and a median survival rate of less than 2 years.[102,103] Due to its heterogeneous and infiltrative nature, GBM displays strong resistance to therapy, which is the most common cause of tumor recurrence.[102,104] Currently, the treatment of GBM is based on surgical removal followed by radiotherapy and the administration of temozolomide as adjuvant therapy,[105] however, the low patient survival rate makes it

USC DE SANTIAGO DE COMPOSTELA

necessary to explore new therapeutic strategies to improve the prognosis of the disease, as well as the quality of life of patients.

Recent studies have revealed the upregulation of $CB_2R$ in endothelial cells of glioblastoma vessels, which may be indicative of the importance of $CB_2R$ impairing tumor growth.[103] Additionally, a study investigating the $CB_2R$ agonist β-caryophyllene in both *in vitro* and *in vivo* model of glioblastoma showed a significant anti-proliferative effect of this compound, reducing cell viability, inhibiting cell cycle, and increasing apoptosis.[105]

The ComBioMed group has recently demonstrated the important role of $CB_2R$ agonists inhibiting cell proliferation in *in vitro* cancer models. This was achieved through the evaluation of a selected group of $CB_2R$ agonists, which are part of a broad library of synthetic cannabinoid receptor agonist analogs, in the U87 glioblastoma cell line.[71] The studied compounds (Figure 1.28) significatively reduced (15-40%) cell proliferation in a dose-dependent manner, particularly at 20 µM. Among these compounds, **IX** emerges as the most promising, reducing glioblastoma proliferation by 40% at 10 µM, outperforming the measured effect of Temozolomide, an orally administered chemotherapeutic agent routinely used in clinical practice,[102,106]

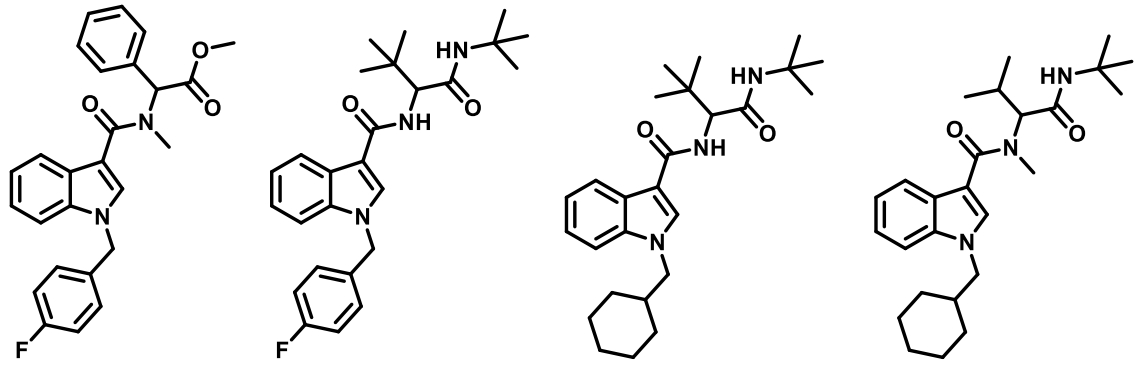



Figure 1.28. Structure and pharmacological data of the SCRA analogs studied in a glioblastoma model.

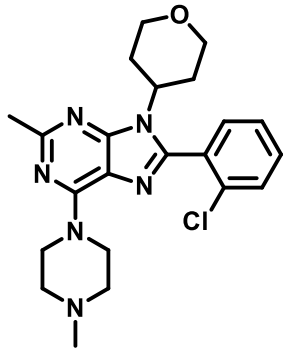
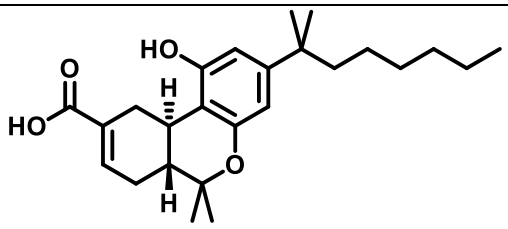
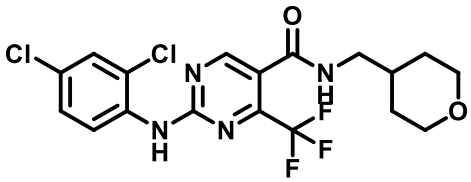
### 1.6.5 $CB_2R$ ligands in clinical trials

The challenges inherent in the quest to discover and refine selective $CB_2R$ agonists are evident in the limited number of candidates that have progressed to clinical trials.[107] A summary of $CB_2R$ compounds currently under investigation is provided in Table 1.1. Clinical

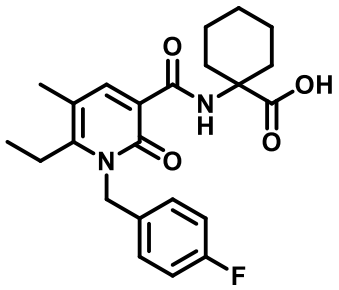
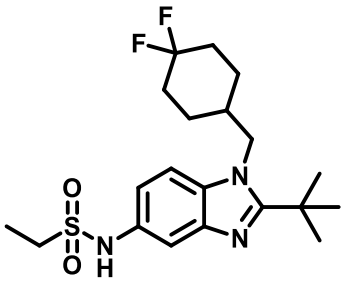
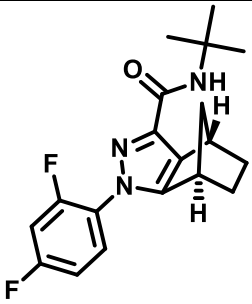
USC UNIVERSIDADE DE SANTIAGO DE COMPOSTELA

research primarily centers on pain relief and osteoarthritis, although recent studies, encompassing both preclinical and clinical phases, are increasingly oriented toward cancer treatment.[87,92,93,97–99,101,107]

Table 1.1. $CB_2R$ ligands in clinical trials.

| Name | Activity | Therapeutical indication | Clinical status |
|---|---|---|---|
|  **LY2828360 (Eli Lilli)** | Agonist | Osteoarthritic knee pain | Phase II[107,108] |
|  **JBT-101 (JB Therapeutics)** | Agonist | Systemic lupus erythematosus (SLE) | Phase II[108] |
|  **GW-842166 (GlaxoSmithKlane)** | Agonist | Osteoarthritis | Phase II[108] |

USC UNIVERSIDADE DE SANTIAGO DE COMPOSTELA

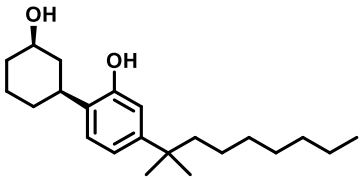
| | | | |
|---|---|---|---|
|  **S-777469 (Shionogi)** | Agonist | Atopic dermatitis | Phase II[108] |
| **TT-816** | Antagonist | Cancer | Phase II[108] |
|  **AZD1940 (AstraZeneca)** | Agonist | Pain | Phase II[108] |
|  **Tedalinab (Glenmark Pharmaceuticals)** | Agonist | Osteoarthritis pain | Phase II[107] |
| **KHK-6188** | Agonist | Neuropathic pain | Phase II[107] |
| **ABT-521** | Agonist | Neuropathic pain | Phase II[107] |

### 1.6.6 Synthetic cannabinoid receptor agonists (SCRAs)

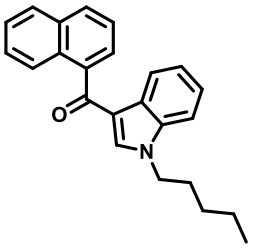
In 2008, the first examples of synthetic cannabinoid receptor agonists (SCRAs) were identified as new psychoactive substances (NPS), and they have proliferated exponentially since then.[109] Along with synthetic cathinones, SCRAs are one of the largest and most defiant classes of NPS because of its great structural diversity and dangerousness. Like $\Delta^9$-THC,

SCRAs are all intended to activate the $CB_1R$, and most also act as agonists of the $CB_2R$, although they are completely different chemically and pharmacologically. Activation of the $CB_1R$ accounts for the psychoactivity of these substances.[109] Because of their ability to mimic the psychotropic effects of $\Delta^9$-THC, SCRAs have been introduced within the illicit drug market to create pseudo-legal or unregulated alternatives to Cannabis, and are usually advertised as synthetic marijuana.[71]

The first SCRA NPS reported back in 2008 was the phytocannabinoid-like CP 47,497-C8, alongside JWH-018 (Figure 1.29), however, the subsequent structural evolution of this class has tended away from natural products scaffolds.[110]




**CP 47,497-C8**
$CB_1R$ $K_i$ = 2.1 nM
$IC_{50}$ ($CB_1R$) = 15.4 nM




**JWH-018**
$CB_1R$ $K_i$ = 9.00 ± 5.00 nM
$EC_{50}$ ($CB_1R$) = 102 nM
$CB_2R$ $K_i$ = 2.94 ± 2.65 nM
$EC_{50}$ ($CB_2R$) = 133 nM

Figure 1.29 First examples of SCRAs NPS: CP 47,497-C8 and JWH-018.

Originally designed in the context of drug discovery programs, SCRAs have evolved into a significant public health issue due to their adverse effects and restricted safety record.[111] In the mid-2000s, SCRAs entered the illicit drug market as herbal blends, gaining popularity for their perception as a lawful and cost-effective substitute for cannabis.[111] In 2014, 5F-AMB-PICA (also known as 5F-AMBICA, Figure 1.30) came to the attention of the European Monitoring Centre for Drugs and Drug Addiction (EMCDDA) when it was identified in Hungary and Sweden. Concurrently, its indazole analogue, 5F-AMB-PINACA (5F-AMB), was also found in Hungary. Subsequently, in 2015, the *tert*-leucinate analog of 5F-AMB, known as 5F-ADB, was detected in both Hungary and Japan. Furthermore, the indole derivative MDMB-FUBICA was uncovered in Hungary and Sweden in 2015, and AMB-FUBINACA was reported to the EMCDDA in Sweden during the same period.[109] These compounds constantly undergo structural changes and diversification, making the task of detecting them quite challenging. Prior to their initial identification by forensic chemists, numerous SCRAs remain undisclosed and their effects on human activity are largely

unknown. The lack of comprehensive information concerning the pharmacological and toxicological characteristics of newly emerging SCRAs presents a continuous obstacle for scientists, healthcare professionals, and policymakers throughout the globe.[109] As a result, there has been a growing effort to characterize the ever-evolving structures of new SCRAs that emerge worldwide. This effort has led to the creation of numerous libraries containing SCRAs analogs, which have offered valuable insights into their structure-activity relationship, as well as their metabolism.[109,111,112]

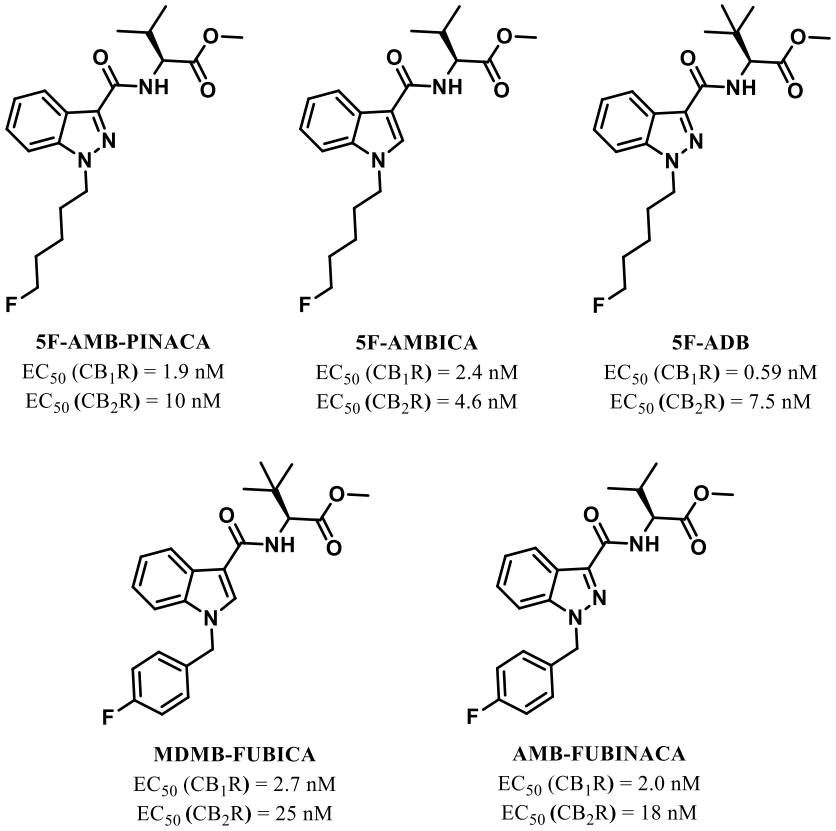



Figure 1.30 Detected SCRAs between 2014-2015.

Despite exhibiting chemical heterogeneity, the majority of SCRA NPS can be classified under a generic Markush structure (Figure 1.31) that consists of four distinct subunits: a core group (blue), a linker group (orange), a tail group (red), and a head group (green).[110] Due to the plasticity of the $CB_1R$ orthosteric site, various combinations of these subunits yield viable SCRA compounds, and emerging SCRA NPS frequently exhibit unconventional arrangements of both new and previously identified subunits.[110] Notably, the identified aromatic cores predominantly include indoles or azaindoles (such as indazole, benzimidazole, and pyrrolopyridine), although pyrroles, napthalenes, and thiazoles have also been reported.

The tail subunit is capable of accommodating diverse physicochemical properties, encompassing alkyl, alicyclic, heterocyclic, aromatic, and heteroaromatic moieties. Ketones, amides, and esters are the most encountered linkers, although simple alkyl ethers and thiazoles have also been observed. Lastly, the head groups exhibit the greatest variability in terms of composition and structure.[110]

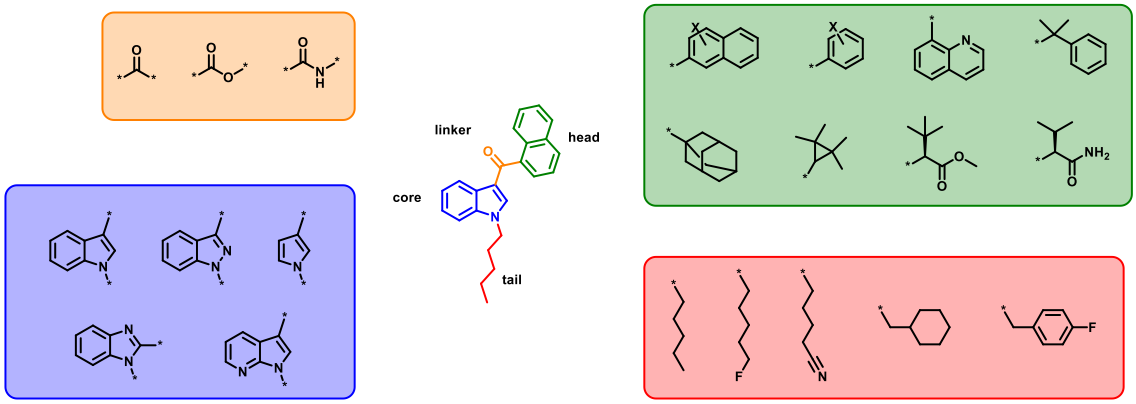



Figure 1.31 General Markush representation for SCRAs based on JWH-018 scaffold.[110]

Two core structures that are receiving increasing attention in the realm of synthetic cannabinoids are indoles and indazoles, the use of which has been linked to severe adverse health effects.[109] Notably, one of the most prevalent categories of synthetic cannabinoids falls under the 1-alkyl-1*H*-indazole-3-carboxamide group, characterized by the inclusion of valinamide and *tert*-leucinamide pendant groups.[109] This category includes examples like AB-FUBINACA and ADB-PINACA. After the Drug Enforcement Administration (DEA) in the United States designated several members of this class as Schedule I substances, newer variants of indole and indazole-3-carboxamides have emerged (Figure 1.32). These new derivatives are gaining popularity and feature substituents like 5-fluoropentyl, 4-fluorobenzyl, cyclohexyl methyl, or pentyl at the 1-position, along with valinate and *tert*-leucinate methyl ester side chains. These developments are noteworthy due to their impact on the landscape of recreational drug use.[109] The most prevalent SCRA families contain a stereocenter in their structure (Figure 1.32). The stereo disposition within the group in the linker remains an intriguing characteristic feature of SCRAs, with reported data so far being somewhat underexplored and contradictory.[71]

USC UNIVERSIDADE DE SANTIAGO DE COMPOSTELA

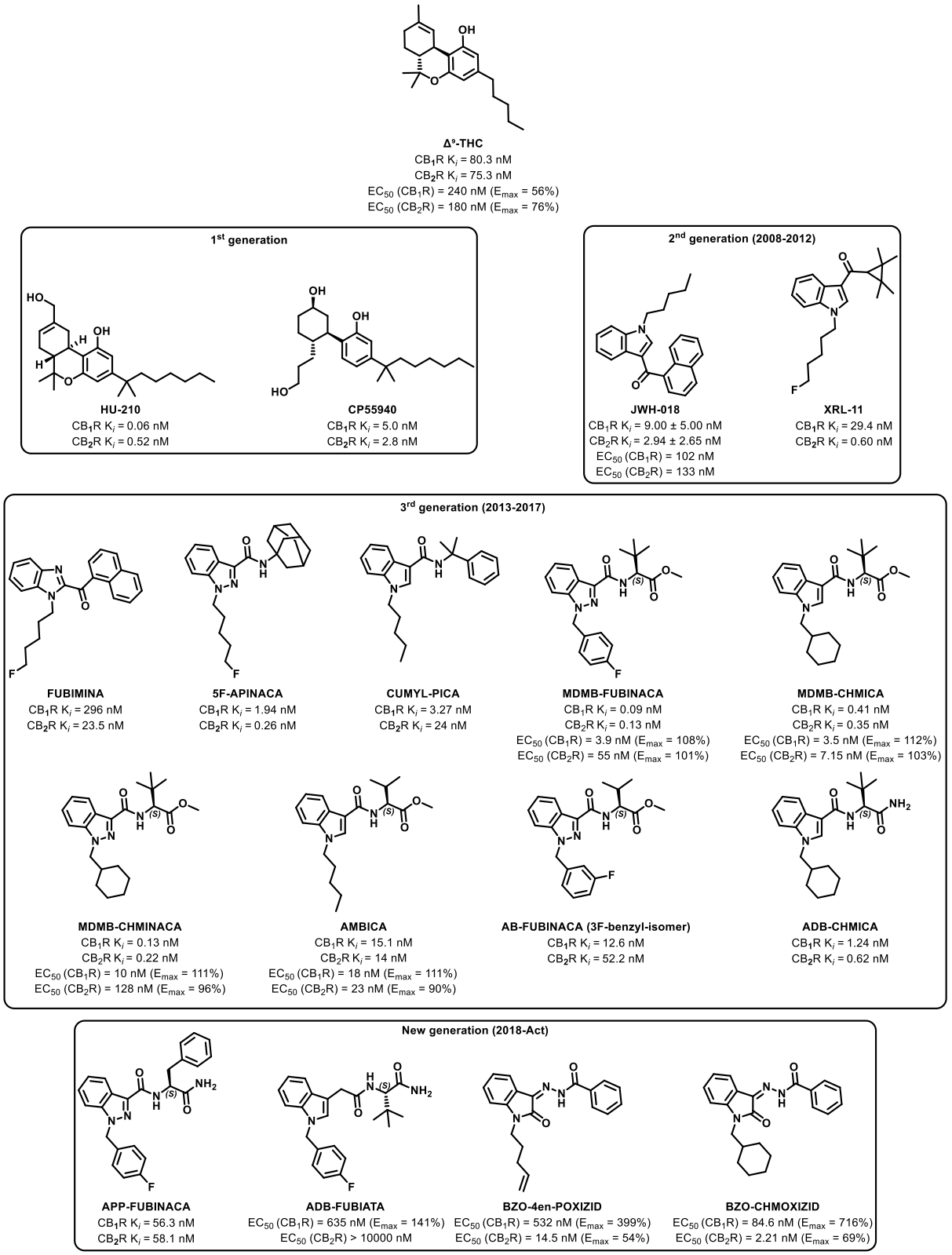



Figure 1.32. Structure and pharmacological data of representative SCRAs.[71]

USC UNIVERSIDADE DE SANTIAGO DE COMPOSTELA

Pfizer compound AB-FUBINACA and all the SCRAs within the illicit market are (*S*) enantiomers; the (*R*) enantiomer of these compounds had not been evaluated in the literature until the ComBioMed group recently published the cannabimimetic data of 32 novel SCRAs containing an (*R*) configuration at this stereogenic center.[71,111] Furthermore, the work of Claudia Gioè offered valuable pharmacological insights into the structure-activity and structure-selectivity relationships of the SCRAs family, leading to the identification of new agonists that selectively target the $CB_2R$.[71] This study was inspired by the SCRAs pharmacophoric model, and utilized a previously unexplored Ugi-based synthetic approach that facilitated the convergent and high-throughput synthesis of 168 new derivatives. The rationale behind this procedure is the resemblance between the SCRAs pharmacophore and the chemical structure of Ugi adducts (acylamino amide, Figure 1.33).

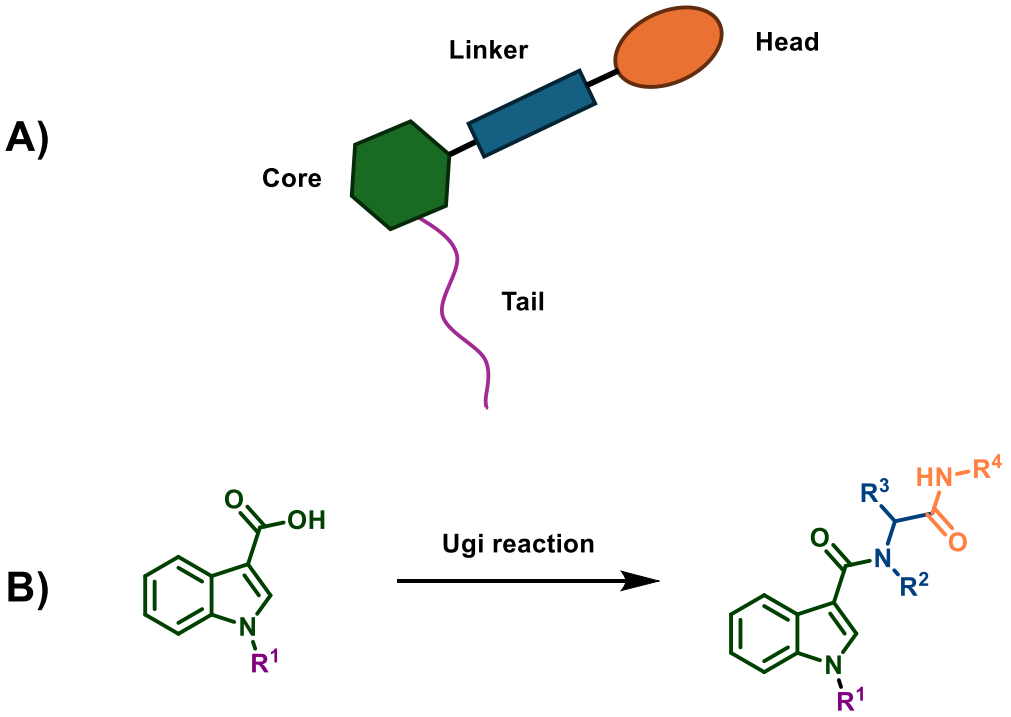



Figure 1.33. Structural resemblance between A) Pharmacophoric model of SCRAs and B) Chemical structure of Ugi adducts.

From a structural standpoint, the Ugi reaction retains the pharmacophoric elements, including the linker between the central core and the head of the pharmacophoric model, thus enabling the modification and exploration at four different positions.[71]

The results of this work allowed the identification of several ligands combining remarkably affinity ($CB_2R$ $K_i$ < 100 nM) and exquisite selectivity (>100-fold over $CB_1R$) that

were used to study the role of $CB_2R$ agonists in the context of cancer therapy. Four of the best ligands were tested in a model tumor cell line (U87) to evaluate their antiproliferative activity and demonstrated to significantly reduce cell proliferation of glioblastoma in a dose-dependent manner (see Section 1.6.4.5. "$CB_2R$ and glioblastoma"). Figure 1.34 shows the structure and pharmacological data of some of the best ligands obtained in this work, characterized by their high affinity for $CB_2R$ and complete selectivity towards $CB_1R$.[71]

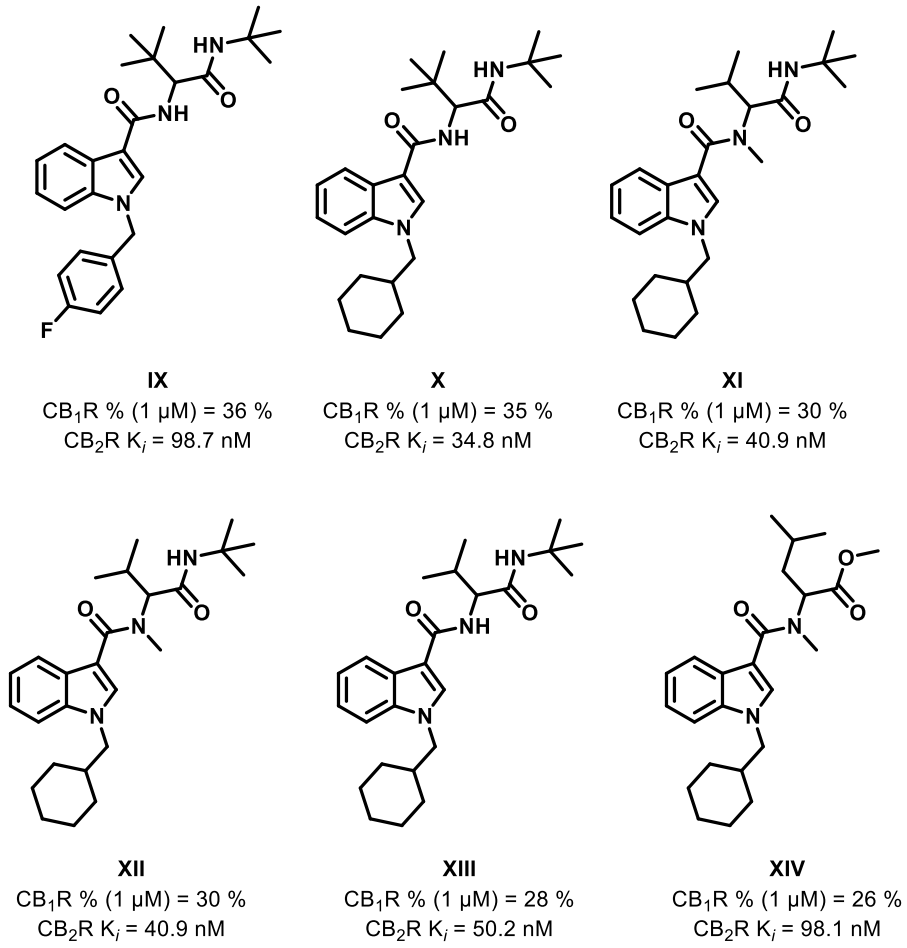



Figure 1.34. Structure and pharmacological data of potent and selective $CB_2R$ agonists obtained through the Ugi reaction.[71]

In this Doctoral Thesis, we will use these scaffolds and capitalize on the SAR and SSR trends revealed in Gioè's work to develop novel series of $CB_2R$ selective agonists.

USC UNIVERSIDADE DE SANTIAGO DE COMPOSTELA

## 1.7 MCRs

The importance of small organic molecules in current chemical biology and medicinal chemistry is undeniable. The study of their interaction with biological systems and the changes they can cause within them are crucial to understanding the fundamental processes involved in health and disease. Organic synthesis provides access to multiple families of structurally complex and functionally diverse compounds, thus providing the raw material for advances in medicinal chemistry. The goal is to identify powerful and selective molecular modulators for all cellular processes, including the ever-increasing number of non-classical biological targets considered "undruggable", that is, which cannot be reached with medication. However, finding even a single one of these modulators in the vastness of chemical space is not an easy task. This chemical space is defined as a representation of all small molecules in a multidimensional space in which the descriptors can be any property other than the molecular structure.[113] These can include, for example, molecular weight, polarity, solubility, membrane permeability, binding constants, hydrogen-bonding properties, etc. Consequently, the molecular diversity within a compounds family is represented by its dispersion in chemical space. Starting from a handful of elements (C, H, N, O, S), the estimation of the total number of possible small molecules that can be prepared goes from $10^{60}$ to $10^{200}$, numbers that clearly escape our comprehension.[113] In order to surmount this challenge, there is a requirement for tools and synthetic methods that can expedite the process.

Classical organic synthesis methods rely on stepwise multistep sequences that enable the progressive introduction of diversity to afford the target structure. Recently, multicomponent reactions (MCRs), those involving the reaction of three or more starting materials where the final product retains significant portions of all reactants, have emerged as tailored synthetic approaches, particularly in medicinal chemistry.[114] Classical examples of MCRs are the Biginelli reaction or the Ugi reaction. MCRs are one-pot transformations that offer convergent, efficient, and eco-friendly alternatives to classical linear multi-step synthesis during the preparation of highly diverse pharmacologically active libraries. MCRs exhibit a high bond economy, making them highly efficient from cost and time points of view. As a result, there is less waste or side products generation compared to sequential synthesis. The concomitant bond-forming efficiency, the low-cost separation and purification of products, and the structural diversity of the resulting products make this sustainable approach a

USC UNIVERSIDADE DE SANTIAGO DE COMPOSTELA

powerful tool for the synthesis of biologically active molecules and optimization processes in the pharmaceutical research.[115] They offer greener alternatives to produce molecular diversity in parallel synthesis, and, in many cases, may be adapted to automation. The variety of chemical reactions involved in MCRs adds the opportunity to obtain many different molecular-skeletons through elegant and efficient approaches.[116] MCRs strategies for synthesis of diverse organic structures have been well known for a long time, but it has only recently started gaining more attention and there are an increasing number of research articles emphasizing on the synthesis of biologically relevant organic molecules via this approach.[115]

### 1.7.1 Isocyanide-based multicomponent reactions.

One of the most well-known categories of multicomponent reactions involves the participation of an isocyanide. These multicomponent reactions, known as isocyanide-based multicomponent reactions (IMCRs), were among the earliest discovered and continue to be extensively explored.[117] Isocyanides (Figure 1.35), also referred to as isonitriles, constitute a class of compounds characterized by an extraordinary functional group. The unique valence structure and reactivity of these compounds have been subject of discussion for more than a century and a half. Among stable organic compounds, they excel as the only class with a formally divalent carbon.[118]

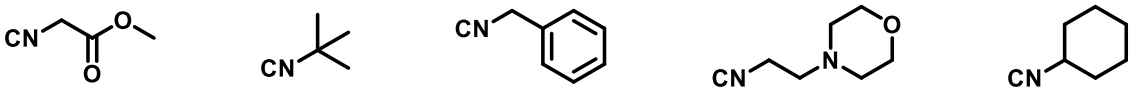



Figure 1.35. Examples of diverse isocyanides.

Due to its distinctive reactivity, the isocyanide stands out as highly peculiar and an intriguing functional group in the realm of organic chemistry. Its chameleonic nature renders its carbon atom notably versatile, making it a focal point for a myriad of reactions. Remarkably, it can function as a nucleophile, attacking activated electrophiles; as an electrophile, being intercepted by various nucleophiles; as a carbene engaged in formal [4 + 1] cycloaddition; and as a radical acceptor, leading to the formation of imidoyl radicals as reaction intermediates. Furthermore, the lone pair on the terminal carbon atom contributes to its robust metal coordinative properties, enabling the preparation of an extensive array of coordination complexes.[119] With a length of only 1.167 Å, the small isocyanide is a linear functional group which can exist in two main resonance forms. Computational studies suggested that the carbenoid form is the most stable (Figure 1.36).[119]

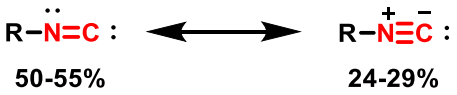



Figure 1.36. The two most important resonance forms of isocyanide account for the 84% of the weight of all resonance forms.[119]

Having an equivalent spatial size to nitrile, isocyanides demonstrate a closely aligned dipole moment (e.g., phenyl isocyanide, 3.44 D; benzonitrile, 4.51 D; methyl isocyanide, 3.83 D; and acetonitrile, 3.92 D). Despite the lipophilic nature of isocyanide compounds, their substantial dipole moment plays a pivotal role in fostering favorable interactions within protein binding pockets and augmenting connections with charged metalloproteins. In contrast to nitriles, which have been found to be inadequate coordinating groups in metal complexes, isocyanides exhibit robust chelating capabilities. Additionally, it has been proposed that the faint fruity odor of acetonitrile, as opposed to the unpleasant scent of methyl isocyanide, is attributed to the strong ability of isocyanides to form complexes with metal ions in olfactory receptors.[119]

### 1.7.2 Ugi four component reaction (U-4CR).

The Ugi four component reaction is an efficient and highly convergent isocyanide-based multicomponent transformation.[120] The reaction displays outstanding efficiency in terms of both atomic and bond economies. Furthermore, the U-4CR is remarkably robust, experimentally simple and exploratory, making it an ideal choice for medicinal chemistry studies.[118,121,122] The classical Ugi reaction involves a carboxylic acid, an amine, a carbonyl compound and an isocyanide to obtain an α-acylaminoamide (Figure 1.37).[120]

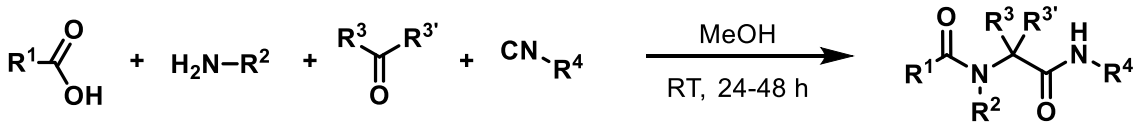



Figure 1.37. Ugi reaction

USC UNIVERSIDADE DE SANTIAGO DE COMPOSTELA

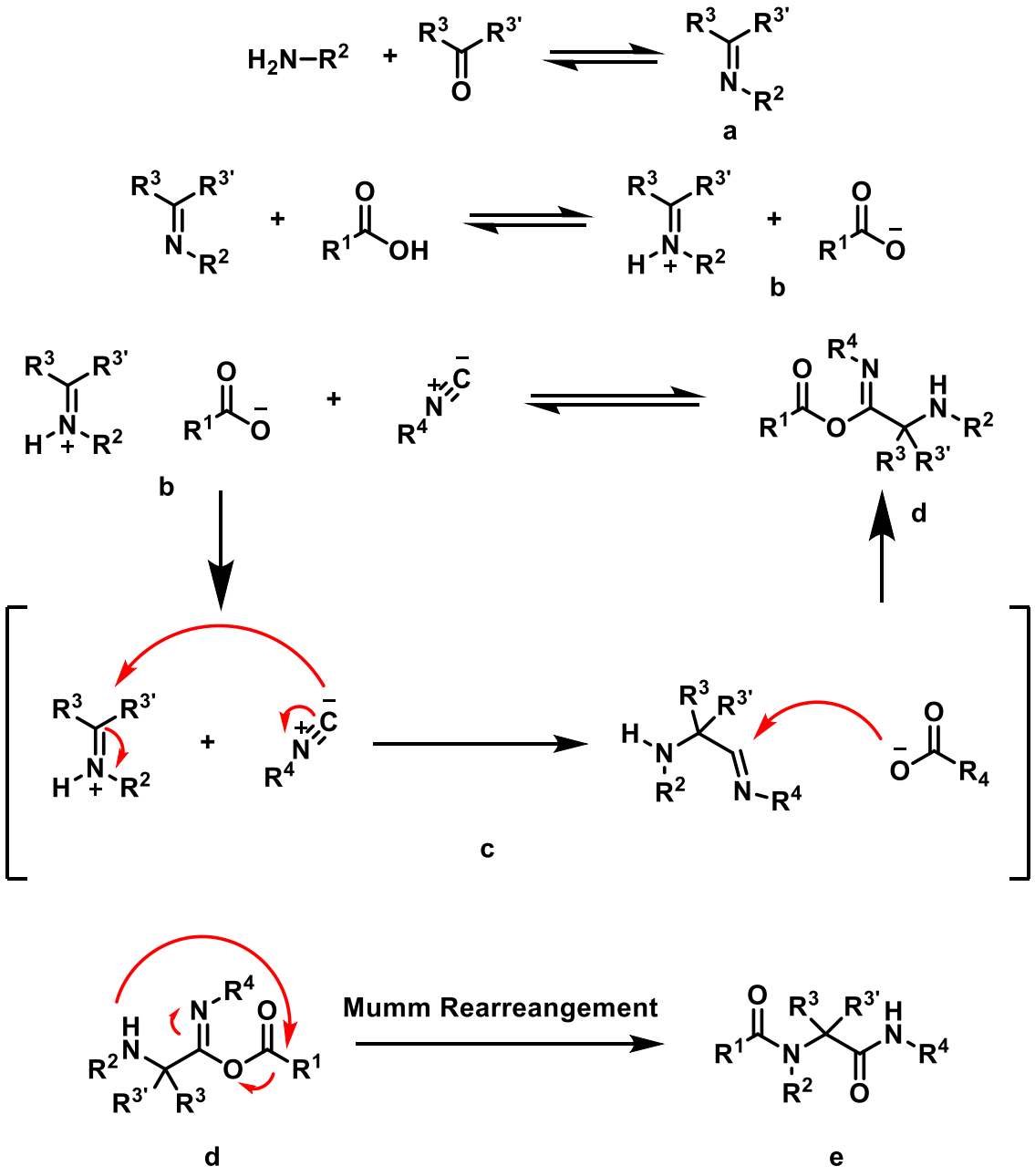



Figure 1.38. Most accepted mechanism of the U-4CR.

Figure 1.38 shows the most accepted mechanism of the U-4CR.[118] The initial step involves the condensation of the carbonyl component (either an aldehyde or a ketone) with the amine, resulting in the formation of an imine intermediate (a). Subsequently, the carboxylic acid protonates the nitrogen within the imine, leading to the creation of an iminium ion (b). The protonation of the imine is critical since it increases the electrophilic nature of the C=N bond. Then, the isocyanide can attack the iminium ion, producing an α-adduct (c) containing a significantly electrophilic center (nitrile ion). Simultaneously, this electrophilic

center is targeted by the carboxylate ion. The structural resemblance between the α-adduct (d) and acid anhydrides (one oxygen atom has been substituted by an N-R group) explains their behavior within the reaction medium. Both the anhydrides and their nitrogenous counterparts (d) serve as acylating agents. Given that the amine's nitrogen atom is the closest atom available for acylation, an intramolecular acylation process, coupled with tautomerization, yields the Ugi adduct.

The final step of the reaction involves the intramolecular acylation, known as the Mumm rearrangement.[118] Throughout the entire sequence, all steps are reversible except for this pivotal one. This conclusive, irreversible step results in the formation of a very stable acyl-amino-amide (e), that shifts the reaction's equilibrium decisively towards its formation.

The typical experimental procedure for the U-4CR involves a straightforward process. Initially, the starting materials are dissolved in methanol (MeOH) and subjected to stirring at room temperature, which lasts for a period ranging from 24 to 48 hours. This transformation can be executed in either a one-pot manner, utilizing all four components simultaneously, or in a stepwise approach. In the stepwise method, the amine and the carbonyl compound are first condensed, followed by the addition of the acid component and the isocyanide.

Methanol is the most used solvent for U-4CR,[121,123] whose polarity can stabilize the reaction intermediates. In addition, the limited solubility of the Ugi adduct in methanol usually facilitates its precipitation and isolation.[121,124] The U-4CR usually takes place under atmospheric pressure and without the need for anhydrous conditions (solvent or inert atmosphere) or catalysts. By utilizing sets of the four functional precursors, a virtually infinite array of structures can be synthesized. It is worth noting that Ugi adducts produced from aldehydes (except formaldehyde) and asymmetrically substituted ketones in the U-4CR generally result in racemic mixtures and are typically isolated as such due to the presence of a stereogenic center.

The isocyanide plays a pivotal role in the U-4CR, but its use in organic synthesis has been significantly restricted due to its strong and unpleasant odor. To address this issue, the ComBioMed group has devised a simple and effective method involving solid-phase extraction, which allows for the capture of any unreacted isocyanide.[121] In this process, a *p*-toluensulfonic resin is employed to trap the surplus isocyanide within the reaction and convert it into the corresponding amine sulphonic salt. This resin also facilitates the solid-phase extraction of compounds that contain a basic component, employing a catch-and-release

USC
DE SANTIAGO
DE COMPOSTELA

approach that typically expedites and simplifies the isolation and purification of Ugi adducts containing basic functional groups.[121,122]

Ugi's groundbreaking contributions to isocyanide multicomponent reactions sparked increased enthusiasm for the application of combinatorial chemistry as a valuable tool in drug discovery.[117] Furthermore, the interest in multicomponent reactions in drug discovery and their utilization in industrially relevant synthetic processes has been propelled by their efficiency, high convergence, and atom economy.[117] One of the first examples is lidocaine (Xylocaine®), a local anesthetic that functions by obstructing $Na^+$ neuronal channels, inducing depolarization. This compound was synthesized using a variant of the Ugi reaction (U-3CR), in a single synthetic step, combining diethylamine, formaldehyde, and 2,6-xylyl isocyanide (Figure 1.39).[117]

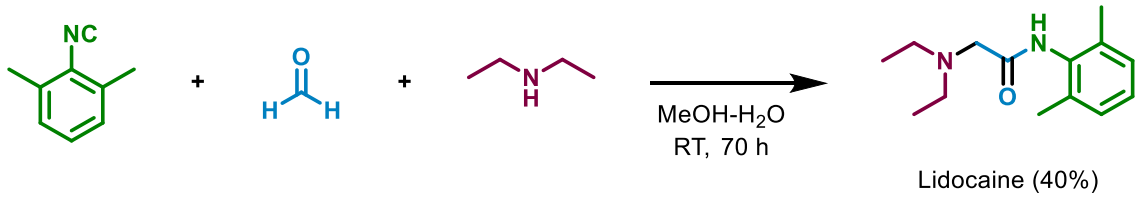



Figure 1.39. Synthesis of Lidocaine by an Ugi-3CR.[117]

Another example of drugs in clinical use prepared using this strategy is Carfentanil, a μ-opioid agonist used as an analgesic, synthesized by a direct U-4CR (Figure 1.40). In this case, the convertible isocyanide was subsequently transformed into the required ester through treatment with acetyl chloride in methanol.[117]

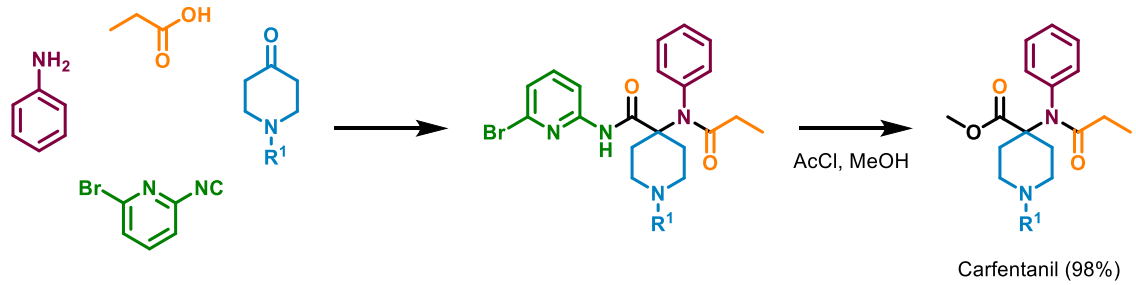



Figure 1.40. Synthesis of Carfentanil by U-4CR.[117]

Similarly, Clopidogrel, an inhibitor of platelet aggregation, Atorvastatin, a blockbuster drug used to reduce cholesterol levels in plasma, or Ivosidenib, an anticancer drug acting by inhibition of isocitrate dehydrogenase-1, can all be obtained by procedures based on the U-4CR, proving the utility and versatility of multicomponent reactions (Figure 1.41).[117]

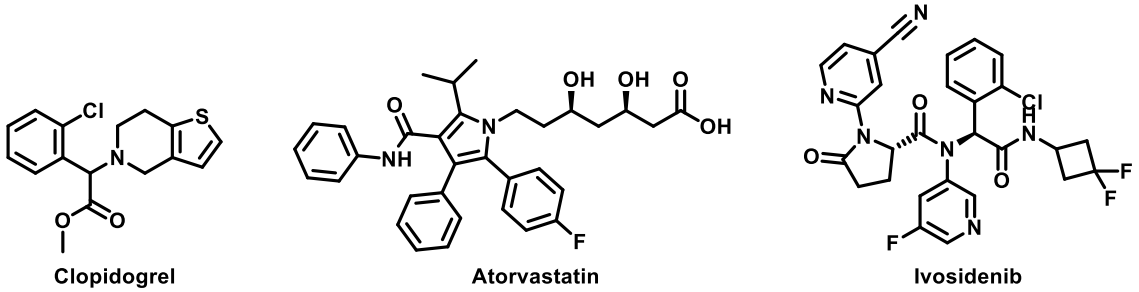



Figure 1.41. Examples of drugs synthesized by the U-4CR.[117]

### 1.7.3 Passerini reaction and PADAM synthetic route

The Passerini reaction, discovered by Mario Passerini in Florence in 1921, stands as the earliest known isocyanide-based multicomponent reaction.[125] This chemical process involves the reaction of a carboxylic acid, an aldehyde (or ketone), and an isocyanide to produce α-acyloxyamides, as depicted in Figure 1.42. Despite being nearly four decades older than the Ugi reaction, the Passerini reaction remained relatively underutilized through the 1990s. This may be attributed to the fact that esters were deemed less appealing than amides in the field of medicinal chemistry. However, a resurgence of interest in this reaction was sparked by expanding its applicability beyond simple α-acyloxyamides to encompass a diverse range of products, including heterocycles and peptidomimetics.[125]

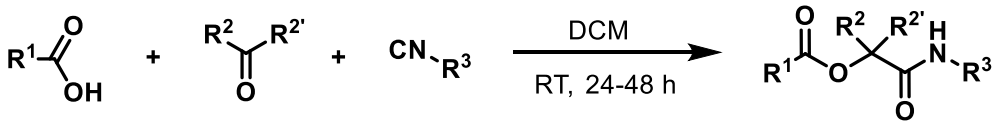



Figure 1.42. Passerini reaction.

In the Passerini reaction (Figure 1.43), an isocyanide is condensed with a carbonyl compound and a carboxylic acid to afford α-acyloxyamides (d). When the carbonyl compound is prochiral, a new stereogenic center is generated. It is generally accepted that the reaction proceeds through intermediate (c), which rearranges to the product. The way this intermediate is formed is more debated. A possibility is a concerted non-ionic mechanism involving a transition state (b). Since the simultaneous union of three molecules is not a very likely process, another possibility is a stepwise mechanism, with the intermediacy of a loosely bonded adduct (a) between the carbonyl compound and the carboxylic acid. Since all three components are involving in rate-determining steps, in principle asymmetric induction may be achieved when at least one of them is chiral.[120,125]

USC
DE COMPOSTELA

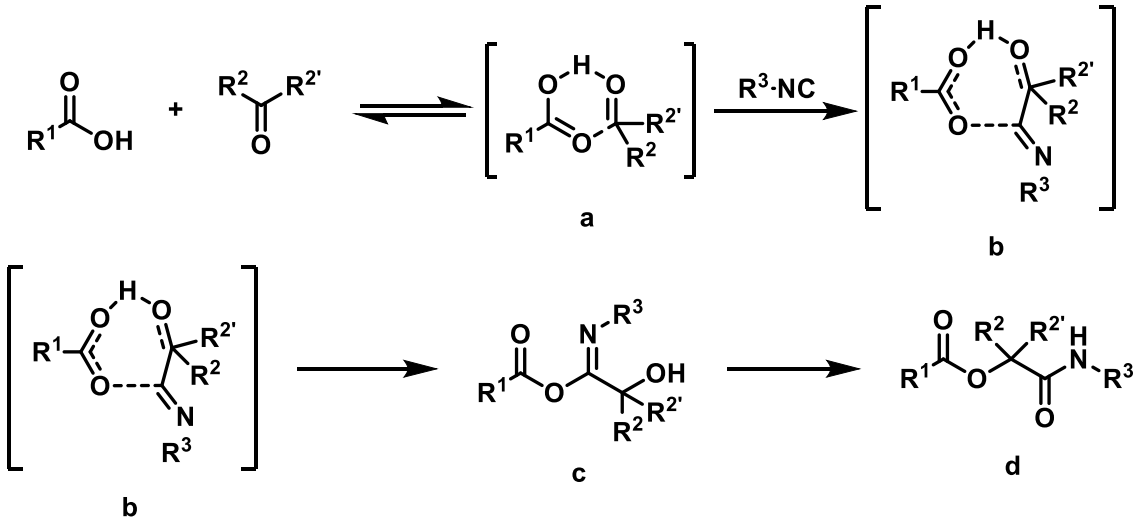



Figure 1.43. Most accepted mechanism of the Passerini reaction.

The standard experimental procedure of the Passerini reaction is typically simple and shares similarities with the U-4CR. This reaction, known for its expedited performance in low-polarity environments, is commonly conducted using solvents like dichloromethane, ethyl acetate, diethyl ether, and tetrahydrofuran. In contrast to the related Ugi reaction, alcohols are less suitable as reaction solvents in the Passerini reaction.[125] The Passerini reaction is carried out at room temperature, with reaction times ranging from a few hours to several days, especially in the case of ketones. When dealing with bulky ketones, the reaction may proceed very slowly. Consequently, aldehydes tend to yield better results overall. This reaction occurs under mild conditions in a slightly acidic medium, allowing for the tolerance of a wide range of functional groups. However, it does not accept electron-poor phenols or primary and secondary amines.[125]

As mentioned earlier, the conventional products resulting from the Passerini reaction are acyclic depsipeptides, which, from a medicinal chemistry perspective, are not particularly intriguing due to the susceptibility of ester groups under physiological conditions.[125] In order to transform the Passerini products in more valuable compounds, the group of Prof. Banfi and Prof. Basso from the University of Genova has developed a synthetic strategy involving a condensation between a *N*-protected α-aminoaldehyde, a carboxylic acid and an isocyanide, followed by amine deprotection and intramolecular acyl migration (PADAM, Figure 1.44).[126–128]

USC UNIVERSIDADE DE SANTIAGO DE COMPOSTELA

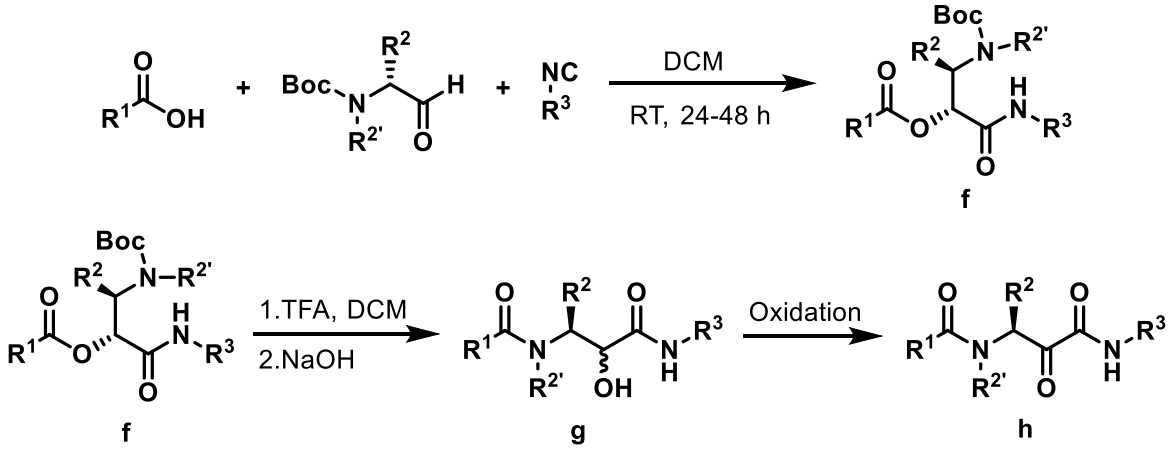



Figure 1.44. PADAM synthetic route.

The overall approach is illustrated in the figure above and encompasses the condensation of the specified *N*-Boc-protected α-aminoaldehydes with diverse isocyanides and carboxylic acids. Subsequently, a one-pot process is employed for Boc deprotection and acyl migration. This two-step procedure yields intricate peptide-like compounds (g), characterized by a central α-hydroxy-β-amino acid unit. Furthermore, a straightforward oxidation step can transform these compounds into oligopeptides (h), which feature an even more appealing α-oxo-β-amino acid structure.[127]

Recognizing the merit of this approach, numerous instances exist where marketed bioactive compounds have been synthesized utilizing the Passerini reaction and its variations. One example is Ubenimex, more commonly known as Bestatin,[129] a competitive, reversible protease inhibitor that can be easily synthesized *via* a Passerini 3 component reaction (Figure 1.45).

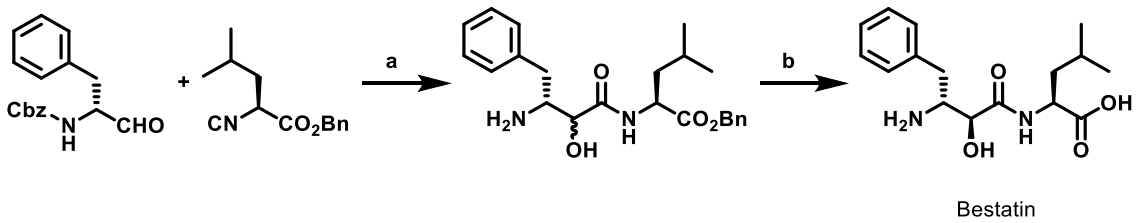



Figure 1.45. Synthesis of Bestatin through the Passerini reaction. a) TFA, pyridine, DCM, 0 ºC to RT, 65%; b) $H_2$, Pd/C; c) HPLC separation, 29%.[120]

Another example is the use of the Seebach Ti (IV) variation of the Passerini reaction to obtain Mandipropamid, an agrochemical compound acting as a fungicide and employed for the control of foliar oomycete pathogens in a range of crops (Figure 1.46).

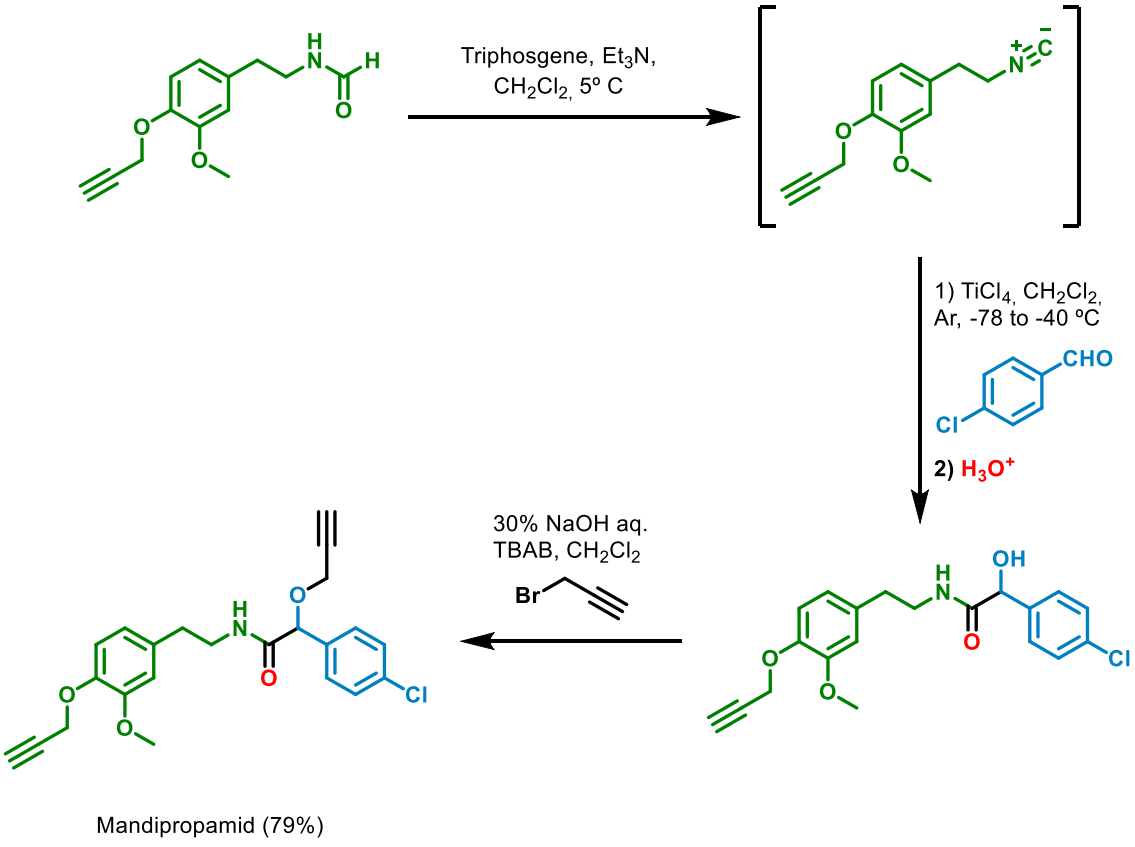



Figure 1.46. Synthesis of Mandipropamid by a Passerini-Seebach approach.[117]

Regarding the PADAM synthetic route, one of the most well-known instances of bioactive compounds prepared using this strategy is the synthesis of Eurystatins A and B (Figure 1.47). These 13-membered macrocyclic natural products are isolated from *Streptomyces eurythermus* R353-21 and feature leucine, ornithine, and α-ketoalaninamide subunits. They have been identified as potent inhibitors of the serine protease prolyl endopeptidase (PEP). Due to their relatively simple structure, they present appealing targets for the development of new methodologies involving α-hydroxy-β-amino amide and α-ketoamide.[128]

USC UNIVERSIDADE DE SANTIAGO DE COMPOSTELA

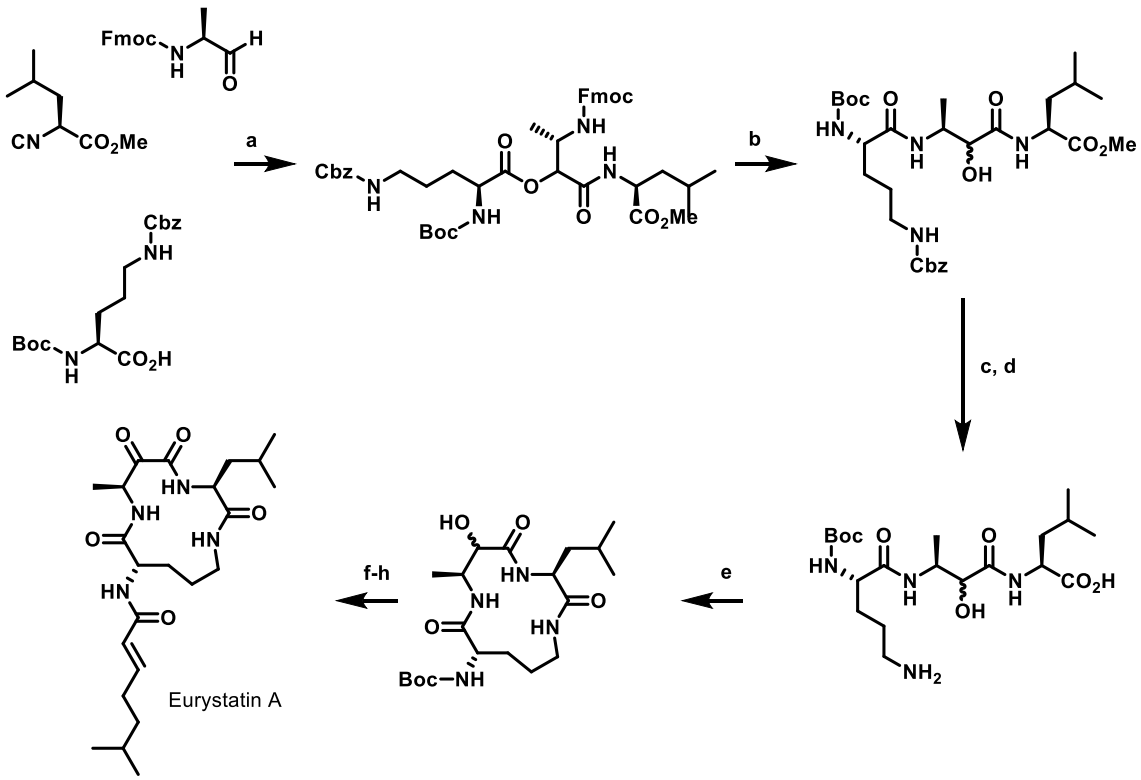



Figure 1.47. Synthesis of Eurystatin A. Reagents and conditions: (a) $CH_2Cl_2$, 0°C to RT, 3–5 days; 75%; (b) $Et_2NH$, RT, $CH_2Cl_2$, 12 h, 92%; (c) LiOH, MeOH, $H_2O$, RT, 95%; (d) $H_2$, Pd/C, MeOH, 45 psi, 3 days, quant. (e) DPPA, DMF, $NaHCO_3$, 0–4°C, 5 days, (0.005–0.01 M), 75–85% or HBTU, HOBt, DMF, RT, 3 days, (0.005 M), 50%; (f) HCl, AcOEt, 0°C to RT, quant.; (g) (E)-6-methyl-2-heptenoic acid, EDC, HOAt, DMF, RT, 93%; (h) Pyr·$SO_3$, DMSO, $Et_3N$, 5°C to RT, 75%.[128]

USC UNIVERSIDADE DE SANTIAGO DE COMPOSTELA

# 2 OBJECTIVES

As introduced in this Thesis, multicomponent reactions constitute valuable tools for the rapid generation of highly diverse chemical libraries required during preliminary drug discovery programs. They offer an efficient, time-effective, and environmentally friendly alternative to traditional linear synthetic methods in medicinal chemistry.

The ComBioMed group has developed a multicomponent-assisted platform dedicated to discovering and optimizing new drug candidates. Over the past decade, our team has made significant contributions to uncovering innovative drugs, pharmacological tools, and fluorescent ligands targeting a range of GPCRs, including $A_1AR$, $A_{2A}AR$, $A_{2B}AR$, $A_3AR$, dopamine $D_2R$, cannabinoid $CB_1R$ and $CB_2R$, serotonin 5-$HT_{2A}R$, and 5-$HT_{2B}R$. These GPCRs play a crucial role in severe pathologies for which current treatments are often ineffective, such as Parkinson's disease[33,35,39], glaucoma[130], diabetes[131], schizophrenia[45,48], pain[73], inflammation[77], and cancer[5,98].

This PhD thesis focuses on discovering and optimizing potent, highly selective ligands for two of these disease-relevant targets: the dopamine $D_2R$ and the cannabinoid $CB_2R$. This research is part of an ongoing, long-term project aimed at applying multicomponent strategies to the drug discovery process. The project comprises two main chapters, each targeting a specific receptor and having distinct objectives. A summary of the primary goals for each chapter is provided below.

**Chapter I** (Section 3.1) deals with the design, synthesis, and optimization of novel melanostatin analogues as allosteric modulators of the $D_2R$. This chapter is divided into three parts covering specific aims:

**A Multicomponent approach to assembly Melanostatin analogues:** Proof of concept via Ugi reaction. The initial series of experiments focused on establishing the feasibility of employing multicomponent strategies for the synthesis of analogues of Melanostatin. The primary goal is to improve the classical linear synthetic procedure by employing a multicomponent approach that is both time and cost-effective compared to traditional synthesis. The similarities between the peptidomimetic structure of melanostatin and the

USC UNIVERSIDADE DE SANTIAGO DE COMPOSTELA

chemical features of the Ugi adducts (acylamino amides) would enable us to explore four different diversity points within this scaffold.

**Ugi-assisted exploration of bioisosteric replacements in Melanostatin.** The second part of this chapter focuses on identifying optimal bioisosteres for the L-proline residue. Inspired by recent data on aromatic heterocycles, specifically from references 62 and 63, 23 cyclic residues are proposed herein to discover new proline bioisosteric surrogates that enhance the efficacy and activity of the model ligand. Furthermore, additional explorations will be carried out for one of the most attractive ligands in the series, including HPLC enantiomeric separation and methylation at the $R^2$ position.

**A PADAM strategy to generate oxo-melanostatin derivatives.** The latest part of this chapter proposes the exploration of the synthesis and biological evaluation of innovative Melanostatin derivatives (oxo- and hydroxy- analogues). To access these series, a novel MCR approach based on the Passerini reaction was conceived and implemented. This synthetic strategy, known as the PADAM (Passerini reaction, amine deprotection, acyl migration) synthetic route, maintains the pharmacophoric elements while adding a new diversity point to be explored. These analogues are characterized by the introduction of an additional carbon atom into their structure, accompanied by either a carbonyl group or a hydroxy group. The main objective is to study the effect that this structural change has on the allosteric activity.

USC
UNIVERSIDADE DE SANTIAGO DE COMPOSTELA

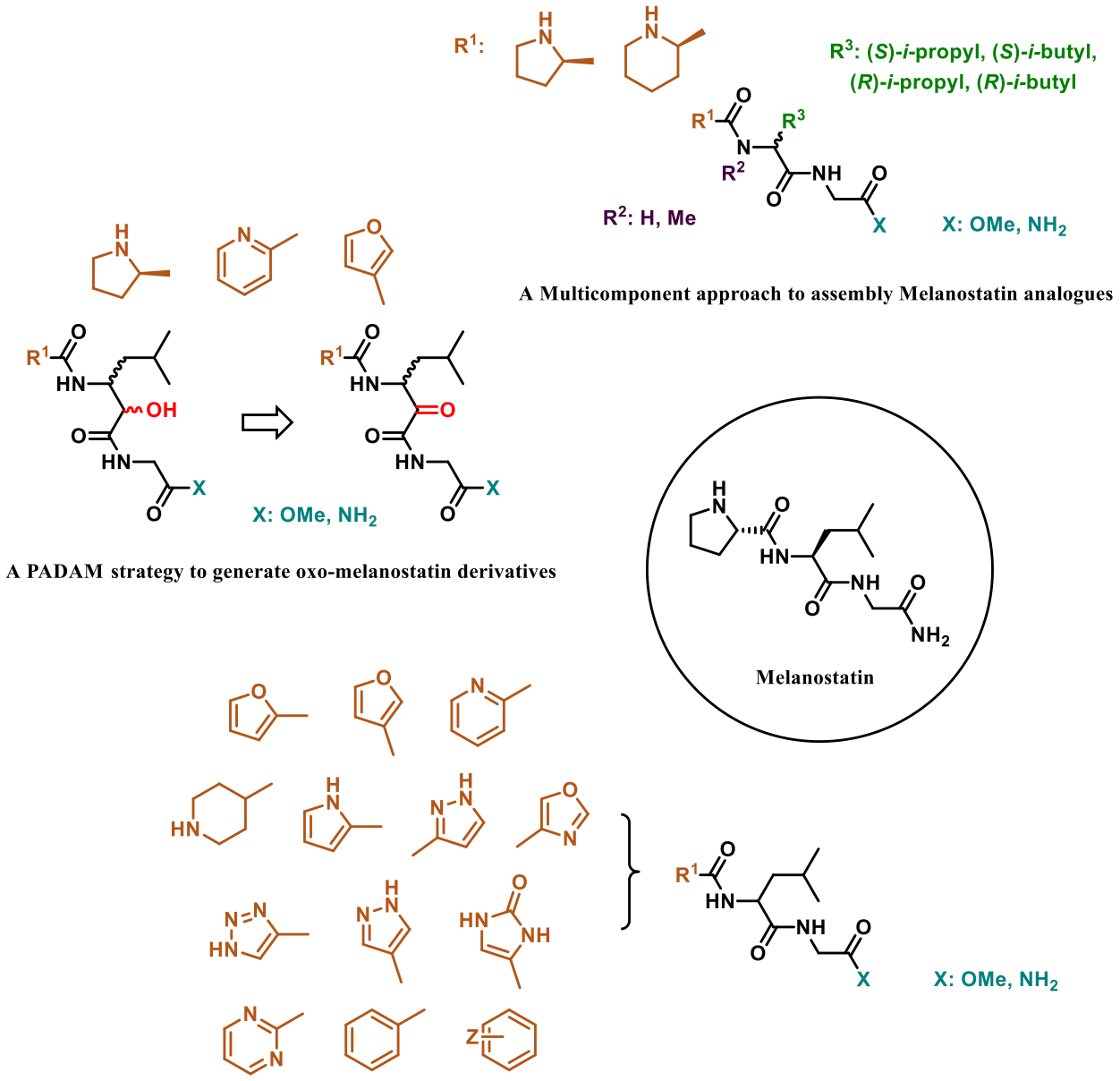



Figure 2.1 Design strategy and diversity points explored during Chapter I of this Doctoral Thesis.

**Chapter II** (Section 3.2) focuses on the design, synthesis, and optimization of a novel series of potent and highly selective $CB_2R$ agonists. Inspired by the promiscuous profile of the Synthetic Cannabinoid Receptor Agonists (SCRAs) family of designed drugs, a pharmacomodulation process was conceived to tailor $CB_2R$ affinity and eliminate the $CB_1R$ agonistic profile (responsible for deleterious psychoactive side effects). Two nitrogenated scaffolds (indole and indazole) were selected as molecular platforms to explore the

programmed MCR-based pharmacomodulation process. Building upon previous efforts of our group in this area, we aimed to explore novel oxo- and hydroxy- analogues of privileged scaffolds that could be readily assembled by a PADAM strategy based on the reliable Passerini reaction (Figure 2.2).

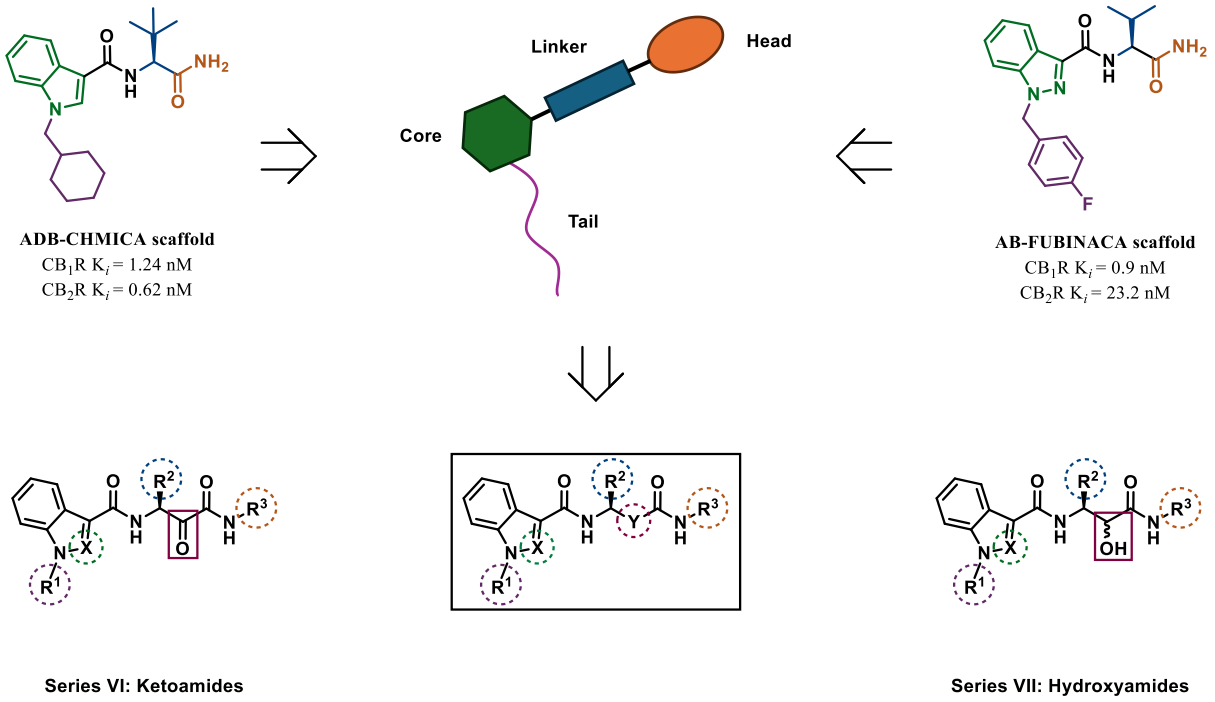



Figure 2.2. Design strategy and diversity points explored during Chapter II of this Doctoral Thesis.

From a structural standpoint, the PADAM pathway produces libraries that introduce unexplored modifications to the pharmacophore while providing an opportunity to modify binding modes and pharmacological profiles, thus generating selective $CB_2R$ agonists. The designed series are grouped into two main subsets. Series **VI** focuses on oxo-amides, while Series **VII** explores hydroxy-amides. Both series explore the SAR trends of the selected scaffolds (core group, tail group, linker, and head group) through a systematic MCR-assisted pharmacomodulation process. The analysis of the biological profile of the obtained libraries will include binding studies to evaluate potency, as well as functional experiments to profile the selected $CB_2R$ ligands as agonists or antagonists. Additionally, we propose a detailed study of the signaling pathways affected by these compounds (biased or unbiased) and provide preliminary evidence of the effectiveness of representative ligands in reducing the proliferation of highly aggressive central nervous system cancer (glioblastoma).

USC UNIVERSIDADE DE SANTIAGO DE COMPOSTELA

# 3 RESULTS AND DISCUSSION

## 3.1 CHAPTER I

Melanostatin, also known as L-Prolyl-L-Leucyglycinamide (PLG), represents a rare example of a neuropeptide functioning as a positive allosteric modulator (PAM) of the $D_2R$. It was initially discovered in 1971 from bovine hypothalamic tissue.[21]

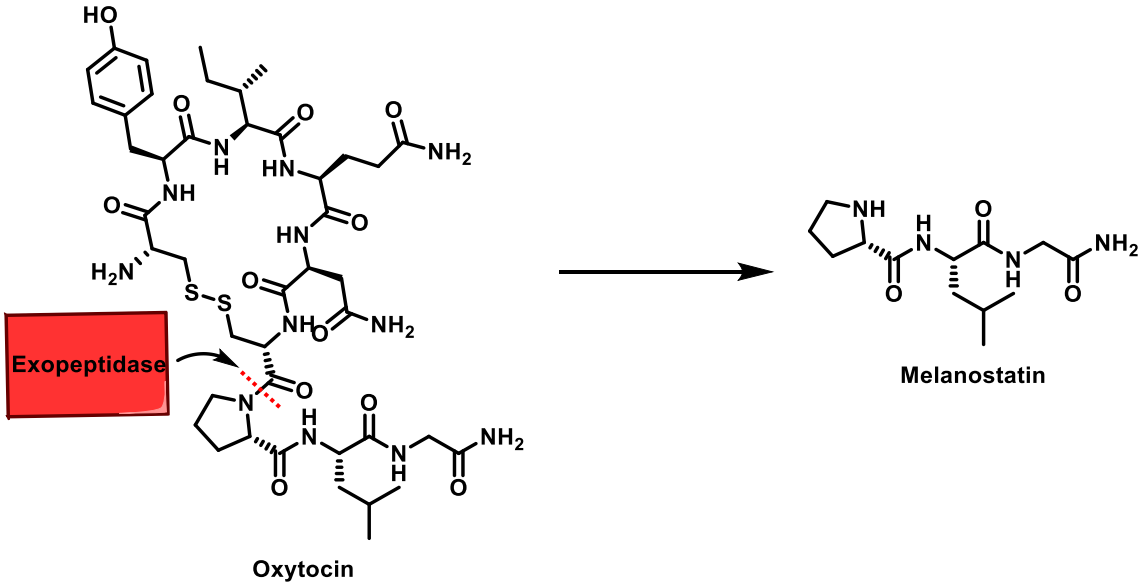



Figure 3.1. Biosynthesis of melanostatin.

Melanostatin, formed by cleavage of oxytocin hormone through the action of the enzyme exopeptidase (Figure 3.1), is found in the central nervous system, where it exerts its biological function through the nigrostriatal pathway.[62–64] With its ability to modulate $D_2R$ and its selectivity for these receptors, melanostatin has emerged as an attractive candidate for drug development aimed at addressing central nervous system-related neurodegenerative conditions that involve sensitivity to dopamine receptors. These conditions include Parkinson's disease, schizophrenia, tardive dyskinesia, and Gilles de la Tourette syndrome.[62]

USC UNIVERSIDADE DE SANTIAGO DE COMPOSTELA

While melanostatin's initial pharmacological profile hinted at its potential for addressing neurological conditions, its peptide-based nature posed inherent limitations for drug development. Consequently, there have been concerted efforts to engineer peptidomimetic analogues of melanostatin, aiming to craft agents that can retain PLG's therapeutic effects while improving their pharmacokinetic properties.[132] This endeavor has been recently spearheaded by Professor Sampaio-Dias and his research group at the University of Porto, with the development of a broad library of melanostatin peptidomimetics. Their pioneering work has established the proline core as an ideal site for derivatization, allowing for the incorporation of heteroaromatic rings at this position in melanostatin (Figure 3.2).[62–64]

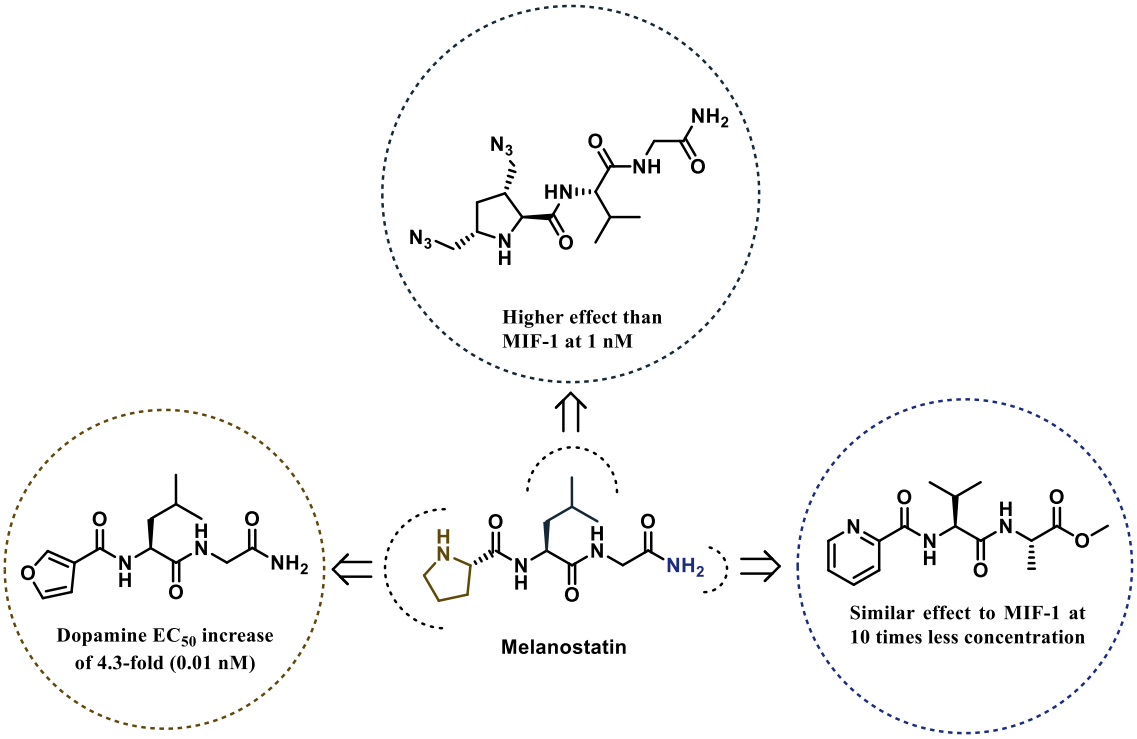


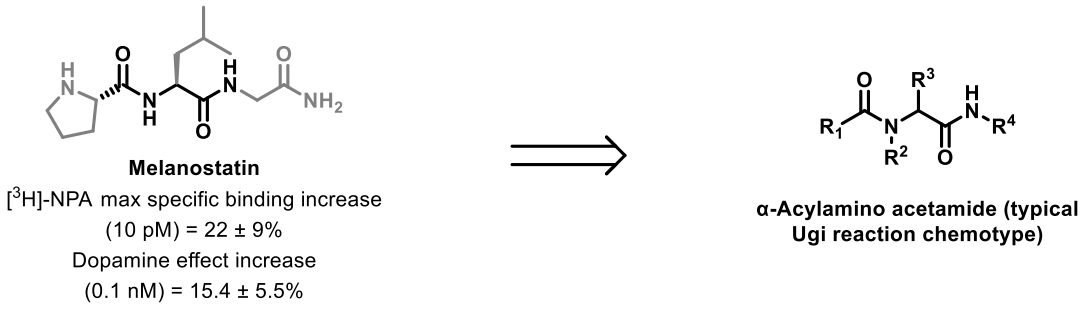

Figure 3.2. Structure of melanostatin and representative peptidomimetics generated through residue substitution.[63,64,133]

In addition to these studies, there are numerous examples of peptidomimetic libraries created through substitutions in the other two residues, namely leucine and glycine (Figure 3.2).[133] The identification of several lead compounds in these research endeavors provides encouragement to embark on a more comprehensive exploration of melanostatin analogues. However, traditional linear synthetic methods only permit the modification of one residue at a time, which can lead to lengthy and expensive processes. As a result, our primary objective in this pharmacomodulation program is to construct an expansive library of melanostatin

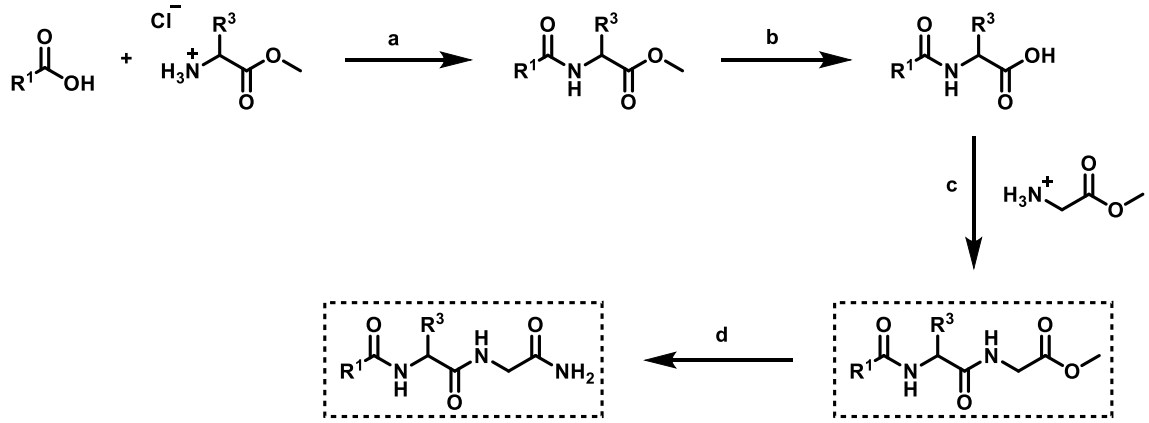
analogs that systematically explore all aspects of its structural diversity, in a time-efficient and cost-effective manner, employing a multicomponent strategy.

### 3.1.1 Design

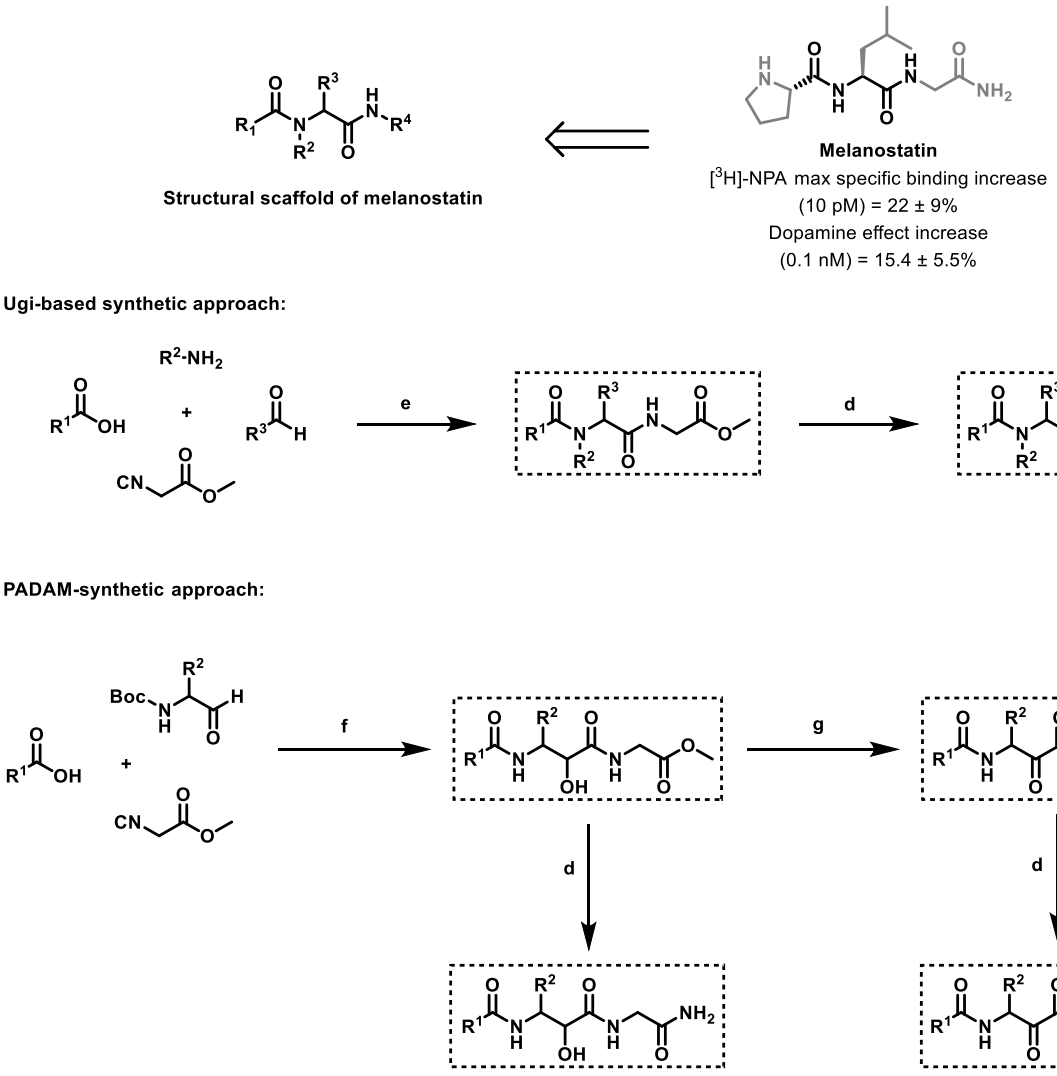
The novel series were conceived in the context of our ongoing projects exploiting multicomponent reactions in medicinal chemistry. In this chapter we aimed to develop selective $D_2R$ allosteric modulators, starting from the melanostatin scaffold as a prototype ligand. The MCR-based strategies herein documented were conceived to rapidly assemble large libraries of melanostatin analogues, thus enabling the exhaustive exploration of the SAR in these series and the identification of novel $D_2R$ selective allosteric modulators. To better evaluate the advantages of the strategies described in Scheme 3.2, we present in Scheme 3.1 the classical linear approach employed for the assembly of the targeted compounds. The main drawbacks of this pathway are related to its limitations in diversity and the higher number of steps required for the route.




**Classical synthetic approach:**




Scheme 3.1. Melanostatin as model ligand and classical synthetic process. a) EDC, HOBt, DMF, RT, 24 h. b) NaOH 2M, Dioxane/$H_2O$, RT, 2 h. c) EDC, HOBt, DMF, RT, 24 h. d) $NH_3$ (2M), MeOH, RT, 24 h.



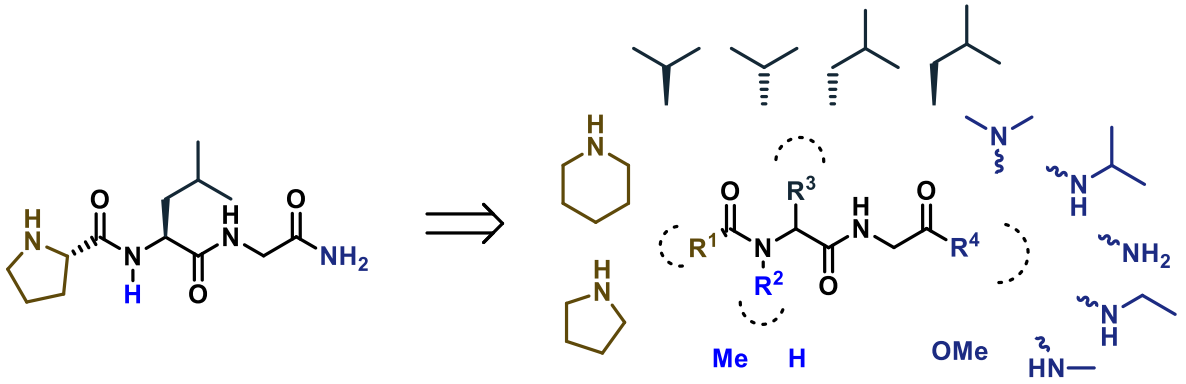

Scheme 3.2. Melanostatin as model ligand and the herein documented multicomponent approaches. d) $NH_3$ (2M), MeOH, RT, 24 h. e) MeOH, RT, 24 h. f) 1) DCM, RT, 24 – 48 h, 2) TFA (15 %), DCM, RT, 2 h. g) Dess-Martin periodinane, DMF, 0 °C, 2 h.

In this context, we have designed three different subsets of melanostatin analogues, each targeting different structural modifications:

**Proof of concept via Ugi reaction (Series I and II)**: Our first approach involves the validation of the Ugi-based strategy designed for synthesizing melanostatin derivatives. In line with this objective, we have designed 16 analogues through the following structural modifications (Scheme 3.3): 1) introducing L-proline and L-homoproline ($R^1$), 2) adding hydrogen or a methyl group at $R^2$, 3) introducing (*S)*-isobutyl and (*R)*-isobutyl ($R^3$), and 4)

USC UNIVERSIDADE DE SANTIAGO DE COMPOSTELA

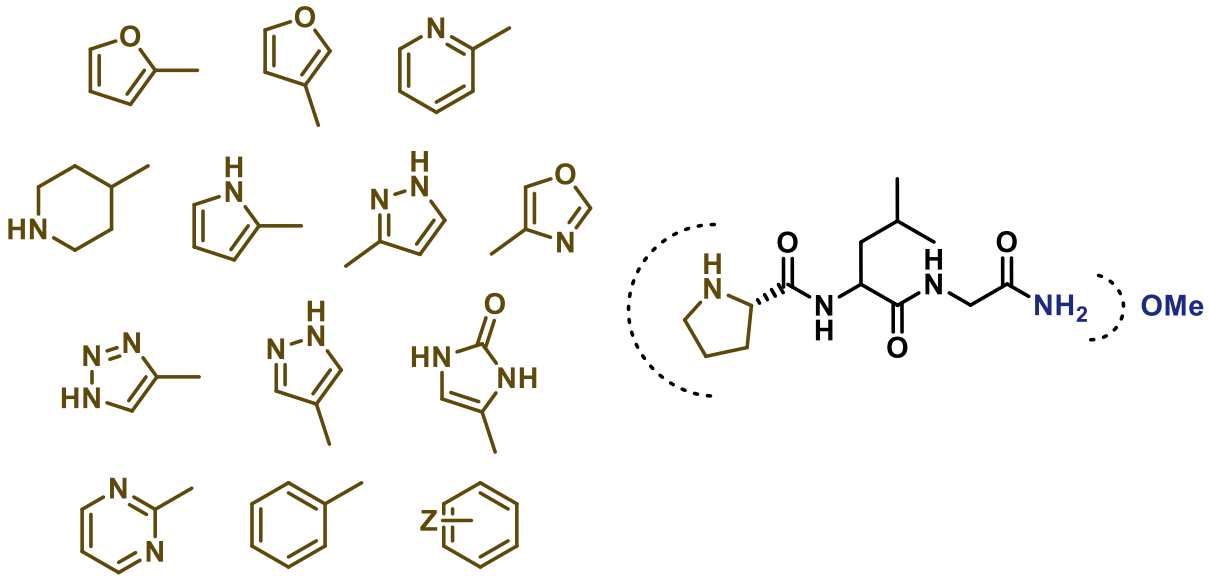
introducing methyl ester or unsubstituted amide ($R^4$). Further substitution of the isobutyl group with isopropyl enables us to obtain 16 additional derivatives.




Scheme 3.3. Structural modifications conceived for Series **I** and **II**.

Finally, melanostatin was employed as model to explore the effect of introducing an alkyl substituent in the terminal amide, rendering 4 new analogues.

**Ugi-assisted bioisosteric replacements in melanostatin (Series III):** Considering the proline residue a perfect spot for derivatization, and inspired by previous explorations carried out by Professor Dias' group, Series **III** of this chapter focuses on exploring substitution at this position with 23 different hetero- and carbocycles (Scheme 3.4).

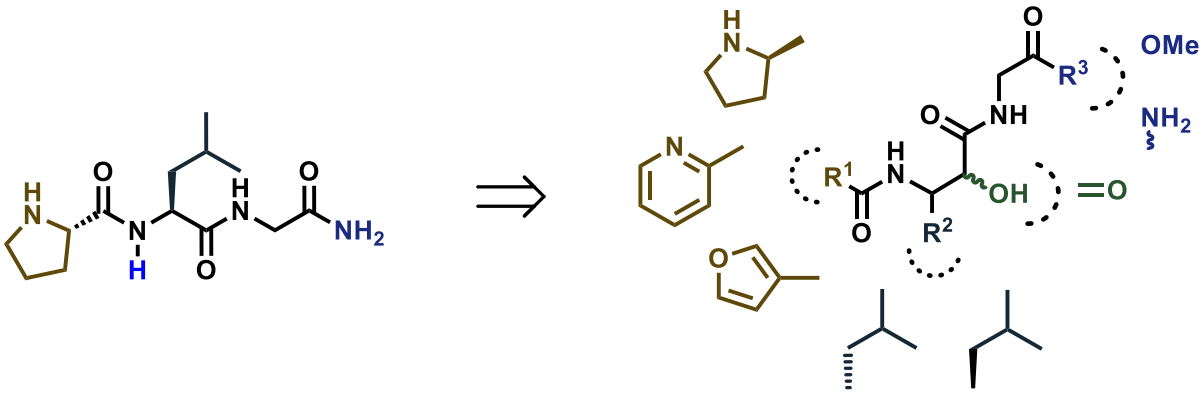



Scheme 3.4. Structural modifications conceived for Series **III**.

Given that the terminal amide has been recently shown to not be a requisite for $D_2R$ allosteric modulation,[64] and for comparison purposes, every surrogate was tested as methyl

ester and primary amide, making this series contain 46 different analogues. Two additional explorations were planned for the most attractive compound: 1) the enantiomeric separation and 2) the methylation of the secondary amide nitrogen.

**A PADAM strategy to generate oxo-melanostatin derivatives (Series IV and V)**: In addition to the Ugi-4CR, we designed novel series of melanostatin oxo-analogues using a variant of the Passerini reaction, specifically a modification of the Passerini reaction (PADAM strategy) developed by Banfi et al.[127] that involves the use of an aldehyde bearing a protected amine, that upon deprotection promotes acyl migration. Different, but conceptually homologous to the Ugi reaction, this MCR enabled the rapid assembly of a subset of unexplored melanostatin derivatives. The principal novelty observed in this series pertains to the incorporation of an additional carbon atom into the structural framework (Scheme 3.5). This new carbon holds a hydroxy group that can be further oxidized to the carbonyl form. In the case of hydroxyamides, a new stereocenter is created in the introduced carbon atom. This stereocenter remained unresolved in Series **IV**, resulting in these compounds being mixtures of diastereomers. Furthermore, some of the structural modifications employed in the first two series are present here as well, namely: the use of proline and two of the most interesting surrogates from Series **III** (2-pyridine and 3-furane), exchanging (*S*)-isobutyl with (*R*)-isobutyl, and replacing the terminal amide with a methyl ester. As a result, 24 new analogues conform Series **IV** and **V**.

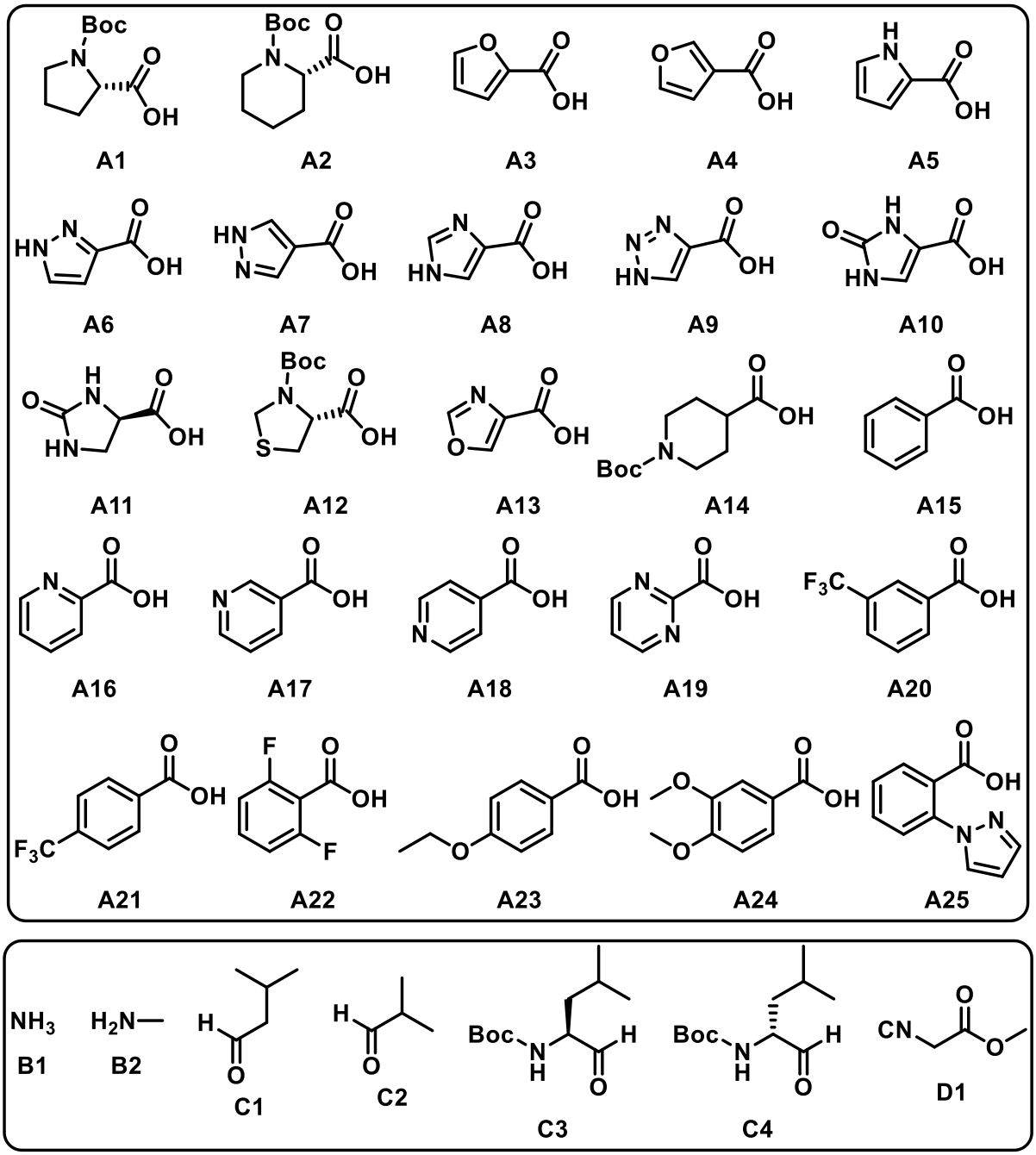



Scheme 3.5. Structural modifications conceived for Series **IV** and **V**.

USC
UNIVERSIDADE DE SANTIAGO DE COMPOSTELA

### 3.1.2 Chemistry

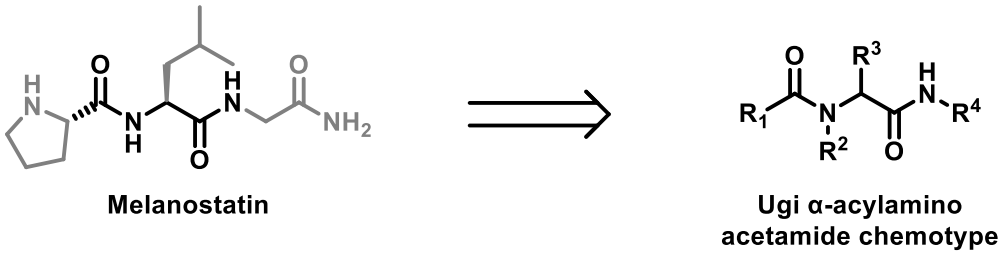
The MCR-based strategies documented here were designed to quickly develop extensive libraries of melanostatin analogues, facilitating thorough exploration of the SAR within these series and the discovery of novel allosteric modulators for $D_2R$. Scheme 3.6 shows the precursors employed in Chapter I of this Doctoral Thesis.




Scheme 3.6. Synthetic precursors employed in Chapter I of this Doctoral Thesis. A: carboxylic acids, B: amines, C: aldehydes, and D: isocyanides.

USC UNIVERSIDADE DE SANTIAGO DE COMPOSTELA

**Proof of concept via Ugi reaction (Series I and II)**: A four-component synthetic approach based on the robust and efficient Ugi reaction (i.e., the four-component reaction of a carboxylic acid, an amine, an aldehyde or ketone and an isocyanide) enabled a time- and cost-effective assembly of the large collection obtained within the two first series of this chapter. For the design of these series, we took advantage of the peptidomimetic structure of the Ugi adducts (α-acylamino acetamide) and its analogy to the structure of melanostatin.

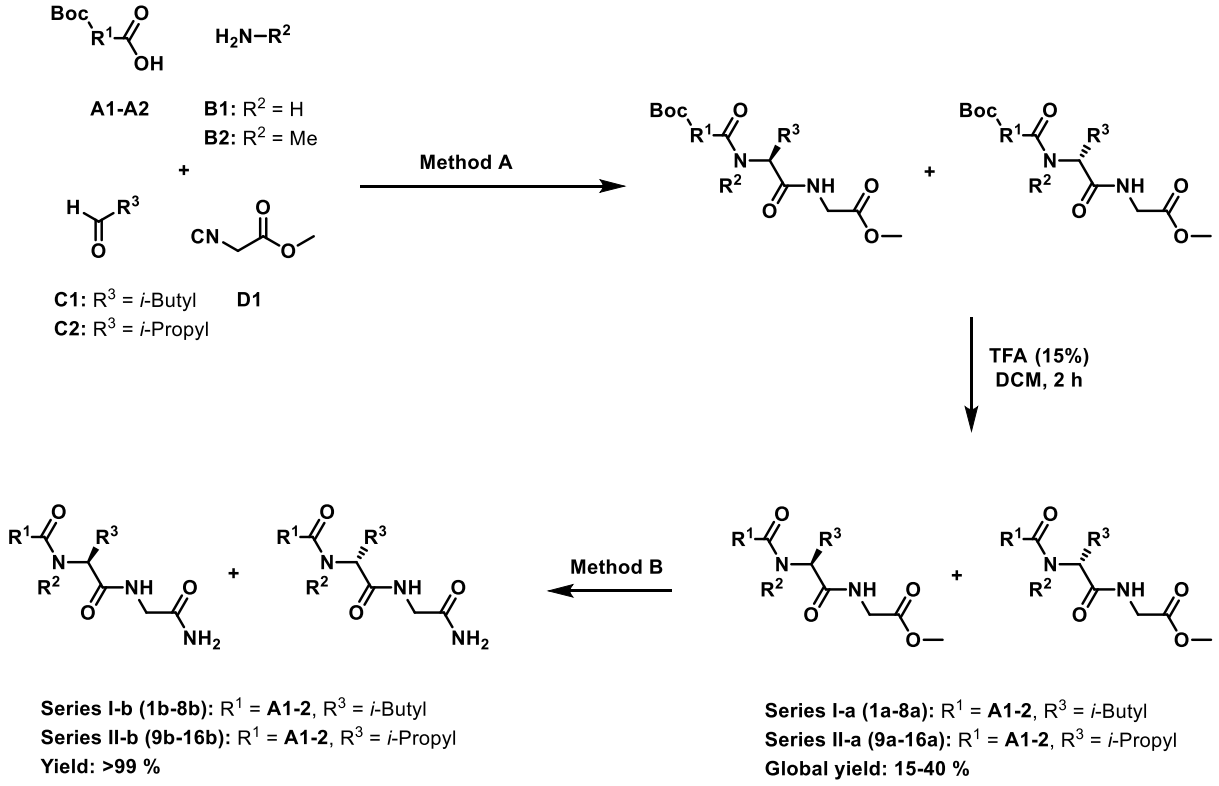



Scheme 3.7. Structural similarity between melanostatin and Ugi reaction products.

*N*-Boc-L-proline (**A1**) and (*S*)-1-Boc-piperidine-2-carboxylic acid (**A2**), in combination with ammonia (**B1**) or methyl amine (**B2**), isovaleraldehyde (**C1**) or isobutyraldehyde (**C2**), and methyl-2-isocyanoacetate (**D1**) were employed as precursors to validate the proof of concept. The targeted melanostatin analogues (**1a-16a**) were obtained as depicted in Scheme 3.8. The starting materials, dissolved in MeOH, were submitted to orbital stirring at room temperature for 24 h (Method A). After completion of the reaction, the solvent was evaporated under reduced pressure to afford an oil residue, which was purified by chromatography on silica gel using MeOH/DCM mixtures. The Ugi reaction produces the two expected diastereomers, that can be separated by column chromatography. An additional step of hydrolysis was required to remove the Boc protecting group. After the Ugi reaction was completed and evaporation of the solvent, the crude product was redissolved in DCM and TFA (15%) was added. The reaction was stirred at room temperature for 2 h. Following completion, the solution was treated with NaOH 2M and the product was extracted with ethyl acetate. The organic phase was dried over $MgSO_4$ and evaporated under reduced pressure to afford an oil residue, which was purified by column chromatography on silica gel. The targeted methyl ester derivatives were obtained in moderate yields (15-40%) and were used as precursors for the synthesis of the corresponding amides (**1b-16b**). For the synthesis of amides, the starting material (methyl glycinate) was dissolved in a solution of $NH_3$ 2M in MeOH (3 mL) and magnetically stirred at room temperature overnight (Method B). Following

USC UNIVERSIDADE DE SANTIAGO DE COMPOSTELA

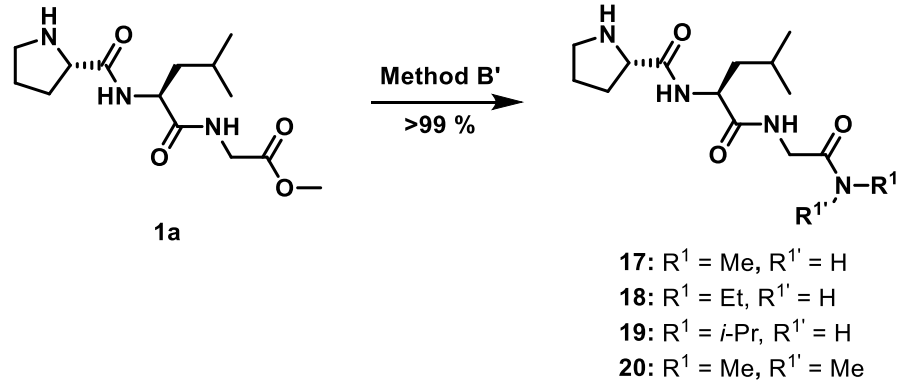
completion, the solvent was evaporated under reduced pressure to afford a pure white solid that was washed with diethyl ether without further purification. The targeted carboxamide derivatives were obtained in quantitative yields (99%).




Scheme 3.8. Ugi-based synthetic route. Method A) MeOH, RT, 24 h. Method B) $NH_3$, RT, 24 h.

In Series **I**, an additional modification was implemented for compound **1a** (methyl ester analogue of melanostatin, Scheme 3.9). By employing a slightly modified version of Method B, the ester group was transformed into four distinct alkyl-substituted amides. The starting material was dissolved in a solution of the corresponding amine (methylamine, ethylamine, isopropyl amine, or dimethylamine) 2M in MeOH and was magnetically stirred at room temperature overnight (Scheme 3.9). After completion of the reaction, the solvent was evaporated under reduced pressure to afford an oil residue, which was purified by chromatography on silica gel using MeOH/DCM mixtures. All reactions were monitored by thin-layer chromatography (TLC). A detailed description of the synthetic methods and the complete structural, spectroscopic, and analytical data for all compounds are provided in the Experimental Section.

USC UNIVERSIDADE DE SANTIAGO DE COMPOSTELA




Scheme 3.9. Synthesis of alkyl substituted amide derivatives of melanostatin. Method B') $MeNH_2$/$EtNH_2$/*i*-$PrNH_2$/$(CH_3)_2NH$, RT, 24 h.

The collection of melanostatin analogues synthesized in Series **I** and **II** is illustrated below.

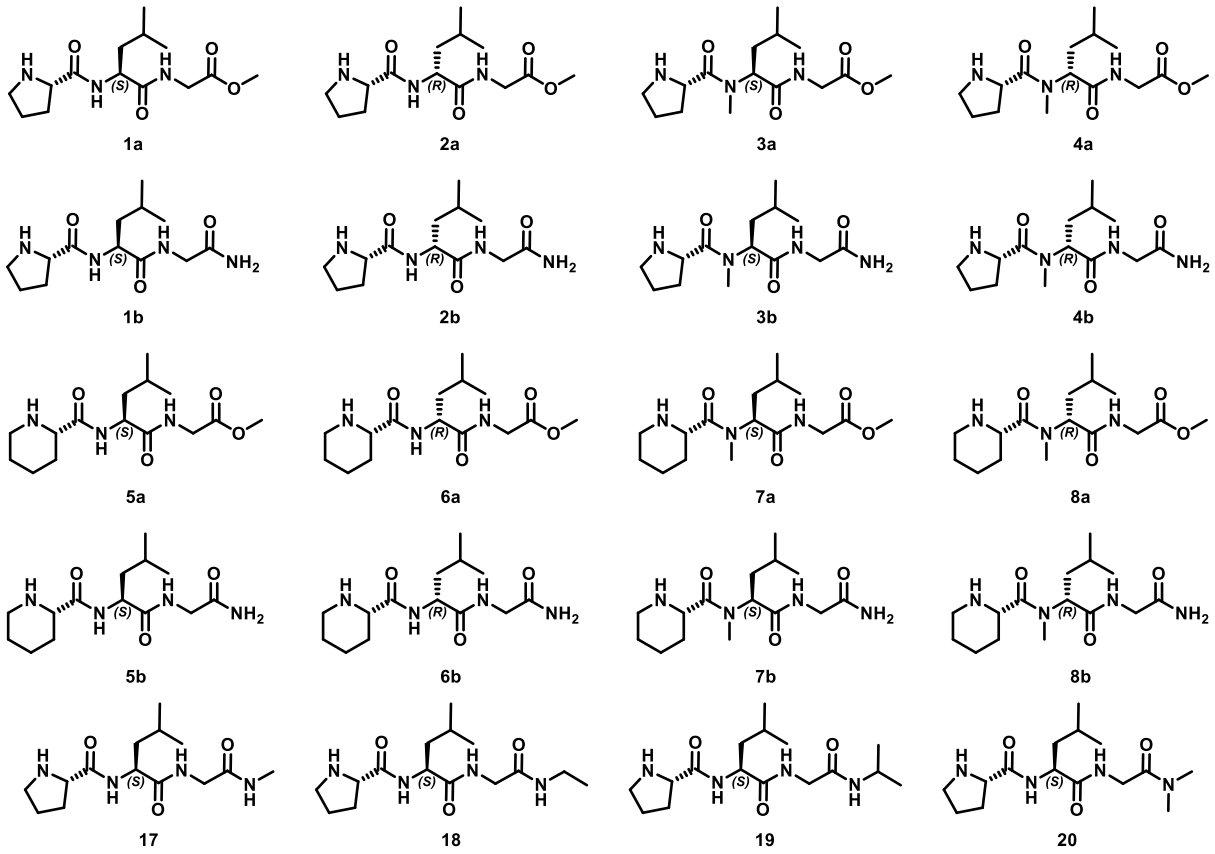



Figure 3.3. Structure of compounds belonging to Series **I**.

USC UNIVERSIDADE DE SANTIAGO DE COMPOSTELA

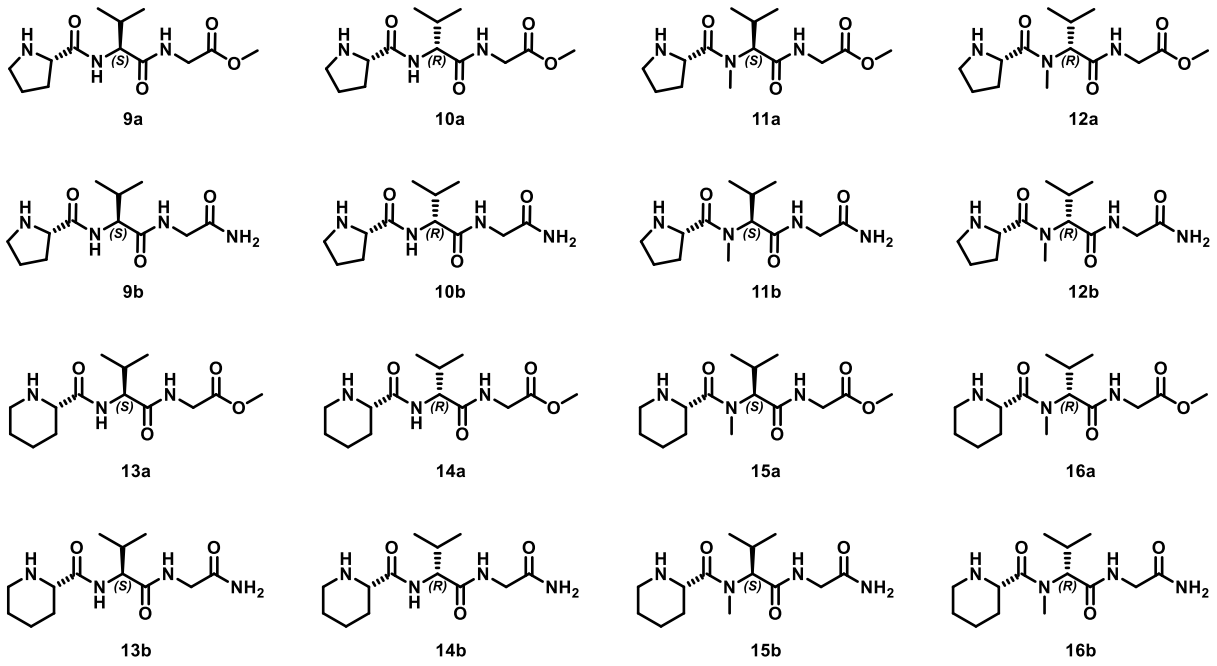
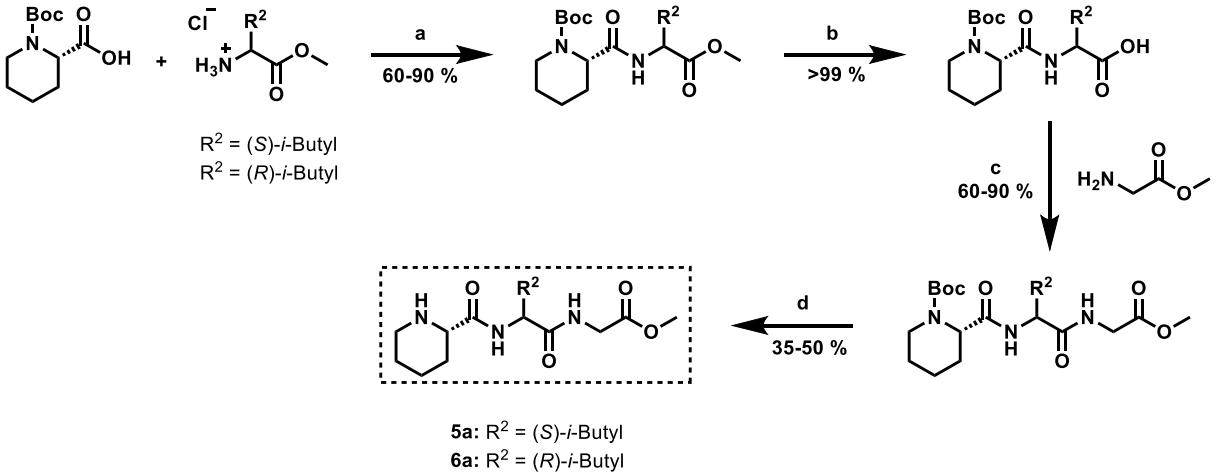



Figure 3.4. Structure of compounds belonging to Series **II**.

One of the structural signature elements of the Ugi adducts is the presence of a stereocenter, thus producing racemic mixtures. In Series **I** and **II**, this stereocenter has been successfully resolved, resulting in compounds **1a-16a** and their corresponding amide pairs, **1b-16b**, all being pure diastereomers. To perform an unambiguous structural characterization of each diastereomer, compounds **5a** and **6a** were synthesized using a traditional approach, using enantiopure reactants, and employing direct amide coupling chemistry (Scheme 3.10).




Scheme 3.10. Linear synthesis of reference compounds **5a** and **6a**. a) EDC, HOBt, DMF, RT, 24 h. b) NaOH 2M, Dioxane/$H_2O$, RT, 2 h. c) EDC, HOBt, DMF, RT, 24 h. d) TFA (15 %), DCM, RT, 2 h.

Analysis of the obtained NMR spectra (Figure 3.5) reveals a noticeable chemical shift difference at the carbon (CH) that carries the $R^2$ group. Specifically, the $R^2$ (*S*) diastereomer exhibits a greater chemical shift (4.7 ppm) compared to the (*R*) diastereomer (4.5 ppm).

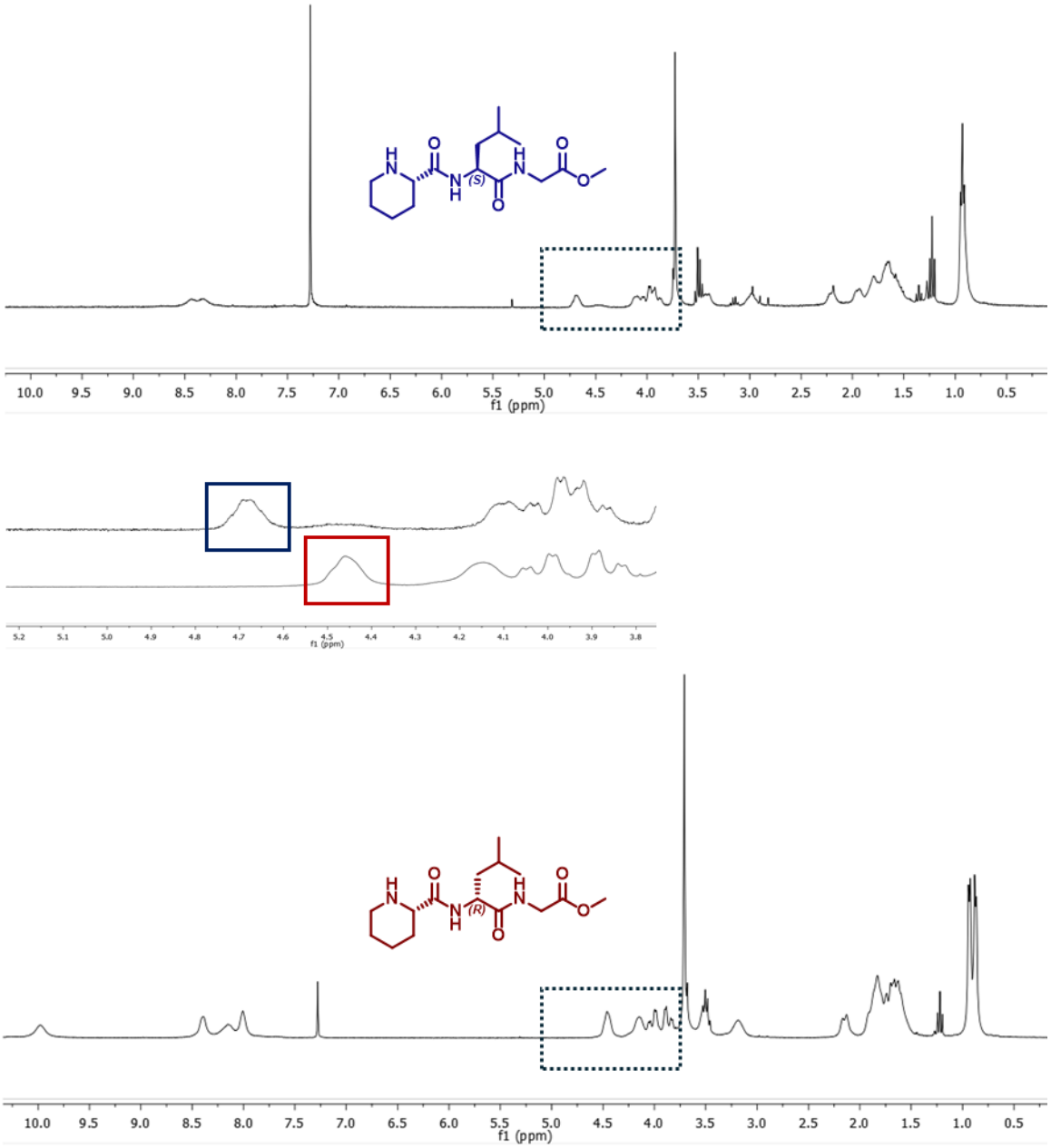



Figure 3.5. Chemical shifts change in asymmetric carbon between diastereomer pair **5a** (blue) and **6a** (red). Both NMR spectra were registered in $CDCl_3$.

USC
UNIVERSIDADE DE SANTIAGO DE COMPOSTELA

In addition, molecules **5a** and **6a** serve as valuable enantiopure standards in circular dichroism (CD) spectroscopy. When analyzing their CD spectra (Figure 3.6), it becomes evident that these molecules exhibit opposite Cotton effect at 220 nm. Since the only difference between compounds **5a** and **6a** is the stereodisposition of the isobutyl group, this structural feature was used to preliminary assign the absolute stereochemistry at this position.

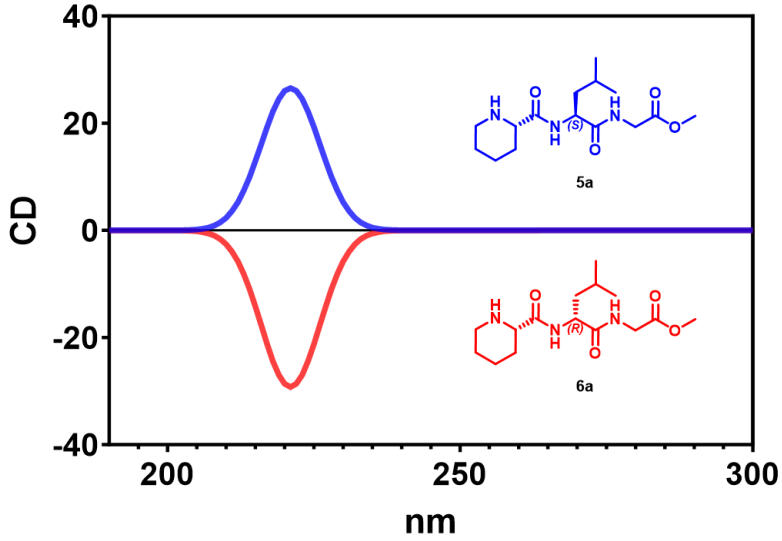



Figure 3.6. CD spectra of molecules **5a** (blue) and **6a** (red).

Molecule **5a** (with an (*S*) configuration, shown in blue) displays a positive Cotton effect at 220 nm, while molecule **6a** (with an (*R*) configuration, shown in red) exhibits a negative Cotton effect at the same wavelength. This empirical validation, in combination with NMR, establishes the reliability of molecules **5a** and **6a** as reference standards, ensuring the accurate assignation of the stereochemistry of the new chiral center of compounds **1-16**.

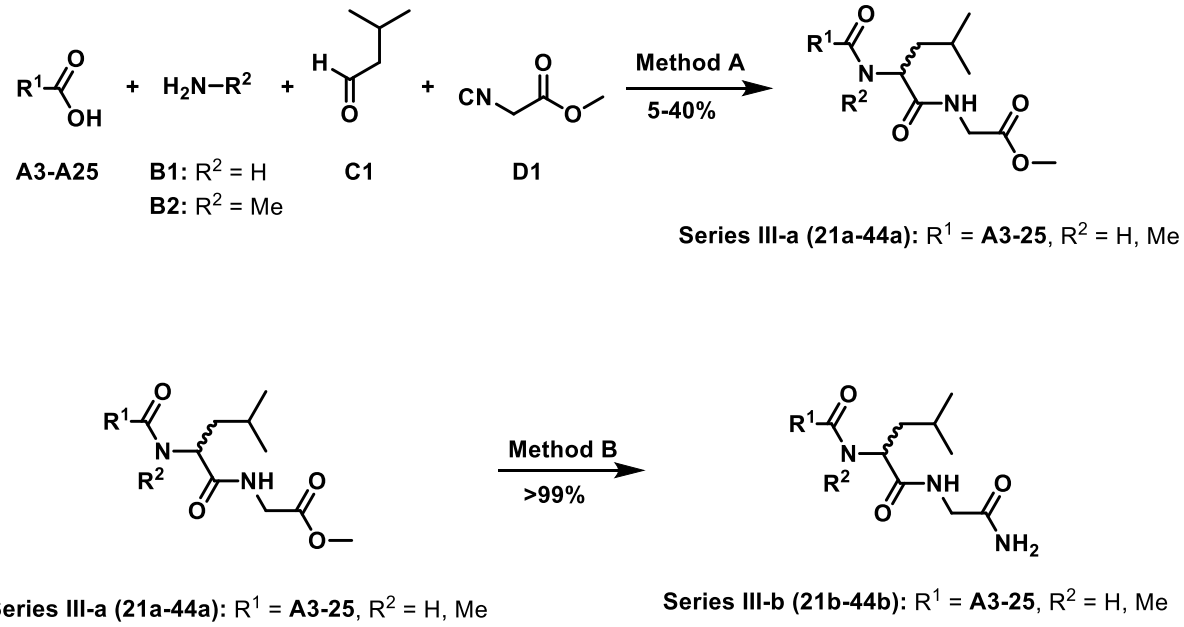
**Ugi-assisted bioisosteric replacements in melanostatin (Series III):** Like Series **I** and **II**, Series **III** was developed using a multicomponent approach based on the robust Ugi reaction. For the design of this series, we also took advantage of the peptidomimetic structure of the Ugi adducts (α-acylamino acetamide) and its analogy to the structure of melanostatin, focusing on the substitution of the proline residue with 23 cyclic groups.

A set of (cyclic, heterocyclic, and aromatic) carboxylic acids (**A3-25**), in combination with ammonia (**B1**) or methyl amine (**B2**), isobutyraldehyde (**C2**), and methyl-2-isocyanoacetate (**D1**) were employed as precursors. The targeted esters (**21a-44a**) were obtained as depicted in Scheme 3.11. The starting materials, dissolved in MeOH, were

USC UNIVERSIDADE DE SANTIAGO DE COMPOSTELA

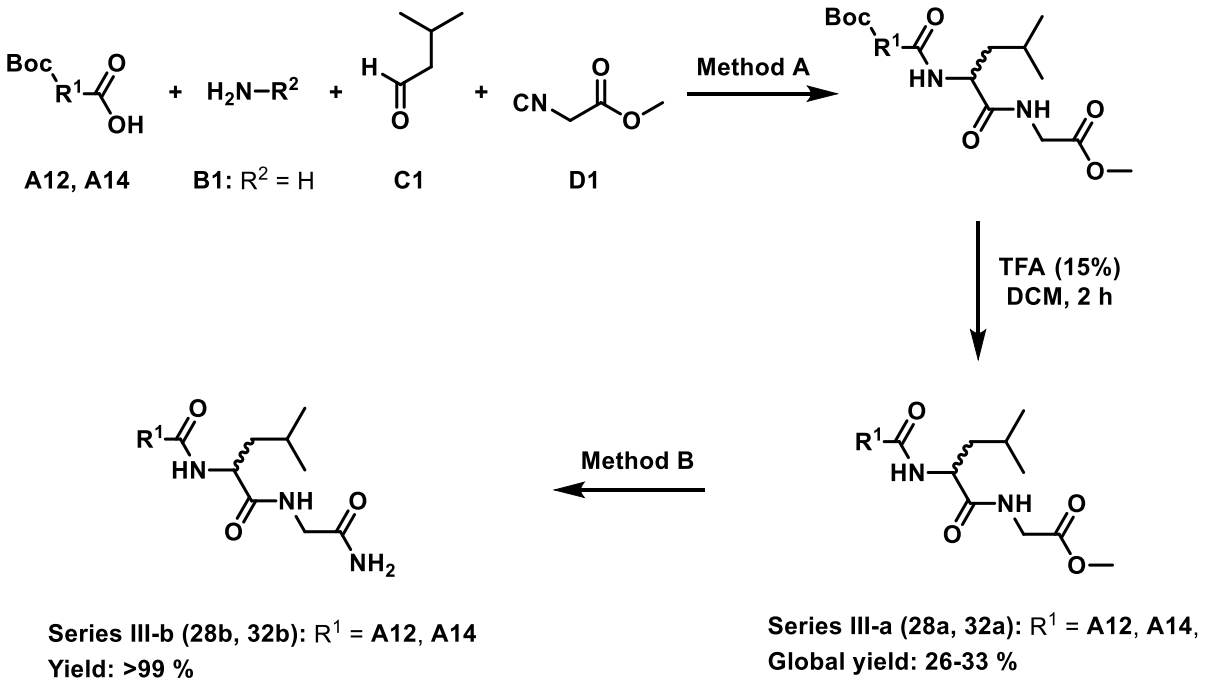
submitted to orbital stirring at room temperature for 24 h (Scheme 3.11, Method A). After completion of the reaction, the solvent was evaporated under reduced pressure to afford an oil residue, which was purified by chromatography on silica gel using MeOH/DCM mixtures.

In the case of carboxylic acids bearing a Boc protecting group (**A12, A14**), an additional step of hydrolysis was required (Scheme 3.12). After the Ugi reaction was completed and evaporation of the solvent, the crude product was redissolved in DCM and TFA (15%) was added. The reaction was stirred at room temperature for 2 h. Following completion, the solution was treated with NaOH 2M and the product was extracted with ethyl acetate. The organic phase was dried over $MgSO_4$ and evaporated under reduced pressure to afford an oil residue, which was purified by column chromatography on silica gel. The targeted methyl glycinate derivatives were obtained in moderate yields (15-40%) and were used as precursors for the synthesis of the corresponding amides (**21b**-**44b**).




Scheme 3.11. Ugi-based synthetic route. Method A) MeOH, RT, 24 h. Method B) $NH_3$, RT, 24 h.

USC UNIVERSIDADE DE SANTIAGO DE COMPOSTELA




Scheme 3.12. Ugi-based synthetic route for Boc-protected carboxylic acids. Method A) MeOH, RT, 24 h. Method B) $NH_3$, RT, 24 h.

For the synthesis of amides, the starting material (methyl glycinate) was dissolved in a solution of $NH_3$ 2M in MeOH (3 mL) and magnetically stirred at room temperature overnight (Scheme 3.11, Method B). Following completion, the solvent was evaporated under reduced pressure to afford a pure white solid that was washed with diethyl ether without further purification. The targeted carboxamide derivatives were obtained in quantitative yields (99%). All reactions were monitored by thin-layer chromatography (TLC). A detailed description of the synthetic methods and the complete structural, spectroscopic, and analytical data for all compounds are provided in the Experimental Section.

USC UNIVERSIDADE DE SANTIAGO DE COMPOSTELA

The collection of melanostatin analogues synthesized in Series **III** is illustrated below.

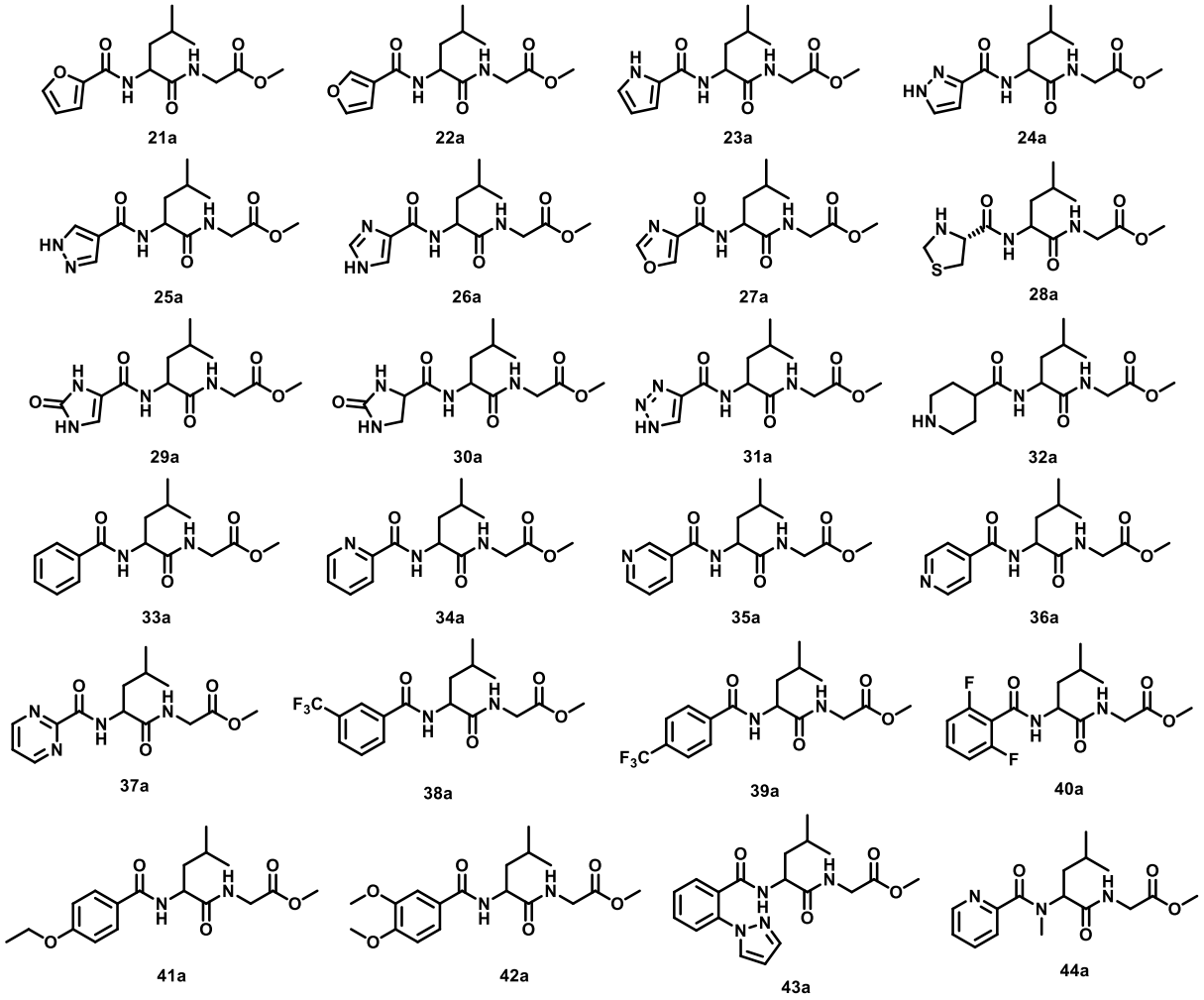



Figure 3.7. Structure of compounds belonging to Series **III-a**.

USC
UNIVERSIDADE DE SANTIAGO DE COMPOSTELA

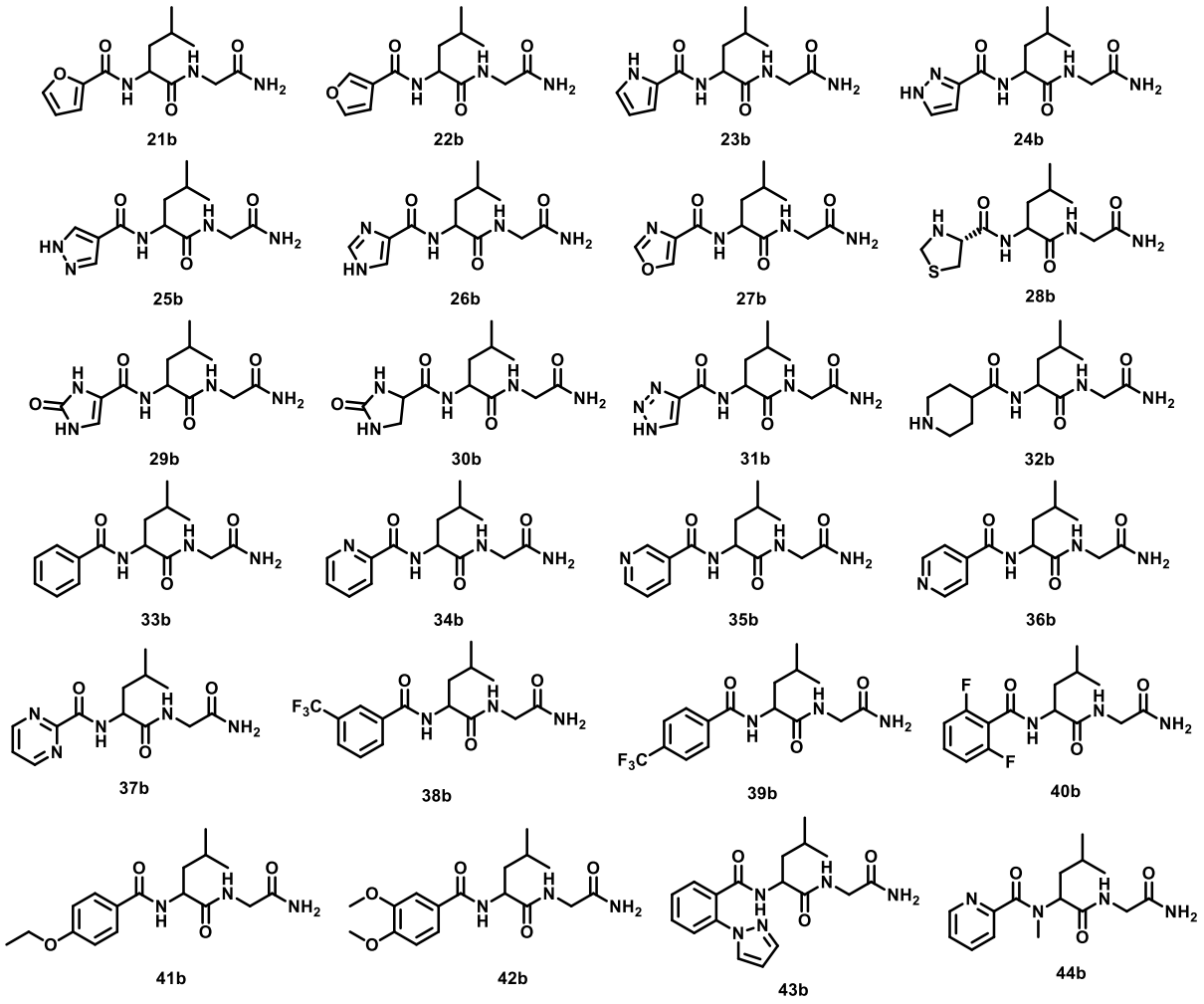
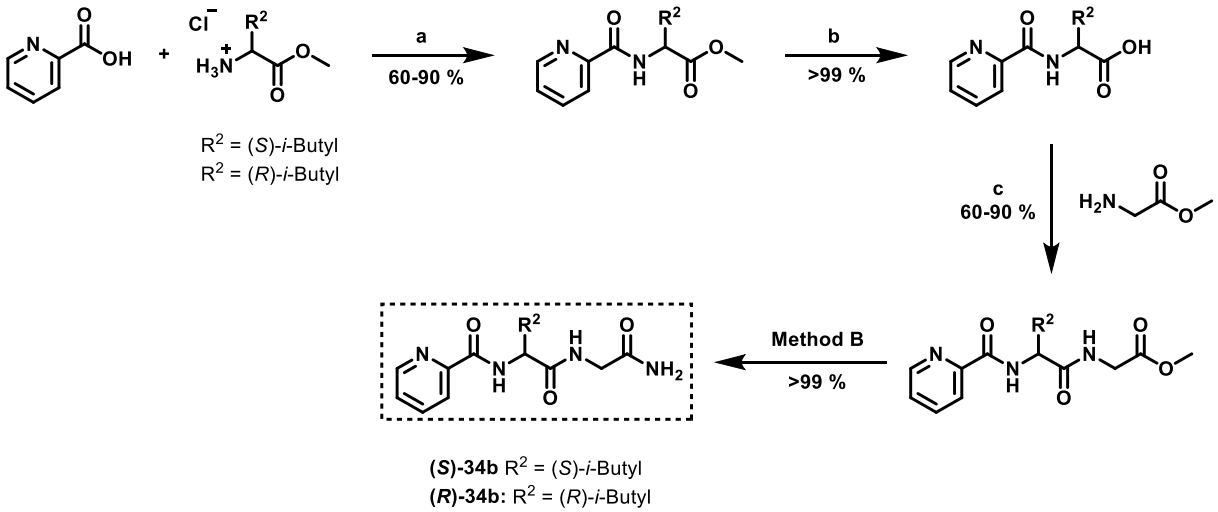



Figure 3.8. Structure of compounds belonging to Series **III-b**.

As mentioned previously, the Ugi reaction leads to the formation of a stereocenter in the final product. Contrary to Series **I** and **II**, where unambiguous structural characterization was performed for all compounds, in Series **III** this stereocenter remained unresolved as we aimed to rapidly explore as much diversity as possible. Consequently, these compounds were isolated and tested as racemic mixtures. The only exception is compound **34b**, which has been separated into its two enantiomers (**(*S*)-34b**, **(*R*)-34b**) through chiral HPLC (refer to Experimental Section). Similarly to the previous series, the lack of an unequivocal assignment protocol for the enantiomer pair of compound **34b** prompted us to prepare standard reference compounds using the same linear approach. Beginning with enantiopure starting materials, compounds **(*S*)-34b** and **(*R*)-34b** were obtained through direct amide coupling synthesis (Scheme 3.13).

USC UNIVERSIDADE DE SANTIAGO DE COMPOSTELA




Scheme 3.13. Linear synthesis of reference compounds **(*S*)-34b** and **(*R*)-34b**. a) EDC, HOBt, DMF, RT, 24 h. b) NaOH 2M, Dioxane/$H_2O$, RT, 2 h. c) EDC, HOBt, DMF, RT, 24 h.

Additionally, molecules **(*S*)-34b** and **(*R*)-34b** serve as valuable chiral standards in circular dichroism (CD) spectroscopy.

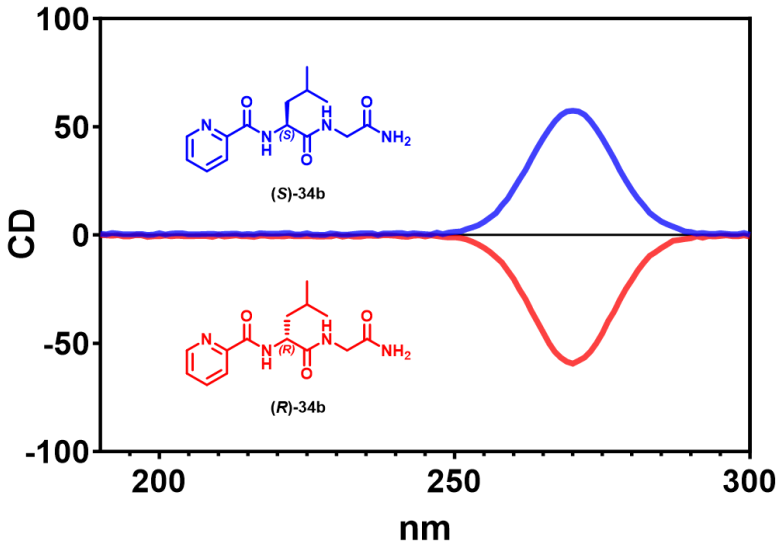


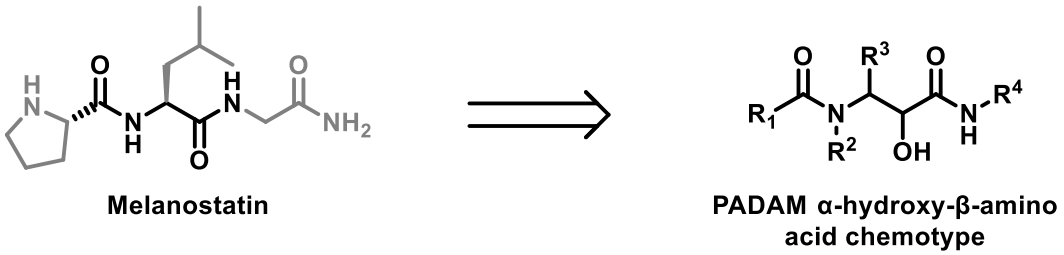

Figure 3.9. CD spectra of molecules **(*S*)-34b** (blue) and **(*R*)-34b** (red).

When analyzing their CD spectra (Figure 3.9), it becomes evident that enantiomers exhibit opposite Cotton effect at 270 nm. Consistent with Series **I** and **II**, the (*S*)-enantiomer displayed a positive Cotton effect, while the (*R*)-enantiomer exhibited a negative Cotton effect. This empirical confirmation establishes the reliability of molecules **(*S*)-34b** and **(*R*)-**

USC
DE SANTIAGO
DE COMPOSTELA

**34b** as reference standards, ensuring the accurate determination of the stereochemistry of future enantiomer separation within Series **III**.

**A PADAM strategy to generate oxo-melanostatin derivatives (Series IV and V)**: We expanded our multicomponent-based synthetic approach beyond the Ugi-4CR by implementing a PADAM strategy. This method, developed by Banfi et al.,[127] is conceptually related to the Ugi reaction and allowed for the rapid synthesis of a subset of melanostatin analogues, introducing into the structure an additional carbon atom carrying a hydroxy group. This hydroxy group, which can be further oxidized to a carbonyl group, offers a new diversity point. For the design of the new sets of molecules (Series **IV** and Series **V**) we took advantage of the structural analogy of melanostatin and the chemical architecture characteristic of the PADAM resulting products (α-hydroxy-β-amino acids or α-oxo-β-amino acids, Scheme 3.14).

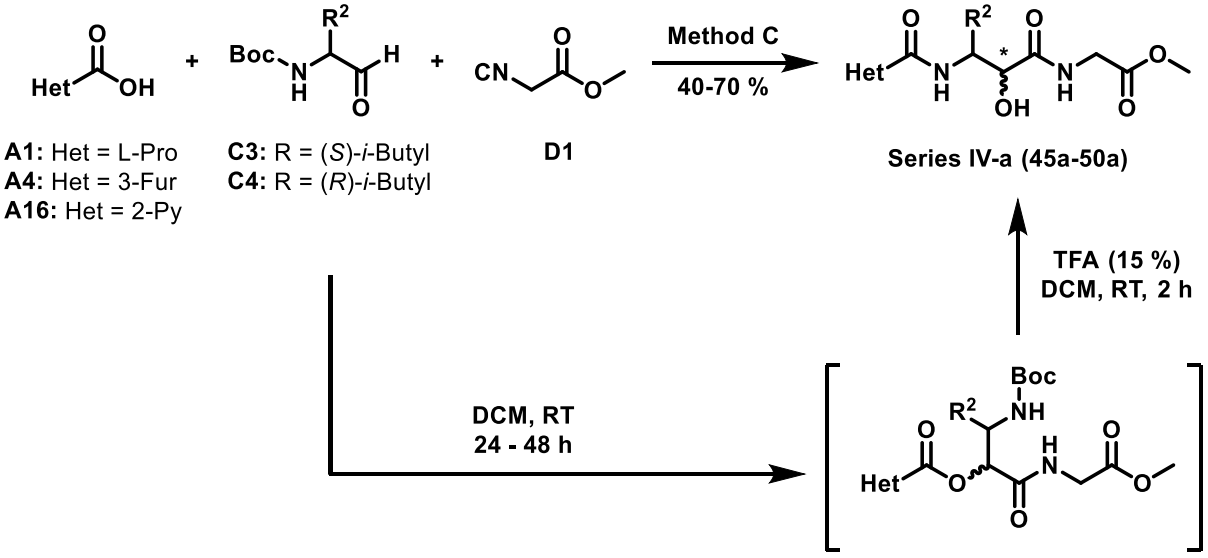



Scheme 3.14. Structural similarity between melanostatin and PADAM synthetic route products.

The methyl esters (**45a-50a**) were obtained as depicted in Scheme 3.15. A three-component synthesis, based on a post-transformation of the robust and efficient Passerini reaction (i.e., the three-component reaction of a carboxylic acid, an aldehyde or ketone, and an isocyanide), known as the PADAM synthetic route, enabled a time- and cost-effective assembly of Series **IV** and Series **V** of this chapter. Additionally, this synthetic strategy introduces one extra carbon atom into the chemical skeleton, with either a carbinol group or a carbonyl group attached, thus allowing the modification and the exploration of the melanostatin scaffold at five different positions. A representative set of heterocyclic carboxylic acids (**A1, A4** and **A16**), α-Boc-amino aldehydes (**C3-4**) and 2-methyl-isocyanoacetate (**D1**) were employed as precursors. The starting materials, dissolved in DCM, were submitted to orbital stirring at room temperature for 24 to 48 h (Method C) to yield the ester intermediate (Scheme 3.15). After completion of the reaction, trifluoroacetic acid was added to the mixture and the reaction was stirred at room temperature for an additional 2 h to promote the amine deprotection and transacylation. Following completion, the solution was

USC UNIVERSIDADE DE SANTIAGO DE COMPOSTELA

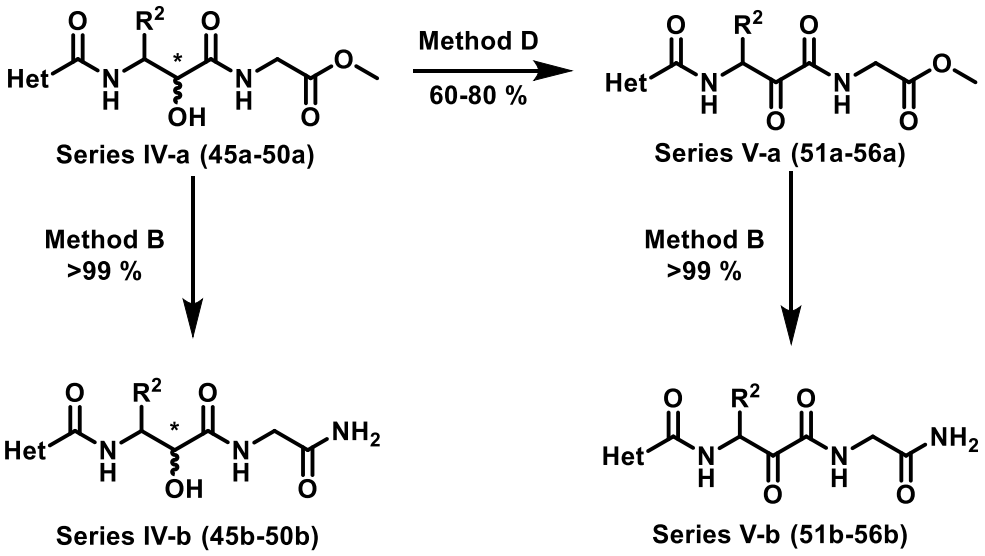
treated with NaOH 2M and the product was extracted with ethyl acetate. The organic phase was dried over $MgSO_4$ and evaporated under reduced pressure to afford an oil residue, which was purified by column chromatography on silica gel. The targeted hydroxyamide derivatives (**45a**-**50a**) were obtained in moderate yields (40-70%) as mixtures of diastereomers and were used as precursors for the synthesis of the oxoamides (**51a**-**56a**, Scheme 3.16).




Scheme 3.15. PADAM synthetic route to Series **IV-a**. Method C) 1) DCM, RT, 24-48 h, 2) TFA, DCM, RT, 2 h.

For the oxidation step, the starting material (**45a**-**50a**) was dissolved in DMF under inert atmosphere and, at 0 ºC, was treated with Dess-Martin periodinane for 2 h (Scheme 3.16, Method D). After completion of the reaction, the solution was treated with $NaHCO_3$ sat. and $Na_2S_2O_3$ (15% aq.) and stirred at room temperature for an additional 15 minutes. The product was extracted with ethyl acetate, and the organic phase was washed with water and brine. The organic phase was dried over $MgSO_4$ and evaporated under reduced pressure to afford an oil residue, which was purified by chromatography on silica gel using MeOH/DCM mixtures. The targeted oxoamide derivatives were obtained in satisfactory yields (60-80%). Equivalently to the previous series, both Series **IV-a** and Series **V-a** were used as precursors for the synthesis of Series **IV-b** (**45b**-**50b**) and Series **V-b** (**51b**-**56b**) using the Method B described above (Scheme 3.16), with similar results. All reactions were monitored by thin-layer chromatography (TLC). A detailed description of the synthetic methods and the complete structural, spectroscopic, and analytical data for all compounds are provided in the Experimental Section.

USC UNIVERSIDADE DE SANTIAGO DE COMPOSTELA




Scheme 3.16. Oxidation step and synthetic procedure of Series **IV-b** and **V-b**. Method D) Dess-Martin periodinane, DMF, 0 ºC, 2 h. Method B) $NH_3$, RT, 24 h.

The collection of melanostatin analogues synthesized in Series **IV** and **V** is illustrated below.

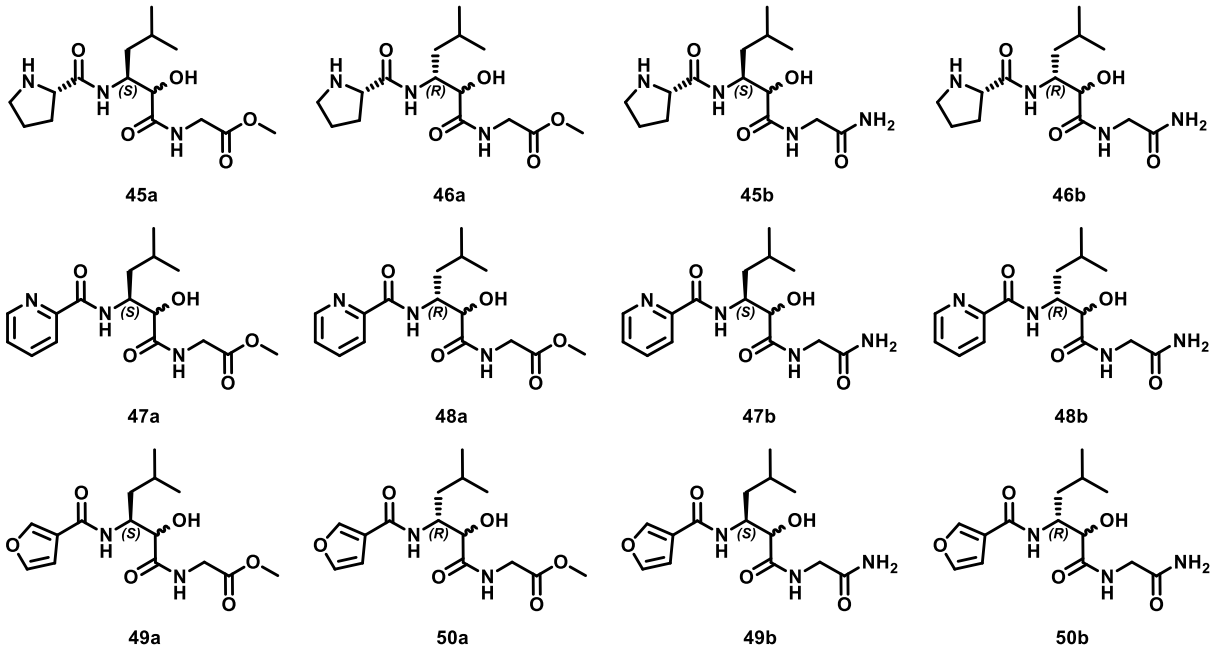



Figure 3.10. Structure of compounds belonging to Series **IV**.

USC UNIVERSIDADE DE SANTIAGO DE COMPOSTELA

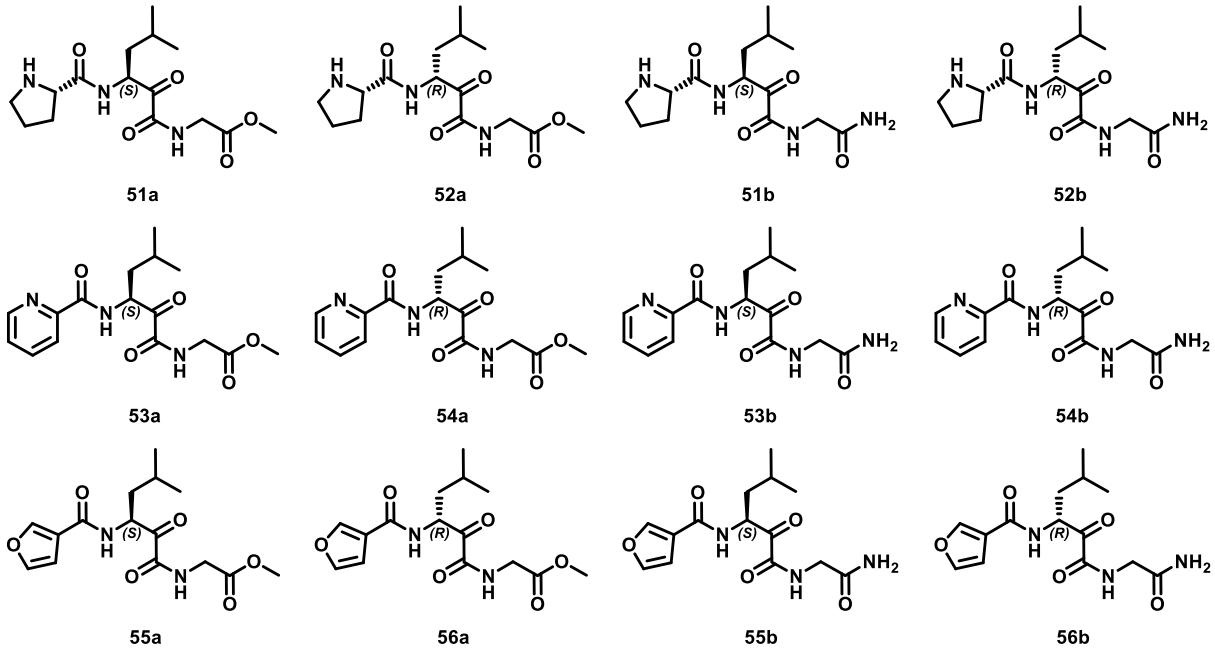



Figure 3.11. Structure of compounds belonging to Series **V**.

USC
UNIVERSIDADE DE SANTIAGO DE COMPOSTELA

### 3.1.3 Biological evaluation

The allosteric modulation activity of the 110 melanostatin analogues synthesized in this chapter was evaluated *in vitro* at human $D_2R$ expressed in CHO cells by measuring cAMP mobilization by means of HTRF measurements (Cisbio cAMP kit). 5000 cells/well were seeded in a 96-well black plate in stimB buffer provided in the kit in the presence of 500 µM IBMX. Then, test compounds and dopamine were added and incubated for 10 min at 37 ºC. Last, 10 µM forskolin was incubated for 5 min. Then, the kit reagents were added and incubated for 1 h at RT and HTRF signal was measured in a Tecan M1000 Pro multilabel reader. The compounds were evaluated at 0.01 nM and 1 nM over 0.1 µM dopamine. Data was converted to cAMP by employing a standard cAMP curve. A dopamine curve was included as positive control in all the assays. The activity of the compounds was expressed as the percentage of increase of the activity of 0.1 µM dopamine. The data for Series **IV** (**45**-**50**) was evaluated using diastereomeric mixtures resulting from the PADAM synthetic process. Data represent the mean ± SD of three independent assays. Table 3.1 to Table 3.7 contain the data obtained for Series **I**-**V**.

USC UNIVERSIDADE DE SANTIAGO DE COMPOSTELA

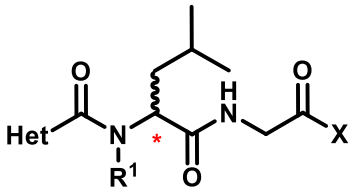



Table 3.1. Structure and variation in the dopamine effect data for Series **I-a** and **I-b**.

| Compound | Het | * | $R^1$ | X | 0.1 µM dopamine effect increase ($D_2R$) | |
|---|---|---|---|---|---|---|
| | | | | | 0.01 nM (%) | 1 nM (%) |
| **1a** | L-Proline | (*S*) | H | OMe | 5.22 ± 6.84 | 22.32 ± 4.63 |
| **2a** | L-Proline | (*R*) | H | OMe | 3.54 ± 8.29 | -11.65 ± 0.99 |
| **3a** | L-Proline | (*S*) | Me | OMe | 3.56 ± 13.6 | -0.84 ± 1.17 |
| **4a** | L-Proline | (*R*) | Me | OMe | 9.31 ± 0.57 | 11.32 ± 5.77 |
| **1b** | L-Proline | (*S*) | H | $NH_2$ | -7.6 ± 11.09 | 6.15 ± 15.64 |
| **2b** | L-Proline | (*R*) | H | $NH_2$ | 5.68 ± 15.62 | -12.67 ± 10.7 |
| **3b** | L-Proline | (*S*) | Me | $NH_2$ | -2.16 ± 9.37 | 19.23 ± 5.35 |
| **4b** | L-Proline | (*R*) | Me | $NH_2$ | -8.65 ± 0.3 | 14.02 ± 4.94 |
| **5a** | L-Homoproline | (*S*) | H | OMe | 11.26 ± 0.12 | 12.23 ± 6.26 |
| **6a** | L-Homoproline | (*R*) | H | OMe | -12.89 ± 4.39 | 5.33 ± 9.46 |
| **7a** | L-Homoproline | (*S*) | Me | OMe | -3.37 ± 8.63 | -1.3 ± 8.43 |
| **8a** | L-Homoproline | (*R*) | Me | OMe | 6 ± 13.25 | 10.79 ± 0.12 |
| **5b** | L-Homoproline | (*S*) | H | $NH_2$ | 22.04 ± 10.44 | 16.39 ± 5.41 |
| **6b** | L-Homoproline | (*R*) | H | $NH_2$ | -2.7 ± 1.44 | -5 ± 2.13 |
| **7b** | L-Homoproline | (*S*) | Me | $NH_2$ | 13.7 ± 0.42 | -0.87 ± 7.38 |
| **8b** | L-Homoproline | (*R*) | Me | $NH_2$ | -8.4 ± 10.23 | 10.13 ± 1.33 |
| **Melanostatin** | L-Proline | (*S*) | H | $NH_2$ | -11.11 ± 1.75 | 11.75 ± 11.59 |

USC UNIVERSIDADE DE SANTIAGO DE COMPOSTELA

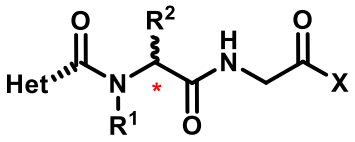



Table 3.2. Structure and variation in the dopamine effect data for Series **II-a** and **II-b**.

| Compound | Het | * | $R^1$ | $R^2$ | X | 0.1 μM dopamine effect increase ($D_2R$) | |
|---|---|---|---|---|---|---|---|
| | | | | | | 0.01 nM (%) | 1 nM (%) |
| **9a** | L-Proline | (*S*) | H | *i*-Pr | OMe | -0.37 ± 9.97 | -17.77 ± 5.57 |
| **10a** | L-Proline | (*R*) | H | *i*-Pr | OMe | 19.30 ± 5.20 | 4.1 ± 3.25 |
| **11a** | L-Proline | (*S*) | Me | *i*-Pr | OMe | -16.82 ± 11.69 | -54.18 ± 8.53 |
| **12a** | L-Proline | (*R*) | Me | *i*-Pr | OMe | -29.03 ± 10.74 | -34.78 ± 11.23 |
| **9b** | L-Proline | (*S*) | H | *i*-Pr | $NH_2$ | 7.06 ± 9.08 | -29.88 ± 5.56 |
| **10b** | L-Proline | (*R*) | H | *i*-Pr | $NH_2$ | -30.05 ± 10.69 | -0.01 ± 11.67 |
| **11b** | L-Proline | (*S*) | Me | *i*-Pr | $NH_2$ | 12.65 ± 8.69 | -20.77 ± 11.31 |
| **12b** | L-Proline | (*R*) | Me | *i*-Pr | $NH_2$ | 5.53 ± 12.64 | -11.88 ± 8.41 |
| **13a** | L-Homoproline | (*S*) | H | *i*-Pr | OMe | -8.86 ± 5.71 | -22.79 ± 6.40 |
| **14a** | L-Homoproline | (*R*) | H | *i*-Pr | OMe | -10.51 ± 6.30 | -1.53 ± 4.08 |
| **15a** | L-Homoproline | (*S*) | Me | *i*-Pr | OMe | 8.00 ± 8.70 | -18.03 ± 8.64 |
| **16a** | L-Homoproline | (*R*) | Me | *i*-Pr | OMe | 2.45 ± 4.59 | -7.54 ± 3.13 |
| **13b** | L-Homoproline | (*S*) | H | *i*-Pr | $NH_2$ | -12.15 ± 0.35 | -0.87 ± 5.19 |
| **14b** | L-Homoproline | (*R*) | H | *i*-Pr | $NH_2$ | -11.55 ± 4.03 | 7.99 ± 3.18 |
| **15b** | L-Homoproline | (*S*) | Me | *i*-Pr | $NH_2$ | 8.44 ± 8.17 | 1.86 ± 3.47 |
| **16b** | L-Homoproline | (*R*) | Me | *i*-Pr | $NH_2$ | -23.70 ± 10.1 | 4.23 ± 1.92 |
| **17** | L-Proline | (*S*) | H | *i*-Bu | NH-Me | 40.02 ± 3.74 | 13.54 ± 8.51 |
| **18** | L-Proline | (*S*) | H | *i*-Bu | NH-Et | 14.9 ± 2.73 | -15.2 ± 17.51 |
| **19** | L-Proline | (*S*) | H | *i*-Bu | NH-*i*-Pr | 20.03 ± 3.86 | 5.65 ± 4.93 |
| **20** | L-Proline | (*S*) | H | *i*-Bu | $N(Me)_2$ | 17.57 ± 11.42 | -21.82 ± 13.24 |
| **Melanostatin** | L-Proline | (*S*) | H | *i*-Bu | $NH_2$ | -11.11 ± 1.75 | 11.75 ± 11.59 |

USC UNIVERSIDADE DE SANTIAGO DE COMPOSTELA

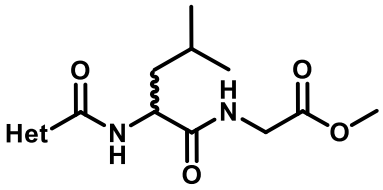



Table 3.3. Structure and variation in the dopamine effect data for Series **III-a**.

| Compound | Het | 0.1 μM dopamine effect increase ($D_2R$) | |
|---|---|---|---|
| | | 0.01 nM (%) | 1 nM (%) |
| **21a** | 2-furyl | -3.56 ± 10.2 | -2.75 ± 1.63 |
| **22a** | 3-furyl | -11.55 ± 3.66 | -13.58 ± 7.97 |
| **23a** | 2-pyrrolyl | 1.36 ± 2.39 | -15.7 ± 0.15 |
| **24a** | 3-pyrazolyl | -6.16 ± 8.69 | -2.41 ± 5.98 |
| **25a** | 4-pyrazolyl | 35.92 ± 14.99 | 5.43 ± 4.09 |
| **26a** | 4-imidazolyl | 5.42 ± 5.3 | -21.77 ± 6.39 |
| **27a** | 4-oxazolyl | 4.69 ± 9.45 | 26.92 ± 10.24 |
| **28a** | (4*R*)-thiazolidin-4-yl | 15.84 ± 7.26 | -12.68 ± 13.76 |
| **29a** | 2-oxo-2,3-dihydro-1*H*-imidazolidin-4-yl | 15.44 ± 7.04 | 22.63 ± 6.66 |
| **30a** | (4*S*)-2-oxoimidazolidin-4-yl | -2.20 ± 6.71 | -4.77 ± 15.36 |
| **31a** | 1,2,3-triazol-4-yl | 28.65 ± 5.61 | 32.87 ± 1.96 |
| **32a** | 4-piperidinyl | 21.41 ± 4.78 | 29.54 ± 7.85 |
| **33a** | Phenyl | -0.38 ± 6.1 | -9.34 ± 9.69 |
| **34a** | 2-Pyridinyl | -4.84 ± 5.61 | -14.07 ± 5.04 |
| **35a** | 3-Pyridinyl | -5.61 ± 5.18 | -10.19 ± 7.41 |
| **36a** | 4-Pyridinyl | 13.85 ± 5.33 | -9.11 ± 7.23 |
| **37a** | 2-Pyrimidinyl | -4.82 ± 5.95 | 0.68 ± 5.24 |
| **38a** | 3-(trifluoromethyl)phenyl | 2.03 ± 9.66 | -34.15 ± 4.24 |
| **39a** | 4-(trifluoromethyl)phenyl | 3.18 ± 7.72 | 5.73 ± 0.94 |
| **40a** | 2,6-difluorophenyl | 4.15 ± 5.77 | 0.03 ± 4.23 |
| **41a** | 4-ethoxyphenyl | -10.53 ± 9.22 | -37.09 ± 3.37 |
| **42a** | 3,4-dimethoxyphenyl | -24.2 ± 6.94 | -49.51 ± 12.98 |
| **43a** | 2-(pyrazol-1-yl)phenyl | -32.13 ± 4.63 | -21.39 ± 6.7 |
| **Melanostatin** | - | -11.11 ± 1.75 | 11.75 ± 11.59 |

USC UNIVERSIDADE DE SANTIAGO DE COMPOSTELA

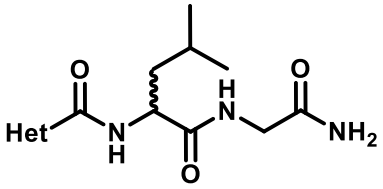



Table 3.4. Structure and variation in the dopamine effect data for Series **III-b**.

| Compound | Het | 0.1 μM dopamine effect increase ($D_2R$) | |
|---|---|---|---|
| | | 0.01 nM (%) | 1 nM (%) |
| **21b** | 2-furyl | 13.64 ± 8.01 | 1.26 ± 7.53 |
| **22b** | 3-furyl | 7.98 ± 6.34 | 4.14 ± 4.64 |
| **23b** | 2-pyrrolyl | 0.16 ± 7.44 | 0.96 ± 0.51 |
| **24b** | 3-pyrazolyl | 4.54 ± 3.42 | -3.58 ± 6.72 |
| **25b** | 4-pyrazolyl | 17.16 ± 8.64 | 24.8 ± 9.24 |
| **26b** | 4-imidazolyl | -15.41 ± 8.93 | 21.62 ± 2.11 |
| **27b** | 4-oxazolyl | 14.02 ± 6.58 | 32.83 ± 4.82 |
| **28b** | (4*R*)-thiazolidin-4-yl | 16.98 ± 7.93 | 10.58 ± 9.37 |
| **29b** | 2-oxo-2,3-dihydro-1*H*-imidazolidin-4-yl | 37.29 ± 8.18 | 16.63 ± 5.89 |
| **30b** | (4*S*)-2-oxoimidazolidin-4-yl | 14.14 ± 1.48 | 1.00 ± 4.97 |
| **31b** | 1,2,3-triazol-4-yl | 39.44 ± 12.62 | 24.93 ± 0.88 |
| **32b** | 4-piperidinyl | 24.43 ± 1.84 | 9.96 ± 7.80 |
| **33b** | Phenyl | 10 ± 5.92 | 2.4 ± 2.32 |
| **34b** | 2-Pyridinyl | -15.77 ± 3.83 | -33.32 ± 13.59 |
| **35b** | 3-Pyridinyl | -5.78 ± 5.85 | -10.36 ± 5.32 |
| **36b** | 4-Pyridinyl | -17.3 ± 1.87 | -5.87 ± 4.67 |
| **37b** | 2-Pyrimidinyl | -6.1 ± 9.8 | -8.87 ± 3.59 |
| **38b** | 3-(trifluoromethyl)phenyl | -24.65 ± 2.33 | -35.6 ± 3.38 |
| **39b** | 4-(trifluoromethyl)phenyl | -0.85 ± 27.33 | 5.76 ± 8.47 |
| **40b** | 2,6-difluorophenyl | -12.63 ± 3.6 | -10.31 ± 3.77 |
| **41b** | 4-ethoxyphenyl | -26.28 ± 4.52 | -35.56 ± 8.59 |
| **42b** | 3,4-dimethoxyphenyl | -10.67 ± 3.3 | -24.70 ± 9.89 |
| **43b** | 2-(pyrazol-1-yl)phenyl | -10.59 ± 8.34 | -31.71 ± 4.14 |
| **Melanostatin** | - | -11.11 ± 1.75 | 11.75 ± 11.59 |

USC UNIVERSIDADE DE SANTIAGO DE COMPOSTELA

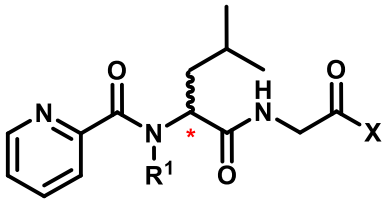


Table 3.5. Structure and variation in the dopamine effect data for enantiomeric separation of compound **34b** and methyl derivatives of compound **34a** and **34b**.

| Compound | $R^1$ | * | X | 0.1 μM dopamine effect increase ($D_2R$) | |
|---|---|---|---|---|---|
| | | | | 0.01 nM (%) | 1 nM (%) |
| **(±)-34b** | H | (*S*) + (*R*) | $NH_2$ | -15.77 ± 3.83 | -33.32 ± 13.59 |
| **(*S*)-34b** | H | (*S*) | $NH_2$ | -18.39 ± 9.1 | -12.76 ± 6.76 |
| **(*R*)-34b** | H | (*R*) | $NH_2$ | 3.83 ± 1.99 | -15.88 ± 8.44 |
| **44b** | Me | (*S*) + (*R*) | $NH_2$ | -38.7 ± 11.28 | -30.27 ± 11.47 |
| **44a** | Me | (*S*) + (*R*) | OMe | -31.77 ± 11.06 | -44.7 ± 8.92 |
| **34a** | H | (*S*) + (*R*) | OMe | -4.84 ± 5.61 | -14.07 ± 5.04 |
| **Melanostatin** | - | - | - | -11.11 ± 1.75 | 11.75 ± 11.59 |

USC UNIVERSIDADE DE SANTIAGO DE COMPOSTELA

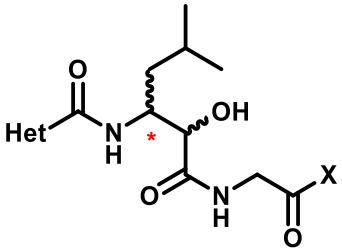



Table 3.6. Structure and variation in the dopamine effect data for Series **IV-a** and **IV-b**.

| Compound | Het | * | X | 0.1 µM dopamine effect increase ($D_2R$) | |
|---|---|---|---|---|---|
| | | | | 0.01 nM (%) | 1 nM (%) |
| **45a** | L-Proline | (*S*) | OMe | 9.16 ± 3.18 | 14.87 ± 4.94 |
| **45b** | L-Proline | (*S*) | $NH_2$ | -27.31 ± 2.73 | 12.22 ± 3.46 |
| **46a** | L-Proline | (*R*) | OMe | 6.46 ± 11.18 | 13.06 ± 6.6 |
| **46b** | L-Proline | (*R*) | $NH_2$ | 0.48 ± 8.26 | 11.73 ± 6.41 |
| **47a** | 2-Pyridinyl | (*S*) | OMe | 7.30 ± 12.92 | 16.70 ± 4.66 |
| **47b** | 2-Pyridinyl | (*S*) | $NH_2$ | -0.67 ± 9.63 | 39.07 ± 4.37 |
| **48a** | 2-Pyridinyl | (*R*) | OMe | 1.90 ± 6.91 | 7.11 ± 2.26 |
| **48b** | 2-Pyridinyl | (*R*) | $NH_2$ | 0.85 ± 10.45 | 15.00 ± 5.21 |
| **49a** | 3-Furyl | (*S*) | OMe | 8.83 ± 3.23 | 28.25 ± 0.11 |
| **49b** | 3-Furyl | (*S*) | $NH_2$ | 3.59 ± 9.93 | -8.24 ± 9.48 |
| **50a** | 3-Furyl | (*R*) | OMe | 14.59 ± 7.24 | -3.43 ± 8.22 |
| **50b** | 3-Furyl | (*R*) | $NH_2$ | 22.03 ± 8.50 | 10.61 ± 12.07 |
| **Melanostatin** | - | - | - | -11.11 ± 1.75 | 11.75 ± 11.59 |

USC
UNIVERSIDADE DE SANTIAGO DE COMPOSTELA

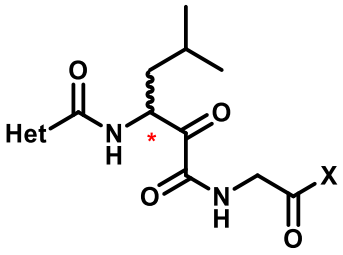



Table 3.7. Structure and variation in the dopamine effect data for Series **V-a** and **V-b**.

| Compound | Het | * | X | 0.1 µM dopamine effect increase ($D_2R$) | |
|---|---|---|---|---|---|
| | | | | 0.01 nM (%) | 1 nM (%) |
| **51a** | L-Proline | (*S*) | OMe | -0.01 ± 12.91 | 12.25 ± 9.52 |
| **51b** | L-Proline | (*S*) | $NH_2$ | 7.28 ± 10.25 | 9.54 ± 6.85 |
| **52a** | L-Proline | (*R*) | OMe | 11.89 ± 6.44 | 25.76 ± 10.03 |
| **52b** | L-Proline | (*R*) | $NH_2$ | 19.81 ± 11.63 | 6.19 ± 10.13 |
| **53a** | 2-Pyridinyl | (*S*) | OMe | 18.16 ± 6.16 | 13.52 ± 3.64 |
| **53b** | 2-Pyridinyl | (*S*) | $NH_2$ | 25.92 ± 5.14 | 7.47 ± 5.97 |
| **54a** | 2-Pyridinyl | (*R*) | OMe | 10.52 ± 8.53 | 12.12 ± 7.18 |
| **54b** | 2-Pyridinyl | (*R*) | $NH_2$ | -6.47 ± 10.83 | -18.48 ± 4.34 |
| **55a** | 3-Furyl | (*S*) | OMe | -23.29 ± 7.87 | 13.16 ± 5.25 |
| **55b** | 3-Furyl | (*S*) | $NH_2$ | 6.44 ± 9.31 | 12.19 ± 6.86 |
| **56a** | 3-Furyl | (*R*) | OMe | -19.34 ± 17.54 | 3.99 ± 2.72 |
| **56b** | 3-Furyl | (*R*) | $NH_2$ | 3.31 ± 0.06 | 7.69 ± 8.48 |
| **Melanostatin** | - | - | - | -11.11 ± 1.75 | 11.75 ± 11.59 |

USC UNIVERSIDADE DE SANTIAGO DE COMPOSTELA

### 3.1.4 Structure-Activity Relationships

In this section, we will analyze and comparatively rationalize the pharmacological data acquired for the herein synthesized series, as presented in Table 3.1 to Table 3.7. The data is presented as the increase in the 0.1 µM dopamine effect exerted by compounds at 0.01 nM and 1 nM, and it represents the mean ± SD of three independent assays. To assess the significance of these results, a one-sample t-test with a 90% confidence level has been performed for all series (refer to Experimental Section). This statistical test helps us determine whether the mean increase in the 0.1 µM dopamine effect, caused by the presence of these compounds, is significantly different from zero (which would correspond to the effect observed when no compound is present). The significance of this analysis lies in the fact that it allows us to distinguish whether the observed changes in the dopamine effect are likely due to the presence of the compounds or if they could have occurred by random chance. Only data falling within this 90% confidence interval will be considered in the subsequent discussion and SAR analysis, ensuring that the effects observed are indeed a result of the compound's presence and not solely due to random variability.

The reference compound and starting point of these series is melanostatin, a well-known endogenous neuropeptide acting as a $D_2R$ PAM.[21] We will refer to it when evaluating the data at hand. Melanostatin was synthesized within Series **I** of this chapter (compound **1b**, Table 3.1), but the data obtained from it are not statistically significant, and thus no conclusions can be drawn from them. To address this issue, we will use the data obtained by Prof. Sampaio-Dias and coworkers,[63] which is summarized in the table below:

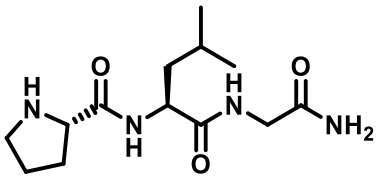



Table 3.8. Increment in the dopamine effect data for reference compound Melanostatin.[63]

| Compound | 0.1 µM dopamine effect increase ($D_2R$) | | |
|---|---|---|---|
| | 0.01 nM (%) | 0.1 nM (%) | 1 nM (%) |
| **Melanostatin** | -11.11 ± 1.75 | 15.40 ± 5.50 | 11.75 ± 11.59 |

USC UNIVERSIDADE DE SANTIAGO DE COMPOSTELA

Melanostatin is considered a reference PAM compound, allowing us to compare the effect that our ligands exert on 0.1 µM dopamine with that of melanostatin. The maximum effect observed for melanostatin occurs at 0.1 nM. Although our data were obtained at two different concentrations (0.01 nM and 1 nM), it serves as a valuable point of comparison. At 1 nM, melanostatin exhibits a moderate increase in the activity of dopamine; however, it fails to increase dopamine activity at 0.01 nM. Therefore, compounds increasing the effect of dopamine at this concentration will be considered as advantageous compared to melanostatin.

**Proof of concept via Ugi reaction (Series I and II)**: Initially, our focus lies in validating a multicomponent strategy tailored specifically for synthesizing derivatives of melanostatin. To this end, we have synthesized 36 analogues through various structural substitutions at the three residues comprising melanostatin (proline, leucine, glycine). The results of these explorations are briefly summarized here, with a more comprehensive analysis provided below.

1. Substitution of L-proline with L-homoproline yields a greater number of active compounds with slightly improved pharmacological profile.
2. Methylation of the secondary amide results in a derivative with enhanced activity compared to melanostatin. However, it does not exhibit a clear trend across Series **I** and Series **II**, leading to a diverse array of results.
3. The stereochemistry of the isobutyl residue influences the pharmacological activity, with (*S*) derivatives exhibiting a positive modulatory effect and (*R*) derivatives exhibiting the opposite effect.
4. Substituting isobutyl with isopropyl leads to an inversion of the allosteric modulatory effect, transitioning from positive to negative with highly active derivatives. The stereochemistry of isopropyl does not significantly affect the activity of the compounds, which maintain negative modulation of dopamine regardless of the stereochemistry at this residue, contrary to the observed effect in Series **I**.
5. Replacing the terminal amide with methyl ester also yields a diverse array of results, similar to methylation of position 2. The positive modulation of dopamine effect is slightly increased in Series **I**, while there is no clear trend throughout Series **II**.
6. Alkylation of the terminal amide improves the PAM activity at low concentrations, which aligns with the results obtained by the group of Sampaio-Dias.[65]

USC UNIVERSIDADE DE SANTIAGO DE COMPOSTELA

Considering the structure of melanostatin (Figure 3.13) and the data from Series **I** (Table 3.1) and Series **II** (Table 3.2), the substitution of the terminal amide with methyl ester results in an increase in activity (**1a** = 22.32 ± 4.63% at 1 nM), which is also higher than the efficacy of melanostatin. Substitution of (*S*)-isobutyl with (*S*)-isopropyl produces an inversion of the effect (**9b** = -29.88 ± 5.56% at 1 nM) with a remarkably negative allosteric modulator activity. Methylation at position 1 improves the PAM activity (**3b** = 19.23 ± 5.35% at 1 nM), also surpassing the efficacy of melanostatin. Substitution of proline with homoproline (**5b** = 16.39 ± 5.41% at 1 nM) results in yet another increase in activity, although this time the effect is similar to that of melanostatin at 0.1 nM. However, this substitution produces an effect at a concentration of 0.01 nM (22.04 ± 10.44%), where melanostatin is inactive, meaning that it is more potent than melanostatin at an even lower concentration. Finally, alkylation of the terminal amide with methyl (**17** = 40.02 ± 3.74%), ethyl (**18** = 14.90 ± 2.73%), or isopropyl (**19** = 20.03 ± 3.86%) results in a significant increase in dopamine effect at 0.01 nM, including the most potent PAM of the chapter at this concentration, compound **17** (Figure 3.13, Het = L-Pro, $R^1$ = H, (*S*)-isobutyl, X = NHMe). These results suggest that alkylation of the terminal amide improves the PAM activity at low concentrations, which aligns with the results obtained by the group of Sampaio-Dias (Figure 3.12).[65]

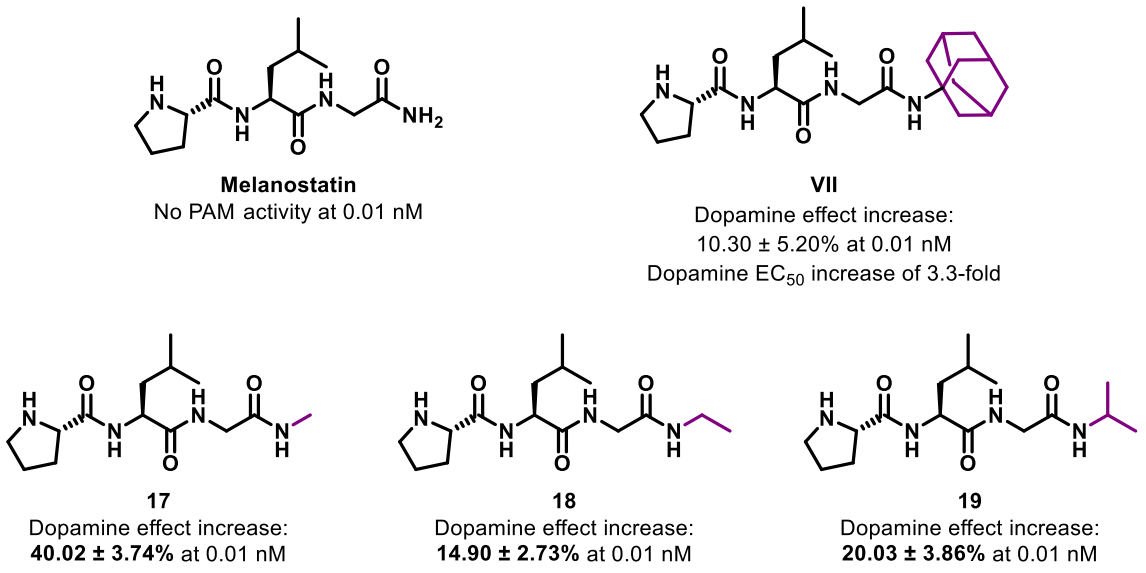



Figure 3.12. Improvement in the PAM activity of melanostatin at low concentration by alkylation of the terminal amide.

USC UNIVERSIDADE DE SANTIAGO DE COMPOSTELA

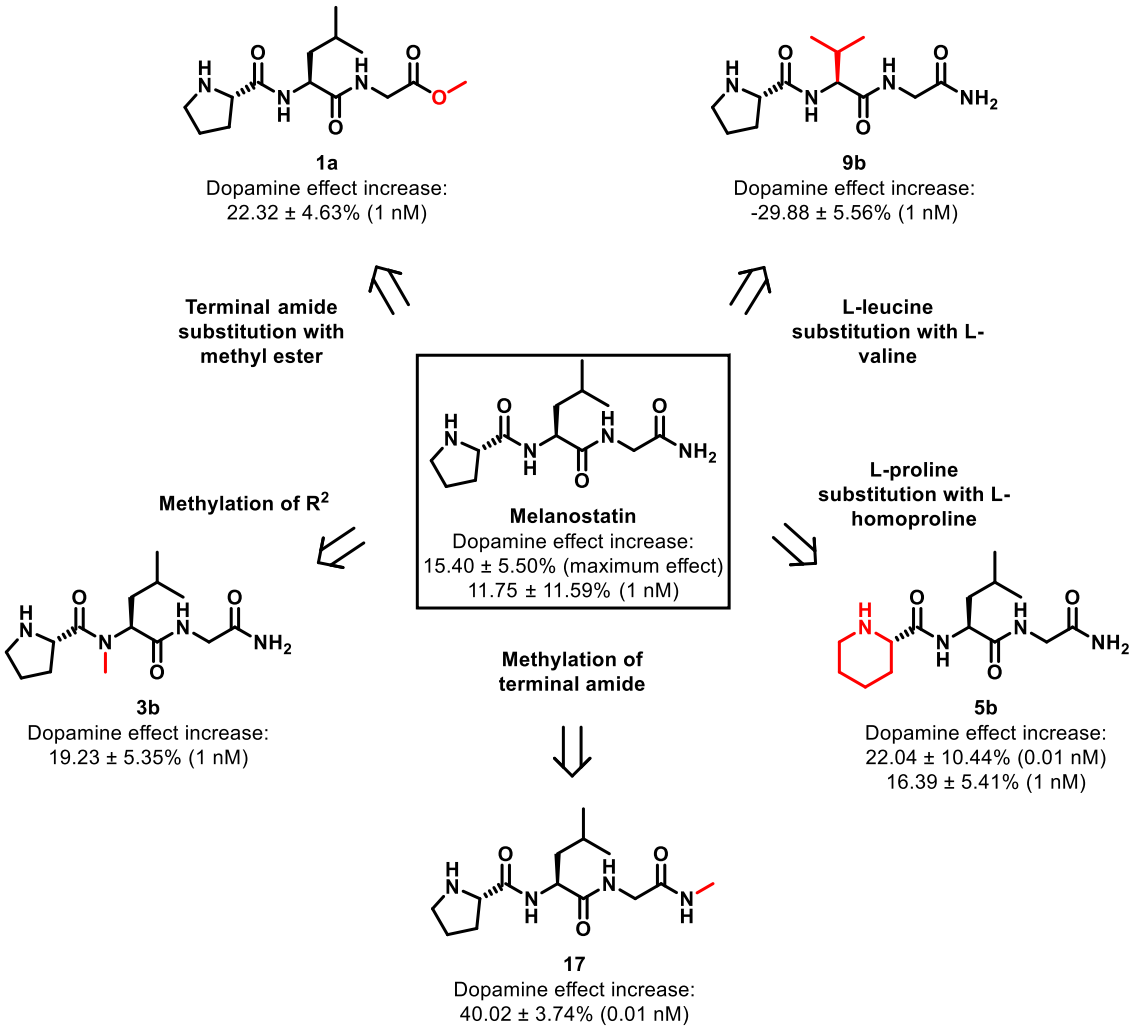



Figure 3.13. Changes in the allosteric modulator activity of melanostatin with derivatization.

In Series **I**, the substitution of proline with homoproline seems to enhance the activity at 0.01 nM, increasing the number of molecules exhibiting a significant effect at this concentration from 2 to 5 (Figure 3.14). Most of these molecules also demonstrate substantial activity, such as **5a** (11.26 ± 0.12% at 0.01 nM, 12.23 ± 6.26% at 1 nM), **6a** (-12.89 ± 4.39% at 0.01 nM), **5b** (22.04 ± 10.44% at 0.01 nM, 16.39 ± 5.41% at 1 nM), and **7b** (13.70 ± 0.42% at 0.01 nM).

USC UNIVERSIDADE DE SANTIAGO DE COMPOSTELA

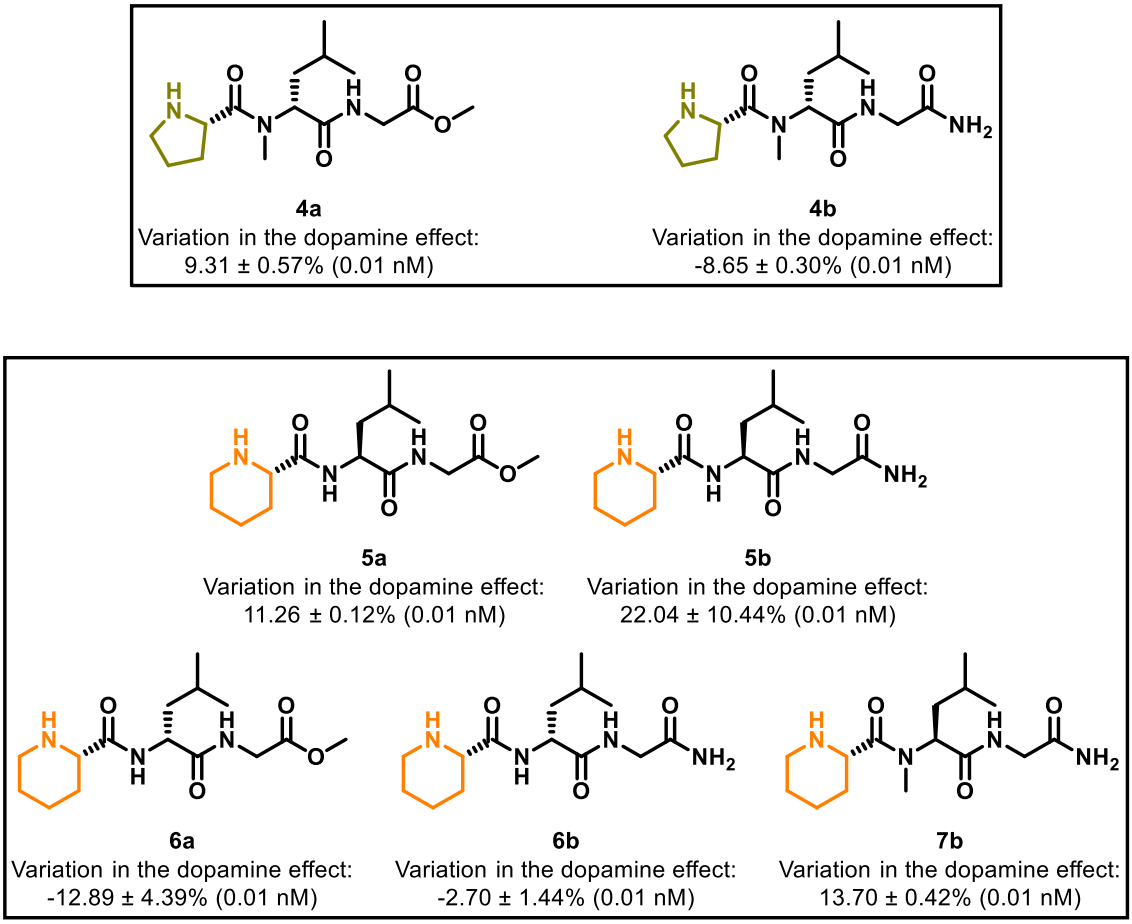



Figure 3.14. Compounds exhibiting activity at 0.01 nM in Series **I**. Substitution of L-proline with L-homoproline yields more derivatives active at this concentration.

Interestingly, the configuration of the isobutyl group appears to influence allosteric activity, as compounds **5a** ((*S*)-isobutyl) and **6a** ((*R*)-isobutyl) exhibit opposing effects (Figure 3.15). This same inversion is observed for compounds **5b** ((*S*)-isobutyl) and **6b** ((*R*)-isobutyl, -2.70 ± 1.44% at 0.01 nM) at both concentrations (Figure 3.15). However, these trends are not observed in Series **II**, where derivatives maintain consistent NAM activity independently of isopropyl configuration, except for compound **10a** (19.30 ± 5.2% at 0.01 nM).

USC UNIVERSIDADE DE SANTIAGO DE COMPOSTELA

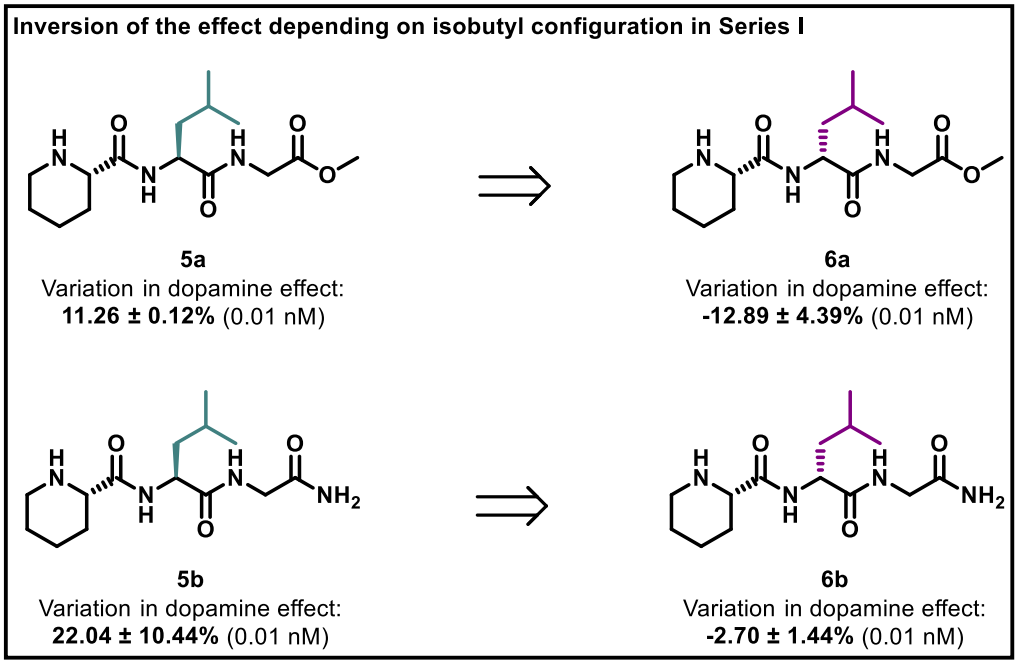
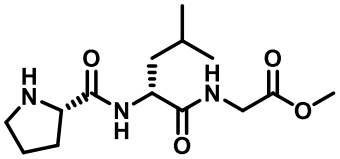



Figure 3.15. Effect of the isobutyl configuration on the allosteric modulatory activity in Series I.

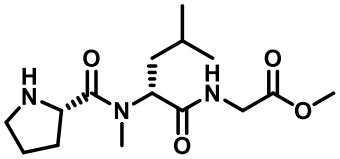
The methylation of $R^2$ appears to have different effects depending on the substrate (Figure 3.16). In Series **I**, the direction of the effect is reversed in the compound pair **2a** and **4a** (11.32 ± 5.77% at 1 nM). On the other hand, in Series **II**, compound **11a** (-54.18 ± 8.53% at 1 nM) exhibits significantly enhanced NAM activity compared to its analog **9a** (-17.77 ± 5.57% at 1 nM), while compound pairs **9b**/**11b** (-29.88 ± 5.56% *vs* -20.77 ± 11.31% at 1 nM), and **13a**/**15a** (-22.79 ± 6.40% *vs* -18.03 ± 8.64% at 1 nM) do not exhibit a significant variation in their effect (Figure 3.16).

A similar pattern emerges when comparing pairs with differing terminal functional groups. Substitution of methyl ester with carboxamide yields slightly better or similar activities throughout Series **I** (**4a**/**4b**, **8a**/**8b**, Figure 3.16), whereas in Series **II**, an enhancement of activity (**9a**/**9b**), a decrease in activity (**11a**, **11b**), and a reversal of activity (**16a**/**16b**) can be observed (Figure 3.16).

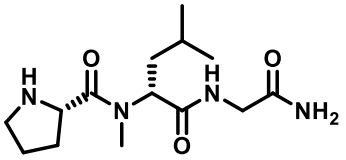
USC UNIVERSIDADE DE SANTIAGO DE COMPOSTELA



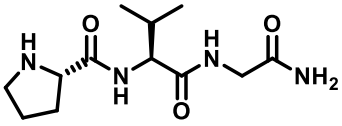
**2a**
Variation in dopamine effect:
-11.65 ± 0.99% at 1 nM



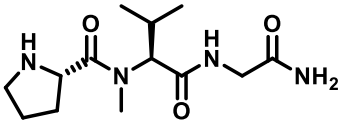
**4a**
Variation in dopamine effect:
11.32 ± 5.77% at 1 nM



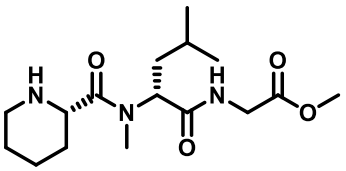
**4b**
Variation in dopamine effect:
14.02 ± 4.94% at 1 nM



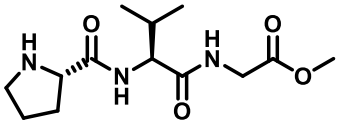
**9b**
Variation in dopamine effect:
-29.88 ± 5.56% at 1 nM



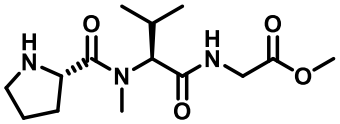
**11b**
Variation in dopamine effect:
-20.77 ± 11.31% at 1 nM



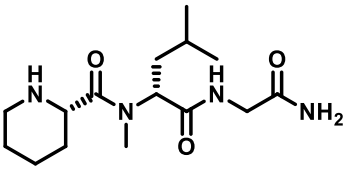
**8a**
Variation in dopamine effect:
10.79 ± 0.12% at 1 nM



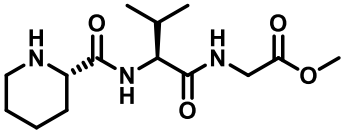
**9a**
Variation in dopamine effect:
-17.77 ± 5.57% at 1 nM



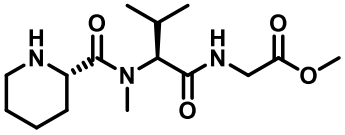
**11a**
Variation in dopamine effect:
-54.18 ± 8.53% at 1 nM



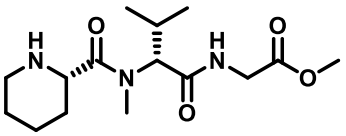
**8b**
Variation in dopamine effect:
10.13 ± 1.33% at 1 nM



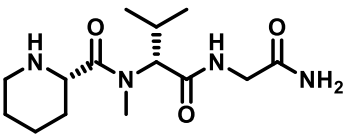
**13a**
Variation in dopamine effect:
-22.79 ± 6.40% at 1 nM



**15a**
Variation in dopamine effect:
-18.03 ± 8.64% at 1 nM



**16a**
Variation in dopamine effect:
-7.54 ± 3.13% at 1 nM



**16b**
Variation in dopamine effect:
4.32 ± 1.92% at 1 nM

Figure 3.16. Effect of methylation at $R^2$ and substitution at $R^4$ on the allosteric modulatory activity of Series **I** and **II**.

USC
UNIVERSIDADE DE SANTIAGO DE COMPOSTELA

The most pronounced trend within both Series **I** and **II** is the inversion of activity resulting from the substitution of isobutyl group with isopropyl group at position 2. While most of the molecules in Series **I** enhance the effect of dopamine (Table 3.1), derivatives in Series **II** exhibit the opposite effect, with remarkably high activity, including the most potent NAM (at 1 nM) identified in the study (**11a**, Figure 3.17).

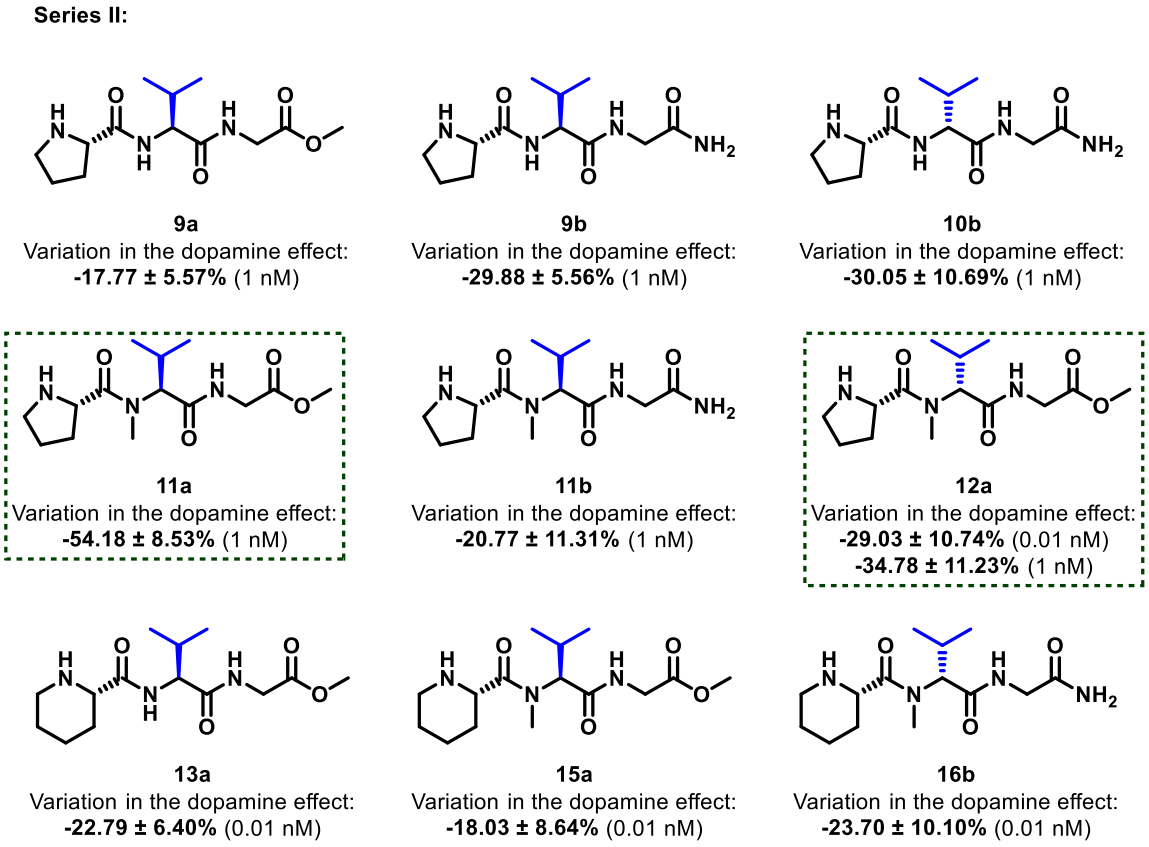



Figure 3.17. Negative allosteric modulatory activity induced by isopropyl, and structure of the best ligands identified during Series **II**.

**<u>Ugi-assisted bioisosteric replacements in melanostatin (Series III):</u>** Drawing inspiration from previous research conducted by Professor Dias' group, Series **III** of this chapter directs its attention to the proline residue, which is deemed ideal for derivatization. The focus lies on investigating substitution at this position with 23 diverse cyclic residues. As previously done in Series **I** and **II**, the main SAR trends found within this subset are summarized here, with a more comprehensive study provided below.

USC UNIVERSIDADE DE SANTIAGO DE COMPOSTELA

1. Pentagonal cycles generally yield compounds that increase the dopamine effect, while substituted phenyl rings provide compounds that decrease the dopamine effect.
2. The presence of strong hydrogen bond acceptors (HBA) within pentagonal cycles enhances the efficacy of the ligands. Furthermore, the increase in efficacy appears to increase with the distance of the HBA to the main chain. Finally, a higher number of HBAs on the ring further enhances the ligands' efficacy.
3. Introducing substituents on the phenyl ring in 6-membered cycle derivatives intensifies the NAM behavior of these compounds. The efficacy of this effect rises with the size of the substituent and is more pronounced in Series **III-a** (esters) than in Series **III-b** (amides).
4. Replacing the unsubstituted terminal amide with an ester group results in an inversion of the activity in some cases.

Analysis of data corresponding to derivatives bearing an unsubstituted terminal amide (Table 3.4) reveals a very intriguing trend. The series is divided into two groups at both concentrations: one group enhances the effect of dopamine, while the other diminishes it. The first group (compounds **21b**-**33b**) includes derivatives substituting L-proline with pentagonal cycles, with only two exceptions featuring a 4-piperidinyl moiety and a phenyl moiety. Conversely, the second group (compounds **34b**-**44b**) comprises derivatives with substituted phenyl rings in place of L-proline, which decrease the effect of dopamine.

The positive effect that 5-membered ring derivatives exert on dopamine activity also provides interesting insights into the SAR within this series. Compounds **21b** (Het = 2-furyl, 13.64 ± 8.01%) and **23b** (Het = 2-pyrrolyl, showing no significant activity) differ only in their heteroatoms (oxygen in furan and nitrogen in pyrrole) within the aromatic ring, yet their activities at 0.01 nM are noticeably different (Figure 3.18). This discrepancy is likely due to the difference between NH and O as hydrogen bond acceptors (HBA), with oxygen being stronger.

USC UNIVERSIDADE DE SANTIAGO DE COMPOSTELA

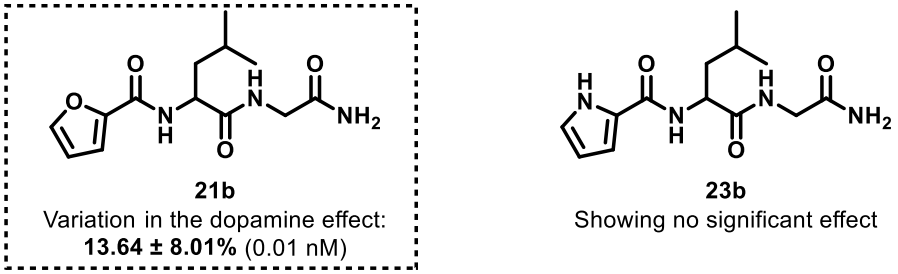



Figure 3.18. Comparative analysis of structure and biological activity of **21b** and **23b**.

Comparisons between compounds **24b** (Het = 3-pyrazolyl, showing no significant activity), **25b** (Het = 4-pyrazolyl, 24.80 ± 9.24% at 1 nM) and **26b** (Het = 4-imidazolyl, 21.62 ± 2.11% at 1 nM) provide interesting information regarding the optimal positions inside the aromatic structure for heteroatom substitution (Figure 3.19). All three compounds feature two nitrogen atoms within the ring, with one serving as a good hydrogen bond acceptor (the lone electron pair is not involved in the aromatic system), while the other exhibits properties similar to those of the nitrogen in the pyrrole ring (i.e., weak hydrogen bond donor and acceptor), but with superior acid character. Compound **24b** stands out as the only one among them that lacks significant activity at either 0.01 nM or 1 nM concentration and is also the only one lacking a nitrogen atom in the furthest position with respect to the amide. This observation suggests that this position is the optimal location for heteroatoms.

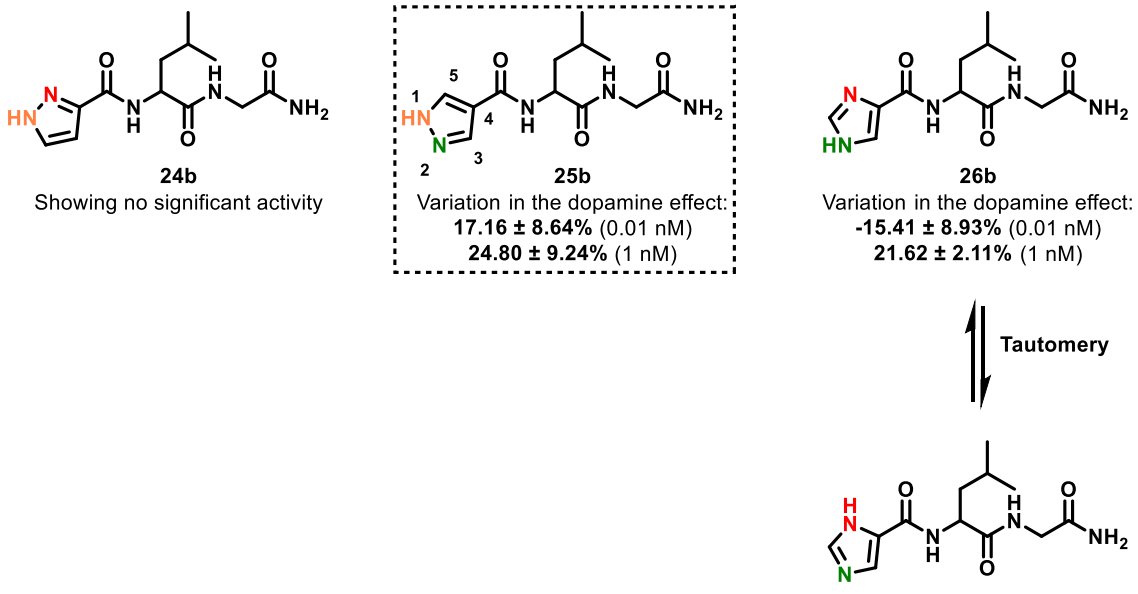



Figure 3.19. SAR analysis of compounds **24b**, **25b**, and **26b**: impact of heteroatom positioning on biological activity.

USC UNIVERSIDADE DE SANTIAGO DE COMPOSTELA

In addition, compound **27b** (Het = 4-oxazolyl, 32.83 ± 4.82% at 1 nM) replaces the nitrogen located farther from the amide with oxygen (Figure 3.20), a stronger HBA (hydrogen bond acceptor). Notably, it exhibits better activity compared to its analogue **26b** at 1 nM. This substitution also renders compound **27b** active in increasing the dopamine effect at 0.01 nM concentration, supporting the idea that this most distant position with respect to the amide is crucial for achieving positive allosteric modulatory activity. Finally, both **25b** and **26b** (Figure 3.19) demonstrate similar activity at 1 nM, but **25b** additionally enhances the dopamine effect at 0.01 nM, indicating a preference for incorporating heteroatoms at position 1 (in this specific structure), rather than position 5.

Compound **28b** (Het = (4*R*)-thiazolidin-4-yl, 16.98 ± 7.93% at 0.01 nM) lacks aromaticity, and thus the nitrogen within the ring has the lone pair available for hydrogen bonding, making it a good HBA and HBD. Additionally, the oxygen in the farthest position with respect to the amide in compound **27b** has been replaced with sulfur, which is less electronegative and a weaker HBA. In comparison to **28b**, **27b** retains similar activity at 0.01 nM but experiences a noticeable reduction in the enhancement of the dopamine effect at 1 nM. Overall, these results suggest that, as emphasized earlier, the presence of a strong HBA in the most distant position to the main chain is crucial for achieving allosteric activity, although an improvement in the hydrogen bonding properties of the heteroatom in position 3 appears to partially compensate for the substitution of sulfur instead of oxygen (Figure 3.20).

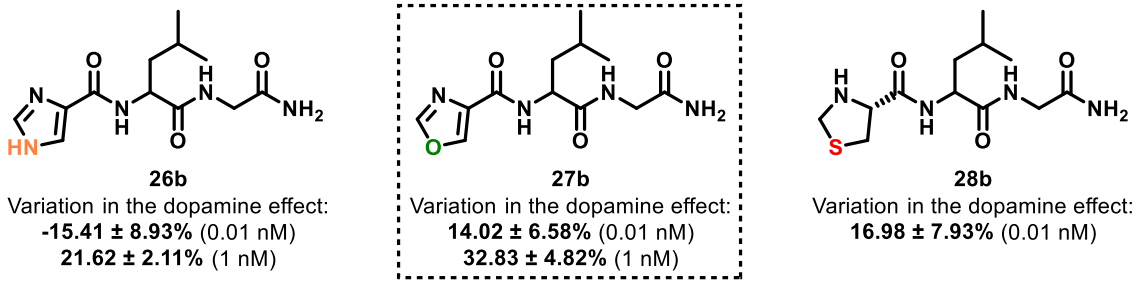



Figure 3.20. SAR analysis of compounds **26b**, **27b**, and **28b**: impact of heteroatom hydrogen bonding strength on biological activity.

Compound **29b** (Het = 2-oxo-2,3-dihydro-1*H*-imidazolidin-4-yl, 37.29 ± 8.18% at 0.01 nM) is the hydroxyderivative of **26b**. The predominant tautomeric form (keto) favors a strong HBA in the form of a carbonyl group and increases the acid character of both NH groups (Figure 3.21). The oxygen atom in this core features additional partial negative charge due to delocalization of nitrogen lone pairs. Furthermore, both nitrogen atoms are good HBD in

compound **29b**. This contributes to a remarkably high enhancement of the dopamine effect at both concentrations, particularly at 0.01 nM. Interestingly, the removal of the double bond within the ring in compound **30b** (Het = (4*S*)-2-oxoimidazolidin-4-yl, 14.14 ± 1.48%) results in a significant decrease in activity at both concentrations (Figure 3.21). This data suggests that conjugation between this double bond and the carbonyl group of the central structure is important to increase its HBA properties.

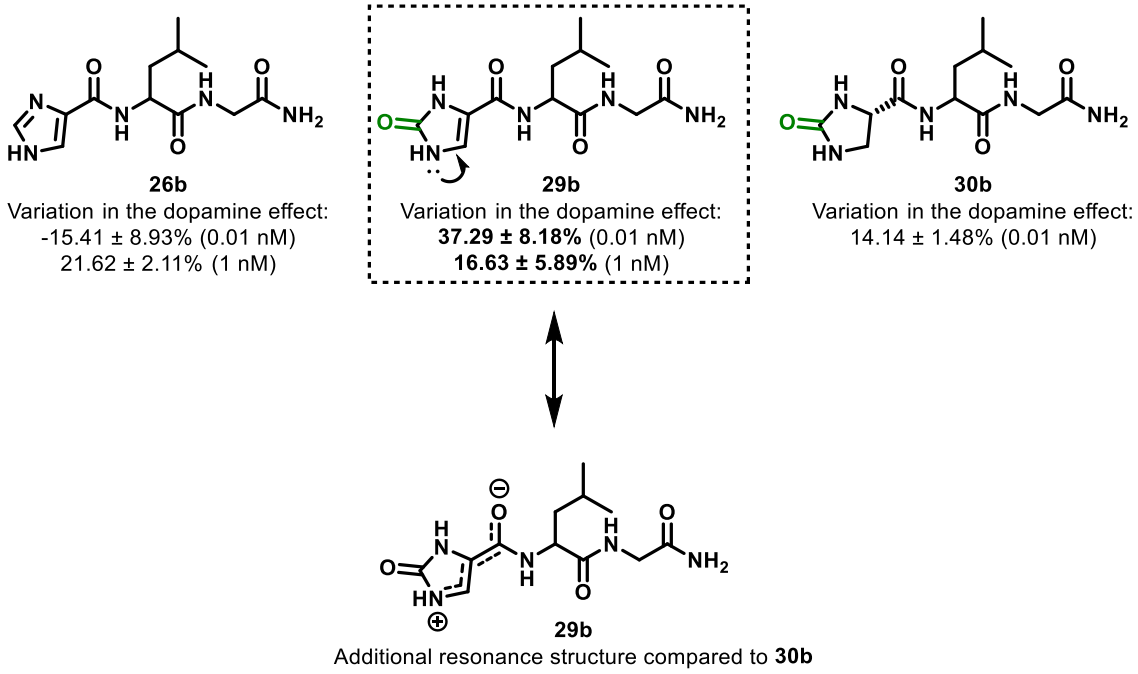



Figure 3.21. SAR analysis of compounds **26b**, **29b**, and **30b**: impact of additional heteroatoms on biological activity.

Compound **31b** (Het = 1,2,3-triazol-4-yl, 39.44 ± 12.62% at 0.01 nM, 24.93 ± 0.88% at 1 nM) exhibits the best pharmacological profile of the series, significantly enhancing the dopamine effect at both concentrations (Figure 3.22).

USC UNIVERSIDADE DE SANTIAGO DE COMPOSTELA

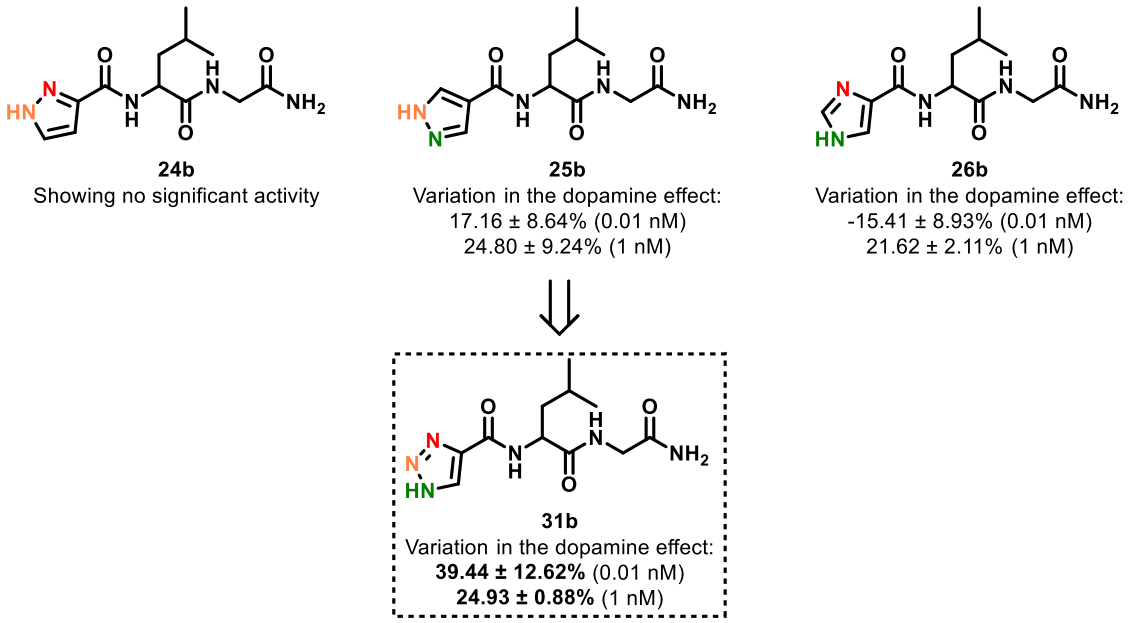



Figure 3.22. SAR analysis of compounds **24b**, **25b**, **26b**, and **31b**: impact of additional heteroatoms within the ring on biological activity.

Structurally, compound **31b** introduces one extra nitrogen atom into the ring compared to compounds **24b**, **25b** and **26b** and it clearly improves their activity as allosteric modulators. This suggests that while heteroatom substitution in the farthest position with respect to the amide is the most important factor for achieving activity, all three of them contribute to the overall effect.

Compounds **32b** (Het = 4-piperidinyl, 24.43 ± 1.84% at 0.01 nM) and **33b** (Het = phenyl, 10.00 ± 5.92% at 0.01 nM) are the only 6-membered ring derivatives that enhance the effect of dopamine in Series **III-b** (Figure 3.23). Compound **32b** is structurally analogous to **5b** and **6b** in Series **I** and exhibits similar activity at 0.01 nM as **5b**, although the latter also increases the dopamine effect at 1 nM. However, considering that compound **32b** is a racemic mixture, and that stereoselectivity is an important factor in allosteric activity (**6b** barely decreases the dopamine effect), it is reasonable to assume that there is still room for improvement in the pharmacological profile of compound **32b**. The significant activity displayed by this derivative can be attributed to the nitrogen located in the farthest position with respect to the amide, as explained earlier. In contrast, compound **33b** does not feature any heteroatom within the ring and, consequently, exhibits lower activity.

USC UNIVERSIDADE DE SANTIAGO DE COMPOSTELA

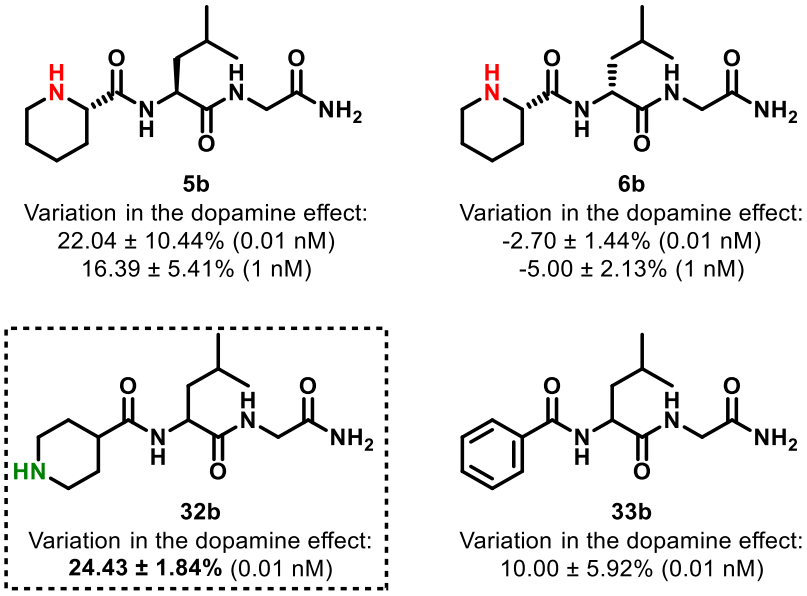



Figure 3.23. SAR and biological activity of 6-membered ring derivatives. Comparison with Series I.

The second part of the data exhibits compounds that decrease the dopamine effect and consists solely of derivatives featuring proline surrogates consisting of substituted 6-membered rings. All of these compounds are aromatic derivatives, and an analysis of their substituents reveals some intriguing trends (Figure 3.24). It is interesting to highlight that insertion of a nitrogen atom within the phenyl ring reverses the observed effect in 33b. Substituting phenyl with pyridine yields compound **34b** (Het = 2-piridinyl, -15.77 ± 3.83% at 0.01 nM, -33.32 ± 13.59% at 1 nM), which shows a remarkable decrease in dopamine effect at both concentrations. The significant decrease in activity exhibited by its isomeric compounds **35b** (Het = 3-piridinyl, -10.36 ± 5.32% at 1 nM) and **36b** (Het = 4-piridinyl, -17.30 ± 1.87% at 0.01 nM) suggests that, in this case, position 2 of the ring is optimal for nitrogen insertion (CH/N bioisosteric substitution), in contrast to the trend observed in pentagonal compounds. Although suboptimal, CH/N substitution at position 3 and 4 of the ring still exhibits noticeable activity. However, the introduction of a second nitrogen atom at position 6 in compound **37b** (Het = 2-pyrimidinyl, -8.87 ± 3.59% at 1 nM) results in a more moderate reduction of dopamine effect.

USC UNIVERSIDADE DE SANTIAGO DE COMPOSTELA

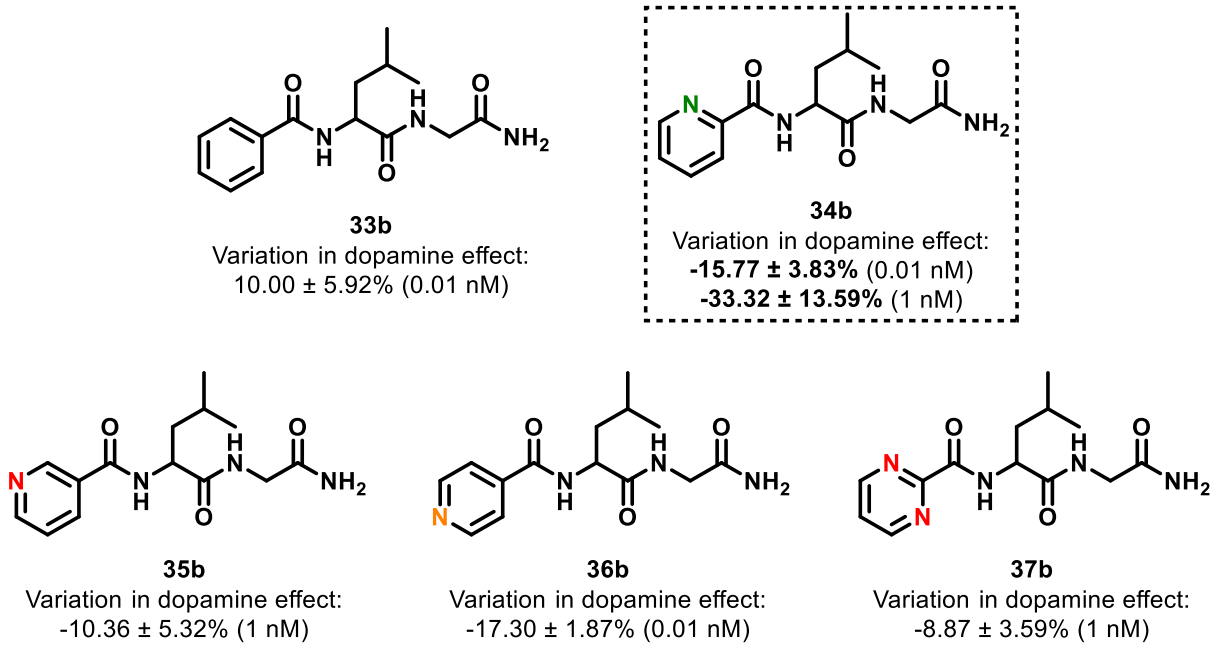



Figure 3.24. SAR analysis of compounds **34b**, **35b**, **36b**, and **37b**: impact of heteroatom positioning on biological activity.

The remarkable activity of compound **34b**, in combination with the findings from Sampaio-Dias' group showing 2-pyridine as a suitable proline surrogate (Figure 3.25, compound **III**),[63] made this derivative an appropriate candidate for further structural explorations, such as methylation of the nitrogen belonging to the amide adjacent to the aromatic ring or the enantiomeric separation of the racemic mixture formed during the Ugi reaction.

Methylating $R^2$ led to the formation of compound **44b** (Figure 3.25). This compound demonstrated significantly enhanced activity at a concentration of 0.01 nM, and its activity was comparable to that of compound **34b** at 1 nM. This trend mirrors the findings in Series **I**, where the methylated derivative of melanostatin (compound **3b**) also showed an enhancement in allosteric modulatory activity. These results indicate that methylation may serve as an effective strategy for improving the activity of allosteric modulators, paving the way for further investigations in this series.

Enantiomeric separation of compound **34b** resulted in the isolation of two isomers, **(*S*)-34b** and **(*R*)-34b** (Figure 3.25). Both enantiomers exhibit comparable activities at 1 nM. However, the (*S*)-enantiomer displays a notable modulatory effect on the action of dopamine even at a lower concentration of 0.01 nM, where the isomer **(*R*)-34b** fails to exert any

significant effect. This suggests a preference for the (*S*) configuration at the isobutyl residue, although the data from compound **(*S*)-34b** does not show improved activity compared to the racemic mixture. Compound **(±)-34b** exhibits a similar decrease in the dopamine effect at 0.01 nM than compound **(*S*)-34b** and shows significantly improved negative allosteric modulation activity at 1 nM.

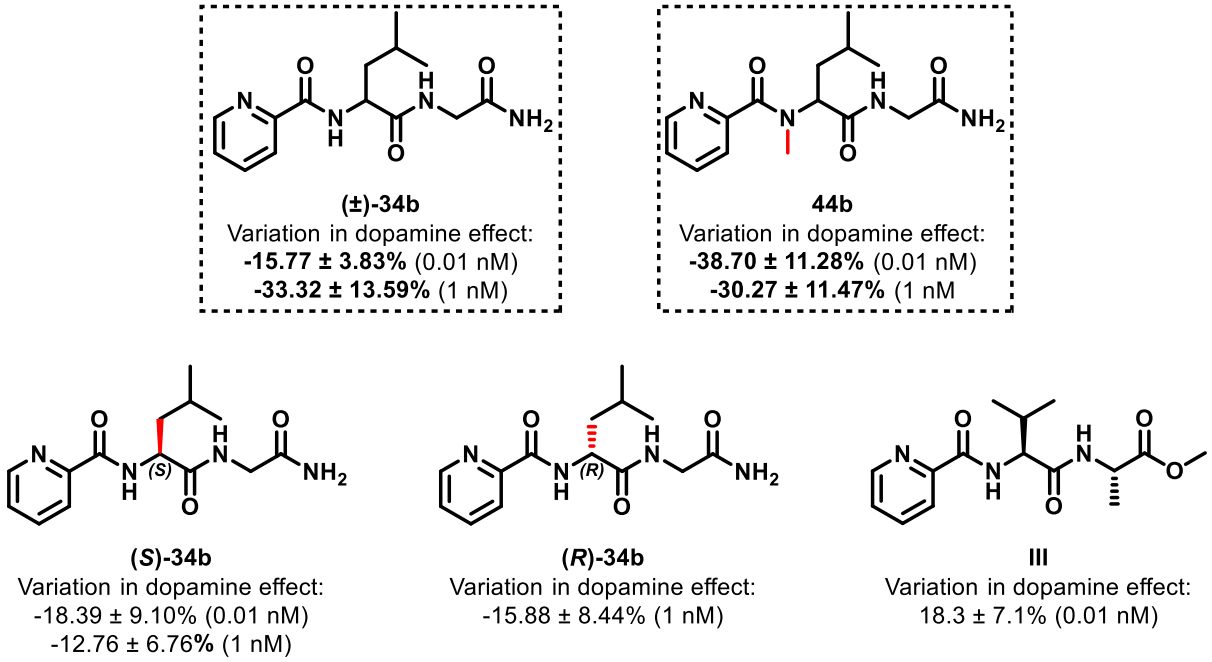



Figure 3.25. SAR analysis of compounds **34b**, **(*S*)-34b**, **(*R*)-34b**, and **44b**: impact of stereochemistry and methylation on biological activity.

The introduction of different groups at the phenyl ring generally resulted in derivatives displaying negative modulation of the dopamine activity, with moderate to high efficacy (Figure 3.26).

USC UNIVERSIDADE DE SANTIAGO DE COMPOSTELA

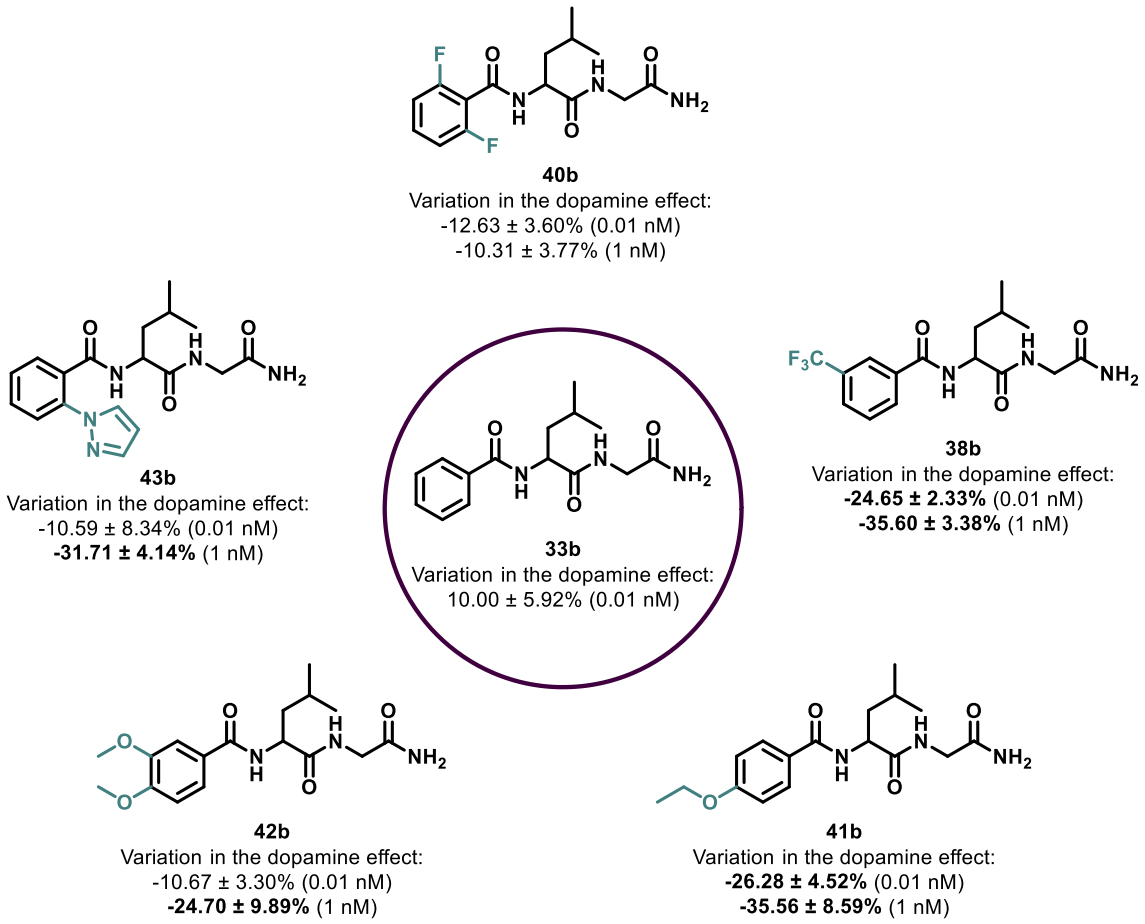


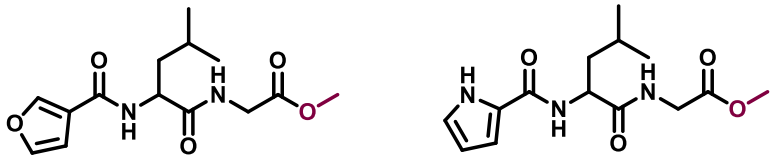

Figure 3.26. Analysis of the allosteric modulatory activity in a series of phenyl substituted derivatives.

Compound **38b** (Het = 3-(trifluoromethyl)phenyl, -24.65 ± 2.33% at 0.01 nM, -35.60 ± 3.38% at 1 nM) features a trifluoromethyl substituent in position 3 of the ring and exhibits one of the most consistent pharmacological profiles of the subset, decreasing the effect of dopamine at both concentrations. The introduction of this trifluoromethyl results in an inversion of the modulatory effect compared to compound **33b**, with a remarkably high activity. The same effect on the allosteric activity is produced by the introduction of different substituents regardless of their electronic effects (EWG or EDG). Among them, the introduction of an ethoxy group yields a ligand with similar activity to compound **38b**, compound **41b** (Het = 4-ethoxyphenyl, -26.28 ± 4.52% at 0.01 nM, -35.56 ± 8.59% at 1 nM). Both display a remarkably high reduction in dopamine effect at both concentrations, despite bearing their respective substituents at different positions, which indicates that the key factor for achieving high negative modulation of the dopamine effect might be the size of the proline surrogate. Compounds **42b** (Het = 3,4-dimethoxyphenyl, -24.70 ± 9.89% at 1 nM) and **43b**

USC UNIVERSIDADE DE SANTIAGO DE COMPOSTELA

(Het = 2-(pyrazol-1-yl)phenyl, -31.71 ± 4.14% at 1 nM) further support this idea, as they incorporate bulky substituents at distinct positions on the aromatic ring, resulting in a substantial reduction of the dopamine effect. It appears that the pharmacological profile of the ligands remains unaffected by both the electronic nature of the substituents and their placement on the aromatic ring. On the other hand, compound **40b** (Het = 2,6-difluorophenyl, -12.63 ± 3.60% at 1 nM) contains smaller substituents at positions 2 and 6 (two fluorine atoms), and as a result, it exhibits lower activity at both concentrations. Nevertheless, the introduction of fluorine atoms leads to a reversal of the modulatory activity of compound **33b**, shifting it from positive to negative.

These trends are generally well preserved within Series **III-a** in terms of overall effectiveness, although replacing the unsubstituted terminal amide with a methyl ester leads to a reversal in the response in some cases. Compounds containing furan and pyrrole as proline surrogates, such as **22a** (Het = 3-furyl, -13.58 ± 7.97% at 1 nM) and **23a** (Het = 2-pyrrolyl, -15.70 ± 0.15% at 1 nM), exemplify this inversion of the activity, as they reduce the effect of dopamine on the $D_2R$.



**22a**
Variation in the dopamine effect:
**-11.55 ± 3.66%** (0.01 nM)
**-13.58 ± 7.97%** (1 nM)



**23a**
Variation in the dopamine effect:
**-15.70 ± 0.15%** (1 nM)

Figure 3.27. Comparative analysis of structure and pharmacological data of compounds **22a** and **23a**.

In general, small pentagonal cycles that performed well in the amide series also exhibit strong activity in the methyl ester form (Figure 3.28). Compounds **24a** (Het = 3-pyrazolyl, showing no significant activity), **25a** (Het = 4-pyrazolyl, 35.92 ± 14.99% at 0.01 nM), and **26a** (Het = 4-imidazolyl, -21.77 ± 6.39% at 1 nM) follow the same nitrogen substitution patterns observed before (i.e., the order of importance of the heteroatom position being 1 > 2 > 5). Similar to Series **III-b**, the 4-pyrazolyl derivative demonstrates the greatest activity of the trio (Figure 3.28).

USC
UNIVERSIDADE DE SANTIAGO DE COMPOSTELA

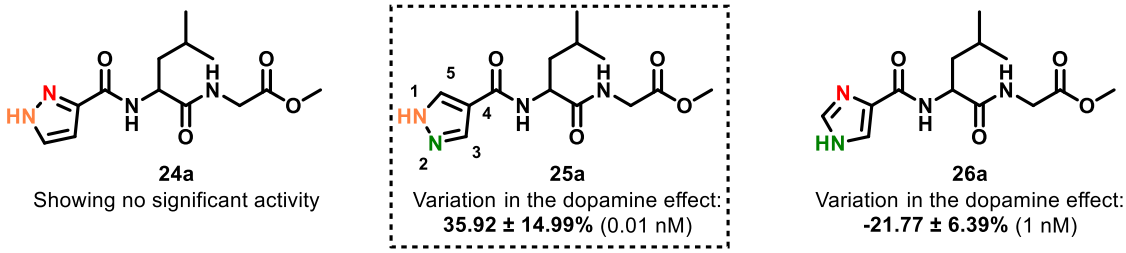



Figure 3.28. SAR analysis of compounds **24a**, **25a**, and **26a**: impact of heteroatom positioning on biological activity.

Substituting nitrogen with oxygen in compound **26a** yields a derivative with similar yet opposing activity (Figure 3.29), compound **27a** (Het = 4-oxazolyl, 26.92 ± 10.24% at 1 nM). In Series **III-b**, the replacement of nitrogen with a stronger HBA improved the positive allosteric modulatory activity, and this trend carries over into Series **III-a**. In this case, both compounds exhibit similar overall activity, but the oxazole derivative displays a positive modulation effect on dopamine at the $D_2R$. Subsequently replacing oxygen with sulfur yields compound **28a** (Het = (4*R*)-thiazolidin-4-yl, 15.84 ± 7.26% at 0.01 nM). Much like the observed effect on Series **III-b**, this substitution leads to a reduction in the modulatory activity of compound **28a** compared to compound **27a**.

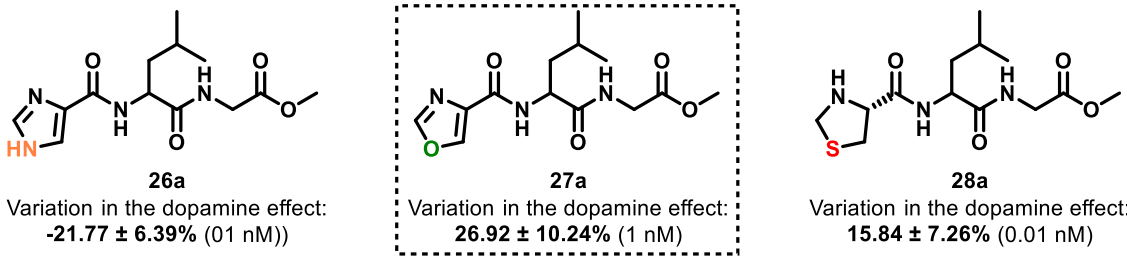



Figure 3.29. SAR analysis of compounds **26a**, **27a**, and **28a**: impact of heteroatom hydrogen bonding strength on biological activity.

Compound **29a** (Het = 2-oxo-2,3-dihydro-1*H*-imidazolidin-4-yl, 15.44 ± 7.04% at 0.01 nM, 22.63 ± 6.66% at 1 nM) is the hydroxyderivative of **26b** (Figure 3.30). The predominant tautomeric form (keto) favors a strong HBA in the form of a carbonyl group and increases the acid character of both NH groups. The improvement in the positive modulation on dopamine effect observed between these two compounds mirrors that seen in Series **III-b** between compounds **26b** and **29b**. Similarly, the removal of the double bond within the ring structure in compound **29a** results in a significant loss of activity in compound **30a** (Het = (4*S*)-2-

USC UNIVERSIDADE DE SANTIAGO DE COMPOSTELA

oxoimidazolidin-4-yl, showing no significant activity). This decline in activity likely arises from the same reasons explained earlier in previous series.

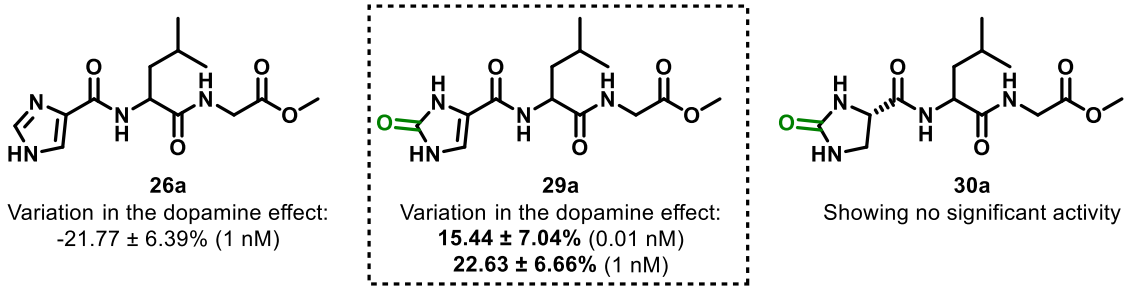



Figure 3.30. SAR analysis of compounds **26b**, **29b**, and **30b**: impact of additional heteroatoms on biological activity.

Parallel to Series **III-b**, the triazole derivative, compound **31a** (Het = 1,2,3-triazol-4-yl, 28.65 ± 5.61% at 0.01 nM, 32.87 ± 1.96% at 1 nM), stands out as the ligand with the most favorable positive allosteric modulatory profile within Series **III-a** (Figure 3.31).

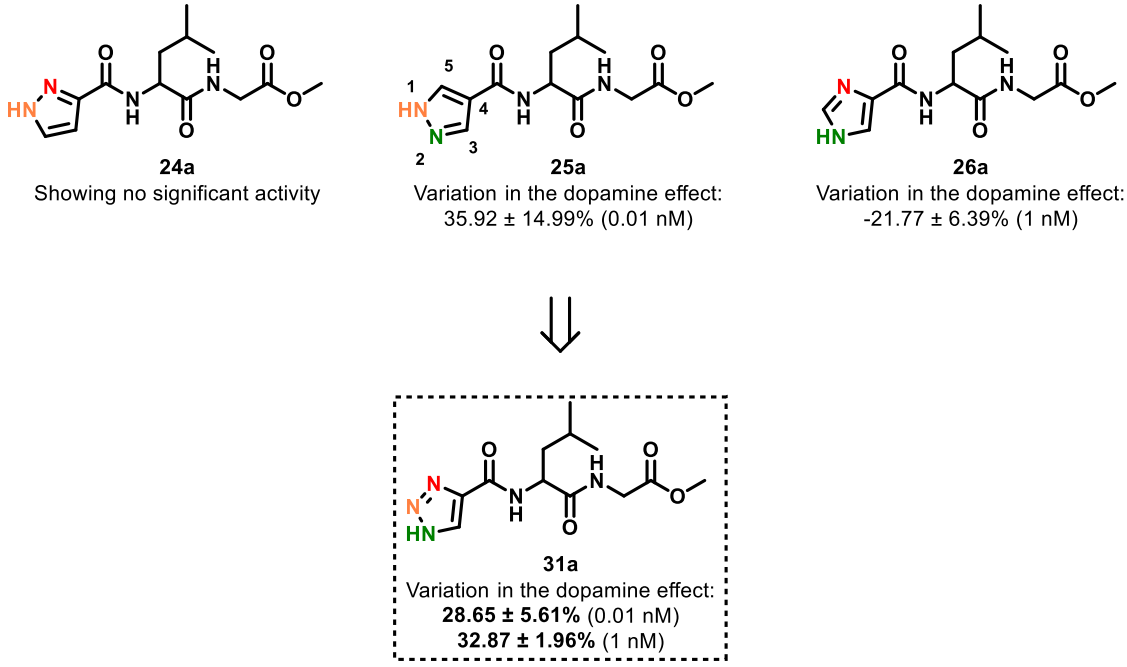



Figure 3.31. SAR analysis of compounds **24a**, **25a**, **26a**, and **31a**: impact of additional heteroatoms within the ring on biological activity.

The inclusion of three nitrogen atoms in the ring structure provides this compound with the highest positive activity within the subset. Compounds **24a**, **25a**, and **26a**, which are analogues of compound **31a** with two nitrogen atoms in the ring structure, all exhibit lower

USC UNIVERSIDADE DE SANTIAGO DE COMPOSTELA

activities, thus reinforcing the idea introduced in Series **III-b** that all three ring positions (1, 2, and 5) contribute to the overall activity.

Finally, the two 6-membered ring derivatives that demonstrated positive modulation of the dopamine effect in Series **III-b** consisted of 4-piperidinyl and phenyl (Figure 3.32).

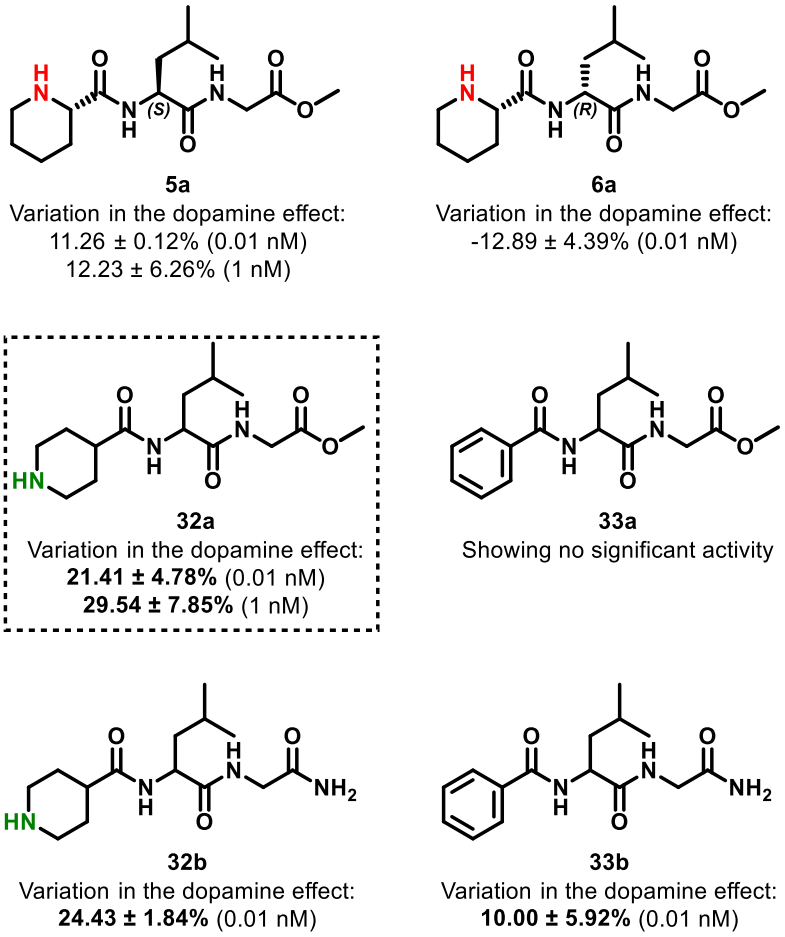



Figure 3.32. SAR and biological activity of 6-membered ring derivatives. Comparison with Series **I** and Series **III-b**.

Compound **32a** (Het = 4-piperidinyl, 21.41 ± 4.78% at 0.01 nM, 29.54 ± 7.85% at 1 nM) exhibits an improved pharmacological profile compared to compound **32b**, displaying remarkable activity at both concentrations. On the other hand, compound **33a** (Het = phenyl, showing no significant activity) does not elicit a significant effect on dopamine activity at the $D_2R$, in contrast to compound **33b**. Furthermore, compound **32a** is structurally analogous to compounds **5a** and **6a** in Series **I**. The difference lie in the stereochemistry (**32a** is a racemic mixture, while Series **I** compounds **5a** and **6a** are pure diastereomers) and the positioning of the nitrogen atom in the ring. This last factor seems to be crucial for achieving activity, as the

USC
DE SANTIAGO
DE COMPOSTELA

pharmacological profile of **32a** is significantly more favorable than that of compounds **5a** and **6a**. This improvement in activity is achieved despite the fact that **32a** is a racemic mixture, and stereochemistry has been shown to be important in modulating dopamine effect. Compounds **5a** and **6a** feature opposing stereochemistry and exhibit inverse activities.

Pyridines (**34a**, **35a**, **36a**) and pyrimidine (**37a**) exhibit reduced effectiveness in Series **III-a** compared to Series **III-b**, although the substituent trends remain unaltered. Thus, compound **34a** (Het = 2-pyridinyl, -14.07 ± 5.04% at 1 nM) displays better pharmacological profile than its analogs **35a** (Het = 3-pyridinyl, showing no significant activity) and **36a** (Het = 4-pyridinyl, 13.85 ± 5.33% at 0.01 nM), and the introduction of a second nitrogen atom in the aromatic ring results in compound **37a** (Het = 2-pyrimidinyl, showing no significant activity), which exhibits no significant variation in the dopamine effect.

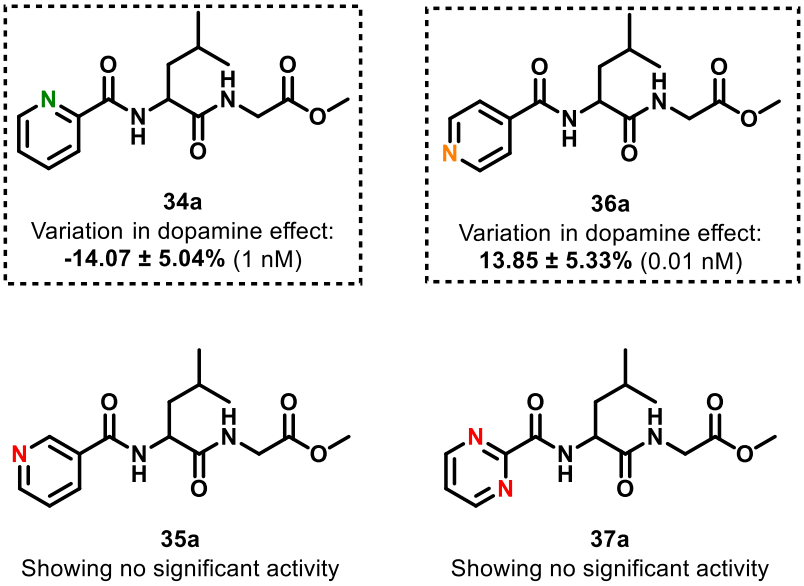



Figure 3.33. SAR analysis of compounds **34a**, **35a**, **36a**, and **37a**: impact of heteroatom positioning on biological activity.

In this case, the 2-pyridine derivative (**34a**) displays an overall similar activity (although opposing) to that of the 4-pyridine derivative. Compound **34a** was selected to explore methylation in the amide adjacent to the ring, as was done with compound **34b** in Series **III-b**. The results are shown in Figure 3.34.

USC
UNIVERSIDADE DE SANTIAGO DE COMPOSTELA

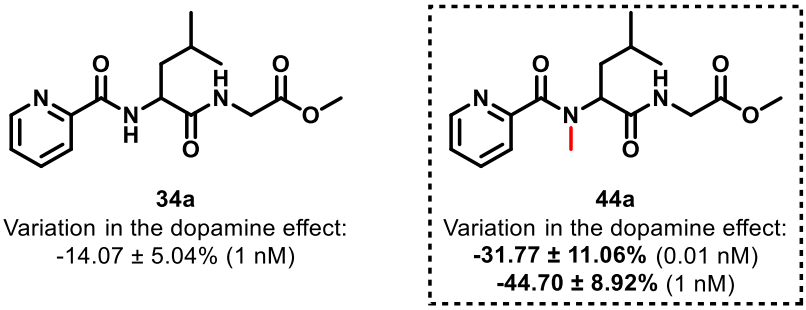



Figure 3.34. SAR analysis of compounds **34a** and **44a**: impact of methylation on biological activity.

Methylating the leucine residue resulted in the formation of compound **44a** which demonstrated significantly enhanced activity at both concentrations. This trend mirrors the findings in Series **I**, where the methylated derivative of melanostatin (compound **3b**) also exhibited enhanced allosteric modulation activity, and in Series **III-b**, where the methylated derivative of compound **34b** (compound **44b**) displayed a more favorable pharmacological profile. These results reinforce the notion that methylation may serve as an effective strategy for improving the activity of allosteric modulators.

The introduction of substituents at the phenyl ring yielded derivatives that negatively modulate the activity of dopamine in Series **III-b**. Likewise, in Series **III-a**, the introduction of bulky substituents to the phenyl ring (Figure 3.35) results in derivatives that substantially reduce the effect of dopamine at the $D_2R$, such as trifluoromethyl in compound **38a** (Het = 3-trifluoromethylphenyl, -34.15 ± 4.24% at 1 nM), an ethoxy group in compound **41a** (Het = 4-ethoxyphenyl, -37.09 ± 3.37% at 1 nM), a 3,4-dimethoxy group in compound **42a** (Het = 3,4-dimethoxyphenyl, -24.20 ± 6.94% at 0.01 nM, -49.51 ± 12.98% at 1 nM), or 2-pyrazol in compound **43a** (Het = 3,4-dimethoxyphenyl, -32.13 ± 4.63% at 0.01 nM, -21.39 ± 6.70% at 1 nM). However, the size of the substituent plays a more significant role on activity in Series **III-a**. In this case, the introduction of two fluorine atoms is insufficient to achieve significant activity in compound **40a**, while substitution with larger residues results in derivatives (compounds **42a** and **43a**) with higher activity than those of Series **III-b**.

USC UNIVERSIDADE DE SANTIAGO DE COMPOSTELA

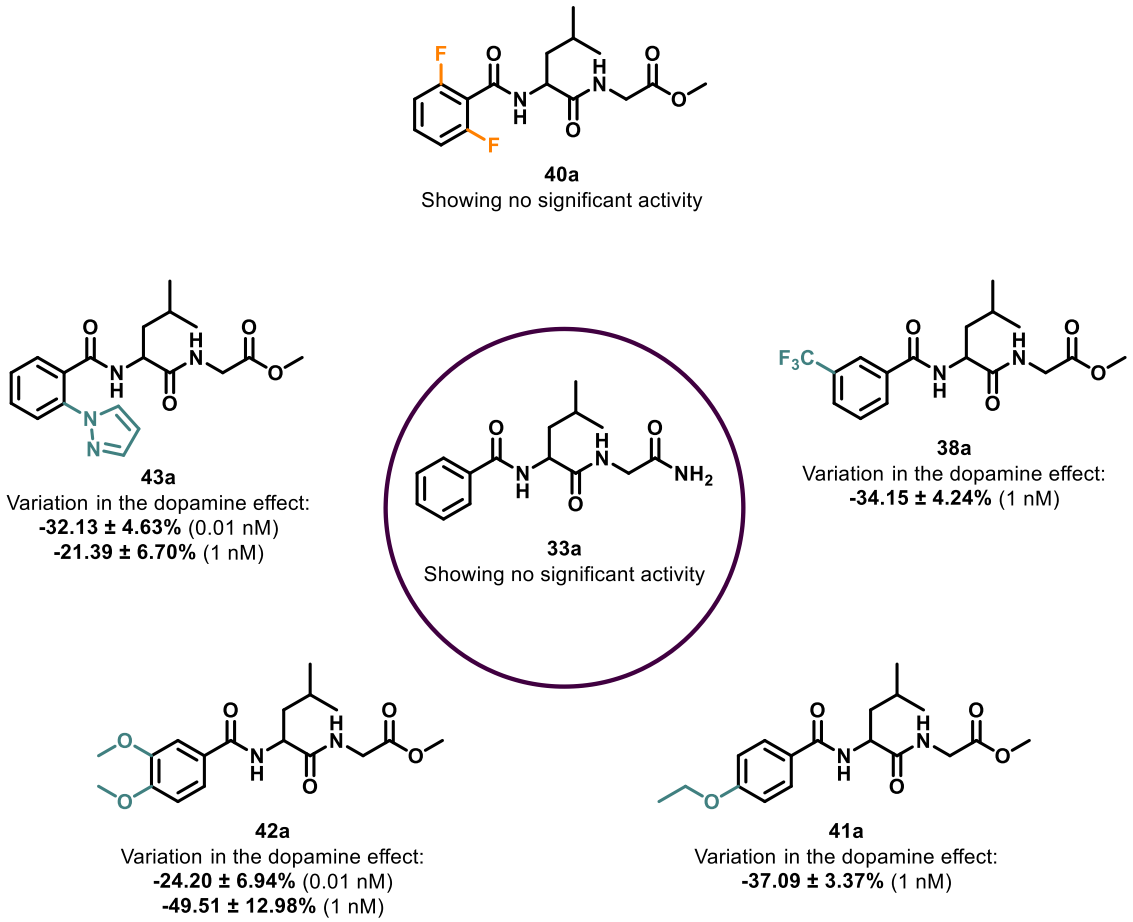



Figure 3.35. SAR analysis of 6-membered ring derivatives: impact of phenyl ring substitution on allosteric modulator activity.

**A PADAM strategy to generate oxo-melanostatin derivatives (Series IV and V)**: These series were developed using the synthetic strategy known as PADAM, which introduces an extra carbon atom within the structure, either with a hydroxy group (Series **IV**) or a carbonyl group (Series **V**) as substituent. Similar structural modifications to those seen in the first three series are also incorporated here, including: the use of proline and two of the most interesting surrogates according to literature (2-pyridine and 3-furane),[63,64] exchanging (*S*)-isobutyl with (*R*)-isobutyl, and replacing the terminal amide with a methyl ester. The main SAR trends found within this subset are summarized below, with a more comprehensive analysis provided later.

USC UNIVERSIDADE DE SANTIAGO DE COMPOSTELA

1. The structural scaffold resulting from the PADAM synthetic route shows a clear tendency to yield compounds that clearly potentiate the dopamine effect.
2. Hydroxyamide derivatives provide compounds with a better pharmacological profile than ketoamides in the L-proline subset.
3. (*S*)-isobutyl exhibited a better pharmacological profile than (*R*)-isobutyl in the 2-pyridine subset.

Within these series, a noticeable trend emerges as the majority of compounds positively modulate the effect of dopamine at the $D_2R$, specially at 1 nM. This tendency contrasts with that observed in Series **III**, where the presence of bulky aromatic heterocycles at position $R^1$ generally lead to a reduction in dopamine effect. The consistent positive modulation of dopamine activity in Series **IV** and **V** underscores the success of the structural modification involving the introduction of an additional carbon atom as an effective scaffold for achieving positive allosteric modulator activity. For instance, among the 24 derivatives in these series, only four compounds showed no significant activity at neither concentration.

Comparisons between melanostatin and the corresponding oxidized PADAM product with the same substitution ($R^1$ = L-proline, (*S*)-isobutyl, X = $NH_2$) are not meaningful since compound **51b** does not show significant allosteric activity (Figure 3.36).

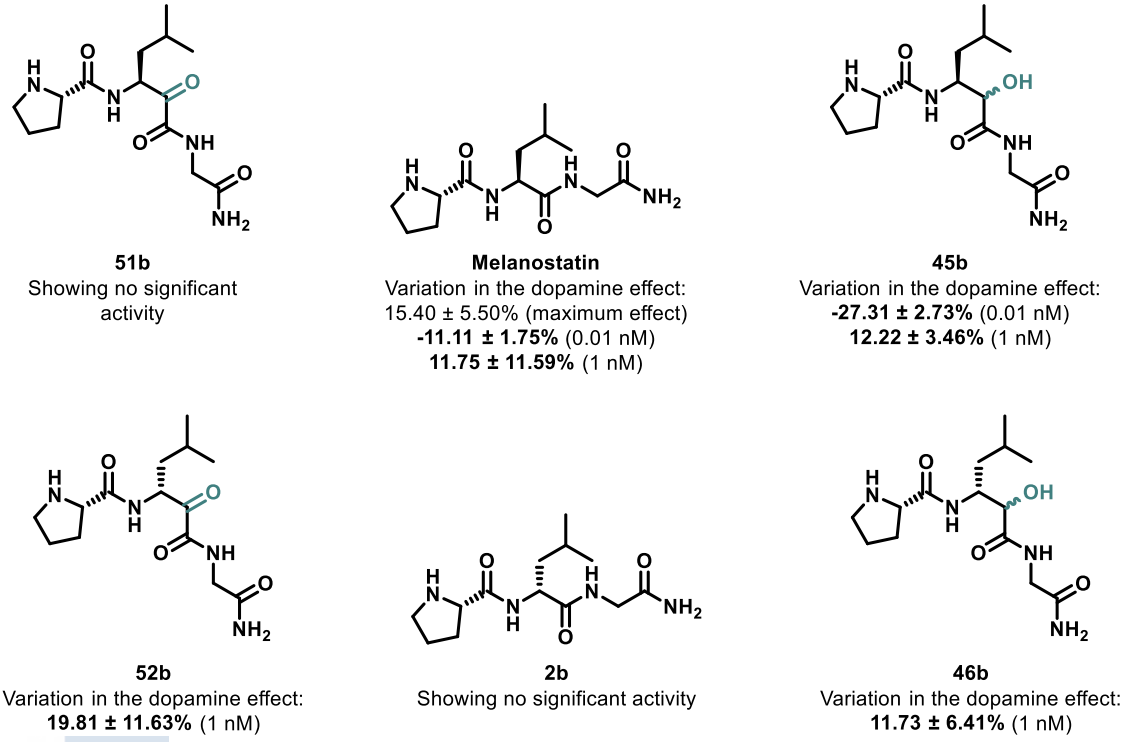
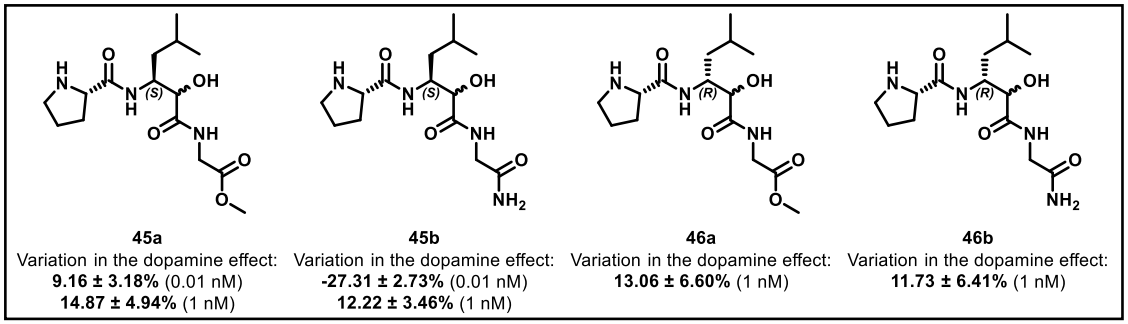



Figure 3.36. Retention of the allosteric modulator activity in the PADAM derivatives of melanostatin.

However, the hydroxyamide derivative **45b** (-27.31 ± 2.73% at 0.01 nM, 12.22 ± 3.46% at 1 nM) demonstrates a greater reduction in dopamine activity at 0.01 nM compared to melanostatin, while exhibiting similar activity at 1 nM (Figure 3.36). This observation further highlights the effectiveness of the PADAM approach and the introduction of an additional carbon atom into the structure in retaining the allosteric modulator profile. The corresponding diastereomer pairs that feature (*R*)-isobutyl substitution, compounds **46b** (11.73 ± 6.41% at 1 nM) and **52b** (19.81 ± 11.63% at 0.01 nM), both demonstrate the ability to enhance the dopamine effect (Figure 3.36). This stands in contrast to the (*R*)-isobutyl diastereomer of melanostatin, compound **2b**, which showed no significant activity. Notably, while **46b** exhibits a comparable effect to melanostatin, **52b** demonstrates even higher activity at lower concentrations (Figure 3.36).

Similar to Series **I** and Series **II**, the methyl ester form of these derivatives yields more favorable results in terms of increasing the dopamine effect (Figure 3.37).



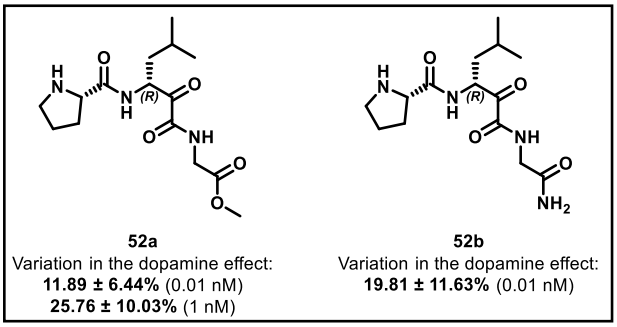




Figure 3.37. SAR analysis of L-proline derivatives in Series **IV** and **V**.

Compounds **45a** (9.16 ± 3.18% at 0.01 nM, 14.87 ± 4.94% at 1 nM) and **46a** (13.06 ± 6.6% at 1 nM) exhibit activities at 1 nM comparable to that of melanostatin, with compound **45a** displaying activity even at a lower concentration. Additionally, compound **52a** (11.89 ± 6.44% at 0.01 nM, 25.76 ± 10.03% at 1 nM) surpasses the efficacy of melanostatin at 1 nM and also enhances the dopamine effect at 0.01 nM (Figure 3.37).

USC UNIVERSIDADE DE SANTIAGO

Overall, the hydroxyamide derivatives within the L-proline subset of Series **IV** and **V** display a more favorable pharmacological profile, with all four derivatives demonstrating activity at least at one concentration (Figure 3.37). In contrast, the two (*S*)-isobutyl carboxamides do not exhibit significant activity. Both methyl ester and unsubstituted terminal amide yield an equal number of active compounds, although methyl ester derivatives display activity at a lower concentration. Finally, the (*R*) configuration at the isobutyl residue appears to offer a slightly advantageous pharmacological profile, as (*S*)-isobutyl carboxamides fail to significantly modulate the activity of dopamine on the $D_2R$ However, it is noteworthy that the (*S*)-isobutyl derivatives do display activity at a lower concentration compared to their (*R*) counterparts.

The 2-pyridine heterocycle serves as a proline surrogate in Series **IV** and **V**, parallel to Series **III**, allowing for direct comparisons between the Ugi adducts and the PADAM products. In Series **III**, enantiomeric separation of the stereocenter resulting from the Ugi reaction was performed, revealing a slight preference for the (*S*)-isobutyl configuration. This preference is upheld in the current series, where the (*S*) configuration at this residue yields superior results for the hydroxyamide derivatives **47a** (16.70 ± 4.66% at 1 nM) and **47b** (39.07 ± 4.37% at 1 nM) compared to the (*R*)-derivatives **48a** (7.11 ± 2.26% at 1 nM) and **48b** (15.00 ± 5.21% at 1 nM), including the compound exhibiting the highest increase in the dopamine effect of this subset, compound **47b (**Figure 3.38**)**.

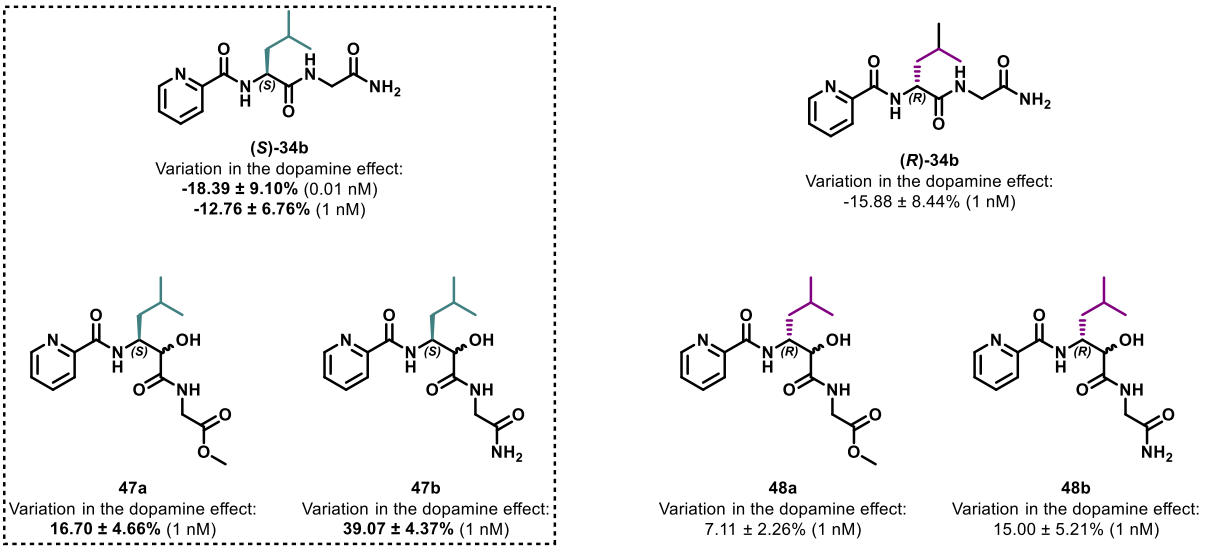



Figure 3.38. SAR analysis of 2-pyridinil derivatives in Series **IV**: impact of the isobutyl residue configuration on biological activity, and comparison with Series **III**.

In the case of carboxamides, a similar trend is observed (Figure 3.39). Compounds **53a** (18.16 ± 6.16% at 0.01 nM, 13.52 ± 3.64% at 1 nM) and **53b** (25.92 ± 5.14% at 0.01 nM) both significantly enhance the dopamine effect at 0.01 nM, a concentration at which melanostatin reduces the dopamine effect. Conversely, compound **54a** (12.12 ± 7.18% at 1 nM) exhibits a lower enhancement of dopamine activity, while compound **54b** (-18.48 ± 4.34% at 1 nM) demonstrates a reversal of the effect.

Comparisons of hydroxyamide derivatives (Series **IV**) with ketoamide derivatives (Series **V**), and of methyl ester derivatives with unsubstituted terminal amide derivatives, reveal no discernible differences in their pharmacological profiles, as all substituents result in derivatives with similar activities. However, in Series **III**, both methyl ester and unsubstituted terminal amide derivatives with 2-pyridinil substitution at position 1 reduced the dopamine effect. In these series, the introduction of an additional carbon atom resulted in a reversal of this trend, generally yielding allosteric modulators that enhance the dopamine effect. This inversion illustrates the overall tendency discussed at the beginning of the analysis of Series **IV** and **V**, which primarily consist of derivatives that increase the effect of dopamine on the $D_2R$.

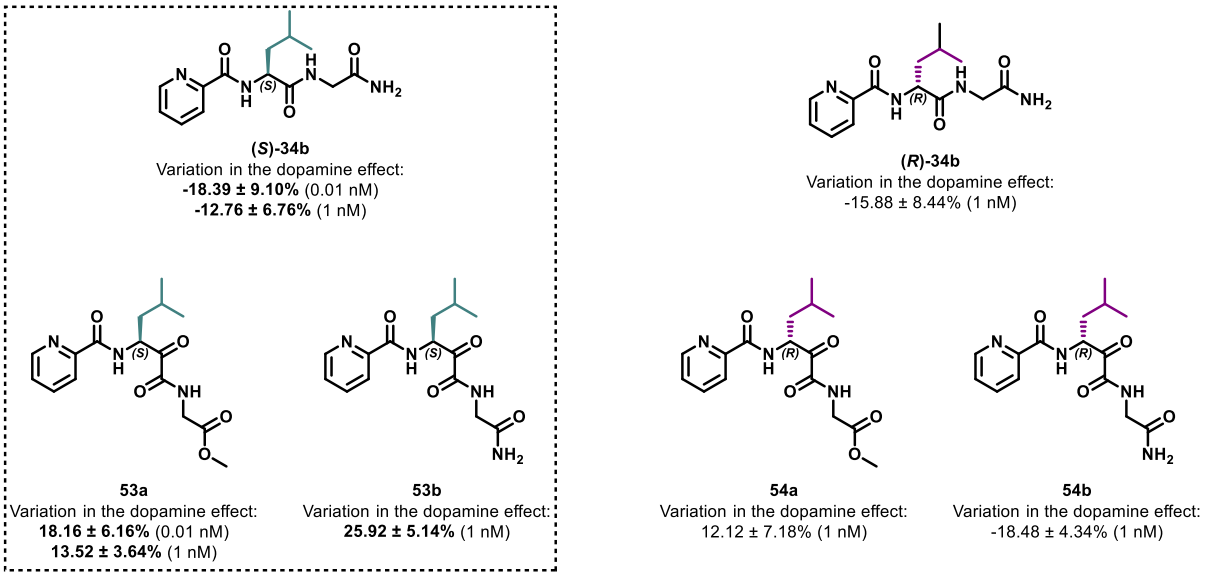
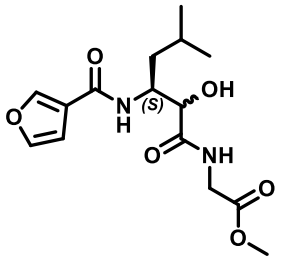


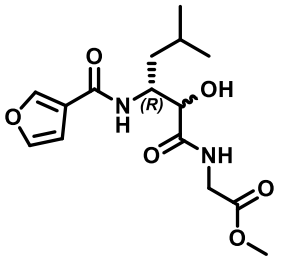

Figure 3.39. SAR analysis of 2-pyridinil derivatives in Series **V**: impact of the isobutyl residue configuration on biological activity, and comparisons with Series **III**.

USC UNIVERSIDADE DE SANTIAGO DE COMPOSTELA

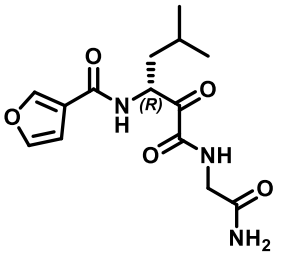
Derivatives featuring 3-furyl as a proline surrogate exhibit a wide range of results that do not conform to any of the trends observed thus far. In this subset, both (*S*) and (*R*) isobutyl configurations, as well as both methyl ester and unsubstituted terminal amide, produce favorable results without a clear discernible pattern. For instance, compound **49a** (8.83 ± 3.23% at 0.01 nM, 28.25 ± 0.11% at 1 nM) represents one of the highest enhancements of the dopamine effect within the series, while also exhibiting positive activity at 0.01 nM. Its (*R*) counterpart, compound **50a** (14.59 ± 7.24% at 0.01 nM), exhibits a positive modulation of the dopamine effect at the lowest concentration, as does the unsubstituted terminal amide derivative, compound **50b** (22.03 ± 8.50% at 0.01 nM).



**49a**
Variation in the dopamine effect:
**8.83 ± 3.23%** (0.01 nM)
**28.25 ± 0.11%** (1 nM)



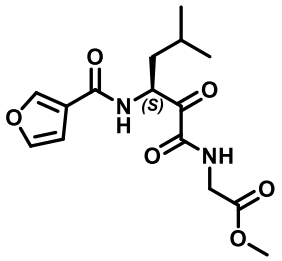
**50a**
Variation in the dopamine effect:
**14.59 ± 7.24%** (0.01 nM)



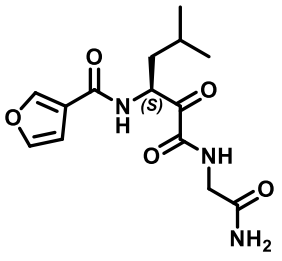
**50b**
Variation in the dopamine effect:
**22.03 ± 8.50%** (0.01 nM)

Figure 3.40. SAR analysis of 3-furyl derivatives in Series **IV.**

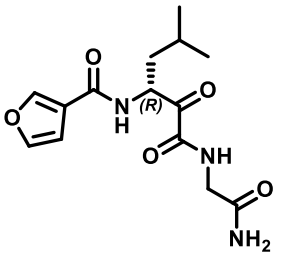
Among the carboxamides, compound **55a** (-23.29 ± 7.87% at 0.01 nM, 13.16 ± 5.25% at 1 nM) demonstrates a profile similar to melanostatin, decreasing the dopamine effect at 0.01 nM and enhancing it at 1 nM, with comparable values. Additionally, compound **55b** (12.19 ± 6.86% at 1 nM) increases the dopamine effect at 1 nM in a manner similar to melanostatin, while compound **56b** (3.31 ± 0.06% at 0.01 nM) exhibits activity at 0.01 nM.



**55a**
Variation in the dopamine effect:
**-23.29 ± 7.87%** (0.01 nM)
**13.16 ± 5.25%** (1 nM)



**55b**
Variation in the dopamine effect:
**12.69 ± 6.86%** (1 nM)



**56b**
Variation in the dopamine effect:
**3.31 ± 0.06%** (0.01 nM)

Figure 3.41. SAR analysis of 3-furyl derivatives in Series **V.**

USC DE SANTIAGO DE COMPOSTELA

Series **III** also employed 3-furyl as a proline surrogate, allowing for direct comparisons between the Ugi adduct and derivatives in the current series (Figure 3.42). The general trend observed is a reversal of the effect, transitioning from a negative modulation of the dopamine effect in compound **22a** to an enhancement of its activity in compounds **49a**, **50a**, and **55a**. This tendency has consistently been observed throughout Series **IV** and **V**. In terms of effectiveness, there is an improvement in compound **49a** at 1 nM, but overall, these derivatives modulate the effect of dopamine in a similar manner.

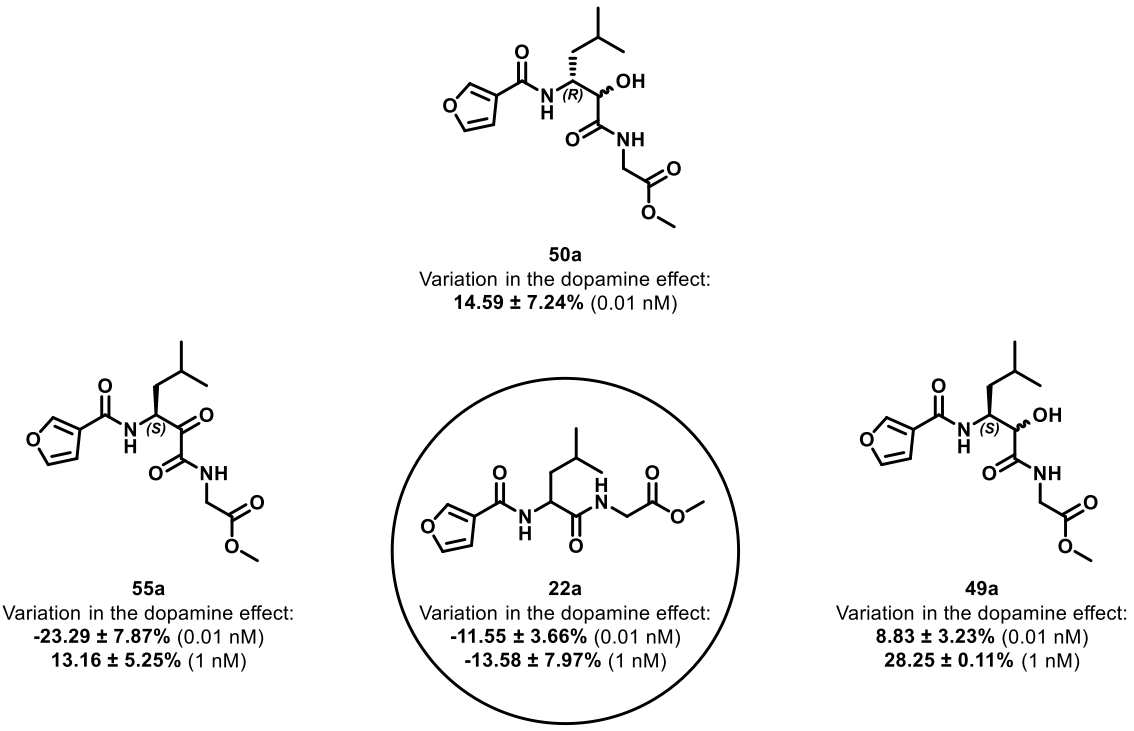
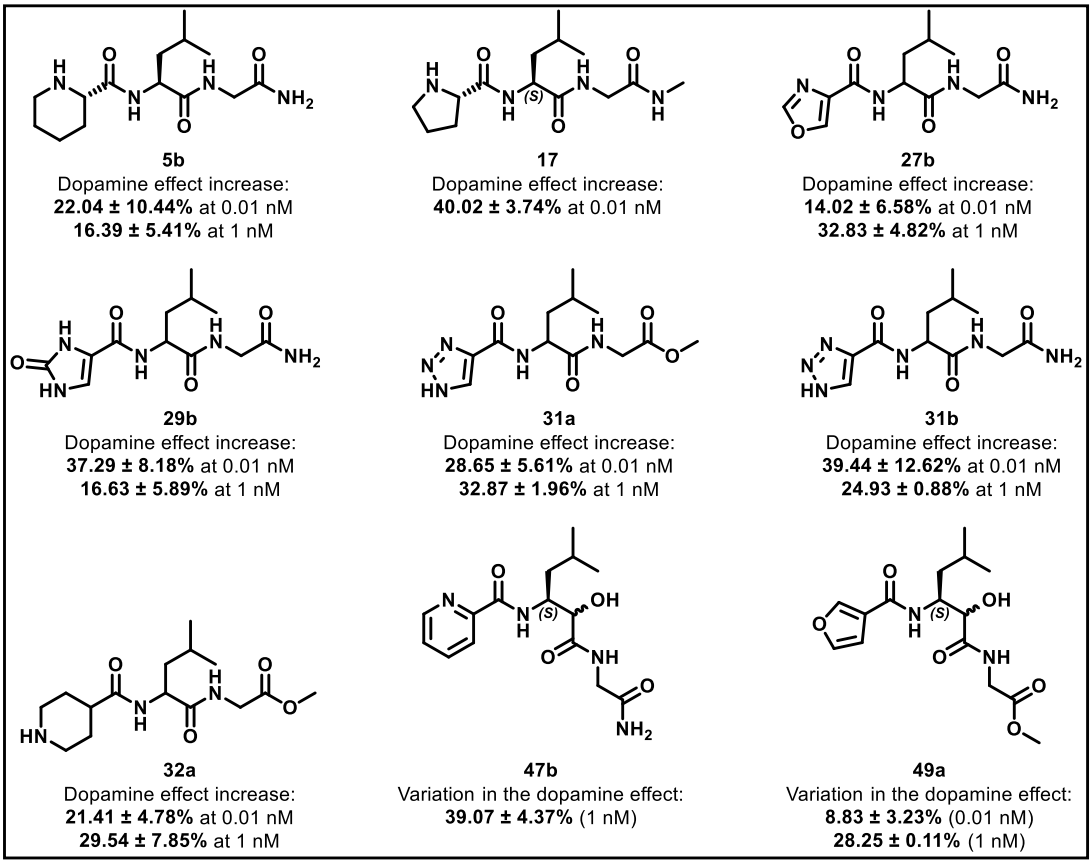



Figure 3.42. Comparisons between 3-furyl derivatives from Series **III** and Series **IV** and **V**.

In conclusion, we have successfully demonstrated the feasibility of using multicomponent reactions to synthesize melanostatin analogues in Series **I** and **II**, identifying several ligands with allosteric modulation effectiveness equal to or greater than melanostatin at the tested concentrations. Building on the pioneering work of Sampaio-Dias's group, we have discovered new heterocycles and aromatic heterocycles as proline substitutes, resulting in derivatives that effectively modulate dopamine activity both positively and negatively. Moreover, the PADAM synthetic route has emerged as an effective strategy for producing melanostatin analogues that positively modulate dopamine activity, in both hydroxyamide and ketoamide forms. The most successful compounds obtained in this chapter are depicted below.



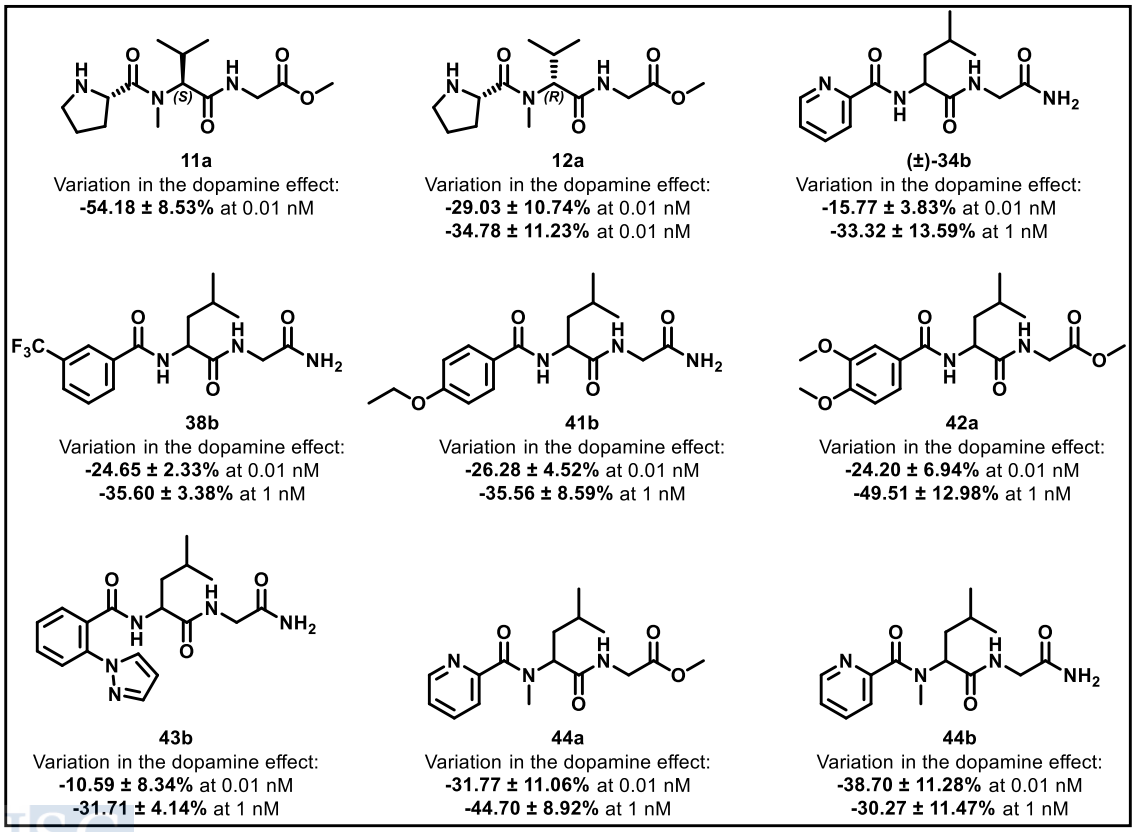




Figure 3.43. Structure and pharmacological data of the most attractive compounds of Chapter I.

## 3.2 CHAPTER II

Cannabis, originated in central Asia, holds the distinction of being one of humanity's earliest known psychotropic substances.[134] Its multifaceted utility, encompassing both recreational and medical purposes, has catalyzed sustained research endeavors aimed at unraveling the intricacies of the endocannabinoid system—a captivating native responder to this remarkable compound.[134,135] Cannabinoids are pharmacologically active components of cannabis (phytocannabinoids) and synthetic ligands that interact with two known subtypes of cannabinoid receptors, $CB_1R$ and $CB_2R$.[135] Activation of $CB_1R$, expressed mainly in the nervous system, has been reported to produce anxiolytic, analgesic, neuroprotective, and anti-nausea effects, and its ligands have been proposed for therapeutic use.[71] However, psychotropic adverse effects induced by the activation of $CB_1R$ by ligands limit their therapeutical applications.[136] Conversely, $CB_2R$ is predominantly distributed in peripheral tissues, particularly in the immune and skeletal systems.[84] Pharmaceutical investigations have unveiled the remarkable therapeutic potential of $CB_2R$ ligands across a spectrum of ailments,[136] encompassing immune-related disorders, pain management, inflammation mitigation, osteoporosis treatment, neurodegenerative disease intervention, and cancer therapy. Consequently, $CB_2R$-selective ligands have garnered heightened attention in recent years, largely due to their ability to exert therapeutic effects within the peripheral system while circumventing the influence of the central nervous system. This heightened focus underscores their potential as a promising avenue for pharmaceutical development.[136,137]

The therapeutic opportunities arising from $CB_2R$ modulation have driven the development of selective $CB_2R$ agonists by academic research laboratories or pharmaceutical companies, such as Hoffman-La Roche and Boehringer Ingelheim.[107] Some of these compounds are based on traditional phytocannabinoids, (HU-308, GW405833, JWH-015), while some others are more structurally diverse, such as the $CB_2R$ inverse agonist JTE-907 (Figure 3.44).[136] Despite extensive efforts in the development of $CB_2R$ ligands, they have not yet reached the market. Consequently, the medicinal chemistry community is in need of fresh approaches that will lead to a fitting $CB_2R$ agonist candidate.

USC UNIVERSIDADE DE SANTIAGO DE COMPOSTELA

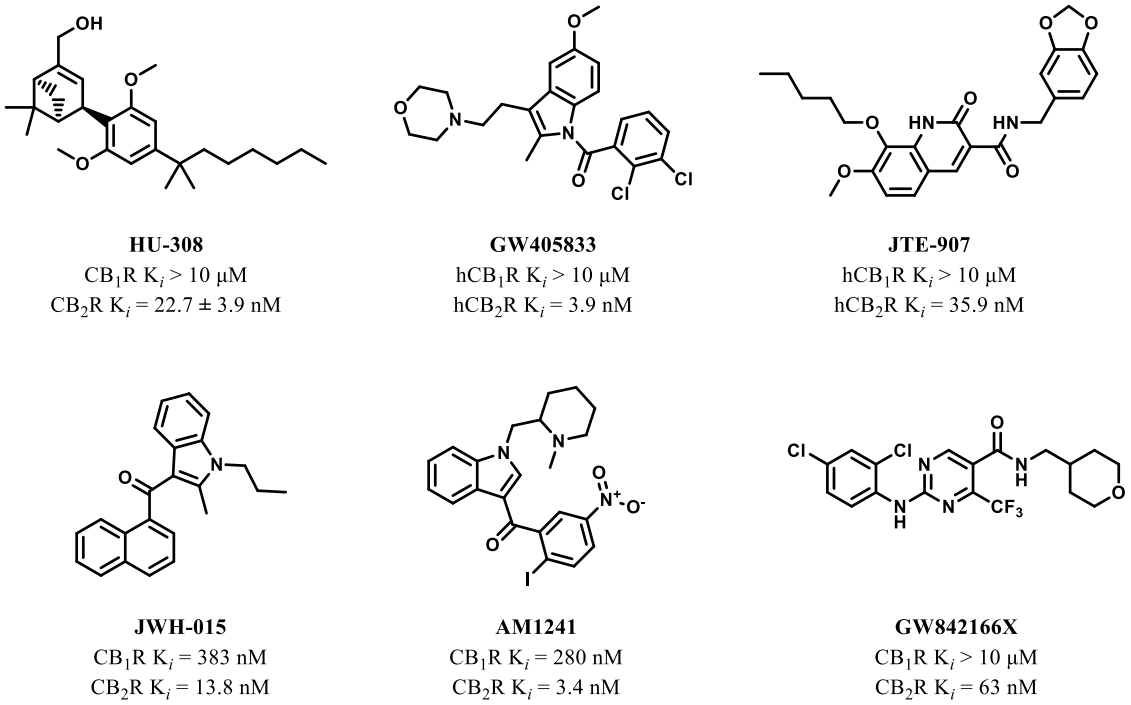



Figure 3.44 Selected examples of traditional (JWH-015) and structurally diverse (JTE-907) $CB_2R$ agonists.

Synthetic cannabinoid receptor agonists (SCRAs) represent one of the most expansive categories within the realm of new psychoactive substances (NPS).[109] Initially conceived for therapeutic purposes,[111] SCRAs have become a major public health concern due to their adverse effects, limited safety profile, evolving structure and diversity.[71] Despite this diversity, a substantial proportion of SCRAs can be categorized under a fundamental Markush structure comprising four discrete subunits: a core group, a linker group, a tail group, and a head group (Figure 3.45).[110]

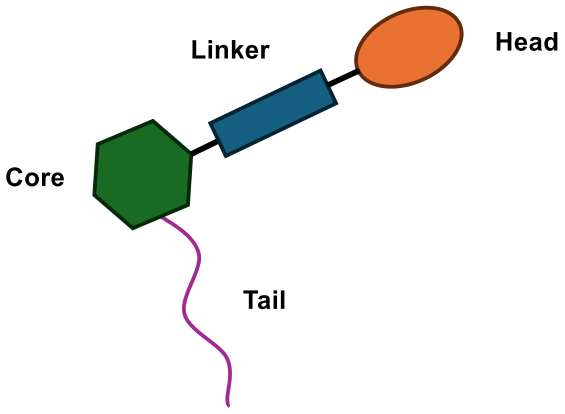



Figure 3.45. Markush representation of SCRAs' chemical structure.

USC UNIVERSIDADE DE SANTIAGO DE COMPOSTELA

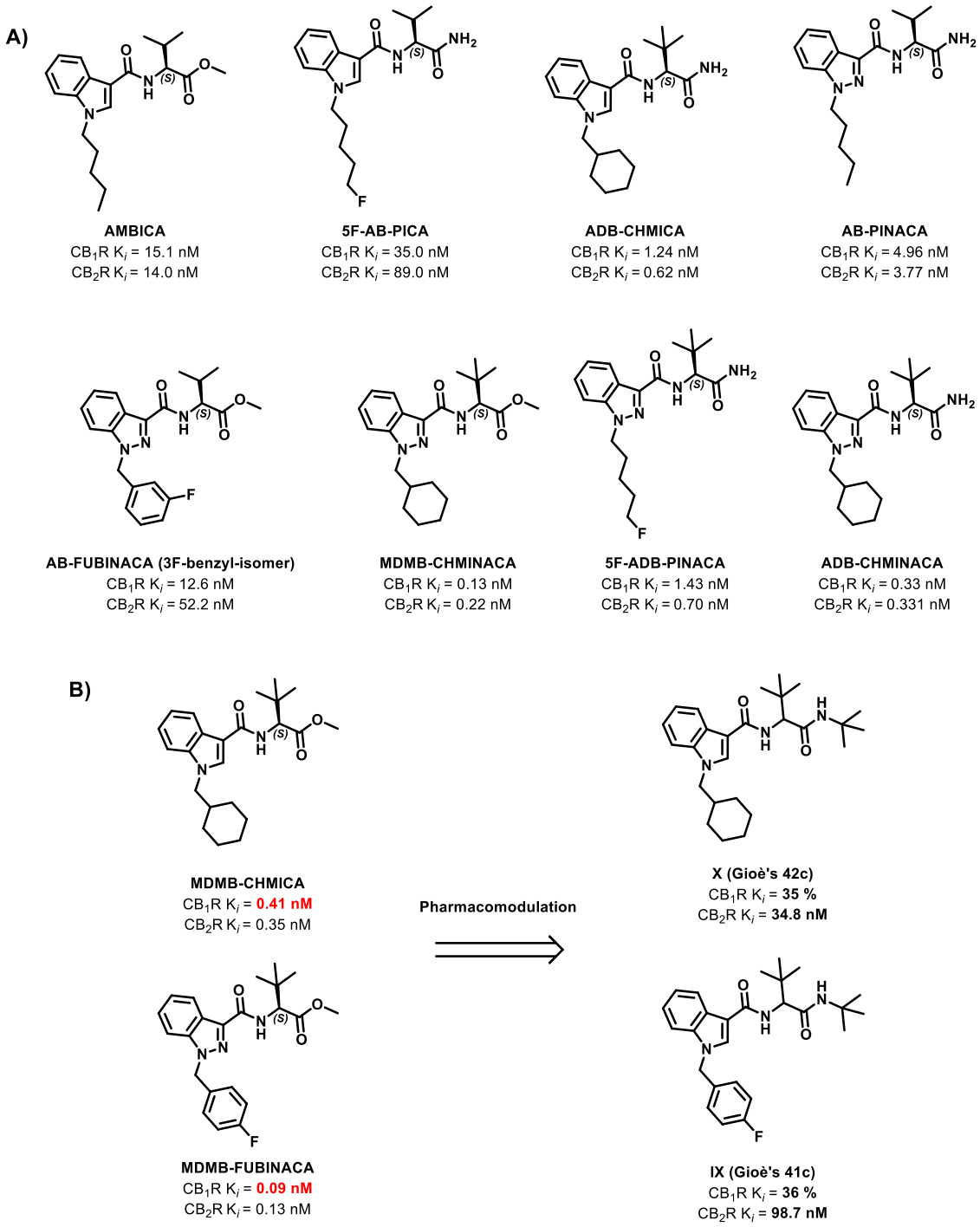



Figure 3.46. A) Representative indole and indazole-based synthetic cannabinoid receptor agonists. B) Ugi-4CR-based pharmacomodulation generating $CB_2R$ selective ligands.

These compounds share a non-selective (promiscuous) $CB_2R$ profile resulting in the activation of the $CB_1R$. Nevertheless, a noteworthy feature is that most of them also function as agonists for the $CB_2R$.[110] Based on the most recently characterized SCRAs scaffolds (Figure 3.46), the ComBioMed group synthesized a broad series of SCRAs analogues aiming

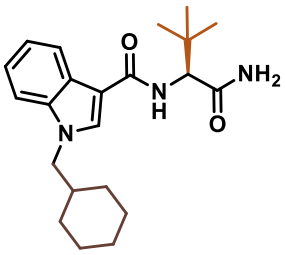
at the development of new $CB_2R$ ligands with improved selectivity towards the $CB_1R$.[71] The library was constructed employing an unexplored multicomponent approach based on the Ugi-4 component reaction that allowed the exploration of four diversity points within the structure. The subsequent pharmacomodulation transformed the promiscuous selectivity profile of the SCRAs into fully selective ligands, while preserving their characteristic potency (Figure 3.46). The results showed the identification of several ligands with remarkably high affinity for the $CB_2R$ ($K_i$ < 100 nM) and complete selectivity towards $CB_1R$,[71] demonstrating the effectiveness of multicomponent approaches in the search of new potent and selective $CB_2R$ agonists.

Therefore, our primary aim in this chapter is to achieve a selective modulation of the $CB_2R$, accomplished through judicious structural modifications in the four subunits that make up their composition, similar to the approach employed by the ComBioMed group in their previous work.

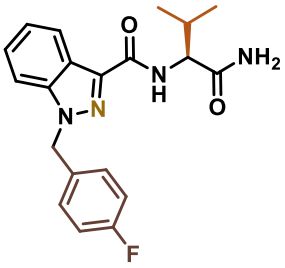
USC UNIVERSIDADE DE SANTIAGO DE COMPOSTELA

### 3.2.1 Design

These novel series were conceived in the context of our ongoing project to develop selective $CB_2R$ agonists, starting from the SCRAs scaffolds represented by ADB-CHMICA and AB-FUBINACA (Figure 3.47) as prototype ligands.

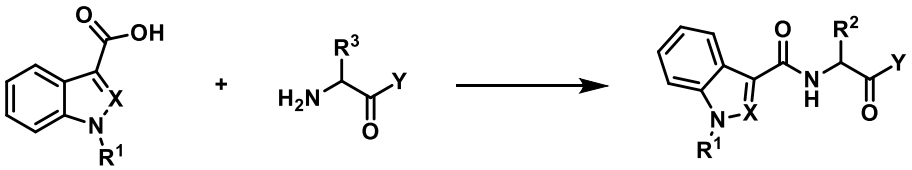


**ADB-CHMICA scaffold**
$CB_1R$ $K_i$ = 1.24 nM
$CB_2R$ $K_i$ = 0.62 nM

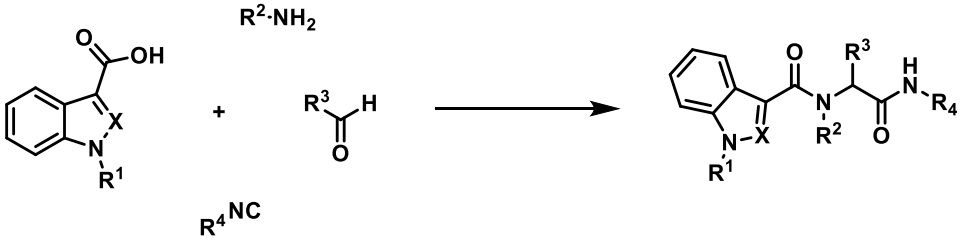


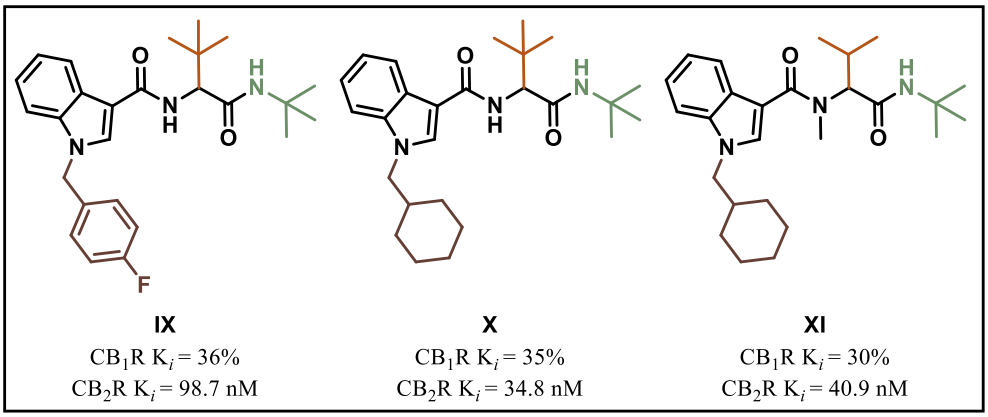
**AB-FUBINACA scaffold**
$CB_1R$ $K_i$ = 0.9 nM
$CB_2R$ $K_i$ = 23.2 nM

**Classical synthetic approach:**



**Ugi-based synthetic approach (Gioè's thesis):**





**IX**
$CB_1R$ $K_i$ = 36%
$CB_2R$ $K_i$ = 98.7 nM

**X**
$CB_1R$ $K_i$ = 35%
$CB_2R$ $K_i$ = 34.8 nM

**XI**
$CB_1R$ $K_i$ = 30%
$CB_2R$ $K_i$ = 40.9 nM

Figure 3.47. Model ligands, diversity points explored, and representative $CB_2R$ selective agonists obtained in the ComBioMed group library created via Ugi-4CR.

Inspired by the successful application of the Ugi-4CR in developing potent and selective $CB_2R$ agonists (Figure 3.47),[71] the MCR-based strategy herein documented (Figure 3.48) was conceived to rapidly assemble large libraries of SCRAs analogues bearing novelty elements (C=O, CHOH), thus enabling the exhaustive exploration of the SAR in these series and the identification of novel $CB_2R$ selective agonists. Different, but conceptually analogous to the Ugi-4CR, the multicomponent reaction employed in this chapter of the Doctoral Thesis is the Passerini reaction, and more specifically the Passerini reaction-amine deprotection-acyl migration (PADAM) strategy.

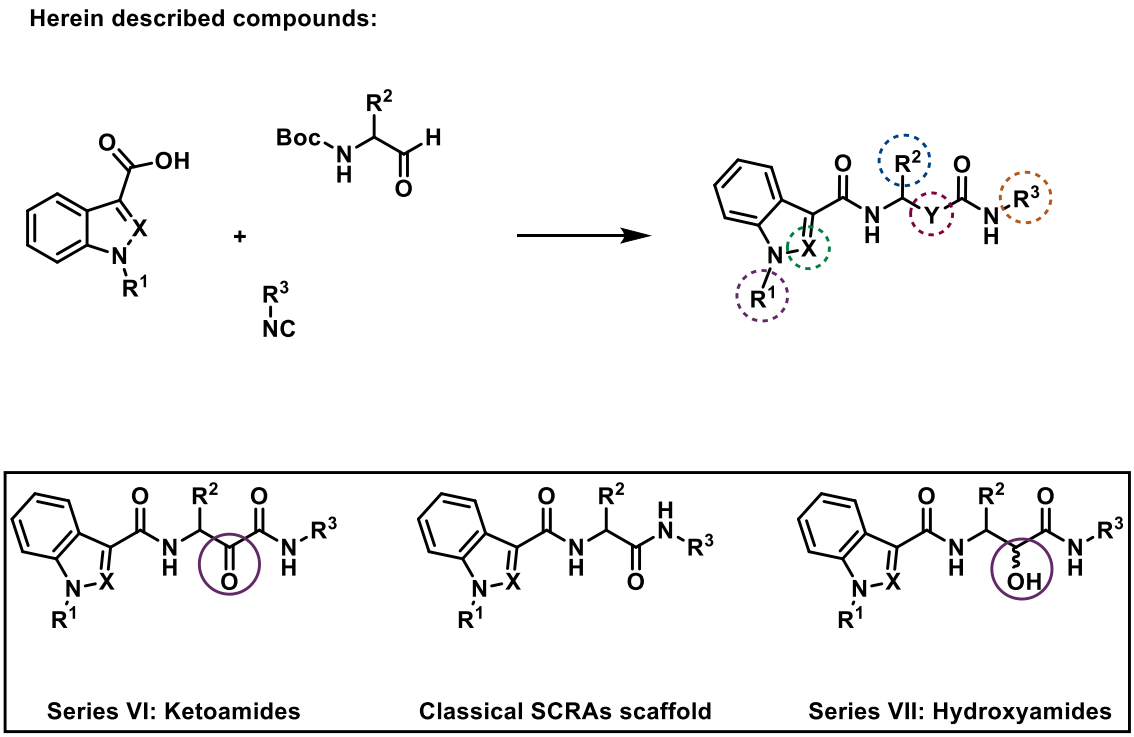



Figure 3.48. Design of Series **VI** and Series **VII** via PADAM synthetic approach and comparison with classical SCRAs scaffold.

From a structural standpoint, the PADAM synthetic route introduces an additional carbon atom in the final product compared to the Ugi adducts synthesized in Gioè's work. This inclusion not only preserves the pharmacophoric elements but also provides an additional point of diversity, enabling modifications and exploration at five different positions.

Based on the published structural information of SCRAs, the new synthetic procedure developed by our group, and the emerging trends in the structure-activity relationships identified during Dr. Gioe's thesis (ComBioMed 2023), in this work we designed two new compound series that contain one additional carbon atom in the exocyclic chain. These new

sets of molecules, namely ketoamides (Series **VI**) and hydroxyamides, (Series **VII**), introduce structural innovation with the potential to enhance the selectivity profile and refine the SAR models within these series. Additionally, the designed compounds can be prepared following the efficient and experimentally simple PADAM sequence studied in Chapter I of this thesis.

To investigate the main SAR trends in both subsets, we selected the most commonly used groups from Figure 3.47 for each diversity point (Figure 3.49). Banister et al. showed that molecules bearing cyclohexyl methyl and 4-fluorobenzyl groups at position 1 of the heterocycle exhibited attenuated affinity for $CB_1R$.[109] Consequently, $R^1$ substitution primarily hinged upon the integration of these two moieties, although a few analogues featuring 5-fluoropentyl and pentyl were also subjected to examination. For $R^2$, we explored substitution with (*S*)-2-aminobutanoic acid, in addition to (*S*)-valinate and (*S*)-*tert*-leucinate, which are the most prevalent linkers within SCRAs, to achieve comprehensive substitution at this position. Among the core groups, indoles yielded the most favorable results based on Gioè's work, and we also introduced indazoles. Finally, $R^3$ was investigated through the incorporation of five different diversities: hydrogen, *tert*-butyl, methoxy carbonyl methyl, benzyl, and 4-morpholinoethyl.

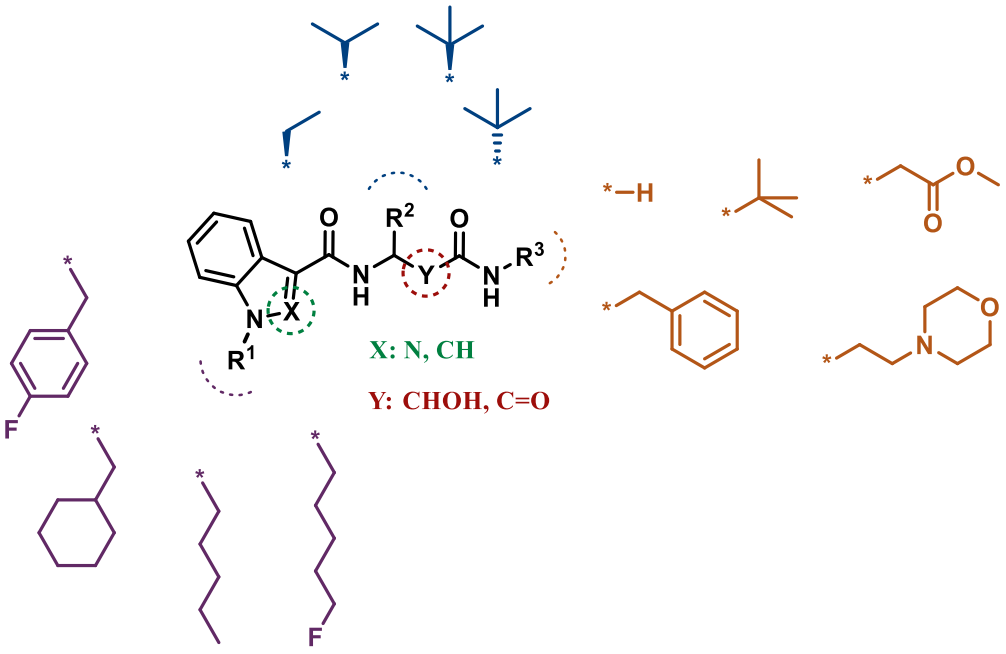



Figure 3.49. General structure and diversity space explored in Chapter II.

Being aware of the significance of a detailed SAR study within this molecular scaffold, we systematically designed all conceivable permutations of the previously delineated

substituents. These exhaustive iterations culminated in two distinct subsets, each comprising 60 molecules. In order to expand the scope of our exploration, we generated specific analogues featuring 5-fluoropentyl and pentyl groups at position 1. In addition, two selected methyl ester derivatives were employed to replace the ester group with an unsubstituted amide. Esters are known to undergo rapid hydrolytic metabolism, and they are typically avoided during the optimization of drug candidates. Nonetheless, their ready availability offers valuable insights into the incorporation of polar substituents within the ligand's structure. Transforming them into amides serves as a conventional approach to address their metabolic challenges. Finally, we assessed the impact of stereochemistry on the pharmacological profile using two distinct approaches, each related to a different stereocenter. We synthesized a set of 16 analogs, all featuring the (*R*) configuration of the most effective linker ($R^2$), *tert*-leucinate, to investigate the influence of configuration at this position. Furthermore, we conducted diastereomeric separation for a subset of hydroxyamide compounds to assess how the orientation of the hydroxy group affects the affinity and selectivity profiles.

USC
UNIVERSIDADE DE SANTIAGO DE COMPOSTELA

### 3.2.2 Chemistry

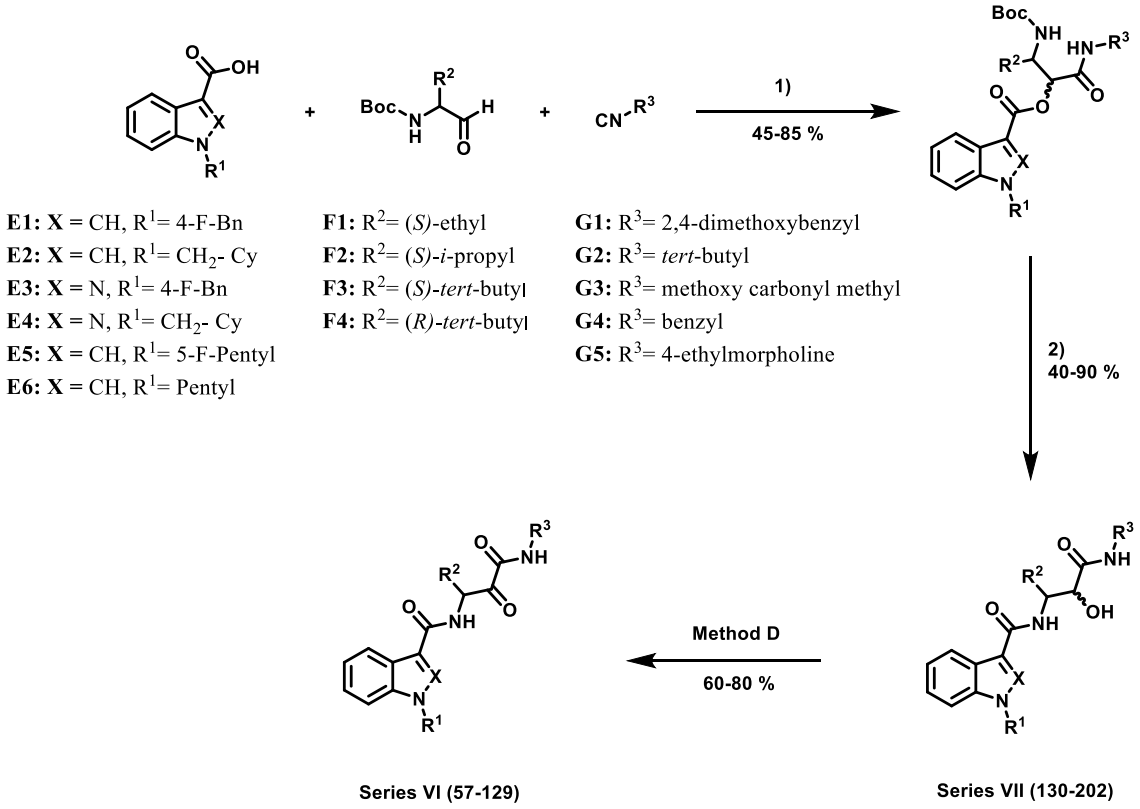
The MCR-based strategy herein documented was conceived to rapidly assemble large libraries of SCRA analogues, thus enabling the exhaustive exploration of the SAR in these series and the identification of novel $CB_2R$ selective agonists. As shown in Figure 3.48 and Figure 3.49, for the design of the new sets of molecules (Series **VI** and Series **VII**) we took advantage of the structural analogy of the SCRAs pharmacophore and the chemical architecture characteristic of the PADAM resulting products (α-hydroxy-β-amino acids or α-oxo-β-amino acids). From a structural point of view, the PADAM synthetic route maintains the pharmacophoric elements, with the linker between the central core and the head of the pharmacophoric model. Additionally, this synthetic strategy introduces one extra carbon atom into the chemical skeleton, with either a carboxy group or a hydroxy group attached, thus allowing the modification and the exploration at five different positions (Figure 3.49).

The *N*-(1-(alkylamino)-2-hydroxy-4-alkyl-1-oxopentan-3-yl)-1-alkyl-1*H*-heteroaryl-3-carboxamides (**130-202**) were obtained as depicted in Scheme 3.17. A three-component synthesis, based on a post-modification of the robust and efficient Passerini reaction (i.e., the three-component reaction of a carboxylic acid, an aldehyde or ketone, and an isocyanide), known as the PADAM synthetic route, enabled a time- and cost-effective assembly of the large collection obtained. A set of 3-carboxylic acid indoles and indazoles (**E1-6**) and α-boc-amino aldehydes (**F1-4**), providing optimal substituents for positions 1 and 2, in combination with five isocyanides (**G1-5**) were employed as precursors (Scheme 3.17). The starting materials, dissolved in DCM, were submitted to orbital stirring at room temperature for 24 to 48 h (Method C, **Series VII**). Once the Passerini reaction had finished, trifluoroacetic acid was added to the mixture and the reaction was stirred at room temperature for an additional 2 h. Following completion, the solution was treated with NaOH 2M and the product was extracted with ethyl acetate. The organic phase was dried over $MgSO_4$ and evaporated under reduced pressure to afford an oil residue, which was purified by column chromatography on silica gel. The targeted hydroxyamide derivatives (Series **VII**) were obtained in moderate to satisfactory yields (20-70%), used as precursors for the synthesis of *N*-(1-(alkylamino)-4-alkyl-1,2-dioxopentan-3-yl)-1-alkyl-1*H*-heteroaryl-3-carboxamides (**57-129**), and employed for pharmacological evaluation.

For the oxidation step, the starting material was dissolved in DMF under inert atmosphere and, at 0 ºC, was treated with Dess-Martin periodinane for 2 h (Method D, **Series VI**). After

USC UNIVERSIDADE DE SANTIAGO DE COMPOSTELA

completion of the oxidation, the solution was treated with $NaHCO_3$ sat. and $Na_2S_2O_3$ (15% aq.) and stirred at room temperature for an additional 15 minutes. The product was extracted with ethyl acetate, and the organic phase was washed with water and brine. The organic phase was dried over $MgSO_4$ and evaporated under reduced pressure to afford an oil residue, which was purified by chromatography on silica gel using MeOH/DCM mixtures. The targeted ketoamides (Series **VI**) were obtained in satisfactory yields (60-80%). All reactions were monitored by thin-layer chromatography (TLC). A detailed description of the synthetic methods and the complete structural, spectroscopic, and analytical data for all compounds are provided in the Experimental Section.




**E1:** **X** = CH, $R^1$= 4-F-Bn
**E2:** **X** = CH, $R^1$= $CH_2$- Cy
**E3:** **X** = N, $R^1$= 4-F-Bn
**E4:** **X** = N, $R^1$= $CH_2$- Cy
**E5:** **X** = CH, $R^1$= 5-F-Pentyl
**E6:** **X** = CH, $R^1$= Pentyl

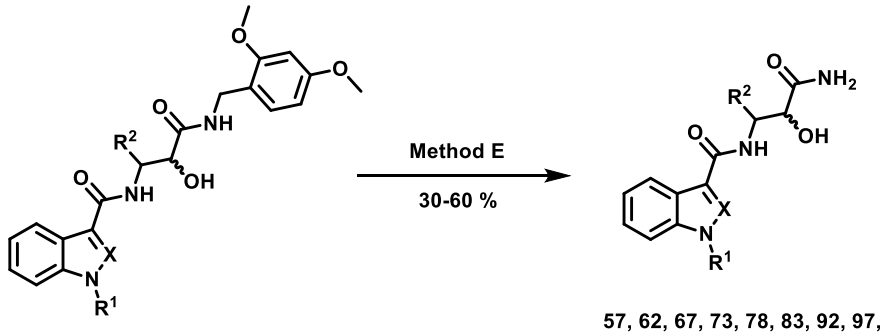
**F1:** $R^2$= (*S*)-ethyl
**F2:** $R^2$= (*S*)-*i*-propyl
**F3:** $R^2$= (*S*)-*tert*-butyl
**F4:** $R^2$= (*R*)-*tert*-butyl

**G1:** $R^3$= 2,4-dimethoxybenzyl
**G2:** $R^3$= *tert*-butyl
**G3:** $R^3$= methoxy carbonyl methyl
**G4:** $R^3$= benzyl
**G5:** $R^3$= 4-ethylmorpholine

Scheme 3.17. PADAM synthetic route to hydroxyamides (Series **VII**) and ketoamides (Series **VI**). Method C) 1) DCM, RT, 24-48 h, 2) TFA, DCM, RT, 2 h. Method D) Dess-Martin periodinane, DMF, 0 ºC, 2 h.

USC UNIVERSIDADE DE SANTIAGO DE COMPOSTELA

An extra step before oxidation (Scheme 3.18) was needed to afford unsubstituted terminal amide derivatives *N*-(1-amino-2-hydroxy-4-alkyl-1-oxopentan-3-yl)-1-alkyl-1*H*-heteroaryl-3-carboxamides (**57, 62, 67, 73, 78, 83, 92, 97, 102, 107, 112, 117, 122-125**) by removing the 2,4-dimethoxybenzyl group. The corresponding PADAM product bearing this protector group was dissolved in toluene, and *p*-toluensulfonic acid was added to the solution. The mixture was magnetically stirred at 110 ºC for 1 h. After completion of the de-benzylation, the solution was treated with $NaHCO_3$, and the product was extracted with ethyl acetate. The organic phase was dried over $Na_2SO_4$ and evaporated under reduced pressure to afford an oil residue, which was purified by chromatography on silica gel using MeOH/DCM mixtures.




**E1: X** = CH, $R^1$= 4-F-Bn
**E2: X** = CH, $R^1$= $CH_2$-Cy
**E3: X** = N, $R^1$= 4-F-Bn
**E4: X** = N, $R^1$= $CH_2$-Cy
**E5: X** = CH, $R^1$= 5-F-Pentyl
**E6: X** = CH, $R^1$= Pentyl

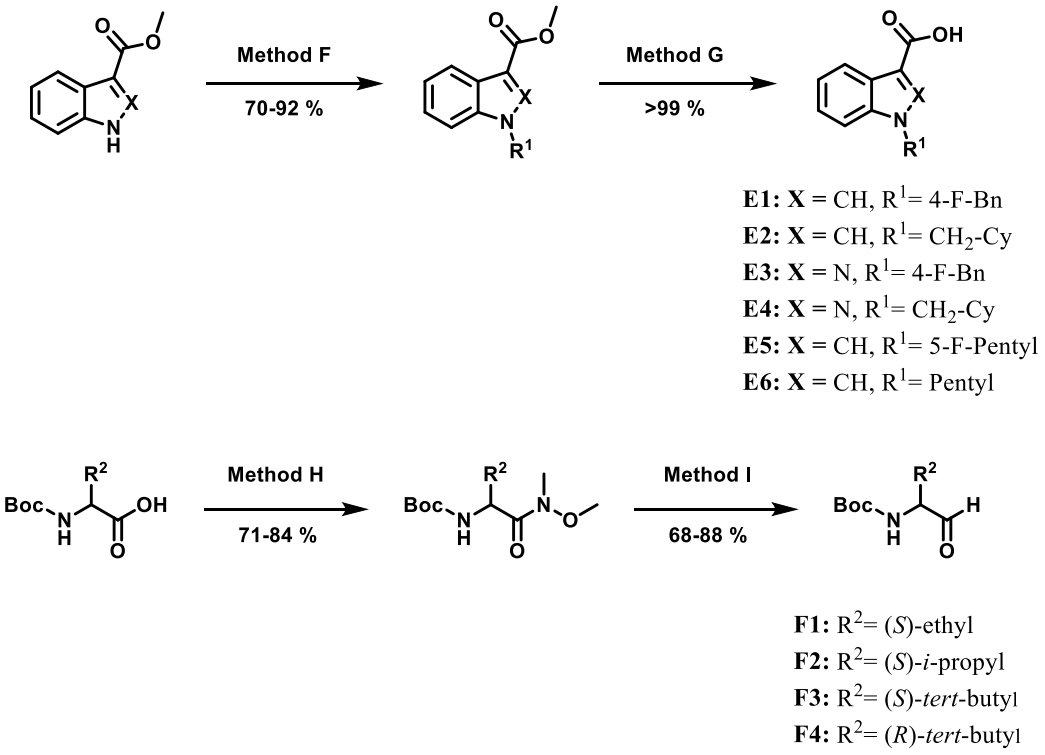
**F1:** $R^2$= (*S*)-ethyl
**F2:** $R^2$= (*S*)-*i*-propyl
**F3:** $R^2$= (*S*)-*tert*-butyl
**F4:** $R^2$= (*R*)-*tert*-butyl

Scheme 3.18. 2,4-dimethoxybenzyl moiety deprotection. Method E) *p*-toluensulfonic acid, toluene, 110 ºC, 1 h.

The required carboxylic acids (**E1**-**E6**) were prepared by saponification of the corresponding *N*-alkylated esters (Scheme 3.19, Method G). The esters were obtained by alkylation of methyl 3-indolecarboxylate and methyl 3-indazolecarboxylate with four alkyl halides under basic conditions (Scheme 3.19, Method F). The two regioisomers obtained during the alkylation of methyl 3-indazolecarboxylate were separated by chromatographic techniques. The unambiguous identity of the major $N^1$-alkylated compound (3:1 ratio) was confirmed by NMR experiments.

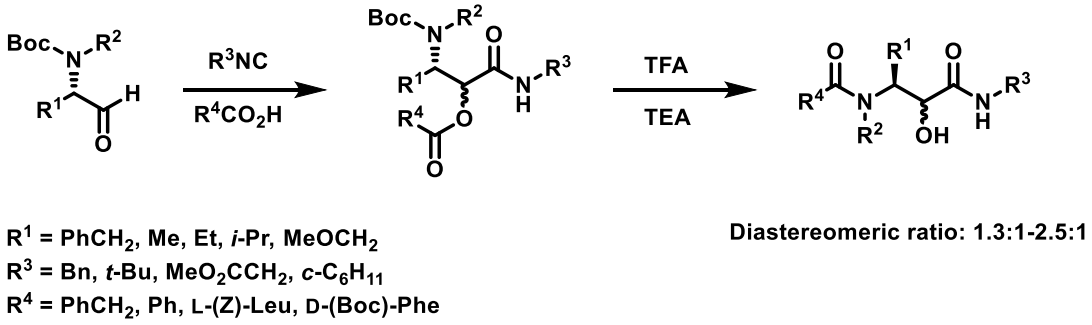
The required α-boc-amino aldehydes (**F1**-**F4**) were prepared by reduction of the corresponding Weinreb amide with lithium aluminum hydride (Scheme 3.19, Method I). The Weinreb amides were obtained by nucleophilic addition of N,O-Dimethylhydroxylamine to the corresponding N-boc-protected amino acid (Scheme 3.19, Method H).

USC UNIVERSIDADE DE SANTIAGO




Scheme 3.19. Synthetic scheme of carboxylic acids **E** and α-boc-amino aldehydes **F**. Method F) Br-$R^1$, NaH, DMF, RT, 24 h. Method G) NaOH, dioxane, 120 ºC, 12 h. Method H) CDI, N,O-dimethyl hydroxylamine, DCM, RT, 24 h. Method I) $LiAlH_4$, THF, -10 ºC, 30 min.

When starting with chiral precursors, some diastereoselectivity may be observed during the Passerini reaction. For example, Banfi et al. studied the diastereoselectivity when using six different *N*-protected α-aminoaldehydes in combination with achiral isocyanides and chiral or achiral carboxylic acids.[126] They found that the diastereoselectivity varied between 1.3:1 and 2.5:1 (Scheme 3.20).




Scheme 3.20. Synthetic procedure and some of the substituents employed by Banfi et al. in their study of PADAM diastereoselectivity.

USC UNIVERSIDADE DE SANTIAGO DE COMPOSTELA

Other groups using the PADAM approach have reported similar diastereoselectivity in the Passerini reaction.[126–128,138–142] The results obtained in our work fit into this range of diastereoselectivity for reactions using α-boc-aminoaldehydes **F1** and **F2**, but the diastereomer rate observed for reactions using the *tert*-butyl derivatives (**F3** and **F4**) is much higher and, to our knowledge, has never been reported without the use of a chiral auxiliar. Representative results from the Passerini reaction of different substrates are shown in Table 3.9.

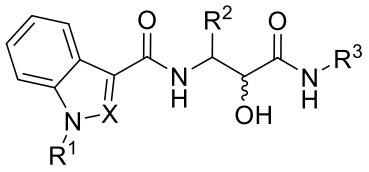



Table 3.9. Diastereomeric ratios for selected compounds.

| CODE | X | $R^1$ | $R^2$ | $R^3$ | RATIO |
|---|---|---|---|---|---|
| **167** | N | 4-F-Bn | (*S*)-Et | $CH_2$-$CO_2Me$ | 26:74 |
| **168** | N | 4-F-Bn | (*S*)-Et | Bn | 34:66 |
| **182** | N | $CH_2$-Cy | (*S*)-Et | $CH_2$-$CO_2Me$ | 32:68 |
| **183** | N | $CH_2$-Cy | (*S*)-Et | Bn | 34:66 |
| **154** | H | $CH_2$-Cy | (*S*)-*i*-Pr | Bn | 22:78 |
| **173** | N | 4-F-Bn | (*S*)-*i*-Pr | Bn | 29:71 |
| **188** | N | $CH_2$-Cy | (*S*)-*i*-Pr | Bn | 25:75 |
| **177** | N | 4-F-Bn | (*S*)-*t*-Bu | $CH_2$-$CO_2Me$ | 9:91 |
| **178** | N | 4-F-Bn | (*S*)-*t*-Bu | Bn | 10:90 |
| **191** | N | $CH_2$-Cy | (*S*)-*t*-Bu | *t*-Bu | 6:94 |
| **193** | N | $CH_2$-Cy | (*S*)-*t*-Bu | Bn | 11:89 |
| **194** | N | $CH_2$-Cy | (*S*)-*t*-Bu | $CH_2CH_2$-Morph | 1:99 |

Given the variety of carboxylic acids and isocyanides employed, and in line with the results of other groups,[138] it is plausible to assume that the prochiral carbonyl compound (α-boc-amino aldehyde) is the main contributor to the observed diastereoselectivity. When possible, the diastereomeric Passerini products were separated by column chromatography prior to deprotection and migration. No racemization of the stereogenic centers was observed during the deprotection-migration sequence, as routinely checked by chiral HPLC.

To explain the stereoselectivity outcome of the Passerini reaction, we propose a rationalization based on treating the reaction as a simple nucleophilic addition of the isocyanide to the α-aminoaldehyde and applying the chelation-controlled Felkin-Anh model. First, we convert the structure of our α-aminoaldehyde into the Newman projection (Figure 3.50):

USC UNIVERSIDADE DE SANTIAGO DE COMPOSTELA

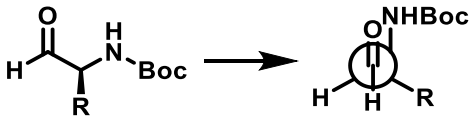



Figure 3.50. Newman projection of α-aminoaldehyde.

Following the Felkin-Anh model, the conformation of the α-substituted carbon for carbonyl conformations must adhere to two rules:

1. Avoid all eclipsed interactions.
2. Have the largest substituent oriented perpendicular to the plane of the carbonyl.

However, as observed for certain simple nucleophilic addition reactions to mono-substituted α-aminoaldehydes,[143] hydrogen bonding between the amine proton and the aldehyde carbonyl oxygen atom stabilizes a different conformation:

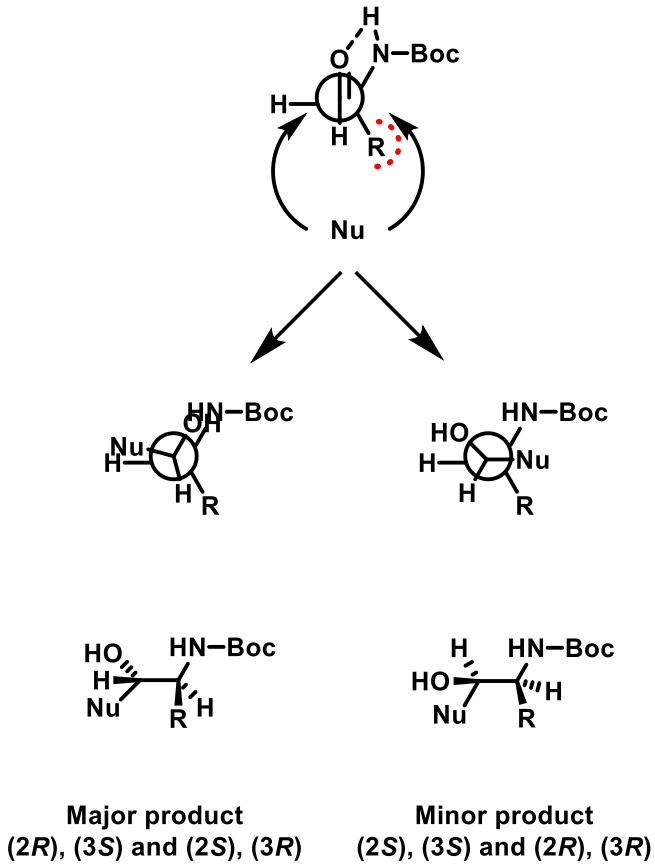
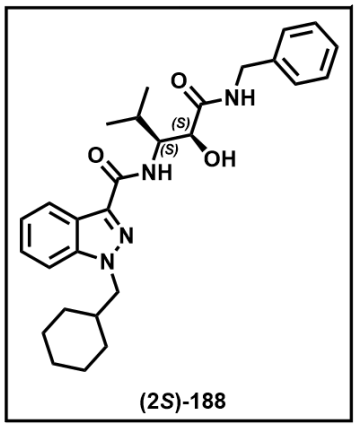



Figure 3.51. Isocyanide nucleophilic attack (Nu) on α-aminoaldehyde most stable conformation.

The nucleophile then attacks the carbonyl at an angle of approximately 107º, which is close to the tetrahedral bond angle. This trajectory approach is termed the Burgi-Dunitz trajectory. Not surprisingly, the nucleophile prefers to attack away from the largest group and

close to the smallest one, resulting in the formation of the *anti*-diastereomer as the preferred product. This model is supported by the work of Riva et al.,[142] who found that the addition of the chelating Lewis acid $ZnBr_2$ to Passerini reactions conducted on an *N*-benzyl-azetidine-derived aldehyde lacking an amino proton also led to the *anti*-Felkin-Anh product. Additionally, the research of Zimuwandeyi et al.,[138] who characterized the major and minor products of the Passerini reaction using α-aminoaldehydes, revealed that, as in our case, the major product was the *anti*-Felkin-Anh product. The R size-dependent stereoselectivity observed in our series could be thus explained with this model.

To gain insights into the impact of stereochemistry on the affinity and selectivity profile of Series **VII**, we evaluated the binding profile of a set of 9 diastereomeric pairs (see Biological Evaluation section). Additionally, unambiguous structural characterization of each diastereomer was carried out through a combination of X-ray diffraction and $^{13}C$ NMR techniques. Single crystal X-ray diffraction confirmed the (*S*)-configuration at the newly formed stereogenic carbon for the **188** minor diastereomer (Figure 3.52 and Experimental Section).



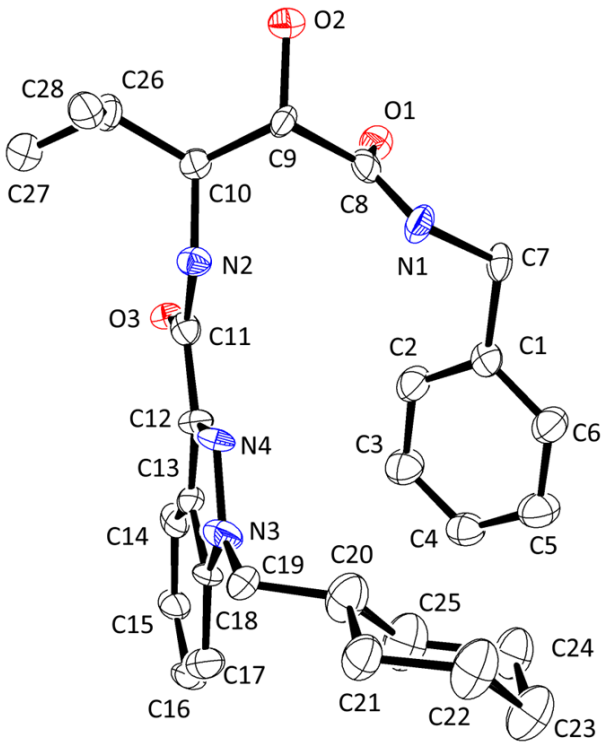




Figure 3.52. Structure and ORTEP diagram (X-ray crystallography) of **(2*S*)-188**.

USC UNIVERSIDADE DE SANTIAGO DE COMPOSTELA

This stereochemistry aligns with that of the *syn* diastereomer, which was predicted to be the minority product according to the Felkin-Anh framework, thereby providing support for the model. To elucidate the stereochemistry of the remaining diastereomer pairs, the assignment is based on the $^{13}C$ NMR chemical shift values observed for the new stereogenic center. Similar to the observations made by Zimuwandeyi et al.[138], this chemical shift value is further upfield for the minor diastereomer than that for the corresponding major diastereomer (Figure 3.53 and Table 3.10), indicating the (*S*) and (*R*) configurations, respectively.

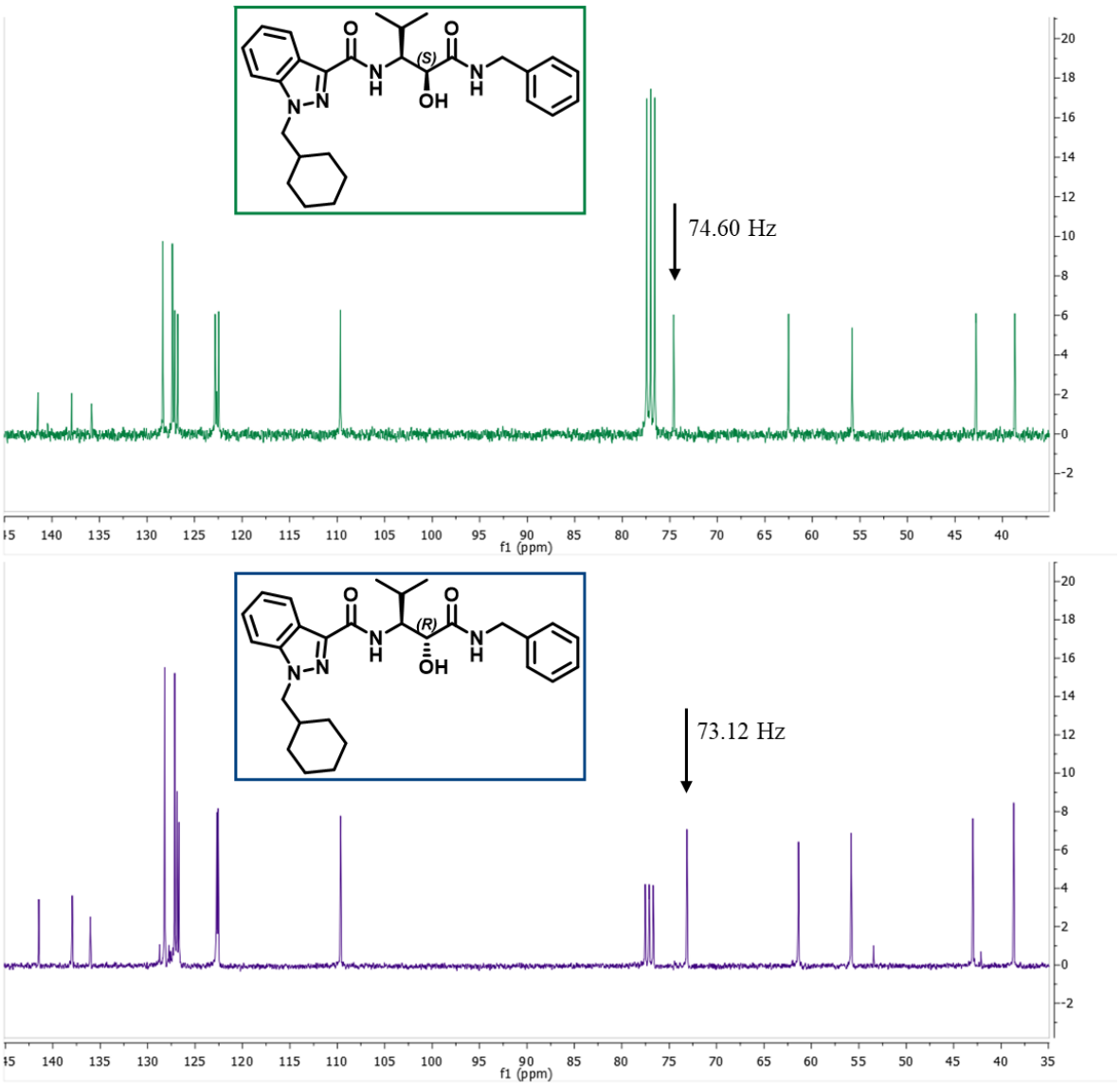



Figure 3.53. Chemical shifts change in the asymmetric carbon between diastereomer pair **(2*S*)-188** (green) and **(2*R*)-188** (blue).

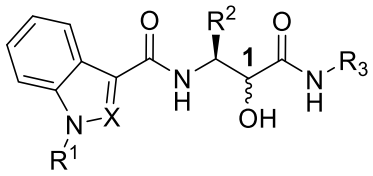


Table 3.10. $^{13}C$ NMR chemical shift values comparison between diastereomeric pairs.

| CODE | Diastereomer | C-1 $^{13}C$ NMR shift (ppm) |
|---|---|---|
| **(2*S*)-168** | Minor | 75.81 |
| **(2*R*)-168** | Major | 74.00 |
| **(2*S*)-182** | Minor | 75.68 |
| **(2*R*)-182** | Major | 73.97 |
| **(2*S*)-183** | Minor | 75.79 |
| **(2*R*)-183** | Major | 74.10 |
| **(2*S*)-173** | Minor | 74.51 |
| **(2*R*)-173** | Major | 72.96 |
| **(2*S*)-188** | Minor | 74.60 |
| **(2*R*)-188** | Major | 73.12 |
| **(2*S*)-177** | Minor | 74.65 |
| **(2*R*)-177** | Major | 71.17 |
| **(2*S*)-178** | Minor | 74.65 |
| **(2*R*)-178** | Major | 71.12 |
| **(2*S*)-191** | Minor | 74.88 |
| **(2*R*)-191** | Major | 71.60 |
| **(2*S*)-193** | Minor | 74.76 |
| **(2*R*)-193** | Major | 71.78 |

The biological evaluation of the selected compounds revealed an improved profile for the diastereomer eliciting the (*R*) configuration at the carbinol center, which displayed a superior affinity profile without affecting selectivity (see Structure-Activity Relationship section). In all nine cases, this diastereomer corresponds to the major product in the PADAM sequence. With this information at hand, it was decided to refine the synthetic procedure and exclusively isolate the eutomer.

USC UNIVERSIDADE DE SANTIAGO DE COMPOSTELA

### 3.2.3 Biological evaluation

The cannabinoid binding profile (affinity and selectivity) of the 158 novel hydroxy carboxamides and ketocarboxamides synthesized in this chapter was evaluated *in vitro* using radioligand binding assays at the two human CBR subtypes. Human CBRs were expressed in transfected cell lines [e.g., Chinese hamster ovary (CHO) cells ($CB_1R$), and human embryonic kidney (HEK-293) cells ($CB_2R$)]. [$^3$H]-CP55940 was employed as radioligand for both receptor subtypes. The binding data for Series **VII** (**130**-**202**) was evaluated using diastereomerically pure hydroxyamides that correspond to the major diastereomer obtained from the PADAM sequence. The binding data is presented as $K_i$ in nM (n = 3) obtained by fitting the data by non-linear regression using Prism 5.0 software (GraphPad, San Diego, CA), or as specific binding inhibition percentage at 1 μM (n = 2) for those compounds that did not reach a minimum of 60 % of radioligand displacement at such concentration. Table 3.13 to Table 3.18 contain the binding data obtained for Series **VI**. Table 3.19 to Table 3.26 contain the binding data obtained for Series **VII**. Table 3.11 and Table 3.12 contain the data of reference compounds from literature or previously obtained by the ComBioMed group for comparison purposes. The original articles detailing the already described compounds are also listed in the corresponding tables. To facilitate the identification of the most salient features of the structure-selectivity relationship throughout the series, the selectivity index (SI), calculated using the affinity data ($K_i$ $CB_1R$/$K_i$ $CB_2R$), is also reported in Table 3.11 to Table 3.26. As previously indicated, ligands bearing an ester group were conceived to be transformed into the corresponding carboxamides, work that is currently in progress in our laboratory.

USC UNIVERSIDADE DE SANTIAGO DE COMPOSTELA

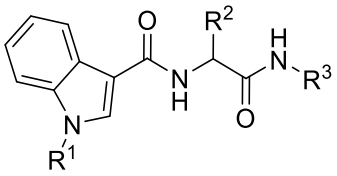


Table 3.11. Structure and cannabinoid receptor affinity data of reference compounds for Series **VI-a**, **VII-a**, **VI-b**, **VII-b**, **VI-c,** and **VII-c**.

| Compound | $R^1$ | $R^2$ | $R^3$ | $K_i$ (nM) or % at 1 μM | | SI |
|---|---|---|---|---|---|---|
| | | | | $hCB_1R$[a)] | $hCB_2R$[b)] | |
| **XV (AB-FUBICA)**[144] | 4-F-Bn | (*S*)-*i*-Pr | H | 35.2 nM | 83.2 nM | 0.42 |
| **XVI**[71] | 4-F-Bn | *i*-Pr | *t*-Bu | 16% | 276 nM | > 100 |
| **XVII**[71] | 4-F-Bn | *i*-Pr | Bn | 10% | 571 nM | > 100 |
| **XVIII (ADB-FUBICA)**[144] | 4-F-Bn | (*S*)-*t*-Bu | H | 53.8 nM | 5.15 nM | 10.4 |
| **XIX**[71] | 4-F-Bn | (*S*)-*t*-Bu | *t*-Bu | 39% | 60.1 nM | > 100 |
| **XX**[71] | 4-F-Bn | *t*-Bu | $CH_2$-$CO_2$Me | 80.6 nM | 15.3 nM | 5.27 |
| **XXI**[71] | 4-F-Bn | *t*-Bu | Bn | 123 nM | 35.8 nM | 3.44 |
| **XXII**[71] | 4-F-Bn | *t*-Bu | $CH_2$-$CH_2$-Morph | 31% | 42.7 nM | > 100 |
| **XXIII (AB-CHMICA)**[145] | $CH_2$-Cy | (*S*)-*i*-Pr | H | 2.43 nM | 35.3 nM | 0.069 |
| **XII**[71] | $CH_2$-Cy | *i*-Pr | *t*-Bu | 38% | 50.2 nM | > 100 |
| **XXIV**[71] | $CH_2$-Cy | *i*-Pr | Bn | 37% | 109 nM | > 100 |
| **XXV (ADB-CHMICA)**[145] | $CH_2$-Cy | (*S*)-*t*-Bu | H | 1.10 nM | 0.76 nM | 1.45 |
| **X**[71] | $CH_2$-Cy | *t*-Bu | *t*-Bu | 59% | 34.8 nM | > 100 |
| **XXVI**[71] | $CH_2$-Cy | *t*-Bu | Bn | 28.4 nM | 7.60 nM | 3.74 |
| **XXVII**[71] | $CH_2$-Cy | *t*-Bu | $CH_2$-$CH_2$-Morph | 108 nM | 13.8 nM | 7.83 |
| **XXVIII**[71] | 5-F-Pentyl | *t*-Bu | *t*-Bu | 26% | 104 nM | > 100 |
| **XXIX**[71] | Pentyl | *t*-Bu | *t*-Bu | 22% | 99.2 nM | > 100 |
| **Surinabant** | - | - | - | 3.00 nM | 400 nM | 0.0075 |
| **GW405833** | - | - | - | 4772 nM | 5.80 nM | 822 |

[a)] Displacement of specific [$^3$H]-CP55940 binding in human CHO cells expressed as $K_i$ in nM (n = 3) or percentage displacement of specific binding at a concentration of 1 $\mu$M (n = 2). [b)] Displacement of specific [$^3$H]-CP55940 binding in human HEK-293 cells expressed as $K_i$ in nM (n = 3) or percentage displacement of specific binding at a concentration of 1 $\mu$M (n = 2).

USC UNIVERSIDADE DE SANTIAGO DE COMPOSTELA

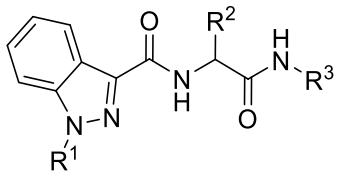


Table 3.12. Structure and cannabinoid receptor affinity data of reference compounds for Series **VI-d**, **VII-d**, **VI-e,** and **VII-e**.

| Compound | $R^1$ | $R^2$ | $R^3$ | $K_i$ (nM) or % at 1 μM | | SI |
|---|---|---|---|---|---|---|
| | | | | $hCB_1R$[a)] | $hCB_2R$[b)] | |
| **XXX (AB-FUBINACA)**[144] | 4-F-Bn | (*S*)-*i*-Pr | H | 2.31 nM | 1.17 nM | 1.97 |
| **XXXI (ADB-FUBINACA)**[144] | 4-F-Bn | (*S*)-*t*-Bu | H | 0.83 nM | 0.14 nM | 5.93 |
| **XXXII (AB-CHMINACA)**[145] | $CH_2$-Cy | (*S*)-*i*-Pr | H | 0.90 nM | 1.10 nM | 0.82 |
| **XXXIII (ABD-CHMINACA)**[145] | $CH_2$-Cy | (*S*)-*t*-Bu | H | 0.98 nM | 0.60 nM | 1.63 |
| **Surinabant** | - | - | - | 3.00 | 400 | 0.0075 |
| **GW405833** | - | - | - | 4772 | 5.80 | 822 |

[a)] Displacement of specific [$^3$H]-CP55940 binding in human CHO cells expressed as $K_i$ in nM (n = 3) or percentage displacement of specific binding at a concentration of 1 $\mu$M (n = 2). [b)] Displacement of specific [$^3$H]-CP55940 binding in human HEK-293 cells expressed as $K_i$ in nM (n = 3) or percentage displacement of specific binding at a concentration of 1 $\mu$M (n = 2).

USC UNIVERSIDADE DE SANTIAGO DE COMPOSTELA

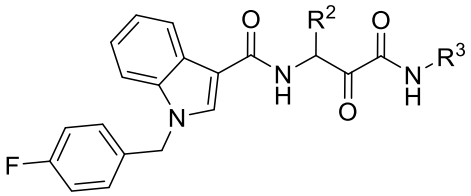


Table 3.13. Structure and cannabinoid receptor affinity data of Series **VI-a** (Cmpds **57-72**).

| Compound | $R^2$ | $R^3$ | Ki (nM) or % at 1 μM | | SI |
|---|---|---|---|---|---|
| | | | $hCB_1R$[a)] | $hCB_2R$[b)] | |
| **57** | (*S*)-Et | H | 315 nM | 44.2 nM | 7.13 |
| **58** | (*S*)-Et | *t*-Bu | 4% | 711 nM | > 100 |
| **59** | (*S*)-Et | $CH_2$-$CO_2Me$ | 5% | 588 nM | > 100 |
| **60** | (*S*)-Et | Bn | 7% | 172 nM | > 100 |
| **61** | (*S*)-Et | $CH_2$-$CH_2$-Morph | 20% | 33% | - |
| **62** | (*S*)-*i*-Pr | H | 11.1 nM | 1.90 nM | 5.84 |
| **63** | (*S*)-*i*-Pr | *t*-Bu | 30% | 229 nM | > 100 |
| **64** | (*S*)-*i*-Pr | $CH_2$-$CO_2Me$ | 17% | 148 nM | > 100 |
| **65** | (*S*)-*i*-Pr | Bn | 42% | 69.0 nM | > 100 |
| **66** | (*S*)-*i*-Pr | $CH_2$-$CH_2$-Morph | 24% | 270 nM | > 100 |
| **67** | (*S*)-*t*-Bu | H | 42.3 nM | 2.70 nM | 15.7 |
| **68** | (*S*)-*t*-Bu | *t*-Bu | 28% | 130 nM | > 100 |
| **69** | (*S*)-*t*-Bu | $CH_2$-$CO_2Me$ | 47% | 65.0 nM | > 100 |
| **70** | (*S*)-*t*-Bu | $CH_2$-$CO_2NH_2$ | 46% | 60.7 nM | > 100 |
| **71** | (*S*)-*t*-Bu | Bn | 280 nM | 8.60 nM | 32.6 |
| **72** | (*S*)-*t*-Bu | $CH_2$-$CH_2$-Morph | 32% | 46.4 nM | > 100 |
| **Surinabant** | - | - | 3.00 nM | 400 nM | 0.0075 |
| **GW405833** | - | - | 4772 nM | 5.80 nM | 822 |

[a)] Displacement of specific [$^3$H]-CP55940 binding in human CHO cells expressed as $K_i$ in nM (n = 3) or percentage displacement of specific binding at a concentration of 1 $\mu$M (n = 2). [b)] Displacement of specific [$^3$H]-CP55940 binding in human HEK-293 cells expressed as $K_i$ in nM (n = 3) or percentage displacement of specific binding at a concentration of 1 $\mu$M (n = 2).

USC UNIVERSIDADE DE SANTIAGO DE COMPOSTELA

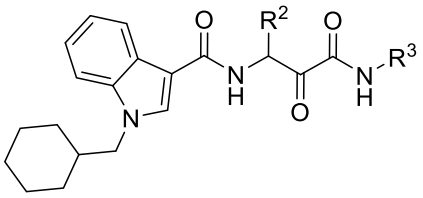


Table 3.14. Structure and cannabinoid receptor affinity data of Series **VI-b** (Cmpds **73-87**).

| Compound | $R^2$ | $R^3$ | $K_i$ (nM) or % at 1 μM | | SI |
|---|---|---|---|---|---|
| | | | $hCB_1R$[a)] | $hCB_2R$[b)] | |
| **73** | (*S*)-Et | H | 53.8 nM | 12.0 nM | 4.48 |
| **74** | (*S*)-Et | *t*-Bu | 18% | 277 nM | > 100 |
| **75** | (*S*)-Et | $CH_2$-$CO_2Me$ | 833 nM | 68.5 nM | 12.2 |
| **76** | (*S*)-Et | Bn | 970 nM | 70.6 nM | 13.7 |
| **77** | (*S*)-Et | $CH_2$-$CH_2$-Morph | 13% | 41% | - |
| **78** | (*S*)-*i*-Pr | H | 3.70 nM | 0.66 nM | 5.61 |
| **79** | (*S*)-*i*-Pr | *t*-Bu | 26% | 137 nM | > 100 |
| **80** | (*S*)-*i*-Pr | $CH_2$-$CO_2Me$ | 48.6 nM | 4.10 nM | 11.9 |
| **81** | (*S*)-*i*-Pr | Bn | 200 nM | 16.4 nM | 12.2 |
| **82** | (*S*)-*i*-Pr | $CH_2$-$CH_2$-Morph | 34% | 42.4 nM | > 100 |
| **83** | (*S*)-*t*-Bu | H | 8.50 nM | 14.4 nM | 0.59 |
| **84** | (*S*)-*t*-Bu | *t*-Bu | 45% | 41.5 nM | > 100 |
| **85** | (*S*)-*t*-Bu | $CH_2$-$CO_2Me$ | 75.3 nM | 3.30 nM | 22.8 |
| **86** | (*S*)-*t*-Bu | Bn | 31.8 nM | 4.60 nM | 6.91 |
| **87** | (*S*)-*t*-Bu | $CH_2$-$CH_2$-Morph | 45% | 18.6 nM | > 100 |
| **Surinabant** | - | - | 3.00 nM | 400 nM | 0.0075 |
| **GW405833** | - | - | 4772 nM | 5.80 nM | 822 |

[a)] Displacement of specific [$^3$H]-CP55940 binding in human CHO cells expressed as $K_i$ in nM (n = 3) or percentage displacement of specific binding at a concentration of 1 $\mu$M (n = 2). [b)] Displacement of specific [$^3$H]-CP55940 binding in human HEK-293 cells expressed as $K_i$ in nM (n = 3) or percentage displacement of specific binding at a concentration of 1 $\mu$M (n = 2).

USC UNIVERSIDADE DE SANTIAGO DE COMPOSTELA

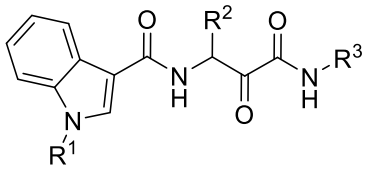


Table 3.15. Structure and cannabinoid receptor affinity data of Series **VI-c** (Cmpds **88-91**).

| Compound | $R^1$ | $R^2$ | $R^3$ | $K_i$ (nM) or % at 1 μM | | SI |
|---|---|---|---|---|---|---|
| | | | | $hCB_1R$[a)] | $hCB_2R$[b)] | |
| **88** | 5-F-Pentyl | (*S*)-*t*-Bu | *t*-Bu | 50% | 27.2 nM | > 100 |
| **89** | 5-F-Pentyl | (*S*)-*t*-Bu | Bn | 80.1 nM | 3.60 nM | 22.6 |
| **90** | Pentyl | (*S*)-*t*-Bu | *t*-Bu | 33% | 30.6 nM | > 100 |
| **91** | Pentyl | (*S*)-*t*-Bu | Bn | 92.9 nM | 14.1 nM | 6.59 |
| **Surinabant** | - | - | - | 3.00 nM | 400 nM | 0.0075 |
| **GW405833** | - | - | - | 4772 nM | 5.80 nM | 822 |

[a)] Displacement of specific [$^3$H]-CP55940 binding in human CHO cells expressed as $K_i$ in nM (n = 3) or percentage displacement of specific binding at a concentration of 1 $\mu$M (n = 2). [b)] Displacement of specific [$^3$H]-CP55940 binding in human HEK-293 cells expressed as $K_i$ in nM (n = 3) or percentage displacement of specific binding at a concentration of 1 $\mu$M (n = 2).

USC UNIVERSIDADE DE SANTIAGO DE COMPOSTELA

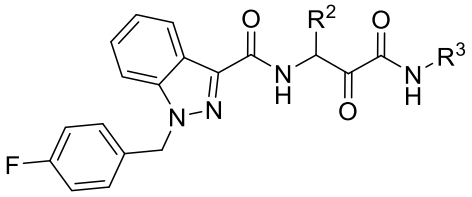


Table 3.16. Structure and cannabinoid receptor affinity data of Series **VI-d** (Cmpds **92-106**).

| Compound | $R^2$ | $R^3$ | $K_i$ (nM) or % at 1 μM | | SI |
|---|---|---|---|---|---|
| | | | $hCB_1R$[a)] | $hCB_2R$[b)] | |
| **92** | (*S*)-Et | H | 9.00 nM | 3.20 nM | 2.81 |
| **93** | (*S*)-Et | *t*-Bu | 36% | 234 nM | > 100 |
| **94** | (*S*)-Et | $CH_2$-$CO_2Me$ | 55% | 102 nM | > 100 |
| **95** | (*S*)-Et | Bn | 114 nM | 26.0 nM | 4.38 |
| **96** | (*S*)-Et | $CH_2$-$CH_2$-Morph | 31% | 164 nM | > 100 |
| **97** | (*S*)-*i*-Pr | H | 0.88 nM | 0.27 nM | 3.25 |
| **98** | (*S*)-*i*-Pr | *t*-Bu | 104 nM | 4.60 nM | 22.7 |
| **99** | (*S*)-*i*-Pr | $CH_2$-$CO_2Me$ | 18.9 nM | 1.60 nM | 11.8 |
| **100** | (*S*)-*i*-Pr | Bn | 28.4 nM | 1.00 nM | 28.4 |
| **101** | (*S*)-*i*-Pr | $CH_2$-$CH_2$-Morph | 227 nM | 18.6 nM | 12.2 |
| **102** | (*S*)-*t*-Bu | H | 1.70 nM | 0.11 nM | 15.5 |
| **103** | (*S*)-*t*-Bu | *t*-Bu | 140 nM | 3.80 nM | 36.9 |
| **104** | (*S*)-*t*-Bu | $CH_2$-$CO_2Me$ | 3.70 nM | 0.14 nM | 26.4 |
| **105** | (*S*)-*t*-Bu | Bn | 4.40 nM | 0.26 nM | 16.9 |
| **106** | (*S*)-*t*-Bu | $CH_2$-$CH_2$-Morph | 21.2 nM | 0.32 nM | 66.3 |
| **Surinabant** | - | - | 3.00 nM | 400 nM | 0.0075 |
| **GW405833** | - | - | 4772 nM | 5.80 nM | 822 |

[a)] Displacement of specific [$^3$H]-CP55940 binding in human CHO cells expressed as $K_i$ in nM (n = 3) or percentage displacement of specific binding at a concentration of 1 $\mu$M (n = 2). [b)] Displacement of specific [$^3$H]-CP55940 binding in human HEK-293 cells expressed as $K_i$ in nM (n = 3) or percentage displacement of specific binding at a concentration of 1 $\mu$M (n = 2).

USC UNIVERSIDADE DE SANTIAGO DE COMPOSTELA

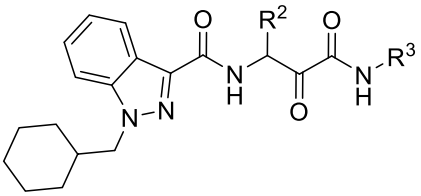


Table 3.17. Structure and cannabinoid receptor affinity data of Series **VI-e** (Cmpds **107-121**).

| Compound | $R^2$ | $R^3$ | $K_i$ (nM) or % at 1 μM | | SI |
|---|---|---|---|---|---|
| | | | $hCB_1R$[a)] | $hCB_2R$[b)] | |
| **107** | (*S*)-Et | H | 10.8 nM | 2.70 nM | 4.00 |
| **108** | (*S*)-Et | *t*-Bu | 34% | 150 nM | > 100 |
| **109** | (*S*)-Et | $CH_2$-$CO_2Me$ | 55% | 59.7 nM | > 100 |
| **110** | (*S*)-Et | Bn | 168 nM | 26.3 nM | 6.39 |
| **111** | (*S*)-Et | $CH_2$-$CH_2$-Morph | 12% | 119 nM | > 100 |
| **112** | (*S*)-*i*-Pr | H | 0.80 nM | 0.20 nM | 4,00 |
| **113** | (*S*)-*i*-Pr | *t*-Bu | 172 nM | 12.0 nM | 14.3 |
| **114** | (*S*)-*i*-Pr | $CH_2$-$CO_2Me$ | 27.8 nM | 1.60 nM | 17.4 |
| **115** | (*S*)-*i*-Pr | Bn | 32.4 nM | 1.90 nM | 17.1 |
| **116** | (*S*)-*i*-Pr | $CH_2$-$CH_2$-Morph | 74.0 nM | 1.40 nM | 52.9 |
| **117** | (*S*)-*t*-Bu | H | 0.80 nM | 0.15 nM | 5.33 |
| **118** | (*S*)-*t*-Bu | *t*-Bu | 65.6 nM | 1.50 nM | 43.7 |
| **119** | (*S*)-*t*-Bu | $CH_2$-$CO_2Me$ | 6.00 nM | 0.52 nM | 11.5 |
| **120** | (*S*)-*t*-Bu | Bn | 2.20 nM | 0.28 nM | 7.86 |
| **121** | (*S*)-*t*-Bu | $CH_2$-$CH_2$-Morph | 30.2 nM | 0.30 nM | > 100 |
| **Surinabant** | - | - | 3.00 | 400 | 0.0075 |
| **GW405833** | - | - | 4772 | 5.80 | 822 |

[a)] Displacement of specific [$^3$H]-CP55940 binding in human CHO cells expressed as $K_i$ in nM (n = 3) or percentage displacement of specific binding at a concentration of 1 $\mu$M (n = 2). [b)] Displacement of specific [$^3$H]-CP55940 binding in human HEK-293 cells expressed as $K_i$ in nM (n = 3) or percentage displacement of specific binding at a concentration of 1 $\mu$M (n = 2).

USC UNIVERSIDADE DE SANTIAGO DE COMPOSTELA

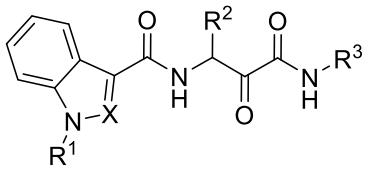


Table 3.18. Structure and cannabinoid receptor affinity data of Series **VI-f** (Cmpds **122-129**).

| Compound | $R^1$ | $R^2$ | $R^3$ | X | $K_i$ (nM) or % at 1 μM | | SI |
|---|---|---|---|---|---|---|---|
| | | | | | $hCB_1R$[a)] | $hCB_2R$[b)] | |
| **122** | 4-F-Bn | (*R*)-*t*-Bu | H | CH | 71.7 nM | 8.10 nM | 8.85 |
| **123** | 4-F-Bn | (*R*)-*t*-Bu | H | N | 4.20 nM | 0.20 nM | 21.0 |
| **124** | $CH_2$-Cy | (*R*)-*t*-Bu | H | CH | 13.7 nM | 1.60 nM | 8.56 |
| **125** | $CH_2$-Cy | (*R*)-*t*-Bu | H | N | 4.20 nM | 0.30 nM | 14.0 |
| **126** | 4-F-Bn | (*R*)-*t*-Bu | *t*-Bu | CH | 3% | 156 nM | > 100 |
| **127** | 4-F-Bn | (*R*)-*t*-Bu | *t*-Bu | N | 45% | 13.6 nM | > 100 |
| **128** | $CH_2$-Cy | (*R*)-*t*-Bu | *t*-Bu | CH | 9% | 44.2 nM | > 100 |
| **129** | $CH_2$-Cy | (*R*)-*t*-Bu | *t*-Bu | N | 43% | 8.90 nM | > 100 |
| **Surinabant** | - | - | - | - | 3.00 nM | 400 nM | 0.0075 |
| **GW405833** | - | - | - | - | 4772 nM | 5.80 nM | 822 |

[a)] Displacement of specific [$^3$H]-CP55940 binding in human CHO cells expressed as $K_i$ in nM (n = 3) or percentage displacement of specific binding at a concentration of 1 $\mu$M (n = 2). [b)] Displacement of specific [$^3$H]-CP55940 binding in human HEK-293 cells expressed as $K_i$ in nM (n = 3) or percentage displacement of specific binding at a concentration of 1 $\mu$M (n = 2).

USC UNIVERSIDADE DE SANTIAGO DE COMPOSTELA

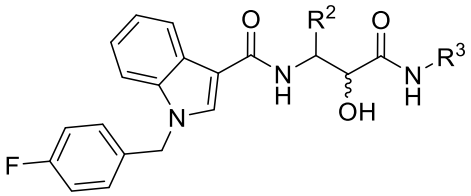


Table 3.19. Structure and cannabinoid receptor affinity data of Series **VII-a** (Cmpds **130-145**).

| Compound | $R^2$ | $R^3$ | Ki (nM) or % at 1 μM | | SI |
|---|---|---|---|---|---|
| | | | $hCB_1R$[a)] | $hCB_2R$[b)] | |
| **130** | (*S*)-Et | H | 5% | 54.8 nM | >100 |
| **131** | (*S*)-Et | *t*-Bu | 1% | 37% | - |
| **132** | (*S*)-Et | $CH_2$-$CO_2Me$ | 2% | 283 nM | >100 |
| **133** | (*S*)-Et | Bn | 3% | 103 nM | >100 |
| **134** | (*S*)-Et | $CH_2$-$CH_2$-Morph | 3% | 5% | - |
| **135** | (*S*)-*i*-Pr | H | 1% | 106 nM | >100 |
| **136** | (*S*)-*i*-Pr | *t*-Bu | 1% | 54% | - |
| **137** | (*S*)-*i*-Pr | $CH_2$-$CO_2Me$ | 3% | 68.0 nM | >100 |
| **138** | (*S*)-*i*-Pr | Bn | 2% | 140 nM | >100 |
| **139** | (*S*)-*i*-Pr | $CH_2$-$CH_2$-Morph | 6% | 43% | - |
| **140** | (*S*)-*t*-Bu | H | 22% | 43.7 nM | >100 |
| **141** | (*S*)-*t*-Bu | *t*-Bu | 2% | 207 nM | >100 |
| **142** | (*S*)-*t*-Bu | $CH_2$-$CO_2Me$ | 15% | 34.5 nM | >100 |
| **143** | (*S*)-*t*-Bu | $CH_2$-$CO_2NH_2$ | 18% | 42.3 nM | >100 |
| **144** | (*S*)-*t*-Bu | Bn | 3% | 84.7 nM | >100 |
| **145** | (*S*)-*t*-Bu | $CH_2$-$CH_2$-Morph | 6% | 55% | - |
| **Surinabant** | - | - | 3.00 nM | 400 nM | 0.0075 |
| **GW405833** | - | - | 4772 nM | 5.80 nM | 822 |

[a)] Displacement of specific [$^3$H]-CP55940 binding in human CHO cells expressed as $K_i$ in nM (n = 3) or percentage displacement of specific binding at a concentration of 1 $\mu$M (n = 2). [b)] Displacement of specific [$^3$H]-CP55940 binding in human HEK-293 cells expressed as $K_i$ in nM (n = 3) or percentage displacement of specific binding at a concentration of 1 $\mu$M (n = 2).

USC UNIVERSIDADE DE SANTIAGO DE COMPOSTELA

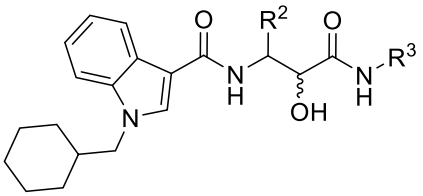


Table 3.20. Structure and cannabinoid receptor affinity data of Series **VII-b** (Cmpds **146-160**).

| Compound | $R^2$ | $R^3$ | $K_i$ (nM) or % at 1 μM | | SI |
|---|---|---|---|---|---|
| | | | $hCB_1R$[a)] | $hCB_2R$[b)] | |
| **146** | (*S*)-Et | H | 3% | 47% | - |
| **147** | (*S*)-Et | *t*-Bu | 5% | 145 nM | >100 |
| **148** | (*S*)-Et | $CH_2$-$CO_2Me$ | 8% | 52.4 nM | >100 |
| **149** | (*S*)-Et | Bn | 22% | 62.4 nM | >100 |
| **150** | (*S*)-Et | $CH_2$-$CH_2$-Morph | 1% | 35% | - |
| **151** | (*S*)-*i*-Pr | H | 20% | 40.8 nM | >100 |
| **152** | (*S*)-*i*-Pr | *t*-Bu | 12% | 197 nM | >100 |
| **153** | (*S*)-*i*-Pr | $CH_2$-$CO_2Me$ | 27% | 22.6 nM | >100 |
| **154** | (*S*)-*i*-Pr | Bn | 51% | 13.9 nM | >100 |
| **155** | (*S*)-*i*-Pr | $CH_2$-$CH_2$-Morph | 7% | 245 nM | >100 |
| **156** | (*S*)-*t*-Bu | H | 49% | 8.50 nM | >100 |
| **157** | (*S*)-*t*-Bu | *t*-Bu | 3% | 142 nM | >100 |
| **158** | (*S*)-*t*-Bu | $CH_2$-$CO_2Me$ | 55% | 6.30 nM | >100 |
| **159** | (*S*)-*t*-Bu | Bn | 8% | 44.0 nM | >100 |
| **160** | (*S*)-*t*-Bu | $CH_2$-$CH_2$-Morph | 5% | 50% | - |
| **Surinabant** | - | - | 3.00 nM | 400 nM | 0.0075 |
| **GW405833** | - | - | 4772 nM | 5.80 nM | 822 |

[a)] Displacement of specific [$^3$H]-CP55940 binding in human CHO cells expressed as $K_i$ in nM (n = 3) or percentage displacement of specific binding at a concentration of 1 $\mu$M (n = 2). [b)] Displacement of specific [$^3$H]-CP55940 binding in human HEK-293 cells expressed as $K_i$ in nM (n = 3) or percentage displacement of specific binding at a concentration of 1 $\mu$M (n = 2).

USC UNIVERSIDADE DE SANTIAGO DE COMPOSTELA

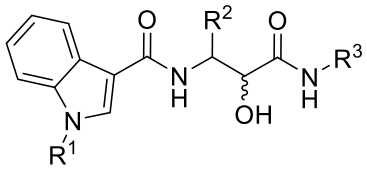


Table 3.21. Structure and cannabinoid receptor affinity data of Series **VII-c** (Cmpds **161-164**).

| Compound | $R^1$ | $R^2$ | $R^3$ | $K_i$ (nM) or % at 1 μM | | SI |
|---|---|---|---|---|---|---|
| | | | | $hCB_1R$[a)] | $hCB_2R$[b)] | |
| **161** | 5-F-Pentyl | (*S*)-*t*-Bu | *t*-Bu | 2% | 277 nM | >100 |
| **162** | 5-F-Pentyl | (*S*)-*t*-Bu | Bn | 3% | 76.5 nM | >100 |
| **163** | Pentyl | (*S*)-*t*-Bu | *t*-Bu | 3% | 105 nM | >100 |
| **164** | Pentyl | (*S*)-*t*-Bu | Bn | 3% | 109 nM | >100 |
| **Surinabant** | - | - | - | 3.00 nM | 400 nM | 0.0075 |
| **GW405833** | - | - | - | 4772 nM | 5.80 nM | 822 |

[a)] Displacement of specific [$^3$H]-CP55940 binding in human CHO cells expressed as $K_i$ in nM (n = 3) or percentage displacement of specific binding at a concentration of 1 μM (n = 2). [b)] Displacement of specific [$^3$H]-CP55940 binding in human HEK-293 cells expressed as $K_i$ in nM (n = 3) or percentage displacement of specific binding at a concentration of 1 μM (n = 2).

USC UNIVERSIDADE DE SANTIAGO DE COMPOSTELA

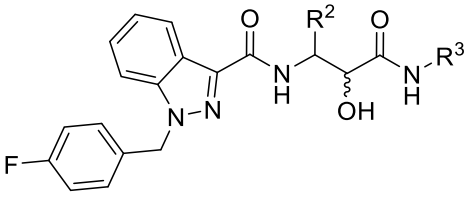


Table 3.22. Structure and cannabinoid receptor affinity data of Series **VII-d** (Cmpds **165-179**).

| Compound | $R^2$ | $R^3$ | $K_i$ (nM) or % at 1 μM | | SI |
|---|---|---|---|---|---|
| | | | $hCB_1R$[a)] | $hCB_2R$[b)] | |
| **165** | (*S*)-Et | H | 54% | 8.80 nM | >100 |
| **166** | (*S*)-Et | *t*-Bu | 4% | 297 nM | >100 |
| **167** | (*S*)-Et | $CH_2$-$CO_2Me$ | 129 nM | 2.20 nM | 58.7 |
| **168** | (*S*)-Et | Bn | 3% | 57.3 nM | >100 |
| **169** | (*S*)-Et | $CH_2$-$CH_2$-Morph | 2% | 17% | - |
| **170** | (*S*)-*i*-Pr | H | 130 nM | 3.60 nM | 36.1 |
| **171** | (*S*)-*i*-Pr | *t*-Bu | 6% | 271 nM | >100 |
| **172** | (*S*)-*i*-Pr | $CH_2$-$CO_2Me$ | 26% | 54.0 nM | >100 |
| **173** | (*S*)-*i*-Pr | Bn | 2% | 46.4 nM | >100 |
| **174** | (*S*)-*i*-Pr | $CH_2$-$CH_2$-Morph | 32% | 115 nM | >100 |
| **175** | (*S*)-*t*-Bu | H | 104 nM | 1.40 nM | 74.7 |
| **176** | (*S*)-*t*-Bu | *t*-Bu | 6% | 112 nM | >100 |
| **177** | (*S*)-*t*-Bu | $CH_2$-$CO_2Me$ | 102 nM | 1.10 nM | 93.0 |
| **178** | (*S*)-*t*-Bu | Bn | 25% | 6.50 nM | >100 |
| **179** | (*S*)-*t*-Bu | $CH_2$-$CH_2$-Morph | 2% | 209 nM | >100 |
| **Surinabant** | - | - | 3.00 nM | 400 nM | 0.0075 |
| **GW405833** | - | - | 4772 nM | 5.80 nM | 822 |

[a)] Displacement of specific [$^3$H]-CP55940 binding in human CHO cells expressed as $K_i$ in nM (n = 3) or percentage displacement of specific binding at a concentration of 1 $\mu$M (n = 2). [b)] Displacement of specific [$^3$H]-CP55940 binding in human HEK-293 cells expressed as $K_i$ in nM (n = 3) or percentage displacement of specific binding at a concentration of 1 $\mu$M (n = 2).

USC UNIVERSIDADE DE SANTIAGO DE COMPOSTELA

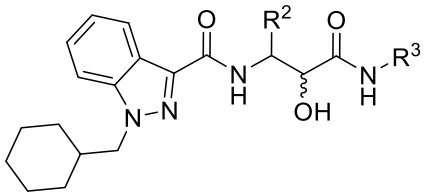


Table 3.23. Structure and cannabinoid receptor affinity data of Series **VII-e** (Cmpds **180-194**).

| Compound | $R^2$ | $R^3$ | $K_i$ (nM) or % at 1 μM | | SI |
|---|---|---|---|---|---|
| | | | $hCB_1R$[a)] | $hCB_2R$[b)] | |
| **180** | (*S*)-Et | H | 162 nM | 8.70 nM | 18.7 |
| **181** | (*S*)-Et | *t*-Bu | 3% | 96.9 nM | >100 |
| **182** | (*S*)-Et | $CH_2$-$CO_2$Me | 29% | 24.2 nM | >100 |
| **183** | (*S*)-Et | Bn | 13% | 39.1 nM | >100 |
| **184** | (*S*)-Et | $CH_2$-$CH_2$-Morph | 3% | 28% | - |
| **185** | (*S*)-*i*-Pr | H | 59.3 nM | 2.70 nM | 22.0 |
| **186** | (*S*)-*i*-Pr | *t*-Bu | 1% | 100 nM | >100 |
| **187** | (*S*)-*i*-Pr | $CH_2$-$CO_2$Me | 84.6 nM | 1.20 nM | 70.5 |
| **188** | (*S*)-*i*-Pr | Bn | 12% | 17.1 nM | >100 |
| **189** | (*S*)-*i*-Pr | $CH_2$-$CH_2$-Morph | 4% | 99.0 nM | >100 |
| **190** | (*S*)-*t*-Bu | H | 80.3 nM | 0.90 nM | 89.2 |
| **191** | (*S*)-*t*-Bu | *t*-Bu | 6% | 54.2 nM | >100 |
| **192** | (*S*)-*t*-Bu | $CH_2$-$CO_2$Me | 81.7 nM | 12.4 nM | 6.60 |
| **193** | (*S*)-*t*-Bu | Bn | 17% | 5.70 nM | >100 |
| **194** | (*S*)-*t*-Bu | $CH_2$-$CH_2$-Morph | 2% | 36.9 nM | >100 |
| **Surinabant** | - | - | 3.00 nM | 400 nM | 0.0075 |
| **GW405833** | - | - | 4772 nM | 5.80 nM | 822 |

[a)] Displacement of specific [$^3$H]-CP55940 binding in human CHO cells expressed as $K_i$ in nM (n = 3) or percentage displacement of specific binding at a concentration of 1 $\mu$M (n = 2). [b)] Displacement of specific [$^3$H]-CP55940 binding in human HEK-293 cells expressed as $K_i$ in nM (n = 3) or percentage displacement of specific binding at a concentration of 1 $\mu$M (n = 2).

USC UNIVERSIDADE DE SANTIAGO DE COMPOSTELA

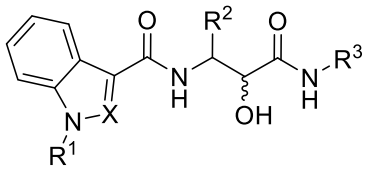


Table 3.24. Structure and cannabinoid receptor affinity data of Series **VII-f** (Cmpds **195-202**).

| Compound | $R^1$ | $R^2$ | $R^3$ | X | $K_i$ (nM) or % at 1 μM | | SI |
|---|---|---|---|---|---|---|---|
| | | | | | $hCB_1R$[a)] | $hCB_2R$[b)] | |
| **195** | 4-F-Bn | (*R*)-*t*-Bu | H | CH | 33% | 18.3 nM | >100 |
| **196** | 4-F-Bn | (*R*)-*t*-Bu | H | N | 24.5 nM | 0.40 nM | 61.3 |
| **197** | $CH_2$-Cy | (*R*)-*t*-Bu | H | CH | 52% | 9.60 nM | >100 |
| **198** | $CH_2$-Cy | (*R*)-*t*-Bu | H | N | 30.3 nM | 0.60 nM | 50.5 |
| **199** | 4-F-Bn | (*R*)-*t*-Bu | *t*-Bu | CH | 32% | 42.4 nM | >100 |
| **200** | 4-F-Bn | (*R*)-*t*-Bu | *t*-Bu | N | 7% | 132 nM | >100 |
| **201** | $CH_2$-Cy | (*R*)-*t*-Bu | *t*-Bu | CH | 2% | 302 nM | >100 |
| **202** | $CH_2$-Cy | (*R*)-*t*-Bu | *t*-Bu | N | 2% | 140 nM | >100 |
| **Surinabant** | - | - | - | - | 3.00 nM | 400 nM | 0.0075 |
| **GW405833** | - | - | - | - | 4772 nM | 5.80 nM | 822 |

[a)] Displacement of specific [$^3$H]-CP55940 binding in human CHO cells expressed as $K_i$ in nM (n = 3) or percentage displacement of specific binding at a concentration of 1 $\mu$M (n = 2). [b)] Displacement of specific [$^3$H]-CP55940 binding in human HEK-293 cells expressed as $K_i$ in nM (n = 3) or percentage displacement of specific binding at a concentration of 1 $\mu$M (n = 2).

USC UNIVERSIDADE DE SANTIAGO DE COMPOSTELA

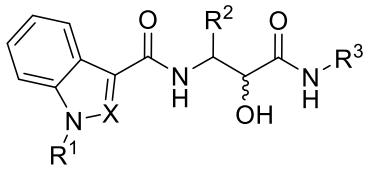


Table 3.25. Structure and cannabinoid receptor affinity data of diastereomeric pairs.

| Compound | X | $R^1$ | $R^2$ | $R^3$ | Ki (nM) or % at 1 μM | | SI |
|---|---|---|---|---|---|---|---|
| | | | | | $hCB_1R$[a)] | $hCB_2R$[b)] | |
| **(±)-168** | N | 4-F-Bn | (*S*)-Et | Bn | 12% | 127 nM | >100 |
| **(2*S*)-168** | N | 4-F-Bn | (*S*)-Et | Bn | 8% | 288 nM | >100 |
| **(2*R*)-168** | N | 4-F-Bn | (*S*)-Et | Bn | 3% | 57.3 nM | >100 |
| **(±)-182** | N | $CH_2$-Cy | (*S*)-Et | $CH_2$-$CO_2$Me | 13% | 58.0 nM | >100 |
| **(2*S*)-182** | N | $CH_2$-Cy | (*S*)-Et | $CH_2$-$CO_2$Me | 3% | 47% | - |
| **(2*R*)-182** | N | $CH_2$-Cy | (*S*)-Et | $CH_2$-$CO_2$Me | 29% | 24.2 nM | >100 |
| **(±)-183** | N | $CH_2$-Cy | (*S*)-Et | Bn | 6% | 94.7 nM | >100 |
| **(2*S*)-183** | N | $CH_2$-Cy | (*S*)-Et | Bn | 12% | 114.5 nM | >100 |
| **(2*R*)-183** | N | $CH_2$-Cy | (*S*)-Et | Bn | 13% | 39.1 nM | >100 |
| **(±)-173** | N | 4-F-Bn | (*S*)-*i*-Pr | Bn | 6% | 103.7 nM | >100 |
| **(2*S*)-173** | N | 4-F-Bn | (*S*)-*i*-Pr | Bn | 9% | 94.9 nM | >100 |
| **(2*R*)-173** | N | 4-F-Bn | (*S*)-*i*-Pr | Bn | 2% | 46.4 nM | >100 |
| **(±)-188** | N | $CH_2$-Cy | (*S*)-*i*-Pr | Bn | 22% | 31.0 nM | >100 |
| **(2*S*)-188** | N | $CH_2$-Cy | (*S*)-*i*-Pr | Bn | 21% | 40.6 nM | >100 |
| **(2*R*)-188** | N | $CH_2$-Cy | (*S*)-*i*-Pr | Bn | 12% | 17.1 nM | >100 |
| **Surinabant** | | | | | 3.00 nM | 400 nM | 0.0075 |
| **GW405833** | | | | | 4772 nM | 5.80 nM | 822 |

[a)] Displacement of specific [$^3$H]-CP55940 binding in human CHO cells expressed as $K_i$ in nM (n = 3) or percentage displacement of specific binding at a concentration of 1 $\mu$M (n = 2). [b)] Displacement of specific [$^3$H]-CP55940 binding in human HEK-293 cells expressed as $K_i$ in nM (n = 3) or percentage displacement of specific binding at a concentration of 1 $\mu$M (n = 2).

USC UNIVERSIDADE DE SANTIAGO DE COMPOSTELA

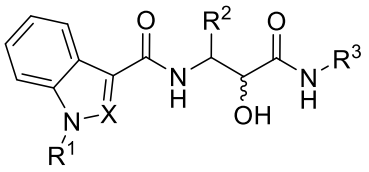


Table 3.26. Structure and cannabinoid receptor affinity data of diastereomeric pairs.

| Compound | X | $R^1$ | $R^2$ | $R^3$ | Ki (nM) or % at 1 μM | | SI |
|---|---|---|---|---|---|---|---|
| | | | | | $hCB_1R$[a)] | $hCB_2R$[b)] | |
| **(±)-177** | N | 4-F-Bn | (*S*)-*t*-Bu | $CH_2$-$CO_2Me$ | 186 nM | 2.30 nM | 80.9 |
| **(2*S*)-177** | N | 4-F-Bn | (*S*)-*t*-Bu | $CH_2$-$CO_2Me$ | 54% | 11.2 nM | >100 |
| **(2*R*)-177** | N | 4-F-Bn | (*S*)-*t*-Bu | $CH_2$-$CO_2Me$ | 102 nM | 1.10 nM | 93.0 |
| **(±)-178** | N | 4-F-Bn | (*S*)-*t*-Bu | Bn | 20% | 20.0 nM | >100 |
| **(2*S*)-178** | N | 4-F-Bn | (*S*)-*t*-Bu | Bn | 30% | 83.6 nM | >100 |
| **(2*R*)-178** | N | 4-F-Bn | (*S*)-*t*-Bu | Bn | 25% | 6.50 nM | >100 |
| **(±)-191** | N | $CH_2$-Cy | (*S*)-*t*-Bu | *t*-Bu | 7% | 89.5 nM | >100 |
| **(2*S*)-191** | N | $CH_2$-Cy | (*S*)-*t*-Bu | *t*-Bu | 7% | 54.2 nM | >100 |
| **(2*R*)-191** | N | $CH_2$-Cy | (*S*)-*t*-Bu | *t*-Bu | 6% | 54.2 nM | >100 |
| **(±)-193** | N | $CH_2$-Cy | (*S*)-*t*-Bu | Bn | 16% | 16.6 nM | >100 |
| **(2*S*)-193** | N | $CH_2$-Cy | (*S*)-*t*-Bu | Bn | 5% | 96.0 nM | >100 |
| **(2*R*)-193** | N | $CH_2$-Cy | (*S*)-*t*-Bu | Bn | 17% | 5.70 nM | >100 |
| **Surinabant** | | | | | 3.00 nM | 400 nM | 0.0075 |
| **GW405833** | | | | | 4772 nM | 5.80 nM | 822 |

[a)] Displacement of specific [$^3$H]-CP55940 binding in human CHO cells expressed as $K_i$ in nM (n = 3) or percentage displacement of specific binding at a concentration of 1 $\mu$M (n = 2). [b)] Displacement of specific [$^3$H]-CP55940 binding in human HEK-293 cells expressed as $K_i$ in nM (n = 3) or percentage displacement of specific binding at a concentration of 1 $\mu$M (n = 2).

USC UNIVERSIDADE DE SANTIAGO DE COMPOSTELA

### 3.2.4 Structure-Activity Relationship

In this section, we will investigate the pharmacological data acquired for the recently synthesized series, as presented in Table 3.13 to Table 3.26. We will also assess how the introduction of the new carbon atom, along with its substituents (hydroxy group or carbonyl), impacts the relationships between structure-activity (SAR) and structure-selectivity (SSR). Comparative studies used as reference the original series presented in Table 3.11 and Table 3.12. Additionally, we will explore the patterns that emerge due to the diverse substituents in the tail group, the linker, and the head group, as well as the influence of the heterocyclic core (indoles or indazoles).

The cannabinergic affinity profiles of the 73 ketoamides are presented in Table 3.13 to Table 3.18. Up to 13 ligands combine attractive $CB_2R$ affinity ($K_i$ < 70 nM) and exquisite subtype selectivity (> 100-fold), including 9 ligands with a $CB_2R$ $K_i$ lower than 50 nM (Figure 3.54). These results evidence the effectiveness of the pharmacomodulation process, which, starting from model dual $CB_1R$-$CB_2R$ prototypes (Figure 3.48), enabled us to dissociate completely the binding profile from these receptors and discover novel and potent ligands that specifically recognize the $CB_2R$.

USC
UNIVERSIDADE DE SANTIAGO DE COMPOSTELA

As observed in Figure 3.54, among the most attractive ligands, ten derivatives belong to the indole series (**65**, **69**, **70**, **72**, **82**, **84**, **87**, **88**, **90**, **128**) and three ligands belong to the indazole series (**109**, **127**, **129**). Ligands **87**, **127**, and **129** stand out for their excellent affinity ($K_i$ < 20 nM) and selectivity profile (> 100-fold).

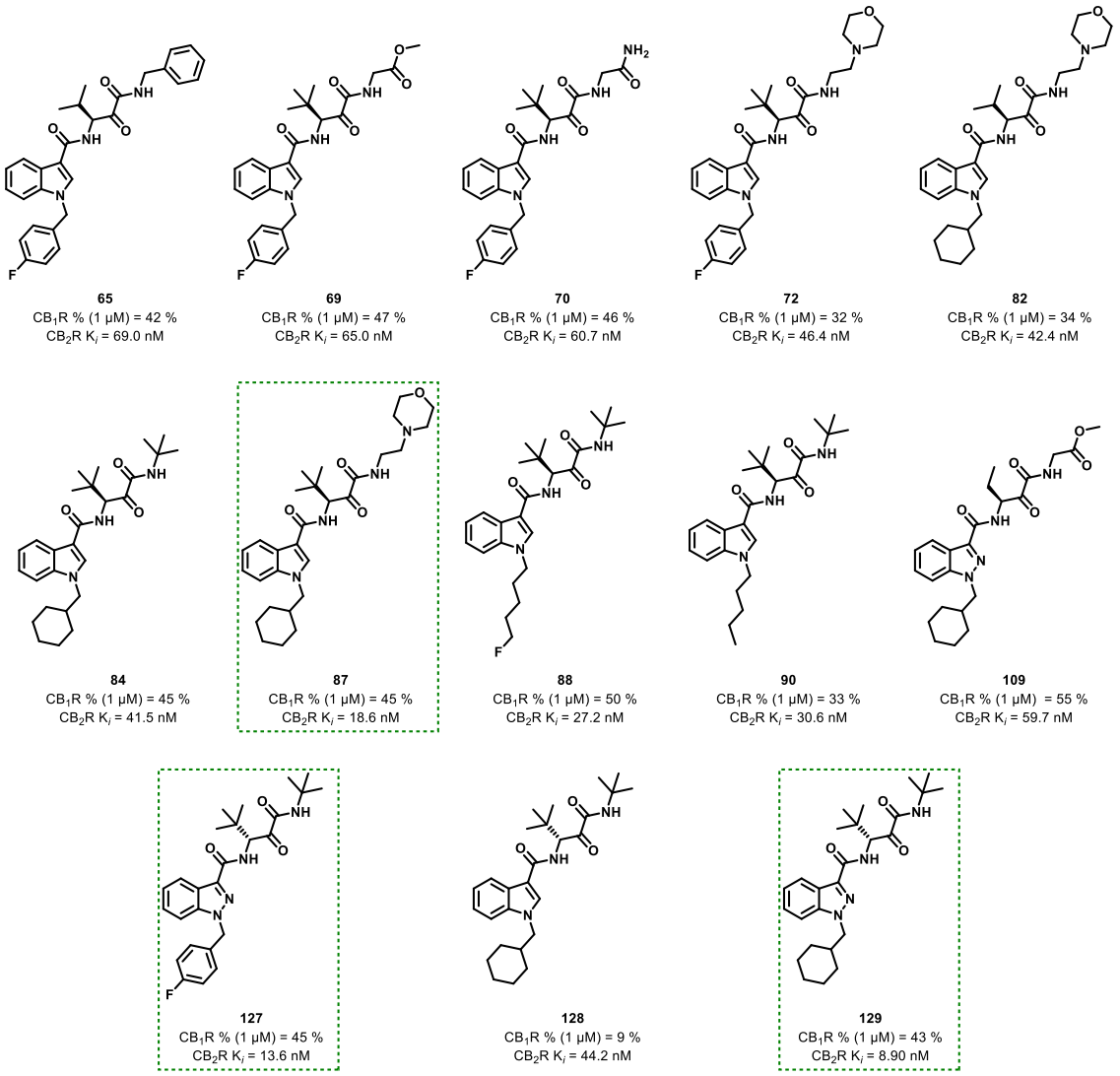



Figure 3.54. Structure and cannabimimetic data of selective $CB_2R$ ligands identified during Series **VI** of this study.

During our study, groups frequently encountered in SCRAs, but also previously unexplored substituents, have been introduced to evaluate the emerging SAR trends. Among the structural distinctions present in these molecules, the primary differentiation revolves around whether their core heterocycle includes an indole or an indazole. Through systematic synthesis of ligand pairs, we can explore the impact of these heterocycles on the affinity for $CB_2R$ and the selectivity towards $CB_1R$. Affinity data for $CB_1R$ and $CB_2R$ are presented in

USC UNIVERSIDADE DE SANTIAGO

Figure 3.55 (4-F-Bn derivatives) and Figure 3.56 ($CH_2$-Cy derivatives). Indoles are presented in purple and indazoles are presented in green.

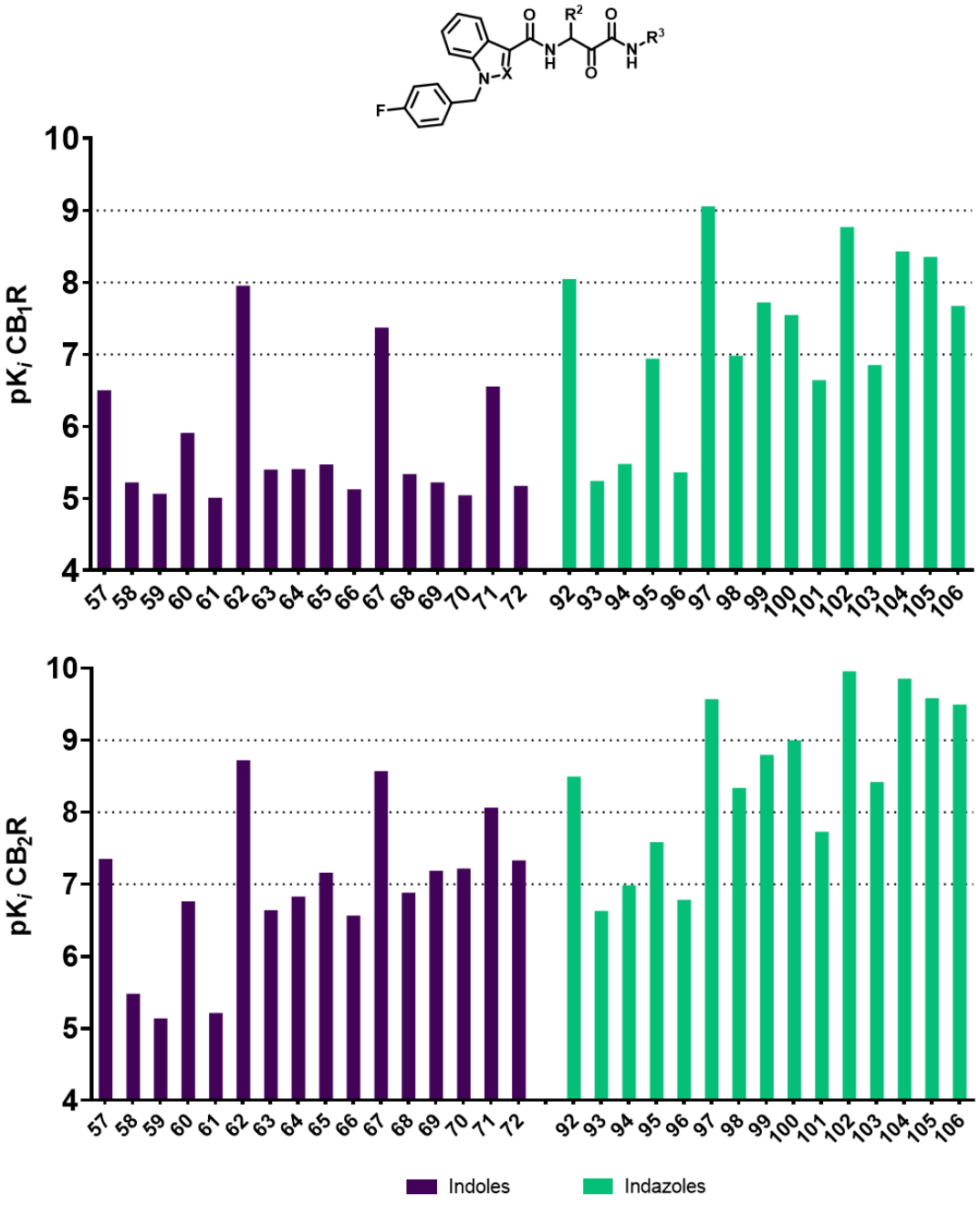



Figure 3.55. Bar chart representation of the SAR trends related to the core group for $R^1$ = 4-F-Bn (Series **VI**). $CB_1R$ affinity data (above) and $CB_2R$ affinity data (bottom) are reported.

USC
UNIVERSIDADE DE SANTIAGO DE COMPOSTELA

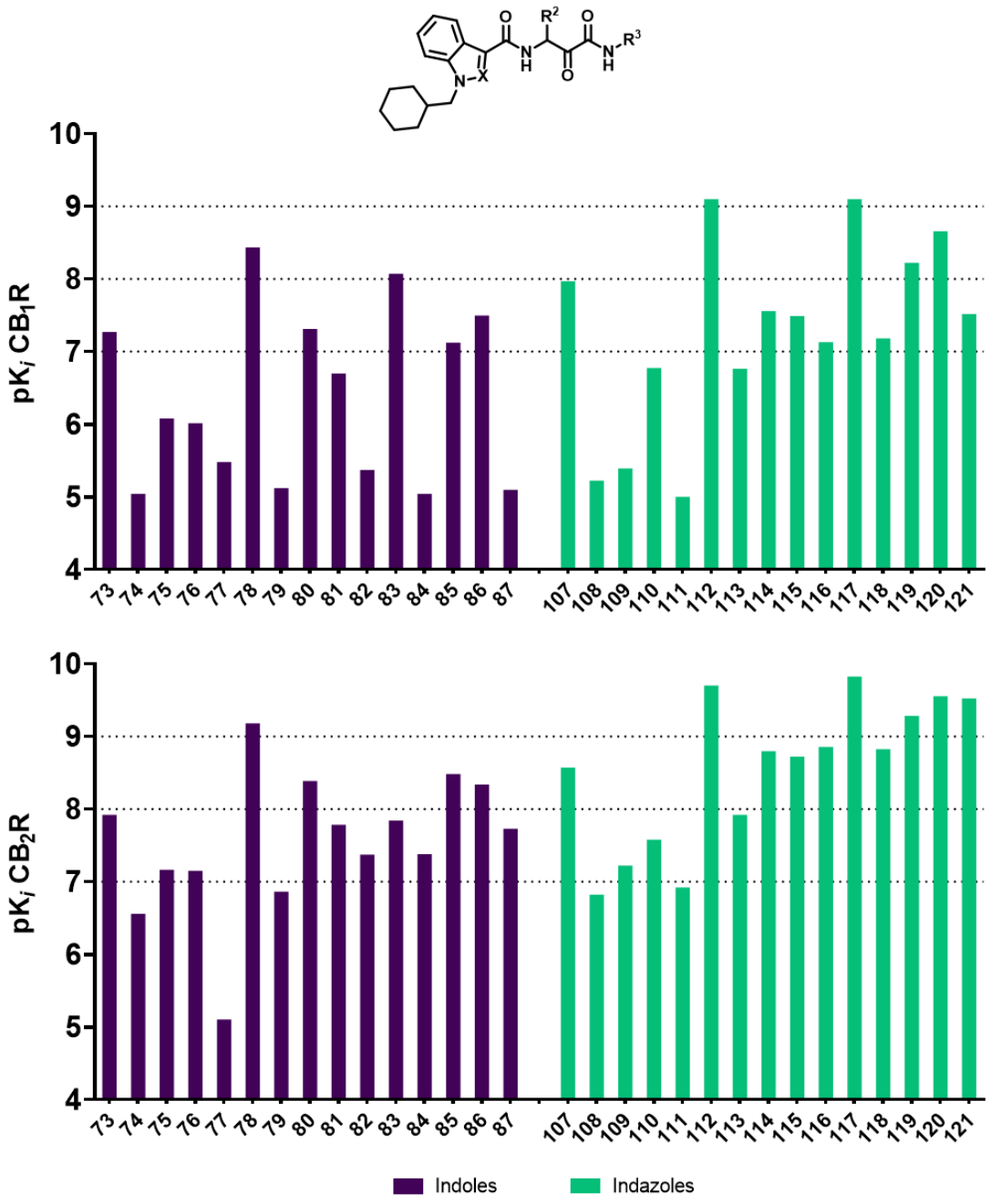



Figure 3.56. Bar chart representation of the SAR trends related to the core group for $R^1$ = $CH_2$-Cy (Series **VI**). $CB_1R$ affinity data (above) and $CB_2R$ affinity data (bottom) are reported.

The charts depicted above illustrate that indazole-based ligands consistently exhibit the highest potency at both $CB_1R$ and $CB_2R$. Of the 30 ligands assessed, 20 of them show a $CB_2R$ $K_i$ value of less than 10 nM, and 11 among them even achieve a remarkable $K_i$ value of less than 1 nM. In contrast, the indole-based ligands show comparatively less potency, with only 7

of them falling below the 10 nM threshold, and just one of those reaching the picomolar range. It's worth noting that all 30 indazole derivatives exhibit at least a moderate affinity for the $CB_2R$ ($pK_i$ > 6), a characteristic that is notably absent in the case of indole derivatives. Nonetheless, the rise in $CB_2R$ potency detected in the indazole derivatives comes with a simultaneous increase in their affinity for the $CB_1R$, resulting in a notable reduction in selectivity that only a few compounds can evade. Figure 3.57 provides a visual representation of both potency and selectivity for reference.

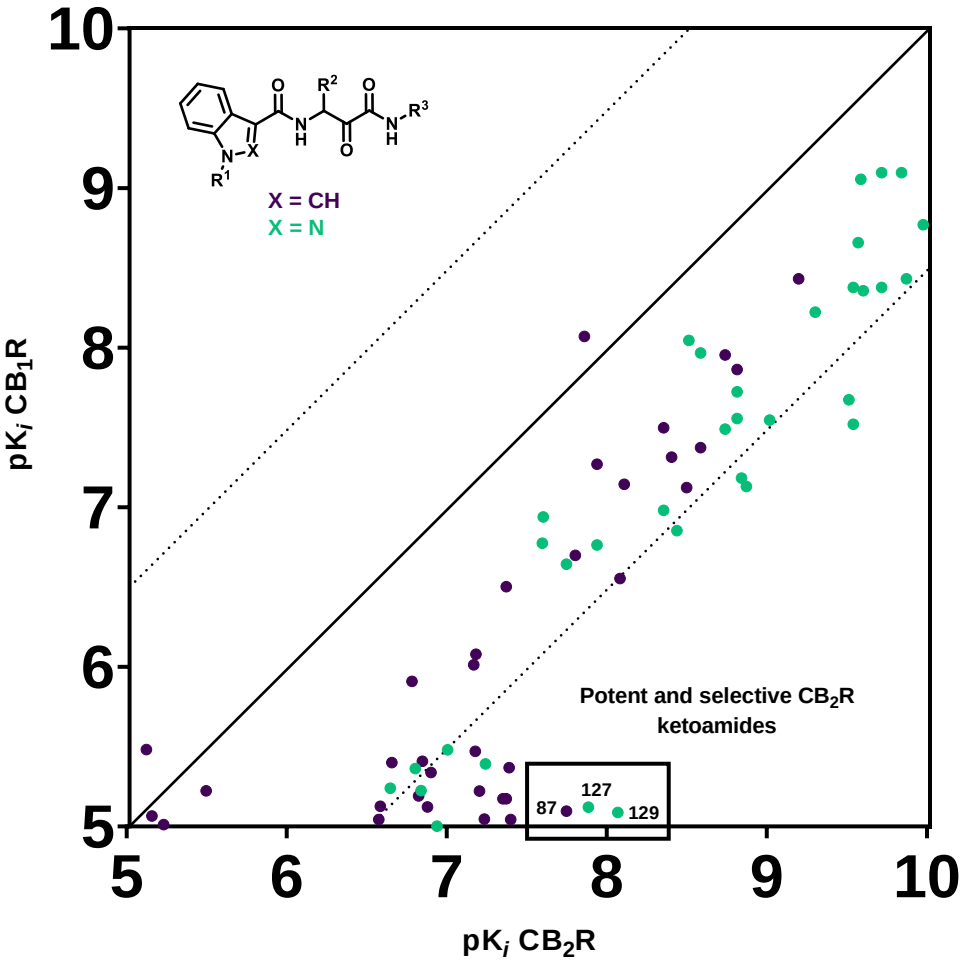



Figure 3.57. $CB_1R$ $pK_i$ [-log($K_i$)] vs $CB_2R$ $pK_i$ [-log($K_i$)] representation of indoles (purple dots) and indazoles (green dots).

For the sake of clarity, the discussion of the structure-activity relationship (SAR) trends, and to a lesser extent of the structure-selectivity relationship (SSR), is made here in an integrated fashion. For a more immediate and efficient analysis of the variation of both affinity and selectivity, the binding data ($pK_i$) are presented graphically as a plot of $pK_i$ $CB_1R$

(*Y* axis) versus $pK_i$ $CB_2R$ (*X* axis) using the same scale and range for both axes (square plot) in Figure 3.57. On the diagonal of this plot (*Y* = *X*) compounds with equal affinities at both receptors will be found, whereas $CB_1R$ or $CB_2R$ selective compounds will be seen above or below the diagonal, respectively. The distance of their $pK_i$ values from the diagonal is a direct measure of their degree of selectivity.

The graph is clearly divided into three sections, each corresponding to a different pharmacological profile. Molecules that are inactive at both receptors appear clustered in the bottom-left corner of the plot, near the axis origin. This group is exclusively comprised of indole derivatives (depicted as purple dots) since they exhibit a lower affinity profile than indazoles. Molecules that exhibit high affinity at both receptors are located in the middle-right part of the representation. These compounds demonstrate the highest affinity for $CB_2R$ in the series but also activate $CB_1R$. This dual $CB_1R/CB_2R$ behavior is primarily displayed by indazole derivatives (depicted as green dots) indicating a poor selectivity profile. Finally, compounds grouped in the lower part of the graph, within the low nanomolar range for $CB_2R$ affinity and on the right side of the dashed line, combine high potency at $CB_2R$ with complete selectivity towards $CB_1R$.

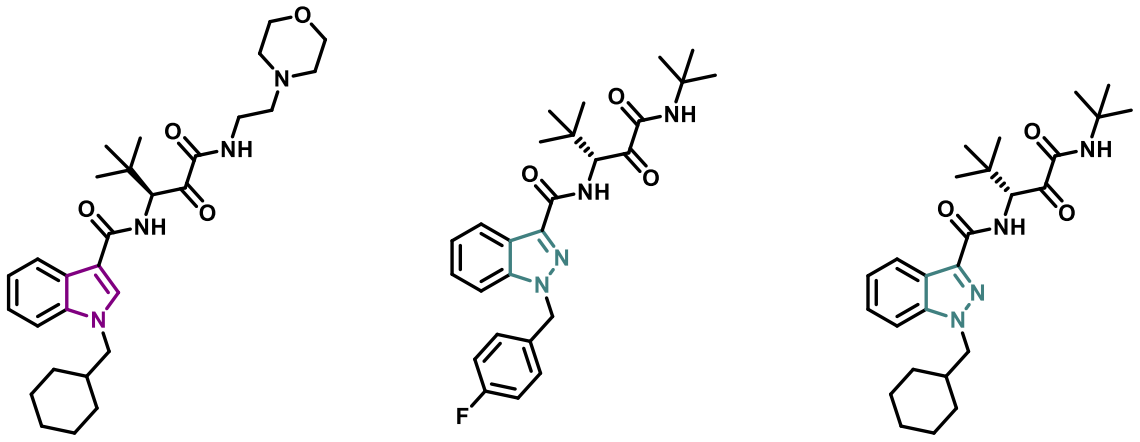



Figure 3.58. Structure of the best $CB_2R$ ligands of Series **VI** depending on their heterocycle group.

The top two compounds in the series feature indazole as the core group: compound **127** ($CB_2R$ $K_i$ = 13.6 nM, SI > 100), and compound **129** ($CB_2R$ $K_i$ = 8.90 nM, SI > 100), while indole **87** stands out as the third best in the series, as it combines a $CB_2R$ $K_i$ value below 20 nM and complete selectivity towards $CB_1R$. Overall, both heterocycles yield good results in

USC DE COMPOSTELA

terms of potent and selective molecules: indoles present a better selectivity profile than indazoles, while the latter exhibit better affinity for $CB_2R$.

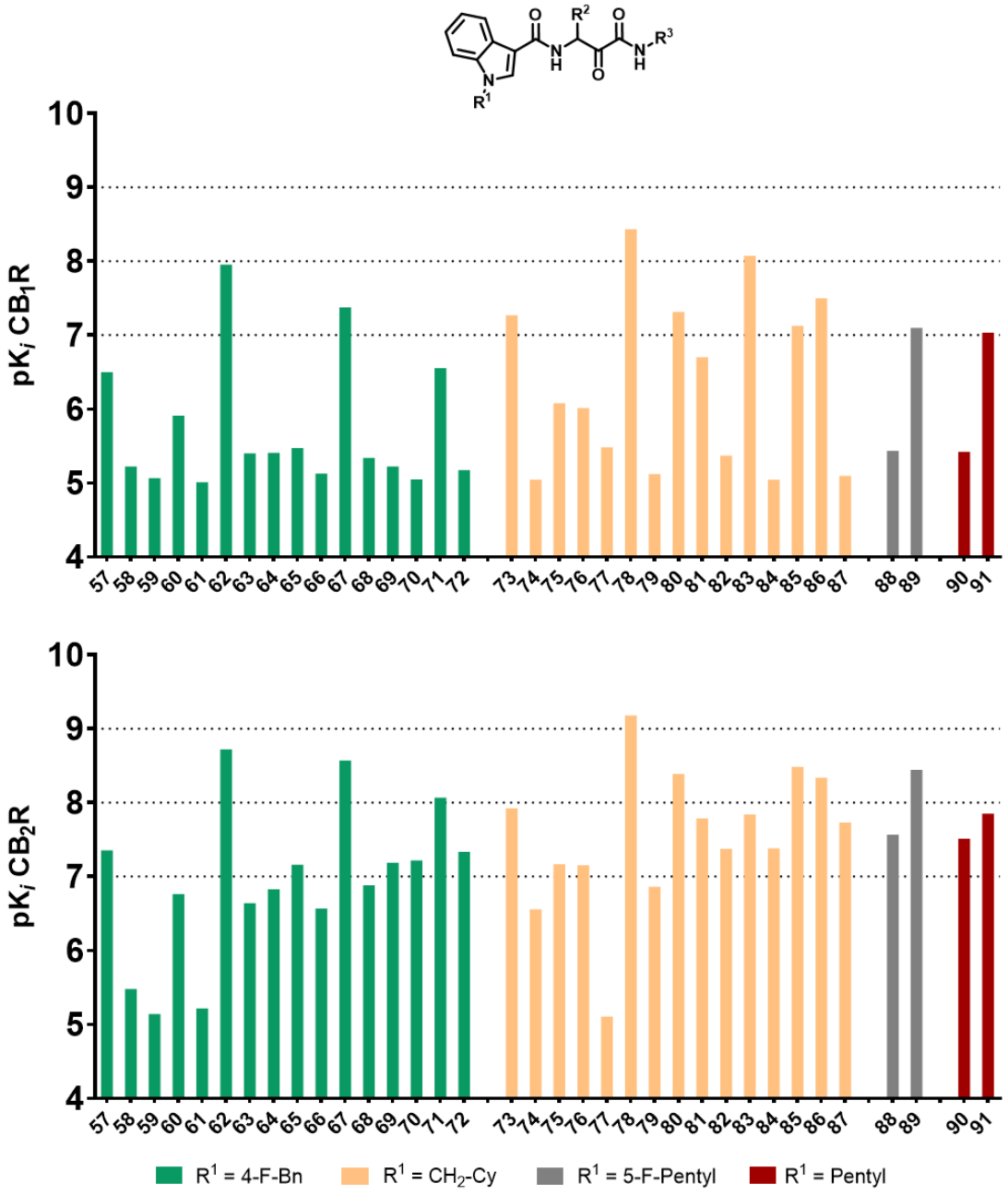



Figure 3.59. Bar chart representation of the SAR trends related to the tail group in the indole derivatives of Series **VI**. $CB_1R$ affinity data (above) and $CB_2R$ affinity data (bottom) are reported.

The second primary distinction among compounds is evident in the tail group, where most molecules were synthesized with either 4-fluorobenzyl or cyclohexyl methyl as substituents at $R^1$. Figure 3.59 shows the affinity data for indole derivatives at $CB_1R$ and

$CB_2R$, separated by their substituent at this position: green represents 4-fluorobenzyl substitution, orange represents cyclohexyl methyl substitution, gray represents 5-fluoropentyl substitution, and red represents pentyl substitution. We will focus on comparisons between the two main residues across the series (4-fluorobenzyl and cyclohexyl methyl), and finally we will study the effect that alkyl chains have on affinity and selectivity. With one exception, derivatives presenting cyclohexyl methyl substitution at position 1 consistently exhibit improved $CB_2R$ affinity in comparison with 4-fluorobenzyl derivatives, even in instances where the latter were found to be inactive. As an example, compounds **82** ($CB_2R$ $K_i$ = 42.4 nM), **84** ($CB_2R$ $K_i$ = 41.5 nM), and **87** ($CB_2R$ $K_i$ = 18.6 nM), all increase the affinity profile for $CB_2R$ compared to their 4-fluorobenzyl homologues **66** ($CB_2R$ $K_i$ = 270 nM), **68** ($CB_2R$ $K_i$ = 130 nM), and **72** ($CB_2R$ $K_i$ = 46.4 nM), respectively. However, substitution with cyclohexyl methyl also results in compounds with enhanced affinity for $CB_1R$, as shown in Figure 3.59.

Additionally, four examples of compounds bearing two different alkyl groups at position 1 were analyzed (Figure 3.60). The ligands were synthesized using indole as core group, (*S*)-*tert*-butyl as linker, and two different $R^3$ substituents for the head group, *tert*-butyl and benzyl. Figure 3.60 shows the results grouped by their substituent at position 3 ($R^3$ = *tert*-butyl on the left part, and $R^3$ = benzyl on the right part).

Molecules with the 5-fluoropentyl substituent exhibited slightly improved affinity for $CB_2R$ in both studied cases, while the removal of the fluor atom resulted in derivatives similarly potent to the original series. Concerning $CB_1R$ affinity, no discernible effect was observed across the different tail groups. Compounds with *tert*-butyl substitution at position 3 were found inactive in all cases, while those with benzyl substitution in position 3 experienced only minor variations and maintained a non-selective profile. Overall, the enhanced affinity for $CB_2R$, coupled with the preservation of complete selectivity ($R^3$ = *tert*-butyl), yielded two compounds with an excellent affinity and selectivity profile: compound **88** ($CB_2R$ $K_i$ = 27.2 nM, SI > 100), and compound **90** ($CB_2R$ $K_i$ = 30.6 nM, SI > 100). Good results were also obtained with cyclohexyl methyl (compound **84**, $CB_2R$ $K_i$ = 41.5 nM, SI > 100). Meanwhile, 4-fluorobenzyl derivative exhibited moderate affinity for $CB_2R$ (compound **68**, $CB_2R$ $K_i$ = 130.7 nM, SI > 100). Furthermore, by comparing the performance of the eight compounds with various tail groups in our study, we can start to observe one of the initial trends that will be discussed later in this text, specifically regarding substitutions at $R^3$.

USC DE SANTIAGO DE COMPOSTELA

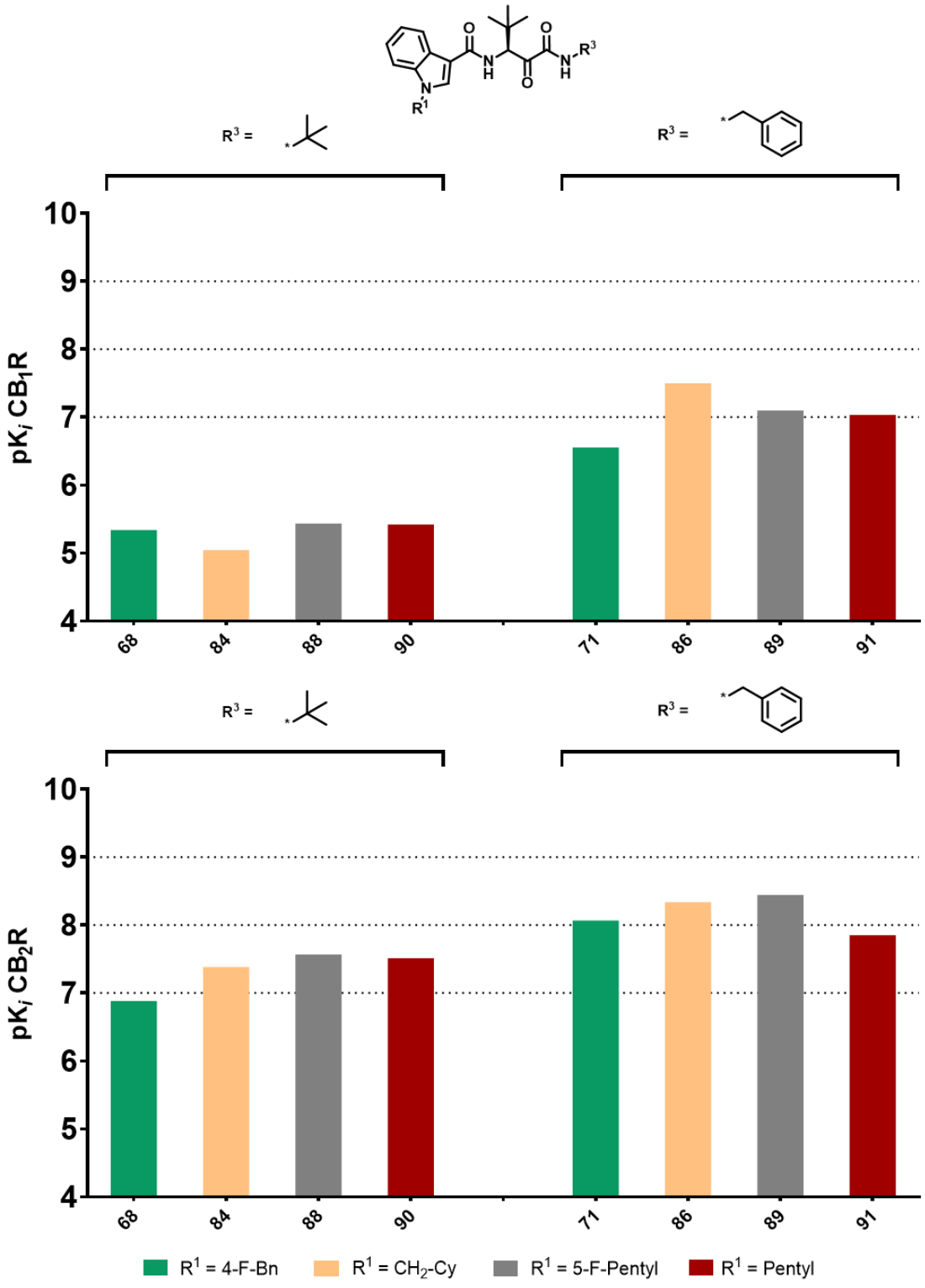



Figure 3.60. Bar chart representation of the SAR trends related to the tail group in the indole derivatives of Series **VI**. $CB_1R$ affinity data (above) and $CB_2R$ affinity data (bottom) are reported.

USC UNIVERSIDADE DE SANTIAGO DE COMPOSTELA

The data presented in Figure 3.60 clearly demonstrates the significantly superior selectivity of *tert*-butyl over benzyl. While the former exhibits lower affinity for $CB_2R$, none of the four compounds with *tert*-butyl as a head group substituent are active in $CB_1R$. In contrast, benzyl derivatives show much higher affinity for $CB_1R$, indicating a non-selective profile.

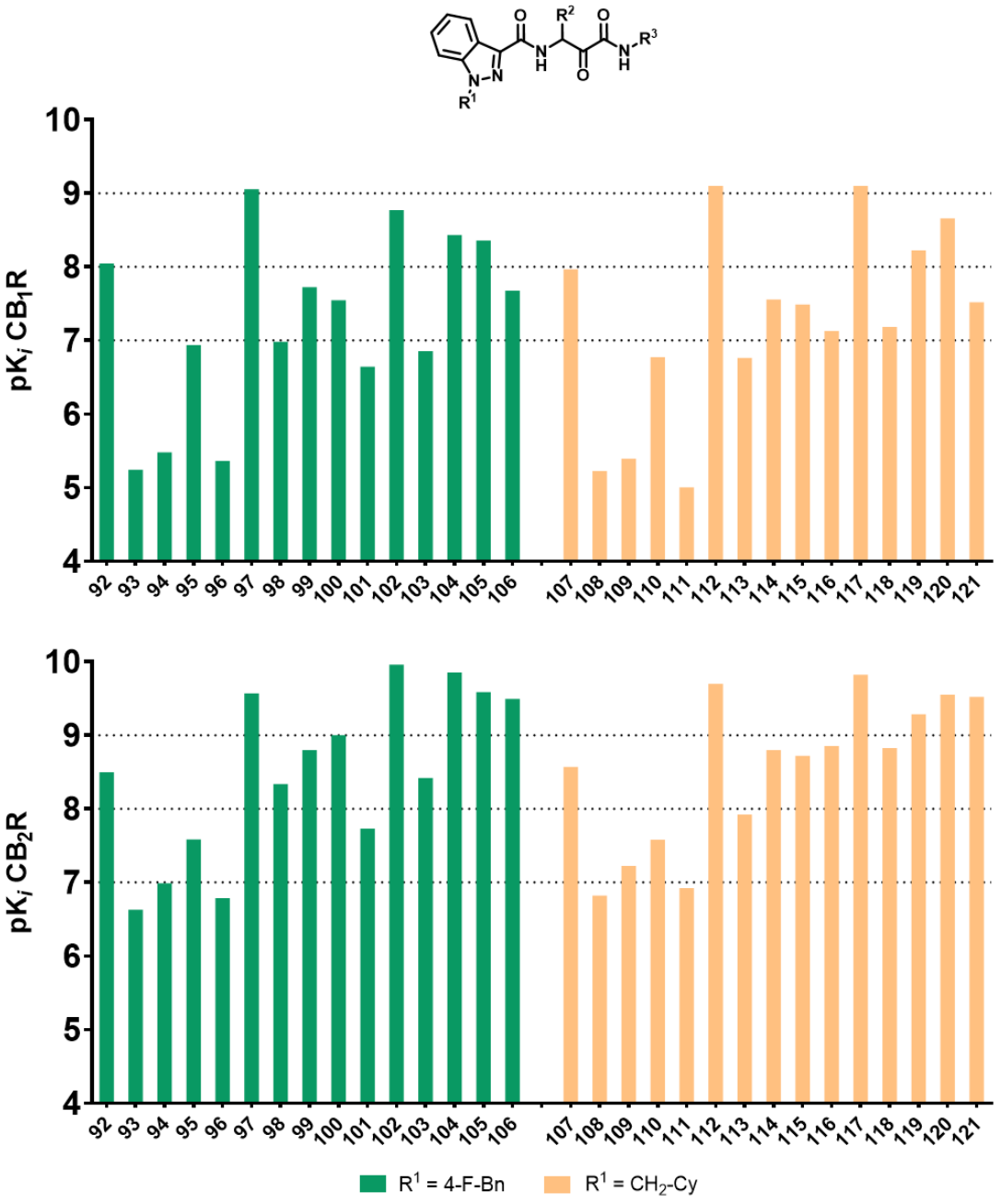



Figure 3.61. Bar chart representation of the SAR trends related to the tail group in the indazole derivatives of Series **VI**. $CB_1R$ affinity data (above) and $CB_2R$ affinity data (bottom) are reported.

USC UNIVERSIDADE DE SANTIAGO DE COMPOSTELA

Figure 3.61 shows the affinity data obtained for indazole derivatives at $CB_1R$ and $CB_2R$ grouped by their substituent at position 1: 4-fluorobenzyl derivatives being represented by green bars, while orange represents cyclohexyl methyl substitution.

Contrary to the observed trends for the indoles, in the case of indazole pairs the effect of the tail group in the $CB_1R$ and $CB_2R$ affinity profile is minimal. The fact that their affinity for both receptors is already significantly higher due to the core group effect may overshadow the impact of substitution at position 1. In contrast, a slight improvement in the selectivity profile is observed for substitution of cyclohexyl methyl with 4-fluorobenzyl. Figure 3.62 shows the affinity trends explained above and provides valuable insights into the selectivity profile of each series of $R^1$ substituents.

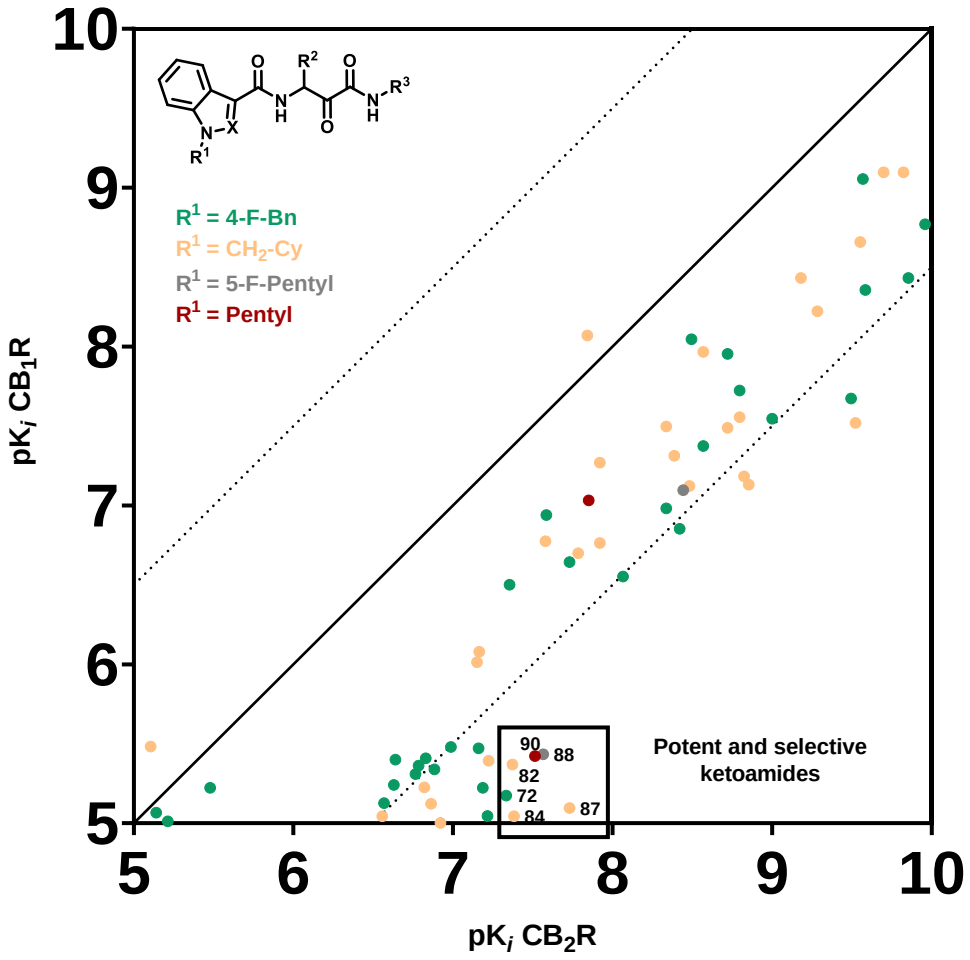



Figure 3.62. $CB_1R$ $pK_i$ [-log($K_i$)] vs $CB_2R$ $pK_i$ [-log($K_i$)] representation of substitution at position 1. 4-F-Bn: green dots, $CH_2$-Cy: orange dots, 5-F-Pentyl: Gray dots, and Pentyl: red dots.

USC UNIVERSIDADE DE SANTIAGO DE COMPOSTELA

As mentioned earlier, cyclohexyl methyl derivatives appear closer to the right-end part of the graph than 4-fluorobenzyl derivatives, meaning a higher $CB_2R$ affinity. In contrast, their worse selectivity profile shifts them upwards, near the identity line. The section next to the origin axis further supports this trend, exhibiting three 4-fluorobenzyl ligands for just one cyclohexyl methyl derivative. The most interesting part of the representation is the middle-bottom part of the graph. Molecules with high potency for $CB_2R$ and complete selectivity towards $CB_1R$ will be plotted here. This group of molecules is primarily formed by compounds with a tail group comprised of 4-fluorobenzyl (12 derivatives), accounting for their better selectivity profile. However, only one such derivative (compound **72**, Figure 3.64) is among the best six molecules of the series, which are predominantly comprised of cyclohexyl methyl derivatives (compounds **82**, **84**, and **87,** Figure 3.64), along with two of the 5-fluoropentyl and pentyl derivatives (compounds **88** and **90,** Figure 3.64). In summary, cyclohexyl methyl presents a better affinity profile, while 4-fluorobenzyl exhibits improved selectivity (Figure 3.63).

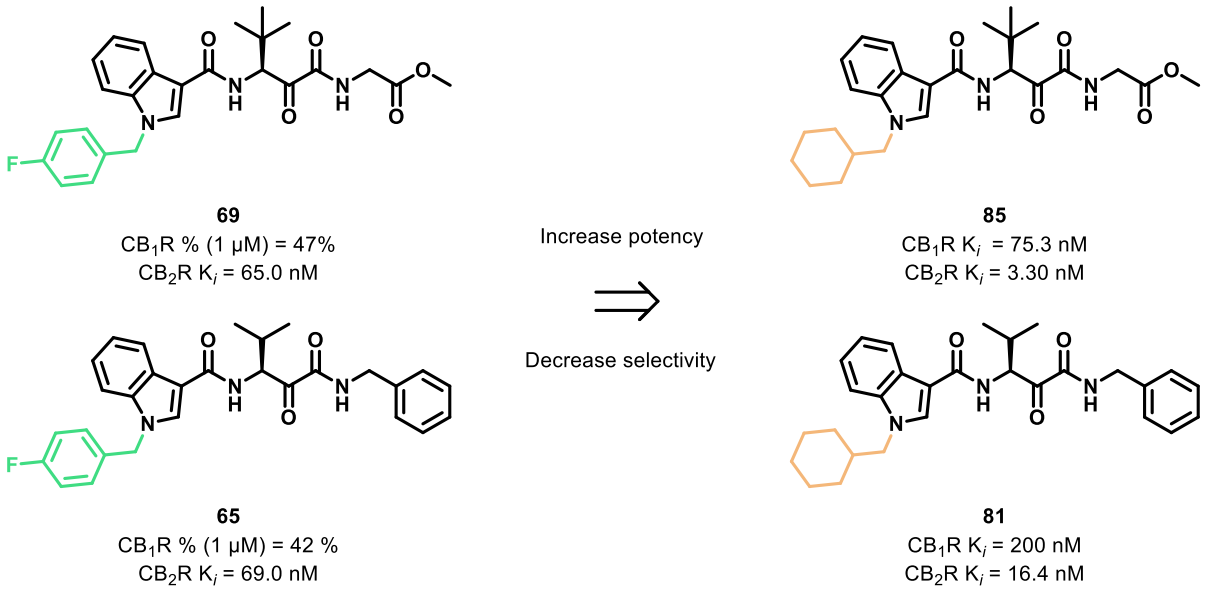



Figure 3.63. Change in the binding profile through substitution of the tail group.

USC UNIVERSIDADE DE SANTIAGO DE COMPOSTELA

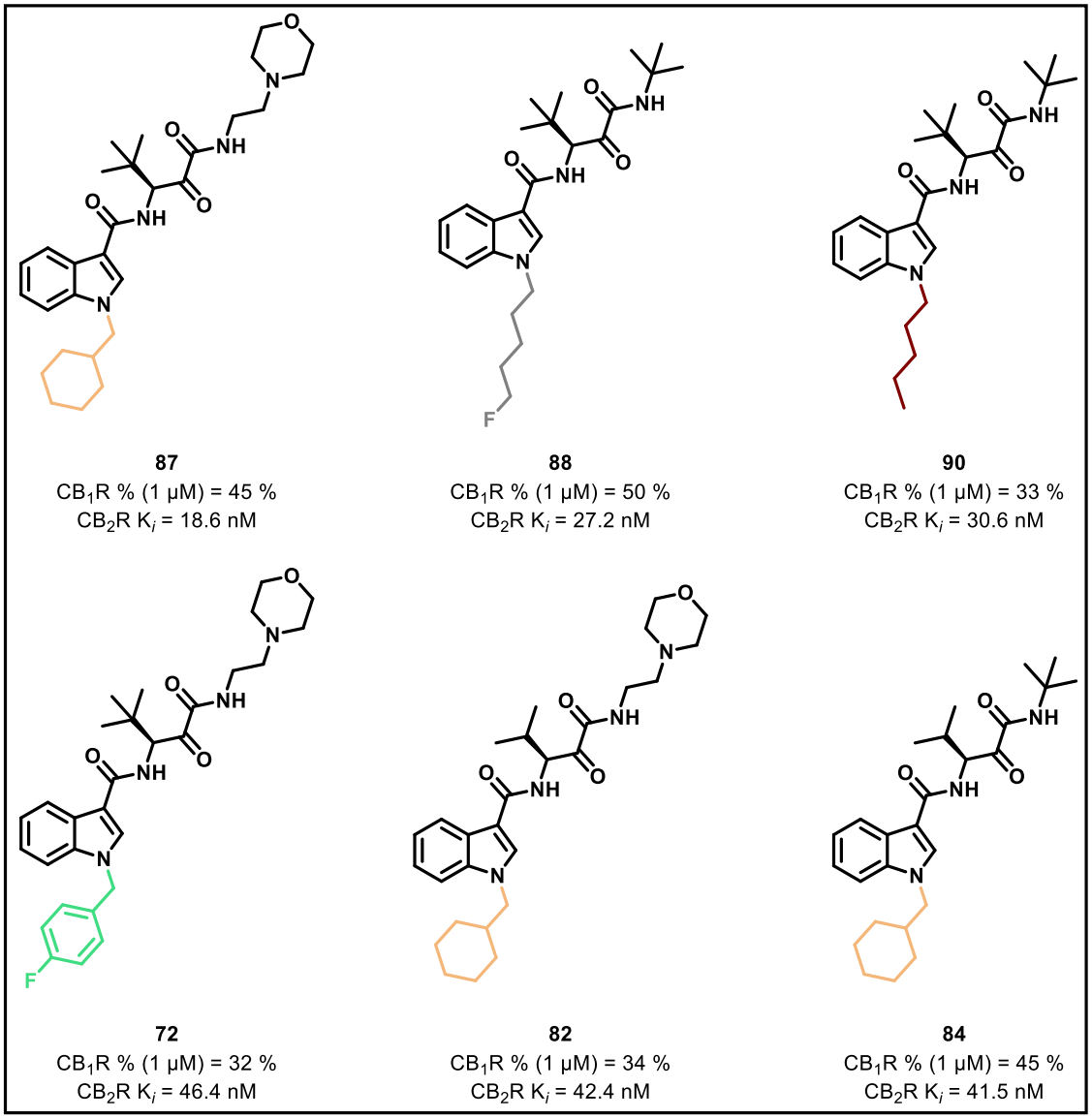



Figure 3.64. Structure of the best ligands obtained through optimization of the tail group in Series **VI**.

USC
UNIVERSIDADE DE SANTIAGO DE COMPOSTELA

To better understand the impact of substitution at $R^2$, we will compare sets of three ligands, with the only variation being in this specific residue. Figure 3.65 displays a chosen selection of results.

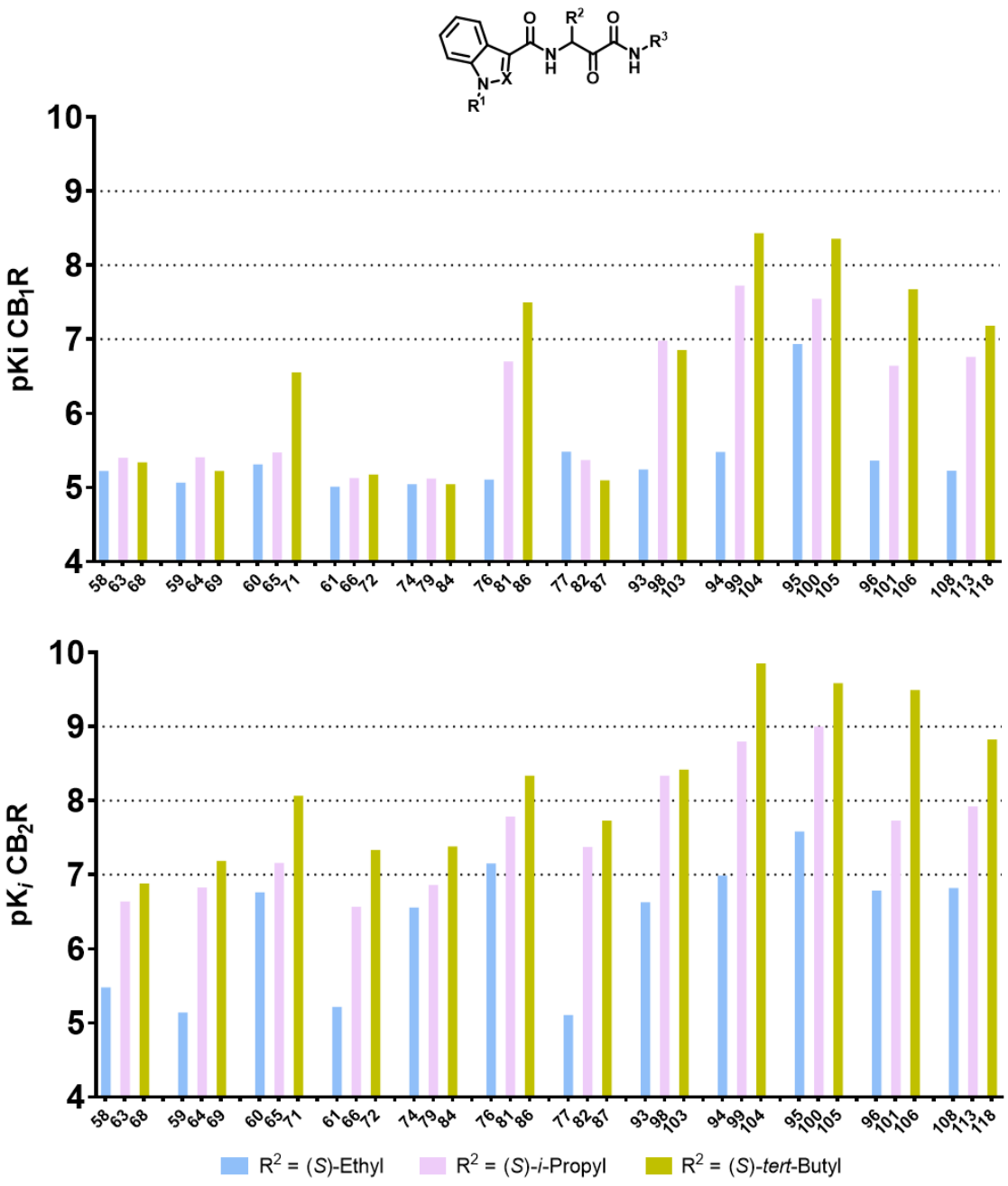



Figure 3.65. Bar chart representation of the SAR trends related to the linker in Series **VI**. $CB_1R$ affinity data (above) and $CB_2R$ affinity data (bottom) are reported. Blue: (*S*)-ethyl substitution, Pale pink: (*S*)-*i*-propyl substitution and ochre: (*S*)-*tert*-butyl substitution.

USC UNIVERSIDADE DE SANTIAGO DE COMPOSTELA

A clear trend emerges, with $CB_2R$ affinity increasing alongside the size of the substituent. Among these ligands, those incorporating *tert*-butyl substituents demonstrate the highest potency at both receptors in this series, followed by those with *i*-propyl substituents. Conversely, the ethyl-substituted ligands fall behind, displaying the lowest affinity for $CB_1R$ and $CB_2R$. The disparity in affinity between the ethyl-bearing ligands and the preceding two groups is notably more pronounced.

$CB_1R$ affinity also increases with the size of the substituent at position 2; however, there is a large number of derivatives that retain complete selectivity despite the presence of (*S*)-*tert*-butyl as the linker. This trend suggests that $CB_2R$ affinity increases more rapidly than $CB_1R$ affinity with bulky substituents at $R^2$.

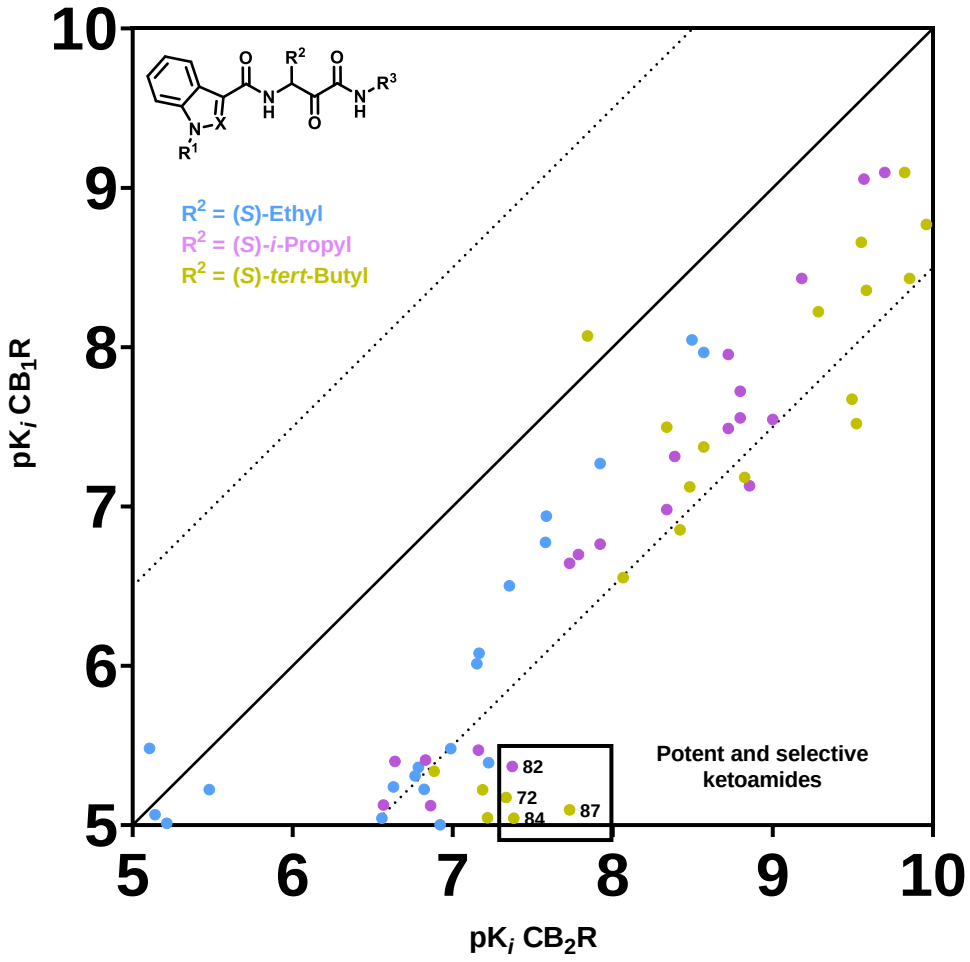



Figure 3.66. $CB_1R$ $pK_i$ [-log($K_i$)] vs $CB_2R$ $pK_i$ [-log($K_i$)] representation of substitution at position 2. Blue: (*S*)-ethyl substitution, Purple: (*S*)-*i*-propyl substitution and ochre: (*S*)-*tert*-butyl substitution.

USC UNIVERSIDADE DE SANTIAGO DE COMPOSTELA

Figure 3.66 shows a graphical representation of potency and selectivity focused on $R^2$ substitution. As observed in the plot, all compounds with the (*S*)-*tert*-butyl residue exhibit affinity at $CB_2R$, and their high binding for this receptor is accompanied by an increase in affinity for $CB_1R$. Consequently, these derivatives are distributed across two regions on the graph: those in the upper-right section, representing non-selective molecules with high affinity for both $CB_1R$ and $CB_2R$, and those in the lower-right section, representing potent and selective compounds, where they contribute with the best three compounds of the analysis (compounds **72**, **84**, **87**). (*S*)-*i*-propyl derivatives follow a similar distribution pattern, but they are slightly skewed to the left and lower section of the graph compared to (*S*)-*tert*-butyl derivatives, indicating lower affinity for both receptors. Among the top four derivatives in this study, we find one representative of (*S*)-*i*-propyl substitution, which is compound **82**. Finally, derivatives with (*S*)-ethyl substitution exhibit modest affinity for both receptors and include a group clustered around the origin of the axis, indicating inactive compounds at both $CB_1R$ and $CB_2R$.

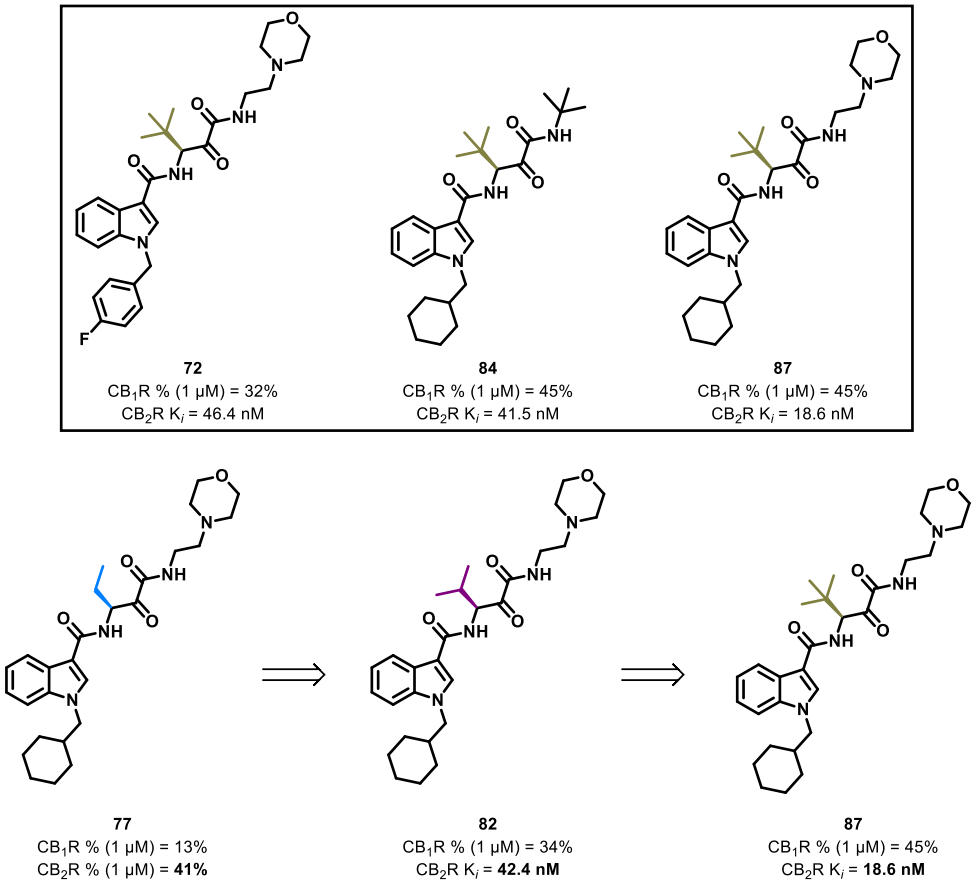



Figure 3.67. Structure of potent and selective $CB_2R$ ligands depending on their linker and increase in $CB_2R$ affinity with $R^2$ substitution size.

Once these trends were stablished, we examined the effect of the linker stereochemistry on the affinity and selectivity profiles. Consequently, we synthesized a small collection of 16 derivatives (8 ketoamides and 8 hydroxyamides) bearing the (*R*) configuration at $R^2$. To develop this subset of compounds, we utilized the linker with the best pharmacological profile, namely (*S*)-*tert*-butyl. We synthesized both indole and indazole derivatives, along with the main tail groups of this work, 4-fluorobenzyl and cyclohexyl methyl. Finally, we selected unsubstituted terminal amide and *tert*-butyl as head groups. Restricting the diversity at this position to just two options allows for more meaningful comparisons within the set. The data corresponding to the hydroxyamide compounds will be analyzed later in the text. The results of this set of compounds are presented in Figure 3.68, alongside the data for their (*S*)-*tert*-butyl counterparts.

Apart from one case, the (*S*) configuration shows slightly higher affinity for both $CB_1R$ and $CB_2R$. This enhanced affinity for $CB_1R$ results in a more favorable selectivity profile for compounds bearing the (*R*) configuration at position 2, exemplified by the presence of three compounds in this set that meet the affinity and selectivity criteria: compound **127** ($CB_2R$ $K_i$ = 13.6 nM, SI > 100), compound **128** ($CB_2R$ $K_i$ = 44.2 nM, SI > 100) and compound **129** ($CB_2R$ $K_i$ = 8.90 nM, SI > 100). Meanwhile, the (*S*) configuration only features one such compound (**84**, $CB_2R$ $K_i$ = 41.5 nM, SI > 100). In overall assessment, the sample size is insufficient for drawing substantial conclusions, but it appears that both configurations yield promising results.

Comparisons between these sets of molecules ((*S*)- and (*R*)-linker derivatives) also offer valuable insights into the impact of the head group, which will be further explored later in the text. As observed in Figure 3.68, unsubstituted terminal amide derivatives exhibit significantly higher affinity at both receptors compared to those with *tert*-butyl substitution at position 3. The increase in affinity is particularly pronounced in $CB_1R$, where most of the *tert*-butyl $R^3$-substituted derivatives are inactive. Consequently, compounds lacking a $R^3$ substituent display a non-selective profile similar to that of SCRAs. In contrast, compounds with a *tert*-butyl residue as the head group achieve complete selectivity while still maintaining most of their potency for $CB_2R$, which make these molecules potent and selective $CB_2R$ ligands.

USC UNIVERSIDADE DE SANTIAGO DE COMPOSTELA

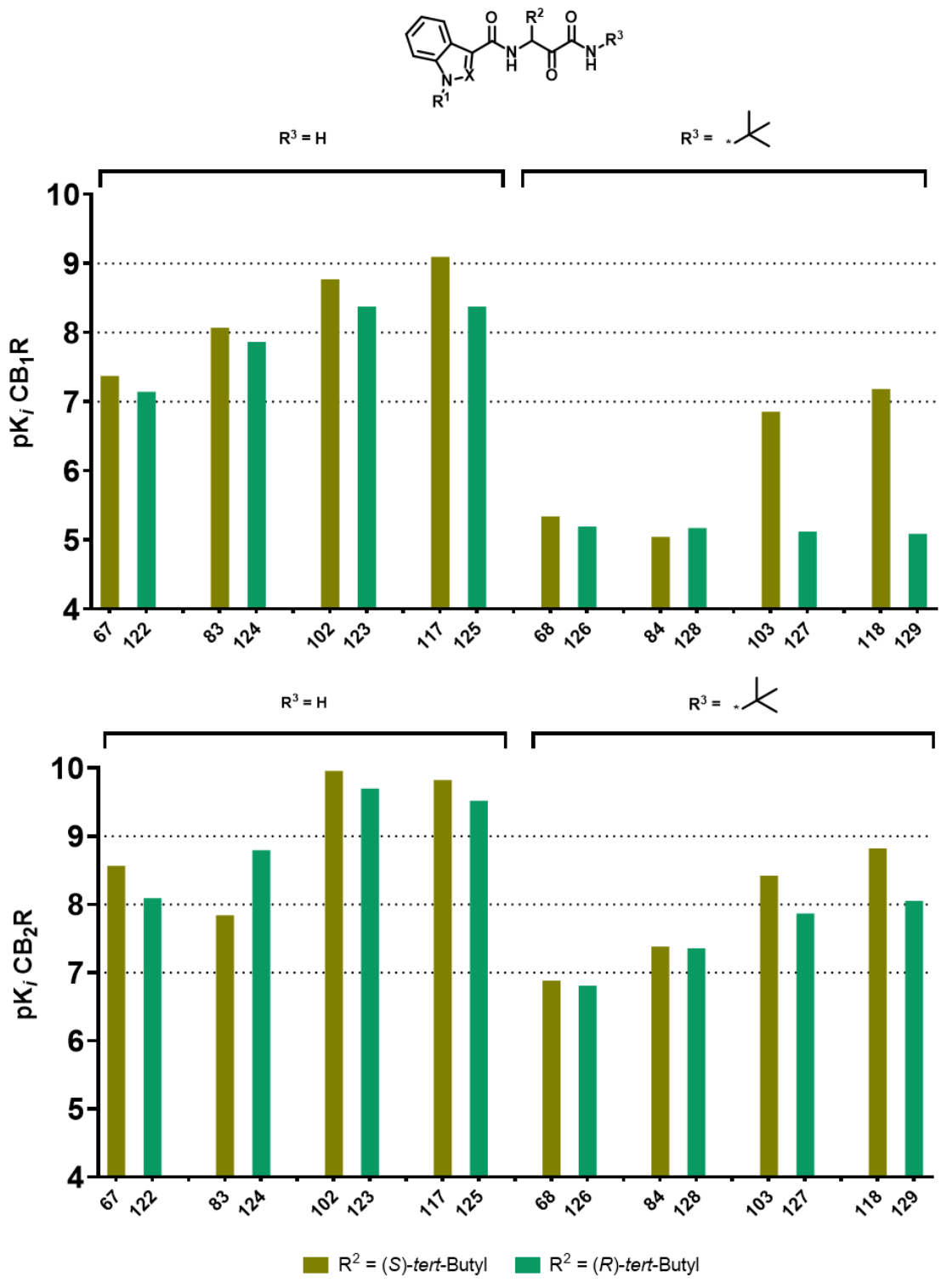



Figure 3.68. Bar chart representation of the SAR trends related to the linker configuration in Series **VI**. $CB_1R$ affinity data (above) and $CB_2R$ affinity data (bottom) are reported. Ochre: (*S*)-tert-butyl substitution, and green: (*R*)-*tert*-butyl substitution.

USC UNIVERSIDADE DE SANTIAGO DE COMPOSTELA

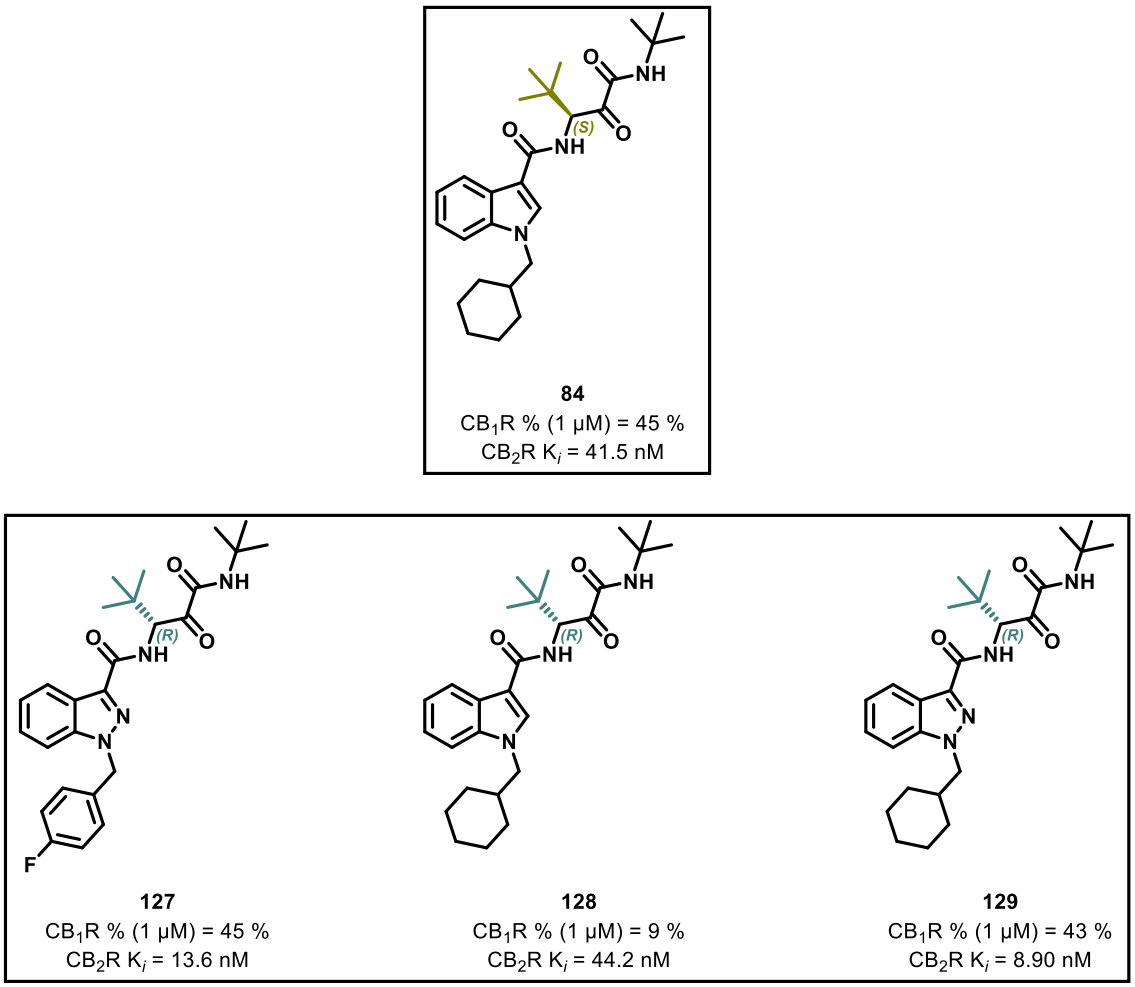



Figure 3.69. Structure and cannabimimetic data for top compounds of Series **VI** based on their linker stereochemistry.

USC
UNIVERSIDADE DE SANTIAGO DE COMPOSTELA

The greatest structural diversity is found at position 3, and the patterns are less distinct than in earlier studies due to the array of results (Figure 3.70).

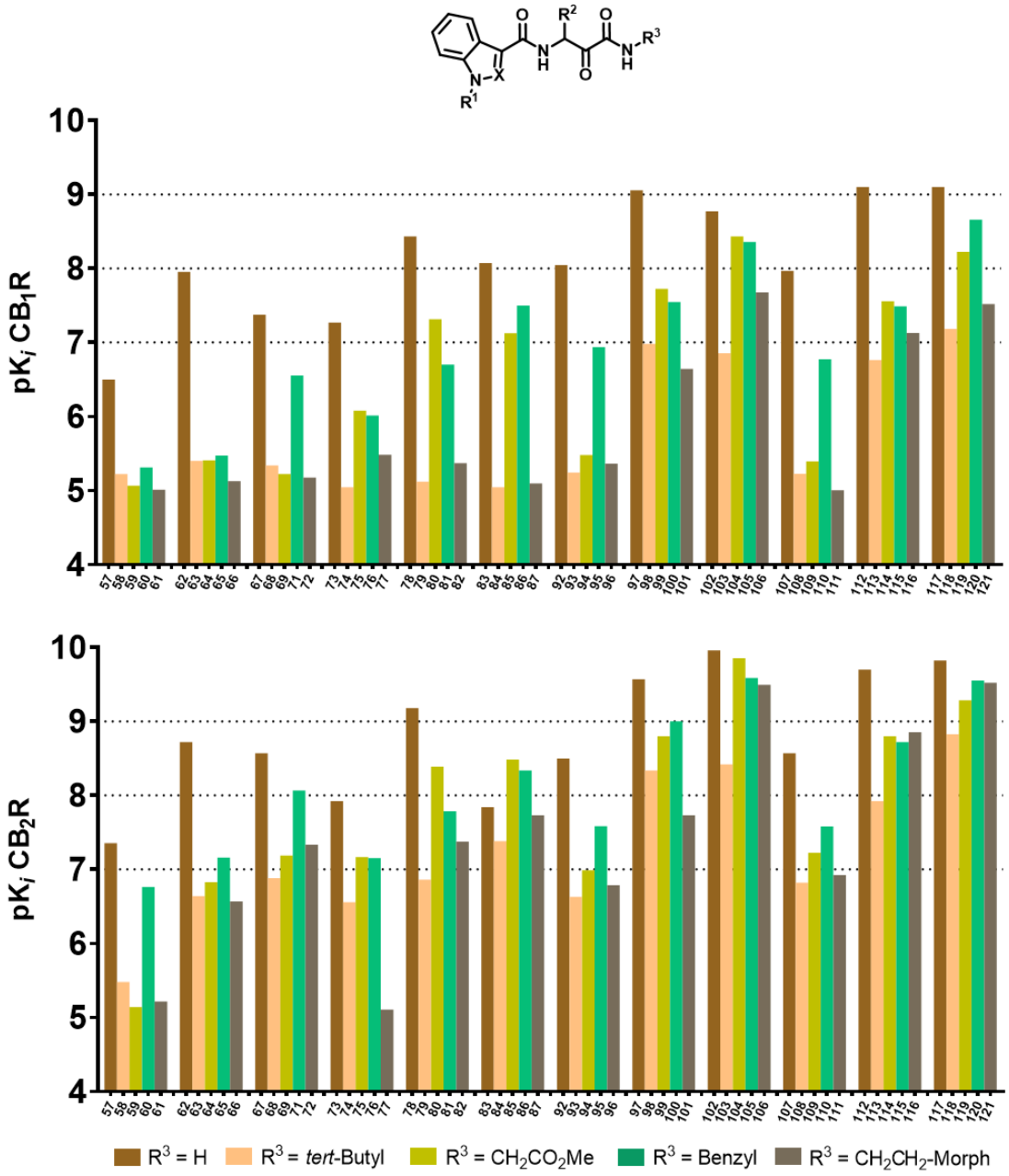



Figure 3.70. Bar chart representation of the SAR trends related to the head group in Series **VI**. $CB_1R$ affinity data (above) and $CB_2R$ affinity data (bottom) are reported. Brown: H, Pink: *tert*-Butyl, Ochre: $CH_2CO_2Me$, Green: Benzyl, and Gray: $CH_2CH_2$-Morph.

Position $R^3$ encompasses six different substituents, although there is only one instance with acetamide as the head group. The five primary residues at $R^3$ are: hydrogen, *tert*-butyl,

methoxycarbonyl methyl, benzyl, and morpholinoethyl. Affinity data for Series **VI** at $CB_1R$ and $CB_2R$ are shown in Figure 3.70 as a bar chart where compounds sharing the same core group, tail group, and linker are represented together. In this representation the sole distinction between compounds within a bar set lies in the head group ($R^3$). Substitution at position 3 is represented in the graph as follows: brown: H, pink: *tert*-butyl, ochre: $CH_2CO_2Me$, green: benzyl, and gray: $CH_2CH_2$-Morph.

As observed in the chart, the unsubstituted terminal amide yields the most potent derivatives in the series, displaying the highest $CB_2R$ affinity among all. For instance, compounds **97** ($CB_2R$ $K_i$ = 0.27 nM, SI = 3.25) or **117** ($CB_2R$ $K_i$ = 0.15 nM, SI = 5.33), even reach the picomolar range in terms of affinity. However, they also exhibit the highest $CB_1R$ affinity of this subset, with binding values very similar to those for $CB_2R$. Consequently, these compounds are non-selective, with a selectivity index barely reaching 15 in the best cases. Their similarity to the original SCRAs explains why they are active at both receptors. These results reinforce our design strategy of introducing groups ($R^3$) at the terminal amide.

$CH_2CO_2Me$ and benzyl exhibit a comparable pharmacological profile. Both substituents yield potent $CB_2R$ derivatives, occasionally matching the affinity of unsubstituted amides (compounds **119**, $CB_2R$ $K_i$ = 0.52 nM, SI = 11.5, or **120**, $CB_2R$ $K_i$ = 0.28 nM, SI = 7.85). However, their affinity for $CB_1R$ is also notably high, generally categorizing them as non-selective ligands.

Similarly, *tert*-butyl and morpholinoethyl exhibit common binding characteristics. Derivatives bearing these substituents in position 3 rank as the least potent for the $CB_2R$ among all compounds, consistently falling behind in every comparison. However, in contrast to previous substitutions, *tert*-butyl and morpholinoethyl also demonstrate the lowest affinity for $CB_1R$, contributing to the majority of potent and completely selective ligands within this series. Interestingly, the best compounds in the series (**87**, **121**, **127**, **129**) feature either *tert*-butyl or morpholinoethyl as a substituent. This implies that distinctions among residues at this structural position have a minor impact on the affinity profile, as it is predominantly determined by the core group (indoles/indazoles) and substitution at $R^2$ (bulky substituents). Consequently, the principal significance of this diversity resides in its influence on selectivity. Figure 3.71 shows the square plot representing the binding data at $CB_1R$ and $CB_2R$ simultaneously.

USC UNIVERSIDADE DE SANTIAGO DE COMPOSTELA

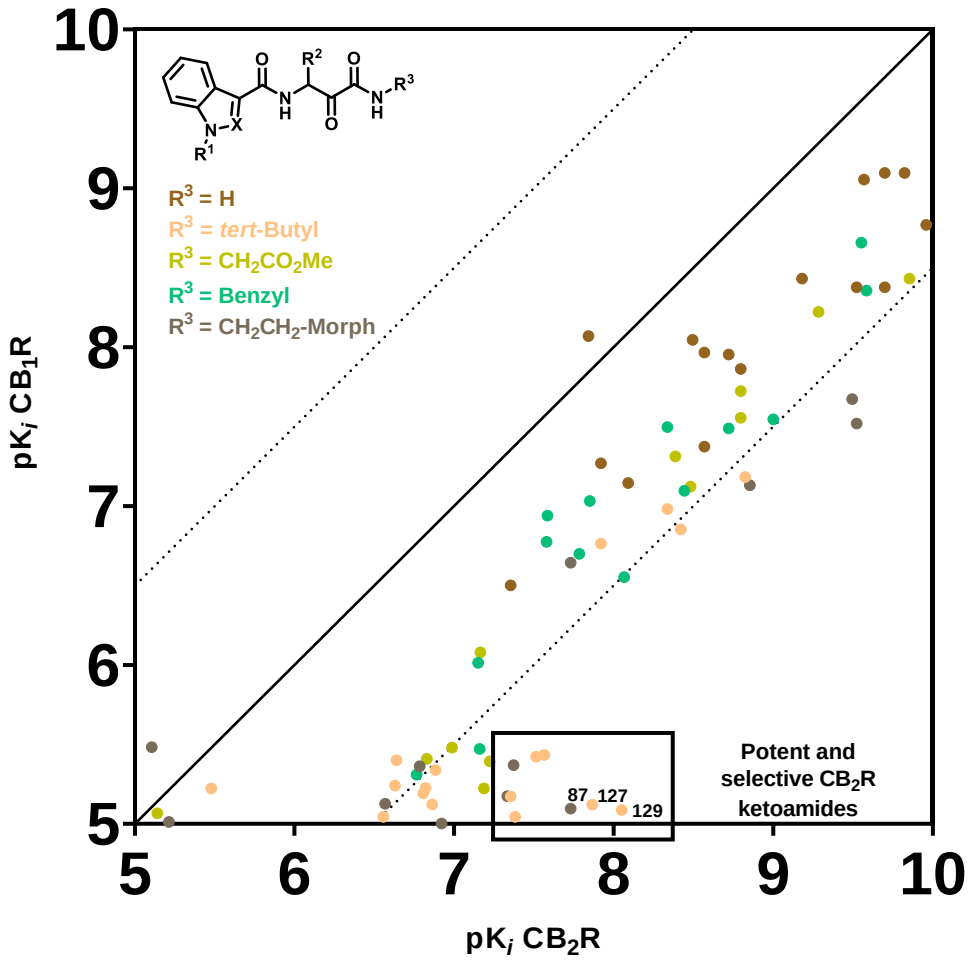



Figure 3.71. $CB_1R$ $pK_i$ [-log($K_i$)] vs $CB_2R$ $pK_i$ [-log($K_i$)] representation of substitution at position 3. Brown: H, Pink: *tert*-Butyl, Ochre: $CH_2CO_2Me$, Green: Benzyl, and Gray: $CH_2CH_2$-Morph.

As previously noted, molecules featuring an unsubstituted amide at position 3 (brown dots) are located at the upper end of the graph, signifying the highest potency within the series. However, this positioning also implies poor selectivity, as they are situated near the identity line, and, consequently, exhibit a dual $CB_1R/CB_2R$ profile. Compounds demonstrating strong selectivity towards $CB_1R$ are situated closer to the lower dashed line. In this context, the substituents $CH_2CO_2Me$ and benzyl each contribute four compounds positioned along this line, while the remaining ligands are located between the identity line and the lower dashed line. This distribution indicates a still relatively modest selectivity profile, although significantly better compared to unsubstituted amides. Six compounds in this group meet the selectivity criteria, with some of them exhibiting remarkably high affinity for

USC UNIVERSIDADE DE SANTIAGO DE COMPOSTELA

$CB_2R$. For example, compounds **65** ($CB_2R$ $K_i$ = 65 nM) and **109** ($CB_2R$ $K_i$ = 59.7 nM) combine a $CB_2R$ $K_i$ value lower than 70 nM and complete selectivity towards $CB_1R$.

Esters are recognized for their rapid metabolism within the body, and as a result, they are usually avoided during the drug candidate optimization process. However, their easy accessibility provides valuable insights into incorporating polar substituents within the ligand's structure. To tackle this metabolic issue, we opted to transform one of the compounds containing $CH_2CO_2Me$ into its corresponding amide form and then assess the pharmacological profile of the new derivative **70**. The results are shown in Figure 3.72.

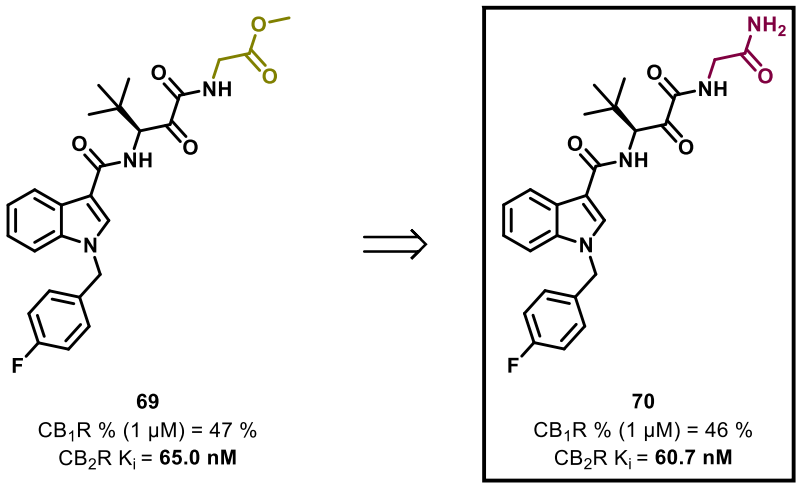



Figure 3.72. Pharmacomodulation of $CH_2CO_2Me$ derivative **69** and change in the affinity and selectivity profile.

As shown in the figure, their binding profiles are nearly identical, with no significant change in affinity for $CB_2R$ and the retention of complete selectivity. While this is just one example of substituting the methyl ester with the corresponding amide, the results appear promising and suggest a viable solution to any metabolic issues associated with esters. We are currently transforming all the methyl esters obtained in this chapter into their corresponding amides.

Lastly, *tert*-butyl and morpholinoethyl yield the derivatives with the lowest affinity for $CB_2R$. However, their distribution throughout the diagonal plot indicates a much more favorable selectivity profile. Out of 30 ligands bearing any of these head groups, only eight display significant activity at the $CB_1R$. The remaining compounds are clustered in the lower-mid zone of the graph (with three exceptions that show no activity at any receptor), indicating a combination of complete selectivity towards $CB_1R$ with high affinity for $CB_2R$ (in the range of 8 nM – 200 nM). This makes a total of 19 potent and highly $CB_2R$-selective ligands,

USC
DE SANTIAGO
DE COMPOSTELA

revealing tert-butyl and morpholinoethyl as the optimal substituents in the head group for achieving selectivity. Furthermore, the fact that the substituents displaying the lowest affinity for $CB_2R$ yield the compounds with the best pharmacological profile (**87**, **88**, **90**, **127**, **129**) suggests that pharmacomodulation of the head group is key for achieving selectivity, while its role in affinity is less important. Potency at $CB_2R$ is provided by the SCRA scaffold, and is strongly determined by the core group and the linker, similar to the observed trend in Gioè's work. Figure 3.73 shows the most interesting ligands obtained in Series **VI**, and summarizes the optimal substituents in each position:

1. The core group can consist of both indole or indazole.
2. Each tail group exhibits specific characteristics, but all four are suitable for achieving high potency and selectivity.
3. Bulky substituents as linker promote a favorable pharmacological profile, and both configurations yield positive outcomes.
4. *Tert*-butyl and morpholinoethyl provide the most selective ligands.

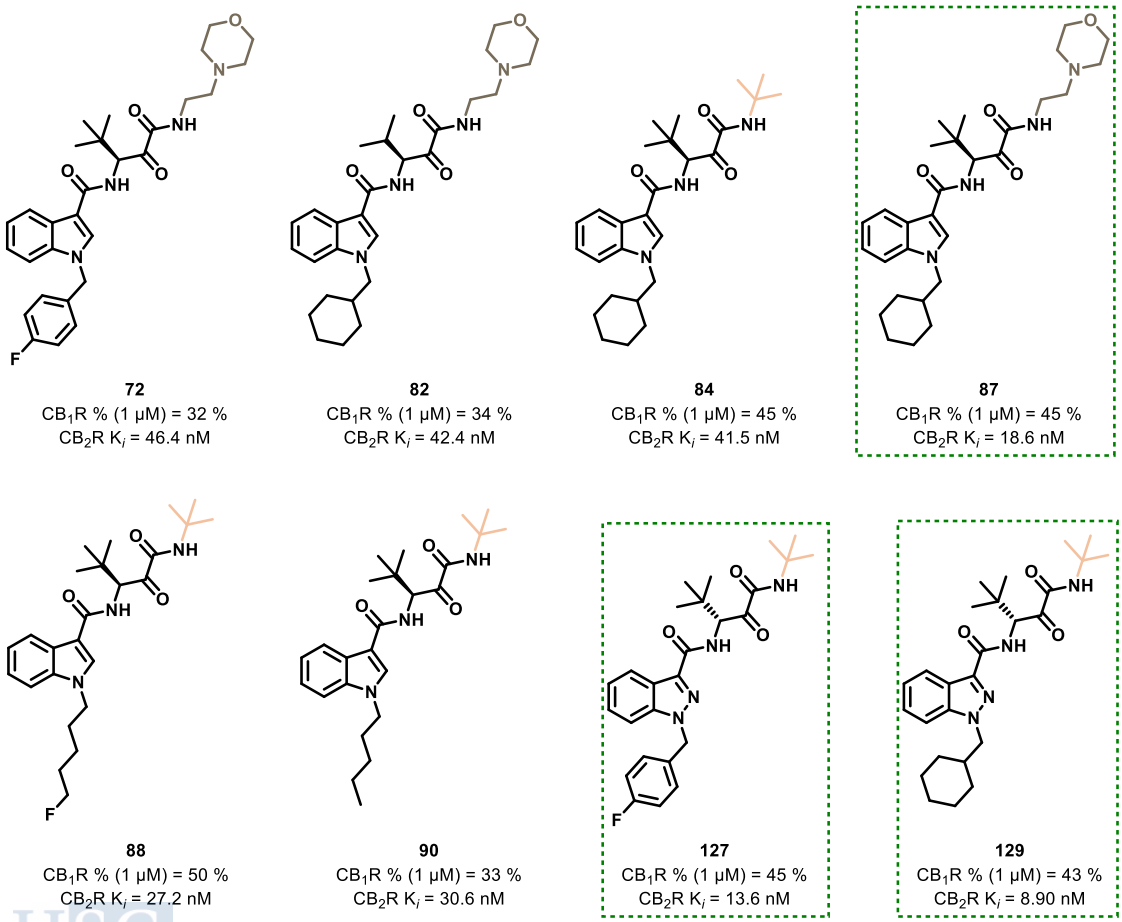



Figure 3.73. Structure of the best ligands identified in Series **VI**.

The cannabinergic affinity profiles of the 82 hydroxy carboxamides are presented in Table 3.19 to Table 3.26. Up to 28 ligands exhibit attractive affinity for $CB_2R$ ($K_i$ < 70 nM) and exceptional subtype selectivity (> 100-fold), including 20 ligands combining complete selectivity with a $CB_2R$ $K_i$ lower than 50 nM and 11 ligands with a similar selectivity profile and a $CB_2R$ $K_i$ lower than 20 nM. The various trends investigated in the preceding series remain consistent in the current one. However, this series introduces nearly twice as many molecules that combine high potency and complete selectivity towards $CB_1R$. Moreover, while Series **VI** featured three molecules with a $CB_2R$ $K_i$ lower than 20 nM and complete selectivity, nine hydroxyamides now meet these criteria. The improvement is not attributable to the affinity profile, which is superior in Series **VI** compared to Series **VII**. Instead, it is the substantial increase in selectivity resulting from the hydroxy substituent in place of the carbonyl group. To put this in perspective, more than half of the carboxamides in Series **VI** (42 molecules) exhibit $CB_1R$ affinity at a level deemed non-selective, whereas only 11 hydroxyamides fall within this range of $CB_1R$ potency. The results of this series further evidence the effectiveness of the pharmacomodulation process, which, starting from model dual $CB_1R$-$CB_2R$ prototypes, enabled us to dissociate completely the binding profile from these receptors and discover novel and potent ligands that specifically recognize the $CB_2R$. Within the hydroxyamide series, we have isolated the predominant diastereomer corresponding to the (*R*) configuration, according to the structural characterization data. As observed in Figure 3.74 and Figure 3.75, among the most attractive ligands, 17 derivatives belong to the indole series (**130**, **137**, **140**, **142**, **143**, **144**, **148**, **149**, **151**, **153**, **154**, **156**, **158**, **159**, **195**, **197**, **199**) and 11 ligands belong to the indazole series (**165**, **168**, **172**, **173**, **178**, **182**, **183**, **188**, **191**, **193**, **194**). Ligands **154**, **156**, **158**, **195**, **197**, **165**, **178**, **188** and **193** stand out for their excellent potency ($K_i$ < 20 nM) and selectivity profile (> 100-fold).

USC
UNIVERSIDADE DE SANTIAGO DE COMPOSTELA

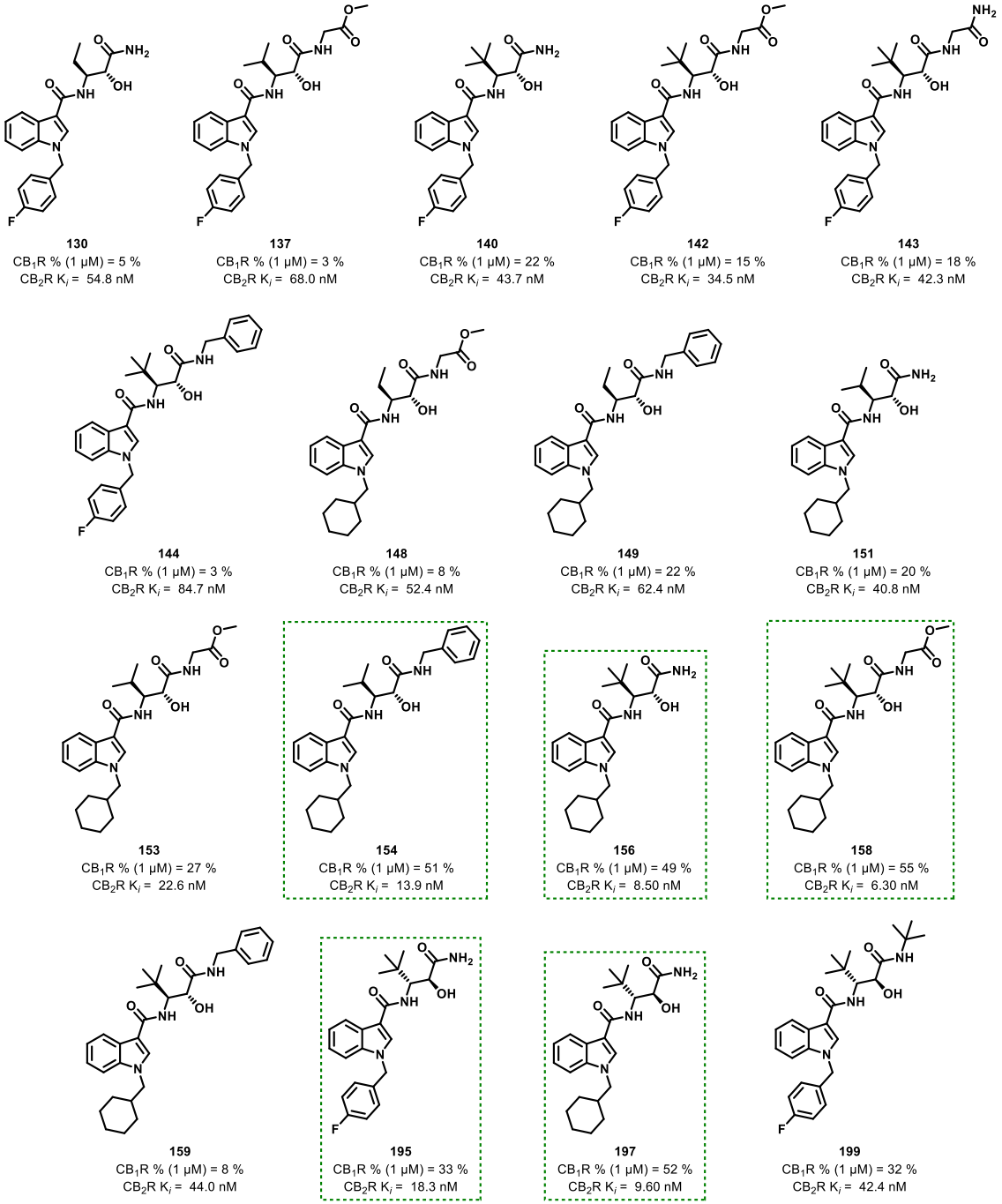



Figure 3.74. Structure and cannabimimetic data of most attractive selective $CB_2R$ indole ligands (Series **VII**) identified during this study.

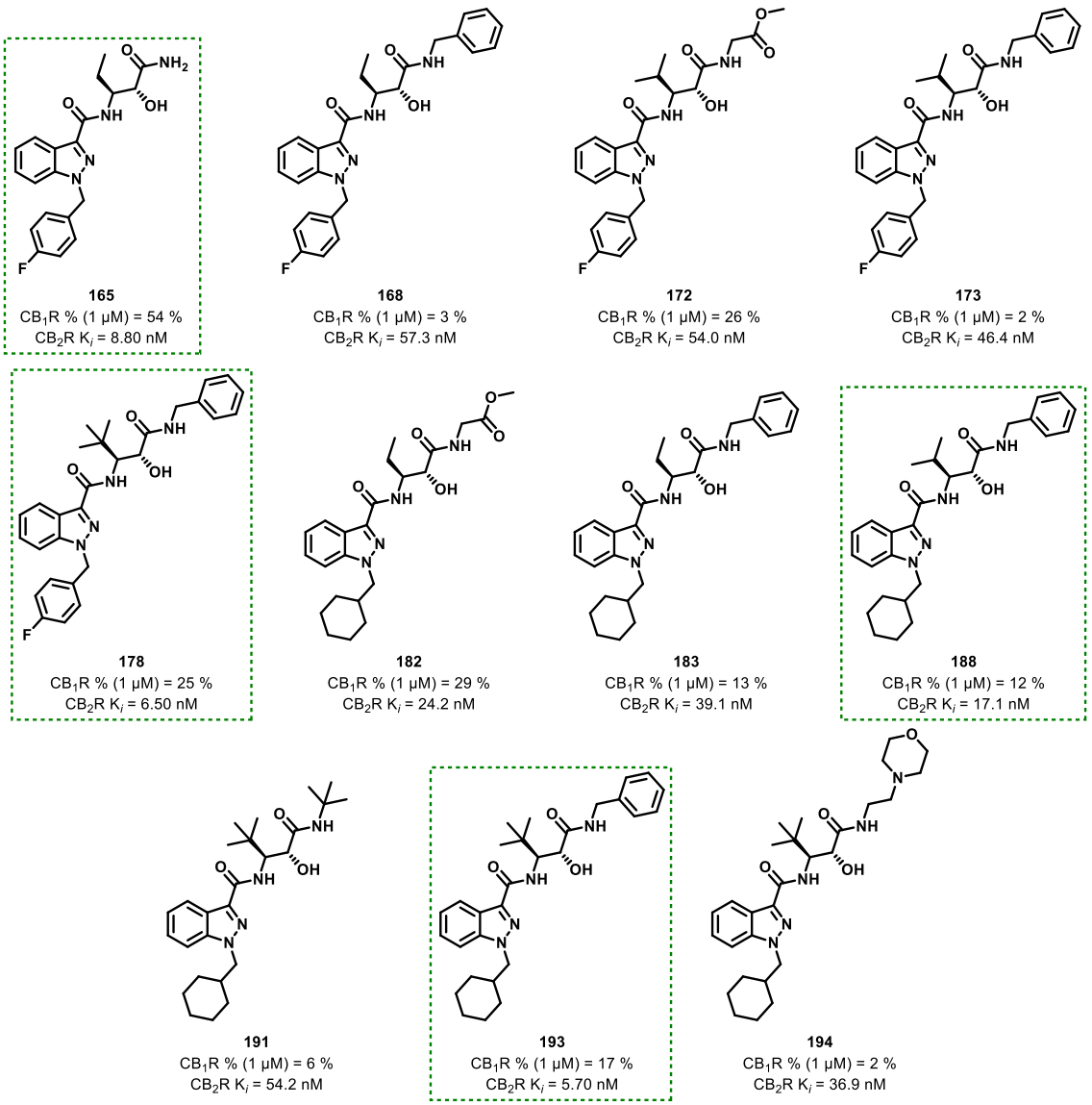



Figure 3.75. Structure and cannabimimetic data of most attractive selective $CB_2R$ indazole ligands (Series **VII**) identified during this study.

During the PADAM sequence to yield the hydroxyamides (**130**-**202**) a new stereocenter is created. As outlined in the chemistry section, we first investigated the impact of the configuration of this asymmetrical carbon on the affinity and selectivity profile of Series **VII**. Our goal was to identify the eutomer and focus our efforts on obtaining the most pharmacologically interesting diastereomer. To achieve this, a set of nine compounds was synthesized and both diastereomers were purified and isolated following the procedure detailed in the experimental section. Stereochemistry assignment was mostly based on $^{13}C$ NMR techniques, relying on information obtained from a single crystal X-ray crystallography

USC UNIVERSIDADE DE SANTIAGO DE COMPOSTELA

of compound **(2*S*)-188**, as explained in the chemistry section. The results are presented in Table 3.25, Table 3.26, and Figure 3.76.

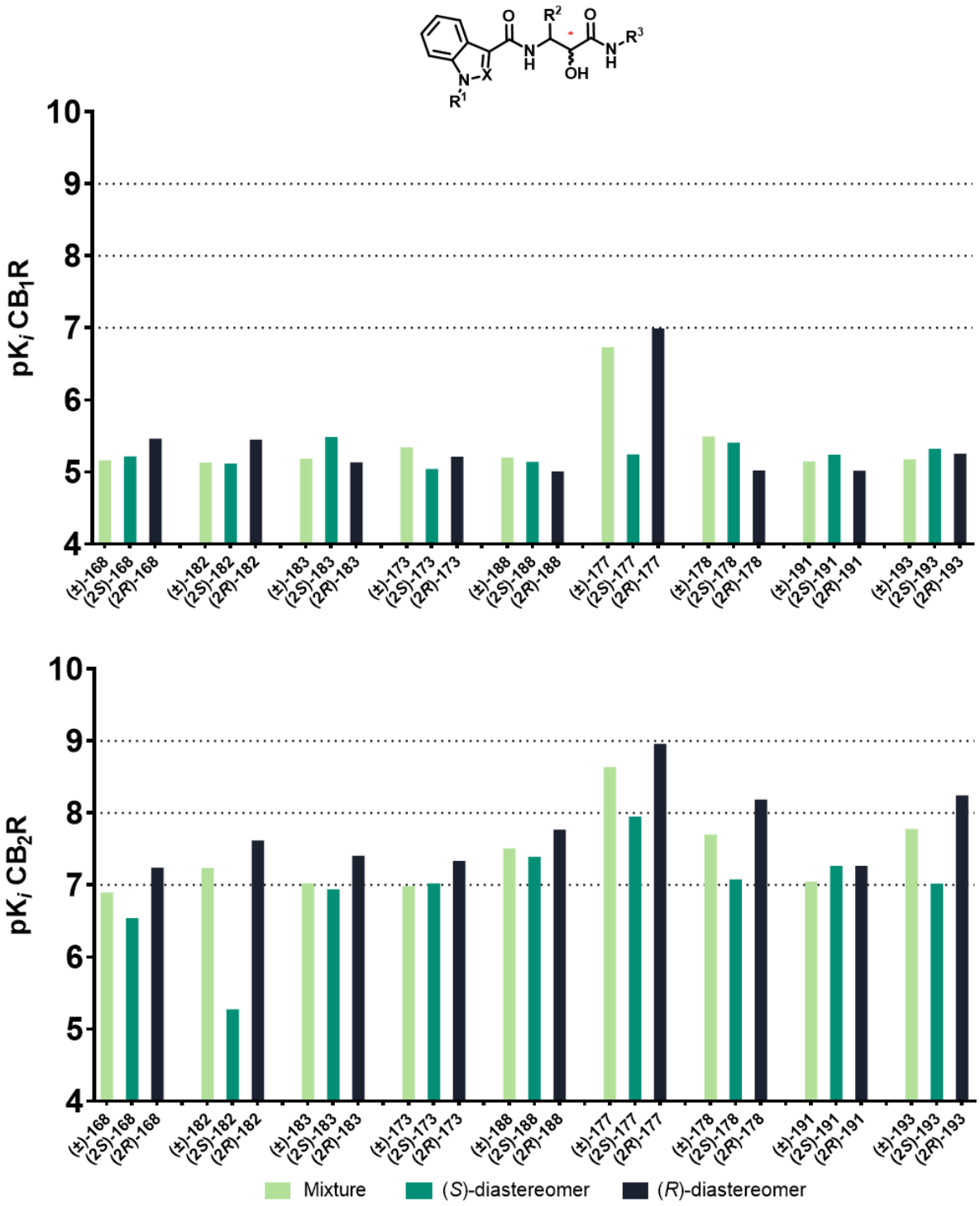



Figure 3.76. Bar chart representation of the SAR trends related to stereochemistry of the PADAM asymmetric carbon (Series **VII**). $CB_1R$ affinity data (above) and $CB_2R$ affinity data (bottom) are reported.

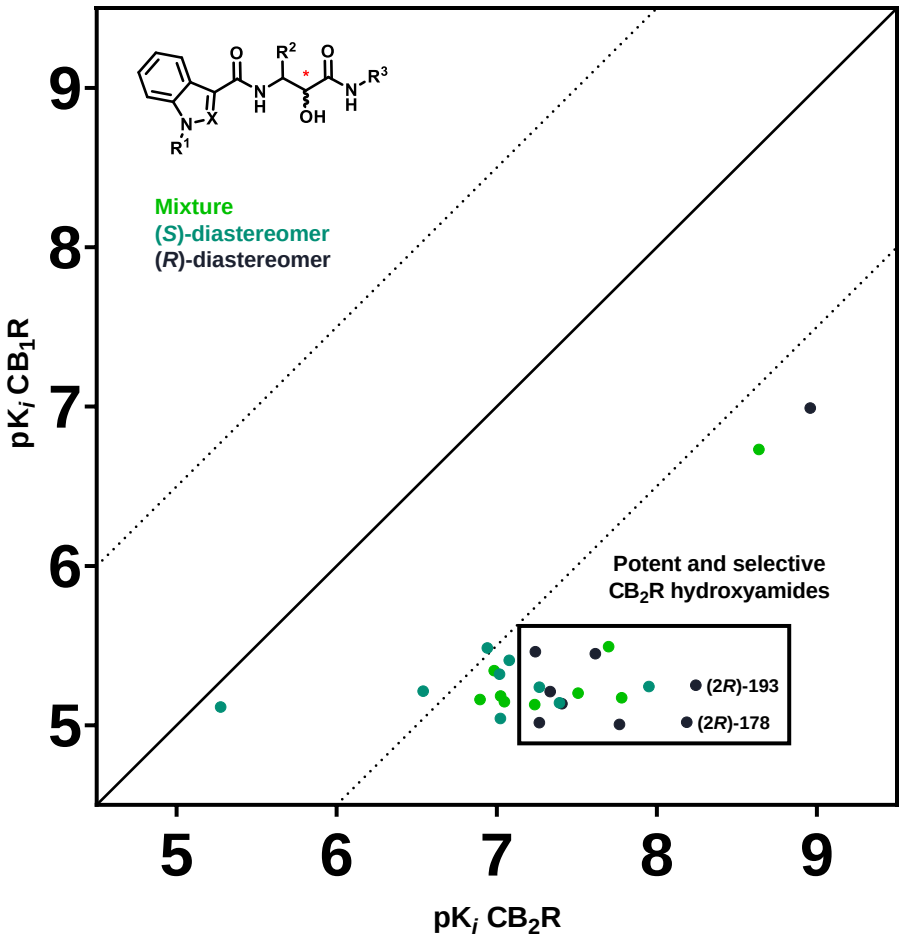



Figure 3.77. $CB_1R$ $pK_i$ [-log($K_i$)] vs $CB_2R$ $pK_i$ [-log($K_i$)] representation of hydroxy group stereochemistry. Green: diastereomeric mixture 1:1. Turquoise: (2*S*)-diastereomer. Dark blue: (2*R*)-diastereomer.

The evaluation of the diastereomeric pairs, along with the 1:1 mixture of both compounds reveals some intriguing trends. Firstly, there is a notable difference in $CB_1R$ affinity compared to the previous analysis conducted in Series **VI**. Out of the nine diastereomeric pairs (comprising 18 compounds), only one exhibits affinity at this receptor, demonstrating a preliminary high selectivity profile for Series **VII**. The favorable $CB_1R$ affinity profile of compound **(2*R*)-177** compared to its diastereomer **(2*S*)-177** suggests an enhanced $CB_1R$ potency for the (*R*) configuration, although the sample is too small to draw significant conclusions.

On the other hand, compounds with the (*R*) configuration at the carbon of the hydroxy group consistently exhibit increased $CB_2R$ affinity among the nine pairs evaluated. For instance, compound **(2*R*)-182** shows a remarkably high $CB_2R$ $K_i$ value of 24.2 nM, while

USC UNIVERSIDADE DE SANTIAGO

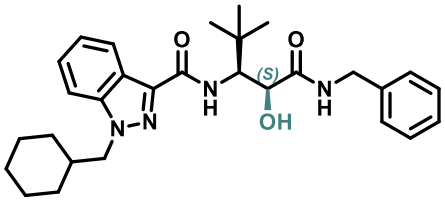
**(2*S*)-182** does not display any significant affinity for this receptor. Furthermore, only two (*S*)-derivatives exhibit a $CB_2R$ $K_i$ value higher than the mixture of both (*S*) and (*R*) diastereomers, indicating the superior affinity profile of (*R*)-derivatives. Figure 3.77 illustrates the representation of both affinity and selectivity for reference.

The diagonal representation perfectly illustrates the trends discussed above. There is only one instance of a compound falling in the inactive region, compound **(2*S*)-182**, which accounts for the high $CB_2R$ affinity profile of the subset and indicates a lower potency for derivatives with the (*S*)-configuration at the carbon bearing the hydroxy group. On the other hand, only one compound falls within the dual $CB_1R/CB_2R$ region (along with its corresponding racemic mixture), accounting for the extraordinary selectivity of the subset.

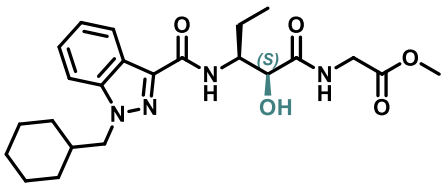
Finally, the lower part of the graph, in the nanomolar range for $CB_2R$ affinity, displays compounds that are potent and completely selective for the $CB_2R$. This is where the majority of the subset is located. The distribution of the compounds throughout this section of the plot reveals the superior affinity profile of the (*R*)-configuration. The three groups of dots are observed to be distributed from right to left as follows: (*R*)-configuration (depicted as dark blue dots), racemic mixture (depicted as green dots), and (*S*)-configuration (depicted as turquoise dots), indicating the affinity profile from higher to lower.

Considering all these trends, it is reasonable to conclude that the (*R*)-diastereomer aligns with the eutomer, which possesses the desired pharmacological profile. Furthermore, in all nine instances, the primary diastereomer obtained from the PADAM route corresponds to the (*R*)-configuration, with ratios reaching up to 1:99, as detailed in the Chemistry section. Given the superior pharmacological profile associated with this diastereomer and the optimization of the synthetic process, which involves isolating only one of the diastereomers, our decision was to exclusively isolate the major diastereomer throughout Series **VII**.

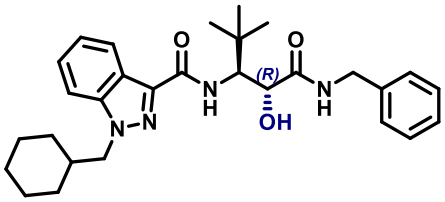
USC
UNIVERSIDADE DE SANTIAGO DE COMPOSTELA



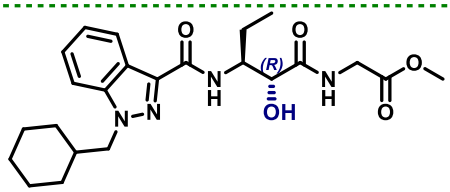
**(2*S*)-193**
$CB_1R$ % (1 μM) = 5 %
$CB_2R$ $K_i$ = **96.0 nM**



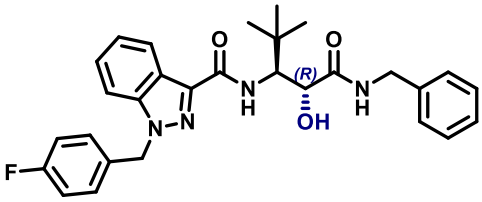
**(2*S*)-182**
$CB_1R$ % (1 μM) = 3 %
$CB_2R$ % (1 μM) = **47 %**



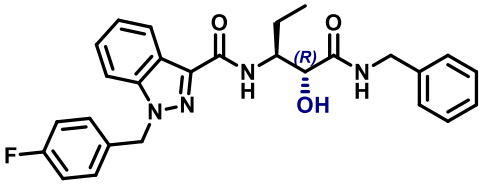
**(2*R*)-193**
$CB_1R$ % (1 μM) = 17 %
$CB_2R$ $K_i$ = **5.70 nM**



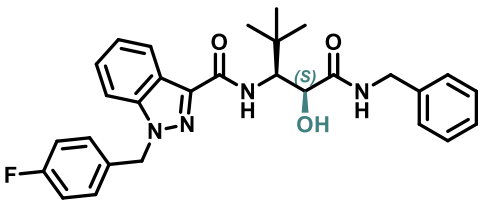
**(2*R*)-182**
$CB_1R$ % (1 μM) = 29 %
$CB_2R$ $K_i$ = **24.2 nM**



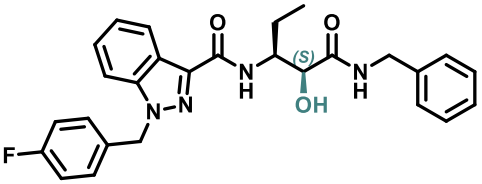
**(2*R*)-178**
$CB_1R$ % (1 μM) = 25 %
$CB_2R$ $K_i$ = **6.50 nM**



**(2*R*)-168**
$CB_1R$ % (1 μM) = 3 %
$CB_2R$ $K_i$ = **57.3 nM**



**(2*S*)-178**
$CB_1R$ % (1 μM) = 30 %
$CB_2R$ $K_i$ = **83.6 nM**



**(2*S*)-168**
$CB_1R$ % (1 μM) = 8 %
$CB_2R$ $K_i$ = **288 nM**

Figure 3.78. Structure and variation in the cannabimimetic affinity data depending on the stereochemistry of the carbon holding the hydroxy group.

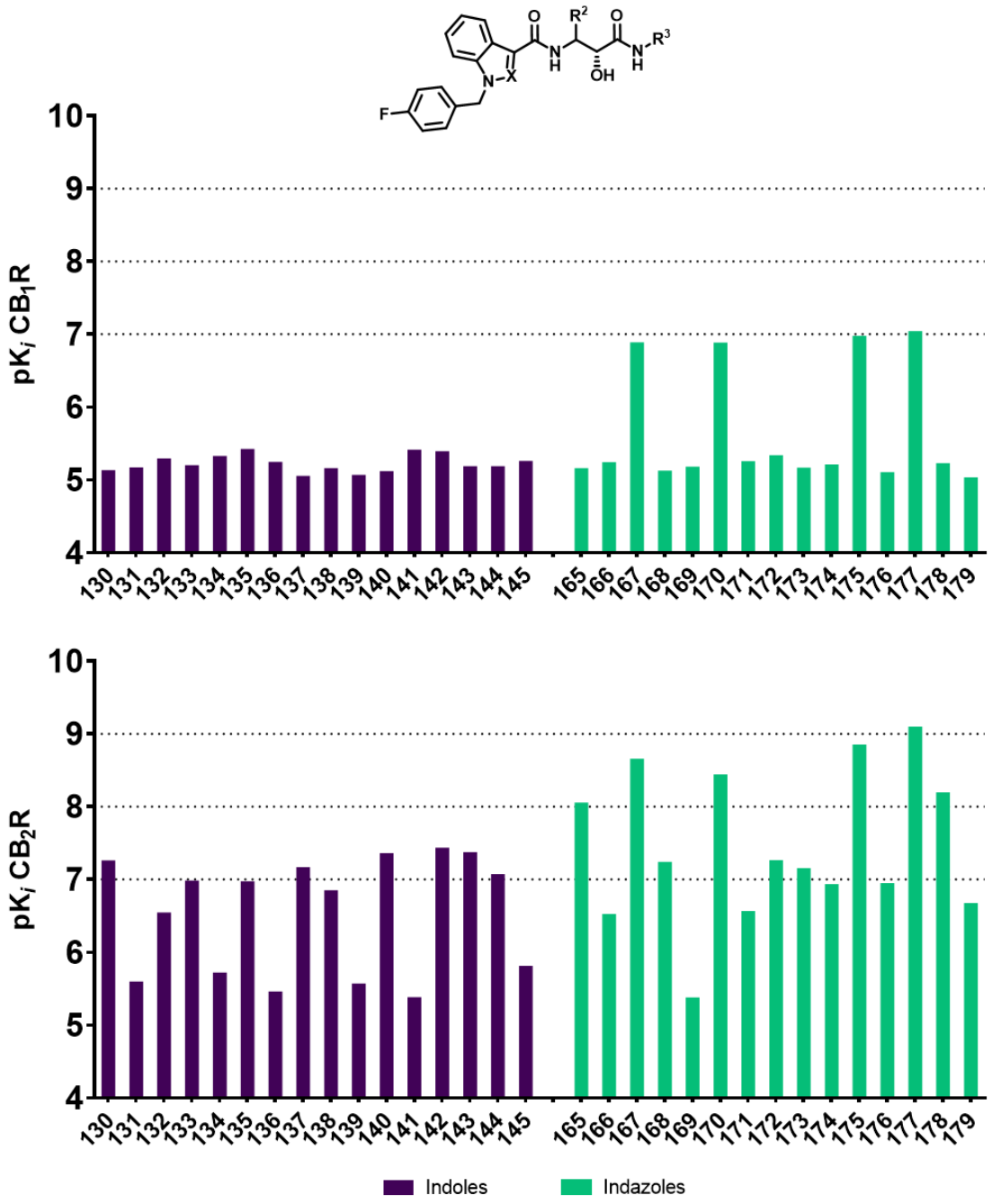



Figure 3.79. Bar chart representation of the SAR trends related to the core group for $R^1$ = 4-F-Bn (Series **VII**). $CB_1R$ affinity data (above) and $CB_2R$ affinity data (bottom) are reported.

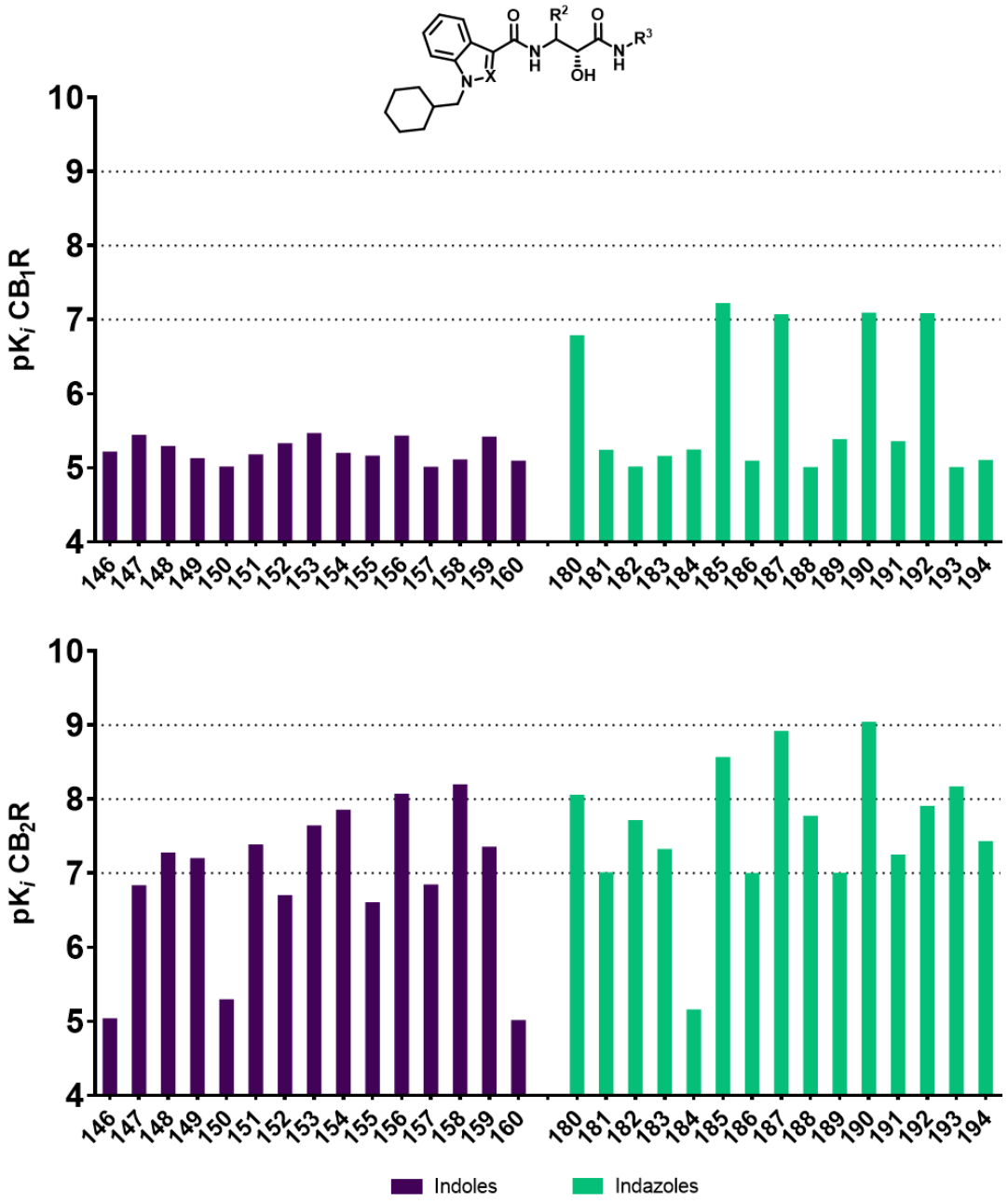



Figure 3.80. Bar chart representation of the SAR trends related to the core group for $R^1$ = $CH_2$-Cy (Series **VII**). $CB_1R$ affinity data (above) and $CB_2R$ affinity data (bottom) are reported.

Similar to the study of the structure-activity and structure-selectivity relationships performed in Series **VI**, we will discuss the trends emerging from the various substitutions at the core group, tail group, linker, and head group for Series **VII**. In addition to the analysis of the linker stereochemistry, we have also evaluated how the configuration of the hydroxy group affects the affinity and selectivity profiles of Series **VII**.

The first structural distinction among compounds lies in the core group, where both heterocycles (indole and indazole) were equally employed to systematically synthesize ligand pairs. As for Series **VI**, the affinity data at $CB_1R$ and $CB_2R$ are shown in Figure 3.79 and Figure 3.80 for 4-fluorobenzyl derivatives and cyclohexyl methyl derivatives, respectively. The results show a significant decrease in affinity compared to Series **VI**, particularly concerning $CB_1R$. Indole derivatives of Series **VII** consistently exhibit inactivity at this receptor while maintaining a good potency profile for $CB_2R$. For instance, compounds like **156** or **158** demonstrate complete selectivity (>100-fold) with a $CB_2R$ $K_i$ value lower than 10 nM. Since the reduction in affinity is much more pronounced at $CB_1R$ than at $CB_2R$, there is a significant increase in selectivity in Series **VII** compared to Series **VI**.

Indazole derivatives were observed to consistently exhibit higher affinity at both receptors in Series **VI**. This increase in $CB_2R$ potency was accompanied by a decrease in the selectivity profile due to the corresponding enhancement in $CB_1R$ affinity. In the case of hydroxyamides, indazoles also show higher $CB_2R$ affinity throughout the series, but the improvement in $CB_1R$ potency is more modest. Out of the 30 molecule pairs studied in this core group analysis (30 indole derivatives and 30 indazole derivatives), only 9 of them display an increase in their affinity for $CB_1R$ when the indole core group is replaced with indazole.

Figure 3.81 provides a visual representation of both potency and selectivity for reference. The three characteristic regions of the graph show clear trends that align with the observed in the previous analysis. The inactive region is primarily comprised of indole derivatives (depicted as purple dots) since they exhibit a lower affinity profile than indazoles, while the position corresponding to dual $CB_1R/CB_2R$ behavior is exclusively displayed by indazole derivatives (depicted as green dots).

Finally, the majority of compounds in Series **VII** are grouped in the lower part of the graph, within the low nanomolar range for $CB_2R$ affinity and on the right side of the dashed line. These are ligands that combine high potency at $CB_2R$ with complete selectivity towards $CB_1R$, demonstrating the success of the pharmacomodulation process. Unlike Series **VI**, where most of the indazoles were positioned around the identity line, the reduction in $CB_1R$ affinity in this subset transformed their promiscuous profile into potent and selective $CB_2R$ ligands. As a result, along with the already selective indoles, we identified several compounds with $CB_2R$ $K_i$ values lower than 10 nM (compounds **156**, **158**, **178**, **193**) and complete selectivity towards $CB_1R$.

USC
DE SANTIAGO
DE COMPOSTELA

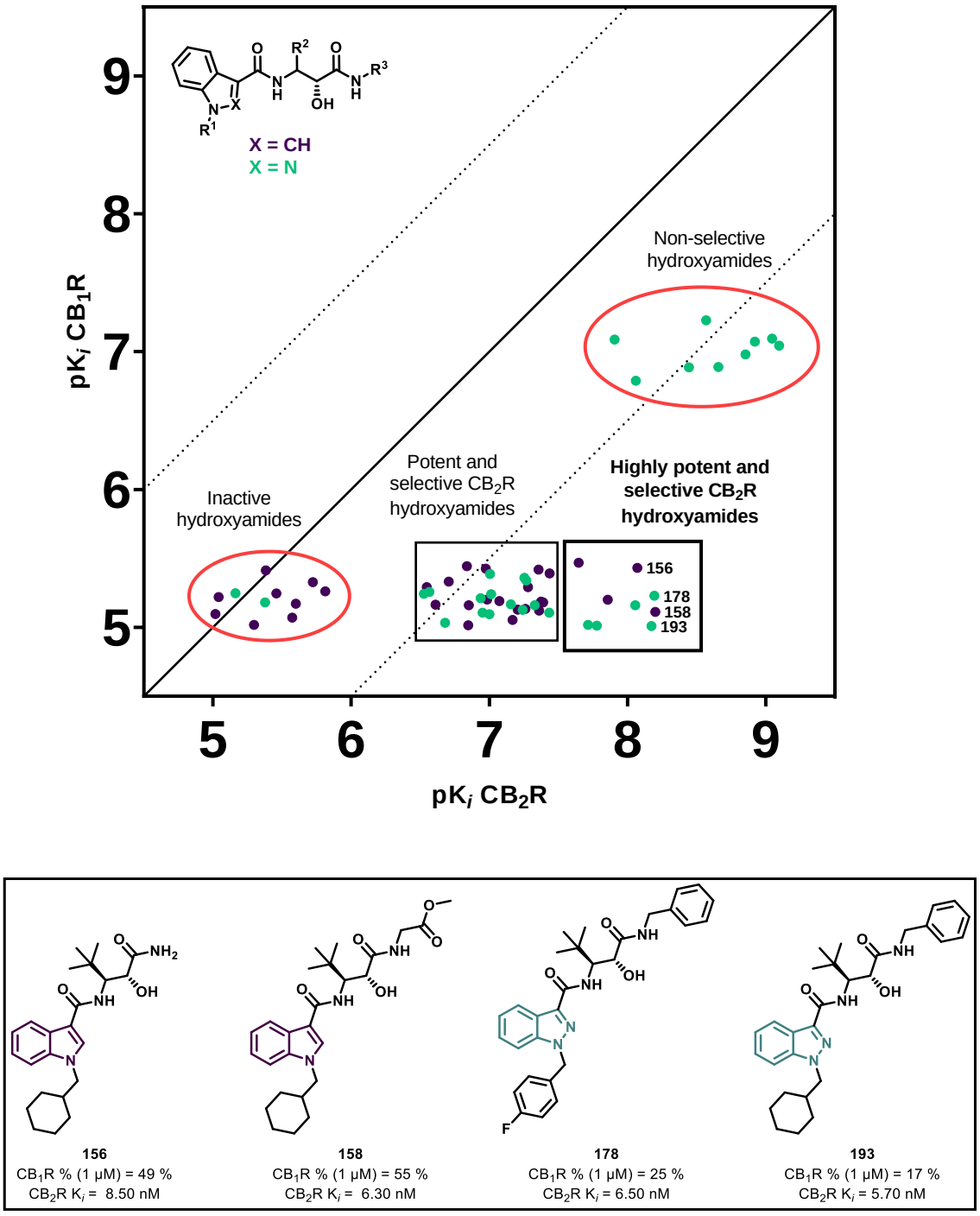



Figure 3.81. $CB_1R$ $pK_i$ [-log($K_i$)] vs $CB_2R$ $pK_i$ [-log($K_i$)] representation of indoles (purple dots) and indazoles (green dots), and the structure of the best $CB_2R$ ligands of Series **VII**.

The second main difference among the compounds is noticeable in the tail group, with the majority of molecules synthesized using either 4-fluorobenzyl or cyclohexyl methyl as substituents at $R^1$. Figure 3.82 shows the affinity data for indole derivatives at $CB_1R$ and

USC UNIVERSIDADE DE SANTIAGO

$CB_2R$, separated by their substituent at position 1: green represents 4-fluorobenzyl substitution, orange represents cyclohexyl methyl substitution, gray represents 5-fluoropentyl substitution, and red represents pentyl substitution.

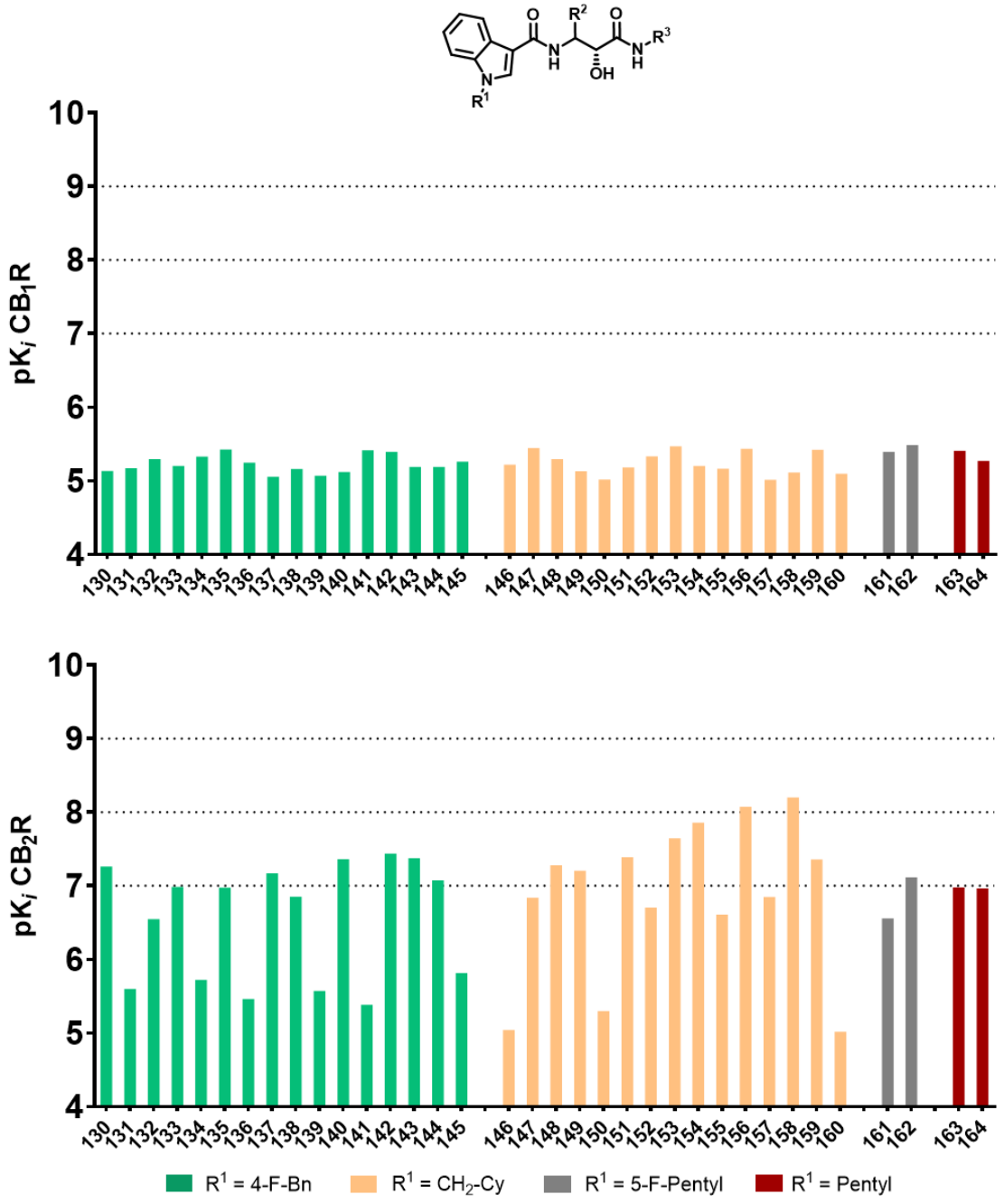



Figure 3.82. Bar chart representation of the SAR trends related to the tail group in the indole derivatives of Series **VII**. $CB_1R$ affinity data (above) and $CB_2R$ affinity data (bottom) are reported.

USC UNIVERSIDADE DE SANTIAGO DE COMPOSTELA

Similar to Series **VI**, we will focus on comparisons between the two main residues across Series **VII** (4-fluorobenzyl and cyclohexyl methyl), and finally we will study the effect that alkyl chains have on affinity and selectivity.

As mentioned earlier in the core group analysis, indole derivatives do not exhibit any affinity for $CB_1R$, so no conclusions can be drawn from the substitution of the tail group regarding selectivity, since all of them are completely selective regardless of substitution at $R^1$. On the other hand, replacing 4-fluorobenzyl with cyclohexyl methyl results in a slight improvement in affinity for $CB_2R$, similar to the observed effect in Series **VI**. In this case, the absence of activity at $CB_1R$ makes the pharmacological profile of cyclohexyl methyl derivatives superior compared to that of 4-fluorobenzyl derivatives. In Series **VI**, both substituents introduced interesting features into the affinity (cyclohexyl methyl) or selectivity (4-fluorobenzyl) profiles. However, the conversion of the entire set of indoles into selective ligands renders the advantages of 4-fluorobenzyl pointless. Nevertheless, with the correct decoration, it was possible to obtain potent $CB_2R$ ligands using 4-fluorobenzyl as the tail group. Figure 3.83 shows the best molecules within this subset and the improvement in the pharmacological profile resulting from cyclohexyl methyl substitution.

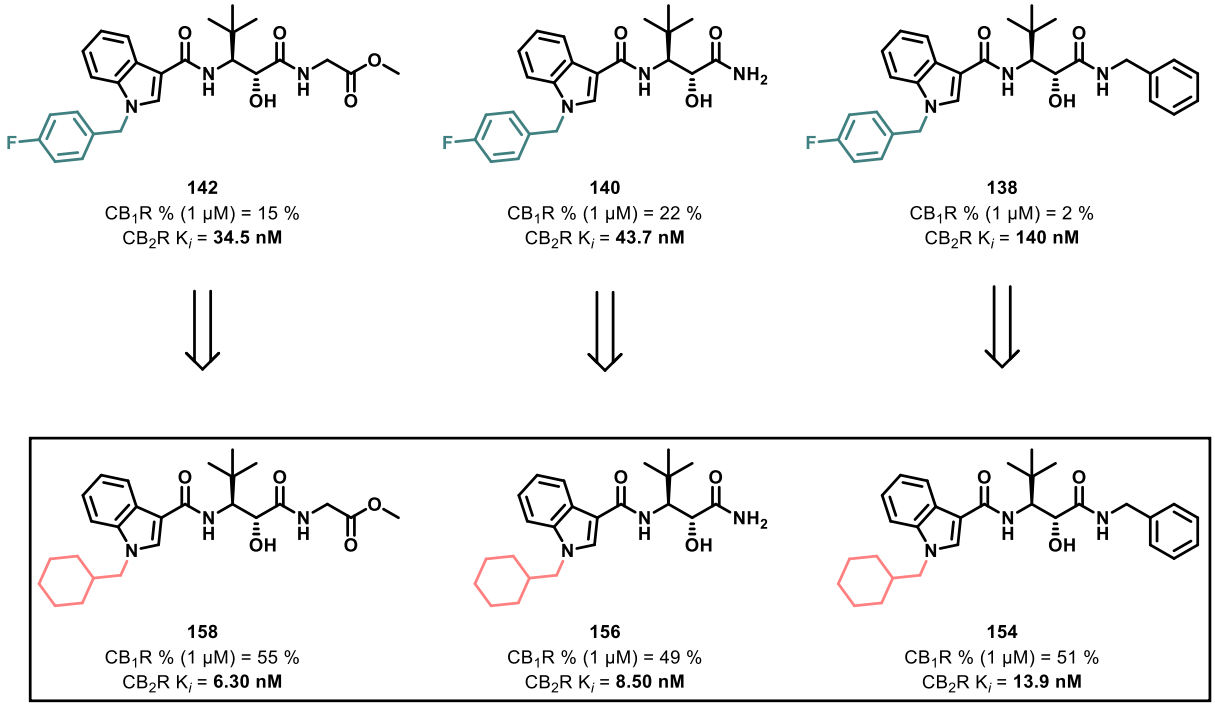



Figure 3.83. Enhancement in $CB_2R$ affinity derived from substitution of 4-fluorobenzyl with cyclohexyl methyl as tail group. Structure of the best ligands identified during this study (bottom).

USC
DE SANTIAGO
DE COMPOSTELA

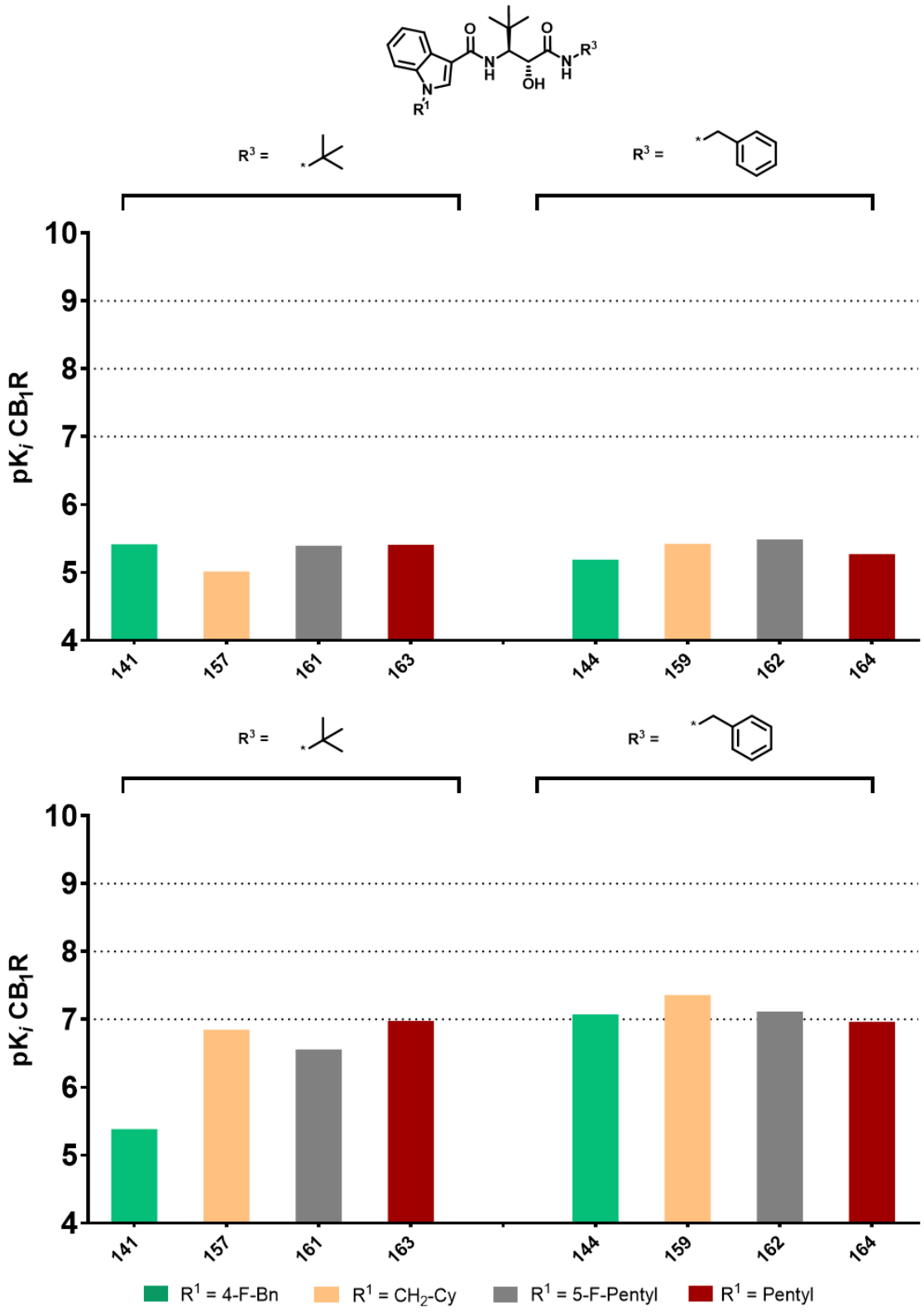



Figure 3.84. Bar chart representation of the SAR trends related to the tail group in the indole derivatives of Series **VII**. $CB_1R$ affinity data (above) and $CB_2R$ affinity data (bottom) are reported.

Additionally, similarly to Series **VI**, four examples of compounds bearing two different alkyl groups at $R^1$ were analyzed. The ligands were synthesized using indole as core group, (*S*)-*tert*-butyl as linker, and two different $R^3$ substituents for the head group, *tert*-butyl and benzyl. Figure 3.84 shows the results grouped by their substituent at position 3 ($R^3$ = *tert*-butyl on the left part, and $R^3$ = benzyl on the right part). Given the indole core structure of the compounds analyzed within this subset, no changes in the $CB_1R$ affinity were observed, as all of them are inactive at this receptor.

Regarding affinity for $CB_2R$, the 4-fluorobenzyl substituent is the least tolerated, as it fails to achieve a good affinity profile at $CB_2R$ when *tert*-butyl is present at the head group. On the contrary, both cyclohexyl methyl and pentyl display similar results with $CB_2R$ $K_i$ values slightly over 100 nM. Finally, the 5-fluoropentyl derivative exhibits a much lower affinity at $CB_2R$. When *tert*-butyl is substituted with benzyl in the head group, the $CB_2R$ affinity trends are altered. The $CB_2R$ $K_i$ values of these compounds are much more similar, ranging from 44 nM to 109 nM, and higher compared to those of the previous subset. The pentyl derivative displays the most modest affinity among them, while cyclohexyl methyl remains the optimal substituent, providing the highest affinity in the group.

The analysis of the affinity and selectivity profile of these subsets also reveals interesting information about the substitution at the head group, which will be exhaustively studied later in the text. Contrary to the observed trends in Series **VI**, where *tert*-butyl exhibits a much more consistent pharmacological profile than benzyl, thanks to its selectivity towards $CB_1R$, in Series **VII,** benzyl shows a superior performance. The conversion of the whole subset of indole derivatives into selective compounds renders the selectivity advantage of *tert*-butyl as a head group pointless, thus making the benzyl derivatives, much more potent, better $CB_2R$ ligands.

Figure 3.85 shows the affinity data for indazole derivatives at $CB_1R$ and $CB_2R$ separated by their substituent at position 1: 4-fluorobenzyl derivatives being represented by green bars, while orange represents cyclohexyl methyl substitution.

USC UNIVERSIDADE DE SANTIAGO DE COMPOSTELA

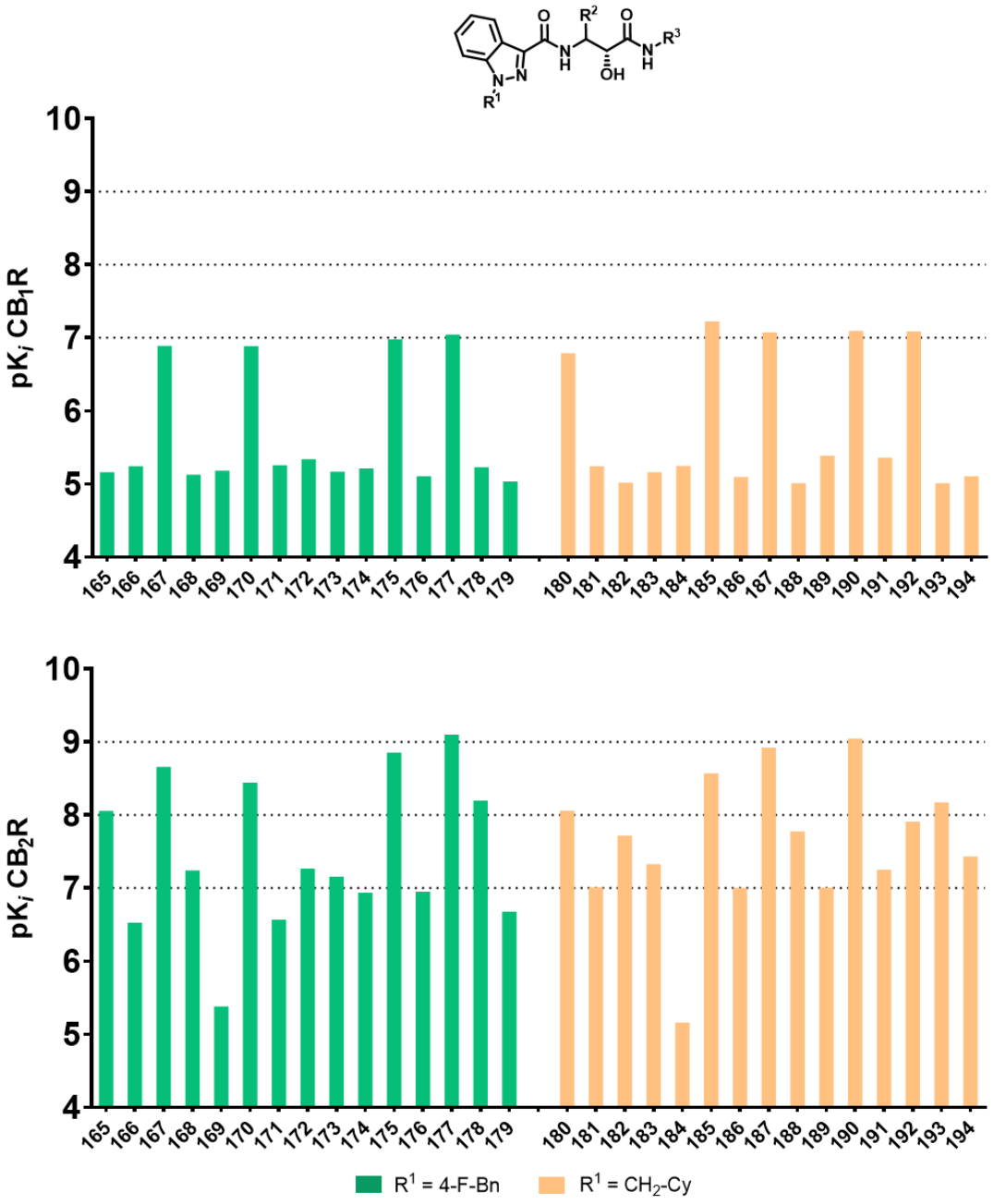



Figure 3.85. Bar chart representation of the SAR trends related to the tail group in the indazole derivatives of Series **VII**. $CB_1R$ affinity data (above) and $CB_2R$ affinity data (bottom) are reported.

In contrast to the previous subset consisting of indole derivatives, compounds bearing indazole as the core group exhibit $CB_1R$ affinity in certain cases, allowing for some comparisons between tail groups. Following the trends observed in Series **VI**, cyclohexyl methyl at position 1 results in derivatives slightly more potent at $CB_1R$ than compounds with 4-fluorobenzyl as the tail group. The difference is rather modest, most likely due to the

increase in the selectivity profile observed within Series **VII**. Affinity for the $CB_2R$ is also enhanced when cyclohexyl methyl is introduced in position 1, generally yielding derivatives more potent at this receptor than those with 4-fluorobenzyl. Despite these differences, both tail groups yield compounds with remarkably high affinity for the $CB_2R$ and complete selectivity towards $CB_1R$. For instance, the best two ligands of Series **VII** include one compound bearing 4-fluorobenzyl in position 1 (compound **178**, $CB_2R$ $K_i$ = 6.50 nM, S.I > 100), while the other compound features cyclohexyl methyl as tail group (compound **193**, $CB_2R$ $K_i$ = 5.70 nM, S.I > 100).

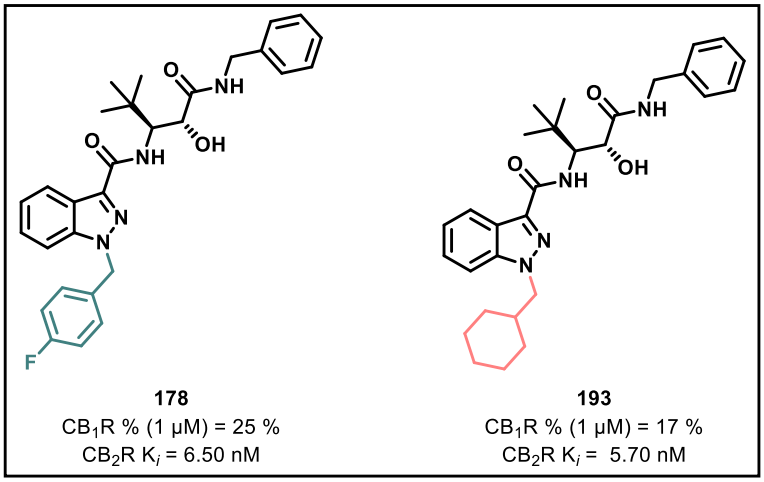



Figure 3.86. Structure and cannabimimetic data of the top two compounds of Series **VII**, each bearing a different tail group.

Figure 3.87 depicts the graphical representation of both potency and selectivity, where compounds are categorized into three different zones based on their pharmacological profile, similar to the observed distribution in earlier studies. The positioning of the various tail groups in the graph perfectly correlates with the trends discussed above. The higher potency of cyclohexyl methyl derivatives is evident in the number of compounds bearing this $R^1$ substituent clustered in the section belonging to potent and selective $CB_2R$ hydroxyamides, where they outnumber 4-fluorobenzyl derivatives by seven to two. Furthermore, there are fewer compounds in the inactive region of the graph with cyclohexyl methyl substitution than there are with 4-fluorobenzyl substitution.

The difference in $CB_1R$ affinity is less pronounced than it is for $CB_2R$ affinity; however, the dual $CB_1R/CB_2R$ section is slightly more represented by compounds with cyclohexyl methyl as the tail group. The small number of compounds with affinity at $CB_1R$, combined

USC UNIVERSIDADE DE SANTIAGO DE COMPOSTELA

with the absence of direct comparisons between analogs differing in the tail group hinders a detailed study of the structure-selectivity relationships. Nevertheless, the presence of more $CB_1R$-active compounds in the cyclohexyl methyl subset, combined with the higher affinity at $CB_2R$ of these particular ligands, suggests that the trends observed in Series **VI** regarding $R^1$ substitution are still applicable in Series **VII**.

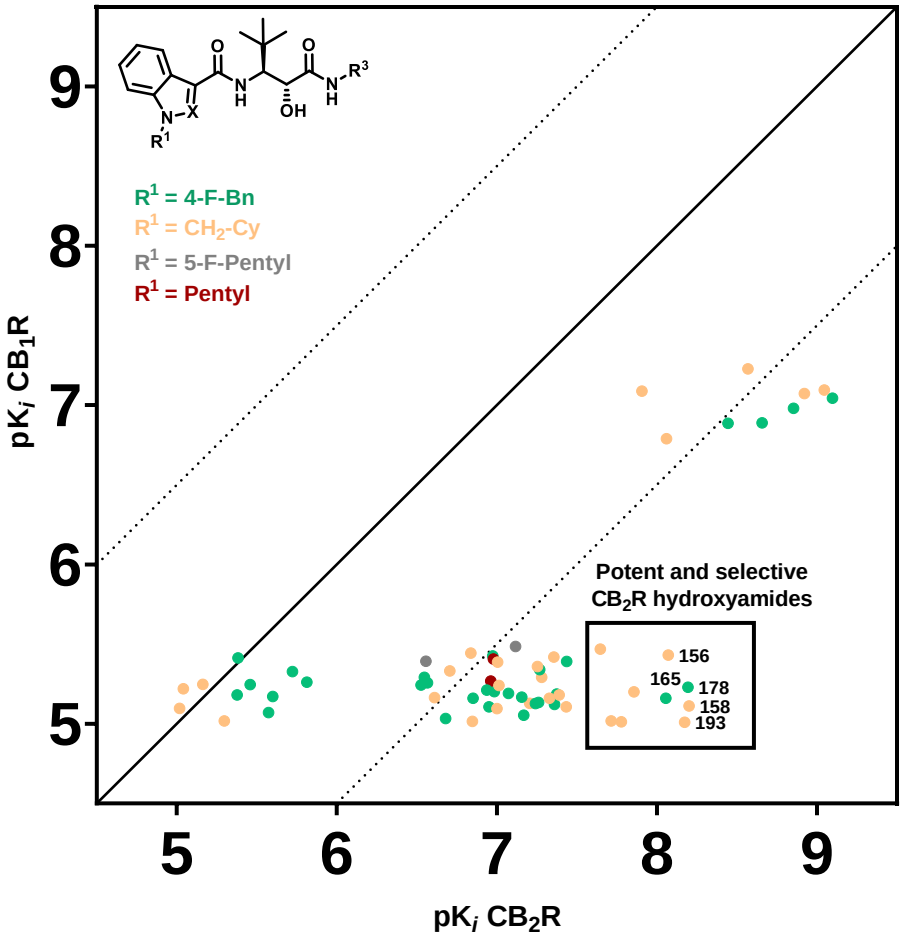



Figure 3.87. $CB_1R$ $pK_i$ [-log($K_i$)] vs $CB_2R$ $pK_i$ [-log($K_i$)] representation of indoles (purple dots) and indazoles (green dots), and the structure of the best $CB_2R$ ligands of Series **VII**.

Similar to the linker studies in Series **VI**, we aim to gain a better understanding of the impact of substituting position 2 by comparing sets of three ligands, where the only variation lies in this specific residue. Figure 3.88 displays a chosen selection of results.

USC UNIVERSIDADE DE SANTIAGO DE COMPOSTELA

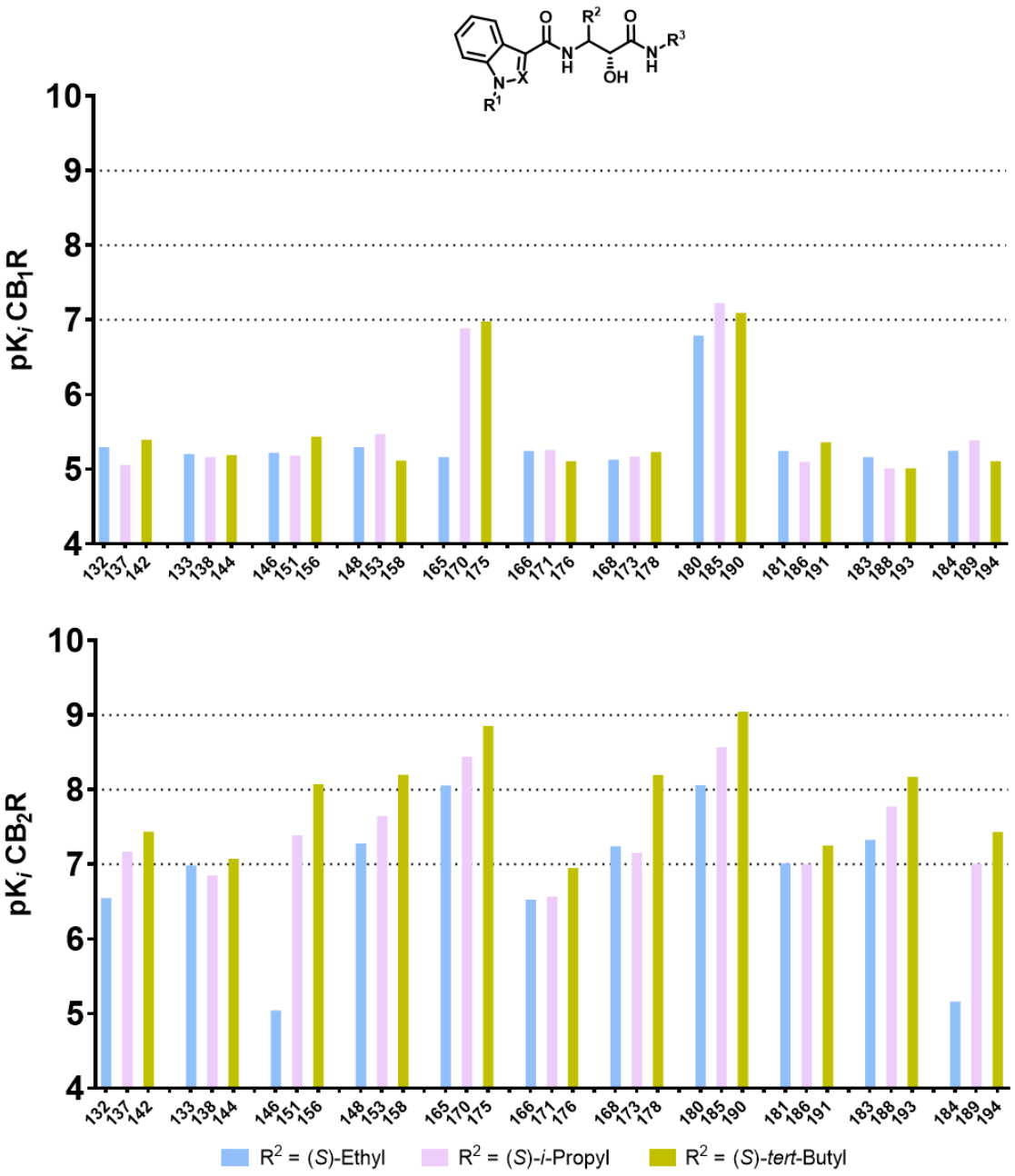



Figure 3.88. Bar chart representation of the SAR trends related to the linker in Series **VII**. $CB_1R$ affinity data (above) and $CB_2R$ affinity data (bottom) are reported.

$CB_2R$ affinity shows an increase with the size of the substituent at position 2, as observed in the carboxamides subset. The (*S*)-*tert*-butyl linker (depicted as ochre) exhibits the highest affinity within the series, followed by (*S*)-*i*-propyl (depicted as pale pink) and (*S*)-ethyl (depicted as blue). However, unlike the significant disparity in potency between (*S*)-*i*-propyl and (*S*)-ethyl derivatives in Series **VI**, the variations in affinity are generally more gradual.

For instance, there are certain groups of three where the (*S*)-ethyl substituent (compound **168**, $CB_2R$ $K_i$ = 57.3 nM) is more potent than its (*S*)-*i*-propyl counterpart (compound **173**, $CB_2R$ $K_i$ = 46.4 nM).

Analysis of $CB_1R$ affinity reveals different trends compared to those observed in Series **VI**, where potency increased along with the size of the substituent at position 2, as did $CB_2R$ affinity. In this case, Figure 3.88 illustrates the characteristic lack of affinity for $CB_1R$ in Series **VII**, except for two cases (groups of compounds **165**, **170**, **175** and compounds **180**, **185**, **190**) where the head group consists of unsubstituted terminal amide. As seen in the analysis of this structural region in Series **VI**, this is the substituent that provides the highest affinity at both receptors (a characteristic of SCRAs), so it is reasonable that these are the instances of compounds active at $CB_1R$. In general, increasing the size of the linker gradually enhance affinity for $CB_2R$ in Series **VII**, with almost no effect in affinity for $CB_1R$.

The square plot representation of Series **VI** focused on its substituent at position 2 is shown in Figure 3.89. As observed in the graph, compounds with (*S*)-ethyl as the linker (represented as blue dots) exhibit the lowest affinity at both receptors. They constitute the majority of molecules clustered in the inactive part of the representation, near the axis origin. Furthermore, in the dual $CB_1R/CB_2R$ region of the graph, (*S*)-ethyl substitution contributes two compounds, while (*S*)-*i*-propyl (depicted as purple dots) and (*S*)-tert-butyl (depicted as ochre dots) introduce three and four compounds, respectively. Finally, despite being the least active among all, two (*S*)-ethyl derivatives are among the top nine ligands of Series **VII**, located in the section corresponding to highly potent and selective $CB_2R$ hydroxyamides.

On the other hand, (*S*)-*tert*-butyl derivatives exhibit the highest potency of the series, and consequently present lower number of compounds in the inactive region (three molecules), and the highest number of compounds in the non-selective and the potent and selective parts of the graph. The top four compounds feature this substituent at position 2 (Figure 3.90). In between them, (*S*)-*i*-propyl derivatives display an intermediate number of compounds in each of the three zones of the graph, contributing three out of the best nine ligands of the series.

USC UNIVERSIDADE DE SANTIAGO DE COMPOSTELA

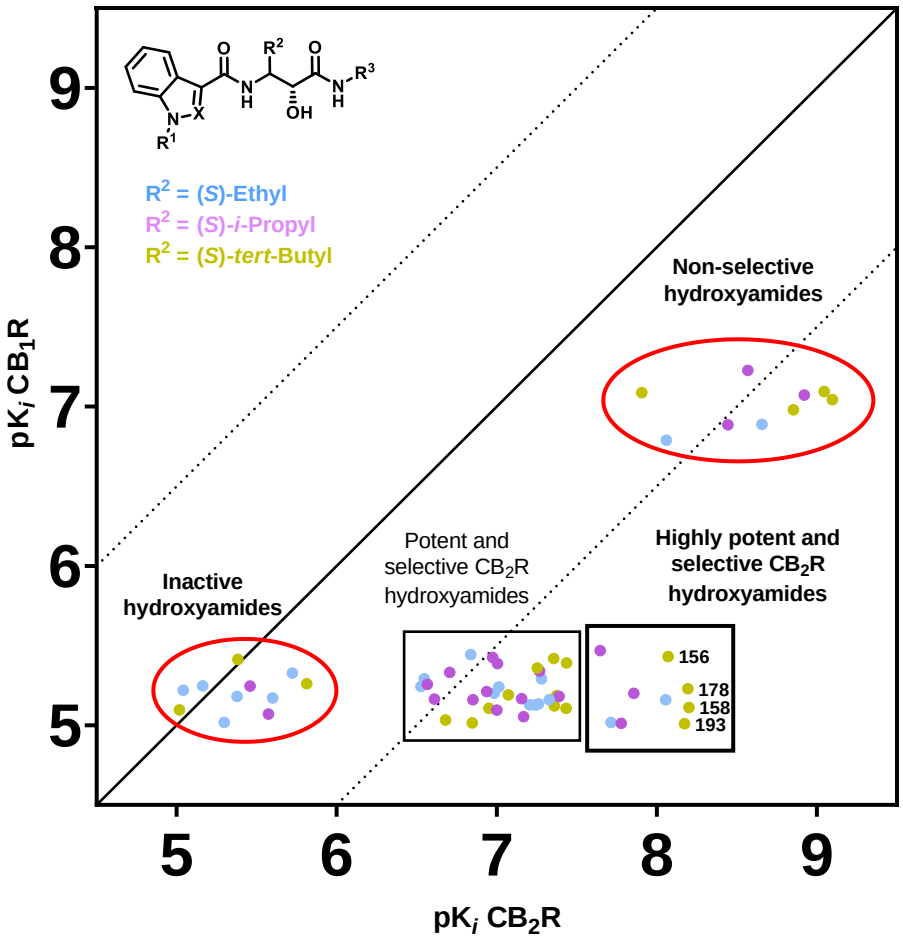



Figure 3.89. $CB_1R$ $pK_i$ [-log($K_i$)] vs $CB_2R$ $pK_i$ [-log($K_i$)] representation of substitution at position 2. Blue: (*S*)-ethyl substitution, Purple: (*S*)-*i*-propyl substitution and ochre: (*S*)-*tert*-butyl substitution.

Figure 3.90 illustrates the best ligands of the subset and the increase in $CB_2R$ affinity with the size of the linker. It is important to highlight that, even though the (*S*)-ethyl derivatives demonstrate the lowest affinity in the series, compound **183** stands out by maintaining absolute selectivity towards $CB_1R$ while achieving a $CB_2R$ $K_i$ value below 40 nM. This exceptional outcome is attributed to the key role played by the hydroxy group in Series **VII** in achieving selectivity. As we will discuss further in this text, the presence of the hydroxy group enables the incorporation of substituents that contribute to the highest affinity for $CB_2R$ across the remaining derivatization sites.

USC UNIVERSIDADE DE SANTIAGO DE COMPOSTELA

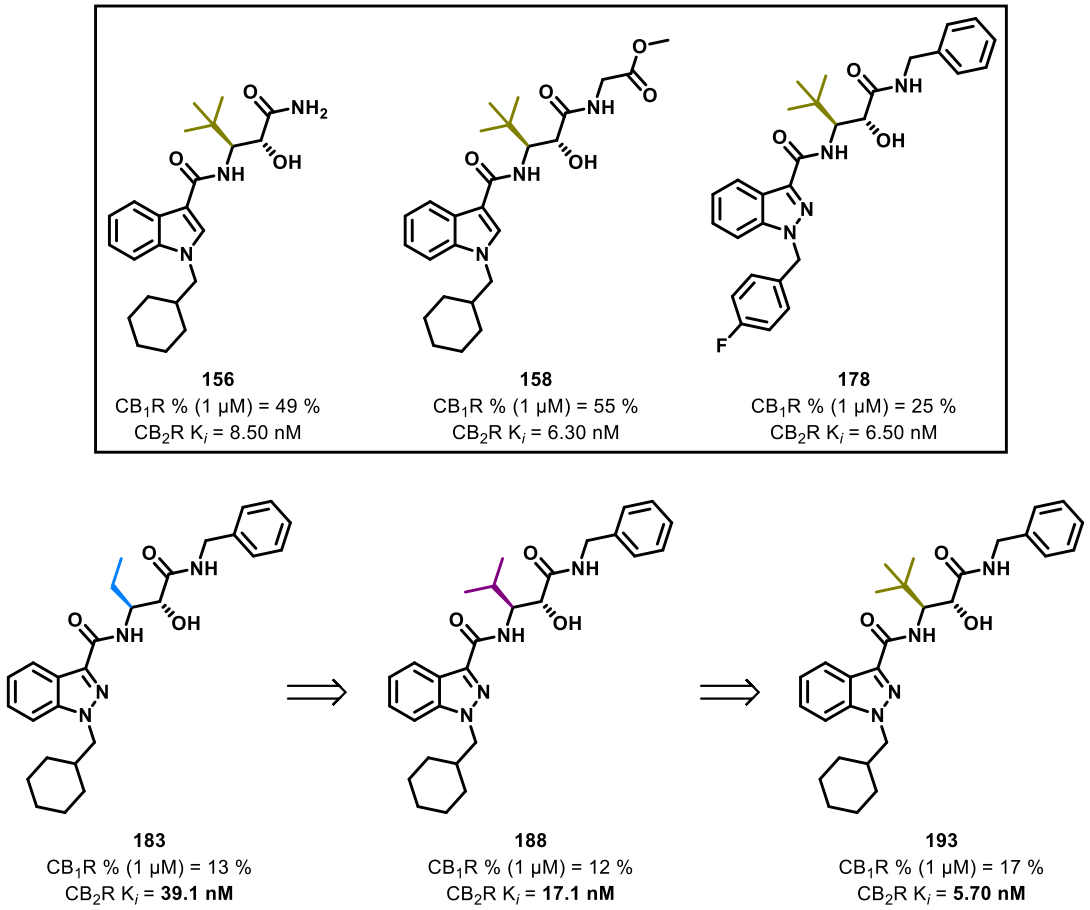



Figure 3.90. Structure of potent and selective $CB_2R$ ligands depending on their linker and increase in $CB_2R$ affinity with $R^2$ substitution size.

Once these trends were stablished, we examined the effect of the linker stereochemistry on the affinity and selectivity profiles. Consequently, we synthesized a small collection of 16 derivatives (8 ketoamides and 8 hydroxyamides) bearing the (*R*) configuration at position 2. To develop this subset of compounds, we utilized the linker with the best pharmacological profile, namely (*S*)-*tert*-butyl. We synthesized both indole and indazole derivatives, along with the main tail groups of this work, 4-fluorobenzyl and cyclohexyl methyl. Finally, we selected unsubstituted terminal amide and *tert*-butyl as head groups. Restricting the diversity at this position to just two options allows for more meaningful comparisons within the set. The results of this set of compounds are presented in Figure 3.91, alongside the data for their (*S*)-*tert*-butyl counterparts.

USC UNIVERSIDADE DE SANTIAGO DE COMPOSTELA

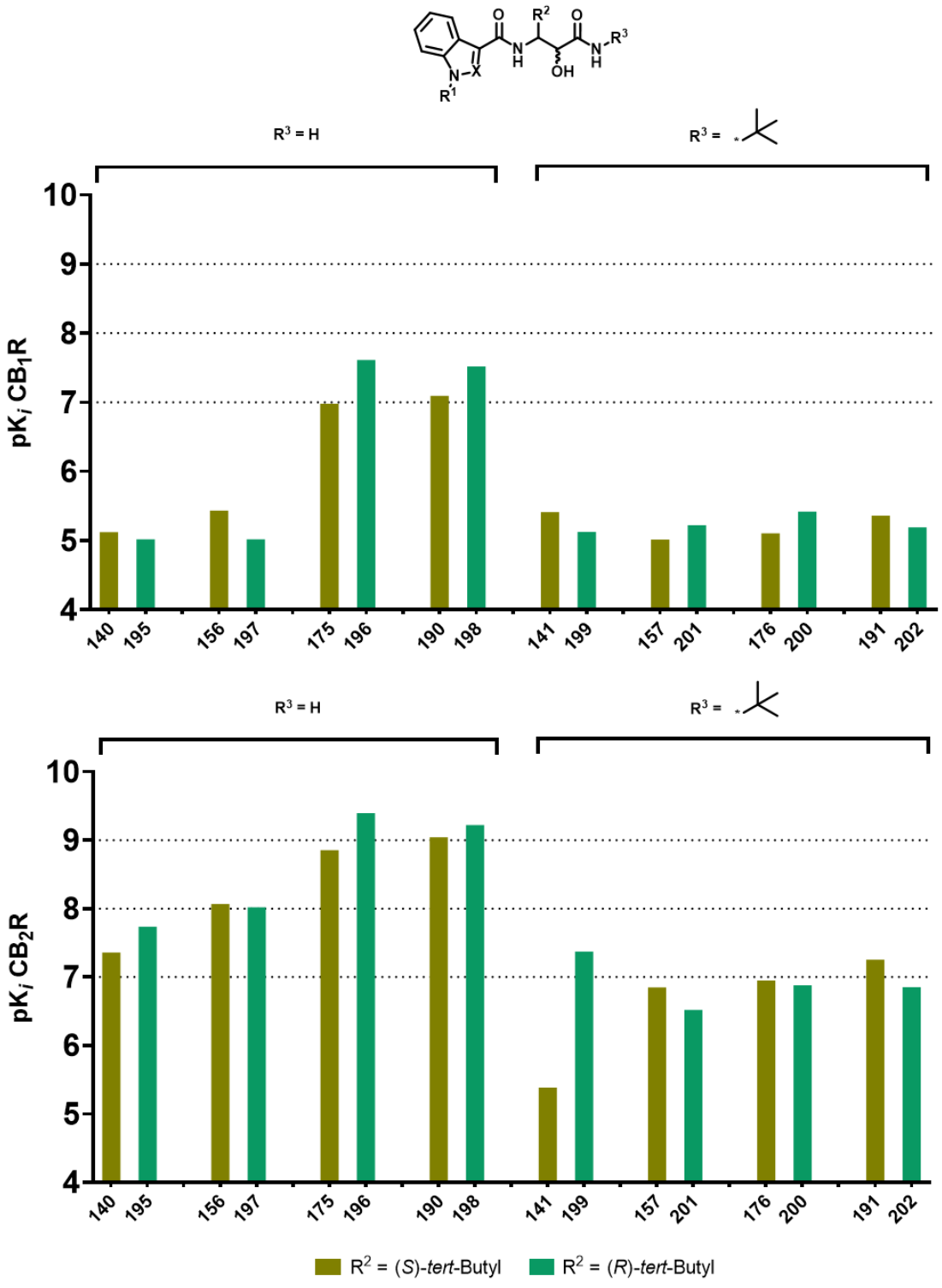



Figure 3.91. Bar chart representation of the SAR trends related to the linker configuration in Series **VII**. $CB_1R$ affinity data (above) and $CB_2R$ affinity data (bottom) are reported. Ochre: (*S*)-tert-butyl substitution, and green: (*R*)-*tert*-butyl substitution.

USC UNIVERSIDADE DE SANTIAGO DE COMPOSTELA

As usual in Series **VII**, most derivatives within this subset are inactive at $CB_1R$, except for the compounds corresponding to indazoles with unsubstituted amide as the head group (compounds **175**, **190**, and compounds **196**, **198**). Comparisons between the two pair of compounds reveal that the (*R*) configuration yield ligands with a slightly higher affinity profile for this receptor, increasing the $CB_1R$ $K_i$ value from 100 nM to 30 nM. Nevertheless, both configurations yield compounds that are generally selective without affinity for the $CB_1R$.

Regarding $CB_2R$ affinity, there is a broader spectrum of results. Substituting (*S*)-*tert*-butyl with (*R*)-*tert*-butyl results in either an increase in the affinity for the $CB_2R$ (compound **141**, showing no significant activity; compound **199**, $CB_2R$ $K_i$ = 42.4 nM), a decrease in potency (compound **191**, $CB_2R$ $K_i$ = 54.2 nM; compound **202**, $CB_2R$ $K_i$ = 140 nM), or has no effect on the affinity profile (compound **156**, $CB_2R$ $K_i$ = 8.50 nM, compound **197**, $CB_2R$ $K_i$ = 9.60 nM). Overall, the variations in the affinity profiles of both $CB_1R$ and $CB_2R$ are not meaningful enough to draw conclusions, and both configurations can be considered to produce favorable results.

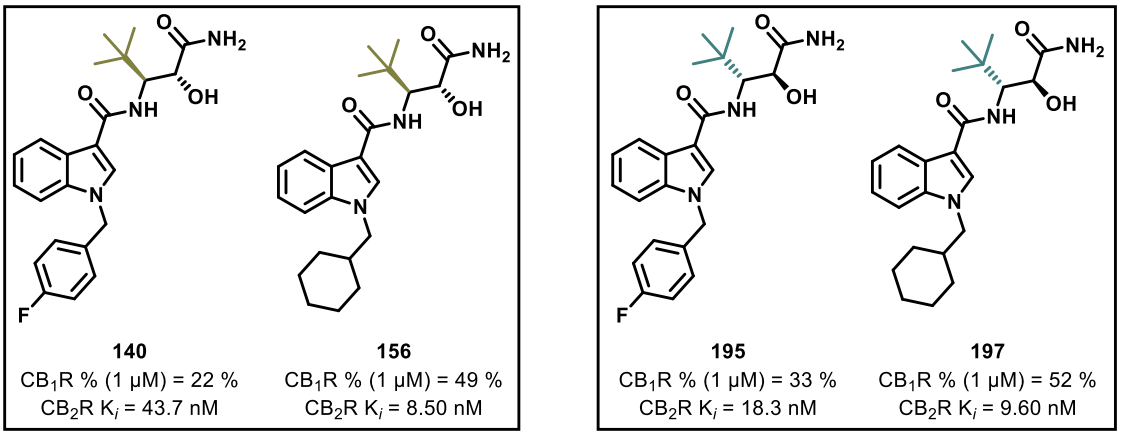



Figure 3.92. Structure and cannabimimetic data for top compounds of Series **VI** based on their linker stereochemistry.

The greatest structural diversity is found at the head group, and the patterns are less distinct than in earlier studies due to the array of results (Figure 3.93).

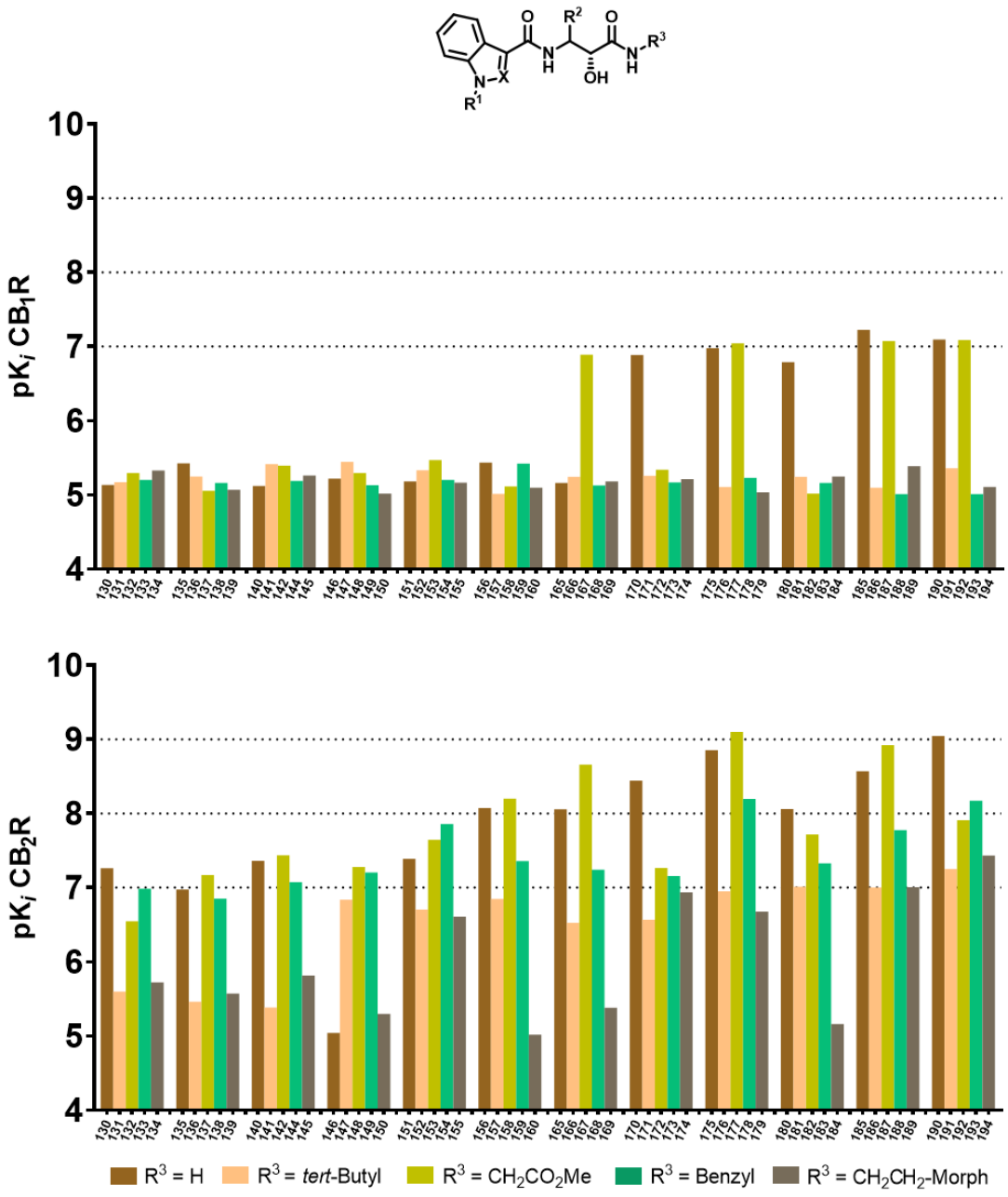



Figure 3.93. Bar chart representation of the SAR trends related to the head group in Series **VII**. $CB_1R$ affinity data (above) and $CB_2R$ affinity data (bottom) are reported.

As evident from the representation, the characteristic absence of $CB_1R$ affinity in Series **VII** is also present here. Out of the five different head groups, only two of them

USC UNIVERSIDADE DE SANTIAGO DE COMPOSTELA

(unsubstituted terminal amide and $CH_2CO_2Me$) yield some derivatives with significant affinity for $CB_1R$. This trend aligns with what was observed in Series **VI** for these substituents, although in the previous series, derivatives bearing benzyl were also generally non-selective due to their high affinity for $CB_1R$. The substitution of the carboxy group introduced in the PADAM synthetic route with a hydroxy group has rendered this subset of compounds inactive at $CB_1R$, resulting in complete selectivity. Furthermore, even though unsubstituted terminal amide and $CH_2CO_2Me$ derivatives are the only ones in the series with affinity for $CB_1R$, the majority of these compounds in Series **VII** do not exhibit any affinity for this receptor, making them highly selective overall. *Tert*-butyl and morpholinoethyl consistently provided derivatives with the lowest $CB_1R$ affinity of Series **VI**, and that pattern persists throughout Series **VII**, where all compounds with these head groups remain inactive at this receptor.

Affinity for $CB_2R$ also mirrors the trends observed in Series **VI**, with unsubstituted terminal amide and $CH_2CO_2Me$ yielding the most potent ligands in Series **VII**. In contrast, *tert*-butyl and morpholinoethyl derivatives consistently exhibit a more modest affinity profile. In Series **VI**, these substituents were deemed optimal due to their selectivity profile, compensating for the reduced potency at $CB_2R$. Since the affinity for this receptor is primarily influenced by other structural elements (core group and linker), their role was to enhance selectivity. However, in this case, the inherent selectivity profile of the hydroxyamides structure is already excellent, rendering the advantages of *tert*-butyl and morpholinoethyl as head groups redundant.

On the other hand, the substitution of position 3 with benzyl in Series **VI** resulted in potent compounds with poor selectivity. The $CB_1R$ affinity issue is addressed here by introducing a hydroxy group from the PADAM synthetic route while retaining high affinity for $CB_2R$. The combination of these factors makes benzyl the ideal substituent for position 3 in achieving potent and entirely selective $CB_2R$ ligands. Figure 3.94 provides a visual representation of both potency and selectivity for reference.

USC
UNIVERSIDADE DE SANTIAGO DE COMPOSTELA

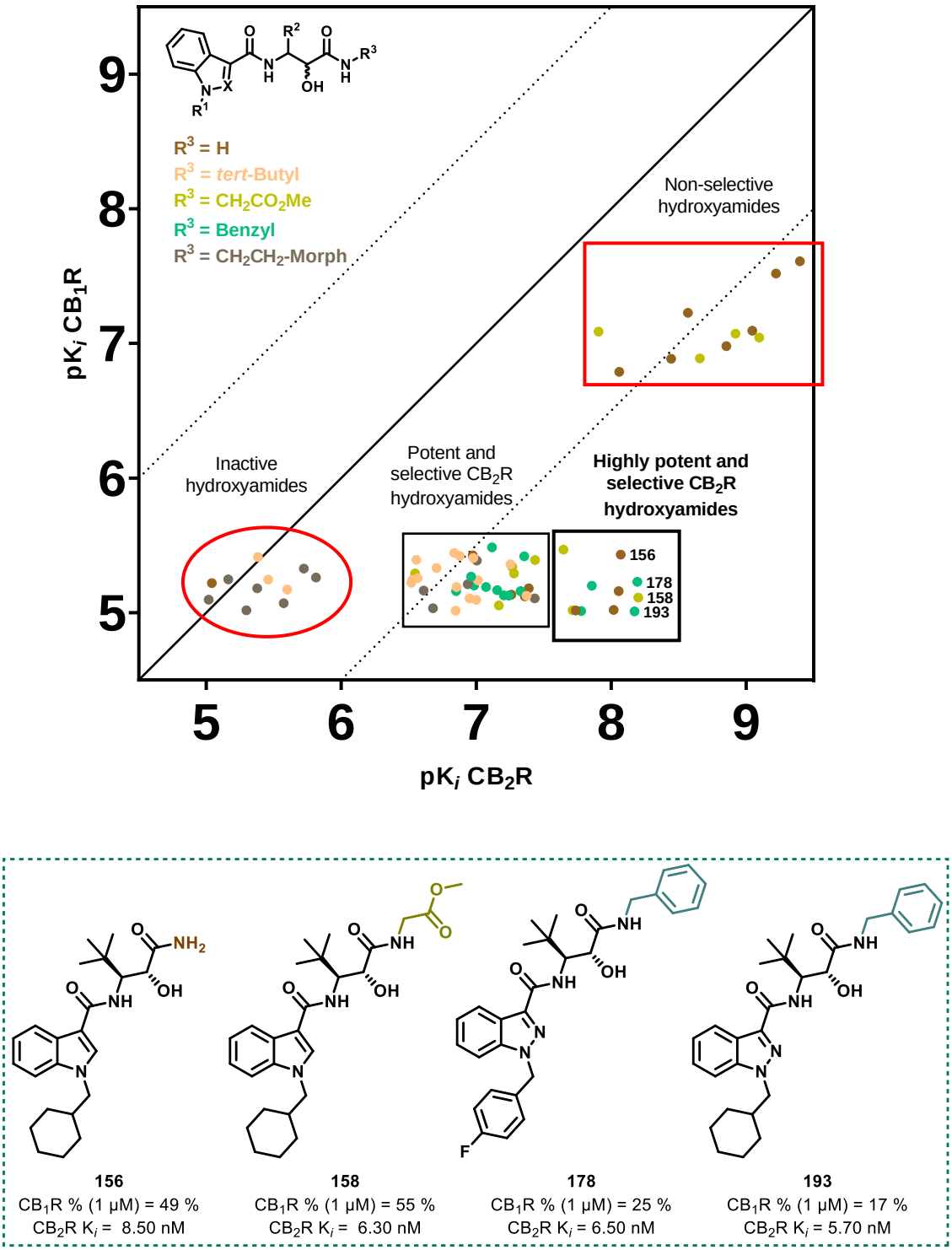



Figure 3.94. $CB_1R$ $pK_i$ [-log($K_i$)] vs $CB_2R$ $pK_i$ [-log($K_i$)] representation of substitution at position 3 and structure of $CB_2R$ potent and selective ligands of Series **VII**. Brown: H, Pink: *tert*-Butyl, Ochre: $CH_2CO_2Me$, Green: Benzyl, and Gray: $CH_2CH_2$-Morph.

USC UNIVERSIDADE DE SANTIAGO DE COMPOSTELA

The structure-activity and structure-selectivity relationship trends mentioned earlier are clearly illustrated in the diagonal plot. The preferred head group substituents of Series **VI**, namely *tert*-butyl and morpholinoethyl, consistently demonstrate complete selectivity towards $CB_1R$. Consequently, they are positioned in the lower section of the graph, and none of their representatives appear in the top-right side of the plot. Their series-lowest affinity profile is evident from the fact that all compounds in the inactive section of the graph belong to these head group subsets, except for one.

The dual $CB_1R/CB_2R$ part of the representation exclusively comprises ligands with unsubstituted terminal amide or $CH_2CO_2Me$ as head groups, as explained earlier in the affinity profile studies. These are the substituents that yielded the most potent ligands in Series **VI**, and they continue to do the same in Series **VII**. Only one of their derivatives appears in the part of the graph corresponding to inactive compounds. Their high potency, combined with the excellent selectivity profile provided by the hydroxyamide structural skeleton, results in seven ligands with complete selectivity towards $CB_1R$ and a $CB_2R$ $K_i$ value under 20 nM, including one of the best $CB_2R$ ligands identified during the study, compound **158** ($R^3 = CH_2CO_2Me$, $CB_2R$ $K_i$ = 6.30 nM).

Finally, the promiscuous profile of benzyl as the head group in Series **VI** has been transformed into a completely selective, yet highly potent subset of ligands in Series **VII**. Benzyl is the only substituent whose derivatives are all placed in the lower section of the graph (indicating no significant affinity for $CB_1R$) and in the low nanomolar range for $CB_2R$ potency. The binding results arising from compounds with benzyl substitution at position 3 are excellent. All compounds evaluated are active at the $CB_2R$, with $K_i$ values ranging from 141 nM to 5.70 nM (compound **193**), and are completely selective towards $CB_1R$, making benzyl the optimal substituent at this position in Series **VII**.

Similar to the transformation process performed in Series **VI**, one $CH_2CO_2Me$ derivative was selected within Series **VII** to be converted into the corresponding amide, to address the metabolic issues associated with esters in the drug discovery process. Figure 3.95 shows the variation in the binding profile arising from this substitution.

USC UNIVERSIDADE DE SANTIAGO DE COMPOSTELA

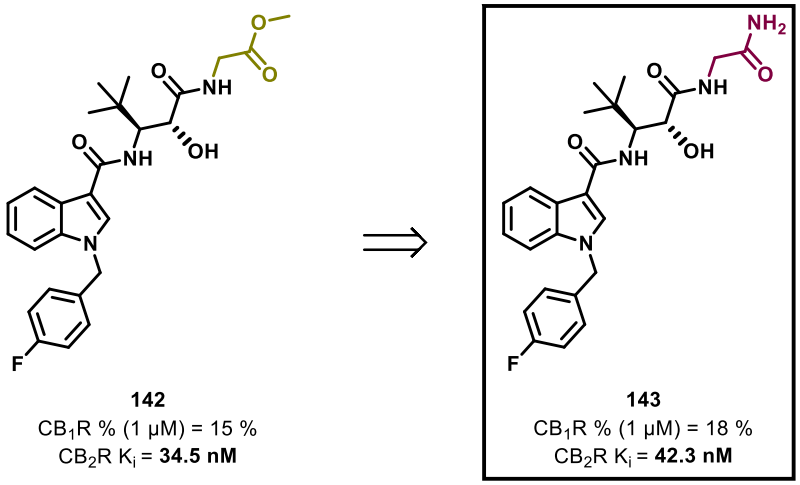



Figure 3.95. Pharmacomodulation of $CH_2CO_2Me$ derivative **142** and change in the affinity and selectivity profile.

As depicted in the figure, their pharmacological profiles are nearly identical, displaying no significant change in affinity for $CB_2R$ and maintaining complete selectivity. These results are consistent with those observed in Series **VI** when the same conversion was carried out. Although these two examples of substituting the methyl ester with the corresponding amide represent a small sample size, the results are promising and suggest it as a potential solution to any metabolic issues associated with esters.

In conclusion, despite some of the substituents having drawbacks such as reduced potency or selectivity, all of them produce exceptional outcomes in the development of potent and entirely selective $CB_2R$ ligands. This underscores the effectiveness of hydroxyamides in achieving selectivity for this receptor and highlights the success of multicomponent reactions in the process of pharmacomodulation. These reactions enabled us to completely separate the dual $CB_1R/CB_2R$ behavior of SCRAs, resulting in potent and completely selective $CB_2R$ ligands. However, certain substituents have proven to be optimal. In Series **VII**, selectivity for $CB_2R$ is provided by the hydroxy group, allowing us to introduce the substituents that yield the highest affinity at $CB_2R$ in the rest of the derivatization sites.

USC
UNIVERSIDADE DE SANTIAGO DE COMPOSTELA

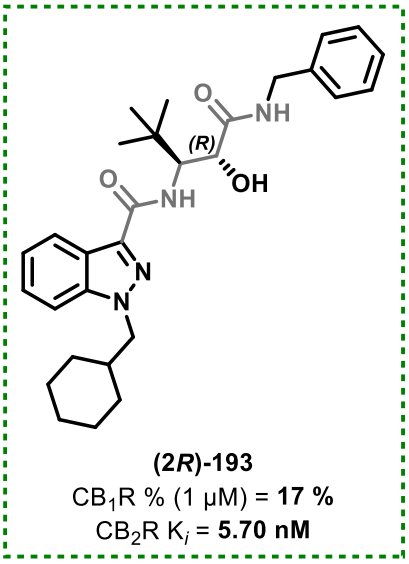



Figure 3.96. Structural features of the most interesting ligand identified in Series **VII**.

Figure 3.96 showcases the most interesting ligand obtained in Series **VII**, and summarizes the optimal substituents in each position:

1. Indazole as the core group.
2. Cyclohexyl methyl as the tail group.
3. Tert-butyl as the linker. In this specific case, $R^2$ bears the (*S*) configuration, although (*R*) substituents appear to exhibit similar results.
4. (*R*) configuration at the carbon holding the hydroxy group.
5. Benzyl as the head group.

Thus far, we have elucidated the diverse trends arising from the various structural motifs within both Series **VI** and Series **VII**, identifying the optimal substituents in each position to achieve potent and selective $CB_2R$ ligands. Both series have yielded excellent results, enhancing the pharmacological profile of the original SCRAs and transitioning from a dual $CB_1R/CB_2R$ behavior to a potent and $CB_2R$-selective scaffold. To assess the changes in the pharmacological profile between Series **VI** and Series **VII**, we will perform the same analysis of the affinity and selectivity profiles as for the previous trends. Figure 3.97 displays the affinity data at $CB_1R$ and $CB_2R$ of a selected subset of compounds from both series.

USC
UNIVERSIDADE DE SANTIAGO DE COMPOSTELA

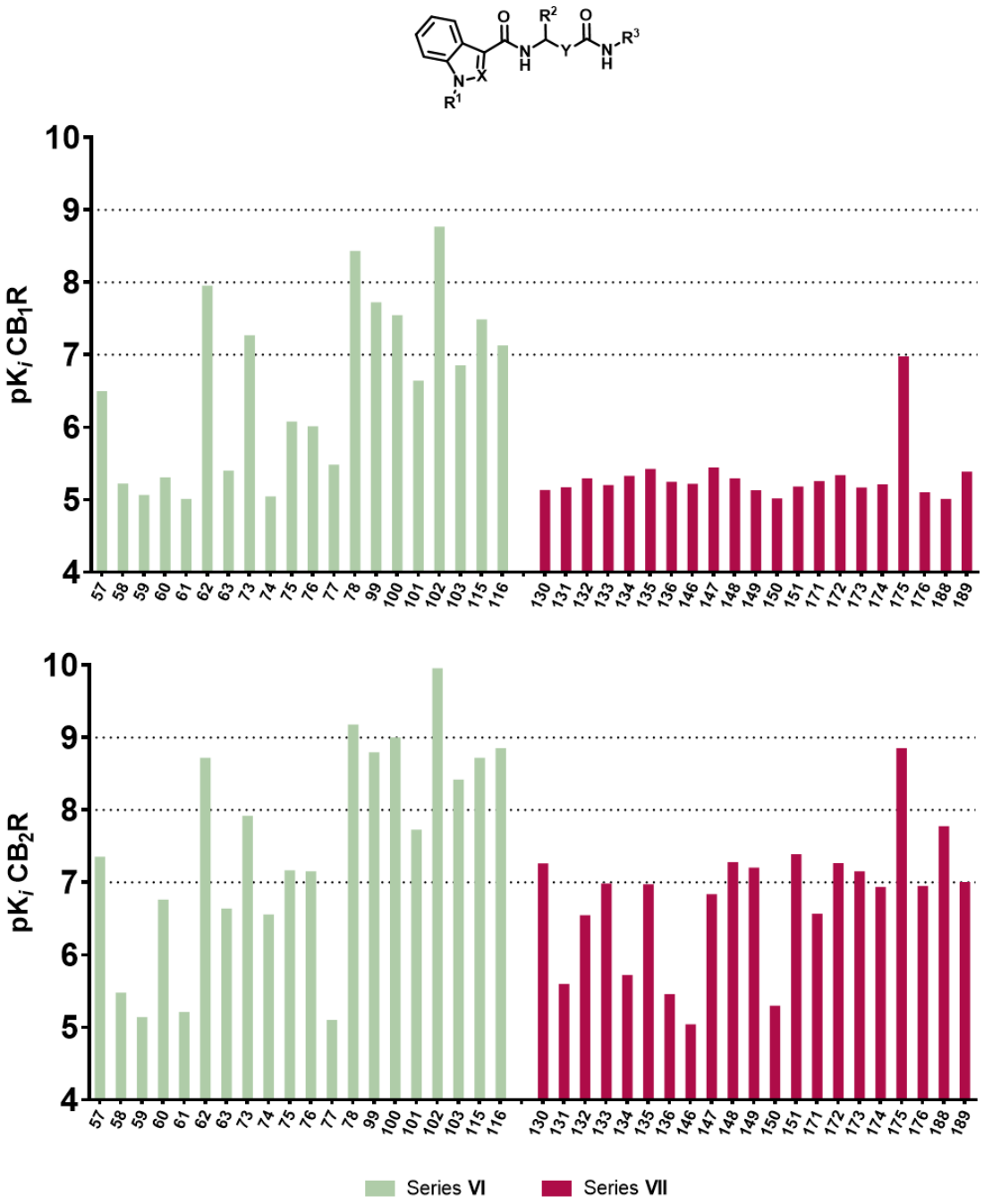



Figure 3.97. Bar chart representation of the SAR trends related to Series **VI** and Series **VII**. $CB_1R$ affinity data (above) and $CB_2R$ affinity data (bottom) are reported.

The comparison of the $CB_1R$ affinity data reveals a distinct difference between the two series. With the exception of compounds in Series **VI** that are inactive at this receptor, Series **VII** reliably exhibits lower affinity for $CB_1R$ than Series **VI**. This trend has been consistently observed throughout the SAR analysis of Series **VII**, where the absence of affinity for $CB_1R$

remained constant. The substitution of the carboxy group in the newly formed carbon atom resulting from the PADAM synthetic route with a hydroxy group completely abolishes affinity at the $CB_1R$.

Likewise, affinity for the $CB_2R$ shows the same tendency, with Series **VI** consistently demonstrating higher affinity for this receptor compared to Series **VII**. However, this difference in potency is much more gradual than the variation in affinity for the $CB_1R$, resulting in compounds with an improved pharmacological profile overall. Additionally, the project's starting point was a highly potent and dual $CB_1R/CB_2R$ scaffold, where potency could be readily achieved through proper decoration of the linker, core, tail, and head groups. Consequently, the primary focus was on enhancing selectivity towards $CB_1R$, and this objective was successfully accomplished. Figure 3.98 shows the representation of both potency and selectivity for reference.

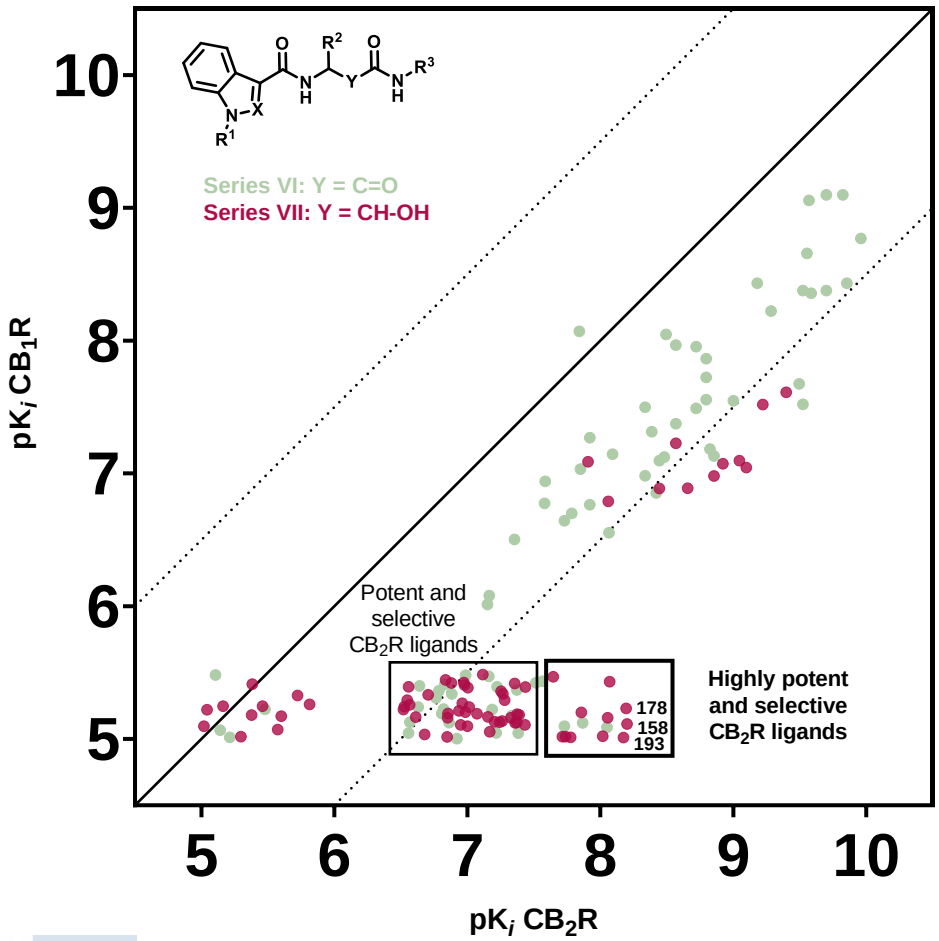



Figure 3.98. $CB_1R$ $pK_i$ [-log($K_i$)] vs $CB_2R$ $pK_i$ [-log($K_i$)] representation of series **VI** and series **VII**.

As mentioned earlier, derivatives from Series **VI** (green dots) are evenly distributed between the top-right part of the graph and the bottom-middle region. While this series has yielded excellent results in terms of potent and selective $CB_2R$ ligands, many of them still exhibit a non-selective profile. On the other hand, derivatives from Series **VII** (red dots) are predominantly clustered in the bottom-middle section of the graph, accounting for their superior selectivity profile. Interestingly, despite Series **VI** providing the most potent ligands in this study, the best ligands belong to Series **VII**. The pharmacomodulation process allowed the introduction of substituents that provided increased potency while still maintaining a good selectivity profile, resulting in the most potent ligands that meet the selectivity criteria (Figure 3.99).

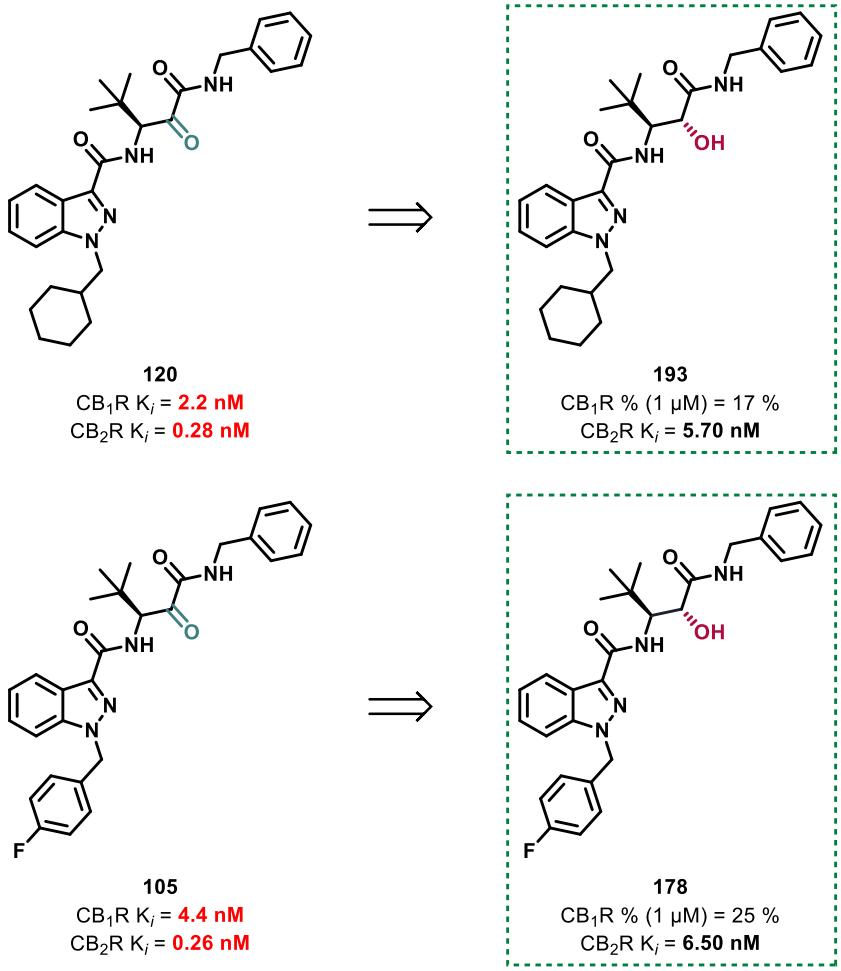



Figure 3.99. Pharmacomodulation improvement of the selectivity profile and structure of the best ligands of Chapter II.

Some of the trends identified during the SAR analysis of Series **VI** and Series **VII** have previously been reported by our group in other studies where a broad library of SCRA

analogs was disclosed.[71,111] Table 3.11 and Table 3.12 present certain derivatives from these studies, along with reference SCRA compounds, serving as a benchmark for evaluating the influence of the newly incorporated carbon atom and its substituent on the SAR and SSR.

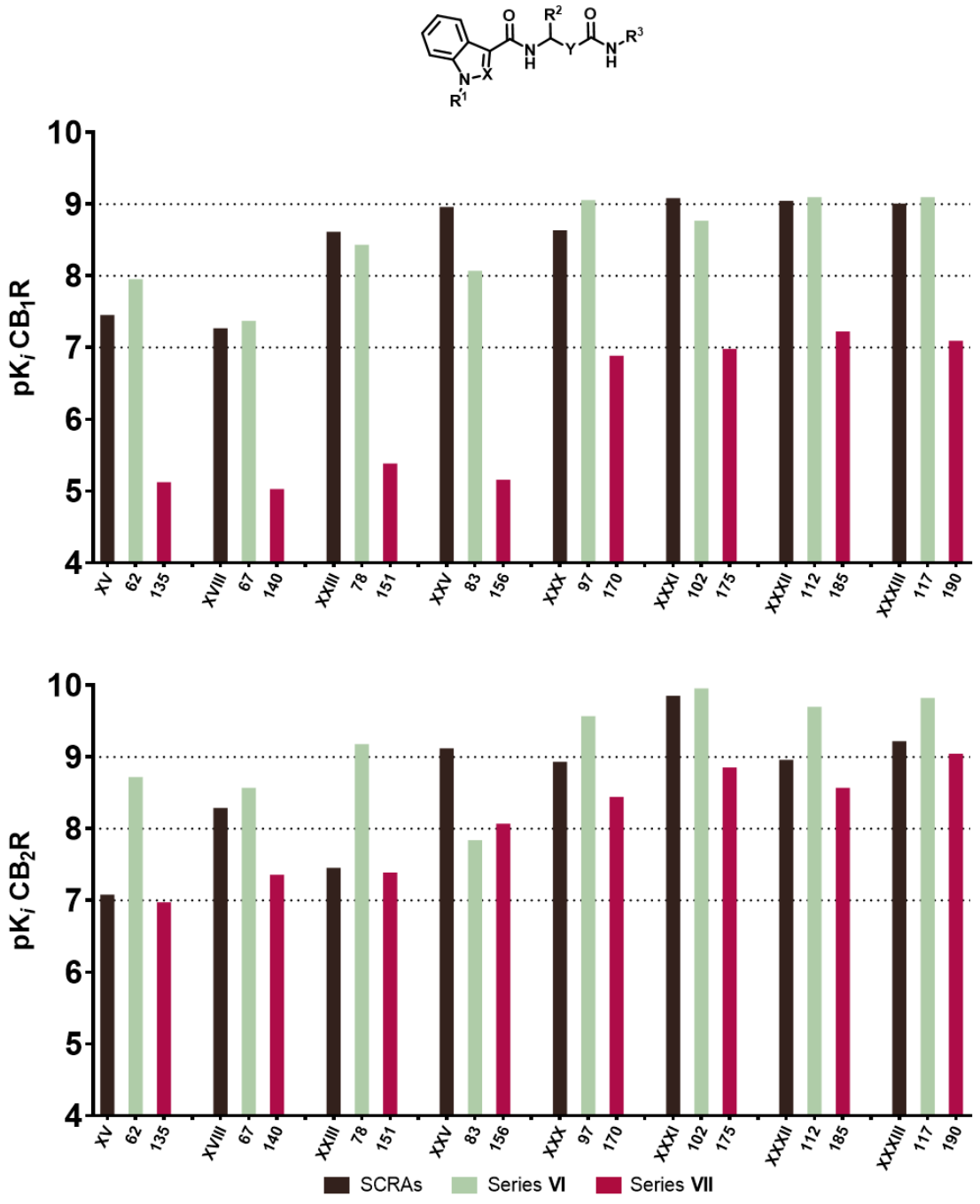



Figure 3.100. Bar chart representation of the SAR trends related to SCRAs, Series **VI** and Series **VII**. $CB_1R$ affinity data (above) and $CB_2R$ affinity data (bottom) are reported.

For direct comparisons, only derivatives sharing the same scaffold decorations will be considered, which means compounds with identical substituents at the core group, tail group, linker, and head group. Figure 3.100 presents a comparison of affinity data among SCRAs, Series **VI**, and Series **VII**. Two distinct trends emerge from this analysis. Firstly, SCRA compounds and Series **VI** derivatives exhibit a similar $CB_1R$ potency, whereas Series **VII** derivatives display a considerably lower affinity profile for $CB_1R$. On the other hand, SCRAs and hydroxyamides exhibit comparable $CB_2R$ potency, while carboxamides demonstrate a significantly higher affinity profile for $CB_2R$. Figure 3.101 shows a visual representation of potency and selectivity for reference.

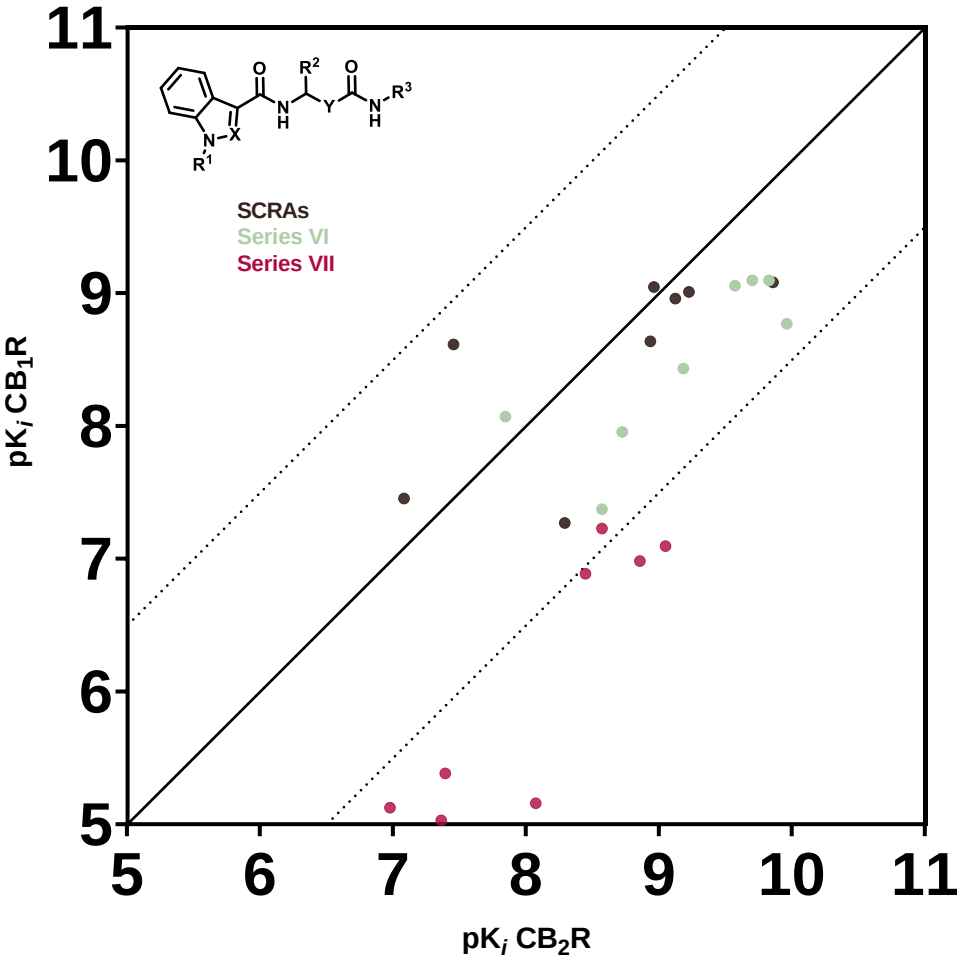



Figure 3.101. $CB_1R$ $pK_i$ [-log($K_i$)] vs $CB_2R$ $pK_i$ [-log($K_i$)] representation of SCRAs, Series **VI**, and Series **VII**.

The trends explained above can be quickly visualized in the diagonal plot. Green dots, representing Series **VI**, are shifted to the right compared to the dark dots (representing the

SCRA compounds). This leads to more potent compounds than the original SCRAs, while also improving their selectivity, as $CB_1R$ affinity remains unchanged. On the other hand, red dots (depicting Series **VII**), are shifted downwards in comparison to the dark dots, indicating an improvement in selectivity (lower $CB_1R$ affinity) without affecting affinity for $CB_2R$. This yields more selective compounds than the original SCRAs, while retaining their characteristic high potency.

In addition to the original series of SCRAs, direct comparisons are possible between our newly synthesized series and those previously reported by the ComBioMed group. Claudia Gioè's research has provided valuable pharmacological insights into the relationships between structure-activity, and structure-selectivity within the SCRAs family. This work has led to the discovery of new agonists that specifically target the $CB_2R$ receptor.[71] Inspired by the success of this work, we proposed a similar multicomponent strategy that incorporates an extra carbon atom into the structure, with either a carbonyl group or a hydroxy group attached to it. Comparisons between selected ligands that bear the same substituents in each position (core group, tail group, linker, and head group) will provide useful understanding of the effect that the extra carbon atom and its substituent have on the pharmacological profile. Figure 3.102 presents a comparison of affinity data among Reference compounds, Series **VI**, and Series **VII**.

In contrast to the earlier analyzed SCRA compounds, in this case, the reference compounds used for comparisons have undergone a pharmacomodulation process, resulting in an enhanced and optimized pharmacological profile. Regarding $CB_1R$ affinity, the reference compounds display the highest potency at this receptor among the three subsets, although Series **VI** shows a similar affinity profile. Series **VII**, conversely, is consistently inactive at the $CB_1R$ in all cases, reaffirming its excellent selectivity profile.

The affinity data at the $CB_2R$ follows a similar pattern. In this case, Series **VI** appears to exhibit slightly higher potency at the $CB_2R$, closely followed by the reference compounds. Similar to the observed trends in the comparison between Series **VI** and Series **VII**, the latter demonstrates a more moderate affinity profile for $CB_2R$.

Overall, the pharmacological profile of the newly synthesized compounds is comparable to that of the compounds in Gioè's work. Series **VI** appears to slightly improve both potency and selectivity compared to the reference compounds, while Series **VII** notably enhances the selectivity profile and the overall pharmacological profile. Considering that the reference

USC UNIVERSIDADE DE SANTIAGO DE COMPOSTELA

compounds have already been optimized, the improvement in their results can be seen as a significant success of the pharmacomodulation process.

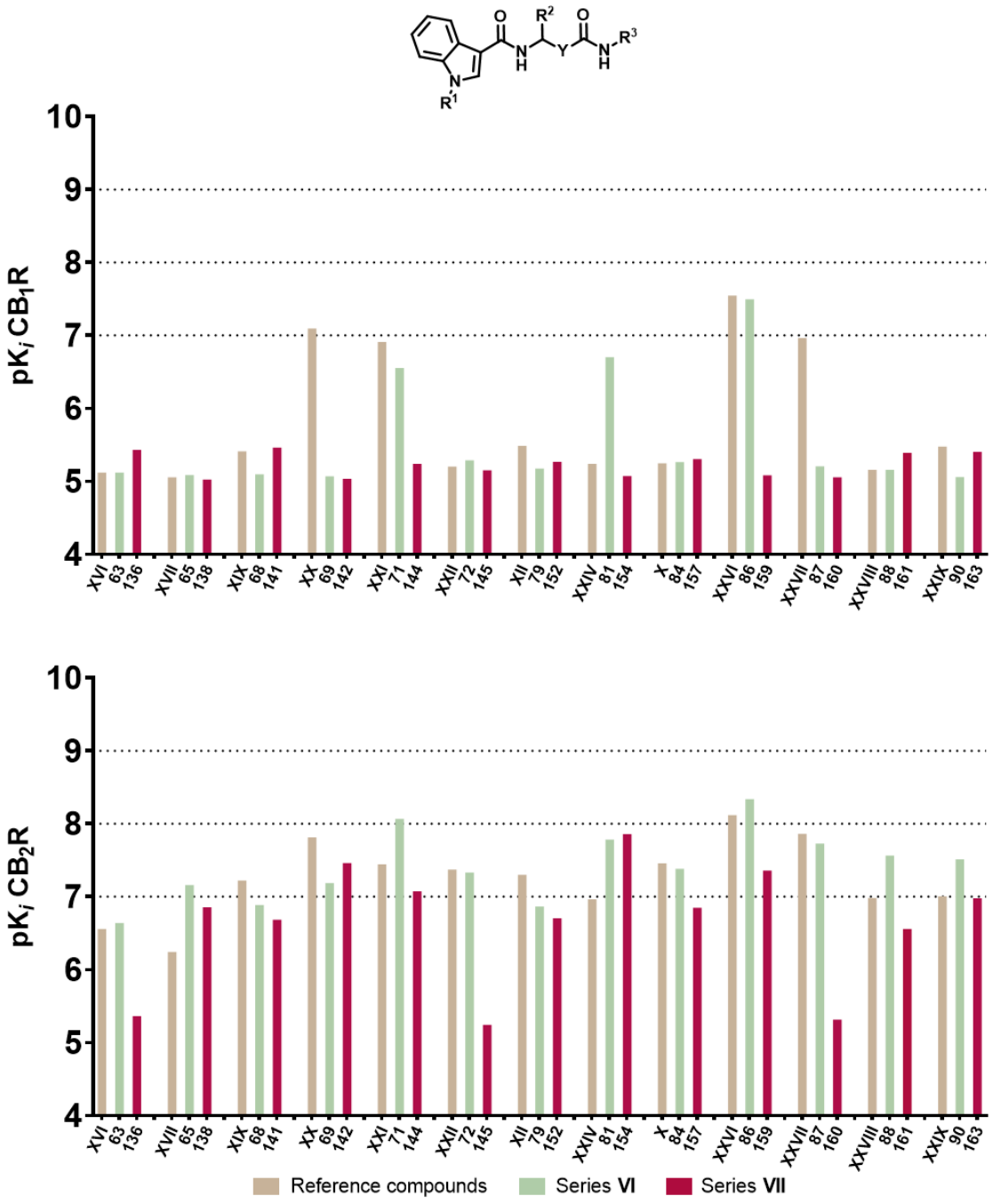



Figure 3.102. Bar chart representation of the SAR trends related to reference compounds, Series **VI**, and Series **VII**. $CB_1R$ affinity data (above) and $CB_2R$ affinity data (bottom) are reported.

Figure 3.103 shows a visual representation of both potency and selectivity for reference. As mentioned previously, the representation shows the slightly improved pharmacological

USC DE SANTIAGO DE COMPOSTELA

profile of Series **VI** and Series **VII** compared to that of the reference compounds. It can be observed that the majority of ligands falling in the top-right section of the graph belong to the reference compounds, alongside derivatives from Series **VI**. Series **VII** does not exhibit any compounds in this section, thanks to its excellent selectivity profile. Furthermore, the bottom part of the graph in the low nanomolar section of $CB_2R$ affinity is predominantly composed of compounds from Series **VI** (three carboxamides) or Series **VII** (five hydroxyamides), with only two derivatives corresponding to the reference compounds.

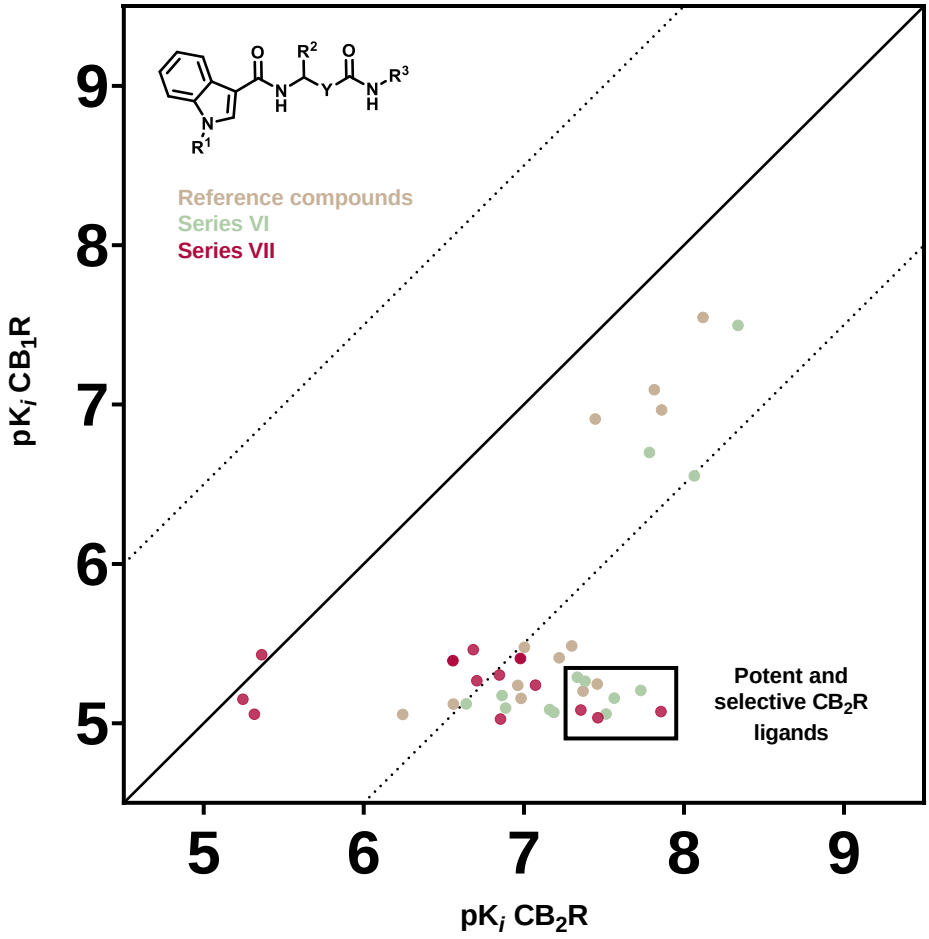



Figure 3.103. $CB_1R$ $pK_i$ [-log($K_i$)] vs $CB_2R$ $pK_i$ [-log($K_i$)] representation of reference compounds, Series **VI**, and Series **VII**.

In conclusion, the PADAM synthetic route has proven to be an effective pharmacological tool for developing extensive libraries of SCRA analogues in a cost-effective and time-efficient manner. Similar to the Ugi-4CR approach, this methodology allowed for a comprehensive exploration of the SAR within both series, leading to the identification of

optimal substituents at each structural motif (core group, tail group, linker, and head group) to achieve potent and selective $CB_2R$ ligands. Furthermore, the introduction of the new carbon atom in the PADAM, along with its substituent (carbonyl or hydroxyl) significantly contributed to improve the selectivity profile of the SCRAs scaffold, especially in the case of hydroxyamides. The specific advantages of Series **VI** and Series **VII**, in comparison to the previously described compounds, are summarized in Figure 3.104.

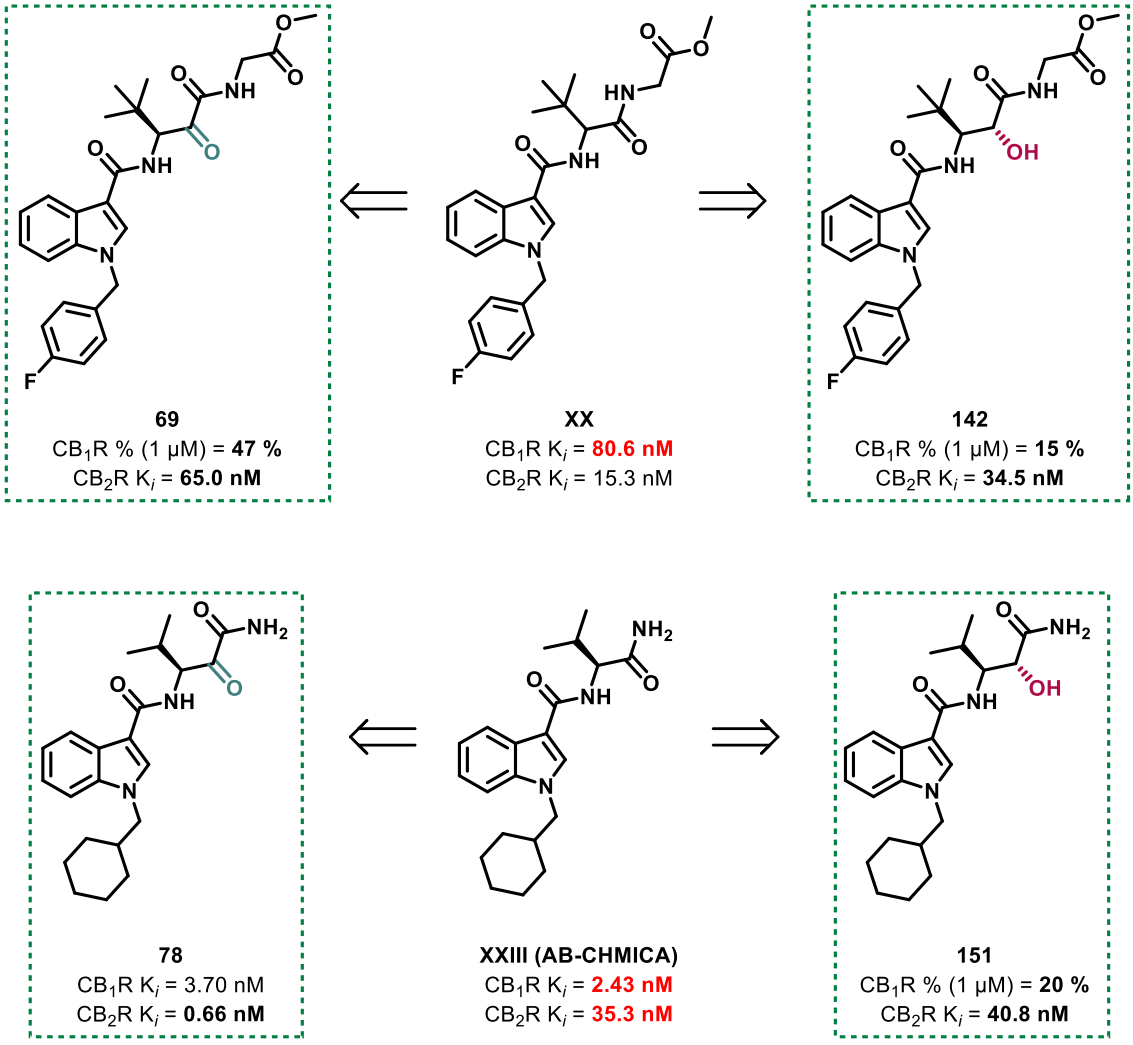



Figure 3.104. Change in the pharmacological profile of SCRAs and reference compounds.

USC UNIVERSIDADE DE SANTIAGO DE COMPOSTELA

### 3.2.5 Molecular docking simulations

Docking assays were conducted on representative indole derivatives (Figure 3.105) on $CB_1R$ (PDB: 5TGZ) and $CB_2R$ (PDB: 5ZTY) to elucidate the structure-activity relationship and complete the binding study of these compounds. The resultant binding mode is in good agreement with the pharmacological data. Small but important differences exist in the orthosteric binding site of $CB_1R$ and $CB_2R$, as shown in Figure 3.106. However, in both receptors, towards the inner side, there are many aromatic amino acids (e.g., phenylalanine and tryptophan) able to stabilize in both cases the aromatic rings of the explored compounds.

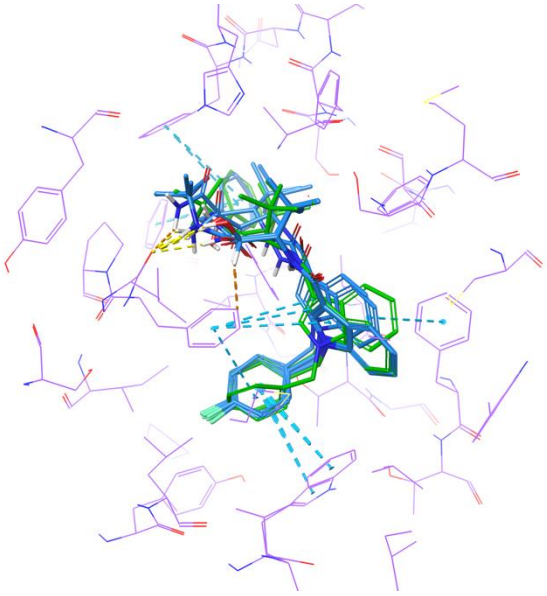


Figure 3.105. Overlapped binding mode of representative ligands in $CB_2R$. In green, model ligands previously described; in blue, oxo-derivatives obtained in this Doctoral Thesis. Yellow dashed lines: hydrogen bonds, blue dashed lines: π-π interactions, orange dashed lines: bad contacts.

To make a preliminary exploration of the binding mode, three representative *N*-(3,3-dimethyl-1-(amino, *tert*-butylamino or benzylamino)-1-oxobutan-2-yl)-1-(4-fluorobenzyl)-1*H*-indole-3-carboxamide (**IV**, **V** or **VII**) were compared with their oxoanalogues (**67**, **68**, **71**) obtained in this Doctoral Thesis in $CB_1R$ and $CB_2R$. This comparison allowed us to explore the effect of the introduction of a carbonyl group in compounds of different sizes on the binding mode. As observed in Figure 3.105, the binding mode is consistent with that already described for model ligands.[71]

USC UNIVERSIDADE DE SANTIAGO DE COMPOSTELA

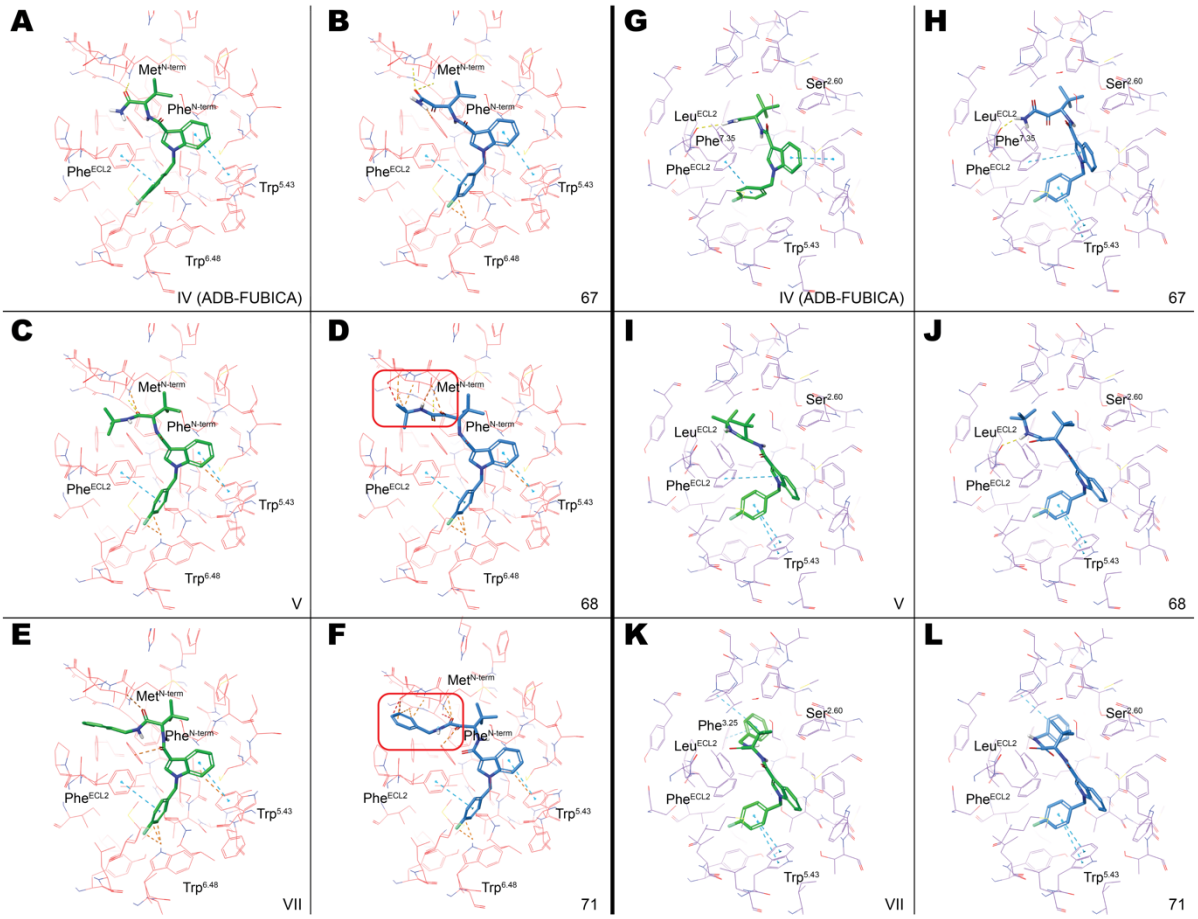



Figure 3.106. Docking-predicted binding mode of A) **ADB-FUBICA** at $CB_1R$, B) **67** at $CB_1R$, C) **V** at $CB_1R$, D) **68** at $CB_1R$, E) **VII** at $CB_1R$, F) **71** at $CB_1R$, G) **ADB-FUBICA** at $CB_2R$, H) **67** at $CB_2R$, I) **V** at $CB_2R$, J) **68** at $CB_2R$, K) **VII** at $CB_2R$, and L) **71** at $CB_2R$. $CB_1R$ (red) and $CB_2R$ (purple) 3D structures are PDB: 5TGZ and 5ZTY respectively. Yellow dashed lines: hydrogen bonds, blue dashed lines: π-π interactions, orange and red dashed lines: bad contacts (highlighted in red rounded square).

Focusing on the comparison of biological data of **ADB-FUBICA** with its oxoderivative, compound **67** ($R^3$ = H, Figure 3.107) we observe that both are unselective $CB_1R/CB_2R$ ligands (**ADB-FUBICA** $CB_1R$ $K_i$ = 53.8 nM, $CB_2R$ $K_i$ = 5.15 nM; **67** $CB_1R$ $K_i$ = 42.3 nM, $CB_2R$ $K_i$ = 2.70 nM). At $CB_1R$, both form a hydrogen bond with $Met^{N\text{-}term}$, in addition to two π-π interactions with $Phe^{ECL2}$ and $Trp^{5.43}$ (Figure 3.106A-B). At $CB_2R$, same π-π interactions are conserved, but in this case both compounds are able to form a hydrogen bond with $Leu^{ECL2}$. As already described,[71] the introduction of a substituent in the amide ($R^3$) causes a change in selectivity, eliminating (or decreasing) $CB_1R$ affinity and keeping $CB_2R$ affinity. A good example of this behavior is the binding mode of compounds **V**, **VII** (Figure 3.106C-D, I-J) compared with **68** and **71** (Figure 3.106E-F, K-L) and their affinity data (Figure 3.107).

USC
DE SANTIAGO
DE COMPOSTELA

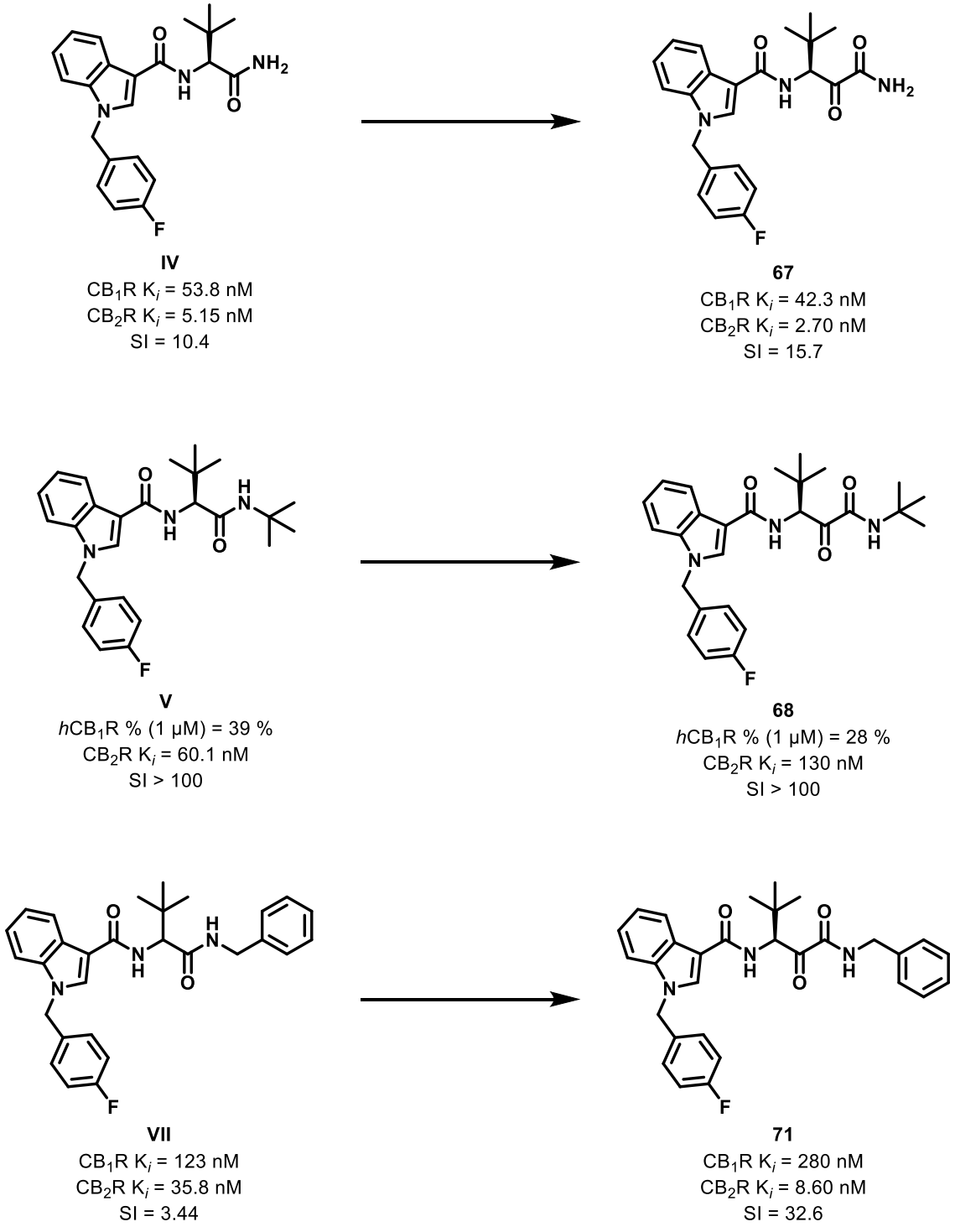



Figure 3.107. Change in the pharmacological profile induced by the introduction of a carbonyl group into the side chain of model compounds.

The incorporation of a carbonyl group into the side chain of model compounds results in an increased molecular size. This increase notably affects the compounds with large substituents at the $R^3$ position, leading to a reduced or completely lost affinity towards $CB_1R$.

In contrast, the affinity for $CB_2R$ is either maintained or experiences only a slight decrease. This differential affinity can be primarily attributed to the size discrepancy between the $CB_1R$ and $CB_2R$, particularly evident in their *N*-terminus, which consist of 111 and 28 amino acids, respectively. The *N*-terminus plays a crucial role in defining the binding site's accessibility from the extracellular region, resulting in a more constricted binding site for $CB_1R$ compared to $CB_2R$.

Another significant modification of the model structure involves replacing a carbonyl group with a hydroxyl group. This alteration, as previously explained, results in a substantial shift in selectivity towards $CB_2R$. This change underscores the critical impact that even minor structural variations can have on the binding affinity and selectivity of these compounds. The transition from a sp2-hybridized carbon (ketone) to a sp3-hybridized carbon (hydroxyl) leads to increased steric clashes with the binding site of $CB_1R$ (Figure 3.108). This structural change results in a decreased or completely abolished affinity for this receptor. Conversely, the $CB_2R$, which possesses a more spacious binding site, continues to accommodate these compounds, thereby retaining their affinity.

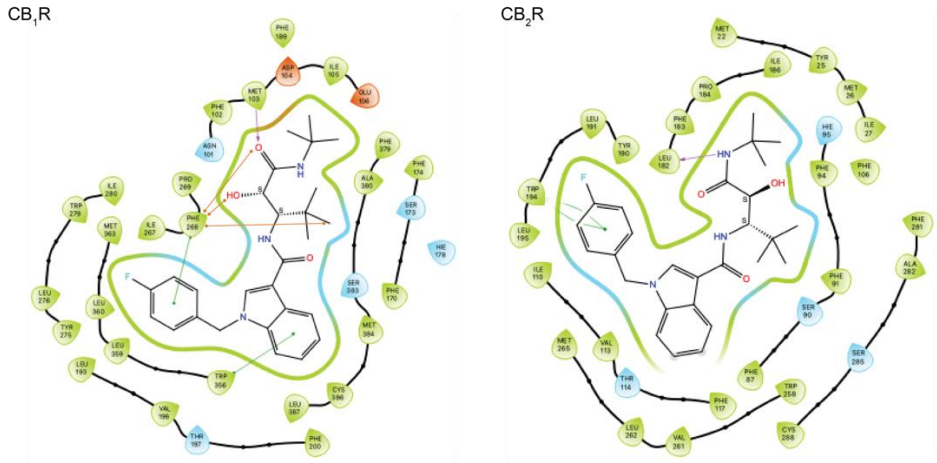



Figure 3.108. Ligand interaction diagram for compound **141** at $CB_1R$ and $CB_2R$. Purple arrows represent hydrogen-bond, green lines represent π-π interactions, and orange lines represent clashes with the receptor.

#### 3.2.5.1 System preparation and MD/FEP simulations

$CB_1R$ and $CB_2R$ 3D structures are PDB: 5TGZ and 5ZTY respectively,[75,146] and here processed using the Protein Preparation Wizard pipeline in Maestro (Schrodinger ver. 2023-1). Subsequently, possible 3D tautomer and protomers at pH 7 ± 2 were generated for each compound using OPLS4 force field[147] and Epik, the lowest energy conformer was chosen for

USC UNIVERSIDADE DE SANTIAGO

molecular docking. A receptor grid was generated with the default Van der Waals radius scaling settings, and it was positioned in the center of geometry of the binding site. Thereafter, Glide SP docking was performed, selecting the best poses in basis of docking score.

USC
UNIVERSIDADE DE SANTIAGO DE COMPOSTELA

### 3.2.6 Functional assays

Five $CB_2R$ selective ligands identified during this project (Figure 3.109) were submitted to functional studies to evaluate their functional behavior (agonist or antagonist). Radioligand binding assays provide valuable information about receptor binding and ligand affinity ($K_i$), but not about the ligand's ability to activate or inhibit receptor signaling pathways. To address the ligand's functional profile, it is required to measure the downstream response of $CB_2R$ activation, e.g., measuring intracellular calcium release, cAMP levels, or phosphorylation of specific signaling proteins.

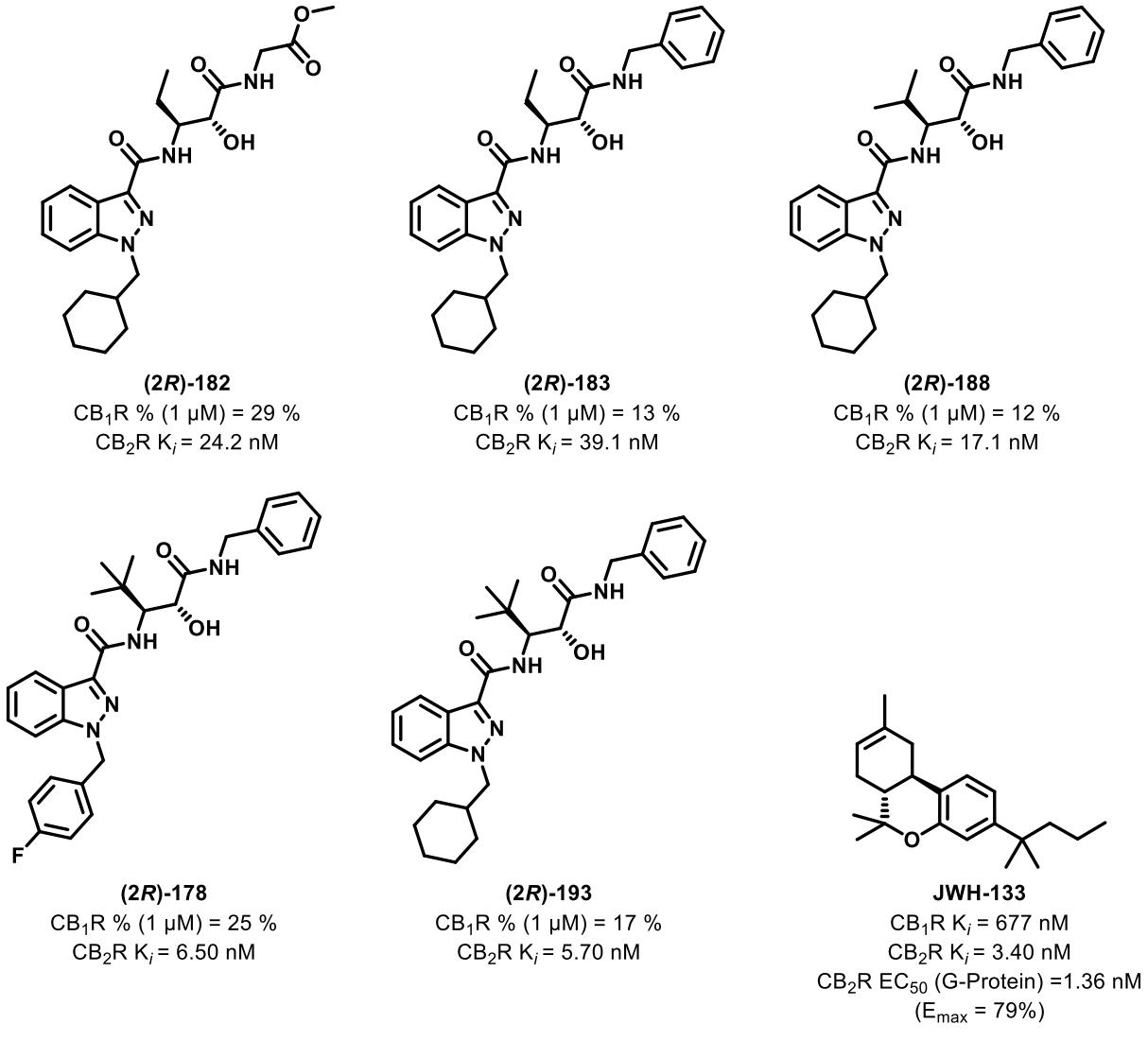



Figure 3.109. Structure of the $CB_2R$ ligands selected for functional studies and JWH-133.

The functional experiments were performed by the group of the Professor Gemma Navarro (University of Barcelona), following established protocols evaluating cAMP

levels.[148] For comparative reasons, JWH-133 (Figure 3.109), a potent and selective $CB_2R$ agonist structurally related to $\Delta^9$-THC, was employed as reference compound and submitted to the same experimental conditions. The results obtained during these experiments are shown in Table 3.27. For comparative purposes, the affinity data of selected ligands was also incorporated. As observed, all compounds were able to increase cAMP concentrations in a dose-dependent manner and exhibit $EC_{50}$ values ranging from 0.007 – 0.07 nM. These results unequivocally validated their agonist behavior. Analysis of the $E_{max}$ data reported in Table 3.27 enabled to confirm that the new compounds herein identified behave as full (Emax > 70%) or partial ($E_{max}$ = 55%) $CB_2R$ agonists. The dose-response curves obtained during this study are presented in Figure 3.110.

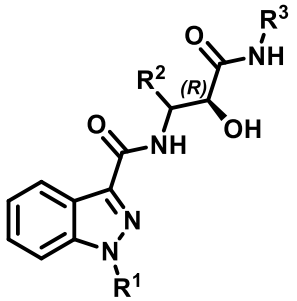



Table 3.27. Structure, binding data, and functional data obtained for representative $CB_2R$ selective ligands.

| Compounds and diversity explored | | | | Binding data | | $CB_2R$ Functional cAMP data | |
|---|---|---|---|---|---|---|---|
| | | | | $CB_1R$ | $CB_2R$ | | |
| Code | $R^1$ | $R^2$ | $R^3$ | % at 1 μM[a)] | $K_i$[b)] | $EC_{50}$[c)] | $E_{max}$[d)] |
| **(2*R*)-178** | 4-F-Bn | (*S*)-*t*-Bu | Bn | 25% | 6.50 nM | 0.05 nM | 73% |
| **(2*R*)-182** | $CH_2$-Cy | (*S*)-Et | $CH_2$-$CO_2$Me | 29% | 24.2 nM | 0.007 nM | 86% |
| **(2*R*)-183** | $CH_2$-Cy | (*S*)-Et | Bn | 13% | 39.1 nM | 0.07 nM | 55% |
| **(2*R*)-188** | $CH_2$-Cy | (*S*)-*i*-Pr | Bn | 12% | 17.1 nM | 0.03 nM | 83% |
| **(2*R*)-193** | $CH_2$-Cy | (*S*)-*t*-Bu | Bn | 17% | 5.70 nM | 0.03 nM | 86% |
| **JWH-133** | - | - | - | 677 nM | 3.40 nM | 1.36 nM | 79% |

[a)] Displacement of specific [$^3$H]-CP55940 binding in human CHO cells expressed as $K_i$ in nM (n = 3) or percentage displacement of specific binding at a concentration of 1 $\mu$M (n = 2). [b)] Displacement of specific [$^3$H]-CP55940 binding in human HEK-293 cells expressed as $K_i$ in nM (n = 3) or percentage displacement of specific binding at a concentration of 1 $\mu$M (n = 2). c) Functional activity assessed in transfected HEK-293T cells by determining cAMP levels after forskolin stimulation. d) $E_{max}$ values were normalized to a maximal efficacious concentration of CP 55,940.

USC UNIVERSIDADE DE SANTIAGO DE COMPOSTELA

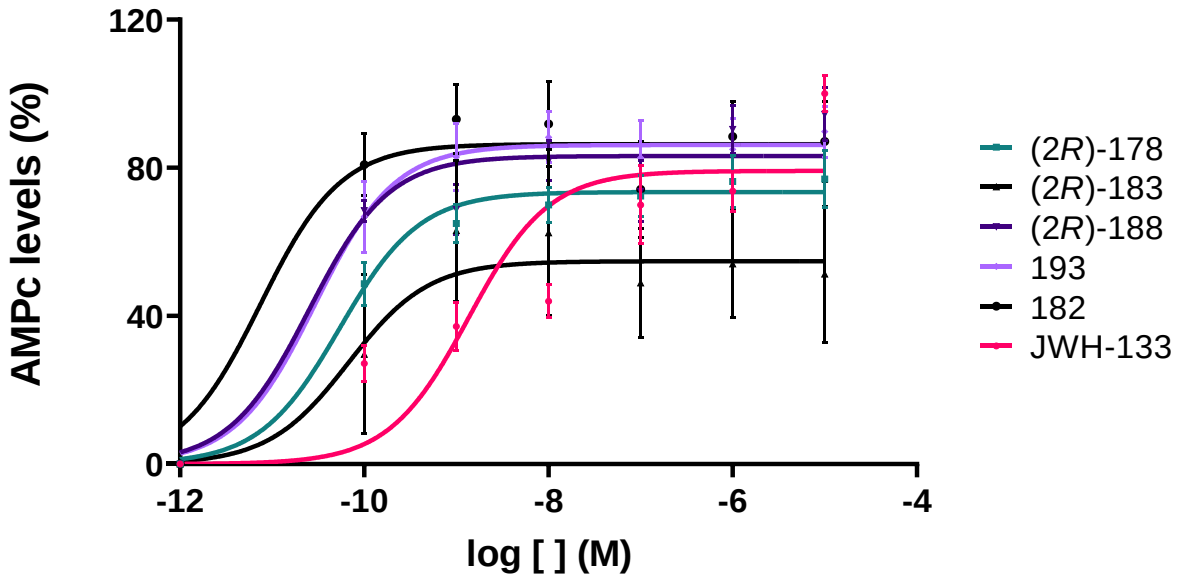



Figure 3.110. Dose-response curves obtained for reference ligand (JWH-133) and selected ligands at $CB_2R$ during cAMP functional assays.

As observed in Table 3.27, the studied ligands differ in efficacy (Emax) and, according to this parameter, can be classified into two groups. Four of the five evaluated compounds (**(2*R*)-178**, **(2*R*)-182**, **(2*R*)-188**, **(2*R*)-193**) behave as full agonists ($E_{max}$ = 73-86%), while compound **(2*R*)-183** behaves as partial agonist ($E_{max}$ = 55%).

### 3.2.6.1 Functional selectivity studies

The concept of bias agonism revolutionized our comprehension of GPCR signaling, reshaping our view of how GPCRs function across various scenarios, notably in drug discovery.[149,150] Functional selectivity can be defined as the ability of a ligand to preferentially signaling through a precise pathway among other possible routes.[151–153] This signaling phenomenon plays a pivotal role in drug development, aiding in the comprehension and differentiation of the adverse effects associated with many drugs.[149–153] However, it's important to note that the biased agonism of a ligand cannot be considered as an absolute description of its action, as it is heavily influenced by factors such as the receptor, reference ligand, and the pathways involved (Figure 3.111).[154]

USC UNIVERSIDADE DE SANTIAGO DE COMPOSTELA

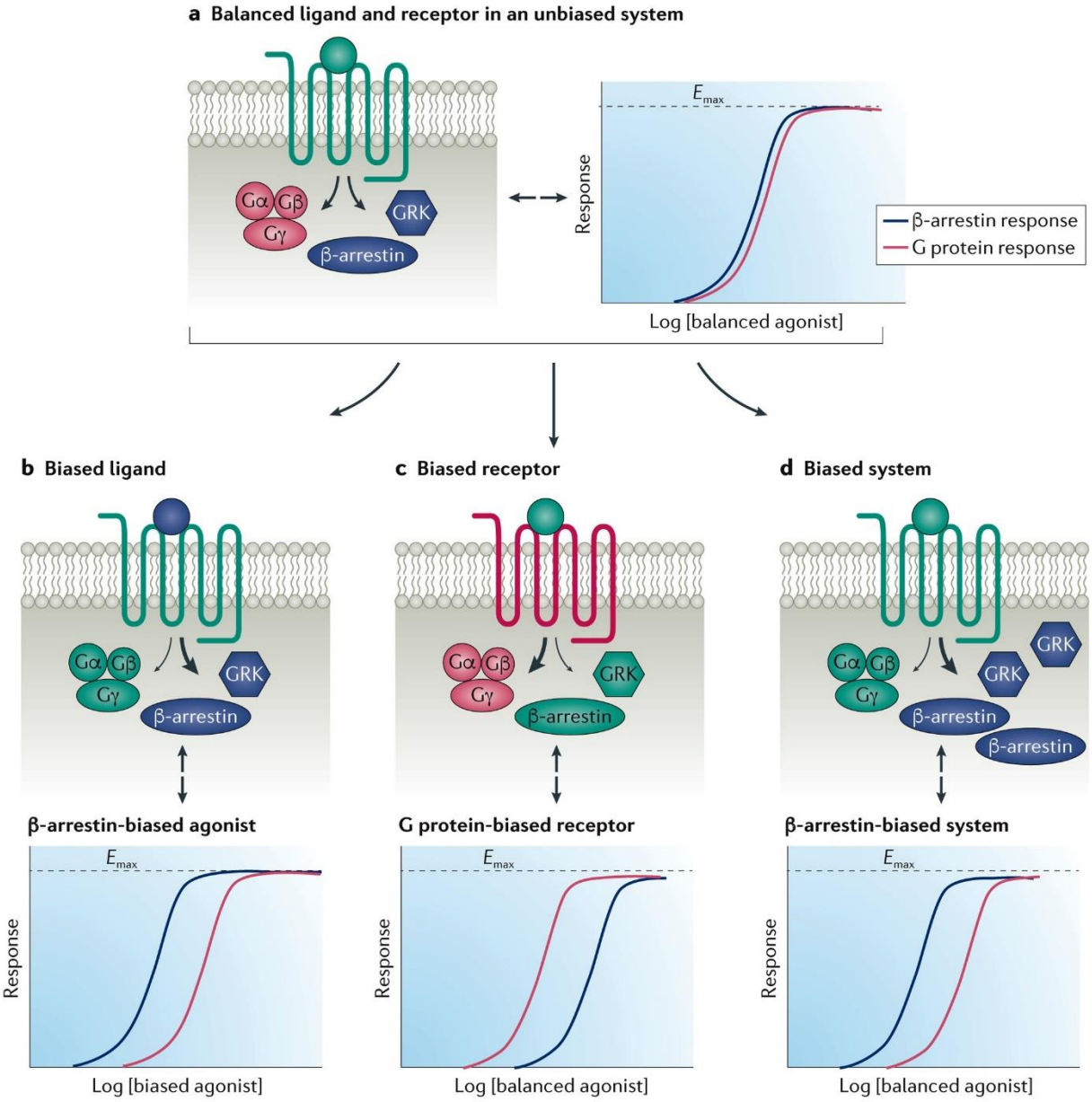



Figure 3.111. Graphical representation of the different facets of the biased signaling phenomena (Figure from Smith, J., Lefkowitz, R. & Rajagopal, S. Biased signaling: from simple switches to allosteric microprocessors. Nat Rev Drug Discov 17, 243–260 (2018). https://doi.org/10.1038/nrd.2017.229).[155]

In the case of the GPCRs concerned within this Thesis (CBRs), the therapeutic profile (advantages/disadvantages) derived from $CB_2R$-biased signaling has not yet been thoroughly investigated. Indeed, only a few truly $CB_2Rs$ biased ligands have been described to date.[152,156,157] The main problem with known biased ligands, both for cannabinoid receptors and other GPCRs, is their lack of selectivity (promiscuity) against other receptor subtypes within the family.[157] Many ligands that exhibit a biased signaling profile at a particular

receptor (e.g., $CB_2R$) are not selective against their congeners (e.g., $CB_1R$). Although these compounds may be useful for studying processes in transfected cells (that express only the receptor of interest), their promiscuity against other subtypes limits their usefulness and the correct interpretation of their effects when used in more complex systems (e.g., cell models, in vivo studies, or drug uses).

This underscores the formidable scientific hurdle in developing ligands that offer both receptor subtype selectivity and biased signaling. The complexity of GPCR signaling further complicates matters. Upon GPCR activation, multiple signaling pathways and downstream effectors can be concurrently engaged. Beyond G proteins, GPCRs can interact with various intracellular signaling molecules including β-arrestins, scaffold proteins, and other signaling mediators.[152,156,157] These molecules can mediate GPCR signaling through alternative pathways, leading to the activation of different downstream effectors and cellular responses. For example, β-arrestins can interact with GPCRs and initiate alternative signaling pathways, such as the mitogen-activated protein kinase (MAPK) pathway, independently of G protein activation.[152,154,156,157] In essence, the intricate interplay between GPCRs and intracellular signaling molecules allows for the coexistence of diverse signaling pathways post-GPCR activation.

The G protein-cAMP (cyclic adenosine monophosphate) pathway is the most common and well-characterized signaling pathway of GPCRs, being considered the “canonical” signaling form of membrane receptors.[152,156] GPCRs typically engage with heterotrimeric G proteins, initiating intracellular signaling cascades upon ligand binding. Activation of a GPCR by a ligand triggers the associated G protein, prompting adenylate cyclase to catalyze the production of cAMP. Subsequently, cAMP acts as a secondary messenger, activating downstream effector proteins such as protein kinase A (PKA) to orchestrate various cellular processes including gene expression and metabolism. The G protein-cAMP pathway has garnered significant attention for its pivotal roles across a spectrum of physiological and pathological contexts.[152,156–158]

β-arrestins are proteins that bind to G protein-coupled receptors (GPCRs) upon activation by a ligand (endogenous or exogenous). Acting as negative regulators of GPCR signaling, β-arrestins intervene in the activated receptor's signaling cascade, leading to desensitization (loss of response) and endocytosis.[152,156–158] Beyond GPCR regulation, β-arrestins participate in various cellular processes such as cell proliferation and migration, serving as modulators of

USC
DE SANTIAGO
DE COMPOSTELA

signaling in other pathways. Moreover, β-arrestins have been implicated in the pathogenesis of various diseases, including cancer, inflammation, and cardiovascular disorders.[152,156–158]

The complexity of GPCR signaling, and the involvement of multiple pathways, make it challenging to identify ligands that exhibit selective biased signaling. Shedding light on the biased signaling profile of new selective $CB_2R$ agonists is crucial for the development of drugs with improved efficacy and safety profiles. This knowledge can help to identify compounds with desirable signaling profiles, which can selectively activate specific pathways while avoiding the activation of others. This can lead to the development of drugs that target diseases more effectively and with fewer side effects. Therefore, investigating the biased signaling profiles of new $CB_2R$ agonists is an important step towards the development of more effective and safer drugs.

After identifying a collection of $CB_2R$-selective ligands in this chapter, it was decided to complete their pharmacological characterization by investigating their functional selectivity profile (biased/unbiased signaling). To accomplish this, five ligands (Figure 3.109) that were previously used to validate the functional (agonist) behavior of the series were employed. To fully characterize the signaling (biased/unbiased) profile of the selected ligands, we evaluated their ability to recruit β-arrestin, that complements the previously evaluated canonical G protein signaling (cAMP). The results of these investigations are presented in Table 3.28 and provide a more complete picture of the signaling landscape of these ligands. The dose-response curves for all studied ligands at each signaling pathway are presented in Figure 3.112.

USC
UNIVERSIDADE DE SANTIAGO DE COMPOSTELA

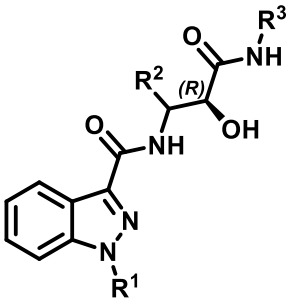


Table 3.28. Binding and functional data of selected $CB_2R$ ligands.

| Compounds and diversity explored | | | | Binding data | | Functional data | | Biased profile |
|---|---|---|---|---|---|---|---|---|
| | | | | $CB_1R$ | $CB_2R$ | | | |
| Code | $R^1$ | $R^2$ | $R^3$ | % at 1 μM[a] | $K_i$[b] | cAMP $EC_{50}$ (nM)[c] [$E_{max}$][d] | B-arrestin $EC_{50}$ (nM)[c] [$E_{max}$][d] | |
| **(2*R*)-178** | 4-F-Bn | (*S*)-*t*-Bu | Bn | 25% | 6.50 nM | 0.05 [73%] | 153 [109%] | G-protein |
| **(2*R*)-182** | $CH_2$-Cy | (*S*)-Et | $CH_2$-$CO_2$Me | 29% | 24.2 nM | 0.007 [86%] | 1024 [130%] | G-protein |
| **(2*R*)-183** | $CH_2$-Cy | (*S*)-Et | Bn | 13% | 39.1 nM | 0.07 [55%] | 1.59 [66%] | G-protein |
| **(2*R*)-188** | $CH_2$-Cy | (*S*)-*i*-Pr | Bn | 12% | 17.1 nM | 0.03 [83%] | 275 [40%] | G-protein |
| **(2*R*)-193** | $CH_2$-Cy | (*S*)-*t*-Bu | Bn | 17% | 5.70 nM | 0.03 [86%] | 1974 [191%] | G-protein |
| **JWH-133** | - | - | - | 677 nM | 3.40 nM | 1.36 [79%] | 1.35 [94%] | Unbiased |

[a] Displacement of specific [$^3$H]-CP55940 binding in human CHO cells expressed as $K_i$ in nM (n = 3) or percentage displacement of specific binding at a concentration of 1 $\mu$M (n = 2). [b] Displacement of specific [$^3$H]-CP55940 binding in human HEK-293 cells expressed as $K_i$ in nM (n = 3) or percentage displacement of specific binding at a concentration of 1 $\mu$M (n = 2). c) Functional activity assessed in transfected HEK-293T cells by determining cAMP levels after forskolin stimulation. d) $E_{max}$ values were normalized to a maximal efficacious concentration of CP 55,940.

USC UNIVERSIDADE DE SANTIAGO DE COMPOSTELA

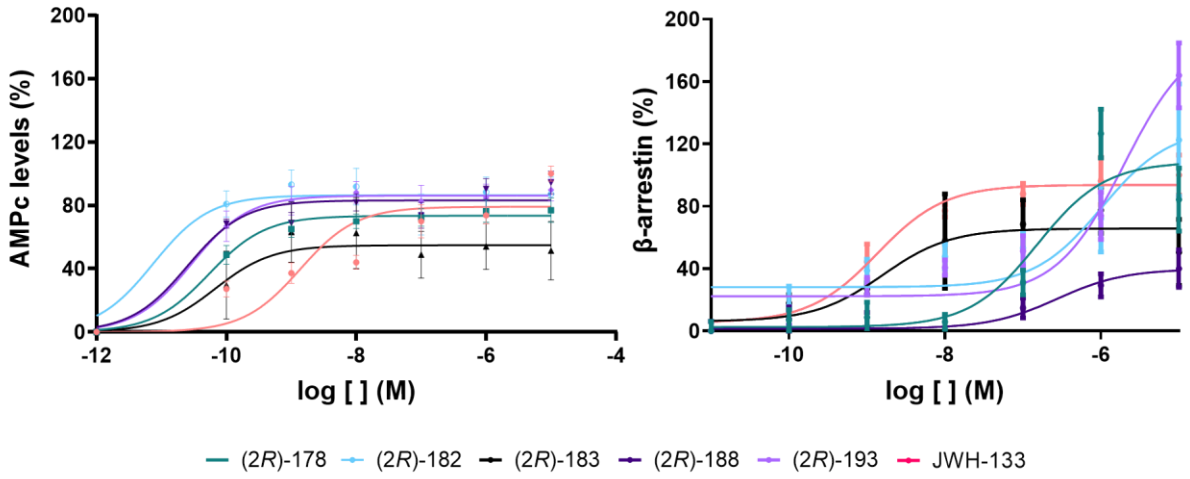



Figure 3.112. Dose-response curves obtained for reference ligand (JWH-133) and selected ligands at $CB_2R$ during functional assays.

In this study, the $CB_2R$ selective ligand JWH-133 has been employed as reference ligand due to the widespread consensus in the scientific community regarding its classification as an unbiased agonist.[153,157] The analysis of the data obtained (Table 3.28) leads us to conclude that the five tested ligands can be classified as G-protein biased ligands. They display excellent activity ($EC_{50}$ < 0.08 nM) and high efficacy (Emax > 55%) in the cAMP pathway, with the former being significantly higher (up to 100.000-fold) than in the β-arrestin pathway.

It is important to note that the exploration of the therapeutic applications of biased $CB_2R$ agonists (in this case, G-protein biased) is still under investigation, and more research is needed to fully understand their efficacy, safety, and clinical potential in these and other disease conditions.[152,156–158] A key factor in addressing the unequivocal validation of the role of biased $CB_2R$ agonists, which would represent an unexplored approach for the treatment of serious pathologies, is the availability of truly selective and biased ligands. The comparative evaluation of the efficacy of the ligands discovered here in advanced pharmacological studies would greatly contribute to a deeper understanding of the true impact of $CB_2R$ biased signaling in various pathologies. Therefore, we firmly believe that the discovery of the compounds identified in this section holds significant value and utility within the drug discovery context. Some of the potential therapeutic applications of these G-protein biased agonists include:

Pain management: G-protein biased $CB_2R$ agonists can be used as analgesics for the treatment of chronic pain, including neuropathic pain and inflammatory pain. By selectively

USC DE COMPOSTELA

activating G-protein signaling pathways, these agonists can modulate pain perception and provide analgesic effects.[152,156–158]

Inflammation and autoimmune diseases: $CB_2Rs$ are predominantly expressed in immune cells, and G-protein biased agonists can target these receptors to modulate immune responses. They may have therapeutic applications in inflammatory conditions (e.g., rheumatoid arthritis, inflammatory bowel disease, multiple sclerosis), and other autoimmune diseases by reducing inflammation and immune cell activation.[152,156–158]

Neurological disorders: G-protein biased $CB_2R$ agonists have shown promise in preclinical studies for the treatment of neurodegenerative disorders (e.g., Alzheimer's, Parkinson's, and Huntington's diseases). These agonists can modulate neuroinflammation and provide neuroprotective effects.[152,156–158]

Cancer therapy: $CB_2Rs$ are expressed in certain cancer cells, and G-protein biased agonists can target these receptors to modulate tumor growth and progression. They may have potential applications in cancer therapy by inhibiting cell proliferation, inducing apoptosis, and reducing tumor angiogenesis.[94,98–101,152,156–158]

To further complement the signaling characterization study and gather additional evidence for upcoming pharmacological evaluations, we also assessed the selected ligands' performance within the MAPK/ERK downstream pathway. The MAPK, also referred to as MAPK/ERK (MAPK: mitogen-activated protein kinases, ERK: signaling regulated kinases), is a vital cellular signaling pathway responsible for regulating a multitude of cellular processes, including cell growth, proliferation, differentiation, and survival.[159,160] The pathway can be activated either by G-protein or β-arrestin signaling and in response to various extracellular signals, such as growth factors and cytokines, and leads to the activation of a cascade of kinases that ultimately phosphorylate and activate the extracellular signal regulated kinases (ERKs). ERKs then translocate to the nucleus and modulate the expression of genes involved in various cellular processes.[159,160] The pathway is responsible for transmitting signals from the cell surface to the nucleus, ultimately influencing multiple cellular functions and contributing to various physiological and pathological processes including inflammation, neurodegeneration, and cancer cell proliferation.[159,160]

The results of these experiments are presented in Table 3.29, and the corresponding dose-response curves are illustrated in Figure 3.113. As observed, all five tested $CB_2R$ selective agonists activate the MAPK/ERK signaling pathway, revealing potent activity (in the sub-

USC UNIVERSIDADE DE SANTIAGO DE COMPOSTELA

nanomolar range), and acting as full agonists ($E_{max}$ = 74-163%). The $EC_{50}$ obtained for these ligands and the significant role of the MAPK/ERK signaling pathway in inflammatory processes and different type of cancer, inspired us to preliminary evaluate compound **(2*R*)-178** in other biological assays.

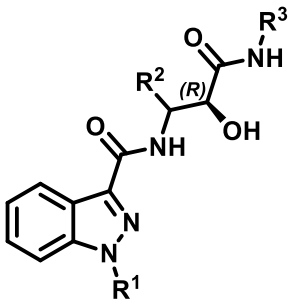



Table 3.29. Binding and functional data of selected $CB_2R$ ligands.

| Compounds and diversity explored | | | | Binding data | | $CB_2R$ Functional MAPK/ERK data | |
|---|---|---|---|---|---|---|---|
| | | | | $CB_1R$ | $CB_2R$ | | |
| Code | $R^1$ | $R^2$ | $R^3$ | % at 1 μM[a)] | $K_i$[b)] | $EC_{50}$[c)] | $E_{max}$[d)] |
| **(2*R*)-178** | 4-F-Bn | (*S*)-*t*-Bu | Bn | 25% | 6.50 nM | 0.07 nM | 87% |
| **(2*R*)-182** | $CH_2$-Cy | (*S*)-Et | $CH_2$-$CO_2$Me | 29% | 24.2 nM | 0.80 nM | 163% |
| **(2*R*)-183** | $CH_2$-Cy | (*S*)-Et | Bn | 13% | 39.1 nM | 0.12 nM | 113% |
| **(2*R*)-188** | $CH_2$-Cy | (*S*)-*i*-Pr | Bn | 12% | 17.1 nM | 0.74 nM | 74% |
| **(2*R*)-193** | $CH_2$-Cy | (*S*)-*t*-Bu | Bn | 17% | 5.70 nM | 0.32 nM | 102% |
| **JWH-133** | - | - | - | 677 nM | 3.40 nM | 2.69 nM | 99% |

[a)] Displacement of specific [$^3$H]-CP55940 binding in human CHO cells expressed as $K_i$ in nM (n = 3) or percentage displacement of specific binding at a concentration of 1 $\mu$M (n = 2). [b)] Displacement of specific [$^3$H]-CP55940 binding in human HEK-293 cells expressed as $K_i$ in nM (n = 3) or percentage displacement of specific binding at a concentration of 1 $\mu$M (n = 2). c) Functional activity assessed in transfected HEK-293T cells by determining cAMP levels after forskolin stimulation. d) $E_{max}$ values were normalized to a maximal efficacious concentration of CP 55,940.

USC UNIVERSIDADE DE SANTIAGO DE COMPOSTELA

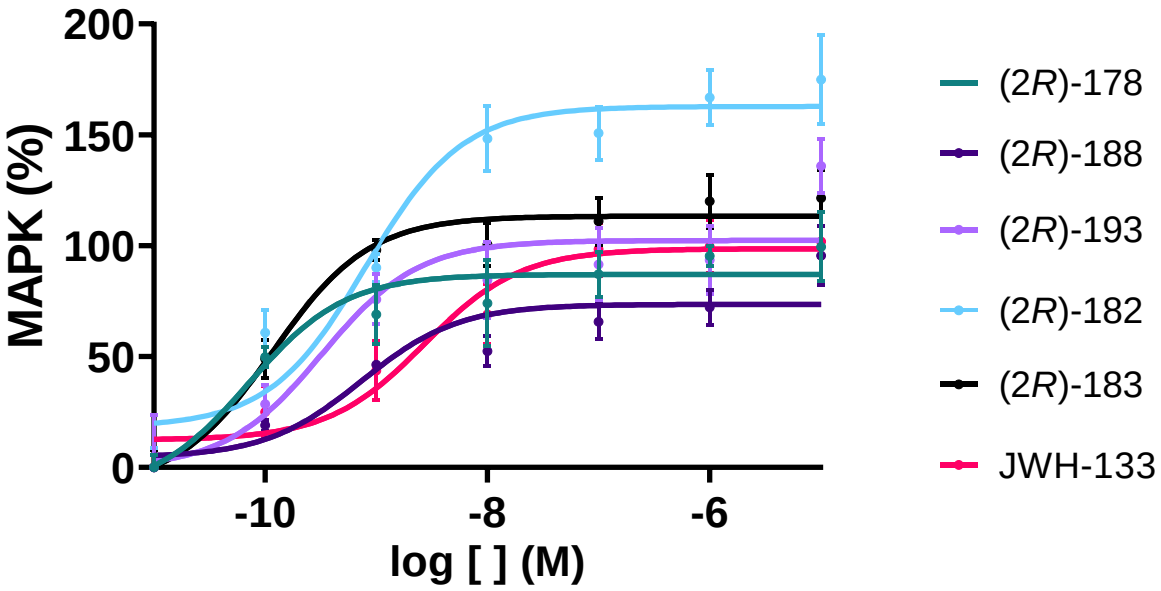



Figure 3.113. Dose-response curves obtained for reference ligand (JWH-133) and selected ligands at $CB_2R$ during cAMP functional assays.

USC
UNIVERSIDADE DE SANTIAGO DE COMPOSTELA

### 3.2.7 Biological assays: antiproliferative effect in the U87 glioblastoma cell line

Motivated by previous studies showcasing the *in vitro* effectiveness of two phytocannabinoids, namely $\Delta^9$-THC and CBD (a non-psychoactive phytocannabinoid), in a glioblastoma cell line,[104,161–163] we chose to utilize this cell line as a substrate for investigating the potential of two selected $CB_2R$ agonists in the context of cancer treatment. Glioblastoma is a tumor of the central nervous system known for its aggressiveness, reduced patient survival, and urgent need for new treatments. The studies were conducted in collaboration with the laboratory of Dr. Miguel Abal and Dr. Jorge Barbazán, from the Institute of Health Research of Santiago (IDIS). The antiproliferative activity of the compounds was assessed in the U87 glioblastoma cell line at three different concentrations (5, 10, and 20 μM).

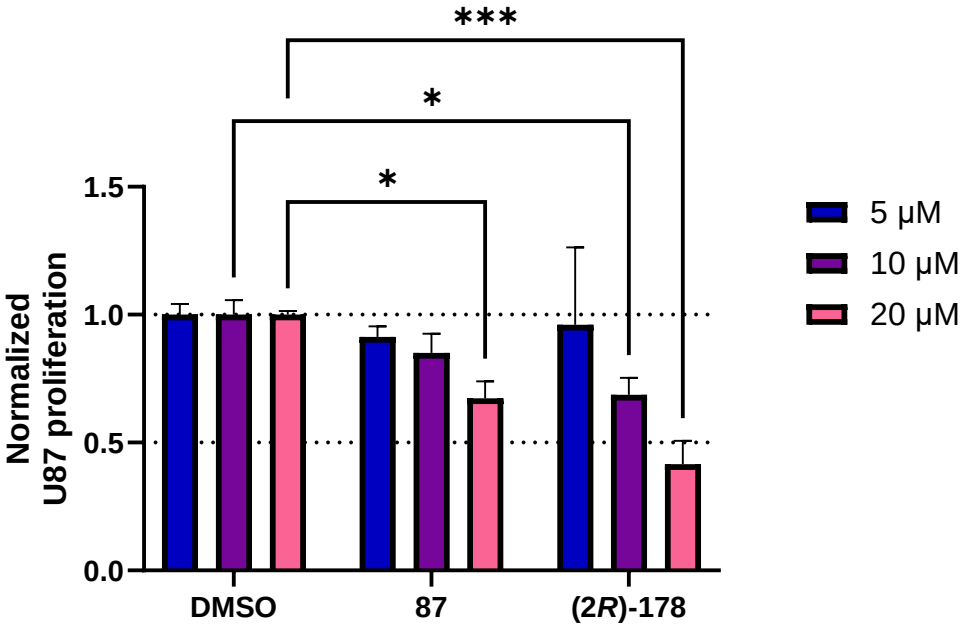



Figure 3.114. Bar chart representation of proliferation assay in U87 cell line. Cells were exposed to compounds for 48 h. Each bar represents the mean ± SEM of three experiments performed in duplicate. Two-Way ANOVA followed by Tukey post-hoc test was applied. Significance of symbols as follows: 1 symbol = p < 0.05; 2 symbols = p < 0.01; 3 symbols = p < 0.001; 4 symbols = p < 0.0001. Legend for symbols as follows: * indicates vs CTRL.

As illustrated in Figure 3.114, compounds **87** and **(2*R*)-178** demonstrated a significant reduction (approximately 30-60%) in the cell proliferation of the U87 glioblastoma cell line in a dose-dependent manner, particularly at 20 μM. Among these compounds, compound **(2*R*)-178** emerges as the most promising, showcasing a 58% reduction in glioblastoma proliferation at a concentration of 20 μM. To contextualize this data, the cytotoxic $IC_{50}$ of

USC UNIVERSIDADE DE SANTIAGO DE COMPOSTELA

Temozolomide, an orally administered chemotherapeutic agent routinely used in clinical practice,[102,106] is 864.1 ± 40.9 nM,[164] a concentration 400 times higher than the maximum concentration used in our assays. Although these findings are very preliminary, the observed inhibition of *in vitro* cell proliferation suggests that the selected $CB_2R$ agonists hold promise as candidates for further investigation in deep exploration and hit-to-lead programs. Furthermore, these results not only validate the crucial role of $CB_2R$ agonism in inhibiting cell proliferation in *in vitro* cancer models but also underscore the significance of the endocannabinoid system (ECS) in cancer treatment.

USC
UNIVERSIDADE DE SANTIAGO DE COMPOSTELA

# 4 CONCLUSIONS

USC
UNIVERSIDADE
DE SANTIAGO
DE COMPOSTELA

- The feasibility of employing multicomponent strategies for the synthesis of analogues of melanostatin has been established. A collection of 86 melanostatin analogues (Series **I**, Series **II**, and Series **III**) has been developed using an Ugi reaction-based synthetic method.
- The identification of the main salient features emerging from the structural-activity relationship (SAR) and the identification of allosteric modulators improving the effectiveness of melanostatin are documented.
- New proline bioisosteric surrogates that yield derivatives improving the effectiveness of melanostatin have been identified. Pentagonal cycles such as 4-pyrazole, 4-oxazole, or 1,2,3-triazole generally yield compounds acting as PAMs. Hexagonal substituted aromatic rings such as 3-trifluoromethylphenyl, 4-ethoxyphenyl, or 3,4-dimethoxyphenyl generally yield compounds acting as NAMs.
- A combination of NMR and circular dichroism techniques provided experimental support to the unambiguous structural characterization performed for diastereomers and enantiomers obtained in Series **I**, Series **II**, and Series **III**.
- Compound **34b**'s (*S*)-enantiomer showed improved pharmacological activity at 0.01 nM than the corresponding (*R*)-enantiomer, which indicates a preference for the (*S*) configuration at the isobutyl residue.
- Methylation of the secondary amide has proven to be an effective strategy for enhancing the activity of allosteric modulators, paving the way for further investigations in this regard.
- As observed by Professor Sampaio-Dias' group, alkylation of the terminal amide improves the PAM activity at low concentrations.
- The PADAM synthetic route has been successfully employed in the development of a collection of 24 melanostatin analogues. The resulting scaffold has shown a promising tendency to yield compounds that act as PAMs.
- A collection of 155 indole and indazole derivatives, which are Synthetic Cannabinoid Receptor Agonist (SCRA) analogues, has been prepared and pharmacologically characterized (binding and functional).
- The identification of the main salient features emerging from the structural-activity relationship (SAR) and the identification of several $CB_2R$ selective ligands are documented.

USC UNIVERSIDADE DE SANTIAGO DE COMPOSTELA

- A pharmacomodulation process enables the transformation of the promiscuous profile ($CB_1R$ and $CB_2R$) of SCRAs into selective $CB_2R$ drugs. Herein, we document a previously unexplored, efficient, and versatile PADAM-based approach that facilitates the rapid generation of novel $CB_2R$ selective ligands. The optimized strategy exemplifies the importance of discovering diverse and previously unexplored moieties in pharmacophoric models. For instance, introducing an additional carbon atom bearing a carbonyl group, and especially a hydroxy group, enables complete dissociation of the binding profile of these receptors ($CB_1R$ and $CB_2R$).
- The introduction of an additional carbon atom into the structure improves the pharmacological profile of the original SCRAs in two different ways, depending on the substituent attached to this carbon atom. Carboxamides exhibit higher affinity for $CB_2R$ without affecting affinity for $CB_1R$, thus yielding compounds that are more potent and selective than the original SCRAs. Hydroxyamides exhibit similar affinity at $CB_2R$ and considerably lower affinity for $CB_1R$, thus yielding compounds that are equally potent but remarkably more selective for $CB_2R$ than the original SCRAs.
- While the carboxamide series contributed numerous potent and selective $CB_2R$ ligands, the most significant achievement of this chapter lies in the hydroxyamide series, where high potency and complete selectivity for $CB_2R$ was attained.
- The study of the structure-activity relationship reveals clear trends of substitution for each pharmacophoric element. Indole, as the central core, provides the highest affinity at both receptors, while indole accounts for better selectivity towards $CB_1R$. Likewise, cyclohexyl methyl as tail group yields compounds more affine at both receptors, while 4-fluorobenzyl yields compounds with higher selectivity for $CB_2R$. Affinity at both receptors increases with the size of the linker ($R^2$), although affinity for $CB_2R$ increases more than affinity for $CB_1R$, maintaining the selectivity profile. Finally, the head group exhibits the highest variability in terms of tolerated substituents. In the carboxamide series (Series **VI**), *tert*-butyl and morpholinoethyl provide the best results, while benzyl is the best substituent for this position in the hydroxyamide series (Series **VII**).
- Binding data analysis reveals that (2*S*) diastereomers are more potent than the corresponding (2*R*) diastereomers at $CB_2R$ in the hydroxyamide series.

USC UNIVERSIDADE DE SANTIAGO DE COMPOSTELA

- Several new ligands combining remarkable affinity ($K_i$ < 100 nM) and exquisite selectivity (> 100-fold over $CB_1R$) were identified.
- Preliminary docking assays allowed a comprehensive understanding of the binding mode and SARs within the series.
- The agonist behavior of representative compounds was corroborated through functional cAMP experiments.
- A detailed study of the signaling pathways that these compounds affect (biased or unbiased) has been conducted. The pharmacological characterization of the new series of compounds enabled the identification of several agonist that elicit excellent $CB_2R$ selectivity and remarkable functional selectivity by the cAMP signaling pathway.
- Given the important role of $CB_2R$ agonists in the context of cancer therapy, two of our best ligands have been tested in a model tumor cell line to study their proliferative activity. It has been observed that our ligands significantly reduced cell proliferation of a glioblastoma (U87) cell line in a dose-dependent manner.
- Jointly, the herein documented results highlight the synthetic potential of multicomponent reactions to accelerate the discovery, optimization, and profiling of new prototypes in Medicinal Chemistry.

USC
UNIVERSIDADE DE SANTIAGO DE COMPOSTELA

# 5 EXPERIMENTAL SECTION

## 5.1 GENERAL CONSIDERATIONS

### 5.1.1 Synthesis and purification

Unless otherwise indicated, all starting materials, reagents and solvents were purchased and used without further purification. The Ugi and Passerini reactions were performed in coated Kimble vials on a PLS (6×4) Organic Synthesizer with orbital stirring. The reactions were monitored by thin-layer chromatography (TLC) on 2.5 mm Merck silica gel GF 254 strips, and the purified compounds each showed a single spot; unless stated otherwise, UV light, iodine vapor, phosphomolybdic acid and/or *p*-anisaldehyde were used to detect compounds. After extraction from aqueous phases, the organic solvents were dried over anhydrous magnesium or sodium sulfate. The purity and identity of all tested compounds were established by a combination of HPLC, mass spectrometry and NMR spectroscopy. Purification of isolated products was carried out by one of following methods: a) column chromatography (Kieselgel 0.040–0.063 mm, E. Merck), b) medium pressure liquid chromatography (MPLC) on a Combi Flash Companion (Teledyne ISCO) with RediSep pre-packed normal-phase silica gel (35–60 μm) columns, or c) preparative chromatography (Uniplate$^{TM}$ Techware 20x20 cm Silica G 1000mm Thick 15μm). The solvent mixtures used in the purification are shown in the sections "Spectroscopic and analytical data for all compounds described" and "Chiral HPLC separation of enantiomers and characterization of **34b**" separately, using the following abbreviations for the solvents: Hex, Hexane; AcOEt, ethyl acetate; MeOH, methanol; DCM, dichloromethane; IPA, *i*-propanol.

### 5.1.2 Structural characterization

Samples were dissolved in deuterated solvent ($CDCl_3$, DMSO-$d_6$ or MeOD) and the NMR spectra were recorded on Bruker AM300 and/or XM500 spectrometers. Chemical shifts are given as $\delta$ values against tetramethyl silane as internal standard and *J* values are given in Hz. The signal multiplicity shown with the abbreviatures s, singlet; d, doublet; t, triplet; q, quartet; p, pentuplet; hept, heptuplet; dd, doublet of doublets; dt, doublet of triplets; td, triplet

USC UNIVERSIDADE DE SANTIAGO DE COMPOSTELA

of doublets; bs, broad singlet; and m, multiplet, followed by number of protons (deduced by integration). The coupling constants (*J*) are deduced in Hertz (Hz). Low-resolution mass spectra (LRMS) were obtained on a Varian MAT-711 instrument (EI, 70 eV) or Agilent 8890 GC coupled to 5977B GC/MSD system (CI). High-resolution mass spectra (HRMS) were obtained on an Autospec Micromass spectrometer. For diastereomer differentiation experiments (Chapter I) CD spectra were recorded on a Jasco-815 system equipped with a Peltier-type thermostatic accessory (CDF-426S, Jasco). Measurements were carried out at 20 °C using a 1 mm quartz cell in a volume of 600 $\mu$L. Compounds (0.5 mg) were dissolved in MeOH (1.0 mL) and then diluted 10-fold in MeOH. The instrument settings were bandwidth, 1.0 nm; data pitch, 1.0 nm; speed, 500 nm/min; accumulation, 10; wavelengths, 300−190 nm. Analytical HPLC was performed on a Water Breeze™ 2 system (binary pump 1525, detector UV/Visible 2489, 7725i Manual Injector Kit 1500 Series) using a Luna 5 µm Silica (2) 100 Å, LC Column 150 x 4.6 mm column with gradient elution using the mobile phases hexane, isopropanol, and a flow rate of 1 ml/min. The structural and spectroscopic data obtained for all compounds described can be found in Spectroscopic and Analytical Data, in the section corresponding to each chapter.

Taking into consideration the quantity of compounds obtained within the framework of this Doctoral Thesis and following the general criteria accepted by the scientific community for the characterization of chemotheques, the general guidelines indicated below have been followed in the structural characterization of the compounds:

All the described compounds have been routinely characterized including:

$^{1}$H-NMR.

Mass spectrometry (LRMS).

Melting point (Mp).

In each series, representative compounds have been chosen for determination of (in addition to the characterization indicated in the previous section):

$^{13}$C-NMR.

HPLC.

High Resolution Mass Spectrometry (HRMS).

For the differentiation of the diastereomer pairs obtained in the same reaction, CD spectroscopy techniques have been used.

USC UNIVERSIDADE DE SANTIAGO DE COMPOSTELA

### 5.1.3 Pharmacological evaluation

#### 5.1.3.1 Allosteric modulation assays

Activity evaluation at human $D_2R$ assays were performed *in vitro* by the group of the Professor Maria I. Loza (University of Santiago de Compostela, Spain). The assay was carried out at human $D_2R$ expressed in CHO cells by measuring cAMP mobilization by means of HTRF measurements (Cisbio cAMP kit). 5000 cells/well were seeded in a 96-well black plate in stimB buffer provided in the kit in the presence of 500 µM IBMX. Then test compounds and dopamine were added and incubated for 10 min at 37 ºC. Last, 10 µM forskolin was incubated for 5 min. Then the kit reagents were added and incubated for 1 h at RT and HTRF signal was measured in a Tecan M1000 Pro multilabel reader. The compounds were evaluated at 0.01 nM and 1 nM over 0.1 µM dopamine. Data was converted to cAMP by employing a standard cAMP curve. A dopamine curve was included as positive control in all the assays. The activity of the compounds was expressed as the percentage of increase of the activity of 0.1 µM dopamine.

#### 5.1.3.2 Radioligand binding competition assays

Radioligand binding competition assays were performed *in vitro* by the group of the Professor Maria I. Loza (University of Santiago de Compostela, Spain) using human CBRs expressed in transfected Chinese hamster ovary (CHO, $CB_1R$), and Human embryonic kidney 293 (HEK-293, $CB_2R$) cells. Cannabinoid $CB_1R$ competition binding experiments were carried out in a polypropylene 96-well plate by incubating 5 µg of membranes from CHO-$CB_1R$ C3 cell line (protein concentration = 4402.88 µg/ml) with 1 nM [$^3$H]-CP55940 (108.5 Ci/mmol, 1 mCi/ml, Perkin Elmer NET1051250UC) and test compounds in binding buffer (50 mM Tris-HCl, 5 mM $MgCl_2$, 1 mM EDTA, 0.5 % BSA, pH:7,4). Non-specific binding was determined in the presence of Rimonabant 10 µM. The reaction mixture (Vt: 250 µl/well) was incubated at 30 °C for 60 min, then 200 µL were transferred to GF/C 96-well plate (Millipore, Madrid, Spain), filtered, and washed four times with 250 µl wash buffer (50 mM Tris-HCl, 5 mM $MgCl_2$, 1 mM EDTA, 0.5 % BSA, pH:7,4). Radioactivity was detected in a microplate beta scintillation counter (Microbeta Trilux, PerkinElmer, Madrid, Spain). Cannabinoid $CB_2R$ competition binding experiments were carried out in a polypropylene 96-well plate by incubating 5 µg of membranes from HEK-$CB_2R$ cell line (protein concentration= 4971.6 µg/ml) with 0.2 nM [$^3$H]-CP55940 (108.5 Ci/mmol, 1 mCi/ml, Perkin Elmer NET1051250UC) and test compounds in binding buffer (50 mM Tris-HCl, 5 mM

USC UNIVERSIDADE DE SANTIAGO

$MgCl_2$, 2.5 mM EGTA, 0.1 % BSA, pH: 7,4). Non-specific binding was determined in the presence of GW405833 10 µM (Sigma G1421). The reaction mixture (Vt: 250 µl/well) was incubated at 30 °C for 90 min, then 200 µL were transferred to GF/C 96-well plate (Millipore, Madrid, Spain), filtered, and washed four times with 250 µl wash buffer (50 mM Tris-HCl, 5 mM $MgCl_2$, 2.5 mM EGTA, 1 % BSA. pH: 7,4). Radioactivity was detected in a microplate beta scintillation counter (Microbeta Trilux, PerkinElmer, Madrid, Spain).

5.1.3.3 Functional assays

**cAMP Determination**. Signaling experiments have been performed as previously described.[165] Two hours before initiating the experiment, HEK-293T cell-culture medium was replaced by serum-starved DMEM medium. Then, cells were detached, resuspended in growing medium containing 50 mM zardaverine (Tocris, Bristol, UK) and placed in 384-well microplates (2,500 cells/well). Cells were pretreated (15 min) with cannabinoid compounds (1 nM to 100 µM) -or vehicle- before adding 0.5 mM forskolin (Tocris, Bristol, UK) to induce cAMP accumulation. Readings were performed after 15 min incubation at 25 ºC. Homogeneous Time Resolved Fluorescence (HTRF) energy transfer measures were performed using the Lance Ultra cAMP kit (PerkinElmer, Waltham, MA, United States). Fluorescence at 665 nm was analyzed in a PHERA star Flagship microplate reader equipped with an HTRF optical module (BMG Lab Technologies, Offenburg, Germany).

**β-Arrestin 2 Recruitment**. Arrestin recruitment was determined as previously described.[158] Briefly, BRET experiments were performed in HEK-293T cells 48 h after transfection with the cDNA corresponding to the $CB_2R$-YFP or $CB_1R$-YFP and 1 mg cDNA corresponding to β-arrestin 2-Rluc. Cells (20 mg protein) were distributed in 96-well microplates (Corning 3600, white plates with white bottom) and were incubated with CBG for 15 min and stimulated with the agonist for 10 min prior to the addition of 5 mM coelenterazine H (Molecular Probes, Eugene, OR, United States). After 1 min of adding coelenterazine H, BRET between β-arrestin 2-Rluc and receptor-YFP was determined and quantified. The readings were collected using a Mithras LB940 (Berthold Technologies, Bad Wildbad, Germany) that allows the integration of the signals detected in the short-wavelength filter at 485 nm and the long-wavelength filter at 530 nm. To quantify protein-RLuc expression luminescence readings were also performed 10 min of adding 5 mM coelenterazine H.

USC UNIVERSIDADE DE SANTIAGO DE COMPOSTELA

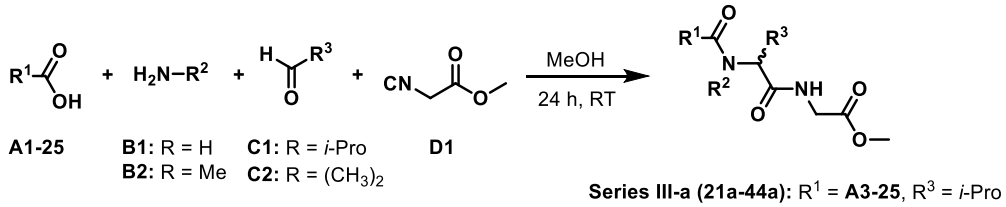
**ERK Phosphorylation Assays**. To determine ERK1/2 phosphorylation, 50,000 HEK-293T cells/well were plated in transparent Deltalab 96-well microplates and kept in the incubator for 24 h. 2 to 4 h before the experiment, the medium was substituted by serum-starved DMEM medium. Then, cells were treated at 25 ºC for 7 min with vehicle or cannabinoid compounds in serum starved DMEM medium. Cells were then washed twice with cold PBS before addition of lysis buffer (20 min treatment). 10 mL of each supernatant were placed in white ProxiPlate 384-well microplates and ERK1/2 phosphorylation was determined using AlphaScreen SureFire kit (Perkin Elmer) following the instructions of the supplier and using an EnSpire Multimode Plate Reader (PerkinElmer, Waltham, MA, United States).

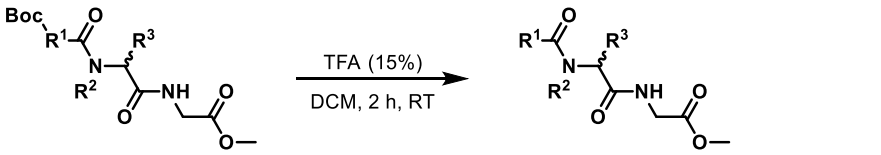
USC
UNIVERSIDADE DE SANTIAGO DE COMPOSTELA

## 5.2 CHAPTER I

### 5.2.1 Synthesis of melanostatin derivatives

**METHOD A.** General procedure for the synthesis of methyl (2-(arylcarboxamido)alkyl)glycinates (**Series I-a** to **III-a**)

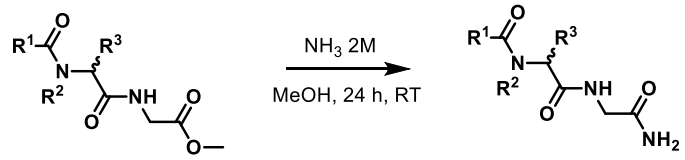



A mixture of the corresponding carboxylic acid (**A1-25**, 1 eq), amine (**B1-2**, 2 eq), aldehyde (**C1-2**, 1.2 eq) and methyl-2-isocyanoacetate **(D1**, 1.2 eq) in methanol (2 mL) was stirred with orbital stirring at room temperature for 24 h. After completion of the reaction, the solvent was evaporated under reduced pressure to afford an oil residue, which was purified by chromatography on silica gel using MeOH/DCM mixtures. In the case of carboxylic acids bearing a Boc protecting group (**A1**, **A2**, **A12**, **A14**), an additional step of hydrolysis was required. After completion of the Ugi reaction and evaporation of the solvent, the crude product was redissolved in DCM and TFA (15%) was added. The reaction was stirred for 2 h. Following completion, the solution was treated with NaOH 2M and the product was extracted with ethyl acetate. The organic phase was dried over $MgSO_4$ and evaporated under reduced pressure to afford an oil residue, which was purified by column chromatography on silica gel.

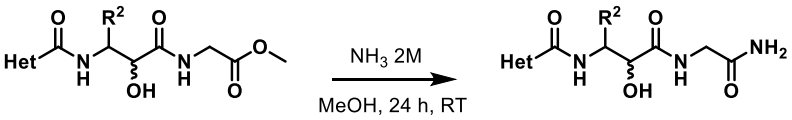
USC UNIVERSIDADE DE SANTIAGO DE COMPOSTELA

**METHOD B.** General procedure for the synthesis of *N*-(1-((2-amino-2-oxoethyl)amino)-1-oxoalkyl)arylcarboxamides (Series **I-b** to **V-b**).

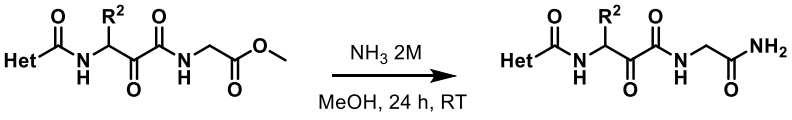



**Series I-a (1a-8a):** $R^1$ = **A1-2**, $R^3$ = *i*-Pro
**Series II-a (9a-16a):** $R^1$ = **A1-2**, $R^3$ = $(CH_3)_2$
**Series III-a (21a-44a):** $R^1$ = **A3-25**, $R^3$ = *i*-Pro

**Series I-b (1b-8b):** $R^1$ = **A1-2**, $R^3$ = *i*-Pro
**Series II-b (9b-16b):** $R^1$ = **A1-2**, $R^3$ = $(CH_3)_2$
**Series III-b (21b-44b):** $R^1$ = **A3-25**, $R^3$ = *i*-Pro




**Series IV-a (45a-50a)** **Series IV-b (45b-50b)**

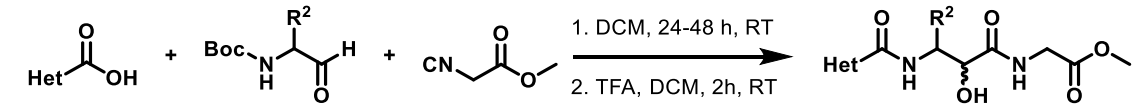



**Series V-a (51a-56a)** **Series V-b (51b-56b)**

The corresponding methylglycinate (**1a-56a**, 1 eq) was solved in a solution of $NH_3$ (2M in MeOH, 3 mL) and magnetically stirred overnight. After completion of the reaction, the solvent was evaporated under reduced pressure to afford a pure white solid without further purification.

USC UNIVERSIDADE DE SANTIAGO DE COMPOSTELA

**METHOD C.** General procedure for the synthesis of methyl (3-(furan-3-carboxamido)-2-hydroxy-5-methylhexanoyl)glycinates (Series **IV-a**).




**A1:** Het = Pro
**A4:** Het = 3-Fur
**A16:** Het = 2-Py

**C3:** R = (*S*)-*i*-Butyl
**C4:** R = (*R*)-*i*-Butyl

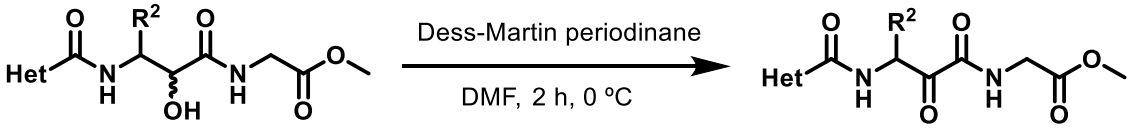
**D1**

**Series IV-a (41a-46a)**

A mixture of the corresponding carboxylic acid (**A1**, **A4**, **A16**, 1 eq), α-boc-amino-aldehyde (**C3-4**, 0.9 eq) and 2-methyl-isocyanoacetate (**D1**, 1.2 eq) in dichloromethane (2 mL) was stirred with orbital stirring at room temperature for 24-48 h. Upon completion, trifluoroacetic acid (45 eq) was added to the reaction pot and the mixture was stirred for an additional 2 h. The solution was treated with NaOH 2M and the product was extracted with ethyl acetate. The organic phase was dried over $MgSO_4$ and evaporated under reduced pressure to afford an oil residue, which was purified by chromatography on silica gel using MeOH/DCM mixtures.

USC UNIVERSIDADE DE SANTIAGO DE COMPOSTELA

**METHOD D.** General procedure for the synthesis of methyl (3-(furan-3-carboxamido)-2-hydroxy-5-methylhexanoyl)glycinates (Series **V-a**).




**Series IV-a (41a-46a)** **Series V-a (47a-52a)**

The corresponding hydroxyamide (**41a-46a**, 1 eq) was solved in DMF (3 mL) under inert atmosphere and, at 0 ºC, then Dess-Martin periodinane (1,5 eq) was added in portions. The reaction mixture was magnetically stirred for 2 h. After completion of the reaction, the solution was treated with $NaHCO_3$ sat. and $Na_2S_2O_3$ (15% aq.) and stirred for an additional 15 minutes. The product was extracted with ethyl acetate, and the organic phase was washed with water and brine. The organic phase was dried over $MgSO_4$ and evaporated under reduced pressure to afford an oil residue, which was purified by chromatography on silica gel using MeOH/DCM mixtures.

USC UNIVERSIDADE DE SANTIAGO DE COMPOSTELA

### 5.2.2 Spectroscopic and analytical data for all compounds described

**methyl L-prolyl-L-leucylglycinate (1a).** Purified by column chromatography (DCM/MeOH 97:3). Yield: 24%. Mp: 172 – 174 ºC. $^1$H NMR (300 MHz, $CDCl_3$) $\delta$ (ppm): 8.18 (d, $J$ = 8.4 Hz, 1H), 7.19 (s, 1H), 4.52 – 4.42 (m, 1H), 4.16 – 4.02 (m, 2H), 3.96 (dd, $J$ = 18.1, 5.0 Hz, 1H), 3.76 (s, 3H), 3.24 – 3.04 (m, 2H), 2.35 – 2.20 (m, 1H), 2.05 – 1.91 (m, 1H), 1.91 – 1.56 (m, 5H), 0.95 (dd, $J$ = 11.9, 6.1 Hz, 6H). LRMS (CI) *m/*z calcd for $C_{14}H_{26}N_3O_4$ $[M+H]^+$: 300.1; found: 300.3.

**(*S*)-*N*-((*S*)-1-((2-amino-2-oxoethyl)amino)-4-methyl-1-oxopentan-2-yl)pyrrolidine-2-carboxamide (1b).** Purified by column chromatography (DCM/MeOH 94:6). Yield: 98%. Mp: 211 – 212 ºC. $^1$H NMR (300 MHz, MeOD) $\delta$ (ppm): 4.27 – 4.19 (m, 1H), 3.95 – 3.66 (m, 2H), 3.39 – 3.31 (m, 1H), 3.05 – 2.95 (m, 2H), 2.19 – 2.05 (m, 1H), 1.84 – 1.70 (m, 4H), 1.65 – 1.50 (m, 2H), 0.90 (dd, $J$ = 13.5, 5.1 Hz, 6H). LRMS (CI) *m/*z calcd for $C_{13}H_{25}N_4O_3$ $[M+H]^+$: 285.1; found: 285.2.

**methyl L-prolyl-D-leucylglycinate (2a).** Purified by column chromatography (DCM/MeOH 97:3). Yield: 21%. Mp: 150 – 152 ºC. $^1$H NMR (300 MHz, $CDCl_3$) $\delta$ (ppm): 8.07 – 7.98 (m, 1H), 6.96 (s, 1H), 4.52 – 4.38 (m, 1H), 4.02 (d, $J$ = 5.4 Hz, 2H), 3.91 (dd, $J$ = 9.1, 5.3 Hz, 1H), 3.75 (s, 3H), 3.17 – 3.04 (m, 1H), 3.04 – 2.87 (m, 2H), 2.29 – 2.11 (m, 1H), 2.10 – 1.88 (m, 1H), 1.85 – 1.54 (m, 5H), 0.95 (dd, $J$ = 12.2, 6.1 Hz, 6H). LRMS (CI) *m/*z calcd for $C_{14}H_{26}N_3O_4$ $[M+H]^+$: 300.1; found: 300.3.

**(*S*)-*N*-((*R*)-1-((2-amino-2-oxoethyl)amino)-4-methyl-1-oxopentan-2-yl)pyrrolidine-2-carboxamide (2b).** Purified by column chromatography (DCM/MeOH 94:6). Yield: 99%. Mp: 175 – 177 ºC. $^1$H NMR (300 MHz, MeOD) $\delta$ (ppm): 4.27 – 4.20 (m, 1H), 4.00 – 3.64 (m, 2H), 3.47 – 3.39 (m, 1H), 3.16 – 3.08 (m, 2H), 2.36 – 2.15 (m, 1H), 1.99 – 1.80 (m, 4H), 1.67 – 1.53 (m, 2H), 0.92 (dd, $J$ = 11.7, 5.4 Hz, 6H). LRMS (CI) *m/*z calcd for $C_{13}H_{25}N_4O_3$ $[M+H]^+$: 285.1; found: 285.2.

**methyl *N*-(L-prolyl)-*N*-methyl-L-leucylglycinate (3a).** Purified by column chromatography (DCM/MeOH 97:3). Yield: 20%. Oil at room temperature. $^1$H NMR (300 MHz, $CDCl_3$) $\delta$ (ppm): 7.90 (s, 1H), 5.30 – 5.22 (m, 1H), 4.70 (s, 1H), 4.09 (dd, $J$ = 17.5, 6.4 Hz, 1H), 3.83 (dd, $J$ = 17.7, 5.3 Hz, 1H), 3.69 (s, 3H), 3.55 – 3.32 (m, 2H), 3.00 (s, 3H), 2.47 – 2.41 (m, 1H), 2.15 – 2.09 (m, 1H), 2.00 – 1.84 (m, 2H), 1.65 (t, $J$ = 13.0 Hz, 1H), 1.42 – 1.22 (m, 2H), 0.99 – 0.84 (m, 6H). LRMS (CI) *m/*z calcd for $C_{15}H_{28}N_3O_4$ $[M+H]^+$: 314.2; found: 314.2.

USC UNIVERSIDADE DE SANTIAGO DE COMPOSTELA

**(*S*)-*N*-((*S*)-1-((2-amino-2-oxoethyl)amino)-4-methyl-1-oxopentan-2-yl)-*N*-methylpyrrolidine-2-carboxamide (3b).** Purified by column chromatography (DCM/MeOH 94:6). Yield: 99%. Mp: 78 – 79 ºC. $^1$H NMR (300 MHz, $CDCl_3$) $\delta$ (ppm): 8.26 (s, 1H), 6.63 (s, 1H), 6.48 (s, 1H), 5.28 – 5.20 (m, 1H), 4.82 – 4.76 (m, 1H), 3.85 – 3.78 (m, 2H), 3.52 – 3.37 (m, 2H), 2.99 (s, 3H), 2.55 – 2.37 (m, 1H), 2.15 – 1.98 (m, 2H), 1.91 – 1.79 (m, 2H), 1.73 – 1.60 (m, 1H), 1.43 – 1.30 (m, 1H), 1.04 – 0.80 (m, 6H). LRMS (CI) *m/*z calcd for $C_{14}H_{27}N_4O_3$ $[M+H]^+$: 299.2; found: 299.5.

**methyl *N*-(L-prolyl)-*N*-methyl-D-leucylglycinate (4a).** Purified by column chromatography (DCM/MeOH 97:3). Yield: 5%. Oil at room temperature. $^1$H NMR (300 MHz, $CDCl_3$) $\delta$ (ppm): 7.20 (bs, 1H), 5.12 – 5.02 (m, 1H), 4.65 – 4.49 (m, 1H), 4.20 – 3.75 (m, 2H), 3.71 (s, 3H), 3.43 – 3.28 (m, 2H), 2.98 (d, $J$ = 23.6 Hz, 3H), 2.50 – 2.37 (m, 1H), 2.12 – 1.90 (m, 3H), 1.78 – 1.61 (m, 2H), 1.55 – 1.39 (m, 1H), 1.04 – 0.82 (m, 6H). LRMS (CI) *m/*z calcd for $C_{15}H_{28}N_3O_4$ $[M+H]^+$: 314.2; found: 314.2.

**(*S*)-*N*-((*R*)-1-((2-amino-2-oxoethyl)amino)-4-methyl-1-oxopentan-2-yl)-*N*-methylpyrrolidine-2-carboxamide (4b).** Purified by column chromatography (DCM/MeOH 94:6). Yield: 99%. Mp: 91 – 93 ºC. $^1$H NMR (300 MHz, $CDCl_3$) $\delta$ (ppm): 7.71 – 7.57 (m, 1H), 6.34 (s, 1H), 5.98 (s, 1H), 5.25 – 5.11 (m, 1H), 4.81 – 4.66 (m, 1H), 4.24 – 4.08 (m, 1H), 3.76 – 3.57 (m, 1H), 3.49 – 3.38 (m, 2H), 3.14 (s, 3H), 2.57 – 2.41 (m, 2H), 2.26 – 2.02 (m, 3H), 1.90 – 1.79 (m, 1H), 1.67 – 1.30 (m, 1H), 1.04 – 0.93 (m, 6H). LRMS (CI) *m/*z calcd for $C_{14}H_{27}N_4O_3$ $[M+H]^+$: 299.2; found: 299.5.

**methyl ((*S*)-piperidine-2-carbonyl)-L-leucylglycinate (5a).** Purified by column chromatography (DCM/MeOH 97:3). Yield: 13%. Mp: 107 – 108 ºC. $^1$H NMR (300 MHz, $CDCl_3$) $\delta$ (ppm): 8.17 (d, $J$ = 7.8 Hz, 1H), 7.58 (bs, 1H), 4.55 – 4.40 (m, 1H), 4.06 – 3.88 (m, 2H), 3.79 (d, $J$ = 10.7 Hz, 1H), 3.71 (s, 3H), 3.34 (d, $J$ = 12.6 Hz, 1H), 2.93 (bs, 1H), 2.14 – 2.05 (m, 1H), 1.92 – 1.81 (m, 1H), 1.81 – 1.43 (m, 7H), 0.91 (dd, $J$ = 10.9, 4.9 Hz, 6H). LRMS (CI) *m/*z calcd for $C_{15}H_{28}N_3O_4$ $[M+H]^+$: 314.2; found: 314.2.

**(*S*)-*N*-((*S*)-1-((2-amino-2-oxoethyl)amino)-4-methyl-1-oxopentan-2-yl)piperidine-2-carboxamide (5b).** Purified by column chromatography (DCM/MeOH 94:6). Yield: 99%. Mp: 90 – 91 ºC. $^1$H NMR (300 MHz, MeOD) $\delta$ (ppm): 4.18 – 4.09 (m, 1H), 3.86 (d, $J$ = 17.4 Hz, 1H), 3.59 (d, $J$ = 17.1 Hz, 1H), 3.30 – 3.11 (m, 2H), 2.99 (d, $J$ = 12.2 Hz, 1H), 2.65 – 2.50 (m, 1H), 1.89 – 1.62 (m, 1H), 1.61 – 1.42 (m, 5H), 1.42 – 1.23 (m, 2H), 0.82 (dd, $J$ = 12.5, 5.1 Hz, 6H). LRMS (CI) *m/*z calcd for $C_{14}H_{27}N_4O_3$ $[M+H]^+$: 299.2; found: 299.3.

USC DE SANTIAGO DE COMPOSTELA

**methyl ((*S*)-piperidine-2-carbonyl)-D-leucylglycinate (6a).** Purified by column chromatography (DCM/MeOH 97:3). Yield: 8%. Mp: 147 – 149 ºC. $^1$H NMR (300 MHz, $CDCl_3$) $\delta$ (ppm): 7.94 – 7.83 (m, 1H), 7.57 – 7.46 (m, 1H), 4.51 – 4.38 (m, 1H), 4.22 – 4.11 (m, 1H), 4.02 – 3.92 (m, 2H), 3.72 (s, 3H), 3.50 – 3.39 (m, 1H), 3.30 (d, *J* = 12.8 Hz, 1H), 2.04 – 2.01 (m, 1H), 1.93 – 1.80 (m, 1H), 1.80 – 1.46 (m, 7H), 0.92 (dd, *J* = 14.2, 6.1 Hz, 6H). LRMS (CI) *m/*z calcd for $C_{15}H_{28}N_3O_4$ $[M+H]^+$: 314.2; found: 314.2.

**(*S*)-*N*-((*R*)-1-((2-amino-2-oxoethyl)amino)-4-methyl-1-oxopentan-2-yl)piperidine-2-carboxamide (6b).** Purified by column chromatography (DCM/MeOH 94:6). Yield: 98%. Mp: 84 – 85 ºC. $^1$H NMR (300 MHz, MeOD) $\delta$ (ppm): 4.28 – 4.20 (m, 1H), 3.92 – 3.66 (m, 2H), 3.29 – 3.26 (m, 1H), 3.10 (d, *J* = 13.0 Hz, 1H), 2.66 (t, *J* = 11.7 Hz, 1H), 1.90 – 1.82 (m, 2H), 1.72 – 1.37 (m, 7H), 0.90 (dd, *J* = 14.1, 5.3 Hz, 6H). LRMS (CI) *m/*z calcd for $C_{14}H_{27}N_4O_3$ $[M+H]^+$: 299.2; found: 299.3.

**methyl *N*-methyl-*N*-((*S*)-piperidine-2-carbonyl)-L-leucylglycinate (7a).** Purified by column chromatography (DCM/MeOH 97:3). Yield: 18%. Oil at room temperature. $^1$H NMR (300 MHz, $CDCl_3$) $\delta$ (ppm): 7.94 (s, 1H), 5.27 (dd, *J* = 10.7, 4.7 Hz, 1H), 4.11 – 3.79 (m, 4H), 3.69 (s, 3H), 3.55 (d, *J* = 12.9 Hz, 1H), 2.97 (s, 3H), 2.04 – 1.47 (m, 7H), 1.42 – 1.17 (m, 2H), 0.90 (dd, *J* = 18.8, 6.6 Hz, 6H). $^{13}$C NMR (75 MHz, $CDCl_3$), δ (ppm): 171.7, 170.6, 56.8, 55.0, 52.0, 44.3, 40.9, 36.0, 30.6, 26.9, 24.9, 23.3, 23.1, 22.9, 21.4. LRMS (CI) *m/*z calcd for $C_{16}H_{30}N_3O_4$ $[M+H]^+$: 328.2; found: 328.4.

**(*S*)-*N*-((*S*)-1-((2-amino-2-oxoethyl)amino)-4-methyl-1-oxopentan-2-yl)-*N*-methylpiperidine-2-carboxamide (7b).** Purified by column chromatography (DCM/MeOH 94:6). Yield: 99%. Mp: 158 – 160 ºC. $^1$H NMR (300 MHz, MeOD) $\delta$ (ppm): 7.51 (s, 1H), 6.55 (s, 1H), 6.44 (s, 1H), 5.16 (dd, *J* = 10.6, 5.1 Hz, 1H), 3.96 (dd, *J* = 16.4, 6.2 Hz, 1H), 3.85 (d, *J* = 10.8 Hz, 1H), 3.76 (dd, *J* = 16.4, 5.6 Hz, 1H), 3.22 (d, *J* = 13.6 Hz, 1H), 3.12 (s, 1H), 2.97 (s, 3H), 2.73 (t, *J* = 12.5 Hz, 1H), 1.98 – 1.32 (m, 8H), 0.94 (d, *J* = 6.6 Hz, 3H), 0.87 (d, *J* = 6.5 Hz, 3H). LRMS (CI) *m/*z calcd for $C_{15}H_{29}N_4O_3$ $[M+H]^+$: 313.2; found: 313.2.

USC UNIVERSIDADE DE SANTIAGO DE COMPOSTELA

**methyl *N*-methyl-*N*-((*S*)-piperidine-2-carbonyl)-D-leucylglycinate (8a).** Purified by column chromatography (DCM/MeOH 97:3). Yield: 17%. Oil at room temperature. $^{1}$H NMR (300 MHz, $CDCl_3$) $\delta$ (ppm): 9.02 (bs, 1H), 7.24 – 7.19 (m, 1H), 4.93 (t, *J* = 7.7 Hz, 1H), 4.35 (t, *J* = 7.2 Hz, 1H), 4.19 – 3.88 (m, 2H), 3.80 (dd, *J* = 17.8, 4.9 Hz, 1H), 3.70 (s, 3H), 3.53 (d, *J* = 14.1 Hz, 2H), 3.02 (s, 2H), 2.85 (s, 1H), 2.25 – 2.11 (m, 0H), 2.10 – 1.68 (m, 6H), 1.66 – 1.47 (m, 1H), 1.40 – 1.22 (m, 1H), 0.97 – 0.89 (m, 6H). LRMS (CI) *m/*z calcd for $C_{16}H_{30}N_3O_4$ $[M+H]^+$: 328.2; found: 328.4.

**(*S*)-*N*-((*R*)-1-((2-amino-2-oxoethyl)amino)-4-methyl-1-oxopentan-2-yl)-*N*-methylpiperidine-2-carboxamide (8b).** Purified by column chromatography (DCM/MeOH 94:6). Yield: 99%. Mp: 81 – 82 ºC. $^{1}$H NMR (300 MHz, MeOD) $\delta$ (ppm): 9.54 (bs, 1H), 7.09 (s, 1H), 6.43 (s, 1H), 4.58 (t, *J* = 7.4 Hz, 1H), 4.31 – 4.20 (m, 1H), 3.88 (d, *J* = 5.3 Hz, 1H), 3.68 (d, *J* = 10.8 Hz, 1H), 3.55 – 3.41 (m, 1H), 3.13 (s, 2H), 2.76 (s, 1H), 2.73 – 2.59 (m, 1H), 2.05 – 1.68 (m, 6H), 1.67 – 1.43 (m, 2H), 1.42 – 1.22 (m, 1H), 0.98 – 0.90 (m, 6H). LRMS (CI) *m/*z calcd for $C_{15}H_{29}N_4O_3$ $[M+H]^+$: 313.2; found: 313.2.

**methyl L-prolyl-L-valylglycinate (9a).** Purified by column chromatography (DCM/MeOH 97:3). Yield: 8%. Oil at room temperature. $^{1}$H NMR (300 MHz, $CDCl_3$) $\delta$ (ppm): 8.19 (d, *J* = 9.1 Hz, 1H), 7.29 (s, 1H), 4.31 – 4.19 (m, 1H), 4.11 – 3.90 (m, 2H), 3.75 – 3.68 (m, 3H), 3.68 – 3.59 (m, 2H), 3.17 – 2.87 (m, 2H), 2.28 – 2.10 (m, 2H), 1.97 – 1.84 (m, 1H), 1.84 – 1.68 (m, 2H), 1.02 – 0.86 (m, 6H). $^{13}$C NMR (75 MHz, $CDCl_3$), δ (ppm): 171.8, 171.5, 169.4, 59.6, 59.1, 52.4, 46.6, 40.9, 31.2, 30.6, 24.5, 19.0, 18.0. LRMS (CI) *m/*z calcd for $C_{13}H_{24}N_3O_4$ $[M+H]^+$: 286.1; found: 286.2.

**(*S*)-*N*-((*S*)-1-((2-amino-2-oxoethyl)amino)-3-methyl-1-oxobutan-2-yl)pyrrolidine-2-carboxamide (9b).** Purified by column chromatography (DCM/MeOH 94:6). Yield: 99%. Oil at room temperature. $^{1}$H NMR (300 MHz, MeOD) $\delta$ (ppm): 4.16 (d, *J* = 6.9 Hz, 1H), 3.99 – 3.89 (m, 2H), 3.80 (d, *J* = 16.9 Hz, 1H), 3.36 – 3.29 (m, 1H), 3.20 – 3.00 (m, 2H), 2.35 – 2.19 (m, 1H), 2.19 – 2.07 (m, 1H), 2.04 – 1.70 (m, 3H), 1.07 – 0.96 (m, 6H). $^{13}$C NMR (75 MHz, MeOD), δ (ppm): 172.6, 172.5, 60.0, 59.3, 46.6, 46.5, 41.6, 30.7, 30.5, 30.3, 25.1, 18.3, 17.2. LRMS (CI) *m/*z calcd for $C_{12}H_{23}N_4O_3$ $[M+H]^+$: 271.1; found: 271.1.

USC UNIVERSIDADE DE SANTIAGO DE COMPOSTELA

**methyl L-prolyl-D-valylglycinate (10a).** Purified by column chromatography (DCM/MeOH 97:3). Yield: 12%. Oil at room temperature. $^{1}$H NMR (300 MHz, $CDCl_3$) $\delta$ (ppm): 8.17 (d, $J$ = 9.3 Hz, 1H), 7.23 – 7.13 (m, 1H), 4.28 – 4.17 (m, 1H), 4.09 – 3.87 (m, 2H), 3.76 – 3.65 (m, 5H), 3.04 – 2.83 (m, 2H), 2.23 – 2.01 (m, 1H), 1.93 – 1.80 (m, 1H), 1.79 – 1.61 (m, 3H), 1.01 – 0.84 (m, 6H). $^{13}$C NMR (75 MHz, $CDCl_3$), δ (ppm): 176.0, 174.3, 172.7, 63.9, 63.2, 56.0, 50.3, 44.7, 34.2, 33.9, 28.0, 22.7, 22.0. LRMS (CI) *m/*z calcd for $C_{13}H_{24}N_3O_4$ $[M+H]^+$: 286.1; found: 286.2.

**(*S*)-*N*-((*R*)-1-((2-amino-2-oxoethyl)amino)-3-methyl-1-oxobutan-2-yl)pyrrolidine-2-carboxamide (10b).** Purified by column chromatography (DCM/MeOH 94:6). Yield: 99%. Oil at room temperature. $^{1}$H NMR (300 MHz, MeOD) $\delta$ (ppm): 4.13 (d, $J$ = 6.8 Hz, 1H), 3.93 (d, $J$ = 17.0 Hz, 1H), 3.79 (d, $J$ = 17.2 Hz, 1H), 3.76 – 3.72 (m, 1H), 3.35 – 3.30 (m, 1H), 2.98 (t, $J$ = 6.4 Hz, 2H), 2.22 – 2.06 (m, 2H), 1.89 – 1.69 (m, 3H), 1.08 – 0.92 (m, 6H). $^{13}$C NMR (75 MHz, MeOD), δ (ppm): 176.3, 172.7, 60.1, 59.0, 46.8, 46.7, 41.7, 30.6, 30.4, 25.7, 19.7, 18.3, 17.2. LRMS (CI) *m/*z calcd for $C_{12}H_{25}N_4O_3$ $[M+H]^+$: 271.1; found: 271.1.

**methyl *N*-(L-prolyl)-*N*-methyl-L-valylglycinate (11a).** Purified by column chromatography (DCM/MeOH 97:3). Yield: 11%. Oil at room temperature. $^{1}$H NMR (300 MHz, $CDCl_3$) $\delta$ (ppm): 7.15 – 7.03 (m, 1H), 4.60 (d, $J$ = 11.1 Hz, 1H), 4.00 – 3.79 (m, 3H), 3.65 (s, 3H), 3.16 – 3.05 (m, 1H), 2.93 (s, 3H), 2.83 – 2.70 (m, 2H), 2.33 – 2.19 (m, 1H), 2.18 – 2.05 (m, 1H), 1.83 – 1.50 (m, 3H), 0.92 (d, $J$ = 6.5 Hz, 3H), 0.77 (d, $J$ = 6.7 Hz, 3H). $^{13}$C NMR (75 MHz, $CDCl_3$), δ (ppm): 175.8, 170.3, 170.0, 62.4, 58.6, 52.1, 47.4, 40.8, 30.5, 30.2, 26.4, 25.8, 19.6, 18.3. LRMS (CI) *m/*z calcd for $C_{14}H_{26}N_3O_4$ $[M+H]^+$: 300.1; found: 300.3.

**(*S*)-*N*-((*S*)-1-((2-amino-2-oxoethyl)amino)-3-methyl-1-oxobutan-2-yl)-*N*-methylpyrrolidine-2-carboxamide (11b).** Purified by column chromatography (DCM/MeOH 94:6). Yield: 99%. Oil at room temperature. $^{1}$H NMR (300 MHz, MeOD) $\delta$ (ppm): 4.65 (d, $J$ = 10.9 Hz, 1H), 4.03 (q, $J$ = 8.1, 7.5 Hz, 1H), 3.88 (d, $J$ = 9.9 Hz, 1H), 3.14 (dt, $J$ = 11.6, 6.2 Hz, 1H), 3.06 (s, 3H), 2.89 – 2.75 (m, 2H), 2.37 – 2.19 (m, 2H), 1.94 – 1.59 (m, 3H), 0.99 (d, $J$ = 6.4 Hz, 3H), 0.85 (d, $J$ = 6.6 Hz, 3H). LRMS (CI) *m/*z calcd for $C_{13}H_{25}N_4O_3$ $[M+H]^+$: 285.1; found: 285.4.

USC UNIVERSIDADE DE SANTIAGO DE COMPOSTELA

**methyl *N*-(L-prolyl)-*N*-methyl-D-valylglycinate (12a).** Purified by column chromatography (DCM/MeOH 97:3). Yield: 9%. Oil at room temperature. $^{1}$H NMR (300 MHz, $CDCl_3$) $\delta$ (ppm): 6.92 – 6.75 (m, 1H), 4.56 (d, *J* = 11.1 Hz, 1H), 4.15 – 3.71 (m, 3H), 3.65 (s, 3H), 3.19 – 3.08 (m, 1H), 2.92 (s, 3H), 2.81 – 2.69 (m, 2H), 2.42 – 2.17 (m, 1H), 2.16 – 1.97 (m, 1H), 1.93 – 1.56 (m, 3H), 0.92 (d, *J* = 6.4 Hz, 3H), 0.78 (d, *J* = 6.7 Hz, 3H). $^{13}$C NMR (75 MHz, $CDCl_3$), δ (ppm): 175.9, 170.3, 169.9, 62.7, 58.7, 52.1, 47.9, 40.7, 30.3, 30.0, 26.6, 25.3, 19.5, 18.5. LRMS (CI) *m/*z calcd for $C_{14}H_{26}N_3O_4$ $[M+H]^+$: 300.1; found: 300.3.

**(*S*)-*N*-((*R*)-1-((2-amino-2-oxoethyl)amino)-3-methyl-1-oxobutan-2-yl)-*N*-methylpyrrolidine-2-carboxamide (12b).** Purified by column chromatography (DCM/MeOH 94:6). Yield: 99%. Oil at room temperature. $^{1}$H NMR (300 MHz, MeOD) $\delta$ (ppm): 4.61 (d, *J* = 11.0 Hz, 1H), 3.92 (d, *J* = 16.7 Hz, 1H), 3.73 (d, *J* = 16.9 Hz, 1H), 3.23 – 3.10 (m, 1H), 3.05 (s, 3H), 2.96 – 2.70 (m, 2H), 2.39 – 2.13 (m, 2H), 1.93 – 1.62 (m, 3H), 1.01 (dd, *J* = 13.3, 6.4 Hz, 3H), 0.88 (dd, *J* = 12.3, 6.6 Hz, 3H). $^{13}$C NMR (75 MHz, MeOD), δ (ppm): 170.9, 170.4, 169.9, 63.0, 58.9, 46.1, 41.2, 29.9, 28.6, 26.2, 23.9, 18.4, 17.5. LRMS (CI) *m/*z calcd for $C_{13}H_{25}N_4O_3$ $[M+H]^+$: 285.1; found: 285.4.

**methyl ((*S*)-piperidine-2-carbonyl)-L-valylglycinate (13a).** Purified by column chromatography (DCM/MeOH 97:3). Yield: 12%. Mp: 170 – 171 ºC. $^{1}$H NMR (300 MHz, $CDCl_3$) $\delta$ (ppm): 7.31 (d, *J* = 9.0 Hz, 1H), 6.57 (s, 1H), 4.28 – 4.19 (m, 1H), 4.12 – 3.92 (m, 2H), 3.75 (s, 3H), 3.32 – 3.24 (m, 1H), 3.06 (d, *J* = 12.2 Hz, 1H), 2.69 (t, *J* = 10.5 Hz, 1H), 2.29 – 2.15 (m, 1H), 2.01 – 1.91 (m, 1H), 1.84 – 1.72 (m, 2H), 1.63 – 1.36 (m, 3H), 0.96 (t, *J* = 7.1 Hz, 6H). $^{13}$C NMR (75 MHz, $CDCl_3$), δ (ppm): 174.5, 170.6, 170.1, 60.0, 58.2, 45.7, 41.1, 30.2, 29.8, 26.0, 23.9, 19.4, 18.1. LRMS (CI) *m/*z calcd for $C_{14}H_{26}N_3O_4$ $[M+H]^+$: 300.1; found: 300.2.

**(*S*)-*N*-((*S*)-1-((2-amino-2-oxoethyl)amino)-3-methyl-1-oxobutan-2-yl)piperidine-2-carboxamide (13b).** Purified by column chromatography (DCM/MeOH 94:6). Yield: 99%. Mp: 141 – 142 ºC. $^{1}$H NMR (300 MHz, MeOD) $\delta$ (ppm): 4.13 (dd, *J* = 6.9, 0.7 Hz, 1H), 3.92 (dd, *J* = 17.0, 0.7 Hz, 1H), 3.79 (dd, *J* = 16.9, 0.7 Hz, 1H), 3.16 – 3.05 (m, 2H), 2.75 – 2.61 (m, 1H), 2.27 – 2.06 (m, 1H), 1.96 – 1.85 (m, 2H), 1.68 – 1.42 (m, 4H), 0.99 (d, *J* = 6.9 Hz, 6H). LRMS (CI) *m/*z calcd for $C_{13}H_{25}N_4O_3$ $[M+H]^+$: 285.1; found: 285.1.

USC UNIVERSIDADE DE SANTIAGO DE COMPOSTELA

**methyl ((*S*)-piperidine-2-carbonyl)-D-valylglycinate (14a).** Purified by column chromatography (DCM/MeOH 97:3). Yield: 15%. Mp: 167 – 168 ºC. $^{1}$H NMR (300 MHz, $CDCl_3$) $\delta$ (ppm): 7.35 (d, $J$ = 9.0 Hz, 1H), 6.57 (s, 1H), 4.29 – 4.20 (m, 1H), 4.02 (t, $J$ = 5.3 Hz, 2H), 3.74 (s, 3H), 3.30 – 3.20 (m, 1H), 3.08 – 2.96 (m, 1H), 2.75 – 2.62 (m, 1H), 2.27 – 2.13 (m, 1H), 1.94 (s, 1H), 1.81 – 1.37 (m, 5H), 0.97 (t, $J$ = 6.8 Hz, 6H). $^{13}$C NMR (75 MHz, $CDCl_3$), δ (ppm): 173.0, 171.5, 170.0, 60.2, 58.0, 45.6, 41.1, 30.4, 30.2, 25.9, 24.0, 19.4, 18.1. LRMS (CI) *m/*z calcd for $C_{14}H_{26}N_3O_4$ $[M+H]^+$: 300.1; found: 300.2.

**(*S*)-*N*-((*R*)-1-((2-amino-2-oxoethyl)amino)-3-methyl-1-oxobutan-2-yl)piperidine-2-carboxamide (14b).** Purified by column chromatography (DCM/MeOH 94:6). Yield: 99%. Mp: 171 – 172 ºC. $^{1}$H NMR (300 MHz, MeOD) $\delta$ (ppm): 4.14 – 4.09 (m, 1H), 3.94 (dd, $J$ = 17.0, 0.7 Hz, 1H), 3.77 (dd, $J$ = 17.0, 0.7 Hz, 1H), 3.14 – 3.03 (m, 2H), 2.73 – 2.62 (m, 1H), 2.19 – 2.05 (m, 1H), 1.97 – 1.81 (m, 2H), 1.68 – 1.38 (m, 4H), 1.03 – 0.99 (m, 6H). LRMS (CI) *m/*z calcd for $C_{13}H_{25}N_4O_3$ $[M+H]^+$: 285.1; found: 285.1.

**methyl *N*-methyl-*N*-((*S*)-piperidine-2-carbonyl)-L-valylglycinate (15a).** Purified by column chromatography (DCM/MeOH 97:3). Yield: 20%. Mp: 123 – 124 ºC. $^{1}$H NMR (300 MHz, $CDCl_3$) $\delta$ (ppm): 6.90 – 6.77 (m, 1H), 4.63 (d, $J$ = 11.1 Hz, 1H), 3.90 (d, $J$ = 5.9 Hz, 2H), 3.68 (s, 3H), 3.61 (dd, $J$ = 10.9, 2.7 Hz, 1H), 3.18 – 3.08 (m, 1H), 2.95 (s, 3H), 2.69 – 2.56 (m, 1H), 2.27 (dt, $J$ = 11.2, 6.4 Hz, 1H), 2.14 (s, 1H), 1.88 (d, $J$ = 12.0 Hz, 1H), 1.78 – 1.68 (m, 1H), 1.60 – 1.28 (m, 4H), 0.95 (d, $J$ = 6.4 Hz, 3H), 0.77 (d, $J$ = 6.7 Hz, 3H). $^{13}$C NMR (75 MHz, $CDCl_3$), δ (ppm): 175.3, 170.3, 170.1, 61.9, 56.8, 52.1, 45.6, 40.8, 30.4, 30.0, 26.6, 25.6, 24.5, 19.7, 18.3. LRMS (CI) *m/*z calcd for $C_{15}H_{28}N_3O_4$ $[M+H]^+$: 314.2; found: 314.3.

**(*S*)-*N*-((*S*)-1-((2-amino-2-oxoethyl)amino)-3-methyl-1-oxobutan-2-yl)-*N*-methylpiperidine-2-carboxamide (15b).** Purified by column chromatography (DCM/MeOH 94:6). Yield: 99%. Oil at room temperature. $^{1}$H NMR (300 MHz, MeOD) $\delta$ (ppm): 4.66 (d, $J$ = 10.9 Hz, 1H), 3.83 – 3.68 (m, 2H), 3.15 – 3.07 (m, 1H), 3.05 (s, 3H), 2.73 – 2.60 (m, 2H), 2.35 – 2.19 (m, 1H), 1.97 – 1.80 (m, 2H), 1.69 – 1.26 (m, 4H), 0.98 (d, $J$ = 6.4 Hz, 3H), 0.83 (d, $J$ = 6.8 Hz, 3H). $^{13}$C NMR (75 MHz, MeOD), δ (ppm): 178.7, 176.4, 175.0, 66.1, 60.1, 48.7, 45.5, 33.8, 33.1, 30.1, 29.5, 27.6, 22.6, 21.5. LRMS (CI) *m/*z calcd for $C_{14}H_{27}N_4O_3$ $[M+H]^+$: 299.2; found: 299.5.

USC UNIVERSIDADE DE SANTIAGO DE COMPOSTELA

**methyl *N*-methyl-*N*-((*S*)-piperidine-2-carbonyl)-D-valylglycinate (16a).** Purified by column chromatography (DCM/MeOH 97:3). Yield: 17%. Mp: 127 – 128 ºC. $^{1}$H NMR (300 MHz, $CDCl_3$) $\delta$ (ppm): 6.74 (s, 1H), 4.58 (d, *J* = 11.2 Hz, 1H), 4.09 – 3.76 (m, 2H), 3.69 (s, 3H), 3.63 – 3.55 (m, 1H), 3.48 – 3.40 (m, 1H), 3.16 (t, *J* = 15.0 Hz, 1H), 2.97 (s, 1H), 2.74 (s, 2H), 2.72 – 2.58 (m, 1H), 2.44 – 2.23 (m, 1H), 2.04 – 1.27 (m, 6H), 0.95 (dd, *J* = 6.5, 2.6 Hz, 3H), 0.82 (d, *J* = 6.7 Hz, 3H). $^{13}$C NMR (75 MHz, $CDCl_3$), δ (ppm): 172.0, 170.3, 169.6, 65.5, 57.2, 52.1, 46.6, 41.3, 28.8, 28.4, 27.1, 25.5, 25.4, 23.7, 20.0, 18.4. LRMS (CI) *m/*z calcd for $C_{15}H_{28}N_3O_4$ $[M+H]^+$: 314.2; found: 314.3.

**(*S*)-*N*-((*R*)-1-((2-amino-2-oxoethyl)amino)-3-methyl-1-oxobutan-2-yl)-*N*-methylpiperidine-2-carboxamide (16b).** Purified by column chromatography (DCM/MeOH 94:6). Yield: 99%. Oil at room temperature. $^{1}$H NMR (300 MHz, MeOD) $\delta$ (ppm): 4.58 (d, *J* = 10.9 Hz, 1H), 3.97 – 3.62 (m, 3H), 3.14 – 3.07 (m, 1H), 3.06 (s, 2H), 2.83 (s, 1H), 2.73 – 2.58 (m, 1H), 2.41 – 2.18 (m, 1H), 1.96 – 1.80 (m, 2H), 1.75 – 1.25 (m, 4H), 1.00 (t, *J* = 7.4 Hz, 3H), 0.88 (d, *J* = 6.6 Hz, 3H). $^{13}$C NMR (75 MHz, MeOD), δ (ppm): 178.5, 176.3, 175.2, 66.7, 60.2, 48.7, 45.3, 33.9, 32.7, 29.8, 29.6, 27.5, 22.6, 21.7. LRMS (CI) *m/*z calcd for $C_{14}H_{27}N_4O_3$ $[M+H]^+$: 299.2; found: 299.5.

**(*S*)-*N*-((*S*)-4-methyl-1-((2-(methylamino)-2-oxoethyl)amino)-1-oxopentan-2-yl)pyrrolidine-2-carboxamide (17).** Purified by column chromatography (DCM/MeOH 94:6). Yield: 99%. Mp: 121 – 123 ºC. $^{1}$H NMR (300 MHz, MeOD) $\delta$ (ppm): 4.12 – 4.06 (m, 1H), 3.80 (d, *J* = 16.8 Hz, 1H), 3.72 (dd, *J* = 8.9, 5.4 Hz, 1H), 3.56 (d, *J* = 16.7 Hz, 1H), 2.98 – 2.84 (m, 2H), 2.60 (s, 3H), 2.15 – 1.98 (m, 1H), 1.81 – 1.59 (m, 3H), 1.54 – 1.36 (m, 3H), 0.78 (dd, *J* = 13.4, 5.0 Hz, 6H). $^{13}$C NMR (75 MHz, MeOD), δ (ppm): 174.7, 173.2, 170.1, 59.8, 52.3, 46.7, 42.4, 40.0, 30.3, 25.7, 25.4, 24.6, 22.5, 21.3. LRMS (CI) *m/*z calcd for $C_{14}H_{27}N_4O_3$ $[M+H]^+$: 299.2; found: 299.2.

**(*S*)-*N*-((*S*)-1-((2-(ethylamino)-2-oxoethyl)amino)-4-methyl-1-oxopentan-2-yl)pyrrolidine-2-carboxamide (18).** Purified by column chromatography (DCM/MeOH 94:6). Yield: 99%. Oil at room temperature. $^{1}$H NMR (300 MHz, MeOD) $\delta$ (ppm): 4.26 – 4.22 (m, 1H), 3.98 (dd, *J* = 8.7, 5.6 Hz, 1H), 3.86 – 3.69 (m, 2H), 3.06 (t, *J* = 6.7 Hz, 2H), 2.80 (q, *J* = 7.3 Hz, 2H), 2.26 – 2.10 (m, 1H), 1.89 – 1.69 (m, 3H), 1.55 – 1.36 (m, 3H), 1.13 (t, *J* = 7.3 Hz, 3H), 0.76 (dd, *J* = 11.2, 5.4 Hz, 6H). $^{13}$C NMR (75 MHz, MeOD), δ (ppm): 173.0, 171.1, 170.3, 59.7, 52.1, 46.6, 40.8, 40.5, 34.9, 30.3, 24.7, 24.6, 22.6, 21.5, 12.3. LRMS (CI) *m/*z calcd for $C_{15}H_{29}N_4O_3$ $[M+H]^+$: 313.2; found: 313.3.

USC DE SANTIAGO DE COMPOSTELA

**(*S*)-*N*-((*S*)-1-((2-(isopropylamino)-2-oxoethyl)amino)-4-methyl-1-oxopentan-2-yl)pyrrolidine-2-carboxamide (19).** Purified by column chromatography (DCM/MeOH 94:6). Yield: 99%. Mp: 102 – 104 ºC. $^{1}$H NMR (300 MHz, MeOD) $\delta$ (ppm): 3.95 (t, *J* = 7.2 Hz, 1H), 3.67 (p, *J* = 6.6 Hz, 1H), 3.61 – 3.52 (m, 2H), 3.01 (d, *J* = 2.0 Hz, 1H), 2.77 (t, *J* = 6.6 Hz, 2H), 2.02 – 1.84 (m, 1H), 1.66 – 1.46 (m, 3H), 1.40 – 1.24 (m, 3H), 0.82 (dd, *J* = 9.7, 6.6 Hz, 6H), 0.63 (dd, *J* = 12.3, 5.5 Hz, 6H). $^{13}$C NMR (75 MHz, MeOD), δ (ppm): 174.0, 173.4, 168.6, 59.9, 52.5, 46.7, 42.5, 41.4, 40.2, 30.4, 25.3, 24.7, 22.4, 21.7, 21.2. LRMS (CI) *m/*z calcd for $C_{16}H_{31}N_4O_3$ $[M+H]^+$: 327.2; found: 327.3.

**(*S*)-*N*-((*S*)-1-((2-(dimethylamino)-2-oxoethyl)amino)-4-methyl-1-oxopentan-2-yl)pyrrolidine-2-carboxamide (20).** Purified by column chromatography (DCM/MeOH 94:6). Yield: 99%. Oil at room temperature. $^{1}$H NMR (300 MHz, MeOD) $\delta$ (ppm): 4.29 – 4.20 (m, 1H), 3.84 (s, 2H), 3.72 (dd, *J* = 8.9, 5.7 Hz, 1H), 2.90 (t, *J* = 6.6 Hz, 2H), 2.81 (d, *J* = 12.6 Hz, 6H), 2.14 – 1.99 (m, 1H), 1.79 – 1.58 (m, 3H), 1.54 – 1.36 (m, 3H), 0.76 (dd, *J* = 12.0, 5.1 Hz, 6H). $^{13}$C NMR (75 MHz, MeOD), δ (ppm): 174.2, 172.8, 168.2, 60.0, 51.8, 46.8, 40.9, 40.6, 35.9, 35.5, 30.5, 25.5, 24.8, 22.7, 21.3. LRMS (CI) *m/*z calcd for $C_{15}H_{29}N_4O_3$ $[M+H]^+$: 313.2; found: 313.2.

**(±) methyl (furan-2-carbonyl)leucylglycinate (21a).** Purified by column chromatography (DCM/MeOH 97:3). Yield: 21%. Mp: 134 – 136 ºC. $^{1}$H NMR (300 MHz, $CDCl_3$) $\delta$ (ppm): 7.44 (s, 1H), 7.12 (d, *J* = 3.5 Hz, 1H), 6.81 (s, 1H), 6.75 (d, *J* = 8.5 Hz, 1H), 6.52 – 6.45 (m, 1H), 4.73 – 4.61 (m, 1H), 4.13 – 3.94 (m, 2H), 3.73 (s, 3H), 1.82 – 1.61 (m, 3H), 0.99 – 0.90 (m, 6H). LRMS (CI) *m/*z calcd for $C_{14}H_{21}N_2O_5$ $[M+H]^+$: 297.1; found: 297.2.

**(±) *N*-(1-((2-amino-2-oxoethyl)amino)-4-methyl-1-oxopentan-2-yl)furan-2-carboxamide (21b).** Purified by column chromatography (DCM/MeOH 94:6). Yield: 99%. Mp: 140 – 142 ºC. $^{1}$H NMR (300 MHz, $CDCl_3$) $\delta$ (ppm): 7.67 – 7.57 (m, 1H), 7.44 (s, 1H), 7.20 – 7.06 (m, 2H), 6.79 (bs, 1H), 6.51 – 6.43 (m, 1H), 6.15 (bs, 1H), 4.67 – 4.53 (m, 1H), 4.03 (dd, *J* = 17.1, 6.3 Hz, 1H), 3.79 (dd, *J* = 16.9, 5.1 Hz, 1H), 1.75 – 1.69 (m, 3H), 0.99 – 0.88 (m, 6H). LRMS (CI) *m/*z calcd for $C_{13}H_{20}N_3O_4$ $[M+H]^+$: 282.1; found: 282.1.

USC UNIVERSIDADE DE SANTIAGO DE COMPOSTELA

**(±) methyl (furan-3-carbonyl)leucylglycinate (22a).** Purified by column chromatography (DCM/MeOH 97:3). Yield: 27%. Mp: 176 – 177 ºC. $^1$H NMR (300 MHz, DMSO-$d_6$) $\delta$ (ppm): 8.39 (t, $J$ = 5.9 Hz, 1H), 8.26 – 8.15 (m, 2H), 7.70 (s, 1H), 6.90 (s, 1H), 4.57 – 4.44 (m, 1H), 3.92 – 3.70 (m, 2H), 3.59 (s, 3H), 1.66 – 1.48 (m, 3H), 0.86 (dd, $J$ = 13.4, 6.1 Hz, 6H). LRMS (CI) *m/*z calcd for $C_{14}H_{21}N_2O_5$ $[M+H]^+$: 297.1; found: 297.2.

**(±) *N*-(1-((2-amino-2-oxoethyl)amino)-4-methyl-1-oxopentan-2-yl)furan-3-carboxamide (22b).** Purified by column chromatography (DCM/MeOH 94:6). Yield: 99%. Oil at room temperature. $^1$H NMR (300 MHz, $CDCl_3$) $\delta$ (ppm): 7.95 (s, 1H), 7.63 (bs, 1H), 7.40 – 7.30 (m, 2H), 6.81 (bs, 1H), 6.65 (s, 1H), 6.19 (bs, 1H), 4.63 – 4.53 (m, 1H), 4.06 – 4.00 (m, 1H), 3.83 – 3.69 (m, 1H), 1.71 – 1.65 (m, 3H), 0.91 (t, $J$ = 6.1 Hz, 6H). LRMS (CI) *m/*z calcd for $C_{13}H_{20}N_3O_4$ $[M+H]^+$: 282.1; found: 282.1.

**(±) methyl (1*H*-pyrrole-2-carbonyl)leucylglycinate (23a).** Purified by column chromatography (DCM/MeOH 97:3). Yield: 27%. Mp: 132 – 133 ºC. $^1$H NMR (300 MHz, $CDCl_3$) $\delta$ (ppm): 10.00 (bs, 1H), 7.50 (bs, 1H), 6.90 (s, 1H), 6.82 – 6.62 (m, 2H), 6.21 (s, 1H), 4.89 – 4.69 (m, 1H), 4.21 – 3.86 (m, 2H), 3.72 (s, 3H), 1.76 – 1.58 (m, 3H), 0.90 (t, $J$ = 6.0 Hz, 6H). LRMS (CI) *m/*z calcd for $C_{14}H_{22}N_3O_4$ $[M+H]^+$: 296.1; found: 296.1.

**(±) *N*-(1-((2-amino-2-oxoethyl)amino)-4-methyl-1-oxopentan-2-yl)-1*H*-pyrrole-2-carboxamide (23b).** Purified by column chromatography (DCM/MeOH 94:6). Yield: 99%. Oil at room temperature. $^1$H NMR (300 MHz, $CDCl_3$) $\delta$ (ppm): 10.22 (s, 1H), 7.40 – 7.34 (m, 1H), 6.94 (s, 1H), 6.70 (s, 2H), 6.59 (d, $J$ = 6.6 Hz, 1H), 6.27 – 6.18 (m, 2H), 4.54 – 4.48 (m, 1H), 4.03 (dd, $J$ = 16.9, 6.4 Hz, 1H), 3.80 (dd, $J$ = 17.0, 5.4 Hz, 1H), 1.82 – 1.66 (m, 3H), 0.97 (dd, $J$ = 10.5, 5.5 Hz, 6H). LRMS (CI) *m/*z calcd for $C_{13}H_{21}N_4O_3$ $[M+H]^+$: 281.1; found: 281.3.

**(±) methyl (1*H*-pyrazole-3-carbonyl)leucylglycinate (24a).** Purified by column chromatography (DCM/MeOH 97:3). Yield: 32%. Oil at room temperature. $^1$H NMR (300 MHz, $CDCl_3$) $\delta$ (ppm): 9.17 (d, $J$ = 8.5 Hz, 1H), 7.67 – 7.53 (m, 2H), 6.83 (s, 1H), 4.88 – 4.74 (m, 1H), 4.21 – 3.93 (m, 2H), 3.72 (s, 3H), 1.88 – 1.53 (m, 3H), 1.11 – 0.79 (m, 6H). LRMS (CI) *m/*z calcd for $C_{13}H_{21}N_4O_4$ $[M+H]^+$: 297.1; found: 297.3.

USC UNIVERSIDADE DE SANTIAGO DE COMPOSTELA

**(±) *N*-(1-((2-amino-2-oxoethyl)amino)-4-methyl-1-oxopentan-2-yl)-1*H*-pyrazole-3-carboxamide (24b).** Purified by column chromatography (DCM/MeOH 94:6). Yield: 98%. Mp: 216 – 217 ºC. $^1$H NMR (300 MHz, MeOD) $\delta$ (ppm): 7.56 – 7.50 (m, 1H), 6.77 – 6.71 (m, 1H), 4.48 (t, *J* = 7.3 Hz, 1H), 3.94 (d, *J* = 17.1 Hz, 1H), 3.73 (d, *J* = 17.1 Hz, 1H), 1.76 – 1.59 (m, 3H), 0.95 – 0.86 (m, 6H). LRMS (CI) *m/*z calcd for $C_{12}H_{20}N_5O_3$ $[M+H]^+$: 282.1; found: 282.1.

**(±) methyl (1*H*-pyrazole-4-carbonyl)leucylglycinate (25a).** Purified by column chromatography (DCM/MeOH 97:3). Yield: 26%. Oil at room temperature. $^1$H NMR (300 MHz, DMSO-$d_6$) $\delta$ (ppm): 13.08 (s, 1H), 8.37 – 8.29 (m, 1H), 8.24 (s, 1H), 8.03 (d, *J* = 8.4 Hz, 1H), 7.92 (s, 1H), 4.57 – 4.45 (m, 1H), 3.91 – 3.71 (m, 2H), 3.60 (s, 3H), 1.71 – 1.49 (m, 3H), 0.86 (dd, *J* = 13.4, 6.2 Hz, 6H). $^{13}$C NMR (75 MHz, DMSO-$d_6$), δ (ppm): 173.4, 170.7, 162.5, 139.3, 130.3, 118.0, 52.1, 51.1, 41.1, 41.0, 24.7, 23.5, 22.0. LRMS (CI) *m/*z calcd for $C_{13}H_{21}N_4O_4$ $[M+H]^+$: 297.1; found: 297.3.

**(±) *N*-(1-((2-amino-2-oxoethyl)amino)-4-methyl-1-oxopentan-2-yl)-1*H*-pyrazole-4-carboxamide (25b).** Purified by column chromatography (DCM/MeOH 94:6). Yield: 99%. Mp: 237 – 238 ºC. $^1$H NMR (300 MHz, DMSO-$d_6$) $\delta$ (ppm): 13.11 (s, 1H), 8.22 (s, 1H), 8.19 – 8.07 (m, 2H), 7.92 (s, 1H), 7.15 (s, 1H), 7.02 (s, 1H), 4.44 – 4.31 (m, 1H), 3.64 (dd, *J* = 16.8, 6.0 Hz, 1H), 3.54 (dd, *J* = 16.8, 5.6 Hz, 1H), 1.69 – 1.50 (m, 3H), 0.87 (dd, *J* = 13.8, 6.0 Hz, 6H). $^{13}$C NMR (75 MHz, DMSO-$d_6$), δ (ppm): 173.1, 171.4, 168.5, 138.7, 130.4, 117.9, 51.9, 42.4, 24.8, 23.5, 22.0. LRMS (CI) *m/*z calcd for $C_{12}H_{20}N_5O_3$ $[M+H]^+$: 282.1; found: 282.1.

**(±) methyl (1*H*-imidazole-4-carbonyl)leucylglycinate (26a).** Purified by column chromatography (DCM/MeOH 97:3). Yield: 35%. Mp: 168 – 170 ºC. $^1$H NMR (300 MHz, $CDCl_3$) $\delta$ (ppm): 7.68 (bs, 1H), 7.61 (d, *J* = 8.2 Hz, 1H), 7.56 (d, *J* = 6.7 Hz, 2H), 4.73 – 4.59 (m, 1H), 4.08 – 3.94 (m, 2H), 3.68 (s, 3H), 1.82 – 1.63 (m, 3H), 0.90 (dd, *J* = 9.3, 5.5 Hz, 6H). LRMS (CI) *m/*z calcd for $C_{13}H_{21}N_4O_4$ $[M+H]^+$: 297.1; found: 297.3.

**(±) *N*-(1-((2-amino-2-oxoethyl)amino)-4-methyl-1-oxopentan-2-yl)-1*H*-imidazole-4-carboxamide (26b).** Purified by column chromatography (DCM/MeOH 94:6). Yield: 99%. Mp: 81 – 82 ºC. $^1$H NMR (300 MHz, DMSO-$d_6$) $\delta$ (ppm): 8.24 – 8.18 (m, 1H), 7.81 (d, *J* = 8.3 Hz, 1H), 7.74 (s, 1H), 7.64 (s, 1H), 7.24 (s, 1H), 7.02 (s, 1H), 4.59 – 4.40 (m, 1H), 3.69 (dd, *J* = 16.7, 5.9 Hz, 1H), 3.58 (dd, *J* = 16.7, 5.5 Hz, 1H), 1.67 – 1.54 (m, 3H), 0.99 – 0.85 (m, 6H). LRMS (CI) *m/*z calcd for $C_{12}H_{20}N_5O_3$ $[M+H]^+$: 282.1; found: 282.1.

USC DE SANTIAGO DE COMPOSTELA

**(±) methyl (oxazole-4-carbonyl)leucylglycinate (27a).** Purified by column chromatography (DCM/MeOH 97:3). Yield: 25%. Oil at room temperature. $^{1}$H NMR (300 MHz, $CDCl_3$) $\delta$ (ppm): 8.25 (s, 1H), 7.86 (s, 1H), 7.39 (d, $J$ = 8.6 Hz, 1H), 7.16 – 7.08 (m, 1H), 4.77 – 4.63 (m, 1H), 4.14 – 3.88 (m, 2H), 3.70 (s, 3H), 1.82 – 1.61 (m, 3H), 0.92 (t, $J$ = 5.9 Hz, 6H). $^{13}$C NMR (75 MHz, $CDCl_3$), δ (ppm): 171.9, 170.2, 160.5, 150.7, 141.8, 135.4, 52.3, 51.2, 41.2, 40.9, 24.8, 22.9, 21.9. LRMS (CI) *m/*z calcd for $C_{13}H_{20}N_3O_5$ $[M+H]^+$: 298.1; found: 298.2.

**(±) *N*-(1-((2-amino-2-oxoethyl)amino)-4-methyl-1-oxopentan-2-yl)oxazole-4-carboxamide (27b).** Purified by column chromatography (DCM/MeOH 94:6). Yield: 99%. Mp: 173 – 174 ºC. $^{1}$H NMR (300 MHz, $CDCl_3$) $\delta$ (ppm): 8.26 (s, 1H), 7.88 (s, 1H), 7.39 (d, $J$ = 7.3 Hz, 1H), 6.62 (bs, 1H), 5.88 (bs, 1H), 4.63 – 4.52 (m, 1H), 4.11 – 3.79 (m, 2H), 1.85 – 1.69 (m, 3H), 0.96 (t, $J$ = 6.9 Hz, 6H). LRMS (CI) *m/*z calcd for $C_{12}H_{19}N_4O_4$ $[M+H]^+$: 283.1; found: 283.3.

**(±) methyl ((*R*)-thiazolidine-4-carbonyl)leucylglycinate (28a).** Purified by column chromatography (DCM/MeOH 97:3). Yield: 33%. Mp: 117 – 119 ºC. $^{1}$H NMR (300 MHz, $CDCl_3$) $\delta$ (ppm): 7.56 – 7.46 (m, 1H), 6.87 (d, $J$ = 25.2 Hz, 1H), 4.57 – 4.41 (m, 1H), 4.28 – 4.12 (m, 2H), 4.07 – 3.89 (m, 3H), 3.73 (s, 3H), 3.40 (dd, $J$ = 10.9, 4.3 Hz, 1H), 3.14 – 3.02 (m, 1H), 1.78 – 1.50 (m, 3H), 0.97 – 0.86 (m, 6H). LRMS (CI) *m/*z calcd for $C_{13}H_{24}N_3O_4S$ $[M+H]^+$: 318.1; found: 318.1.

**(±) (4*R*)-*N*-(1-((2-amino-2-oxoethyl)amino)-4-methyl-1-oxopentan-2-yl)thiazolidine-4-carboxamide (28b).** Purified by column chromatography (DCM/MeOH 94:6). Yield: 99%. Mp: 216 – 217 ºC. $^{1}$H NMR (300 MHz, $CDCl_3$) $\delta$ (ppm): 3.96 – 3.71 (m, 2H), 3.68 – 3.50 (m, 2H), 3.25 – 3.11 (m, 3H), 3.07 – 2.87 (m, 1H), 1.56 – 1.36 (m, 3H), 0.85 – 0.71 (m, 6H). LRMS (CI) *m/*z calcd for $C_{12}H_{23}N_4O_3S$ $[M+H]^+$: 303.1; found: 303.2.

**(±) methyl (2-oxo-2,3-dihydro-1*H*-imidazole-4-carbonyl)leucylglycinate (29a).** Purified by column chromatography (DCM/MeOH 97:3). Yield: 33%. Mp: 215 – 216 ºC. $^{1}$H NMR (300 MHz, DMSO-$d_6$) $\delta$ (ppm): 10.26 (s, 1H), 10.17 (s, 1H), 8.42 – 8.34 (m, 1H), 7.82 (d, $J$ = 8.4 Hz, 1H), 7.12 (s, 1H), 4.51 – 4.38 (m, 1H), 3.91 – 3.70 (m, 2H), 3.60 (s, 3H), 1.66 – 1.56 (m, 1H), 1.56 – 1.45 (m, 2H), 0.86 (dd, $J$ = 13.5, 6.3 Hz, 6H). $^{13}$C NMR (75 MHz, DMSO-$d_6$), δ (ppm): 173.2, 170.6, 159.0, 154.2, 117.7, 114.3, 52.1, 51.0, 41.3, 41.0, 24.7, 23.5, 21.9. LRMS (CI) *m/*z calcd for $C_{13}H_{21}N_4O_5$ $[M+H]^+$: 313.1; found: 313.5.

USC UNIVERSIDADE DE SANTIAGO DE COMPOSTELA

**(±) *N*-(1-((2-amino-2-oxoethyl)amino)-4-methyl-1-oxopentan-2-yl)-2-oxo-2,3-dihydro-1*H*-imidazole-4-carboxamide (29b).** Purified by column chromatography (DCM/MeOH 94:6). Yield: 99%. Mp: 215 – 216 ºC. $^1$H NMR (300 MHz, DMSO-$d_6$) $\delta$ (ppm): 10.28 (bs, 2H), 8.20 (s, 1H), 7.95 (s, 1H), 7.15 (bs, 1H), 7.10 (s, 1H), 7.02 (bs, 1H), 4.40 – 4.30 (m, 1H), 3.68 – 3.51 (m, 2H), 1.66 – 1.46 (m, 3H), 0.85 (dd, *J* = 13.2, 6.2 Hz, 6H). LRMS (CI) *m/*z calcd for $C_{12}H_{20}N_5O_4$ $[M+H]^+$: 298.1; found: 298.1.

**(±) methyl ((*S*)-2-oxoimidazolidine-4-carbonyl)leucylglycinate (30a).** Purified by column chromatography (DCM/MeOH 97:3). Yield: 34%. Oil at room temperature. $^1$H NMR (300 MHz, DMSO-$d_6$) $\delta$ (ppm): 8.47 – 8.37 (m, 1H), 7.92 (d, *J* = 8.4 Hz, 1H), 6.49 (d, *J* = 16.2 Hz, 1H), 6.26 (s, 1H), 4.40 – 4.33 (m, 1H), 4.14 – 4.06 (m, 1H), 3.91 – 3.73 (m, 2H), 3.60 (s, 3H), 3.57 – 3.45 (m, 1H), 3.26 – 3.10 (m, 1H), 1.62 – 1.53 (m, 1H), 1.46 (t, *J* = 7.2 Hz, 2H), 0.85 (dd, *J* = 11.9, 6.4 Hz, 6H). LRMS (CI) *m/*z calcd for $C_{13}H_{23}N_4O_5$ $[M+H]^+$: 315.1; found: 315.2.

**(±) (4*S*)-*N*-(1-((2-amino-2-oxoethyl)amino)-4-methyl-1-oxopentan-2-yl)-2-oxoimidazolidine-4-carboxamide (30b).** Purified by column chromatography (DCM/MeOH 94:6). Yield: 99%. Mp: 197 – 198 ºC. $^1$H NMR (300 MHz, DMSO-$d_6$) $\delta$ (ppm): 8.20 – 8.12 (m, 1H), 7.99 (t, *J* = 9.1 Hz, 1H), 7.17 (s, 1H), 7.03 (d, *J* = 7.3 Hz, 1H), 6.48 (d, *J* = 14.6 Hz, 1H), 6.28 (s, 1H), 4.35 – 4.22 (m, 1H), 4.18 – 4.05 (m, 1H), 3.71 – 3.46 (m, 2H), 3.25 – 3.13 (m, 2H), 1.65 – 1.43 (m, 3H), 0.85 (dd, *J* = 11.9, 6.2 Hz, 6H). $^{13}$C NMR (75 MHz, DMSO-$d_6$), δ (ppm): 172.44, 172.34, 172.22, 171.23 (d, *J* = 5.6 Hz), 54.67, 51.65, 44.23 (d, *J* = 7.8 Hz), 42.33 (d, *J* = 5.1 Hz), 24.62, 23.52, 22.05. LRMS (CI) *m/*z calcd for $C_{12}H_{22}N_5O_4$ $[M+H]^+$: 300.1; found: 300.3.

**(±) methyl (1*H*-1,2,3-triazole-4-carbonyl)leucylglycinate (31a).** Purified by column chromatography (DCM/MeOH 97:3). Yield: 17%. Mp: 122 – 124 ºC. $^1$H NMR (300 MHz, $CDCl_3$) $\delta$ (ppm): 8.31 (s, 1H), 8.19 (s, 1H), 6.08 – 6.02 (m, 1H), 4.31 – 4.23 (m, 1H), 4.08 – 4.02 (m, 2H), 3.73 (s, 3H), 1.82 – 1.51 (m, 3H), 0.80 (dd, *J* = 13.3, 5.8 Hz, 6H). LRMS (CI) *m/*z calcd for $C_{12}H_{20}N_5O_4$ $[M+H]^+$: 298.1; found: 298.1.

USC UNIVERSIDADE DE SANTIAGO DE COMPOSTELA

**(±) *N*-(1-((2-amino-2-oxoethyl)amino)-4-methyl-1-oxopentan-2-yl)-1*H*-1,2,3-triazole-4-carboxamide (31b).** Purified by column chromatography (DCM/MeOH 94:6). Yield: 99%. Mp: 140 – 142 ºC. $^1$H NMR (300 MHz, DMSO-$d_6$) $\delta$ (ppm): 8.08 (s, 1H), 7.93 (s, 1H), 7.09 (s, 1H), 6.98 (s, 1H), 3.95 – 3.79 (m, 1H), 3.72 – 3.35 (m, 2H), 1.78 – 1.58 (m, 2H), 1.48 – 1.32 (m, 1H), 0.95 – 0.73 (m, 6H). LRMS (CI) *m/*z calcd for $C_{11}H_{19}N_6O_3$ $[M+H]^+$: 283.1; found: 283.3.

**(±) methyl (piperidine-4-carbonyl)leucylglycinate (32a).** Purified by column chromatography (DCM/MeOH 97:3). Yield: 26%. Mp: 88 – 89 ºC. $^1$H NMR (300 MHz, $CDCl_3$) $\delta$ (ppm): 6.65 (s, 1H), 5.82 (d, $J$ = 8.4 Hz, 1H), 4.61 – 4.47 (m, 1H), 4.04 (dd, $J$ = 5.4, 3.3 Hz, 2H), 3.80 – 3.74 (m, 4H), 2.19 – 2.07 (m, 2H), 1.75 – 1.56 (m, 7H), 1.11 – 0.82 (m, 9H). LRMS (CI) *m/*z calcd for $C_{15}H_{28}N_3O_4$ $[M+H]^+$: 314.2; found: 314.3.

**(±) *N*-(1-((2-amino-2-oxoethyl)amino)-4-methyl-1-oxopentan-2-yl)piperidine-4-carboxamide (32b).** Purified by column chromatography (DCM/MeOH 94:6). Yield: 99%. Mp: 102 – 104 ºC. $^1$H NMR (300 MHz, $CDCl_3$) $\delta$ (ppm): 7.15 – 7.05 (m, 1H), 6.64 (s, 1H), 6.19 (s, 1H), 5.72 (s, 1H), 4.35 (d, $J$ = 7.4 Hz, 1H), 4.07 (td, $J$ = 16.2, 15.4, 6.1 Hz, 1H), 3.84 – 3.71 (m, 2H), 2.18 – 1.99 (m, 2H), 1.78 – 1.48 (m, 7H), 1.06 – 0.82 (m, 9H). LRMS (CI) *m/*z calcd for $C_{14}H_{27}N_4O_3$ $[M+H]^+$: 299.2; found: 299.2.

**(±) methyl benzoylleucylglycinate (33a).** Purified by column chromatography (DCM/MeOH 97:3). Yield: 37%. Mp: 166 – 168 ºC. $^1$H NMR (300 MHz, $CDCl_3$) $\delta$ (ppm): 7.87 – 7.75 (m, 2H), 7.55 – 7.47 (m, 1H), 7.46 – 7.38 (m, 2H), 7.02 (s, 1H), 6.84 (d, $J$ = 8.3 Hz, 1H), 4.86 – 4.71 (m, 1H), 4.15 – 3.91 (m, 2H), 3.72 (s, 3H), 1.92 – 1.58 (m, 3H), 1.03 – 0.87 (m, 6H). LRMS (CI) *m/*z calcd for $C_{16}H_{23}N_2O_4$ $[M+H]^+$: 307.1; found: 307.5.

**(±) *N*-(1-((2-amino-2-oxoethyl)amino)-4-methyl-1-oxopentan-2-yl)benzamide (33b).** Purified by column chromatography (DCM/MeOH 94:6). Yield: 99%. Mp: 144 – 146 ºC. $^1$H NMR (300 MHz, DMSO-$d_6$) $\delta$ (ppm): 8.54 (d, $J$ = 7.6 Hz, 1H), 8.17 (t, $J$ = 5.8 Hz, 1H), 7.95 – 7.86 (m, 2H), 7.61 – 7.42 (m, 3H), 7.17 (s, 1H), 7.06 (s, 1H), 4.55 – 4.39 (m, 1H), 3.69 (dd, $J$ = 16.7, 6.0 Hz, 1H), 3.58 (dd, $J$ = 16.7, 5.6 Hz, 1H), 1.80 – 1.54 (m, 3H), 0.91 (dd, $J$ = 11.0, 6.0 Hz, 6H). LRMS (CI) *m/*z calcd for $C_{15}H_{22}N_3O_3$ $[M+H]^+$: 292.1; found: 292.1.

USC UNIVERSIDADE DE SANTIAGO DE COMPOSTELA

**(±) methyl picolinoylleucylglycinate (34a).** Purified by column chromatography (DCM/MeOH 97:3). Yield: 26%. Mp: 208 – 209 ºC. $^{1}$H NMR (300 MHz, $CDCl_3$) $\delta$ (ppm): 8.57 (d, *J* = 4.7 Hz, 1H), 8.33 (d, *J* = 8.4 Hz, 1H), 8.18 (d, *J* = 7.8 Hz, 1H), 7.89 – 7.81 (m, 1H), 7.47 – 7.41 (m, 1H), 6.80 (s, 1H), 4.74 – 4.63 (m, 1H), 4.04 (d, *J* = 5.3 Hz, 2H), 3.72 (s, 3H), 1.95 – 1.82 (m, 1H), 1.81 – 1.69 (m, 2H), 0.97 (t, *J* = 6.7 Hz, 6H). LRMS (CI) *m/*z calcd for $C_{15}H_{22}N_3O_4$ $[M+H]^+$: 308.1; found: 308.2.

**(±) *N*-(1-((2-amino-2-oxoethyl)amino)-4-methyl-1-oxopentan-2-yl)picolinamide (34b).** Purified by column chromatography (DCM/MeOH 94:6). Yield: 99%. Mp: 149 – 150 ºC. $^{1}$H NMR (300 MHz, $CDCl_3$) $\delta$ (ppm): 8.58 (d, *J* = 4.8 Hz, 1H), 8.37 (d, *J* = 6.8 Hz, 1H), 8.15 (d, *J* = 7.8 Hz, 1H), 7.92 – 7.81 (m, 1H), 7.52 – 7.42 (m, 1H), 6.88 (s, 1H), 6.56 (s, 1H), 5.45 (s, 1H), 4.58 – 4.44 (m, 1H), 4.08 – 3.85 (m, 2H), 1.92 – 1.71 (m, 3H), 0.99 (dd, *J* = 10.9, 6.0 Hz, 6H). $^{13}$C NMR (75 MHz, $CDCl_3$), δ (ppm): 172.4, 171.5, 165.2, 149.0, 148.4, 137.5, 126.7, 122.4, 52.6, 43.0, 40.6, 24.9, 22.9, 21.9. LRMS (CI) *m/*z calcd for $C_{14}H_{21}N_4O_3$ $[M+H]^+$: 293.1; found: 293.3.

**(*S*)-*N*-(1-((2-amino-2-oxoethyl)amino)-4-methyl-1-oxopentan-2-yl)picolinamide ((*S*)-34b).** Purified by column chromatography (DCM/MeOH 94:6). Yield: 99%. Mp: 149 – 150 ºC. $^{1}$H NMR (300 MHz, DMSO-*d6*) $\delta$ (ppm): 8.71 (d, J = 8.7 Hz, 1H), 8.66 (d, J = 4.7 Hz, 1H), 8.30 (t, J = 5.6 Hz, 1H), 8.06 – 7.95 (m, 2H), 7.64 – 7.58 (m, 1H), 7.25 (bs, 1H), 7.03 (bs, 1H), 4.64 – 4.51 (m, 1H), 3.68 (dd, J = 16.7, 5.9 Hz, 1H), 3.54 (dd, J = 16.7, 5.5 Hz, 1H), 1.72 – 1.52 (m, 3H), 0.87 (d, J = 5.6 Hz, 6H). $^{13}$C NMR (75 MHz, DMSO-*d6*), δ (ppm): 172.3, 171.2, 164.0, 150.0, 149.0, 138.4, 127.2, 122.4, 51.7, 42.4, 41.8, 24.9, 23.6, 22.2. LRMS (CI) *m/*z calcd for $C_{14}H_{21}N_4O_3$ $[M+H]^+$: 293.1; found: 293.1.

**(*R*)-*N*-(1-((2-amino-2-oxoethyl)amino)-4-methyl-1-oxopentan-2-yl)picolinamide ((*R*)-34b).** Purified by column chromatography (DCM/MeOH 94:6). Yield: 99%. Mp: 149 – 150 ºC. $^{1}$H NMR (300 MHz, DMSO-*d6*) $\delta$ (ppm): 8.71 (d, J = 8.7 Hz, 1H), 8.66 (d, J = 4.7 Hz, 1H), 8.30 (t, J = 5.9 Hz, 1H), 8.07 – 7.95 (m, 2H), 7.65 – 7.58 (m, 1H), 7.25 (s, 1H), 7.03 (s, 1H), 4.62 – 4.51 (m, 1H), 3.68 (dd, J = 16.8, 6.0 Hz, 1H), 3.54 (dd, J = 16.7, 5.4 Hz, 1H), 1.72 – 1.51 (m, 3H), 0.87 (d, J = 5.6 Hz, 6H). $^{13}$C NMR (75 MHz, DMSO-*d6*), δ (ppm): 172.3, 171.2, 164.0, 150.0, 149.0, 138.4, 127.2, 122.4, 51.7, 42.4, 41.8, 24.9, 23.6, 22.2. LRMS (CI) *m/*z calcd for $C_{14}H_{21}N_4O_3$ $[M+H]^+$: 293.1; found: 293.1.

USC UNIVERSIDADE DE SANTIAGO DE COMPOSTELA

**(±) methyl nicotinoylleucylglycinate (35a).** Purified by column chromatography (DCM/MeOH 97:3). Yield: 31%. Mp: 137 – 138 ºC. $^1$H NMR (300 MHz, $CDCl_3$) $\delta$ (ppm): 9.10 – 9.00 (m, 1H), 8.69 (dd, *J* = 4.9, 1.7 Hz, 1H), 8.18 – 8.08 (m, 1H), 7.59 (d, *J* = 8.3 Hz, 1H), 7.41 – 7.29 (m, 2H), 4.87 – 4.73 (m, 1H), 4.17 – 3.89 (m, 2H), 3.71 (s, 3H), 1.82 – 1.60 (m, 3H), 1.03 – 0.82 (m, 6H). LRMS (CI) *m/*z calcd for $C_{15}H_{22}N_3O_4$ $[M+H]^+$: 308.1; found: 308.2.

**(±) *N*-(1-((2-amino-2-oxoethyl)amino)-4-methyl-1-oxopentan-2-yl)nicotinamide (35b).** Purified by column chromatography (DCM/MeOH 94:6). Yield: 99%. Mp: 119 – 120 ºC. $^1$H NMR (300 MHz, $CDCl_3$) $\delta$ (ppm): 9.03 (s, 1H), 8.66 (d, *J* = 4.9 Hz, 1H), 8.11 (d, *J* = 8.0 Hz, 1H), 7.83 (d, *J* = 7.5 Hz, 1H), 7.57 (s, 1H), 7.33 (dd, *J* = 8.0, 4.9 Hz, 1H), 6.78 (s, 1H), 6.19 (s, 1H), 4.70 – 4.60 (m, 1H), 4.05 (dd, *J* = 17.1, 6.3 Hz, 1H), 3.78 (dd, *J* = 16.9, 5.1 Hz, 1H), 1.74 – 1.67 (m, 3H), 0.97 – 0.87 (m, 6H). LRMS (CI) *m/*z calcd for $C_{14}H_{21}N_4O_3$ $[M+H]^+$: 293.1; found: 293.3.

**(±) methyl isonicotinoylleucylglycinate (36a).** Purified by column chromatography (DCM/MeOH 97:3). Yield: 28%. Mp: 167 – 168 ºC. $^1$H NMR (300 MHz, $CDCl_3$) $\delta$ (ppm): 8.81 (d, *J* = 8.1 Hz, 1H), 8.75 – 8.67 (m, 2H), 8.45 (t, *J* = 5.8 Hz, 1H), 7.83 – 7.75 (m, 2H), 4.59 – 4.50 (m, 1H), 3.93 – 3.71 (m, 2H), 3.60 (s, 3H), 1.75 – 1.53 (m, 3H), 0.87 (dd, *J* = 11.9, 5.8 Hz, 6H). LRMS (CI) *m/*z calcd for $C_{15}H_{22}N_3O_4$ $[M+H]^+$: 308.1; found: 308.2.

**(±) *N*-(1-((2-amino-2-oxoethyl)amino)-4-methyl-1-oxopentan-2-yl)isonicotinamide (36b).** Purified by column chromatography (DCM/MeOH 94:6). Yield: 99%. Oil at room temperature. $^1$H NMR (300 MHz, $CDCl_3$) $\delta$ (ppm): 8.84 (d, *J* = 7.7 Hz, 1H), 8.78 – 8.70 (m, 2H), 8.22 (t, *J* = 5.8 Hz, 1H), 7.84 – 7.76 (m, 2H), 7.15 (s, 1H), 7.05 (s, 1H), 4.58 – 4.41 (m, 1H), 3.75 – 3.53 (m, 2H), 1.77 – 1.56 (m, 3H), 0.91 (dd, *J* = 10.7, 5.9 Hz, 6H). LRMS (CI) *m/*z calcd for $C_{14}H_{21}N_4O_3$ $[M+H]^+$: 293.1; found: 293.3.

**(±) methyl (pyrimidine-2-carbonyl)leucylglycinate (37a).** Purified by column chromatography (DCM/MeOH 97:3). Yield: 34%. Oil at room temperature. $^1$H NMR (300 MHz, $CDCl_3$) $\delta$ (ppm): 9.36 (s, 1H), 8.75 (s, 1H), 8.53 (s, 1H), 8.16 (d, *J* = 8.7 Hz, 1H), 6.93 (s, 1H), 4.81 – 4.67 (m, 1H), 4.15 – 3.93 (m, 2H), 3.72 (s, 3H), 1.89 – 1.64 (m, 3H), 0.98 – 0.92 (m, 6H). LRMS (CI) *m/*z calcd for $C_{14}H_{21}N_4O_4$ $[M+H]^+$: 309.1; found: 309.1.

USC UNIVERSIDADE DE SANTIAGO DE COMPOSTELA

**(±) *N*-(1-((2-amino-2-oxoethyl)amino)-4-methyl-1-oxopentan-2-yl)pyrimidine-2-carboxamide (37b).** Purified by column chromatography (DCM/MeOH 94:6). Yield: 99%. Oil at room temperature. $^1$H NMR (300 MHz, $CDCl_3$) $\delta$ (ppm): 9.34 (s, 1H), 8.76 (s, 1H), 8.55 (s, 1H), 8.20 (d, *J* = 7.6 Hz, 1H), 7.30 (s, 1H), 6.58 (s, 1H), 5.89 (s, 1H), 4.71 – 4.57 (m, 1H), 4.06 (dd, *J* = 16.8, 6.2 Hz, 1H), 3.87 (dd, *J* = 17.1, 5.2 Hz, 1H), 1.92 – 1.65 (m, 3H), 0.97 (t, *J* = 6.5 Hz, 6H). LRMS (CI) *m/*z calcd for $C_{13}H_{20}N_5O_3$ $[M+H]^+$: 294.1; found: 294.2.

**(±) methyl (3-(trifluoromethyl)benzoyl)leucylglycinate (38a).** Purified by column chromatography (DCM/MeOH 97:3). Yield: 20%. Mp: 122 – 123 ºC. $^1$H NMR (300 MHz, $CDCl_3$) $\delta$ (ppm): 8.10 (s, 1H), 7.98 (d, *J* = 7.9 Hz, 1H), 7.75 – 7.64 (m, 2H), 7.49 (t, *J* = 7.8 Hz, 1H), 7.43 – 7.33 (m, 1H), 4.89 – 4.76 (m, 1H), 4.14 – 3.86 (m, 2H), 3.70 (s, 3H), 1.74 – 1.64 (m, 3H), 0.99 – 0.84 (m, 6H). LRMS (CI) *m/*z calcd for $C_{17}H_{22}F_3N_2O_4$ $[M+H]^+$: 375.1; found: 375.2.

**(±) *N*-(1-((2-amino-2-oxoethyl)amino)-4-methyl-1-oxopentan-2-yl)-3-(trifluoromethyl)benzamide (38b).** Purified by column chromatography (DCM/MeOH 94:6). Yield: 99%. Mp: 187 – 189 ºC. $^1$H NMR (300 MHz, DMSO-$d_6$) $\delta$ (ppm): 8.84 (d, *J* = 7.6 Hz, 1H), 8.29 – 8.16 (m, 3H), 7.93 (d, *J* = 7.8 Hz, 1H), 7.74 (t, *J* = 7.8 Hz, 1H), 7.14 (s, 1H), 7.05 (s, 1H), 4.55 – 4.43 (m, 1H), 3.75 – 3.52 (m, 2H), 1.78 – 1.56 (m, 3H), 0.91 (dd, *J* = 11.4, 5.9 Hz, 6H). LRMS (CI) *m/*z calcd for $C_{16}H_{21}F_3N_3O_3$ $[M+H]^+$: 360.1; found: 360.3.

**(±) methyl (4-(trifluoromethyl)benzoyl)leucylglycinate (39a).** Purified by column chromatography (DCM/MeOH 97:3). Yield: 25%. Mp: 166 – 167 ºC. $^1$H NMR (300 MHz, $CDCl_3$) $\delta$ (ppm): 7.90 (d, *J* = 8.0 Hz, 2H), 7.64 (d, *J* = 8.0 Hz, 2H), 7.33 – 7.25 (m, 1H), 7.09 (s, 1H), 4.85 – 4.72 (m, 1H), 4.15 – 3.92 (m, 2H), 3.73 (s, 3H), 1.80 – 1.62 (m, 3H), 0.98 – 0.88 (m, 6H). LRMS (CI) *m/*z calcd for $C_{17}H_{22}F_3N_2O_4$ $[M+H]^+$: 375.1; found: 375.2.

**(±) *N*-(1-((2-amino-2-oxoethyl)amino)-4-methyl-1-oxopentan-2-yl)-4-(trifluoromethyl)benzamide (39b).** Purified by column chromatography (DCM/MeOH 94:6). Yield: 99%. Mp: 106 – 108 ºC. $^1$H NMR (300 MHz, DMSO-$d_6$) $\delta$ (ppm): 8.79 (d, *J* = 7.6 Hz, 1H), 8.21 (t, *J* = 5.8 Hz, 1H), 8.09 (d, *J* = 8.1 Hz, 2H), 7.87 (d, *J* = 8.1 Hz, 2H), 7.15 (s, 1H), 7.05 (s, 1H), 4.55 – 4.42 (m, 1H), 3.75 – 3.52 (m, 2H), 1.78 – 1.54 (m, 3H), 0.91 (dd, *J* = 10.4, 5.8 Hz, 6H). LRMS (CI) *m/*z calcd for $C_{16}H_{21}F_3N_3O_3$ $[M+H]^+$: 360.1; found: 360.3.

USC UNIVERSIDADE DE SANTIAGO DE COMPOSTELA

**(±) methyl (2,6-difluorobenzoyl)leucylglycinate (40a).** Purified by column chromatography (DCM/MeOH 97:3). Yield: 21%. Mp: 131 – 132 ºC. $^1$H NMR (300 MHz, $CDCl_3$) $\delta$ (ppm): 7.43 – 7.27 (m, 1H), 7.02 – 6.86 (m, 3H), 6.77 (d, *J* = 8.5 Hz, 1H), 4.86 – 4.72 (m, 1H), 4.13 – 3.92 (m, 2H), 3.73 (s, 3H), 1.81 – 1.59 (m, 3H), 1.00 – 0.85 (m, 6H). LRMS (CI) *m/*z calcd for $C_{16}H_{21}F_2N_2O_4$ $[M+H]^+$: 343.1; found: 343.2.

**(±) *N*-(1-((2-amino-2-oxoethyl)amino)-4-methyl-1-oxopentan-2-yl)-2,6-difluorobenzamide (40b).** Purified by column chromatography (DCM/MeOH 94:6). Yield: 99%. Mp: 167 – 168 ºC. $^1$H NMR (300 MHz, MeOD) $\delta$ (ppm): 7.45 – 7.29 (m, 1H), 6.93 (t, *J* = 8.2 Hz, 2H), 4.52 (t, *J* = 7.5 Hz, 1H), 4.02 – 3.67 (m, 2H), 1.78 – 1.57 (m, 3H), 0.98 – 0.89 (m, 6H). LRMS (CI) *m/*z calcd for $C_{15}H_{20}F_2N_3O_3$ $[M+H]^+$: 328.1; found: 328.1.

**(±) methyl (4-ethoxybenzoyl)leucylglycinate (41a).** Purified by column chromatography (DCM/MeOH 97:3). Yield: 23%. Mp: 145 – 146 ºC. $^1$H NMR (300 MHz, DMSO-$d_6$) $\delta$ (ppm): 8.27 (d, *J* = 10.2 Hz, 2H), 7.86 (d, *J* = 8.1 Hz, 2H), 6.95 (d, *J* = 7.8 Hz, 2H), 4.57 – 4.46 (m, 1H), 4.12 – 4.00 (m, 2H), 3.81 (t, *J* = 6.4 Hz, 2H), 3.59 (s, 3H), 1.74 – 1.50 (m, 3H), 1.32 (t, *J* = 7.1 Hz, 3H), 0.93 – 0.82 (m, 6H). LRMS (CI) *m/*z calcd for $C_{18}H_{27}N_2O_5$ $[M+H]^+$: 351.1; found: 351.4.

**(±) *N*-(1-((2-amino-2-oxoethyl)amino)-4-methyl-1-oxopentan-2-yl)-4-ethoxybenzamide (41b).** Purified by column chromatography (DCM/MeOH 94:6). Yield: 99%. Mp: 111 – 112 ºC. $^1$H NMR (300 MHz, $CDCl_3$) $\delta$ (ppm): 7.73 (d, *J* = 8.4 Hz, 2H), 6.91 (d, *J* = 8.3 Hz, 2H), 6.84 (s, 1H), 6.57 (s, 1H), 6.49 (d, *J* = 7.1 Hz, 1H), 5.44 (s, 1H), 4.54 – 4.44 (m, 1H), 4.15 – 4.02 (m, 3H), 3.86 (dd, *J* = 17.0, 5.3 Hz, 1H), 1.83 – 1.67 (m, 3H), 1.43 (t, *J* = 7.0 Hz, 3H), 0.98 (t, *J* = 6.8 Hz, 6H). LRMS (CI) *m/*z calcd for $C_{17}H_{26}N_3O_4$ $[M+H]^+$: 336.1; found: 336.1.

**(±) methyl (3,4-dimethoxybenzoyl)leucylglycinate (42a).** Purified by column chromatography (DCM/MeOH 97:3). Yield: 33%. Mp: 160 – 161 ºC. $^1$H NMR (300 MHz, $CDCl_3$) $\delta$ (ppm): 7.42 (s, 1H), 7.37 – 7.32 (m, 1H), 7.06 – 6.99 (m, 1H), 6.87 – 6.80 (m, 2H), 4.80 – 4.70 (m, 1H), 4.07 – 3.99 (m, 2H), 3.90 (s, 6H), 3.72 (s, 3H), 1.82 – 1.62 (m, 3H), 1.00 – 0.90 (m, 6H). LRMS (CI) *m/*z calcd for $C_{18}H_{27}N_2O_6$ $[M+H]^+$: 367.1; found: 367.1.

USC UNIVERSIDADE DE SANTIAGO DE COMPOSTELA

**(±) *N*-(1-((2-amino-2-oxoethyl)amino)-4-methyl-1-oxopentan-2-yl)-3,4-dimethoxybenzamide (42b).** Purified by column chromatography (DCM/MeOH 94:6). Yield: 99%. Mp: 189 – 190 ºC. $^1$H NMR (300 MHz, $CDCl_3$) $\delta$ (ppm): 7.38 (s, 1H), 7.32 (d, *J* = 8.7 Hz, 1H), 6.87 (d, *J* = 8.2 Hz, 2H), 6.56 (d, *J* = 7.0 Hz, 1H), 6.46 (s, 1H), 5.45 (s, 1H), 4.58 – 4.48 (m, 1H), 4.09 (dd, *J* = 17.2, 6.2 Hz, 1H), 3.93 (s, 6H), 3.90 – 3.82 (m, 1H), 1.84 – 1.66 (m, 3H), 0.99 (t, *J* = 5.9 Hz, 6H). LRMS (CI) *m/*z calcd for $C_{17}H_{26}N_3O_5$ $[M+H]^+$: 352.1; found: 352.2.

**(±) methyl (2-(1*H*-pyrazol-1-yl)benzoyl)leucylglycinate (43a).** Purified by column chromatography (DCM/MeOH 97:3). Yield: 37%. Mp: 127 – 128 ºC. $^1$H NMR (300 MHz, $CDCl_3$) $\delta$ (ppm): 7.78 – 7.67 (m, 3H), 7.59 – 7.44 (m, 2H), 7.39 (d, *J* = 7.7 Hz, 1H), 7.12 (s, 1H), 6.63 (d, 1H), 6.47 (s, 1H), 4.64 – 4.46 (m, 1H), 4.12 – 3.88 (m, 2H), 3.73 (s, 3H), 1.82 – 1.64 (m, 2H), 1.57 – 1.36 (m, 1H), 0.94 – 0.85 (m, 6H). LRMS (CI) *m/*z calcd for $C_{19}H_{25}N_4O_4$ $[M+H]^+$: 373.1; found: 373.1.

**(±) *N*-(1-((2-amino-2-oxoethyl)amino)-4-methyl-1-oxopentan-2-yl)-2-(1*H*-pyrazol-1-yl)benzamide (43b).** Purified by column chromatography (DCM/MeOH 94:6). Yield: 99%. Mp: 174 – 175 ºC. $^1$H NMR (300 MHz, $CDCl_3$) $\delta$ (ppm): 7.81 (d, *J* = 2.4 Hz, 1H), 7.72 (s, 1H), 7.68 (d, *J* = 7.4 Hz, 1H), 7.58 (t, *J* = 7.7 Hz, 1H), 7.49 (t, *J* = 7.2 Hz, 1H), 7.40 (d, *J* = 7.9 Hz, 1H), 6.64 (s, 1H), 6.55 – 6.46 (m, 2H), 5.32 (s, 1H), 4.43 – 4.32 (m, 1H), 4.08 (dd, *J* = 17.1, 6.8 Hz, 1H), 3.84 (dd, *J* = 17.0, 5.7 Hz, 1H), 1.86 – 1.42 (m, 3H), 0.94 (t, *J* = 5.9 Hz, 6H). LRMS (CI) *m/*z calcd for $C_{18}H_{24}N_5O_3$ $[M+H]^+$: 358.1; found: 358.2.

**(±) methyl *N*-methyl-*N*-picolinoylleucylglycinate (44a).** Purified by column chromatography (DCM/MeOH 97:3). Yield: 35%. Oil at room temperature. $^1$H NMR (300 MHz, $CDCl_3$) $\delta$ (ppm): 9.50 (s, 1H), 8.68 – 8.62 (m, 1H), 7.91 – 7.83 (m, 1H), 7.81 – 7.74 (m, 1H), 7.46 – 7.38 (m, 1H), 4.61 (dd, *J* = 10.3, 4.8 Hz, 1H), 4.31 – 4.19 (m, 1H), 4.03 – 3.93 (m, 1H), 3.75 (s, 3H), 2.93 (s, 3H), 1.88 – 1.72 (m, 1H), 1.52 – 1.27 (m, 1H), 0.98 – 0.92 (m, 1H), 0.79 (d, *J* = 6.4 Hz, 3H), 0.47 (d, *J* = 6.3 Hz, 3H). $^{13}$C NMR (75 MHz, $CDCl_3$), δ (ppm): 170.7, 170.4, 168.8, 147.4, 138.1, 125.3, 125.0, 58.3, 52.2, 41.5, 36.0, 29.0, 24.0, 23.1, 21.4. LRMS (CI) *m/*z calcd for $C_{16}H_{24}N_3O_4$ $[M+H]^+$: 322.1; found: 322.1.

USC UNIVERSIDADE DE SANTIAGO DE COMPOSTELA

**(±) *N*-(1-((2-amino-2-oxoethyl)amino)-4-methyl-1-oxopentan-2-yl)-*N*-methylpicolinamide (44b).** Purified by column chromatography (DCM/MeOH 94:6). Yield: 99%. Oil at room temperature. $^{1}$H NMR (300 MHz, $CDCl_3$) $\delta$ (ppm): 9.30 (t, $J$ = 5.5 Hz, 1H), 8.60 (d, $J$ = 5.2 Hz, 1H), 7.86 (t, $J$ = 7.7 Hz, 1H), 7.76 (d, $J$ = 7.7 Hz, 1H), 7.43 – 7.36 (m, 1H), 6.69 (s, 1H), 6.10 (s, 1H), 4.61 (dd, $J$ = 10.5, 4.6 Hz, 1H), 4.26 – 4.15 (m, 1H), 3.90 – 3.81 (m, 1H), 2.94 (s, 3H), 1.87 – 1.71 (m, 1H), 1.55 – 1.26 (m, 1H), 0.95 (t, $J$ = 7.0 Hz, 1H), 0.81 (d, $J$ = 6.5 Hz, 3H), 0.47 (d, $J$ = 6.4 Hz, 3H). LRMS (CI) *m/*z calcd for $C_{15}H_{23}N_4O_3$ $[M+H]^+$: 307.1; found: 307.2.

**(±) methyl ((3*S*)-2-hydroxy-5-methyl-3-((*S*)-pyrrolidine-2-carboxamido)hexanoyl)glycinate (45a).** Purified by column chromatography (DCM/MeOH 97:3). Yield: 42%. Mp: 90 – 92 ºC. $^{1}$H NMR (300 MHz, MeOD) $\delta$ (ppm): 4.13 – 3.91 (m, 2H), 3.84 (dd, $J$ = 13.0, 5.6 Hz, 2H), 3.57 (d, $J$ = 8.3 Hz, 3H), 3.26 – 3.01 (m, 3H), 2.25 – 2.11 (m, 1H), 1.90 – 1.68 (m, 3H), 1.52 – 1.01 (m, 3H), 0.83 – 0.65 (m, 6H). $^{13}$C NMR (75 MHz, MeOD), δ (ppm): 174.4, 170.6, 170.3, 73.0, 59.7, 52.0, 46.1, 40.3, 39.5, 29.9, 24.5, 24.3, 23.0, 22.5, 21.4, 20.7. LRMS (CI) *m/*z calcd for $C_{15}H_{28}N_3O_5$ $[M+H]^+$: 330.1; found: 330.2.

**(±) (2*S*)-*N*-((3*S*)-1-((2-amino-2-oxoethyl)amino)-2-hydroxy-5-methyl-1-oxohexan-3-yl)pyrrolidine-2-carboxamide (45b).** Purified by column chromatography (DCM/MeOH 94:6). Yield: 99%. Oil at room temperature. $^{1}$H NMR (300 MHz, MeOD) $\delta$ (ppm): 4.26 – 4.13 (m, 1H), 4.03 – 3.77 (m, 2H), 3.66 – 3.54 (m, 2H), 2.75 – 2.56 (m, 2H), 2.16 – 2.01 (m, 1H), 1.82 – 1.58 (m, 3H), 1.42 – 0.91 (m, 3H), 0.61 (dt, $J$ = 18.1, 6.4 Hz, 6H). LRMS (CI) *m/*z calcd for $C_{14}H_{27}N_4O_4$ $[M+H]^+$: 315.1; found: 315.1.

**(±) methyl ((3*R*)-2-hydroxy-5-methyl-3-((*S*)-pyrrolidine-2-carboxamido)hexanoyl)glycinate (46a).** Purified by column chromatography (DCM/MeOH 97:3). Yield: 50%. Mp: 81 – 82 ºC. $^{1}$H NMR (300 MHz, MeOD) $\delta$ (ppm): 4.19 – 3.71 (m, 3H), 3.58 – 3.48 (m, 4H), 3.19 – 3.05 (m, 3H), 2.27 – 2.10 (m, 1H), 2.02 – 1.67 (m, 3H), 1.49 – 0.95 (m, 3H), 0.80 – 0.60 (m, 6H). LRMS (CI) *m/*z calcd for $C_{15}H_{28}N_3O_5$ $[M+H]^+$: 330.1; found: 330.2.

USC UNIVERSIDADE DE SANTIAGO DE COMPOSTELA

**(±) (2*S*)-*N*-((3*R*)-1-((2-amino-2-oxoethyl)amino)-2-hydroxy-5-methyl-1-oxohexan-3-yl)pyrrolidine-2-carboxamide (46b).** Purified by column chromatography (DCM/MeOH 94:6). Yield: 99%. Oil at room temperature. $^{1}$H NMR (300 MHz, MeOD) $\delta$ (ppm): 4.52 – 3.45 (m, 5H), 3.40 – 3.33 (m, 1H), 2.81 – 2.59 (m, 1H), 2.49 – 2.29 (m, 1H), 2.09 – 1.87 (m, 3H), 1.68 – 1.38 (m, 3H), 1.03 – 0.82 (m, 6H). $^{13}$C NMR (75 MHz, MeOD), δ (ppm): 174.3, 172.5, 172.2, 73.6, 72.8, 41.1, 41.0, 40.2, 24.8, 24.6, 22.5, 22.1, 20.9, 20.2. LRMS (CI) *m/*z calcd for $C_{14}H_{27}N_4O_4$ $[M+H]^+$: 315.1; found: 315.1.

**(±) methyl ((3*S*)-2-hydroxy-5-methyl-3-(picolinamido)hexanoyl)glycinate (47a).** Purified by column chromatography (DCM/MeOH 97:3). Yield: 69%. Mp: 117 – 118 ºC. $^{1}$H NMR (300 MHz, $CDCl_3$) $\delta$ (ppm): 8.63 (d, *J* = 8.9 Hz, 0.5H), 8.58 – 8.52 (m, 1H), 8.36 (d, *J* = 7.7 Hz, 0.5H), 8.13 (t, *J* = 8.3 Hz, 1H), 7.83 (q, *J* = 7.4 Hz, 1H), 7.58 – 7.37 (m, 2H), 4.45 – 4.25 (m, 2H), 4.12 – 3.95 (m, 2H), 3.63 (d, *J* = 16.3 Hz, 3H), 2.01 – 1.76 (m, 1H), 1.74 – 1.39 (m, 2H), 0.93 (q, *J* = 6.3 Hz, 6H). LRMS (CI) *m/*z calcd for $C_{16}H_{24}N_3O_5$ $[M+H]^+$: 338.1; found: 338.3.

**(±) *N*-((3*S*)-1-((2-amino-2-oxoethyl)amino)-2-hydroxy-5-methyl-1-oxohexan-3-yl)picolinamide (47b).** Purified by column chromatography (DCM/MeOH 94:6). Yield: 99%. Oil at room temperature. $^{1}$H NMR (300 MHz, $CDCl_3$) $\delta$ (ppm): 8.56 (s, 1H), 8.54 – 8.29 (m, 1H), 8.12 (dd, *J* = 18.2, 7.8 Hz, 1H), 7.92 – 7.80 (m, 1H), 7.57 (s, 1H), 7.46 (s, 1H), 6.45 (s, 1H), 6.09 (s, 1H), 5.67 – 5.60 (m, 1H), 5.35 – 5.23 (m, 1H), 4.48 – 4.22 (m, 1H), 4.07 – 3.81 (m, 2H), 2.10 – 1.85 (m, 1H), 1.75 – 1.63 (m, 2H), 0.95 (dd, *J* = 11.1, 6.4 Hz, 6H). LRMS (CI) *m/*z calcd for $C_{15}H_{23}N_4O_4$ $[M+H]^+$: 323.1; found: 323.2.

**(±) methyl ((3*R*)-2-hydroxy-5-methyl-3-(picolinamido)hexanoyl)glycinate (48a).** Purified by column chromatography (DCM/MeOH 97:3). Yield: 66%. Oil at room temperature. $^{1}$H NMR (300 MHz, $CDCl_3$) $\delta$ (ppm): 8.63 (d, *J* = 9.2 Hz, 1H), 8.57 – 8.46 (m, 1H), 8.35 (d, *J* = 7.9 Hz, 0H), 8.09 (t, *J* = 7.0 Hz, 1H), 7.85 – 7.72 (m, 1H), 7.69 – 7.59 (m, 1H), 7.43 – 7.32 (m, 1H), 5.73 (d, *J* = 74.6 Hz, 1H), 4.53 – 4.24 (m, 2H), 4.04 – 3.94 (m, 2H), 3.64 (s, 1H), 3.57 (s, 2H), 1.94 – 1.21 (m, 3H), 0.97 – 0.82 (m, 6H). $^{13}$C NMR (75 MHz, $CDCl_3$), δ (ppm): 173.4, 172.3, 170.0, 169.9, 165.8, 165.1, 149.3, 149.1, 148.3, 148.2, 137.4, 137.2, 126.4, 126.2, 122.2, 75.2, 73.8, 52.7, 52.1, 51.4, 40.8, 38.8, 37.6, 24.8, 23.4, 23.2, 21.9, 21.4. LRMS (CI) *m/*z calcd for $C_{16}H_{24}N_3O_5$ $[M+H]^+$: 338.1; found: 338.3.

USC UNIVERSIDADE DE SANTIAGO DE COMPOSTELA

**(±) *N*-((3*R*)-1-((2-amino-2-oxoethyl)amino)-2-hydroxy-5-methyl-1-oxohexan-3-yl)picolinamide (48b).** Purified by column chromatography (DCM/MeOH 94:6). Yield: 99%. Oil at room temperature. $^{1}$H NMR (300 MHz, $CDCl_3$) $\delta$ (ppm): 8.61 – 8.29 (m, 2H), 8.21 – 7.68 (m, 2H), 7.38 (bs, 1H), 6.91 (bs, 1H), 6.30 (bs, 1H), 5.80 (bs, 1H), 4.66 – 4.19 (m, 2H), 4.05 – 3.54 (m, 2H), 3.47 (s, 1H), 2.41 – 2.19 (m, 1H), 1.89 – 1.22 (m, 2H), 0.99 – 0.80 (m, 6H). LRMS (CI) *m/*z calcd for $C_{15}H_{23}N_4O_4$ $[M+H]^+$: 323.1; found: 323.2.

**(±) methyl ((3*S*)-3-(furan-3-carboxamido)-2-hydroxy-5-methylhexanoyl)glycinate (49a).** Purified by column chromatography (DCM/MeOH 97:3). Yield: 49%. Oil at room temperature. $^{1}$H NMR (300 MHz, $CDCl_3$) $\delta$ (ppm): 7.97 (d, $J$ = 14.2 Hz, 1H), 7.69 (t, $J$ = 5.9 Hz, 1H), 7.49 (d, $J$ = 8.8 Hz, 1H), 7.40 – 7.35 (m, 1H), 6.70 (dd, $J$ = 14.4, 1.9 Hz, 1H), 5.27 (s, 1H), 4.42 – 4.08 (m, 2H), 3.99 (d, $J$ = 5.7 Hz, 2H), 3.68 (d, $J$ = 12.6 Hz, 3H), 1.80 – 1.31 (m, 3H), 0.92 – 0.82 (m, 6H). $^{13}$C NMR (75 MHz, $CDCl_3$), δ (ppm): 173.9, 169.7, 163.8, 145.3, 143.7, 122.2, 108.5, 73.7, 52.3, 51.7, 40.7, 37.9, 24.9, 23.3, 21.7. LRMS (CI) *m/*z calcd for $C_{15}H_{23}N_2O_6$ $[M+H]^+$: 327.1; found: 327.1.

**(±) *N*-((3*S*)-1-((2-amino-2-oxoethyl)amino)-2-hydroxy-5-methyl-1-oxohexan-3-yl)furan-3-carboxamide (49b).** Purified by column chromatography (DCM/MeOH 94:6). Yield: 99%. Mp: 78 – 79 ºC. $^{1}$H NMR (300 MHz, MeOD) $\delta$ (ppm): 8.08 (d, $J$ = 10.8 Hz, 1H), 7.58 – 7.50 (m, 1H), 6.90 – 6.75 (m, 1H), 4.64 – 4.46 (m, 1H), 4.26 – 4.10 (m, 1H), 3.99 – 3.71 (m, 2H), 1.76 – 1.54 (m, 2H), 1.52 – 1.19 (m, 1H), 1.04 – 0.84 (m, 6H). $^{13}$C NMR (75 MHz, MeOD), δ (ppm): 178.4, 176.7, 176.5, 167.5, 149.2, 147.7, 126.1, 112.3, 77.9, 77.1, 54.4, 54.0, 45.4, 45.2, 43.7, 41.1, 28.6, 28.5, 26.2, 24.9. LRMS (CI) *m/*z calcd for $C_{14}H_{22}N_3O_5$ $[M+H]^+$: 312.1; found: 312.2.

**(±) methyl ((3*R*)-3-(furan-3-carboxamido)-2-hydroxy-5-methylhexanoyl)glycinate (50a).** Purified by column chromatography (DCM/MeOH 97:3). Yield: 65%. Oil at room temperature. $^{1}$H NMR (300 MHz, $CDCl_3$) $\delta$ (ppm): 7.97 (d, $J$ = 14.0 Hz, 1H), 7.76 (dt, $J$ = 23.8, 6.0 Hz, 1H), 7.44 – 7.31 (m, 2H), 6.73 – 6.60 (m, 1H), 5.21 (d, $J$ = 4.9 Hz, 1H), 4.50 – 4.28 (m, 1H), 4.23 – 4.17 (m, 1H), 4.16 – 3.79 (m, 2H), 3.73 – 3.59 (m, 3H), 1.87 – 1.27 (m, 3H), 0.96 – 0.81 (m, 6H). $^{13}$C NMR (75 MHz, $CDCl_3$), δ (ppm): 174.1, 170.5, 170.0, 163.7, 145.5, 145.3, 143.6, 122.1, 122.0, 108.6, 108.5, 73.8, 52.4, 52.2, 51.2, 50.9, 40.7, 38.5, 38.1, 24.8, 23.2, 21.7, 21.5. LRMS (CI) *m/*z calcd for $C_{15}H_{23}N_2O_6$ $[M+H]^+$: 327.1; found: 327.1.

USC UNIVERSIDADE DE SANTIAGO DE COMPOSTELA

**(±) *N*-((3*R*)-1-((2-amino-2-oxoethyl)amino)-2-hydroxy-5-methyl-1-oxohexan-3-yl)furan-3-carboxamide (50b).** Purified by column chromatography (DCM/MeOH 94:6). Yield: 99%. Oil at room temperature. $^1$H NMR (300 MHz, MeOD) $\delta$ (ppm): 8.08 (d, $J$ = 10.9 Hz, 1H), 7.57 – 7.50 (m, 1H), 6.82 (d, $J$ = 16.9 Hz, 1H), 4.61 – 4.49 (m, 1H), 4.21 (d, $J$ = 3.9 Hz, 0.5H), 4.12 (d, $J$ = 2.6 Hz, 0.5H), 3.98 – 3.72 (m, 2H), 1.76 – 1.56 (m, 2H), 1.54 – 1.14 (m, 1H), 1.02 – 0.86 (m, 6H). LRMS (CI) *m/*z calcd for $C_{14}H_{22}N_3O_5$ $[M+H]^+$: 312.1; found: 312.2.

**methyl ((*S*)-5-methyl-2-oxo-3-((*S*)-pyrrolidine-2-carboxamido)hexanoyl)glycinate (51a).** Purified by column chromatography (DCM/MeOH 99:1). Yield: 76%. Mp: 182 – 183 ºC. $^1$H NMR (300 MHz, $CDCl_3$) $\delta$ (ppm): 7.72 (dd, $J$ = 16.3, 7.4 Hz, 1H), 7.45 – 7.29 (m, 1H), 6.92 (s, 1H), 4.21 (dd, $J$ = 18.4, 6.4 Hz, 1H), 4.02 (dd, $J$ = 18.4, 5.0 Hz, 1H), 3.76 (s, 3H), 3.77 – 3.52 (m, 2H), 3.40 (t, $J$ = 6.5 Hz, 1H), 2.83 – 2.53 (m, 4H), 2.49 – 2.08 (m, 1H), 1.95 – 1.74 (m, 2H), 1.71 – 1.45 (m, 1H), 1.02 – 0.89 (m, 6H). LRMS (CI) *m/*z calcd for $C_{15}H_{26}N_3O_5$ $[M+H]^+$: 328.1; found: 328.1.

**(*S*)-*N*-((*S*)-1-((2-amino-2-oxoethyl)amino)-5-methyl-1,2-dioxohexan-3-yl)pyrrolidine-2-carboxamide (51b).** Purified by column chromatography (DCM/MeOH 96:4). Yield: 99%. Mp: 174 – 175 ºC. $^1$H NMR (300 MHz, MeOD) $\delta$ (ppm): 4.02 – 3.82 (m, 2H), 3.67 (d, $J$ = 7.9 Hz, 1H), 3.48 – 3.38 (m, 1H), 3.33 – 3.28 (m, 1H), 2.95 (dd, $J$ = 13.6, 8.8 Hz, 1H), 2.58 (q, $J$ = 9.1, 8.7 Hz, 1H), 2.52 – 2.41 (m, 1H), 2.32 (dd, $J$ = 13.5, 6.3 Hz, 1H), 2.26 – 2.09 (m, 1H), 2.03 – 1.82 (m, 1H), 1.82 – 1.67 (m, 2H), 0.95 (d, $J$ = 6.6 Hz, 3H), 0.88 (d, $J$ = 6.7 Hz, 3H). LRMS (CI) *m/*z calcd for $C_{14}H_{25}N_4O_4$ $[M+H]^+$: 313.1; found: 313.3.

**methyl ((*R*)-5-methyl-2-oxo-3-((*S*)-pyrrolidine-2-carboxamido)hexanoyl)glycinate (52a).** Purified by column chromatography (DCM/MeOH 99:1). Yield: 64%. Mp: 169 – 170 ºC. $^1$H NMR (300 MHz, $CDCl_3$) $\delta$ (ppm): 7.49 – 7.34 (m, 1H), 7.02 – 6.92 (m, 1H), 4.21 (dd, $J$ = 18.3, 6.4 Hz, 1H), 4.01 (dd, $J$ = 18.4, 5.1 Hz, 1H), 3.76 (s, 3H), 3.75 – 3.63 (m, 2H), 3.47 – 3.35 (m, 1H), 2.82 – 2.70 (m, 1H), 2.68 – 2.51 (m, 4H), 2.29 – 2.11 (m, 1H), 1.98 – 1.75 (m, 2H), 0.95 (dd, $J$ = 17.0, 6.6 Hz, 6H). LRMS (CI) *m/*z calcd for $C_{15}H_{26}N_3O_5$ $[M+H]^+$: 328.1; found: 328.1.

USC UNIVERSIDADE DE SANTIAGO DE COMPOSTELA

**(*S*)-*N*-((*R*)-1-((2-amino-2-oxoethyl)amino)-5-methyl-1,2-dioxohexan-3-yl)pyrrolidine-2-carboxamide (52b).** Purified by column chromatography (DCM/MeOH 96:4). Yield: 99%. Mp: 173 – 174 ºC. $^1$H NMR (300 MHz, MeOD) $\delta$ (ppm): 4.01 – 3.83 (m, 2H), 3.67 (d, *J* = 8.3 Hz, 1H), 3.49 – 3.36 (m, 1H), 3.34 – 3.26 (m, 1H), 2.95 (dd, *J* = 13.4, 8.7 Hz, 1H), 2.60 (t, *J* = 8.4 Hz, 1H), 2.57 – 2.41 (m, 1H), 2.32 (dd, *J* = 13.5, 6.3 Hz, 1H), 2.26 – 2.12 (m, 1H), 2.03 – 1.65 (m, 3H), 0.95 (d, *J* = 6.6 Hz, 3H), 0.88 (d, *J* = 6.8 Hz, 3H). LRMS (CI) *m/*z calcd for $C_{14}H_{25}N_4O_4$ $[M+H]^+$: 313.1; found: 313.3.

**methyl (*S*)-(5-methyl-2-oxo-3-(picolinamido)hexanoyl)glycinate (53a).** Purified by column chromatography (DCM/MeOH 99:1). Yield: 77%. Mp: 140 – 141 ºC. $^1$H NMR (300 MHz, $CDCl_3$) $\delta$ (ppm): 8.57 (dd, *J* = 12.8, 5.0 Hz, 1H), 8.44 (d, *J* = 8.2 Hz, 1H), 8.19 – 8.07 (m, 1H), 7.88 – 7.79 (m, 1H), 7.50 – 7.37 (m, 2H), 5.67 – 5.47 (m, 1H), 4.21 – 4.00 (m, 2H), 3.77 (s, 3H), 1.97 – 1.53 (m, 3H), 1.12 – 0.83 (m, 6H). LRMS (CI) *m/*z calcd for $C_{16}H_{22}N_3O_5$ $[M+H]^+$: 336.1; found: 336.2.

**(*S*)-*N*-(1-((2-amino-2-oxoethyl)amino)-5-methyl-1,2-dioxohexan-3-yl)picolinamide (53b).** Purified by column chromatography (DCM/MeOH 96:4). Yield: 99%. Oil at room temperature. $^1$H NMR (300 MHz, $CDCl_3$) $\delta$ (ppm): 8.59 (s, 1H), 8.50 – 8.40 (m, 1H), 8.24 – 8.07 (m, 1H), 7.93 – 7.77 (m, 1H), 7.55 – 7.36 (m, 1H), 7.21 – 7.01 (m, 1H), 5.62 – 5.36 (m, 1H), 4.60 – 3.75 (m, 2H), 1.92 – 1.54 (m, 3H), 1.00 (td, *J* = 15.1, 14.7, 7.6 Hz, 6H). LRMS (CI) *m/*z calcd for $C_{15}H_{21}N_4O_4$ $[M+H]^+$: 321.1; found: 321.1.

**methyl (*R*)-(5-methyl-2-oxo-3-(picolinamido)hexanoyl)glycinate (54a).** Purified by column chromatography (DCM/MeOH 99:1). Yield: 75%. Mp: 94 – 95 ºC. $^1$H NMR (300 MHz, $CDCl_3$) $\delta$ (ppm): 8.58 (d, *J* = 4.8 Hz, 1H), 8.44 (d, *J* = 8.0 Hz, 1H), 8.13 (d, *J* = 7.8 Hz, 1H), 7.83 (td, *J* = 7.8, 1.7 Hz, 1H), 7.51 – 7.40 (m, 2H), 5.64 – 5.50 (m, 1H), 4.22 – 3.97 (m, 2H), 3.76 (s, 3H), 1.92 – 1.73 (m, 2H), 1.68 – 1.55 (m, 1H), 1.04 (d, *J* = 5.9 Hz, 3H), 0.96 (d, *J* = 6.1 Hz, 3H). $^{13}$C NMR (75 MHz, $CDCl_3$), δ (ppm): 195.6, 169.1, 164.2, 159.3, 149.2, 148.3, 137.3, 126.4, 122.4, 52.9, 52.6, 40.9, 40.4, 25.4, 23.2, 21.4. LRMS (CI) *m/*z calcd for $C_{16}H_{22}N_3O_5$ $[M+H]^+$: 336.1; found: 336.2.

USC UNIVERSIDADE DE SANTIAGO DE COMPOSTELA

**(*R*)-*N*-(1-((2-amino-2-oxoethyl)amino)-5-methyl-1,2-dioxohexan-3-yl)picolinamide (54b).** Purified by column chromatography (DCM/MeOH 96:4). Yield: 99%. Mp: 104 – 106 ºC. $^{1}$H NMR (300 MHz, $CDCl_3$) $\delta$ (ppm): 8.59 (d, $J$ = 5.1 Hz, 1H), 8.44 (d, $J$ = 6.2 Hz, 1H), 8.10 (d, $J$ = 7.9 Hz, 1H), 7.84 (t, $J$ = 7.6 Hz, 1H), 7.57 – 7.40 (m, 2H), 6.24 (bs, 1H), 5.56 (bs, 1H), 5.51 – 5.40 (m, 1H), 4.14 – 4.03 (m, 1H), 4.02 – 3.91 (m, 1H), 1.95 – 1.58 (m, 3H), 1.09 – 0.88 (m, 6H). LRMS (CI) *m/*z calcd for $C_{15}H_{20}N_4O_4$ $[M+H]^+$: 321.1; found: 321.1. LRMS (CI) *m/*z calcd for $C_{15}H_{21}N_2O_6$ $[M+H]^+$: 325.1; found: 325.1.

**methyl (*S*)-(3-(furan-3-carboxamido)-5-methyl-2-oxohexanoyl)glycinate (55a).** Purified by column chromatography (DCM/MeOH 99:1). Yield: 60%. Oil at room temperature. $^{1}$H NMR (300 MHz, $CDCl_3$) $\delta$ (ppm): 7.95 (s, 1H), 7.62 (q, $J$ = 6.0 Hz, 1H), 7.37 (d, $J$ = 2.1 Hz, 1H), 6.87 (d, $J$ = 7.8 Hz, 1H), 6.72 – 6.59 (m, 1H), 5.44 – 5.32 (m, 1H), 4.16 – 3.95 (m, 2H), 3.72 (s, 3H), 1.79 – 1.65 (m, 2H), 1.51 (p, $J$ = 9.2 Hz, 1H), 1.02 – 0.79 (m, 6H). $^{13}$C NMR (75 MHz, $CDCl_3$), δ (ppm): 195.7, 169.2, 162.6, 159.7, 145.3, 143.7, 121.8, 108.4, 53.2, 52.5, 40.9, 40.1, 25.2, 23.1, 21.4. LRMS (CI) *m/*z calcd for $C_{15}H_{21}N_2O_6$ $[M+H]^+$: 325.1; found: 325.2.

**(*S*)-*N*-(1-((2-amino-2-oxoethyl)amino)-5-methyl-1,2-dioxohexan-3-yl)furan-3-carboxamide (55b).** Purified by column chromatography (DCM/MeOH 96:4). Yield: 99%. Oil at room temperature. $^{1}$H NMR (300 MHz, MeOD) $\delta$ (ppm): 8.15 – 8.03 (m, 1H), 7.62 – 7.50 (m, 1H), 6.88 – 6.78 (m, 1H), 4.65 – 4.26 (m, 1H), 4.11 – 3.63 (m, 2H), 1.85 – 1.43 (m, 3H), 1.05 – 0.88 (m, 6H). LRMS (CI) *m/*z calcd for $C_{14}H_{20}N_3O_5$ $[M+H]^+$: 310.1; found: 310.2.

**methyl (*R*)-(3-(furan-3-carboxamido)-5-methyl-2-oxohexanoyl)glycinate (56a).** Purified by column chromatography (DCM/MeOH 99:1). Yield: 75%. Oil at room temperature. $^{1}$H NMR (300 MHz, $CDCl_3$) $\delta$ (ppm): 7.95 (s, 1H), 7.60 – 7.46 (m, 1H), 7.40 (s, 1H), 6.67 – 6.57 (m, 2H), 5.49 – 5.36 (m, 1H), 4.20 – 3.95 (m, 2H), 3.75 (s, 3H), 1.81 – 1.66 (m, 2H), 1.64 – 1.45 (m, 1H), 1.03 – 0.82 (m, 6H). $^{13}$C NMR (75 MHz, $CDCl_3$), δ (ppm): 195.6, 169.2, 162.5, 159.5, 145.2, 143.8, 121.8, 108.4, 53.2, 52.6, 40.9, 40.4, 25.3, 23.1, 21.5. LRMS (CI) *m/*z calcd for $C_{15}H_{21}N_2O_6$ $[M+H]^+$: 325.1; found: 325.2.

USC UNIVERSIDADE DE SANTIAGO DE COMPOSTELA

**(*R*)-*N*-(1-((2-amino-2-oxoethyl)amino)-5-methyl-1,2-dioxohexan-3-yl)furan-3-carboxamide (56b).** Purified by column chromatography (DCM/MeOH 96:4). Yield: 99%. Oil at room temperature. $^{1}$H NMR (300 MHz, MeOD) $\delta$ (ppm): 8.08 (d, $J$ = 10.7 Hz, 1H), 7.60 – 7.49 (m, 1H), 6.88 – 6.77 (m, 1H), 4.61 – 4.32 (m, 1H), 4.07 – 3.68 (m, 2H), 1.83 – 1.42 (m, 3H), 1.04 – 0.87 (m, 6H). LRMS (CI) *m/*z calcd for $C_{14}H_{20}N_3O_5$ $[M+H]^+$: 310.1; found: 310.2.

USC UNIVERSIDADE DE SANTIAGO DE COMPOSTELA

### 5.2.3 Statistical analysis: One sample t-test for all compounds described

This section shows the results of the one-sample t-test conducted in the biological results of Chapter I to evaluate the impact of the compounds on dopamine activity at 0.1 µM. The test was performed using GraphPad Prism 10.1.0, set at a 90% confidence level, and was used to determine if the observed dopamine activity changes were significantly different from zero, which would indicate no compound effect. This statistical approach is pivotal for confirming that any dopamine activity changes are due to the compounds rather than random variability.

Table 5.1. One sample t-test for **Series I** at 0.01 nM.

| Compound | Actual mean | t, df | P value (two tailed) | P value summary | Significant (alpha=0.1) | 90% confidence interval |
|---|---|---|---|---|---|---|
| **1a** | 5,22 | t=1,322, df=2 | 0,3172 | ns | No | -6,311 to 16,75 |
| **2a** | 3,54 | t=0,7396, df=2 | 0,5366 | ns | No | -10,44 to 17,52 |
| **3a** | 3,56 | t=0,4534, df=2 | 0,6947 | ns | No | -19,37 to 26,49 |
| **4a** | 9,31 | t=28,29, df=2 | 0,0012 | ** | Yes | 8,349 to 10,27 |
| **1b** | -7,6 | t=1,187, df=2 | 0,3571 | ns | No | -26,30 to 11,10 |
| **2b** | 5,68 | t=0,6298, df=2 | 0,5932 | ns | No | -20,65 to 32,01 |
| **3b** | -2,16 | t=0,3993, df=2 | 0,7283 | ns | No | -17,96 to 13,64 |
| **4b** | -8,65 | t=49,94, df=2 | 0,0004 | *** | Yes | -9,156 to -8,144 |
| **5a** | 11,26 | t=162,5, df=2 | <0,0001 | **** | Yes | 11,06 to 11,46 |
| **6a** | -12,89 | t=5,086, df=2 | 0,0366 | * | Yes | -20,29 to -5,489 |
| **7a** | -3,37 | t=0,6764, df=2 | 0,5685 | ns | No | -17,92 to 11,18 |
| **8a** | 6 | t=0,7843, df=2 | 0,515 | ns | No | -16,34 to 28,34 |
| **5b** | 22,04 | t=3,657, df=2 | 0,0673 | ns | Yes | 4,440 to 39,64 |
| **6b** | -2,7 | t=3,248, df=2 | 0,0832 | ns | Yes | -5,128 to -0,2724 |
| **7b** | 13,7 | t=56,50, df=2 | 0,0003 | *** | Yes | 12,99 to 14,41 |
| **8b** | -8,4 | t=1,422, df=2 | 0,2909 | ns | No | -25,65 to 8,846 |
| **17** | 40,02 | t=18,53, df=2 | 0,0029 | ** | Yes | 33,71 to 46,33 |
| **18** | 14,9 | t=9,453, df=2 | 0,011 | * | Yes | 10,30 to 19,50 |
| **19** | 20,03 | t=8,988, df=2 | 0,0122 | * | Yes | 13,52 to 26,54 |
| **20** | 17,57 | t=2,665, df=2 | 0,1167 | ns | No | -1,682 to 36,82 |

USC UNIVERSIDADE DE SANTIAGO DE COMPOSTELA

Table 5.2. One sample t-test for **Series I** at 1 nM.

| Compound | Actual mean | t, df | P value (two tailed) | P value summary | Significant (alpha=0.1) | 90% confidence interval |
|---|---|---|---|---|---|---|
| **1a** | 22,32 | t=8,350, df=2 | 0,014 | * | Yes | 14,51 to 30,13 |
| **2a** | -11,65 | t=20,38, df=2 | 0,0024 | ** | Yes | -13,32 to -9,981 |
| **3a** | -0,84 | t=1,244, df=2 | 0,3397 | ns | No | -2,812 to 1,132 |
| **4a** | 11,32 | t=3,398, df=2 | 0,0768 | ns | Yes | 1,593 to 21,05 |
| **1b** | 6,15 | t=0,6811, df=2 | 0,5661 | ns | No | -20,22 to 32,52 |
| **2b** | -12,67 | t=2,051, df=2 | 0,1767 | ns | No | -30,71 to 5,369 |
| **3b** | 19,23 | t=6,226, df=2 | 0,0248 | * | Yes | 10,21 to 28,25 |
| **4b** | 14,02 | t=4,916, df=2 | 0,039 | * | Yes | 5,692 to 22,35 |
| **5a** | 12,23 | t=3,384, df=2 | 0,0773 | ns | Yes | 1,677 to 22,78 |
| **6a** | 5,33 | t=0,9759, df=2 | 0,432 | ns | No | -10,62 to 21,28 |
| **7a** | -1,3 | t=0,2671, df=2 | 0,8144 | ns | No | -15,51 to 12,91 |
| **8a** | 10,79 | t=155,7, df=2 | <0,0001 | **** | Yes | 10,59 to 10,99 |
| **5b** | 16,39 | t=5,247, df=2 | 0,0345 | * | Yes | 7,270 to 25,51 |
| **6b** | -5 | t=4,066, df=2 | 0,0555 | ns | Yes | -8,591 to -1,409 |
| **7b** | -0,87 | t=0,2042, df=2 | 0,8571 | ns | No | -13,31 to 11,57 |
| **8b** | 10,13 | t=13,19, df=2 | 0,0057 | ** | Yes | 7,888 to 12,37 |
| **17** | 13,54 | t=2,756, df=2 | 0,1103 | ns | No | -0,8066 to 27,89 |
| **18** | -15,2 | t=1,504, df=2 | 0,2716 | ns | No | -44,72 to 14,32 |
| **19** | 5,65 | t=1,985, df=2 | 0,1856 | ns | No | -2,661 to 13,96 |
| **20** | -21,82 | t=2,854, df=2 | 0,1039 | ns | No | -44,14 to 0,5007 |

USC UNIVERSIDADE DE SANTIAGO DE COMPOSTELA

Table 5.3. One sample t-test for **Series II** at 0.01 nM.

| Compound | Actual mean | t, df | P value (two tailed) | P value summary | Significant (alpha=0.1) | 90% confidence interval |
|---|---|---|---|---|---|---|
| **9a** | -0,37 | t=0,06428, df=2 | 0,9546 | ns | No | -17,18 to 16,44 |
| **10a** | 19,3 | t=6,429, df=2 | 0,0234 | * | Yes | 10,53 to 28,07 |
| **11a** | -16,82 | t=2,492, df=2 | 0,1303 | ns | No | -36,53 to 2,888 |
| **12a** | -29,03 | t=4,682, df=2 | 0,0427 | * | Yes | -47,14 to -10,92 |
| **9b** | 7,06 | t=1,347, df=2 | 0,3104 | ns | No | -8,248 to 22,37 |
| **10b** | -30,05 | t=4,869, df=2 | 0,0397 | * | Yes | -48,07 to -12,03 |
| **11b** | 12,65 | t=2,521, df=2 | 0,1278 | ns | No | -2,000 to 27,30 |
| **12b** | 5,53 | t=0,7578, df=2 | 0,5277 | ns | No | -15,78 to 26,84 |
| **13a** | -8,86 | t=2,688, df=2 | 0,115 | ns | No | -18,49 to 0,7662 |
| **14a** | -10,51 | t=2,890, df=2 | 0,1018 | ns | No | -21,13 to 0,1109 |
| **15a** | 8 | t=1,593, df=2 | 0,2522 | ns | No | -6,667 to 22,67 |
| **16a** | 2,45 | t=0,9245, df=2 | 0,4528 | ns | No | -5,288 to 10,19 |
| **13b** | -12,15 | t=60,13, df=2 | 0,0003 | *** | Yes | -12,74 to -11,56 |
| **14b** | -11,55 | t=4,964, df=2 | 0,0383 | * | Yes | -18,34 to -4,756 |
| **15b** | 8,44 | t=1,789, df=2 | 0,2155 | ns | No | -5,333 to 22,21 |
| **16b** | -23,7 | t=4,064, df=2 | 0,0555 | ns | Yes | -40,73 to -6,673 |

USC UNIVERSIDADE DE SANTIAGO DE COMPOSTELA

Table 5.4. One sample t-test for **Series II** at 1 nM.

| Compound | Actual mean | t, df | P value (two tailed) | P value summary | Significant (alpha=0.1) | 90% confidence interval |
|---|---|---|---|---|---|---|
| **9a** | -17,77 | t=5,526, df=2 | 0,0312 | * | Yes | -27,16 to -8,380 |
| **10a** | 4,1 | t=2,185, df=2 | 0,1605 | ns | No | -1,379 to 9,579 |
| **11a** | -54,18 | t=11,00, df=2 | 0,0082 | ** | Yes | -68,56 to -39,80 |
| **12a** | -34,78 | t=5,364, df=2 | 0,033 | * | Yes | -53,71 to -15,85 |
| **9b** | -29,88 | t=9,308, df=2 | 0,0113 | * | Yes | -39,25 to -20,51 |
| **10b** | -0,01 | t=0,001484, df=2 | 0,999 | ns | No | -19,68 to 19,66 |
| **11b** | -20,77 | t=3,181, df=2 | 0,0862 | ns | Yes | -39,84 to -1,703 |
| **12b** | -11,88 | t=2,447, df=2 | 0,1342 | ns | No | -26,06 to 2,298 |
| **13a** | -22,79 | t=6,168, df=2 | 0,0253 | * | Yes | -33,58 to -12,00 |
| **14a** | -1,53 | t=0,6495, df=2 | 0,5826 | ns | No | -8,408 to 5,348 |
| **15a** | -18,03 | t=3,614, df=2 | 0,0687 | ns | Yes | -32,60 to -3,464 |
| **16a** | -7,54 | t=4,172, df=2 | 0,0529 | ns | Yes | -12,82 to -2,263 |
| **13b** | -0,87 | t=0,2903, df=2 | 0,7989 | ns | No | -9,620 to 7,880 |
| **14b** | 7,99 | t=4,352, df=2 | 0,049 | * | Yes | 2,629 to 13,35 |
| **15b** | 1,86 | t=0,9284, df=2 | 0,4512 | ns | No | -3,990 to 7,710 |
| **16b** | 4,23 | t=3,816, df=2 | 0,0623 | ns | Yes | 0,9932 to 7,467 |

USC UNIVERSIDADE DE SANTIAGO DE COMPOSTELA

Table 5.5. One sample t-test for **Series III-a** at 0.01 nM.

| Compound | Actual mean | t, df | P value (two tailed) | P value summary | Significant (alpha=0.1) | 90% confidence interval |
|---|---|---|---|---|---|---|
| **21a** | -3,56 | t=0,6045, df=2 | 0,6069 | ns | No | -20,76 to 13,64 |
| **22a** | -11,55 | t=5,466, df=2 | 0,0319 | * | Yes | -17,72 to -5,380 |
| **23a** | 1,36 | t=0,9856, df=2 | 0,4282 | ns | No | -2,669 to 5,389 |
| **24a** | -6,16 | t=1,228, df=2 | 0,3444 | ns | No | -20,81 to 8,490 |
| **25a** | 35,92 | t=4,150, df=2 | 0,0534 | ns | Yes | 10,65 to 61,19 |
| **26a** | 5,42 | t=1,771, df=2 | 0,2185 | ns | No | -3,515 to 14,36 |
| **27a** | 4,69 | t=0,8596, df=2 | 0,4806 | ns | No | -11,24 to 20,62 |
| **28a** | 15,84 | t=3,779, df=2 | 0,0634 | ns | Yes | 3,601 to 28,08 |
| **29a** | 15,44 | t=3,799, df=2 | 0,0628 | ns | Yes | 3,572 to 27,31 |
| **30a** | -2,2 | t=0,5679, df=2 | 0,6274 | ns | No | -13,51 to 9,112 |
| **31a** | 28,65 | t=8,846, df=2 | 0,0125 | * | Yes | 19,19 to 38,11 |
| **32a** | 21,41 | t=7,758, df=2 | 0,0162 | * | Yes | 13,35 to 29,47 |
| **33a** | -0,38 | t=0,1079, df=2 | 0,9239 | ns | No | -10,66 to 9,904 |
| **34a** | -4,84 | t=1,494, df=2 | 0,2737 | ns | No | -14,30 to 4,618 |
| **35a** | -5,61 | t=1,876, df=2 | 0,2015 | ns | No | -14,34 to 3,123 |
| **36a** | 13,85 | t=4,501, df=2 | 0,046 | * | Yes | 4,864 to 22,84 |
| **37a** | -4,82 | t=1,403, df=2 | 0,2957 | ns | No | -14,85 to 5,211 |
| **38a** | 2,03 | t=0,3640, df=2 | 0,7507 | ns | No | -14,26 to 18,32 |
| **39a** | 3,18 | t=0,7135, df=2 | 0,5496 | ns | No | -9,835 to 16,19 |
| **40a** | 4,15 | t=1,246, df=2 | 0,339 | ns | No | -5,577 to 13,88 |
| **41a** | -10,53 | t=1,978, df=2 | 0,1865 | ns | No | -26,07 to 5,014 |
| **42a** | -24,2 | t=6,040, df=2 | 0,0263 | * | Yes | -35,90 to -12,50 |
| **43a** | -32,13 | t=12,02, df=2 | 0,0069 | ** | Yes | -39,94 to -24,32 |
| **44a** | -31,77 | t=4,975, df=2 | 0,0381 | * | Yes | -50,42 to -13,12 |

USC UNIVERSIDADE DE SANTIAGO DE COMPOSTELA

Table 5.6. One sample t-test for **Series III-a** at 1 nM.

| Compound | Actual mean | t, df | P value (two tailed) | P value summary | Significant (alpha=0.1) | 90% confidence interval |
|---|---|---|---|---|---|---|
| **21a** | -2,75 | t=2,922, df=2 | 0,0999 | ns | Yes | -5,498 to -0,002057 |
| **22a** | -13,58 | t=2,951, df=2 | 0,0982 | ns | Yes | -27,02 to -0,1437 |
| **23a** | -15,7 | t=181,3, df=2 | <0,0001 | **** | Yes | -15,95 to -15,45 |
| **24a** | -2,41 | t=0,6980, df=2 | 0,5574 | ns | No | -12,49 to 7,671 |
| **25a** | 5,43 | t=2,300, df=2 | 0,1482 | ns | No | -1,465 to 12,33 |
| **26a** | -21,77 | t=5,901, df=2 | 0,0275 | * | Yes | -32,54 to -11,00 |
| **27a** | 26,92 | t=4,553, df=2 | 0,045 | * | Yes | 9,657 to 44,18 |
| **28a** | -12,68 | t=1,596, df=2 | 0,2515 | ns | No | -35,88 to 10,52 |
| **29a** | 22,63 | t=5,885, df=2 | 0,0277 | * | Yes | 11,40 to 33,86 |
| **30a** | -4,77 | t=0,5379, df=2 | 0,6445 | ns | No | -30,66 to 21,12 |
| **31a** | 32,87 | t=29,05, df=2 | 0,0012 | ** | Yes | 29,57 to 36,17 |
| **32a** | 29,54 | t=6,518, df=2 | 0,0227 | * | Yes | 16,31 to 42,77 |
| **33a** | -9,34 | t=1,669, df=2 | 0,237 | ns | No | -25,68 to 6,996 |
| **34a** | -14,07 | t=4,835, df=2 | 0,0402 | * | Yes | -22,57 to -5,573 |
| **35a** | -10,19 | t=2,382, df=2 | 0,1401 | ns | No | -22,68 to 2,302 |
| **36a** | -9,11 | t=2,182, df=2 | 0,1608 | ns | No | -21,30 to 3,079 |
| **37a** | 0,68 | t=0,2248, df=2 | 0,843 | ns | No | -8,154 to 9,514 |
| **38a** | -34,15 | t=13,95, df=2 | 0,0051 | ** | Yes | -41,30 to -27,00 |
| **39a** | 5,73 | t=10,56, df=2 | 0,0089 | ** | Yes | 4,145 to 7,315 |
| **40a** | 0,03 | t=0,01228, df=2 | 0,9913 | ns | No | -7,101 to 7,161 |
| **41a** | -37,09 | t=19,06, df=2 | 0,0027 | ** | Yes | -42,77 to -31,41 |
| **42a** | -49,51 | t=6,607, df=2 | 0,0222 | * | Yes | -71,39 to -27,63 |
| **43a** | -21,39 | t=5,530, df=2 | 0,0312 | * | Yes | -32,69 to -10,09 |
| **44a** | -44,7 | t=8,680, df=2 | 0,013 | * | Yes | -59,74 to -29,66 |

USC UNIVERSIDADE DE SANTIAGO DE COMPOSTELA

Table 5.7. One sample t-test for **Series III-b** at 0.01 nM.

| Compound | Actual mean | t, df | P value (two tailed) | P value summary | Significant (alpha=0.1) | 90% confidence interval |
|---|---|---|---|---|---|---|
| **21b** | 13,64 | t=2,949, df=2 | 0,0983 | ns | Yes | 0,1363 to 27,14 |
| **22b** | 7,98 | t=2,180, df=2 | 0,1611 | ns | No | -2,708 to 18,67 |
| **23b** | 0,16 | t=0,03725, df=2 | 0,9737 | ns | No | -12,38 to 12,70 |
| **24b** | 4,54 | t=2,299, df=2 | 0,1482 | ns | No | -1,226 to 10,31 |
| **25b** | 17,16 | t=3,440, df=2 | 0,0751 | ns | Yes | 2,594 to 31,73 |
| **26b** | -15,41 | t=2,989, df=2 | 0,0961 | ns | Yes | -30,46 to -0,3553 |
| **27b** | 14,02 | t=3,690, df=2 | 0,0662 | ns | Yes | 2,927 to 25,11 |
| **28b** | 16,98 | t=3,709, df=2 | 0,0656 | ns | Yes | 3,611 to 30,35 |
| **29b** | 37,29 | t=7,896, df=2 | 0,0157 | * | Yes | 23,50 to 51,08 |
| **30b** | 14,14 | t=16,55, df=2 | 0,0036 | ** | Yes | 11,64 to 16,64 |
| **31b** | 39,44 | t=5,413, df=2 | 0,0325 | * | Yes | 18,16 to 60,72 |
| **32b** | 24,43 | t=23,00, df=2 | 0,0019 | ** | Yes | 21,33 to 27,53 |
| **33b** | 10 | t=2,926, df=2 | 0,0997 | ns | Yes | 0,01974 to 19,98 |
| **34b** | -15,77 | t=7,132, df=2 | 0,0191 | * | Yes | -22,23 to -9,313 |
| **35b** | -5,78 | t=1,711, df=2 | 0,2292 | ns | No | -15,64 to 4,082 |
| **36b** | -17,3 | t=16,02, df=2 | 0,0039 | ** | Yes | -20,45 to -14,15 |
| **37b** | -6,1 | t=1,078, df=2 | 0,3937 | ns | No | -22,62 to 10,42 |
| **38b** | -24,65 | t=18,32, df=2 | 0,003 | ** | Yes | -28,58 to -20,72 |
| **39b** | -0,85 | t=0,05387, df=2 | 0,9619 | ns | No | -46,92 to 45,22 |
| **40b** | -12,63 | t=6,077, df=2 | 0,026 | * | Yes | -18,70 to -6,561 |
| **41b** | -26,28 | t=10,07, df=2 | 0,0097 | ** | Yes | -33,90 to -18,66 |
| **42b** | -10,67 | t=5,600, df=2 | 0,0304 | * | Yes | -16,23 to -5,107 |
| **43b** | -10,59 | t=2,199, df=2 | 0,1589 | ns | No | -24,65 to 3,470 |
| **(*S*)-34b** | -18,39 | t=3,500, df=2 | 0,0728 | ns | Yes | -33,73 to -3,049 |
| **(*R*)-34b** | 3,83 | t=3,334, df=2 | 0,0794 | ns | Yes | 0,4751 to 7,185 |
| **44b** | -38,7 | t=5,942, df=2 | 0,0272 | * | Yes | -57,72 to -19,68 |

USC UNIVERSIDADE DE SANTIAGO DE COMPOSTELA

Table 5.8. One sample t-test for **Series III-b** at 1 nM.

| Compound | Actual mean | t, df | P value (two tailed) | P value summary | Significant (alpha=0.1) | 90% confidence interval |
|---|---|---|---|---|---|---|
| **21b** | 1,26 | t=0,2898, df=2 | 0,7992 | ns | No | -11,43 to 13,95 |
| **22b** | 4,14 | t=1,545, df=2 | 0,2623 | ns | No | -3,682 to 11,96 |
| **23b** | 0,96 | t=3,260, df=2 | 0,0826 | ns | Yes | 0,1002 to 1,820 |
| **24b** | -3,58 | t=0,9227, df=2 | 0,4536 | ns | No | -14,91 to 7,749 |
| **25b** | 24,8 | t=4,649, df=2 | 0,0433 | * | Yes | 9,223 to 40,38 |
| **26b** | 21,62 | t=17,75, df=2 | 0,0032 | ** | Yes | 18,06 to 25,18 |
| **27b** | 32,83 | t=11,80, df=2 | 0,0071 | ** | Yes | 24,70 to 40,96 |
| **28b** | 10,58 | t=1,956, df=2 | 0,1897 | ns | No | -5,216 to 26,38 |
| **29b** | 16,63 | t=4,890, df=2 | 0,0394 | * | Yes | 6,700 to 26,56 |
| **30b** | 1 | t=0,3485, df=2 | 0,7607 | ns | No | -7,379 to 9,379 |
| **31b** | 24,93 | t=49,07, df=2 | 0,0004 | *** | Yes | 23,45 to 26,41 |
| **32b** | 9,96 | t=2,212, df=2 | 0,1575 | ns | No | -3,190 to 23,11 |
| **33b** | 2,4 | t=1,792, df=2 | 0,215 | ns | No | -1,511 to 6,311 |
| **34b** | -33,32 | t=4,247, df=2 | 0,0512 | ns | Yes | -56,23 to -10,41 |
| **35b** | -10,36 | t=3,373, df=2 | 0,0778 | ns | Yes | -19,33 to -1,391 |
| **36b** | -5,87 | t=2,177, df=2 | 0,1614 | ns | No | -13,74 to 2,003 |
| **37b** | -8,87 | t=4,279, df=2 | 0,0505 | ns | Yes | -14,92 to -2,818 |
| **38b** | -35,6 | t=18,24, df=2 | 0,003 | ** | Yes | -41,30 to -29,90 |
| **39b** | 5,76 | t=1,178, df=2 | 0,36 | ns | No | -8,519 to 20,04 |
| **40b** | -10,31 | t=4,737, df=2 | 0,0418 | * | Yes | -16,67 to -3,954 |
| **41b** | -35,56 | t=7,170, df=2 | 0,0189 | * | Yes | -50,04 to -21,08 |
| **42b** | -24,7 | t=4,326, df=2 | 0,0495 | * | Yes | -41,37 to -8,027 |
| **43b** | -31,71 | t=13,27, df=2 | 0,0056 | ** | Yes | -38,69 to -24,73 |
| **(*S*)-34b** | -12,76 | t=3,269, df=2 | 0,0822 | ns | Yes | -24,16 to -1,364 |
| **(*R*)-34b** | -15,88 | t=3,259, df=2 | 0,0827 | ns | Yes | -30,11 to -1,651 |
| **44b** | -30,27 | t=4,571, df=2 | 0,0447 | * | Yes | -49,61 to -10,93 |

USC UNIVERSIDADE DE SANTIAGO DE COMPOSTELA

Table 5.9. One sample t-test for **Series IV** and **Series V** at 0.01 nM.

| Compound | Actual mean | t, df | P value (two tailed) | P value summary | Significant (alpha=0.1) | 90% confidence interval |
|---|---|---|---|---|---|---|
| **45a** | 9,16 | t=4,989, df=2 | 0,0379 | * | Yes | 3,799 to 14,52 |
| **45b** | -27,31 | t=17,33, df=2 | 0,0033 | ** | Yes | -31,91 to -22,71 |
| **46a** | 6,46 | t=1,001, df=2 | 0,4223 | ns | No | -12,39 to 25,31 |
| **46b** | 0,48 | t=0,1007, df=2 | 0,929 | ns | No | -13,45 to 14,41 |
| **47a** | 7,3 | t=0,9786, df=2 | 0,431 | ns | No | -14,48 to 29,08 |
| **47b** | -0,67 | t=0,1205, df=2 | 0,9151 | ns | No | -16,90 to 15,56 |
| **48a** | 1,9 | t=0,4763, df=2 | 0,6809 | ns | No | -9,749 to 13,55 |
| **48b** | 0,85 | t=0,1409, df=2 | 0,9009 | ns | No | -16,77 to 18,47 |
| **49a** | 8,83 | t=4,735, df=2 | 0,0418 | * | Yes | 3,385 to 14,28 |
| **49b** | 3,59 | t=0,6262, df=2 | 0,5951 | ns | No | -13,15 to 20,33 |
| **50a** | 14,59 | t=3,490, df=2 | 0,0732 | ns | Yes | 2,384 to 26,80 |
| **50b** | 22,03 | t=4,489, df=2 | 0,0462 | * | Yes | 7,700 to 36,36 |
| **51a** | -0,01 | t=0,001342, df=2 | 0,9991 | ns | No | -21,77 to 21,75 |
| **51b** | 7,28 | t=1,230, df=2 | 0,3437 | ns | No | -10,00 to 24,56 |
| **52a** | 11,89 | t=3,198, df=2 | 0,0854 | ns | Yes | 1,033 to 22,75 |
| **52b** | 19,81 | t=2,950, df=2 | 0,0982 | ns | Yes | 0,2035 to 39,42 |
| **53a** | 18,16 | t=5,106, df=2 | 0,0363 | * | Yes | 7,775 to 28,54 |
| **53b** | 25,92 | t=8,734, df=2 | 0,0129 | * | Yes | 17,25 to 34,59 |
| **54a** | 10,52 | t=2,136, df=2 | 0,1662 | ns | No | -3,860 to 24,90 |
| **54b** | -6,47 | t=1,035, df=2 | 0,4095 | ns | No | -24,73 to 11,79 |
| **55a** | -23,29 | t=5,126, df=2 | 0,036 | * | Yes | -36,56 to -10,02 |
| **55b** | 6,44 | t=1,198, df=2 | 0,3536 | ns | No | -9,255 to 22,14 |
| **56a** | -19,34 | t=1,910, df=2 | 0,1964 | ns | No | -48,91 to 10,23 |
| **56b** | 3,31 | t=95,55, df=2 | 0,0001 | *** | Yes | 3,209 to 3,411 |

USC UNIVERSIDADE DE SANTIAGO DE COMPOSTELA

Table 5.10. One sample t-test for **Series IV** and **Series V** at 1 nM.

| Compound | Actual mean | t, df | P value (two tailed) | P value summary | Significant (alpha=0.1) | 90% confidence interval |
|---|---|---|---|---|---|---|
| **45a** | 14,87 | t=5,214, df=2 | 0,0349 | * | Yes | 6,542 to 23,20 |
| **45b** | 12,22 | t=6,117, df=2 | 0,0257 | * | Yes | 6,387 to 18,05 |
| **46a** | 13,06 | t=3,427, df=2 | 0,0756 | ns | Yes | 1,933 to 24,19 |
| **46b** | 11,73 | t=3,170, df=2 | 0,0868 | ns | Yes | 0,9237 to 22,54 |
| **47a** | 16,7 | t=6,207, df=2 | 0,025 | * | Yes | 8,844 to 24,56 |
| **47b** | 39,07 | t=15,49, df=2 | 0,0041 | ** | Yes | 31,70 to 46,44 |
| **48a** | 7,11 | t=5,449, df=2 | 0,0321 | * | Yes | 3,300 to 10,92 |
| **48b** | 15 | t=4,987, df=2 | 0,0379 | * | Yes | 6,217 to 23,78 |
| **49a** | 28,25 | t=444,8, df=2 | <0,0001 | **** | Yes | 28,06 to 28,44 |
| **49b** | -8,24 | t=1,505, df=2 | 0,2711 | ns | No | -24,22 to 7,742 |
| **50a** | -3,43 | t=0,7227, df=2 | 0,5449 | ns | No | -17,29 to 10,43 |
| **50b** | 10,61 | t=1,523, df=2 | 0,2673 | ns | No | -9,738 to 30,96 |
| **51a** | 12,25 | t=2,229, df=2 | 0,1556 | ns | No | -3,799 to 28,30 |
| **51b** | 9,54 | t=2,412, df=2 | 0,1373 | ns | No | -2,008 to 21,09 |
| **52a** | 25,76 | t=4,448, df=2 | 0,047 | * | Yes | 8,851 to 42,67 |
| **52b** | 6,19 | t=1,058, df=2 | 0,4008 | ns | No | -10,89 to 23,27 |
| **53a** | 13,52 | t=6,433, df=2 | 0,0233 | * | Yes | 7,383 to 19,66 |
| **53b** | 7,47 | t=2,167, df=2 | 0,1625 | ns | No | -2,595 to 17,53 |
| **54a** | 12,12 | t=2,924, df=2 | 0,0998 | ns | Yes | 0,01556 to 24,22 |
| **54b** | -18,48 | t=7,375, df=2 | 0,0179 | * | Yes | -25,80 to -11,16 |
| **55a** | 13,16 | t=4,342, df=2 | 0,0492 | * | Yes | 4,309 to 22,01 |
| **55b** | 12,19 | t=3,078, df=2 | 0,0913 | ns | Yes | 0,6250 to 23,75 |
| **56a** | 3,99 | t=2,541, df=2 | 0,1262 | ns | No | -0,5955 to 8,576 |
| **56b** | 7,69 | t=1,571, df=2 | 0,2568 | ns | No | -6,606 to 21,99 |

USC UNIVERSIDADE DE SANTIAGO DE COMPOSTELA

### 5.2.4 Circular dichroism (CD) of Series I, II and III

CD spectra were recorded on a Jasco-815 system equipped with a Peltier-type thermostatic accessory (CDF-426S, Jasco). Measurements were carried out at 20 °C using a 1 mm quartz cell in a volume of 600 $\mu$L. Compounds (0.5 mg) were dissolved in MeOH (1.0 mL) and then diluted 10-fold in MeOH. The instrument settings were bandwidth, 1.0 nm; data pitch, 1.0 nm; speed, 500 nm/min; accumulation, 10, and wavelengths, 300−190 nm.

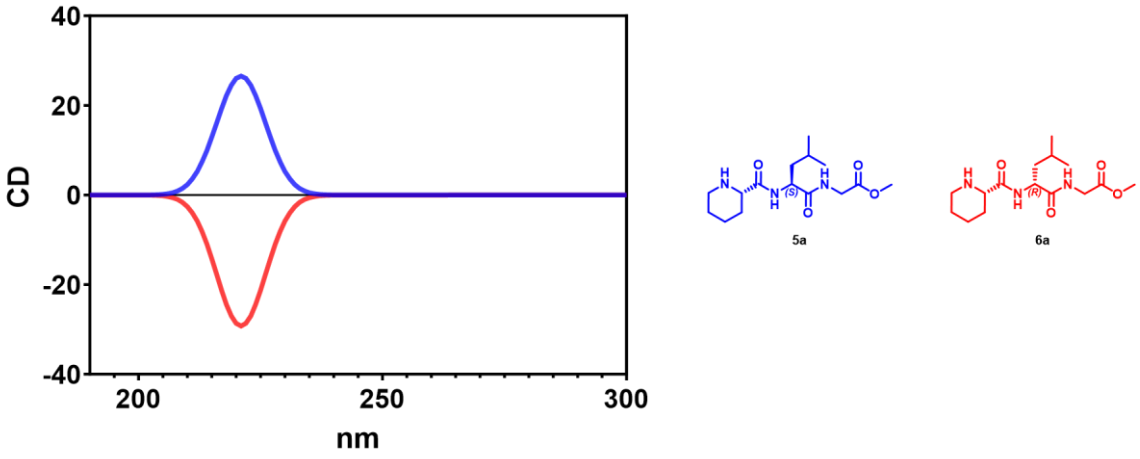



Figure 5.1. Circular dichroism spectra of reference compounds **5a** and **6a**.

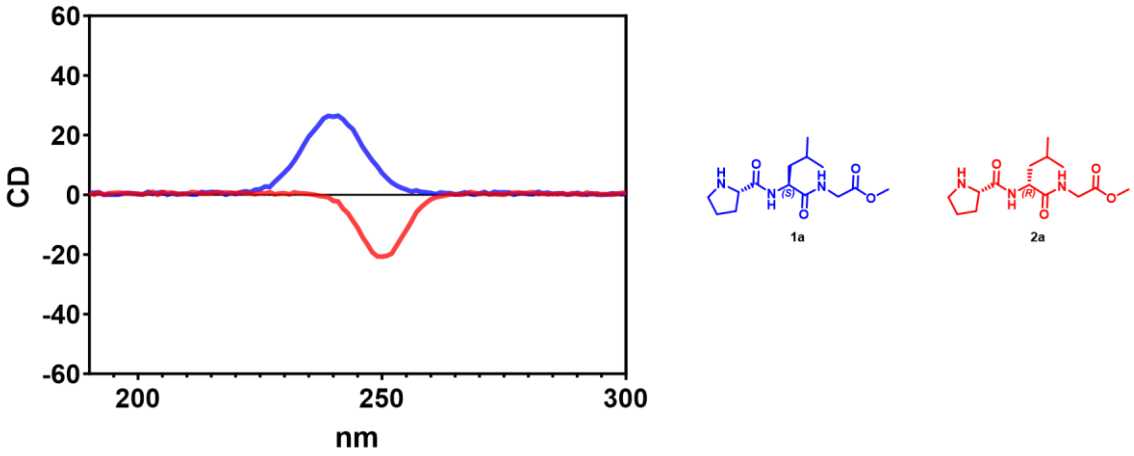



Figure 5.2. Circular dichroism spectra of diastereomeric pair **1a** and **2a**.

USC
UNIVERSIDADE DE SANTIAGO DE COMPOSTELA

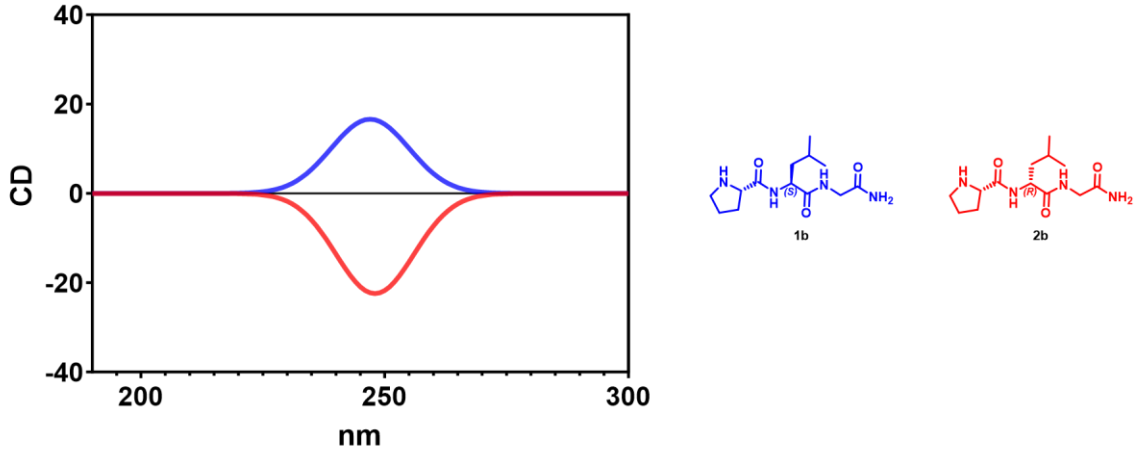



Figure 5.3. Circular dichroism spectra of diastereomeric pair **1b** and **2b**.

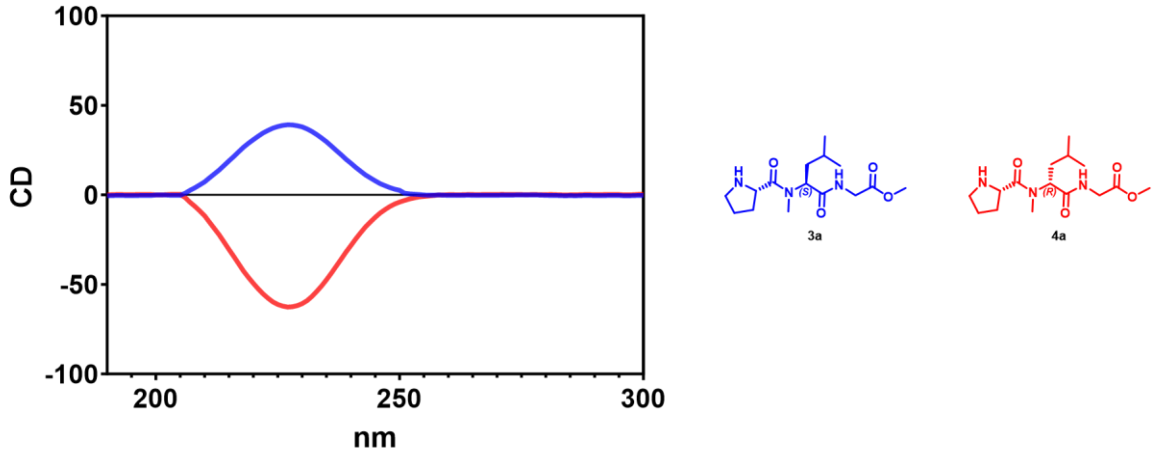



Figure 5.4. Circular dichroism spectra of diastereomeric pair **3a** and **4a**.

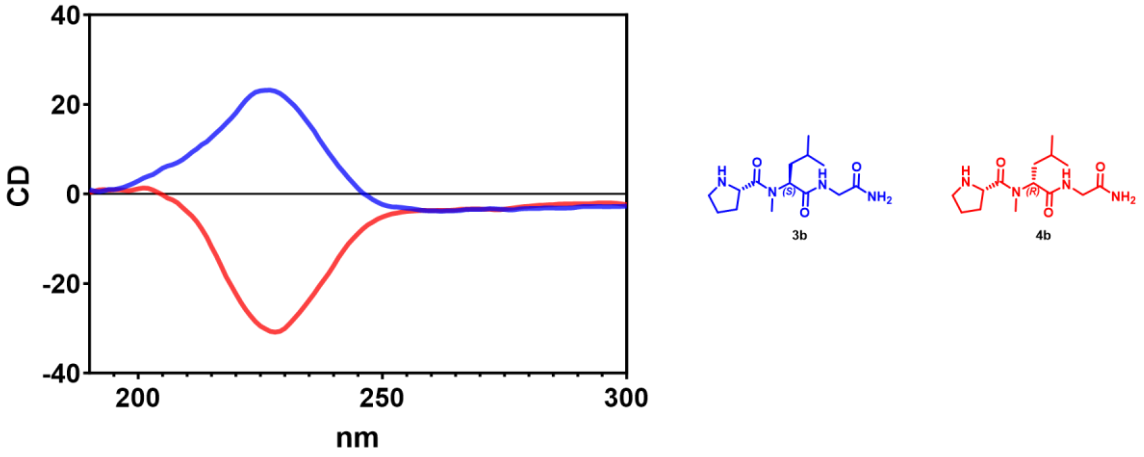



Figure 5.5. Circular dichroism spectra of diastereomeric pair **3b** and **4b**.

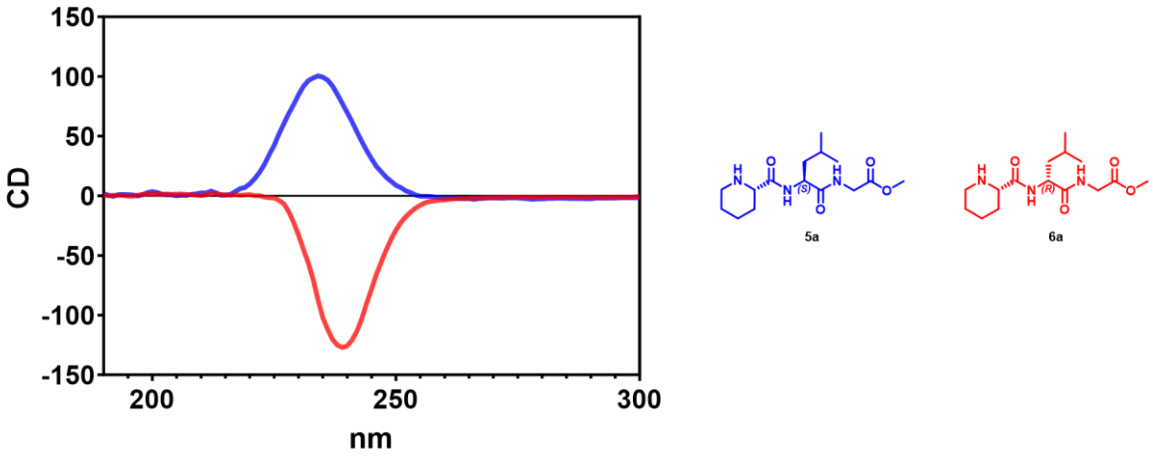



Figure 5.6. Circular dichroism spectra of diastereomeric pair **5a** and **6a**.

USC
UNIVERSIDADE DE SANTIAGO DE COMPOSTELA

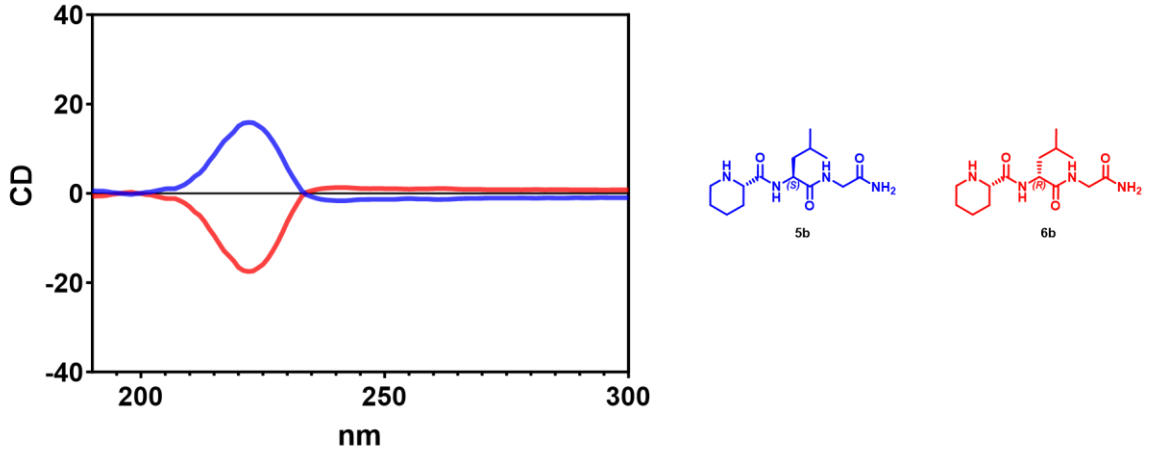



Figure 5.7. Circular dichroism spectra of diastereomeric pair **5b** and **6b**.

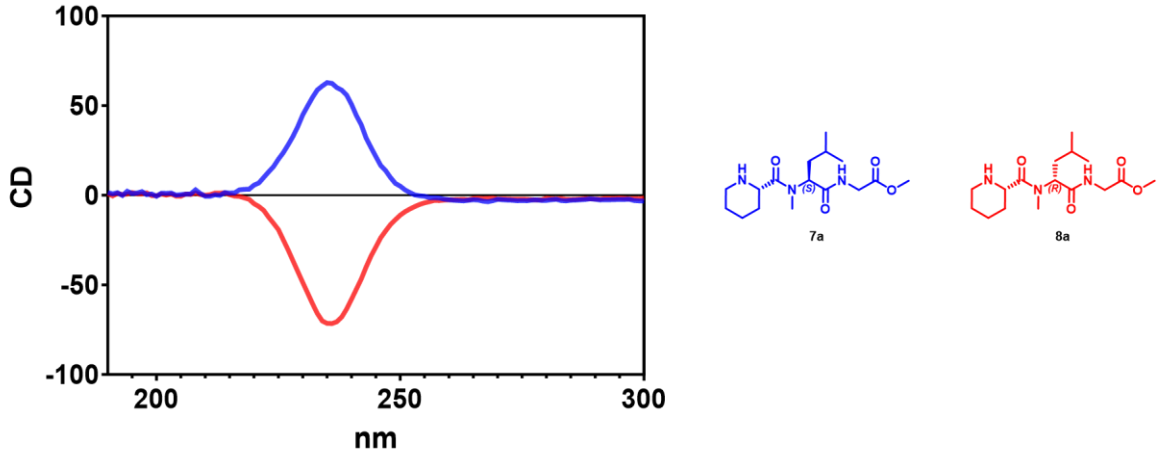



Figure 5.8. Circular dichroism spectra of diastereomeric pair **7a** and **8a**.

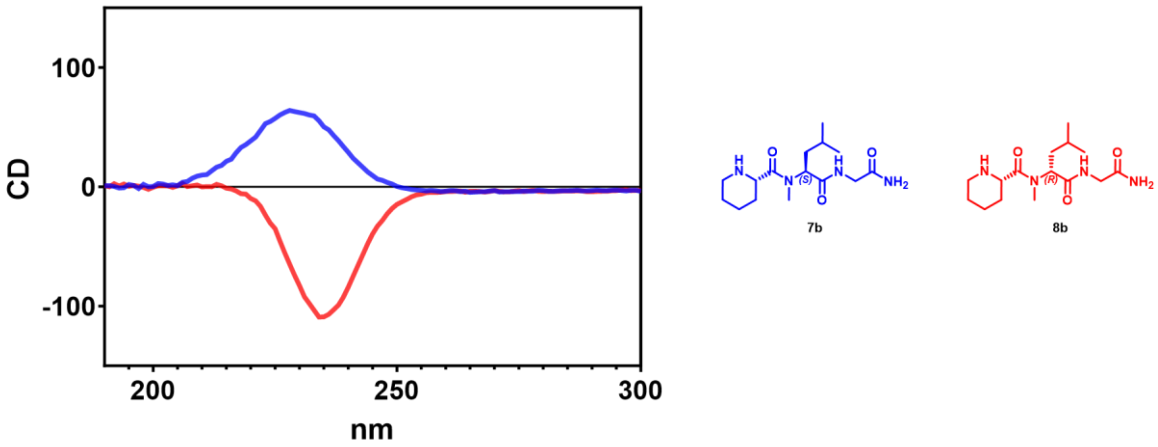



Figure 5.9. Circular dichroism spectra of diastereomeric pair **7b** and **8b**.

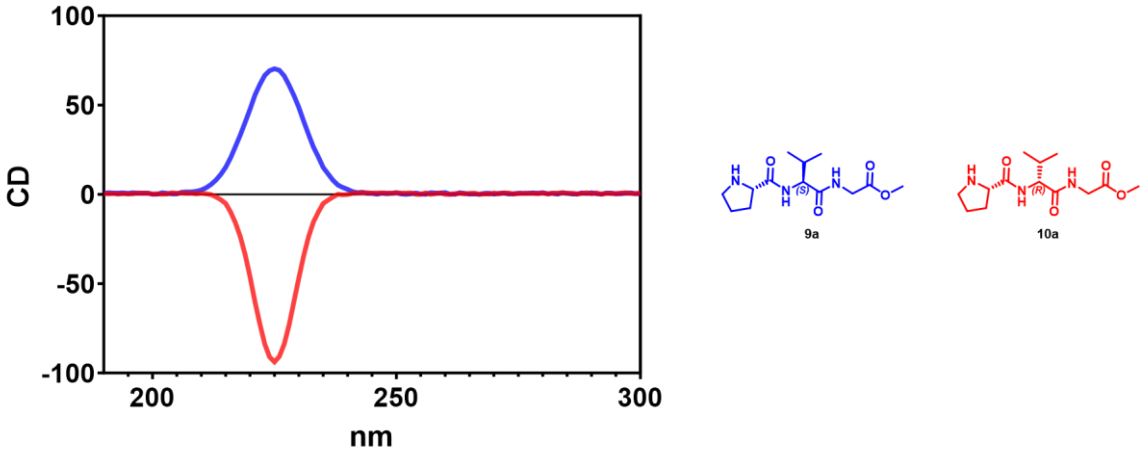



Figure 5.10. Circular dichroism spectra of diastereomeric pair **9a** and **10a**.

USC
UNIVERSIDADE DE SANTIAGO DE COMPOSTELA

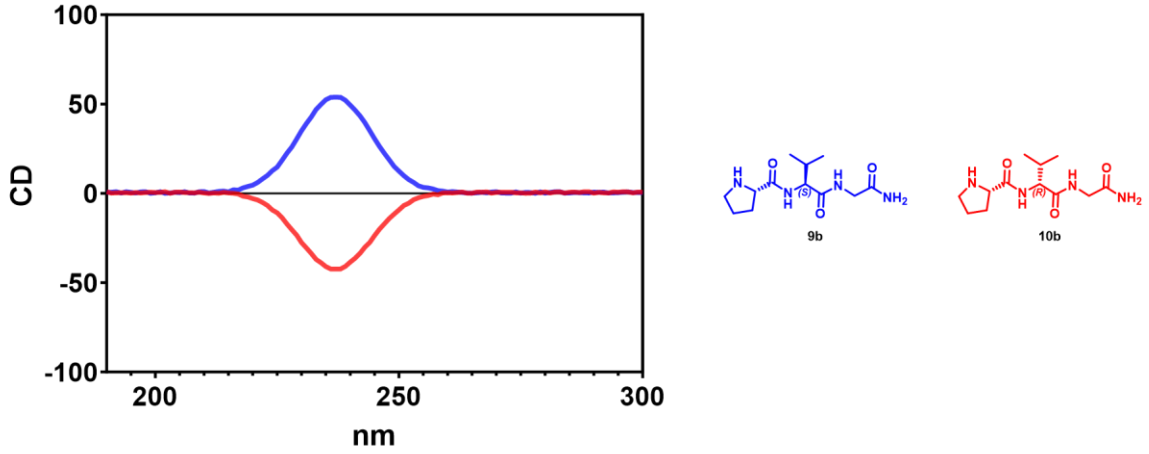



Figure 5.11. Circular dichroism spectra of diastereomeric pair **9b** and **10b**.

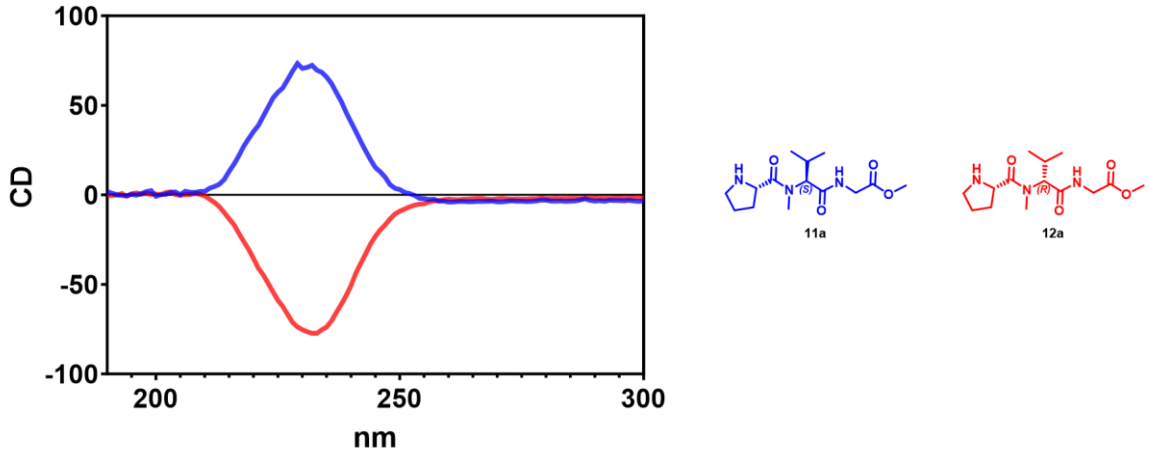



Figure 5.12. Circular dichroism spectra of diastereomeric pair **11a** and 1**2a**.

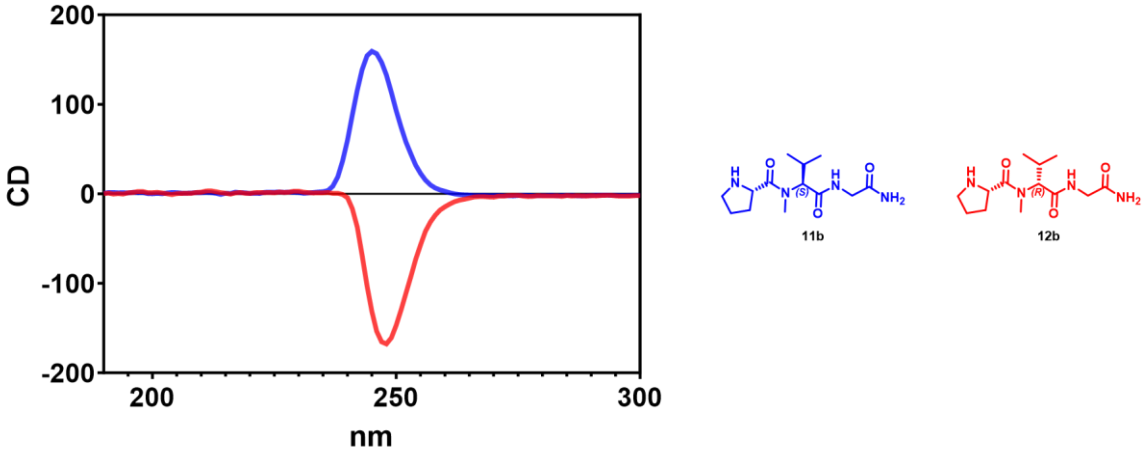



Figure 5.13. Circular dichroism spectra of diastereomeric pair **11b** and 1**2b**.

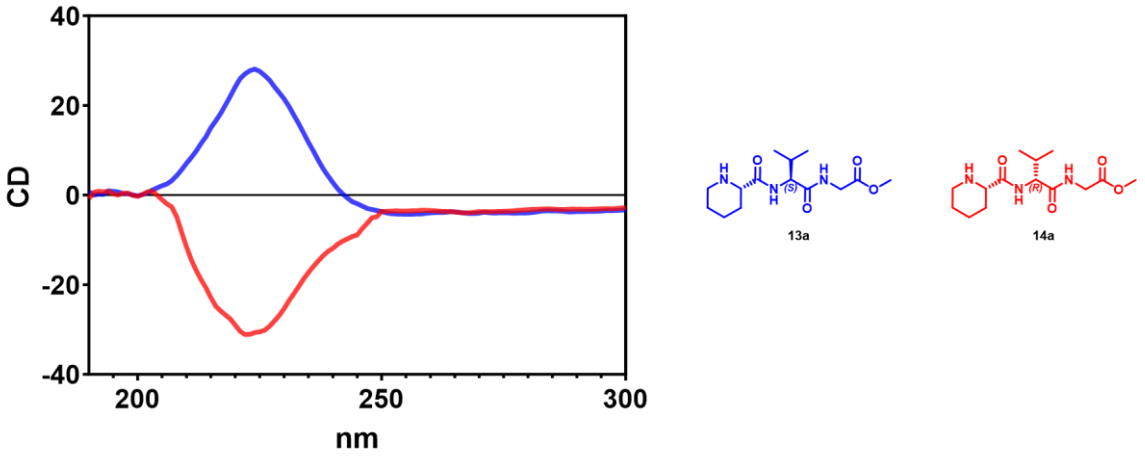



Figure 5.14. Circular dichroism spectra of diastereomeric pair **13a** and **14a**.

USC
UNIVERSIDADE DE SANTIAGO DE COMPOSTELA

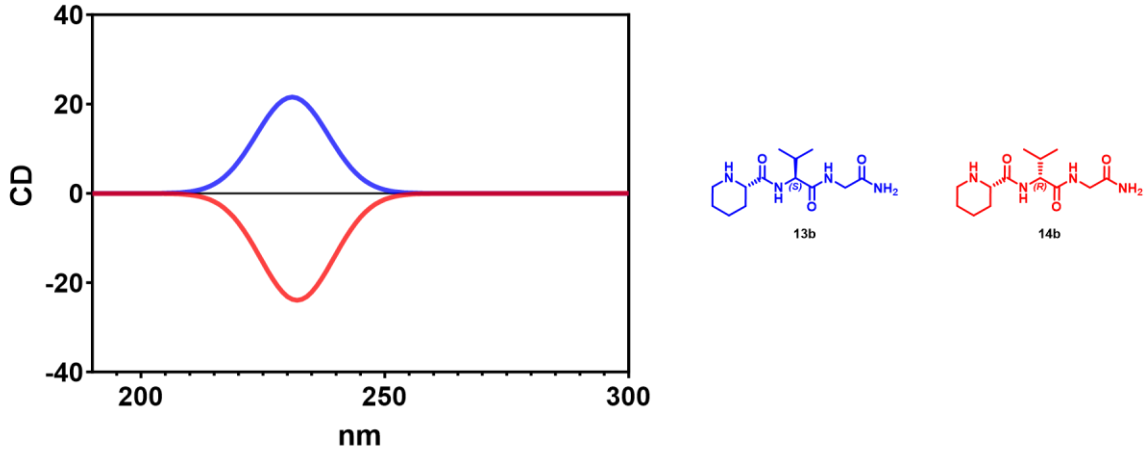



Figure 5.15. Circular dichroism spectra of diastereomeric pair **13b** and **14b**.

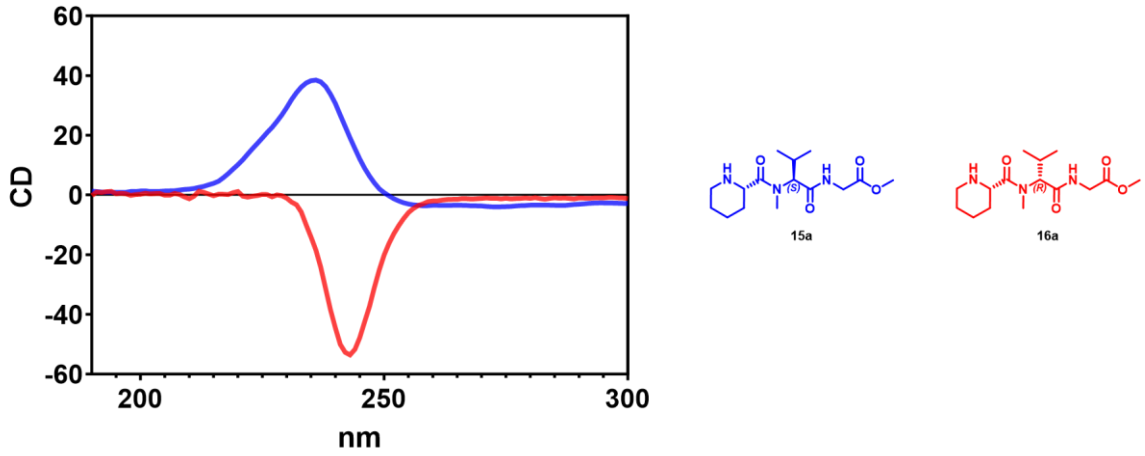



Figure 5.16. Circular dichroism spectra of diastereomeric pair **15a** and **16a**.

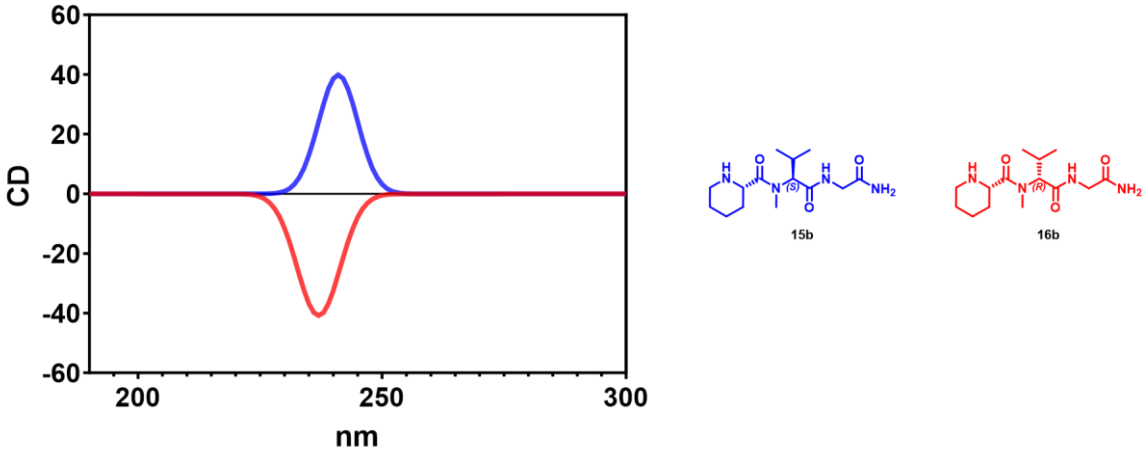



Figure 5.17. Circular dichroism spectra of diastereomeric pair **15b** and **16b**.

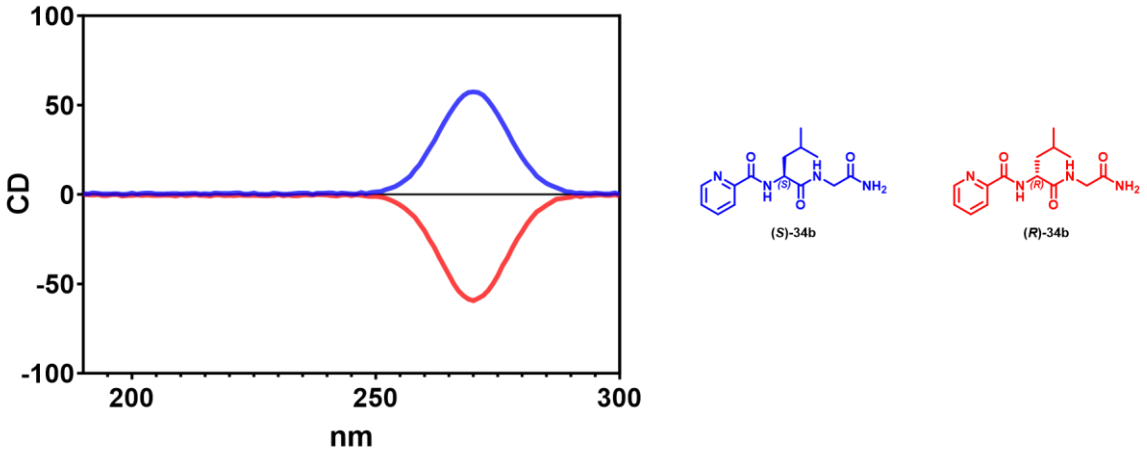



Figure 5.18. Circular dichroism spectra of enantiomeric pair **(*S*)-34b** and **(*R*)-34b**.

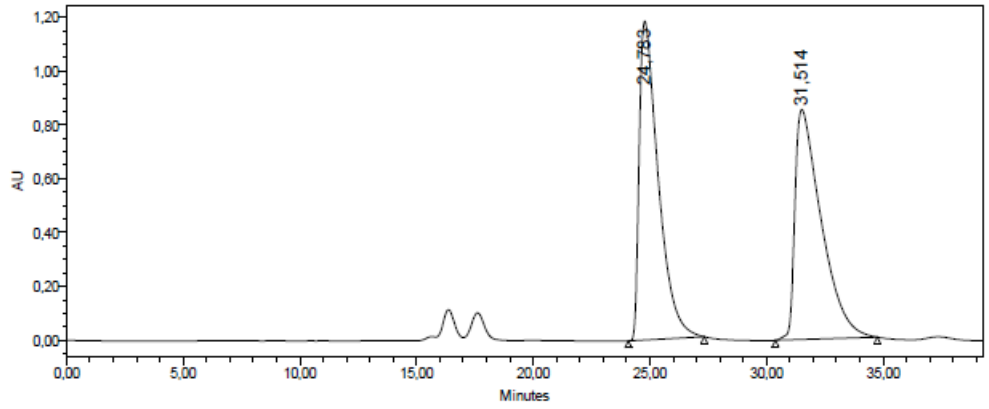
USC
UNIVERSIDADE DE SANTIAGO DE COMPOSTELA

### 5.2.5 Chiral HPLC separation of enantiomers and characterization of 34b

The chiral resolution was performed using a Water Breeze™ 2 (binary pump: 1525, detector UV/Visible 2489, 7725i Manual Injector Kit 1500 Series) using a 250 mm x 20 mm Chiralpak® 5µm IE-3 (DAICEL). The separation was performed at 25 ºC with a mixture of Hex/IPA (1:1) as mobile phase. The enantiomers **(*S*)-34b** and **(*R*)-34b** were isolated and then characterized by $^{1}$H NMR and circular dichroism (CD).

SAMPLE INFORMATION

| | | | |
|---|---|---|---|
| Sample Name: | sy1crg-598 | Acquired By: | Breeze |
| Sample Type: | Unknown | Sample Set Name | |
| Vial: | 1 | Acq. Method: | 50%HexiPAISOF10 set |
| Injection #: | 2 | Date Acquired: | 12/04/2023 16:03:25 CET |
| Run Time: | 40,00 Minutes | Injection Volume: | 500,00 ul |




| | RT (min) | Area (µV*sec) | % Area | Height (µV) |
|---|---|---|---|---|
| 1 | 24,783 | 67275717 | 50,10 | 1185410 |
| 2 | 31,514 | 67005617 | 49,90 | 854662 |

**(±) *N*-(1-((2-amino-2-oxoethyl)amino)-4-methyl-1-oxopentan-2-yl)picolinamide (34b).** Purified by column chromatography (DCM/MeOH 94:6). Yield: 99%. Mp: 149 – 150 ºC. $^{1}$H NMR (300 MHz, $CDCl_3$) $\delta$ (ppm): 8.58 (d, *J* = 4.8 Hz, 1H), 8.37 (d, *J* = 6.8 Hz, 1H), 8.15 (d, *J* = 7.8 Hz, 1H), 7.92 – 7.81 (m, 1H), 7.52 – 7.42 (m, 1H), 6.88 (s, 1H), 6.56 (s, 1H), 5.45 (s, 1H), 4.58 – 4.44 (m, 1H), 4.08 – 3.85 (m, 2H), 1.92 – 1.71 (m, 3H), 0.99 (dd, *J* = 10.9, 6.0 Hz, 6H). $^{13}$C NMR (75 MHz, $CDCl_3$), δ (ppm): 172.4, 171.5, 165.2, 149.0, 148.4, 137.5, 126.7, 122.4, 52.6, 43.0, 40.6, 24.9, 22.9, 21.9. LRMS (CI) *m/*z calcd for $C_{14}H_{21}N_4O_3$ $[M+H]^+$: 293.1; found: 293.3.

**(*S*)-*N*-(1-((2-amino-2-oxoethyl)amino)-4-methyl-1-oxopentan-2-yl)picolinamide ((*S*)-34b).** Purified by column chromatography (DCM/MeOH 94:6). Yield: 99%. Mp: 149 – 150 ºC. $^{1}$H NMR (300 MHz, DMSO-*d6*) $\delta$ (ppm): 8.71 (d, J = 8.7 Hz, 1H), 8.66 (d, J = 4.7 Hz, 1H), 8.30 (t, J = 5.6 Hz, 1H), 8.06 – 7.95 (m, 2H), 7.64 – 7.58 (m, 1H), 7.25 (bs, 1H), 7.03 (bs, 1H), 4.64 – 4.51 (m, 1H), 3.68 (dd, J = 16.7, 5.9 Hz, 1H), 3.54 (dd, J = 16.7, 5.5 Hz, 1H), 1.72 – 1.52 (m, 3H), 0.87 (d, J = 5.6 Hz, 6H). $^{13}$C NMR (75 MHz, DMSO-*d6*), δ (ppm): 172.3, 171.2, 164.0, 150.0, 149.0, 138.4, 127.2, 122.4, 51.7, 42.4, 41.8, 24.9, 23.6, 22.2. LRMS (CI) *m/*z calcd for $C_{14}H_{21}N_4O_3$ $[M+H]^+$: 293.1; found: 293.1.

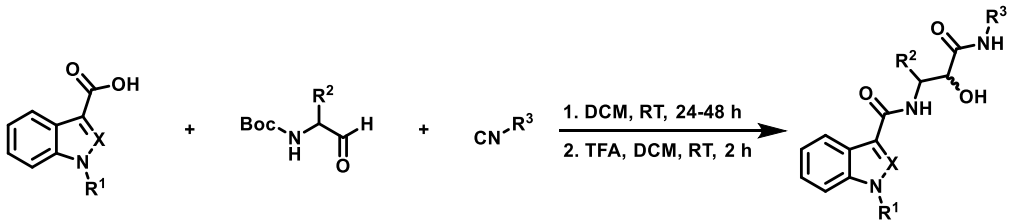
**(*R*)-*N*-(1-((2-amino-2-oxoethyl)amino)-4-methyl-1-oxopentan-2-yl)picolinamide ((*R*)-34b).** Purified by column chromatography (DCM/MeOH 94:6). Yield: 99%. Mp: 149 – 150 ºC. $^{1}$H NMR (300 MHz, DMSO-*d6*) $\delta$ (ppm): 8.71 (d, J = 8.7 Hz, 1H), 8.66 (d, J = 4.7 Hz, 1H), 8.30 (t, J = 5.9 Hz, 1H), 8.07 – 7.95 (m, 2H), 7.65 – 7.58 (m, 1H), 7.25 (s, 1H), 7.03 (s, 1H), 4.62 – 4.51 (m, 1H), 3.68 (dd, J = 16.8, 6.0 Hz, 1H), 3.54 (dd, J = 16.7, 5.4 Hz, 1H), 1.72 – 1.51 (m, 3H), 0.87 (d, J = 5.6 Hz, 6H). $^{13}$C NMR (75 MHz, DMSO-*d6*), δ (ppm): 172.3, 171.2, 164.0, 150.0, 149.0, 138.4, 127.2, 122.4, 51.7, 42.4, 41.8, 24.9, 23.6, 22.2. LRMS (CI) *m/*z calcd for $C_{14}H_{21}N_4O_3$ $[M+H]^+$: 293.1; found: 293.1.

USC UNIVERSIDADE DE SANTIAGO DE COMPOSTELA

## 5.3 CHAPTER II

### 5.3.1 Synthesis of SCRAs analogues

**METHOD C.** General procedure for the synthesis of *N*-(1-(alkylamino)-2-hydroxy-4-alkyl-1-oxopentan-3-yl)-1-alkyl-1*H*-heteroaryl-3-carboxamides.




**E1: X =** CH, $R^1$= 4-F-Bn
**E2: X =** CH, $R^1$= $CH_2$- Cy
**E3: X =** N, $R^1$= 4-F-Bn
**E4: X =** N, $R^1$= $CH_2$- Cy
**E5: X =** CH, $R^1$= 5-F-Pentyl
**E6: X =** CH, $R^1$= Pentyl

**F1:** $R^2$= (*S*)-ethyl
**F2:** $R^2$= (*S*)-*i*-propyl
**F3:** $R^2$= (*S*)-*tert*-butyl
**F4:** $R^2$= (*R*)-*tert*-butyl

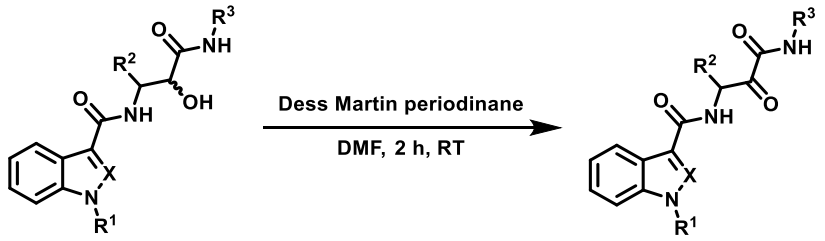
**G1:** $R^3$= 2,4-dimethoxybenzyl
**G2:** $R^3$= *tert*-butyl
**G3:** $R^3$= methyl acetate
**G4:** $R^3$= benzyl
**G5:** $R^3$= 4-ethylmorpholine

**Series VII (130-202)**

A mixture of the corresponding carboxylic acid (**E1-6**, 1 eq), Boc-amino-aldehyde (**F1-4**, 0.9 eq) and isocyanide **(G1-5**, 1.2 eq) in dichloromethane (2 mL) was stirred with orbital stirring at room temperature for 24-48 h. Upon completion, trifluoroacetic acid (45 eq) was added to the reaction pot and the mixture was stirred at room temperature for an additional 2h. The solution was treated with NaOH 2M and the product was extracted with ethyl acetate. The organic phase was dried over $MgSO_4$ and evaporated under reduced pressure to afford an oil residue, which was purified by chromatography on silica gel using MeOH/DCM mixtures.

USC UNIVERSIDADE DE SANTIAGO DE COMPOSTELA

**METHOD D.** General procedure for the synthesis of *N*-(1-(alkylamino)-4-alkyl-1,2-dioxopentan-3-yl)-1-alkyl-1*H*-heteroaryl-3-carboxamides.

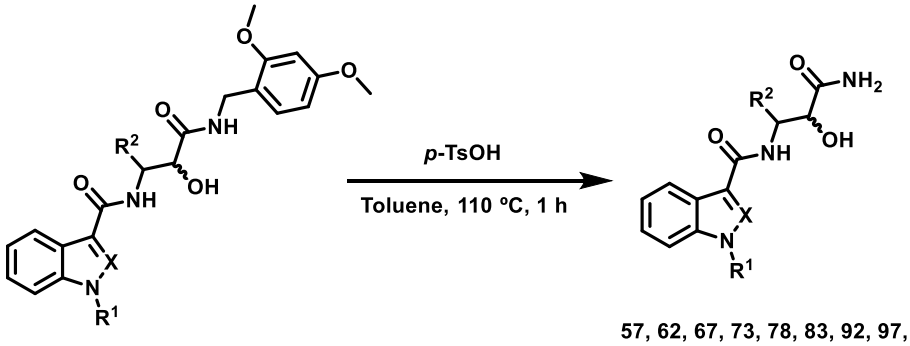



(130-202) Series VI (57-129)

The corresponding hydroxyamide (**130-202**, 1 eq) was dissolved in DMF (3 mL) under inert atmosphere and, at 0 ºC, Dess-Martin periodinane (1,5 eq) was added in portions. The reaction mixture was magnetically stirred at room temperature for 2 h. After completion of the reaction, the solution was treated with $NaHCO_3$ sat. and $Na_2S_2O_3$ (15% aq.) and stirred for an additional 15 minutes. The product was extracted with ethyl acetate, and the organic phase was washed with water and brine. The organic phase was dried over $MgSO_4$ and evaporated under reduced pressure to afford an oil residue, which was purified by chromatography on silica gel using MeOH/DCM mixtures.

USC UNIVERSIDADE DE SANTIAGO DE COMPOSTELA

**METHOD E.** General procedure for the synthesis of N-(1-amino-2-hydroxy-4-alkyl-1-oxopentan-3-yl)-1-alkyl-1H-heteroaryl-3-carboxamides.




**57, 62, 67, 73, 78, 83, 92, 97, 102, 107, 112, 117, 122-125**

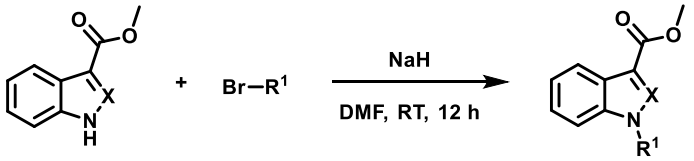
**E1: X =** CH, $R^1$= 4-F-Bn
**E2: X =** CH, $R^1$= $CH_2$-Cy
**E3: X =** N, $R^1$= 4-F-Bn
**E4: X =** N, $R^1$= $CH_2$-Cy
**E5: X =** CH, $R^1$= 5-F-Pentyl
**E6: X =** CH, $R^1$= Pentyl

**F1:** $R^2$= (*S*)-ethyl
**F2:** $R^2$= (*S*)-*i*-propyl
**F3:** $R^2$= (*S*)-*tert*-butyl
**F4:** $R^2$= (*R*)-*tert*-butyl

In a round bottom flask, *p*-TsOH (4 eq) was added to a solution of the PADAM product (1 eq) in toluene (8 mL). The reaction was magnetically stirred at reflux for 1 h. After completion of the reaction, the solution was treated with $NaHCO_3$, and the product was extracted with ethyl acetate. The organic phase was dried over $Na_2SO_4$ and evaporated under reduced pressure to afford an oil residue, which was purified by chromatography on silica gel using MeOH/DCM mixtures.

USC UNIVERSIDADE DE SANTIAGO DE COMPOSTELA

**METHOD F.** General procedure for the synthesis of 1-alkyl-1*H*-indole-3-carboxylates and 1-alkyl-1*H*-indazole-3-carboxylates.




**X** = CH, N

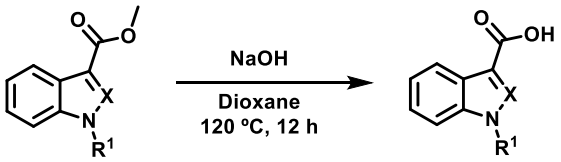
$R^1$ = 4-F-Bn
$R^1$ = $CH_2$-Cy
$R^1$ = 5-F-Pentyl
$R^1$ = Pentyl

**H1: X =** CH, $R^1$ = 4-F-Bn
**H2: X =** CH, $R^1$ = $CH_2$-Cy
**H3: X =** N, $R^1$ = 4-F-Bn
**H4: X =** N, $R^1$ = $CH_2$-Cy
**H5: X =** CH, $R^1$ = 5-F-Pentyl
**H6: X =** CH, $R^1$ = Pentyl

To a solution of methyl 1*H*-indole-3-carboxylate or methyl 1*H*-indazole-3-carboxylate (1 eq) in dry DMF (40 mL), NaH (1.2 eq) was added at 0 ºC. After 30 minutes, the corresponding alkyl bromide (1.2 eq) was added, and the reaction was stirred at room temperature for 24 h. The reaction was quenched with water and extracted with $CH_2Cl_2$. The organic phase was dried over $MgSO_4$, filtered, and concentrated. The resulting product was purified by column chromatography on silica gel using MeOH/$CH_2Cl_2$.

USC UNIVERSIDADE DE SANTIAGO DE COMPOSTELA

**METHOD G.** General procedure for the synthesis of *N*-alkyl-indole-3-carboxylic acids and *N*-alkyl-indazole-3-carboxylic acids.



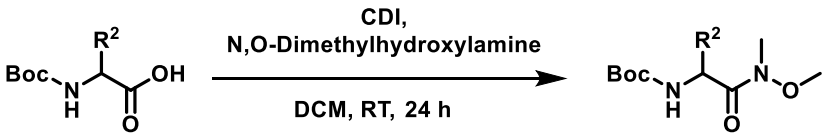

**H1: X** = CH, $R^1$= 4-F-Bn
**H2: X** = CH, $R^1$= $CH_2$-Cy
**H3: X** = N, $R^1$= 4-F-Bn
**H4: X** = N, $R^1$= $CH_2$-Cy
**H5: X** = CH, $R^1$= 5-F-Pentyl
**H6: X** = CH, $R^1$= Pentyl

**E1: X** = CH, $R^1$= 4-F-Bn
**E2: X** = CH, $R^1$= $CH_2$-Cy
**E3: X** = N, $R^1$= 4-F-Bn
**E4: X** = N, $R^1$= $CH_2$-Cy
**E5: X** = CH, $R^1$= 5-F-Pentyl
**E6: X** = CH, $R^1$= Pentyl

To a solution of methyl 1-alkyl-1*H*-indole-3-carboxylate or methyl 1-alkyl-1*H*-indazole-3-carboxylate (1 eq, **H1-6**) in dioxane (100 mL), NaOH (5 eq) was added, and the reaction was stirred a 120 ºC for 12 h. After completion of the reaction, the solvent was removed under reduced pressure and the pH was adjusted to 2 by addition of a solution of HCl 2N. The obtained suspension was filtered. The solid was washed with water and then was purified by column chromatography on silica gel using MeOH/$CH_2Cl_2$.

USC UNIVERSIDADE DE SANTIAGO DE COMPOSTELA

**METHOD H.** General procedure for the synthesis of amino acid derived Weinreb amides.



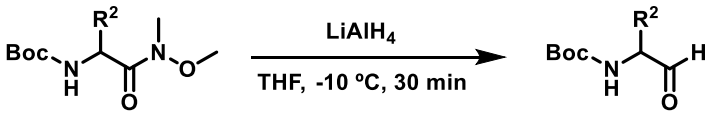

$R^2$ = (*S*)-ethyl
$R^2$ = (*S*)-*i*-propyl
$R^2$ = (*S*)-*tert*-butyl
$R^2$ = (*R*)-*tert*-butyl

**I1**: $R^2$ = (*S*)-ethyl
**I2**: $R^2$ = (*S*)-*i*-propyl
**I3**: $R^2$ = (*S*)-*tert*-butyl
**I4**: $R^2$ = (*R*)-*tert*-butyl

In a round bottom flask, CDI (1.2 eq) was added to a solution of the corresponding amino acid (1 eq) in dry DCM (20 mL). The reaction mixture was magnetically stirred for 1 h at room temperature, and N,O-dimethylhydroxylamine (1.2 eq) was added. After the reaction was completed, the solvent was evaporated under reduced pressure and redissolved in ethyl acetate. The organic phase was washed with HCl 2N, $NaHCO_3$ sat., and brine. The organic phase was dried over $MgSO_4$ and evaporated under reduced pressure to afford an oil residue, which was purified by chromatography on silica gel using MeOH/DCM mixtures.

USC
UNIVERSIDADE DE SANTIAGO DE COMPOSTELA

**METHOD I.** General procedure for the synthesis of α-boc-amino aldehydes.




**I1**: $R^2$ = (*S*)-ethyl
**I2**: $R^2$ = (*S*)-*i*-propyl
**I3**: $R^2$ = (*S*)-*tert*-butyl
**I4**: $R^2$ = (*R*)-*tert*-butyl

**F1**: $R^2$ = (*S*)-ethyl
**F2**: $R^2$ = (*S*)-*i*-propyl
**F3**: $R^2$ = (*S*)-*tert*-butyl
**F4**: $R^2$ = (*R*)-*tert*-butyl

In a round bottom flask, $LiAlH_4$ (2.5 eq) was added to a solution of the corresponding Weinreb amide (1 eq, **I1-4**) in dry THF (20 mL) at -10 ºC. The reaction mixture was magnetically stirred for 30 minutes. Upon completion, the solution was quenched with ethyl acetate and the organic phase was washed with HCl 0,1N, $NaHCO_3$ sat., and brine. The organic phase was dried over $MgSO_4$ and evaporated under reduced pressure to afford an oil residue, which was purified by chromatography on silica gel using MeOH/DCM mixtures.

USC
UNIVERSIDADE DE SANTIAGO DE COMPOSTELA

### 5.3.2 Spectroscopic and analytical data for all compounds described

**(*S*)-*N*-(1-amino-1,2-dioxopentan-3-yl)-1-(4-fluorobenzyl)-1*H*-indole-3-carboxamide (57).** Purified by column chromatography (DCM/MeOH 94:6). Yield: 74%. Mp: 146 – 147 ºC. $^1$H NMR (300 MHz, $CDCl_3$) $\delta$ (ppm): 8.01 (d, *J* = 7.1 Hz, 1H), 7.76 (s, 1H), 7.33 – 7.26 (m, 3H), 7.15 – 7.08 (m, 2H), 6.99 (t, *J* = 8.6 Hz, 2H), 6.84 (brs, 1H), 6.67 (d, *J* = 7.5 Hz, 1H), 5.69 (brs, 1H), 5.49 – 5.41 (m, 1H), 5.29 (s, 2H), 2.24 – 2.11 (m, 1H), 1.96 – 1.82 (m, 1H), 1.04 (t, *J* = 7.4 Hz, 3H). LRMS (CI) *m/*z calcd for $C_{21}H_{21}FN_3O_3$ $[M+H]^+$: 382.2; found: 382.2.

**(*S*)-*N*-(1-(*tert*-butylamino)-1,2-dioxopentan-3-yl)-1-(4-fluorobenzyl)-1*H*-indole-3-carboxamide (58).** Purified by column chromatography (DCM/MeOH 99:1). Yield: 60%. Mp: 149 – 150 ºC. $^1$H NMR (300 MHz, DMSO-*d6*) $\delta$ (ppm): 8.24 (s, 1H), 8.15 (d, *J* = 7.1 Hz, 1H), 8.08 (d, *J* = 7.9 Hz, 1H), 7.78 (s, 1H), 7.53 (d, *J* = 8.0 Hz, 1H), 7.32 – 7.24 (m, 2H), 7.22 – 7.08 (m, 4H), 5.46 (s, 2H), 5.09 – 4.90 (m, 1H), 1.97 – 1.48 (m, 2H), 1.27 (s, 9H), 0.97 (t, *J* = 7.1 Hz, 3H). LRMS (CI) *m/*z calcd for $C_{25}H_{29}FN_3O_3$ $[M+H]^+$: 438.2; found: 438.2.

**methyl (*S*)-(3-(1-(4-fluorobenzyl)-1*H*-indole-3-carboxamido)-2-oxopentanoyl)glycinate (59).** Purified by column chromatography (DCM/MeOH 99:1). Yield: 66%. Mp: 97 – 98 ºC. $^1$H NMR (300 MHz, $CDCl_3$) $\delta$ (ppm): 8.01 (d, *J* = 6.5 Hz, 1H), 7.75 (s, 1H), 7.43 (s, 1H), 7.28 (m, 2H), 7.16 – 7.08 (m, 2H), 7.04 – 6.96 (m, 3H), 6.65 (d, *J* = 7.6 Hz, 1H), 5.58 – 5.48 (m, 1H), 5.30 (s, 2H), 4.23 – 4.01 (m, 2H), 3.78 (s, 3H), 2.23 – 2.13 (m, 1H), 1.94 – 1.84 (m, 1H), 1.04 (t, *J* = 7.4 Hz, 3H). LRMS (CI) *m/*z calcd for $C_{24}H_{25}FN_3O_5$ $[M+H]^+$: 454.2; found: 454.2.

**(*S*)-*N*-(1-(benzylamino)-1,2-dioxopentan-3-yl)-1-(4-fluorobenzyl)-1*H*-indole-3-carboxamide (60).** Purified by column chromatography (DCM/MeOH 99:1). Yield: 75%. Mp: 284 – 285 ºC. $^1$H NMR (300 MHz, $CDCl_3$) $\delta$ (ppm): 8.02 (d, *J* = 7.0 Hz, 1H), 7.74 (s, 1H), 7.36 – 7.21 (m, 7H), 7.15 – 7.09 (m, 3H), 7.05 – 6.94 (m, 3H), 6.69 (d, *J* = 7.6 Hz, 1H), 5.54 – 5.45 (m, 1H), 5.30 (s, 2H), 4.54 – 4.46 (m, 2H), 2.24 – 2.15 (m, 1H), 1.97 – 1.86 (m, 1H), 1.11 – 1.01 (m, 3H). LRMS (CI) *m/*z calcd for $C_{28}H_{27}FN_3O_3$ $[M+H]^+$: 472.2; found: 472.2.

USC UNIVERSIDADE DE SANTIAGO DE COMPOSTELA

**(*S*)-1-(4-fluorobenzyl)-*N*-(1-((2-morpholinoethyl)amino)-1,2-dioxopentan-3-yl)-1*H*-indole-3-carboxamide (61).** Purified by column chromatography (DCM/MeOH 99:1). Yield: 66%. Mp: 291 – 292 ºC. $^{1}$H NMR (300 MHz, $CDCl_3$) $\delta$ (ppm): 8.03 (d, *J* = 7.7 Hz, 1H), 7.75 (s, 1H), 7.42 (s, 1H), 7.34 – 7.29 (m, 3H), 7.12 (t, *J* = 7.0 Hz, 2H), 7.00 (t, *J* = 8.6 Hz, 2H), 6.71 (d, *J* = 7.6 Hz, 1H), 5.56 – 5.43 (m, 1H), 5.30 (s, 2H), 3.75 – 3.66 (m, 4H), 3.46 – 3.37 (m, 2H), 2.54 (t, *J* = 6.0 Hz, 2H), 2.50 – 2.41 (m, 4H), 2.26 – 2.12 (m, 1H), 1.97 – 1.81 (m, 1H), 1.04 (t, *J* = 7.5 Hz, 3H). LRMS (CI) *m/*z calcd for $C_{27}H_{32}FN_4O_4$ $[M+H]^+$: 495.2; found: 495.2.

**(*S*)-*N*-(1-amino-4-methyl-1,2-dioxopentan-3-yl)-1-(4-fluorobenzyl)-1*H*-indole-3-carboxamide (62).** Purified by column chromatography (DCM/MeOH 94:6). Yield: 70%. Mp: 139 – 140 ºC. $^{1}$H NMR (300 MHz, $CDCl_3$) $\delta$ (ppm): 8.03 – 7.97 (m, 1H), 7.77 (s, 1H), 7.33 – 7.26 (m, 2H), 7.15 – 7.08 (m, 2H), 7.03 – 6.95 (m, 2H), 6.86 (brs, 1H), 6.69 (d, *J* = 8.3 Hz, 1H), 5.70 (brs, 1H), 5.43 (dd, *J* = 8.4, 5.7 Hz, 1H), 5.29 (s, 2H), 2.55 – 2.42 (m, 1H), 1.11 (d, *J* = 6.8 Hz, 3H), 0.99 (d, *J* = 6.8 Hz, 3H). $^{13}$C NMR (75 MHz, $CDCl_3$) $\delta$ (ppm): 196.29, 164.91, 162.49 (d, *J* = 246.8 Hz), 161.49, 136.75, 132.28, 128.77 (d, *J* = 8.4 Hz), 125.48, 123.45, 122.91, 122.00, 120.14, 115.94 (d, *J* = 21.9 Hz), 110.66, 102.86, 59.26, 49.99, 30.78, 19.96, 18.01. LRMS (CI) *m/*z calcd for $C_{22}H_{23}FN_3O_3$ $[M+H]^+$: 396.2; found: 396.2.

**(*S*)-*N*-(1-(*tert*-butylamino)-4-methyl-1,2-dioxopentan-3-yl)-1-(4-fluorobenzyl)-1*H*-indole-3-carboxamide (63).** Purified by column chromatography (DCM/MeOH 99:1). Yield: 64%. Mp: 194 – 195 ºC. $^{1}$H NMR (300 MHz, $CDCl_3$) $\delta$ (ppm): 8.02 (d, *J* = 7.2 Hz, 1H), 7.76 (s, 1H), 7.34 – 7.26 (m, 3H), 7.17 – 7.05 (m, 2H), 7.05 – 6.93 (m, 2H), 6.84 – 6.71 (m, 2H), 5.43 (dd, *J* = 8.7, 5.5 Hz, 1H), 5.30 (s, 2H), 2.58 – 2.41 (m, 1H), 1.40 (s, 9H), 1.10 (d, *J* = 6.8 Hz, 3H), 0.97 (d, *J* = 6.9 Hz, 3H). LRMS (CI) *m/*z calcd for $C_{26}H_{31}FN_3O_3$ $[M+H]^+$: 452.2; found: 452.2.

**methyl (*S*)-(3-(1-(4-fluorobenzyl)-1*H*-indole-3-carboxamido)-4-methyl-2-oxopentanoyl)glycinate (64).** Purified by column chromatography (DCM/MeOH 99:1). Yield: 72%. Mp: 112 – 113 ºC. $^{1}$H NMR (300 MHz, $CDCl_3$) $\delta$ (ppm): 8.00 (d, *J* = 8.1 Hz, 1H), 7.79 (s, 1H), 7.48 (s, 1H), 7.38 (s, 1H), 7.32 – 7.24 (m, 1H), 7.12 (t, *J* = 6.9 Hz, 3H), 6.99 (t, *J* = 8.5 Hz, 2H), 6.69 (d, *J* = 8.3 Hz, 1H), 5.53 – 5.42 (m, 1H), 5.30 (s, 2H), 4.22 – 4.00 (m, 2H), 3.77 (s, 3H), 2.54 – 2.41 (m, 1H), 1.11 (d, *J* = 6.7 Hz, 3H), 0.98 (d, *J* = 6.8 Hz, 3H). LRMS (CI) *m/*z calcd for $C_{25}H_{27}FN_3O_5$ $[M+H]^+$: 468.2; found: 468.2.

USC UNIVERSIDADE DE SANTIAGO DE COMPOSTELA

**(*S*)-*N*-(1-(benzylamino)-4-methyl-1,2-dioxopentan-3-yl)-1-(4-fluorobenzyl)-1*H*-indole-3-carboxamide (65).** Purified by column chromatography (DCM/MeOH 99:1). Yield: 78%. Mp: 280 – 281 ºC. $^{1}$H NMR (300 MHz, $CDCl_3$) $\delta$ (ppm): 8.02 (d, $J$ = 7.7 Hz, 1H), 7.76 (s, 1H), 7.36 – 7.19 (m, 7H), 7.17 – 7.06 (m, 3H), 7.06 – 6.93 (m, 3H), 6.76 (d, $J$ = 8.5 Hz, 1H), 5.50 – 5.40 (m, 1H), 5.29 (s, 2H), 4.50 (d, $J$ = 6.3 Hz, 2H), 2.59 – 2.47 (m, 1H), 1.12 (d, $J$ = 6.8 Hz, 3H), 0.99 (d, $J$ = 6.9 Hz, 3H). $^{13}$C NMR (75 MHz, $CDCl_3$) $\delta$ (ppm): 196.56, 165.04, 164.86, 162.48 (d, $J$ = 246.9 Hz), 136.77, 132.19, 131.79, 128.87, 128.81, 128.70, 127.90, 127.83, 125.51, 122.89, 121.98, 120.22, 115.94 (d, $J$ = 21.9 Hz), 110.61, 59.70, 49.98, 43.45, 30.86, 20.03, 18.00. HRMS (ESI) *m/*z calcd for $C_{29}H_{29}FN_3O_3$ $[M+H]^+$: 486.2115; found: 486.2187.

**(*S*)-1-(4-fluorobenzyl)-*N*-(4-methyl-1-((2-morpholinoethyl)amino)-1,2-dioxopentan-3-yl)-1*H*-indole-3-carboxamide (66).** Purified by column chromatography (DCM/MeOH 99:1). Yield: 63%. Mp: 269 – 271 ºC. $^{1}$H NMR (300 MHz, $CDCl_3$) $\delta$ (ppm): 8.02 (d, $J$ = 7.8 Hz, 1H), 7.77 (s, 1H), 7.42 (s, 1H), 7.34 – 7.27 (m, 3H), 7.18 – 7.07 (m, 2H), 7.06 – 6.94 (m, 2H), 6.76 (d, $J$ = 8.5 Hz, 1H), 5.44 (dd, $J$ = 8.6, 5.6 Hz, 1H), 5.31 (s, 2H), 3.74 – 3.66 (m, 4H), 3.46 – 3.36 (m, 2H), 2.54 (d, $J$ = 6.0 Hz, 2H), 2.47 (s, 4H), 1.28 – 1.15 (m, 1H), 1.11 (d, $J$ = 6.8 Hz, 3H), 0.98 (d, $J$ = 6.8 Hz, 3H). LRMS (CI) *m/*z calcd for $C_{28}H_{34}FN_4O_4$ $[M+H]^+$: 509.3; found: 509.3.

**(*S*)-*N*-(1-amino-4,4-dimethyl-1,2-dioxopentan-3-yl)-1-(4-fluorobenzyl)-1*H*-indole-3-carboxamide (67).** Purified by column chromatography (DCM/MeOH 94:6). Yield: 66%. Mp: 121 – 123 ºC. $^{1}$H NMR (300 MHz, $CDCl_3$) $\delta$ (ppm): 7.97 (d, $J$ = 7.8 Hz, 1H), 7.77 (s, 1H), 7.35 – 7.27 (m, 3H), 7.15 – 7.08 (m, 2H), 6.99 (t, $J$ = 8.6 Hz, 2H), 6.87 (s, 1H), 6.84 (brs, 1H), 5.60 (brs, 1H), 5.56 (d, $J$ = 8.0 Hz, 1H), 5.30 (s, 2H), 1.13 (s, 9H). $^{13}$C NMR (75 MHz, $CDCl_3$) $\delta$ (ppm): 191.0, 162.1, 160.8, 132.5, 128.8, 128.7, 127.4, 122.9, 122.7, 122.0, 120.0, 116.1, 115.8, 110.7, 59.6, 50.0, 35.4, 26.9. LRMS (CI) *m/*z calcd for $C_{23}H_{25}FN_3O_3$ $[M+H]^+$: 409.2; found: 409.2.

**(*S*)-*N*-(1-(*tert*-butylamino)-4,4-dimethyl-1,2-dioxopentan-3-yl)-1-(4-fluorobenzyl)-1*H*-indole-3-carboxamide (68).** Purified by column chromatography (DCM/MeOH 99:1). Yield: 77%. Mp: 107 – 108 ºC. $^{1}$H NMR (300 MHz, DMSO-*d6*) $\delta$ (ppm): 8.43 (s, 1H), 8.05 (d, $J$ = 7.3 Hz, 1H), 7.86 (s, 1H), 7.66 (d, $J$ = 7.9 Hz, 1H), 7.51 (d, $J$ = 8.0 Hz, 1H), 7.35 – 7.24 (m, 2H), 7.20 – 7.09 (m, 4H), 5.45 (s, 2H), 5.40 (d, $J$ = 7.8 Hz, 1H), 1.27 (s, 9H), 1.01 (s, 9H). LRMS (CI) *m/*z calcd for $C_{27}H_{33}FN_3O_3$ $[M+H]^+$: 466.2; found: 466.2.

USC UNIVERSIDADE DE SANTIAGO DE COMPOSTELA

**methyl (*S*)-(3-(1-(4-fluorobenzyl)-1*H*-indole-3-carboxamido)-4,4-dimethyl-2-oxopentanoyl)glycinate (69).** Purified by column chromatography (DCM/MeOH 99:1). Yield: 68%. Mp: 167 – 169 ºC. $^1$H NMR (300 MHz, $CDCl_3$) $\delta$ (ppm): 8.01 – 7.93 (m, 1H), 7.76 (s, 1H), 7.49 – 7.40 (m, 1H), 7.33 – 7.28 (m, 2H), 7.16 – 7.08 (m, 3H), 7.05 – 6.94 (m, 3H), 5.58 (d, *J* = 8.0 Hz, 1H), 5.30 (s, 2H), 4.18 – 4.05 (m, 2H), 3.77 (s, 3H), 1.12 (s, 9H). LRMS (CI) *m/*z calcd for $C_{26}H_{29}FN_3O_5$ $[M+H]^+$: 482.2; found: 482.2.

**(*S*)-*N*-(1-((2-amino-2-oxoethyl)amino)-4,4-dimethyl-1,2-dioxopentan-3-yl)-1-(4-fluorobenzyl)-1*H*-indole-3-carboxamide (70).** Purified by column chromatography (DCM/MeOH 94:6). Yield: 66%. Mp: 80 – 81 ºC. $^1$H NMR (300 MHz, $CDCl_3$) $\delta$ (ppm): 8.14 (d, *J* = 7.2 Hz, 1H), 8.01 (s, 1H), 7.93 – 7.72 (m, 1H), 7.34 – 7.27 (m, 2H), 7.15 – 7.08 (m, 2H), 7.01 – 6.93 (m, 2H), 6.42 (brs, 1H), 6.23 (s, 1H), 5.92 (brs, 1H), 5.78 (brs, 1H), 5.28 (d, *J* = 7.4 Hz, 2H), 4.18 – 3.77 (m, 2H), 1.30 (s, 9H). HRMS (ESI) *m/*z calcd for $C_{25}H_{28}FN_4O_4$ $[M+H]^+$: 467.2016; found: 467.2089.

**(*S*)-*N*-(1-(benzylamino)-4,4-dimethyl-1,2-dioxopentan-3-yl)-1-(4-fluorobenzyl)-1*H*-indole-3-carboxamide (71).** Purified by column chromatography (DCM/MeOH 99:1). Yield: 63%. Oil at room temperature. $^1$H NMR (300 MHz, $CDCl_3$) $\delta$ (ppm): 8.01 (d, *J* = 7.0 Hz, 2H), 7.77 (s, 1H), 7.37 – 7.18 (m, 7H), 7.10 (t, *J* = 6.7 Hz, 3H), 7.04 – 6.93 (m, 3H), 5.61 – 5.53 (m, 1H), 5.28 (s, 2H), 4.59 – 4.39 (m, 2H), 1.12 (s, 9H). LRMS (CI) *m/*z calcd for $C_{30}H_{31}FN_3O_3$ $[M+H]^+$: 500.2; found: 500.2.

**(*S*)-*N*-(4,4-dimethyl-1-((2-morpholinoethyl)amino)-1,2-dioxopentan-3-yl)-1-(4-fluorobenzyl)-1*H*-indole-3-carboxamide (72).** Purified by column chromatography (DCM/MeOH 99:1). Yield: 63%. Mp: 140 – 141 ºC. $^1$H NMR (300 MHz, $CDCl_3$) $\delta$ (ppm): 8.01 (d, *J* = 7.8 Hz, 1H), 7.76 (s, 1H), 7.49 – 7.38 (m, 1H), 7.34 – 7.27 (m, 3H), 7.17 – 7.07 (m, 2H), 7.06 – 6.94 (m, 3H), 5.55 (d, *J* = 8.5 Hz, 1H), 5.30 (s, 2H), 3.73 – 3.67 (m, 4H), 3.45 – 3.39 (m, 2H), 2.59 – 2.52 (m, 2H), 2.51 – 2.45 (m, 4H), 1.12 (s, 9H). LRMS (CI) *m/*z calcd for $C_{29}H_{36}FN_4O_4$ $[M+H]^+$: 523.3; found: 523.3.

USC UNIVERSIDADE DE SANTIAGO DE COMPOSTELA

**(*S*)-*N*-(1-amino-1,2-dioxopentan-3-yl)-1-(cyclohexylmethyl)-1*H*-indole-3-carboxamide (73).** Purified by column chromatography (DCM/MeOH 94:6). Yield: 60%. Mp: 162 – 163 ºC. $^1$H NMR (300 MHz, $CDCl_3$) $\delta$ (ppm): 8.01 – 7.94 (m, 1H), 7.71 (s, 1H), 7.37 (m, 1H), 7.30 (m, 1H), 6.86 – 6.77 (m, 1H), 6.65 – 6.57 (m, 1H), 5.51 – 5.42 (m, 2H), 3.96 (d, *J* = 7.1 Hz, 2H), 2.42 – 2.10 (m, 2H), 2.00 – 1.81 (m, 1H), 1.78 – 1.48 (m, 7H), 1.36 – 1.27 (m, 1H), 1.23 – 1.14 (m, 2H), 1.06 (t, *J* = 7.6 Hz, 3H). LRMS (CI) *m/*z calcd for $C_{21}H_{28}N_3O_3$ $[M+H]^+$: 370.2; found: 370.2.

**(*S*)-*N*-(1-(*tert*-butylamino)-1,2-dioxopentan-3-yl)-1-(cyclohexylmethyl)-1*H*-indole-3-carboxamide (74).** Purified by column chromatography (DCM/MeOH 99:1). Yield: 75%. Mp: 193 – 195 ºC. $^1$H NMR (300 MHz, $CDCl_3$) $\delta$ (ppm): 8.02 – 7.95 (m, 1H), 7.70 (s, 1H), 7.41 – 7.34 (m, 1H), 7.29 – 7.27 (m, 2H), 6.78 (s, 1H), 6.68 (d, *J* = 7.9 Hz, 1H), 5.52 – 5.42 (m, 1H), 3.95 (d, *J* = 7.2 Hz, 2H), 2.25 – 2.10 (m, 1H), 1.93 – 1.80 (m, 2H), 1.63 (d, *J* = 9.9 Hz, 6H), 1.40 (s, 9H), 1.34 – 1.12 (m, 3H), 1.04 (t, *J* = 7.4 Hz, 3H), 0.92 (t, *J* = 7.5 Hz, 1H). LRMS (CI) *m/*z calcd for $C_{25}H_{36}N_3O_3$ $[M+H]^+$: 409.2; found: 409.2.

**methyl (*S*)-(3-(1-(cyclohexylmethyl)-1*H*-indole-3-carboxamido)-2-oxopentanoyl)glycinate (75).** Purified by column chromatography (DCM/MeOH 99:1). Yield: 64%. Mp: 208 – 210 ºC. $^1$H NMR (300 MHz, $CDCl_3$) $\delta$ (ppm): 8.24 – 8.19 (m, 1H), 7.93 (s, 1H), 7.42 – 7.37 (m, 1H), 7.34 – 7.29 (m, 1H), 7.10 (s, 1H), 5.86 (s, 1H), 4.12 (dd, *J* = 9.4, 5.2 Hz, 2H), 4.01 (d, *J* = 7.3 Hz, 2H), 3.80 (s, 3H), 3.04 – 2.77 (m, 2H), 1.96 – 1.85 (m, 1H), 1.80 – 1.62 (m, 8H), 1.28 – 1.25 (m, 2H), 1.15 (t, *J* = 7.2 Hz, 3H). LRMS (CI) *m/*z calcd for $C_{24}H_{32}N_3O_5$ $[M+H]^+$: 442.2; found: 442.2.

**(*S*)-*N*-(1-(benzylamino)-1,2-dioxopentan-3-yl)-1-(cyclohexylmethyl)-1*H*-indole-3-carboxamide (76).** Purified by column chromatography (DCM/MeOH 99:1). Yield: 69%. Mp: 105 – 106 ºC. $^1$H NMR (300 MHz, $CDCl_3$) $\delta$ (ppm): 7.99 (d, *J* = 6.4 Hz, 1H), 7.70 (s, 1H), 7.41 – 7.20 (m, 9H), 6.68 (d, *J* = 7.7 Hz, 1H), 5.55 – 5.46 (m, 1H), 4.51 (d, *J* = 6.2 Hz, 2H), 3.95 (d, *J* = 6.9 Hz, 2H), 2.28 – 2.14 (m, 1H), 2.00 – 1.80 (m, 2H), 1.78 – 1.56 (m, 7H), 1.28 – 1.13 (m, 3H), 1.06 (t, *J* = 7.4 Hz, 3H). LRMS (CI) *m/*z calcd for $C_{28}H_{34}N_3O_3$ $[M+H]^+$: 460.3; found: 460.3.

USC UNIVERSIDADE DE SANTIAGO DE COMPOSTELA

**(*S*)-1-(cyclohexylmethyl)-*N*-(1-((2-morpholinoethyl)amino)-1,2-dioxopentan-3-yl)-1*H*-indole-3-carboxamide (77).** Purified by column chromatography (DCM/MeOH 99:1). Yield: 69%. Mp: 169 – 171 ºC. $^1$H NMR (300 MHz, $CDCl_3$) $\delta$ (ppm): 8.03 – 7.96 (m, 1H), 7.71 (s, 1H), 7.45 (s, 1H), 7.41 – 7.35 (m, 1H), 7.31 – 7.28 (m, 2H), 6.69 (d, *J* = 7.8 Hz, 1H), 5.54 – 5.45 (m, 1H), 3.96 (d, *J* = 7.1 Hz, 2H), 3.75 – 3.67 (m, 4H), 3.48 – 3.40 (m, 2H), 2.56 (t, *J* = 5.8 Hz, 2H), 2.52 – 2.46 (m, 4H), 2.25 – 2.14 (m, 1H), 1.96 – 1.82 (m, 2H), 1.75 – 1.58 (m, 7H), 1.22 – 1.12 (m, 3H), 1.08 – 0.99 (m, 3H). LRMS (CI) *m/*z calcd for $C_{27}H_{39}N_4O_4$ $[M+H]^+$: 483.3; found: 483.3.

**(*S*)-*N*-(1-amino-4-methyl-1,2-dioxopentan-3-yl)-1-(cyclohexylmethyl)-1*H*-indole-3-carboxamide (78).** Purified by column chromatography (DCM/MeOH 94:6). Yield: 67%. Mp: 85 – 86 ºC. $^1$H NMR (300 MHz, $CDCl_3$) $\delta$ (ppm): 8.01 – 7.96 (m, 1H), 7.74 (s, 1H), 7.43 – 7.38 (m, 1H), 7.33 – 7.28 (m, 2H), 6.88 (brs, 1H), 6.67 (d, *J* = 8.4 Hz, 1H), 5.67 (brs, 1H), 5.44 (dd, *J* = 8.3, 5.8 Hz, 1H), 3.97 (d, *J* = 7.2 Hz, 2H), 2.58 – 2.44 (m, 1H), 1.95 – 1.81 (m, 1H), 1.78 – 1.59 (m, 8H), 1.25 – 1.16 (m, 2H), 1.14 (d, *J* = 6.8 Hz, 3H), 1.03 (d, *J* = 6.9 Hz, 3H). $^{13}$C NMR (75 MHz, $CDCl_3$) $\delta$ (ppm): 196.3, 165.2, 161.6, 132.9, 122.4, 121.6, 119.9, 110.7, 59.2, 53.4, 38.5, 31.0, 30.8, 26.2, 25.6, 20.0, 18.0. LRMS (CI) *m/*z calcd for $C_{22}H_{30}N_3O_3$ $[M+H]^+$: 384.2; found: 384.2.

**(*S*)-*N*-(1-(*tert*-butylamino)-4-methyl-1,2-dioxopentan-3-yl)-1-(cyclohexylmethyl)-1*H*-indole-3-carboxamide (79).** Purified by column chromatography (DCM/MeOH 99:1). Yield: 74%. Mp: 112 – 113 ºC. $^1$H NMR (300 MHz, $CDCl_3$) $\delta$ (ppm): 7.99 (dd, *J* = 6.1, 3.3 Hz, 1H), 7.71 (s, 1H), 7.42 – 7.33 (m, 1H), 7.31 – 7.26 (m, 2H), 6.80 (s, 1H), 6.73 (d, *J* = 8.7 Hz, 1H), 5.43 (dd, *J* = 8.7, 5.6 Hz, 1H), 3.95 (d, *J* = 7.2 Hz, 2H), 2.49 (m, 1H), 1.93 – 1.78 (m, 1H), 1.77 – 1.55 (m, 7H), 1.40 (s, 9H), 1.24 – 1.14 (m, 3H), 1.10 (d, *J* = 6.8 Hz, 3H), 0.97 (d, *J* = 6.8 Hz, 3H). LRMS (CI) *m/*z calcd for $C_{26}H_{38}N_3O_3$ $[M+H]^+$: 440.3; found: 440.3.

**methyl (*S*)-(3-(1-(cyclohexylmethyl)-1*H*-indole-3-carboxamido)-4-methyl-2-oxopentanoyl)glycinate (80).** Purified by column chromatography (DCM/MeOH 99:1). Yield: 60%. Mp: 171 – 173 ºC. $^1$H NMR (300 MHz, $CDCl_3$) $\delta$ (ppm): 8.24 – 8.18 (m, 1H), 7.92 (s, 1H), 7.42 – 7.35 (m, 1H), 7.34 – 7.28 (m, 1H), 7.09 (s, 1H), 6.02 (s, 1H), 4.11 (dd, *J* = 10.2, 5.2 Hz, 2H), 4.00 (d, *J* = 7.2 Hz, 2H), 3.78 (s, 3H), 3.36 – 3.25 (m, 1H), 1.94 – 1.85 (m, 1H), 1.77 – 1.59 (m, 8H), 1.30 (d, *J* = 6.9 Hz, 3H), 1.22 – 1.18 (m, 1H), 1.14 (d, *J* = 6.7 Hz, 3H), 1.08 – 0.96 (m, 1H). LRMS (CI) *m/*z calcd for $C_{25}H_{34}N_3O_5$ $[M+H]^+$: 456.2; found: 456.3.

USC UNIVERSIDADE DE SANTIAGO DE COMPOSTELA

**(*S*)-*N*-(1-(benzylamino)-4-methyl-1,2-dioxopentan-3-yl)-1-(cyclohexylmethyl)-1*H*-indole-3-carboxamide (81).** Purified by column chromatography (DCM/MeOH 99:1). Yield: 75%. Mp: 245 – 246 ºC. $^{1}$H NMR (300 MHz, $CDCl_3$) $\delta$ (ppm): 8.11 (d, $J$ = 7.9 Hz, 1H), 7.86 (s, 1H), 7.41 – 7.29 (m, 8H), 7.26 – 7.19 (m, 1H), 6.80 (s, 1H), 5.47 (dd, $J$ = 8.5, 5.7 Hz, 1H), 4.53 (m, 2H), 3.98 (d, $J$ = 7.2 Hz, 2H), 2.60 – 2.50 (m, 1H), 1.95 – 1.81 (m, 1H), 1.78 – 1.55 (m, 7H), 1.32 (d, $J$ = 7.1 Hz, 3H), 1.26 – 1.22 (m, 3H), 1.19 (d, $J$ = 7.2 Hz, 3H). LRMS (CI) *m/*z calcd for $C_{29}H_{36}N_3O_3$ $[M+H]^+$: 474.3; found: 474.3.

**(*S*)-1-(cyclohexylmethyl)-*N*-(4-methyl-1-((2-morpholinoethyl)amino)-1,2-dioxopentan-3-yl)-1*H*-indole-3-carboxamide (82).** Purified by column chromatography (DCM/MeOH 99:1-97:3). Yield: 64%. Mp: 133 – 134 ºC. $^{1}$H NMR (300 MHz, $CDCl_3$) $\delta$ (ppm): 8.04 – 7.92 (m, 1H), 7.71 (s, 1H), 7.44 – 7.34 (m, 2H), 7.32 – 7.27 (m, 2H), 6.73 (d, $J$ = 8.6 Hz, 1H), 5.48 – 5.40 (m, 1H), 3.96 (d, $J$ = 7.2 Hz, 2H), 3.73 – 3.66 (m, 4H), 3.46 – 3.38 (m, 2H), 2.53 (t, $J$ = 6.2 Hz, 2H), 2.49 – 2.41 (m, 4H), 1.92 – 1.80 (m, 1H), 1.74 – 1.57 (m, 7H), 1.27 – 1.14 (m, 3H), 1.12 (d, $J$ = 6.8 Hz, 3H), 0.99 (d, $J$ = 6.9 Hz, 3H). $^{13}$C NMR (75 MHz, $CDCl_3$) $\delta$ (ppm): 191.9, 165.1, 159.2, 132.8, 125.6, 125.1, 122.4, 121.6, 119.9, 110.7, 66.9, 59.6, 56.6, 53.3, 38.5, 35.6, 31.0, 30.9, 26.2, 25.6, 20.0, 18.0. LRMS (CI) *m/*z calcd for $C_{28}H_{41}N_4O_4$ $[M+H]^+$: 497.3; found: 497.3.

**(*S*)-*N*-(1-amino-4,4-dimethyl-1,2-dioxopentan-3-yl)-1-(cyclohexylmethyl)-1*H*-indole-3-carboxamide (83).** Purified by column chromatography (DCM/MeOH 94:6). Yield: 78%. Mp: 171 – 172 ºC. $^{1}$H NMR (300 MHz, $CDCl_3$) $\delta$ (ppm): 7.97 – 7.91 (m, 1H), 7.72 (s, 1H), 7.42 – 7.35 (m, 1H), 7.33 – 7.25 (m, 2H), 6.92 – 6.79 (m, 2H), 5.61 – 5.52 (m, 2H), 3.95 (d, $J$ = 7.2 Hz, 2H), 1.85 (s, 1H), 1.77 – 1.57 (m, 7H), 1.26 – 1.16 (m, 1H), 1.13 (s, 9H), 1.08 – 0.90 (m, 2H). $^{13}$C NMR (75 MHz, $CDCl_3$) $\delta$ (ppm): 197.4, 165.0, 162.2, 137.0, 133.1, 122.4, 121.6, 119.7, 110.7, 59.5, 53.4, 38.5, 35.4, 31.0, 26.9, 26.2, 25.6. LRMS (CI) *m/*z calcd for $C_{23}H_{32}N_3O_3$ $[M+H]^+$: 398.2; found: 398.2.

USC UNIVERSIDADE DE SANTIAGO DE COMPOSTELA

**(*S*)-*N*-(1-(*tert*-butylamino)-4,4-dimethyl-1,2-dioxopentan-3-yl)-1-(cyclohexylmethyl)-1*H*-indole-3-carboxamide (84).** Purified by column chromatography (DCM/MeOH 99:1). Yield: 79%. Mp: 284 – 285 ºC. $^{1}$H NMR (300 MHz, $CDCl_3$) $\delta$ (ppm): 8.07 – 7.95 (m, 1H), 7.73 (s, 1H), 7.45 – 7.35 (m, 1H), 7.35 – 7.23 (m, 2H), 7.01 (d, *J* = 8.7 Hz, 1H), 6.82 (s, 1H), 5.60 (d, *J* = 8.7 Hz, 1H), 3.97 (d, *J* = 7.2 Hz, 2H), 1.94 – 1.80 (m, 1H), 1.76 – 1.60 (m, 6H), 1.42 (s, 9H), 1.22 – 1.14 (m, 2H), 1.12 (s, 9H), 1.06 – 0.92 (m, 2H). $^{13}$C NMR (75 MHz, $CDCl_3$) $\delta$ (ppm): 198.7, 164.8, 159.6, 137.0, 132.9, 125.1, 122.3, 121.5, 119.9, 110.6, 110.2, 59.7, 53.4, 51.4, 38.5, 35.7, 31.0, 28.3, 27.0, 26.2, 25.6. HRMS (ESI) *m/*z calcd for $C_{27}H_{40}N_3O_3$ $[M+H]^+$: 454.2991; found: 454.3064.

**methyl (*S*)-(3-(1-(cyclohexylmethyl)-1*H*-indole-3-carboxamido)-4,4-dimethyl-2-oxopentanoyl)glycinate (85).** Purified by column chromatography (DCM/MeOH 99:1). Yield: 61%. Mp: 128 – 129 ºC. $^{1}$H NMR (300 MHz, $CDCl_3$) $\delta$ (ppm): 8.24 – 8.17 (m, 1H), 7.92 (s, 1H), 7.43 – 7.37 (m, 1H), 7.35 – 7.30 (m, 1H), 6.98 (s, 1H), 6.28 (s, 1H), 4.12 (dd, *J* = 11.2, 5.3 Hz, 2H), 4.01 (d, *J* = 7.2 Hz, 2H), 3.78 (s, 3H), 1.99 – 1.85 (m, 1H), 1.81 – 1.63 (m, 4H), 1.59 (s, 4H), 1.36 (s, 9H), 1.31 – 1.18 (m, 1H), 0.93 – 0.82 (m, 1H). LRMS (CI) *m/*z calcd for $C_{26}H_{36}N_3O_5$ $[M+H]^+$: 470.3; found: 470.3.

**(*S*)-*N*-(1-(benzylamino)-4,4-dimethyl-1,2-dioxopentan-3-yl)-1-(cyclohexylmethyl)-1*H*-indole-3-carboxamide (86).** Purified by column chromatography (DCM/MeOH 99:1). Yield: 63%. Mp: 111 – 112 ºC. $^{1}$H NMR (300 MHz, $CDCl_3$) $\delta$ (ppm): 8.06 – 7.93 (m, 1H), 7.73 (s, 1H), 7.43 – 7.37 (m, 1H), 7.36 – 7.28 (m, 7H), 6.97 (d, *J* = 8.3 Hz, 1H), 5.60 (d, *J* = 8.3 Hz, 1H), 4.61 – 4.45 (m, 2H), 3.97 (d, *J* = 7.2 Hz, 2H), 1.94 – 1.82 (m, 1H), 1.78 – 1.60 (m, 7H), 1.21 – 1.18 (m, 2H), 1.15 (s, 9H), 1.06 – 0.98 (m, 1H). LRMS (CI) *m/*z calcd for $C_{30}H_{38}N_3O_3$ $[M+H]^+$: 488.3; found: 488.3.

**(*S*)-1-(cyclohexylmethyl)-*N*-(4,4-dimethyl-1-((2-morpholinoethyl)amino)-1,2-dioxopentan-3-yl)-1*H*-indole-3-carboxamide (87).** Purified by column chromatography (DCM/MeOH 99:1-97:3). Yield: 62%. Mp: 290 – 292 ºC. $^{1}$H NMR (300 MHz, $CDCl_3$) $\delta$ (ppm): 8.16 (d, *J* = 6.7 Hz, 1H), 7.89 (s, 1H), 7.42 – 7.35 (m, 1H), 7.34 – 7.26 (m, 2H), 7.04 – 6.97 (m, 1H), 6.28 (s, 1H), 3.99 (d, *J* = 7.1 Hz, 2H), 3.45 – 3.34 (m, 6H), 2.53 – 2.44 (m, 2H), 2.42 – 2.31 (m, 4H), 1.92 – 1.80 (m, 1H), 1.78 – 1.54 (m, 7H), 1.33 (s, 9H), 1.24 – 1.14 (m, 2H), 1.09 – 0.94 (m, 1H). LRMS (CI) *m/*z calcd for $C_{29}H_{43}N_4O_4$ $[M+H]^+$: 511.3; found: 511.3.

USC UNIVERSIDADE DE SANTIAGO DE COMPOSTELA

**(*S*)-*N*-(1-(*tert*-butylamino)-4,4-dimethyl-1,2-dioxopentan-3-yl)-1-(5-fluoropentyl)-1*H*-indole-3-carboxamide (88).** Purified by column chromatography (DCM/MeOH 99:1). Yield: 74%. Mp: 272 – 273 ºC. $^{1}$H NMR (300 MHz, $CDCl_3$) $\delta$ (ppm): 8.07 – 8.00 (m, 1H), 7.77 (s, 1H), 7.44 – 7.37 (m, 1H), 7.35 – 7.28 (m, 2H), 7.03 (d, *J* = 8.7 Hz, 1H), 6.83 (s, 1H), 5.61 (d, *J* = 8.7 Hz, 1H), 4.52 (t, *J* = 5.9 Hz, 1H), 4.36 (t, *J* = 5.9 Hz, 1H), 4.18 (t, *J* = 7.1 Hz, 2H), 1.94 (p, *J* = 7.2 Hz, 2H), 1.83 – 1.63 (m, 3H), 1.54 – 1.44 (m, 1H), 1.43 (s, 9H), 1.13 (s, 9H). $^{13}$C NMR (75 MHz, $CDCl_3$) $\delta$ (ppm): 198.7, 164.7, 159.6, 136.6, 132.1, 122.5, 121.7, 120.1, 110.6, 110.3, 84.7, 82.5, 59.8, 51.4, 46.7, 35.7, 30.1, 29.8, 29.6, 28.3, 27.0, 22.9, 22.8. HRMS (ESI) *m/*z calcd for $C_{25}H_{37}FN_3O_3$ $[M+H]^+$: 446.2741; found: 446.2815.

**(*S*)-*N*-(1-(benzylamino)-4,4-dimethyl-1,2-dioxopentan-3-yl)-1-(5-fluoropentyl)-1*H*-indole-3-carboxamide (89).** Purified by column chromatography (DCM/MeOH 99:1). Yield: 60%. Mp: 82 – 83 ºC. $^{1}$H NMR (300 MHz, $CDCl_3$) $\delta$ (ppm): 8.06 – 7.99 (m, 1H), 7.77 (s, 1H), 7.43 – 7.38 (m, 1H), 7.36 – 7.27 (m, 8H), 7.02 (d, *J* = 8.3 Hz, 1H), 5.60 (d, *J* = 8.3 Hz, 1H), 4.61 – 4.45 (m, 3H), 4.35 (t, *J* = 5.9 Hz, 1H), 4.17 (t, *J* = 7.1 Hz, 2H), 1.93 (p, *J* = 7.3 Hz, 2H), 1.82 – 1.62 (m, 2H), 1.53 – 1.41 (m, 2H), 1.16 (s, 9H). $^{13}$C NMR (75 MHz, $CDCl_3$) $\delta$ (ppm): 197.59, 164.85, 160.30, 136.84 (d, *J* = 29.2 Hz), 132.11, 128.83, 127.85, 127.82, 125.30, 122.55, 121.73, 120.07, 110.33, 83.63 (d, *J* = 165.0 Hz), 60.19, 46.72, 43.51, 35.62, 29.93 (d, *J* = 19.8 Hz), 29.62, 27.02, 22.82 (d, *J* = 5.0 Hz). LRMS (CI) *m/*z calcd for $C_{28}H_{35}FN_3O_3$ $[M+H]^+$: 480.3; found: 480.3.

**(*S*)-*N*-(1-(*tert*-butylamino)-4,4-dimethyl-1,2-dioxopentan-3-yl)-1-pentyl-1*H*-indole-3-carboxamide (90).** Purified by column chromatography (DCM/MeOH 99:1). Yield: 62%. Mp: 229 – 231 ºC. $^{1}$H NMR (300 MHz, $CDCl_3$) $\delta$ (ppm): 8.07 – 8.00 (m, 1H), 7.78 (s, 1H), 7.44 – 7.37 (m, 1H), 7.35 – 7.16 (m, 2H), 7.04 (d, *J* = 8.7 Hz, 1H), 6.85 (s, 1H), 5.62 (d, *J* = 8.3 Hz, 1H), 4.18 – 4.10 (m, 2H), 1.94 – 1.81 (m, 2H), 1.43 (s, 9H), 1.39 – 1.27 (m, 4H), 1.13 (s, 9H), 0.96 – 0.86 (m, 3H). $^{13}$C NMR (75 MHz, $CDCl_3$) $\delta$ (ppm): 198.72, 164.78, 159.69, 136.68, 132.20, 128.63 (d, *J* = 61.1 Hz), 125.28, 122.37, 121.57, 120.01, 110.38, 59.75, 51.43, 46.87, 35.73, 29.63, 28.99, 28.27, 27.00, 22.26, 13.87. HRMS (ESI) *m/*z calcd for $C_{25}H_{38}N_3O_3$ $[M+H]^+$: 428.2835; found: 428.2908.

USC UNIVERSIDADE DE SANTIAGO DE COMPOSTELA

**(*S*)-*N*-(1-(benzylamino)-4,4-dimethyl-1,2-dioxopentan-3-yl)-1-pentyl-1*H*-indole-3-carboxamide (91).** Purified by column chromatography (DCM/MeOH 99:1). Yield: 74%. Mp: 108 – 109 ºC. $^1$H NMR (300 MHz, $CDCl_3$) $\delta$ (ppm): 8.01 – 7.95 (m, 1H), 7.75 (s, 1H), 7.43 – 7.35 (m, 1H), 7.30 (d, *J* = 4.8 Hz, 8H), 6.96 (d, *J* = 8.3 Hz, 1H), 5.58 (d, *J* = 8.3 Hz, 1H), 4.59 – 4.42 (m, 2H), 4.13 (t, *J* = 7.3 Hz, 2H), 1.87 (q, *J* = 7.4 Hz, 2H), 1.39 – 1.25 (m, 4H), 1.13 (s, 9H), 0.93 – 0.84 (m, 3H). LRMS (CI) *m/*z calcd for $C_{28}H_{36}N_3O_3$ $[M+H]^+$: 462.3; found: 462.3.

**(*S*)-*N*-(1-amino-1,2-dioxopentan-3-yl)-1-(4-fluorobenzyl)-1*H*-indazole-3-carboxamide (92).** Purified by column chromatography (DCM/MeOH 94:6). Yield: 62%. Mp: 163 – 164 ºC. $^1$H NMR (300 MHz, $CDCl_3$) $\delta$ (ppm): 8.33 (d, *J* = 8.1 Hz, 1H), 7.54 (d, *J* = 7.6 Hz, 1H), 7.40 – 7.23 (m, 2H), 7.22 – 7.15 (m, 3H), 7.00 (t, *J* = 8.4 Hz, 2H), 6.86 (brs, 1H), 5.77 (brs, 1H), 5.59 (s, 2H), 5.54 – 5.47 (m, 1H), 2.26 – 2.11 (m, 1H), 1.95 – 1.79 (m, 1H), 1.06 (t, *J* = 7.4 Hz, 3H). LRMS (CI) *m/*z calcd for $C_{20}H_{20}FN_4O_3$ $[M+H]^+$: 383.1; found: 383.1.

**(*S*)-*N*-(1-(*tert*-butylamino)-1,2-dioxopentan-3-yl)-1-(4-fluorobenzyl)-1*H*-indazole-3-carboxamide (93).** Purified by column chromatography (DCM/MeOH 99:1). Yield: 63%. Oil at room temperature. $^1$H NMR (300 MHz, $CDCl_3$) $\delta$ (ppm): 8.35 (d, *J* = 8.0 Hz, 1H), 7.54 (d, *J* = 8.0 Hz, 1H), 7.39 – 7.28 (m, 2H), 7.23 – 7.15 (m, 2H), 7.00 (t, *J* = 8.2 Hz, 2H), 6.77 (s, 1H), 5.59 (s, 2H), 5.57 – 5.50 (m, 1H), 2.27 – 2.12 (m, 1H), 1.92 – 1.76 (m, 1H), 1.40 (s, 9H), 1.06 (t, *J* = 7.3 Hz, 3H). LRMS (CI) *m/*z calcd for $C_{24}H_{28}FN_4O_3$ $[M+H]^+$: 439.2; found: 439.2.

**methyl (*S*)-(3-(1-(4-fluorobenzyl)-1*H*-indazole-3-carboxamido)-2-oxopentanoyl)glycinate (94).** Purified by column chromatography (DCM/MeOH 99:1). Yield: 66%. Mp: 219 – 221 ºC. $^1$H NMR (300 MHz, $CDCl_3$) $\delta$ (ppm): 8.33 (d, *J* = 8.1 Hz, 1H), 7.55 (d, *J* = 7.5 Hz, 1H), 7.47 – 7.28 (m, 3H), 7.23 – 7.15 (m, 3H), 7.01 (t, *J* = 8.6 Hz, 2H), 5.59 (s, 2H), 5.56 (s, 1H), 4.16 – 4.08 (m, 2H), 3.78 (s, 3H), 2.27 – 2.12 (m, 1H), 1.95 – 1.79 (m, 1H), 1.06 (t, *J* = 7.5 Hz, 3H). LRMS (CI) *m/*z calcd for $C_{23}H_{24}FN_4O_5$ $[M+H]^+$: 455.2; found: 455.2.

**(*S*)-*N*-(1-(benzylamino)-1,2-dioxopentan-3-yl)-1-(4-fluorobenzyl)-1*H*-indazole-3-carboxamide (95).** Purified by column chromatography (DCM/MeOH 99:1). Yield: 74%. Mp: 146 – 148 ºC. $^1$H NMR (300 MHz, $CDCl_3$) $\delta$ (ppm): 8.34 (d, *J* = 8.0 Hz, 1H), 7.56 (d, *J* = 7.4 Hz, 1H), 7.40 – 7.23 (m, 8H), 7.22 – 7.15 (m, 3H), 7.00 (t, *J* = 8.5 Hz, 2H), 5.59 (s, 2H), 5.57 – 5.51 (m, 1H), 4.51 (d, *J* = 6.0 Hz, 2H), 2.30 – 2.15 (m, 1H), 1.98 – 1.82 (m, 1H), 1.07 (t, *J* = 7.4 Hz, 3H). LRMS (CI) *m/*z calcd for $C_{27}H_{26}FN_4O_3$ $[M+H]^+$: 473.2; found: 473.2.

USC UNIVERSIDADE DE SANTIAGO DE COMPOSTELA

**(*S*)-1-(4-fluorobenzyl)-*N*-(1-((2-morpholinoethyl)amino)-1,2-dioxopentan-3-yl)-1*H*-indazole-3-carboxamide (96).** Purified by column chromatography (DCM/MeOH 99:1-97:3). Yield: 80%. Mp: 260 – 262 ºC. $^1$H NMR (300 MHz, $CDCl_3$) $\delta$ (ppm): 8.34 (d, *J* = 8.0 Hz, 1H), 7.56 (d, *J* = 7.8 Hz, 1H), 7.45 – 7.27 (m, 3H), 7.23 – 7.15 (m, 2H), 7.00 (t, *J* = 8.3 Hz, 2H), 5.59 (s, 2H), 5.56 – 5.50 (m, 1H), 3.72 – 3.66 (m, 4H), 3.45 – 3.38 (m, 2H), 2.53 (t, *J* = 6.0 Hz, 2H), 2.49 – 2.42 (m, 4H), 2.27 – 2.15 (m, 1H), 1.95 – 1.84 (m, 1H), 1.06 (t, *J* = 7.4 Hz, 3H). LRMS (CI) *m/*z calcd for $C_{26}H_{31}FN_5O_4$ $[M+H]^+$: 496.2; found: 496.2.

**(*S*)-*N*-(1-amino-4-methyl-1,2-dioxopentan-3-yl)-1-(4-fluorobenzyl)-1*H*-indazole-3-carboxamide (97).** Purified by column chromatography (DCM/MeOH 94:6). Yield: 61%. Mp: 140 – 142 ºC. $^1$H NMR (300 MHz, $CDCl_3$) $\delta$ (ppm): 8.34 (d, *J* = 8.1 Hz, 1H), 7.57 (d, *J* = 8.6 Hz, 1H), 7.39 – 7.27 (m, 3H), 7.23 – 7.15 (m, 2H), 7.01 (t, *J* = 8.5 Hz, 2H), 6.85 (brs, 1H), 5.72 (brs, 1H), 5.60 (s, 2H), 5.57 – 5.46 (m, 1H), 2.58 – 2.45 (m, 1H), 1.12 (d, *J* = 6.7 Hz, 3H), 0.99 (d, *J* = 6.9 Hz, 3H). LRMS (CI) *m/*z calcd for $C_{21}H_{22}FN_4O_3$ $[M+H]^+$: 397.2; found: 397.2.

**(*S*)-*N*-(1-(*tert*-butylamino)-4-methyl-1,2-dioxopentan-3-yl)-1-(4-fluorobenzyl)-1*H*-indazole-3-carboxamide (98).** Purified by column chromatography (DCM/MeOH 99:1). Yield: 70%. Oil at room temperature. $^1$H NMR (300 MHz, $CDCl_3$) $\delta$ (ppm): 8.35 (d, *J* = 8.1 Hz, 1H), 7.61 (d, *J* = 8.9 Hz, 1H), 7.41 – 7.15 (m, 5H), 7.00 (t, *J* = 8.2 Hz, 2H), 6.78 (s, 1H), 5.60 (s, 2H), 5.54 (dd, *J* = 9.0, 5.0 Hz, 1H), 2.59 – 2.47 (m, 1H), 1.40 (s, 9H), 1.12 (d, *J* = 6.8 Hz, 3H), 0.96 (d, *J* = 6.9 Hz, 3H). LRMS (CI) *m/*z calcd for $C_{25}H_{30}FN_4O_3$ $[M+H]^+$: 453.2; found: 453.2.

**methyl (*S*)-(3-(1-(4-fluorobenzyl)-1*H*-indazole-3-carboxamido)-4-methyl-2-oxopentanoyl)glycinate (99).** Purified by column chromatography (DCM/MeOH 99:1). Yield: 60%. Oil at room temperature. $^1$H NMR (300 MHz, $CDCl_3$) $\delta$ (ppm): 8.34 (d, *J* = 8.1 Hz, 1H), 7.58 (d, *J* = 8.5 Hz, 1H), 7.46 – 7.24 (m, 4H), 7.23 – 7.15 (m, 2H), 7.00 (t, *J* = 8.6 Hz, 2H), 5.60 (s, 2H), 5.59 – 5.53 (m, 1H), 4.26 – 4.01 (m, 2H), 3.77 (s, 3H), 2.59 – 2.42 (m, 1H), 1.12 (d, *J* = 6.8 Hz, 3H), 0.98 (d, *J* = 6.9 Hz, 3H). LRMS (CI) *m/*z calcd for $C_{24}H_{26}FN_4O_5$ $[M+H]^+$: 469.2; found: 469.2.

USC UNIVERSIDADE DE SANTIAGO DE COMPOSTELA

**(*S*)-*N*-(1-(benzylamino)-4-methyl-1,2-dioxopentan-3-yl)-1-(4-fluorobenzyl)-1*H*-indazole-3-carboxamide (100).** Purified by column chromatography (DCM/MeOH 99:1). Yield: 64%. Oil at room temperature. $^1$H NMR (300 MHz, $CDCl_3$) $\delta$ (ppm): 8.36 (d, $J$ = 8.1 Hz, 1H), 7.64 (d, $J$ = 8.5 Hz, 1H), 7.40 – 7.24 (m, 8H), 7.23 – 7.15 (m, 3H), 7.00 (t, $J$ = 8.4 Hz, 2H), 5.59 (s, 2H), 5.58 – 5.54 (m, 1H), 4.51 (d, $J$ = 6.0 Hz, 2H), 2.66 – 2.49 (m, 1H), 1.15 (d, $J$ = 6.7 Hz, 3H), 1.00 (d, $J$ = 6.8 Hz, 3H). LRMS (CI) *m/*z calcd for $C_{28}H_{28}FN_4O_3$ $[M+H]^+$: 487.2; found: 487.2.

**(*S*)-1-(4-fluorobenzyl)-*N*-(4-methyl-1-((2-morpholinoethyl)amino)-1,2-dioxopentan-3-yl)-1*H*-indazole-3-carboxamide (101).** Purified by column chromatography (DCM/MeOH 99:1-97:3). Yield: 75%. Mp: 179 – 180 ºC. $^1$H NMR (300 MHz, $CDCl_3$) $\delta$ (ppm): 8.35 (d, $J$ = 8.1 Hz, 1H), 7.65 – 7.59 (m, 1H), 7.42 – 7.29 (m, 4H), 7.24 – 7.18 (m, 2H), 7.02 (t, $J$ = 8.5 Hz, 2H), 5.61 (s, 2H), 5.52 (dd, $J$ = 8.7, 5.4 Hz, 1H), 3.73 – 3.67 (m, 4H), 3.48 – 3.38 (m, 2H), 2.54 (t, $J$ = 6.0 Hz, 2H), 2.49 – 2.44 (m, 4H), 1.14 (d, $J$ = 6.8 Hz, 3H), 0.99 (d, $J$ = 7.0 Hz, 3H). LRMS (CI) *m/*z calcd for $C_{27}H_{33}FN_5O_4$ $[M+H]^+$: 510.2; found: 510.2.

**(*S*)-*N*-(1-amino-4,4-dimethyl-1,2-dioxopentan-3-yl)-1-(4-fluorobenzyl)-1*H*-indazole-3-carboxamide (102).** Purified by column chromatography (DCM/MeOH 99:1-97:3). Yield: 60%. Mp: 180 – 182 ºC. $^1$H NMR (300 MHz, $CDCl_3$) $\delta$ (ppm): 8.33 (d, $J$ = 8.1 Hz, 1H), 7.68 (d, $J$ = 7.8 Hz, 1H), 7.39 – 7.29 (m, 2H), 7.29 – 7.24 (m, 1H), 7.23 – 7.14 (m, 3H), 7.00 (t, $J$ = 8.4 Hz, 2H), 6.85 (s, 1H), 5.72 – 5.67 (m, 1H), 5.60 (s, 2H), 1.12 (s, 9H). LRMS (CI) *m/*z calcd for $C_{22}H_{24}FN_4O_3$ $[M+H]^+$: 411.2; found: 411.2.

**(*S*)-*N*-(1-(*tert*-butylamino)-4,4-dimethyl-1,2-dioxopentan-3-yl)-1-(4-fluorobenzyl)-1*H*-indazole-3-carboxamide (103).** Purified by column chromatography (DCM/MeOH 99:1). Yield: 80%. Oil at room temperature. $^1$H NMR (300 MHz, $CDCl_3$) $\delta$ (ppm): 8.36 (d, $J$ = 8.3 Hz, 1H), 7.81 – 7.72 (m, 1H), 7.39 – 7.29 (m, 2H), 7.23 – 7.15 (m, 2H), 7.00 (t, $J$ = 8.4 Hz, 3H), 6.77 (s, 1H), 5.75 (d, $J$ = 9.1 Hz, 1H), 5.60 (s, 2H), 1.40 (s, 9H), 1.10 (s, 9H). LRMS (CI) *m/*z calcd for $C_{26}H_{32}FN_4O_3$ $[M+H]^+$: 467.2; found: 467.2.

**methyl (*S*)-(3-(1-(4-fluorobenzyl)-1*H*-indazole-3-carboxamido)-4,4-dimethyl-2-oxopentanoyl)glycinate (104).** Purified by column chromatography (DCM/MeOH 99:1). Yield: 78%. Oil at room temperature. $^1$H NMR (300 MHz, $CDCl_3$) $\delta$ (ppm): 8.33 (d, $J$ = 8.0 Hz, 1H), 7.69 (d, $J$ = 8.4 Hz, 1H), 7.46 – 7.13 (m, 6H), 7.00 (t, $J$ = 8.6 Hz, 2H), 5.71 (d, $J$ = 8.4 Hz, 1H), 5.59 (s, 2H), 4.26 – 4.12 (m, 1H), 4.12 – 3.99 (m, 1H), 3.77 (s, 3H), 1.11 (s, 9H). LRMS (CI) *m/*z calcd for $C_{25}H_{28}FN_4O_5$ $[M+H]^+$: 483.2; found: 483.2.

USC DE SANTIAGO DE COMPOSTELA

**(*S*)-*N*-(1-(benzylamino)-4,4-dimethyl-1,2-dioxopentan-3-yl)-1-(4-fluorobenzyl)-1*H*-indazole-3-carboxamide (105).** Purified by column chromatography (DCM/MeOH 99:1). Yield: 63%. Mp: 86 – 87 ºC. $^{1}$H NMR (300 MHz, $CDCl_3$) $\delta$ (ppm): 8.35 (d, *J* = 8.0 Hz, 1H), 7.74 (d, *J* = 9.3 Hz, 1H), 7.38 – 7.28 (m, 7H), 7.23 – 7.16 (m, 3H), 7.00 (t, *J* = 8.5 Hz, 3H), 5.73 (d, *J* = 8.4 Hz, 1H), 5.60 (s, 2H), 4.53 (t, *J* = 5.8 Hz, 2H), 1.13 (s, 9H). LRMS (CI) *m/*z calcd for $C_{29}H_{30}FN_4O_3$ $[M+H]^+$: 501.2; found: 501.2.

**(*S*)-*N*-(4,4-dimethyl-1-((2-morpholinoethyl)amino)-1,2-dioxopentan-3-yl)-1-(4-fluorobenzyl)-1*H*-indazole-3-carboxamide (106).** Purified by column chromatography (DCM/MeOH 99:1-97:3). Yield: 62%. Mp: 113 – 115 ºC. $^{1}$H NMR (300 MHz, $CDCl_3$) $\delta$ (ppm): 8.33 (d, *J* = 8.1 Hz, 1H), 7.74 (d, *J* = 8.6 Hz, 1H), 7.40 – 7.27 (m, 4H), 7.23 – 7.15 (m, 2H), 7.04 – 6.96 (m, 2H), 5.70 (d, *J* = 8.3 Hz, 1H), 5.59 (s, 2H), 3.73 – 3.66 (m, 4H), 3.47 – 3.38 (m, 2H), 2.53 (t, *J* = 6.2 Hz, 2H), 2.49 – 2.43 (m, 4H), 1.11 (s, 9H). LRMS (CI) *m/*z calcd for $C_{28}H_{35}FN_5O_4$ $[M+H]^+$: 524.3; found: 524.3.

**(*S*)-*N*-(1-amino-1,2-dioxopentan-3-yl)-1-(cyclohexylmethyl)-1*H*-indazole-3-carboxamide (107).** Purified by column chromatography (DCM/MeOH 94:6). Yield: 67%. Mp: 163 – 165 ºC. $^{1}$H NMR (300 MHz, $CDCl_3$) $\delta$ (ppm): 8.31 (d, *J* = 8.2 Hz, 1H), 7.52 (d, *J* = 7.6 Hz, 1H), 7.43 – 7.35 (m, 2H), 7.25 – 7.21 (m, 1H), 6.88 (brs, 1H), 5.88 (brs, 1H), 5.56 – 5.46 (m, 1H), 4.22 (d, *J* = 7.3 Hz, 2H), 2.25 – 2.11 (m, 1H), 2.09 – 1.97 (m, 1H), 1.94 – 1.82 (m, 1H), 1.76 – 1.55 (m, 7H), 1.29 – 1.15 (m, 3H), 1.06 (t, *J* = 7.5 Hz, 3H). $^{13}$C NMR (75 MHz, $CDCl_3$) $\delta$ (ppm): 196.2, 162.6, 161.4, 141.4, 136.4, 126.6, 122.7, 122.7, 122.6, 109.5, 55.7, 54.9, 38.7, 30.9, 26.2, 25.6, 25.0, 10.1. LRMS (CI) *m/*z calcd for $C_{20}H_{27}N_4O_3$ $[M+H]^+$: 371.2; found: 371.2.

**(*S*)-*N*-(1-(*tert*-butylamino)-1,2-dioxopentan-3-yl)-1-(cyclohexylmethyl)-1*H*-indazole-3-carboxamide (108).** Purified by column chromatography (DCM/MeOH 99:1). Yield: 68%. Mp: 102 – 103 ºC. $^{1}$H NMR (300 MHz, $CDCl_3$) $\delta$ (ppm): 8.32 (d, *J* = 8.4 Hz, 1H), 7.52 (d, *J* = 8.3 Hz, 1H), 7.43 – 7.35 (m, 2H), 7.24 – 7.20 (m, 1H), 6.77 (s, 1H), 5.57 – 5.49 (m, 1H), 4.22 (d, *J* = 7.3 Hz, 2H), 2.26 – 2.13 (m, 1H), 2.08 – 1.95 (m, 1H), 1.90 – 1.78 (m, 1H), 1.76 – 1.55 (m, 7H), 1.39 (s, 9H), 1.27 – 1.15 (m, 3H), 1.11 – 1.01 (m, 3H). LRMS (CI) *m/*z calcd for $C_{24}H_{35}N_4O_3$ $[M+H]^+$: 427.3; found: 427.3.

USC UNIVERSIDADE DE SANTIAGO DE COMPOSTELA

**methyl (*S*)-(3-(1-(cyclohexylmethyl)-1*H*-indazole-3-carboxamido)-2-oxopentanoyl)glycinate (109).** Purified by column chromatography (DCM/MeOH 99:1). Yield: 71%. Oil at room temperature. $^{1}$H NMR (300 MHz, $CDCl_3$) $\delta$ (ppm): 8.31 (d, $J$ = 8.2 Hz, 1H), 7.52 (d, $J$ = 7.7 Hz, 1H), 7.46 – 7.35 (m, 2H), 7.25 – 7.21 (m, 1H), 7.20 – 7.14 (m, 1H), 5.60 – 5.51 (m, 1H), 4.22 (d, $J$ = 7.2 Hz, 2H), 4.12 (dd, $J$ = 10.5, 5.6 Hz, 2H), 3.78 (s, 3H), 2.25 – 2.11 (m, 1H), 2.09 – 1.97 (m, 1H), 1.94 – 1.81 (m, 1H), 1.77 – 1.55 (m, 7H), 1.27 – 1.15 (m, 3H), 1.06 (t, $J$ = 7.5 Hz, 3H). $^{13}$C NMR (75 MHz, $CDCl_3$) $\delta$ (ppm): 195.7, 169.1, 162.6, 159.4, 141.4, 136.4, 126.6, 122.7, 122.7, 122.5, 109.5, 55.7, 54.9, 52.6, 41.0, 38.7, 30.9, 26.2, 25.6, 25.0, 10.1. HRMS (ESI) *m/*z calcd for $C_{23}H_{31}N_4O_5$ $[M+H]^+$: 443.2216; found: 443.2289.

**(*S*)-*N*-(1-(benzylamino)-1,2-dioxopentan-3-yl)-1-(cyclohexylmethyl)-1*H*-indazole-3-carboxamide (110).** Purified by column chromatography (DCM/MeOH 99:1). Yield: 60%. Mp: 129 – 131 ºC. $^{1}$H NMR (300 MHz, $CDCl_3$) $\delta$ (ppm): 8.31 (d, $J$ = 8.2 Hz, 1H), 7.55 (d, $J$ = 7.6 Hz, 1H), 7.43 – 7.36 (m, 2H), 7.33 – 7.21 (m, 6H), 7.19 – 7.14 (m, 1H), 5.58 – 5.50 (m, 1H), 4.50 (d, $J$ = 6.0 Hz, 2H), 4.21 (d, $J$ = 7.2 Hz, 2H), 2.28 – 2.15 (m, 1H), 2.07 – 1.96 (m, 1H), 1.96 – 1.83 (m, 1H), 1.75 – 1.55 (m, 7H), 1.28 – 1.15 (m, 3H), 1.12 – 1.03 (m, 3H). LRMS (CI) *m/*z calcd for $C_{27}H_{33}N_4O_3$ $[M+H]^+$: 461.3; found: 461.3.

**(*S*)-1-(cyclohexylmethyl)-*N*-(1-((2-morpholinoethyl)amino)-1,2-dioxopentan-3-yl)-1*H*-indazole-3-carboxamide (111).** Purified by column chromatography (DCM/MeOH 99:1-97:3). Yield: 79%. Mp: 107 – 109 ºC. $^{1}$H NMR (300 MHz, $CDCl_3$) $\delta$ (ppm): 8.30 (d, $J$ = 8.1 Hz, 1H), 7.60 (s, 1H), 7.53 (d, $J$ = 7.7 Hz, 1H), 7.42 – 7.34 (m, 2H), 7.25 – 7.20 (m, 1H), 5.62 – 5.48 (m, 1H), 4.22 (d, $J$ = 7.2 Hz, 2H), 3.80 – 3.68 (m, 4H), 3.56 – 3.44 (m, 2H), 2.75 – 2.55 (m, 6H), 2.27 – 2.11 (m, 1H), 2.09 – 1.95 (m, 1H), 1.95 – 1.79 (m, 1H), 1.78 – 1.54 (m, 7H), 1.31 – 1.14 (m, 3H), 1.06 (t, $J$ = 7.4 Hz, 3H). LRMS (CI) *m/*z calcd for $C_{26}H_{38}N_5O_4$ $[M+H]^+$: 484.3; found: 484.3.

USC UNIVERSIDADE DE SANTIAGO DE COMPOSTELA

**(*S*)-*N*-(1-amino-4-methyl-1,2-dioxopentan-3-yl)-1-(cyclohexylmethyl)-1*H*-indazole-3-carboxamide (112).** Purified by column chromatography (DCM/MeOH 94:6). Yield: 77%. Mp: 158 – 160 ºC. $^{1}$H NMR (300 MHz, $CDCl_3$) $\delta$ (ppm): 8.31 (d, *J* = 8.1 Hz, 1H), 7.55 (d, *J* = 8.5 Hz, 1H), 7.43 – 7.37 (m, 2H), 7.25 – 7.20 (m, 1H), 6.87 (brs, 1H), 5.74 (brs, 1H), 5.54 – 5.46 (m, 1H), 4.22 (d, *J* = 7.2 Hz, 2H), 2.58 – 2.45 (m, 1H), 2.09 – 1.96 (m, 1H), 1.77 – 1.56 (m, 7H), 1.27 – 1.16 (m, 3H), 1.12 (d, *J* = 6.8 Hz, 3H), 0.99 (d, *J* = 6.8 Hz, 3H). $^{13}$C NMR (75 MHz, $CDCl_3$) $\delta$ (ppm): 196.3, 162.8, 161.4, 141.4, 136.4, 126.6, 122.7, 122.5, 109.5, 58.3, 55.7, 38.7, 30.9, 30.6, 26.2, 25.6, 20.0, 17.7. LRMS (CI) *m/*z calcd for $C_{21}H_{29}N_4O_3$ $[M+H]^+$: 385.2; found: 385.2.

**(*S*)-*N*-(1-(*tert*-butylamino)-4-methyl-1,2-dioxopentan-3-yl)-1-(cyclohexylmethyl)-1*H*-indazole-3-carboxamide (113).** Purified by column chromatography (DCM/MeOH 99:1). Yield: 62%. Oil at room temperature. $^{1}$H NMR (300 MHz, $CDCl_3$) $\delta$ (ppm): 8.32 (d, *J* = 8.2 Hz, 1H), 7.59 (d, *J* = 8.8 Hz, 1H), 7.42 – 7.35 (m, 2H), 7.24 – 7.21 (m, 1H), 6.78 (s, 1H), 5.52 (dd, *J* = 8.9, 5.1 Hz, 1H), 4.22 (d, *J* = 7.2 Hz, 2H), 2.59 – 2.47 (m, 1H), 2.03 (s, 1H), 1.76 – 1.54 (m, 7H), 1.39 (s, 9H), 1.28 – 1.15 (m, 3H), 1.11 (d, *J* = 6.8 Hz, 3H), 0.96 (d, *J* = 6.8 Hz, 3H). LRMS (CI) *m/*z calcd for $C_{25}H_{37}N_4O_3$ $[M+H]^+$: 441.3; found: 441.3.

**methyl (*S*)-(3-(1-(cyclohexylmethyl)-1*H*-indazole-3-carboxamido)-4-methyl-2-oxopentanoyl)glycinate (114).** Purified by column chromatography (DCM/MeOH 99:1). Yield: 80%. Oil at room temperature. $^{1}$H NMR (300 MHz, $CDCl_3$) $\delta$ (ppm): 8.31 (d, *J* = 8.2 Hz, 1H), 7.56 (d, *J* = 8.5 Hz, 1H), 7.45 – 7.35 (m, 2H), 7.25 – 7.21 (m, 1H), 7.19 – 7.14 (m, 1H), 5.55 (dd, *J* = 8.6, 5.3 Hz, 1H), 4.22 (d, *J* = 7.3 Hz, 2H), 4.12 (t, *J* = 6.8 Hz, 2H), 3.78 (s, 3H), 2.56 – 2.44 (m, 1H), 2.09 – 1.96 (m, 1H), 1.76 – 1.56 (m, 7H), 1.26 – 1.16 (m, 3H), 1.12 (d, *J* = 6.7 Hz, 3H), 0.98 (d, *J* = 6.8 Hz, 3H). LRMS (CI) *m/*z calcd for $C_{24}H_{33}N_4O_5$ $[M+H]^+$: 457.2; found: 457.2.

**(*S*)-*N*-(1-(benzylamino)-4-methyl-1,2-dioxopentan-3-yl)-1-(cyclohexylmethyl)-1*H*-indazole-3-carboxamide (115).** Purified by column chromatography (DCM/MeOH 99:1). Yield: 79%. Mp: 119 – 121 ºC. $^{1}$H NMR (300 MHz, $CDCl_3$) $\delta$ (ppm): 8.32 (d, *J* = 8.2 Hz, 1H), 7.60 (d, *J* = 8.5 Hz, 1H), 7.45 – 7.36 (m, 2H), 7.35 – 7.22 (m, 6H), 7.19 – 7.15 (m, 1H), 5.54 (dd, *J* = 8.6, 5.4 Hz, 1H), 4.50 (d, *J* = 6.1 Hz, 2H), 4.22 (d, *J* = 7.2 Hz, 2H), 2.63 – 2.49 (m, 1H), 2.10 – 1.95 (m, 1H), 1.77 – 1.56 (m, 7H), 1.27 – 1.17 (m, 3H), 1.14 (d, *J* = 6.8 Hz, 3H), 0.99 (d, *J* = 6.7 Hz, 3H). LRMS (CI) *m/*z calcd for $C_{28}H_{35}N_4O_3$ $[M+H]^+$: 475.3; found: 475.3.

USC DE SANTIAGO DE COMPOSTELA

**(*S*)-1-(cyclohexylmethyl)-*N*-(4-methyl-1-((2-morpholinoethyl)amino)-1,2-dioxopentan-3-yl)-1*H*-indazole-3-carboxamide (116).** Purified by column chromatography (DCM/MeOH 99:1-97:3). Yield: 68%. Mp: 238 – 240 ºC. $^1$H NMR (300 MHz, $CDCl_3$) $\delta$ (ppm): 9.25 (s, 1H), 8.30 (d, *J* = 8.0 Hz, 1H), 7.55 (d, *J* = 9.1 Hz, 1H), 7.40 (s, 2H), 5.66 – 5.46 (m, 1H), 4.41 (m, 1H), 4.22 (d, *J* = 7.2 Hz, 2H), 3.89 (s, 1H), 3.80 (d, *J* = 12.9 Hz, 2H), 3.69 (s, 2H), 3.53 (s, 1H), 3.32 (s, 3H), 2.49 (d, *J* = 21.1 Hz, 2H), 2.08 – 1.94 (m, 1H), 1.91 – 1.55 (m, 7H), 1.28 – 1.16 (m, 2H), 1.15 – 1.09 (m, 3H), 1.09 – 1.01 (m, 1H), 0.97 (t, *J* = 6.5 Hz, 3H). LRMS (CI) *m/*z calcd for $C_{27}H_{40}N_5O_4$ $[M+H]^+$: 498.3; found: 498.3.

**(*S*)-*N*-(1-amino-4,4-dimethyl-1,2-dioxopentan-3-yl)-1-(cyclohexylmethyl)-1*H*-indazole-3-carboxamide (117).** Purified by column chromatography (DCM/MeOH 94:6). Yield: 60%. Mp: 80 – 81 ºC. $^1$H NMR (300 MHz, $CDCl_3$) $\delta$ (ppm): 8.31 (d, *J* = 8.2 Hz, 1H), 7.65 (d, *J* = 8.2 Hz, 1H), 7.42 – 7.34 (m, 2H), 7.24 – 7.19 (m, 1H), 6.87 (brs, 1H), 5.79 (brs, 1H), 5.68 (d, *J* = 8.2 Hz, 1H), 4.22 (d, *J* = 7.3 Hz, 2H), 2.07 – 1.95 (m, 1H), 1.80 – 1.55 (m, 7H), 1.26 – 1.16 (m, 3H), 1.12 (s, 9H). $^{13}$C NMR (75 MHz, $CDCl_3$) $\delta$ (ppm): 197.7, 162.5, 162.0, 141.4, 136.4, 126.6, 122.7, 122.5, 109.5, 57.9, 55.7, 38.7, 35.5, 30.9, 26.7, 26.2, 25.6. LRMS (CI) *m/*z calcd for $C_{22}H_{31}N_4O_3$ $[M+H]^+$: 399.2; found: 399.2.

**(*S*)-*N*-(1-(*tert*-butylamino)-4,4-dimethyl-1,2-dioxopentan-3-yl)-1-(cyclohexylmethyl)-1*H*-indazole-3-carboxamide (118).** Purified by column chromatography (DCM/MeOH 99:1). Yield: 80%. Oil at room temperature. $^1$H NMR (300 MHz, $CDCl_3$) $\delta$ (ppm): 8.33 (d, *J* = 8.2 Hz, 1H), 7.73 (d, *J* = 9.0 Hz, 1H), 7.42 – 7.33 (m, 2H), 7.24 – 7.20 (m, 1H), 6.77 (s, 1H), 5.74 (d, *J* = 8.9 Hz, 1H), 4.22 (d, *J* = 7.2 Hz, 2H), 2.07 – 1.97 (m, 1H), 1.76 – 1.54 (m, 7H), 1.40 (s, 9H), 1.28 – 1.15 (m, 3H), 1.10 (s, 9H). LRMS (CI) *m/*z calcd for $C_{26}H_{39}N_4O_3$ $[M+H]^+$: 455.3; found: 455.3.

**methyl (*S*)-(3-(1-(cyclohexylmethyl)-1*H*-indazole-3-carboxamido)-4,4-dimethyl-2-oxopentanoyl)glycinate (119).** Purified by column chromatography (DCM/MeOH 99:1). Yield: 60%. Oil at room temperature. $^1$H NMR (300 MHz, $CDCl_3$) $\delta$ (ppm): 8.30 (d, *J* = 8.1 Hz, 1H), 7.66 (d, *J* = 8.2 Hz, 1H), 7.47 – 7.35 (m, 2H), 7.23 – 7.20 (m, 1H), 7.19 – 7.13 (m, 1H), 5.70 (d, *J* = 8.1 Hz, 1H), 4.21 (d, *J* = 7.3 Hz, 2H), 4.20 – 3.99 (m, 2H), 3.77 (s, 3H), 2.09 – 1.94 (m, 1H), 1.76 – 1.54 (m, 7H), 1.26 – 1.16 (m, 3H), 1.11 (s, 9H). LRMS (CI) *m/*z calcd for $C_{25}H_{35}N_4O_5$ $[M+H]^+$: 471.3; found: 471.3.

USC UNIVERSIDADE DE SANTIAGO DE COMPOSTELA

**(*S*)-*N*-(1-(benzylamino)-4,4-dimethyl-1,2-dioxopentan-3-yl)-1-(cyclohexylmethyl)-1*H*-indazole-3-carboxamide (120).** Purified by column chromatography (DCM/MeOH 99:1). Yield: 64%. Mp: 85 – 86 ºC. $^{1}$H NMR (300 MHz, $CDCl_3$) $\delta$ (ppm): 8.33 (d, $J$ = 8.2 Hz, 1H), 7.72 (d, $J$ = 8.4 Hz, 1H), 7.43 – 7.35 (m, 2H), 7.33 – 7.22 (m, 6H), 7.20 – 7.15 (m, 1H), 5.74 (d, $J$ = 8.4 Hz, 1H), 4.60 – 4.44 (m, 2H), 4.22 (d, $J$ = 7.3 Hz, 2H), 2.09 – 1.94 (m, 1H), 1.76 – 1.55 (m, 7H), 1.28 – 1.16 (m, 3H), 1.13 (s, 9H). LRMS (CI) *m/*z calcd for $C_{29}H_{37}N_4O_3$ $[M+H]^+$: 489.3; found: 489.3.

**(*S*)-1-(cyclohexylmethyl)-*N*-(4,4-dimethyl-1-((2-morpholinoethyl)amino)-1,2-dioxopentan-3-yl)-1*H*-indazole-3-carboxamide (121).** Purified by column chromatography (DCM/MeOH 99:1-97:3). Yield: 69%. Mp: 222 – 223 ºC. $^{1}$H NMR (300 MHz, $CDCl_3$) $\delta$ (ppm): 8.31 (d, $J$ = 8.2 Hz, 1H), 7.71 (d, $J$ = 8.6 Hz, 1H), 7.43 – 7.33 (m, 3H), 7.24 – 7.19 (m, 1H), 5.70 (d, $J$ = 8.5 Hz, 1H), 4.22 (d, $J$ = 7.2 Hz, 2H), 3.73 – 3.65 (m, 4H), 3.43 (q, $J$ = 5.8 Hz, 2H), 2.53 (t, $J$ = 6.0 Hz, 2H), 2.49 – 2.44 (m, 4H), 2.08 – 1.96 (m, 1H), 1.83 – 1.55 (m, 8H), 1.32 – 1.16 (m, 2H), 1.12 (s, 9H). LRMS (CI) *m/*z calcd for $C_{28}H_{42}N_5O_4$ $[M+H]^+$: 512.3; found: 512.3.

**(*R*)-*N*-(1-amino-4,4-dimethyl-1,2-dioxopentan-3-yl)-1-(4-fluorobenzyl)-1*H*-indole-3-carboxamide (122).** Purified by column chromatography (DCM/MeOH 94:6). Yield: 77%. Mp: 121 – 123 ºC. $^{1}$H NMR (300 MHz, $CDCl_3$) $\delta$ (ppm): 8.20 – 8.10 (m, 1H), 7.93 (s, 1H), 7.36 – 7.21 (m, 2H), 7.22 – 7.08 (m, 3H), 7.01 (t, $J$ = 8.4 Hz, 2H), 6.41 (s, 1H), 6.19 (s, 1H), 5.88 (s, 1H), 5.38 – 5.29 (m, 1H), 5.30 (s, 2H), 1.33 (s, 9H). $^{13}$C NMR (75 MHz, $CDCl_3$) $\delta$ (ppm): 208.27, 167.60, 162.57 (d, $J$ = 247.7 Hz), 162.31, 135.34, 131.26, 128.84 (d, $J$ = 8.3 Hz), 123.53, 122.75, 121.61, 116.07 (d, $J$ = 21.8 Hz), 110.52, 105.79, 73.47, 50.25, 44.95, 26.60. LRMS (CI) *m/*z calcd for $C_{23}H_{25}FN_3O_3$ $[M+H]^+$: 410.2; found: 410.2.

**(*R*)-*N*-(1-amino-4,4-dimethyl-1,2-dioxopentan-3-yl)-1-(4-fluorobenzyl)-1*H*-indazole-3-carboxamide (123).** Purified by column chromatography (DCM/MeOH 94:6). Yield: 78%. Mp: 180 – 182 ºC. $^{1}$H NMR (300 MHz, $CDCl_3$) $\delta$ (ppm): 8.33 (d, $J$ = 8.1 Hz, 1H), 7.68 (d, $J$ = 8.3 Hz, 1H), 7.39 – 7.13 (m, 5H), 7.00 (t, $J$ = 8.5 Hz, 2H), 6.88 (s, 1H), 5.92 (s, 1H), 5.69 (d, $J$ = 8.3 Hz, 1H), 5.59 (s, 2H), 1.11 (s, 9H). $^{13}$C NMR (75 MHz, $CDCl_3$) $\delta$ (ppm): 197.65, 162.48 (d, $J$ = 246.8 Hz), 162.25, 162.02, 140.78, 137.14, 131.71, 128.95 (d, $J$ = 8.2 Hz), 127.12, 123.28, 122.93 (d, $J$ = 2.9 Hz), 115.79 (d, $J$ = 21.9 Hz), 109.42, 57.98, 52.92, 35.57, 26.73. LRMS (CI) *m/*z calcd for $C_{22}H_{24}FN_4O_3$ $[M+H]^+$: 411.2; found: 411.2.

USC UNIVERSIDADE DE SANTIAGO DE COMPOSTELA

**(*R*)-*N*-(1-amino-4,4-dimethyl-1,2-dioxopentan-3-yl)-1-(cyclohexylmethyl)-1*H*-indole-3-carboxamide (124).** Purified by column chromatography (DCM/MeOH 94:6). Yield: 73%. Mp: 171 – 172 ºC. $^{1}$H NMR (300 MHz, $CDCl_3$) $\delta$ (ppm): 8.18 – 8.08 (m, 1H), 7.86 (s, 1H), 7.43 – 7.26 (m, 4H), 6.36 (s, 1H), 6.21 (s, 1H), 5.63 (s, 1H), 3.98 (d, *J* = 6.6 Hz, 2H), 1.87 (s, 1H), 1.79 – 1.48 (m, 6H), 1.33 (s, 9H), 1.30 – 1.10 (m, 3H), 1.10 – 0.94 (m, 1H). LRMS (CI) *m/*z calcd for $C_{23}H_{32}N_3O_3$ $[M+H]^+$: 398.2; found: 398.2.

**(*R*)-*N*-(1-amino-4,4-dimethyl-1,2-dioxopentan-3-yl)-1-(cyclohexylmethyl)-1*H*-indazole-3-carboxamide (125).** Purified by column chromatography (DCM/MeOH 94:6). Yield: 79%. Mp: 80 – 81 ºC. $^{1}$H NMR (300 MHz, $CDCl_3$) $\delta$ (ppm): 8.31 (d, *J* = 8.3 Hz, 1H), 7.65 (d, *J* = 8.3 Hz, 1H), 7.39 (s, 1H), 7.24 – 7.14 (m, 2H), 6.93 – 6.85 (m, 1H), 5.93 (s, 1H), 5.68 (d, *J* = 8.2 Hz, 1H), 4.22 (d, *J* = 7.2 Hz, 2H), 2.11 – 1.93 (m, 1H), 1.78 – 1.54 (m, 5H), 1.29 – 1.14 (m, 4H), 1.12 (s, 9H), 1.09 – 1.00 (m, 1H). $^{13}$C NMR (75 MHz, $CDCl_3$) $\delta$ (ppm): 197.7, 162.5, 162.1, 141.4, 136.4, 129.0, 128.2, 126.6, 122.7, 122.5, 109.5, 57.9, 55.7, 38.7, 35.5, 30.9, 27.6, 26.7, 26.2, 25.6. LRMS (CI) *m/*z calcd for $C_{22}H_{31}N_4O_3$ $[M+H]^+$: 399.2; found: 399.2.

**(*R*)-*N*-(1-(*tert*-butylamino)-4,4-dimethyl-1,2-dioxopentan-3-yl)-1-(4-fluorobenzyl)-1*H*-indole-3-carboxamide (126).** Purified by column chromatography (DCM/MeOH 99:1-97:3). Yield: 80%. Mp: 107 – 108 ºC. $^{1}$H NMR (300 MHz, $CDCl_3$) $\delta$ (ppm): 8.03 (d, *J* = 8.0 Hz, 1H), 7.77 (s, 1H), 7.34 – 7.21 (m, 3H), 7.20 – 7.02 (m, 3H), 6.98 (t, *J* = 8.5 Hz, 2H), 6.82 (s, 1H), 5.59 (d, *J* = 8.7 Hz, 1H), 5.28 (s, 2H), 1.40 (s, 9H), 1.10 (s, 9H). $^{13}$C NMR (75 MHz, $CDCl_3$) $\delta$ (ppm): 198.63, 164.57, 162.46 (d, *J* = 247.0 Hz), 159.63, 136.74, 132.31, 129.04, 128.75 (d, *J* = 8.1 Hz), 128.23, 125.46, 125.30, 122.81, 121.93, 120.15, 115.90 (d, *J* = 21.8 Hz), 111.27, 110.61, 59.81, 51.45, 49.94, 35.73, 28.25, 26.98. LRMS (CI) *m/*z calcd for $C_{27}H_{33}FN_3O_3$ $[M+H]^+$: 466.2; found: 466.2.

USC UNIVERSIDADE DE SANTIAGO DE COMPOSTELA

**(*R*)-*N*-(1-(*tert*-butylamino)-4,4-dimethyl-1,2-dioxopentan-3-yl)-1-(4-fluorobenzyl)-1*H*-indazole-3-carboxamide (127).** Purified by column chromatography (DCM/MeOH 99:1-97:3). Yield: 74%. Oil at room temperature. $^{1}$H NMR (300 MHz, $CDCl_3$) $\delta$ (ppm): 8.36 (d, *J* = 8.1 Hz, 1H), 7.77 (d, *J* = 9.0 Hz, 1H), 7.39 – 7.13 (m, 5H), 6.99 (t, *J* = 8.6 Hz, 2H), 6.78 (s, 1H), 5.77 (d, *J* = 9.0 Hz, 1H), 5.59 (s, 2H), 1.40 (s, 9H), 1.10 (s, 9H). $^{13}$C NMR (75 MHz, $CDCl_3$) $\delta$ (ppm): 199.05, 162.46 (d, *J* = 246.9 Hz), 162.11, 159.38, 140.78, 137.38, 131.78 (d, *J* = 3.2 Hz), 129.03, 128.92, 128.23, 127.06, 125.30, 123.29, 122.92 (d, *J* = 15.4 Hz), 115.76 (d, *J* = 21.7 Hz), 109.38, 57.92, 52.86, 51.41, 35.82, 28.26, 26.78. HRMS (ESI) *m/*z calcd for $C_{26}H_{32}FN_4O_3$ $[M+H]^+$: 467.2380; found: 467.2453.

**(*R*)-*N*-(1-(*tert*-butylamino)-4,4-dimethyl-1,2-dioxopentan-3-yl)-1-(cyclohexylmethyl)-1*H*-indole-3-carboxamide (128).** Purified by column chromatography (DCM/MeOH 99:1-97:3). Yield: 72%. Mp: 284 – 285 ºC. $^{1}$H NMR (300 MHz, $CDCl_3$) $\delta$ (ppm): 8.03 – 7.95 (m, 1H), 7.71 (s, 1H), 7.42 – 7.33 (m, 1H), 7.32 – 7.23 (m, 2H), 7.04 – 6.94 (m, 1H), 6.81 (s, 1H), 5.59 (d, *J* = 8.6 Hz, 1H), 3.94 (d, *J* = 7.2 Hz, 2H), 1.93 – 1.77 (m, 1H), 1.76 – 1.57 (m, 6H), 1.39 (s, 9H), 1.28 – 1.13 (m, 3H), 1.10 (s, 9H), 1.06 – 0.87 (m, 1H). $^{13}$C NMR (75 MHz, $CDCl_3$) $\delta$ (ppm): 198.7, 164.8, 159.7, 137.0, 132.9, 125.1, 122.3, 121.5, 119.9, 110.6, 110.2, 59.7, 53.3, 51.4, 38.5, 35.7, 31.0, 28.3, 27.0, 26.2, 25.6. HRMS (ESI) *m/*z calcd for $C_{27}H_{40}N_3O_3$ $[M+H]^+$: 454.2991; found: 454.3064.

**(*R*)-*N*-(1-(*tert*-butylamino)-4,4-dimethyl-1,2-dioxopentan-3-yl)-1-(cyclohexylmethyl)-1*H*-indazole-3-carboxamide (129).** Purified by column chromatography (DCM/MeOH 99:1-97:3). Yield: 77%. Oil at room temperature. $^{1}$H NMR (300 MHz, $CDCl_3$) $\delta$ (ppm): 8.32 (d, *J* = 8.2 Hz, 1H), 7.73 (d, *J* = 9.0 Hz, 1H), 7.43 – 7.32 (m, 2H), 7.29 – 7.18 (m, 1H), 6.77 (s, 1H), 5.74 (d, *J* = 8.9 Hz, 1H), 4.21 (d, *J* = 7.2 Hz, 2H), 2.09 – 1.92 (m, 1H), 1.77 – 1.53 (m, 6H), 1.39 (s, 9H), 1.32 – 1.14 (m, 2H), 1.09 (s, 9H), 1.03 – 0.81 (m, 2H). $^{13}$C NMR (75 MHz, $CDCl_3$) $\delta$ (ppm): 199.1, 162.4, 159.4, 141.4, 136.6, 126.5, 122.8, 122.7, 122.4, 109.4, 57.8, 55.6, 51.4, 38.7, 35.8, 30.9, 28.3, 26.8, 26.2, 25.6. HRMS (ESI) *m/*z calcd for $C_{26}H_{39}N_4O_3$ $[M+H]^+$: 455.2944; found: 455.3017.

USC UNIVERSIDADE DE SANTIAGO DE COMPOSTELA

***N*-((3*S*)-1-amino-2-hydroxy-1-oxopentan-3-yl)-1-(4-fluorobenzyl)-1*H*-indole-3-carboxamide (130).** Purified by column chromatography (DCM/MeOH 97:3-94:6). Yield: 24%. Mp: 262 – 263 ºC. $^1$H NMR (300 MHz, $CDCl_3$) $\delta$ (ppm): 8.10 – 8.02 (m, 1H), 7.74 (s, 1H), 7.25 – 7.21 (m, 3H), 7.15 – 7.02 (m, 4H), 6.95 (t, *J* = 8.6 Hz, 2H), 6.33 (bs, 1H), 5.73 (bs, 1H), 5.20 (s, 2H), 4.32 – 4.25 (m, 1H), 4.24 – 4.14 (m, 1H), 2.05 – 1.83 (m, 2H), 1.01 (t, *J* = 7.4 Hz, 3H). LRMS (CI) *m/*z calcd for $C_{21}H_{23}FN_3O_3$ $[M+H]^+$: 384.1; found: 384.1.

***N*-((3*S*)-1-(*tert*-butylamino)-2-hydroxy-1-oxopentan-3-yl)-1-(4-fluorobenzyl)-1*H*-indole-3-carboxamide (131).** Purified by column chromatography (DCM/MeOH 99:1-97:3). Yield: 35%. Mp: 85 – 86 ºC. $^1$H NMR (300 MHz, $CDCl_3$) $\delta$ (ppm): 8.07 – 8.00 (m, 1H), 7.71 (s, 1H), 7.31 – 7.22 (m, 3H), 7.12 – 7.04 (m, 2H), 6.97 (t, *J* = 8.6 Hz, 2H), 6.92 – 6.82 (m, 2H), 6.15 (d, *J* = 6.3 Hz, 1H), 5.27 (s, 2H), 4.19 – 4.06 (m, 2H), 1.98 – 1.85 (m, 2H), 1.27 (s, 9H), 1.02 (t, *J* = 7.4 Hz, 3H). LRMS (CI) *m/*z calcd for $C_{25}H_{31}FN_3O_3$ $[M+H]^+$: 440.2; found: 440.2.

**methyl ((3*S*)-3-(1-(4-fluorobenzyl)-1*H*-indole-3-carboxamido)-2-hydroxypentanoyl)glycinate (132).** Purified by column chromatography (DCM/MeOH 99:1-97:3). Yield: 39%. Mp: 255 – 256 ºC. $^1$H NMR (300 MHz, $CDCl_3$) $\delta$ (ppm): 8.18 (t, *J* = 7.9 Hz, 1H), 7.99 (d, *J* = 20.5 Hz, 1H), 7.45 (s, 1H), 7.34 – 7.20 (m, 4H), 7.17 – 7.07 (m, 2H), 7.06 – 6.89 (m, 2H), 5.55 (d, *J* = 2.5 Hz, 1H), 5.39 (d, *J* = 5.2 Hz, 1H), 5.26 (s, 2H), 4.25 – 4.05 (m, 1H), 4.02 – 3.86 (m, 1H), 3.69 (s, 3H), 3.41 – 3.24 (m, 1H), 1.88 – 1.41 (m, 2H), 1.11 – 0.93 (m, 3H). $^{13}$C NMR (75 MHz, $CDCl_3$) $\delta$ (ppm): 170.29, 169.48, 165.16 (d, *J* = 162.2 Hz), 163.45 (d, *J* = 11.6 Hz), 136.72, 135.32 (d, *J* = 8.0 Hz), 131.70, 131.48 (d, *J* = 3.2 Hz), 128.78 (d, *J* = 8.0 Hz), 126.83, 123.37, 122.62 (d, *J* = 4.3 Hz), 121.64, 115.96 (d, *J* = 21.7 Hz), 110.53 (d, *J* = 3.8 Hz), 75.63 (d, *J* = 86.5 Hz), 54.65 (d, *J* = 4.7 Hz), 52.33, 50.19, 40.95 (d, *J* = 4.2 Hz), 26.44 (d, *J* = 51.5 Hz), 10.73 (d, *J* = 21.4 Hz). LRMS (CI) *m/*z calcd for $C_{24}H_{27}FN_3O_5$ $[M+H]^+$: 456.2; found: 456.3.

***N*-((3*S*)-1-(benzylamino)-2-hydroxy-1-oxopentan-3-yl)-1-(4-fluorobenzyl)-1*H*-indole-3-carboxamide (133).** Purified by column chromatography (DCM/MeOH 99:1-97:3). Yield: 29%. Mp: 94 – 96 ºC. $^1$H NMR (300 MHz, $CDCl_3$) $\delta$ (ppm): 8.20 – 8.12 (m, 1H), 8.07 – 8.03 (m, 1H), 7.35 – 7.22 (m, 9H), 7.20 – 7.10 (m, 2H), 7.06 – 6.91 (m, 3H), 5.60 (d, *J* = 2.6 Hz, 1H), 5.48 (d, *J* = 5.0 Hz, 1H), 5.34 – 5.30 (m, 2H), 4.51 (dd, *J* = 5.9, 3.4 Hz, 2H), 3.47 – 3.36 (m, 1H), 2.20 – 1.50 (m, 2H), 1.12 – 0.98 (m, 3H). LRMS (CI) *m/*z calcd for $C_{28}H_{29}FN_3O_3$ $[M+H]^+$: 474.2; found: 474.2.

USC
DE SANTIAGO
DE COMPOSTELA

**1-(4-fluorobenzyl)-*N*-((3*S*)-2-hydroxy-1-((2-morpholinoethyl)amino)-1-oxopentan-3-yl)-1*H*-indole-3-carboxamide (134).** Purified by column chromatography (DCM/MeOH 99:1-97:3). Yield: 38%. Oil at room temperature. $^1$H NMR (300 MHz, DMSO-*d6*) $\delta$ (ppm): 8.50 (s, 0.4H), 8.43 (s, 0.3H), 8.15 (s, 0.4H), 8.09 – 7.96 (m, 1H), 7.91 – 7.65 (m, 1H), 7.52 (d, *J* = 14.1 Hz, 1H), 7.39 – 7.26 (m, 3H), 7.25 – 7.09 (m, 4H), 6.02 (d, *J* = 5.7 Hz, 1H), 5.47 (d, *J* = 24.4 Hz, 2H), 5.05 – 4.96 (m, 1H), 4.19 – 4.08 (m, 0.5H), 3.98 (s, 0.5H), 3.47 – 3.34 (m, 6H), 2.36 – 2.27 (m, 4H), 2.23 – 2.11 (m, 2H), 1.74 – 1.30 (m, 2H), 0.99 – 0.85 (m, 3H). LRMS (CI) *m/*z calcd for $C_{27}H_{34}FN_4O_4$ $[M+H]^+$: 497.3; found: 497.3.

***N*-((3*S*)-1-amino-2-hydroxy-4-methyl-1-oxopentan-3-yl)-1-(4-fluorobenzyl)-1*H*-indole-3-carboxamide (135).** Purified by column chromatography (DCM/MeOH 97:3-94:6). Yield: 36%. Mp: 164 – 165 ºC. $^1$H NMR (300 MHz, $CDCl_3$) $\delta$ (ppm): 7.98 – 7.91 (m, 1H), 7.67 (s, 1H), 7.33 – 7.27 (m, 4H), 7.18 – 7.09 (m, 2H), 7.01 (t, *J* = 8.4 Hz, 2H), 6.65 – 6.58 (m, 1H), 6.50 – 6.42 (m, 1H), 5.49 – 5.40 (m, 1H), 5.28 (s, 2H), 4.47 – 4.38 (m, 1H), 3.79 – 3.66 (m, 1H), 2.66 – 2.52 (m, 1H), 1.12 (d, *J* = 6.7 Hz, 3H), 1.05 (d, *J* = 6.6 Hz, 3H). LRMS (CI) *m/*z calcd for $C_{22}H_{25}FN_3O_3$ $[M+H]^+$: 398.2; found: 398.2.

***N*-((3*S*)-1-(*tert*-butylamino)-2-hydroxy-4-methyl-1-oxopentan-3-yl)-1-(4-fluorobenzyl)-1*H*-indole-3-carboxamide (136).** Purified by column chromatography (DCM/MeOH 99:1-97:3). Yield: 58%. Mp: 182 – 183 ºC. $^1$H NMR (300 MHz, DMSO-*d6*) $\delta$ (ppm): 8.25 (s, 1H), 8.10 – 8.04 (m, 1H), 7.54 (d, *J* = 7.8 Hz, 1H), 7.32 (t, *J* = 7.0 Hz, 2H), 7.26 – 7.09 (m, 6H), 5.78 (d, *J* = 6.2 Hz, 1H), 5.46 (s, 2H), 4.06 (d, *J* = 5.6 Hz, 1H), 4.01 (d, *J* = 9.6 Hz, 1H), 2.03 – 1.89 (m, 1H), 1.10 (s, 9H), 1.01 (d, *J* = 6.6 Hz, 3H), 0.93 (d, *J* = 6.7 Hz, 3H). LRMS (CI) *m/*z calcd for $C_{26}H_{33}FN_3O_3$ $[M+H]^+$: 454.2; found: 454.2.

**methyl ((3*S*)-3-(1-(4-fluorobenzyl)-1*H*-indole-3-carboxamido)-2-hydroxy-4-methylpentanoyl)glycinate (137).** Purified by column chromatography (DCM/MeOH 97:3-94:6). Yield: 40%. Mp: 205 – 206 ºC. $^1$H NMR (300 MHz, $CDCl_3$) $\delta$ (ppm): 7.99 (d, *J* = 7.0 Hz, 1H), 7.74 (s, 1H), 7.66 (t, *J* = 5.8 Hz, 1H), 7.31 – 7.21 (m, 1H), 7.16 – 7.06 (m, 3H), 7.04 – 6.88 (m, 4H), 5.25 (s, 2H), 4.45 (s, 1H), 3.95 (d, *J* = 5.7 Hz, 2H), 3.77 – 3.66 (m, 2H), 3.51 (s, 3H), 2.67 – 2.48 (m, 1H), 1.09 (d, *J* = 6.6 Hz, 3H), 1.03 (d, *J* = 6.7 Hz, 3H). HRMS (ESI) *m/*z calcd for $C_{25}H_{29}FN_3O_5$ $[M+H]^+$: 470.2013; found: 470.2099.

USC UNIVERSIDADE DE SANTIAGO DE COMPOSTELA

***N*-((3*S*)-1-(benzylamino)-2-hydroxy-4-methyl-1-oxopentan-3-yl)-1-(4-fluorobenzyl)-1*H*-indole-3-carboxamide (138).** Purified by column chromatography (DCM/MeOH 97:3-94:6). Yield: 59%. Oil at room temperature. $^{1}$H NMR (300 MHz, $CDCl_3$) $\delta$ (ppm): 8.20 – 8.11 (m, 1H), 8.10 – 7.91 (m, 1H), 7.37 – 7.21 (m, 8H), 7.18 – 7.09 (m, 2H), 7.04 – 6.96 (m, 3H), 6.88 – 6.70 (m, 1H), 5.71 (d, *J* = 2.4 Hz, 2H), 5.41 (d, *J* = 6.9 Hz, 1H), 5.31 (s, 2H), 4.54 – 4.46 (m, 2H), 3.24 – 3.17 (m, 1H), 2.20 – 1.99 (m, 0H), 1.16 – 0.90 (m, 6H). LRMS (CI) *m/*z calcd for $C_{29}H_{31}FN_3O_3$ $[M+H]^+$: 488.2; found: 488.2.

**1-(4-fluorobenzyl)-*N*-((3*S*)-2-hydroxy-4-methyl-1-((2-morpholinoethyl)amino)-1-oxopentan-3-yl)-1*H*-indole-3-carboxamide (139).** Purified by column chromatography (DCM/MeOH 99:1-97:3). Yield: 53%. Oil at room temperature. $^{1}$H NMR (300 MHz, DMSO-*d6*) $\delta$ (ppm): 8.52 (s, 0.4H), 8.38 (s, 0.3H), 8.18 (s, 0.4H), 8.05 – 7.95 (m, 2H), 7.80 – 7.48 (m, 2H), 7.39 – 7.27 (m, 2H), 7.24 – 7.09 (m, 4H), 6.04 (d, *J* = 6.3 Hz, 1H), 5.46 (d, *J* = 25.6 Hz, 2H), 5.17 – 5.11 (m, 0.5H), 5.01 – 4.95 (m, 0.5H), 4.10 (s, 0.5H), 3.96 (s, 0.5H), 3.48 – 3.30 (m, 6H), 2.38 – 2.23 (m, 4H), 2.18 – 1.93 (m, 2H), 1.73 – 1.60 (m, 1H), 1.01 – 0.94 (m, 3H), 0.92 – 0.80 (m, 3H). LRMS (CI) *m/*z calcd for $C_{28}H_{36}FN_4O_4$ $[M+H]^+$: 511.3; found: 511.3.

***N*-((3*S*)-1-amino-2-hydroxy-4,4-dimethyl-1-oxopentan-3-yl)-1-(4-fluorobenzyl)-1*H*-indole-3-carboxamide (140).** Purified by column chromatography (DCM/MeOH 97:3-94:6). Yield: 48%. Mp: 240 – 242 ºC. $^{1}$H NMR (300 MHz, $CDCl_3$) $\delta$ (ppm): 8.26 – 8.15 (m, 0.5H), 8.00 – 7.86 (m, 1H), 7.72 (s, 0.5H), 7.37 – 7.21 (m, 4H), 7.19 – 7.09 (m, 2H), 7.08 – 6.96 (m, 2H), 6.60 (d, *J* = 10.2 Hz, 1H), 5.84 (s, 1H), 5.54 (bs, 1H), 5.32 (d, *J* = 14.2 Hz, 2H), 4.53 (s, 0.5H), 4.31 (d, *J* = 9.7 Hz, 0.5H), 3.49 (d, *J* = 6.4 Hz, 1H), 1.17 (s, 7H), 1.01 (s, 2H). $^{13}$C NMR (75 MHz, $CDCl_3$) $\delta$ (ppm): 177.30, 165.39, 162.39 (d, *J* = 246.7 Hz), 136.73, 132.31, 132.08, 128.71 (d, *J* = 8.3 Hz), 125.37, 122.73, 121.78, 119.75, 115.67 (d, *J* = 21.7 Hz), 110.72, 69.79, 58.07, 49.79, 35.55, 27.10. HRMS (ESI) *m/*z calcd for $C_{23}H_{27}FN_3O_3$ $[M+H]^+$: 412.1958; found: 412.2031.

USC UNIVERSIDADE DE SANTIAGO DE COMPOSTELA

***N*-((3*S*)-1-(*tert*-butylamino)-2-hydroxy-4,4-dimethyl-1-oxopentan-3-yl)-1-(4-fluorobenzyl)-1*H*-indole-3-carboxamide (141).** Purified by column chromatography (DCM/MeOH 97:3-94:6). Yield: 60%. Mp: 189 – 190 ºC. $^{1}$H NMR (300 MHz, DMSO-*d6*) $\delta$ (ppm): 8.27 (s, 1H), 8.03 – 7.97 (m, 1H), 7.54 – 7.47 (m, 1H), 7.34 – 7.26 (m, 2H), 7.18 – 7.08 (m, 4H), 6.98 (s, 1H), 6.88 (d, *J* = 9.8 Hz, 1H), 5.75 (d, *J* = 6.0 Hz, 1H), 5.44 (s, 2H), 4.20 – 4.10 (m, 2H), 1.03 (s, 9H), 0.99 (s, 9H). LRMS (CI) *m/*z calcd for $C_{27}H_{35}FN_3O_3$ $[M+H]^+$: 468.3; found: 468.3.

**methyl ((3*S*)-3-(1-(4-fluorobenzyl)-1*H*-indole-3-carboxamido)-2-hydroxy-4,4-dimethylpentanoyl)glycinate (142).** Purified by column chromatography (DCM/MeOH 97:3-94:6). Yield: 30%. Mp: 223 – 224 ºC. $^{1}$H NMR (300 MHz, $CDCl_3$) $\delta$ (ppm): 7.96 (d, *J* = 7.1 Hz, 1H), 7.73 (s, 1H), 7.37 – 7.21 (m, 4H), 7.11 (t, *J* = 7.0 Hz, 2H), 6.98 (t, *J* = 8.4 Hz, 2H), 6.71 (d, *J* = 9.4 Hz, 1H), 5.28 (d, *J* = 6.5 Hz, 1H), 5.25 (s, 2H), 4.58 (s, 1H), 4.29 (d, *J* = 9.5 Hz, 1H), 4.06 – 3.88 (m, 2H), 3.57 (d, *J* = 2.2 Hz, 3H), 1.13 (s, 9H). $^{13}$C NMR (75 MHz, $CDCl_3$) $\delta$ (ppm): 173.91, 169.89, 165.51, 163.00 (d, *J* = 163.7 Hz), 150.07, 136.71, 135.25, 131.98, 128.77 (d, *J* = 8.4 Hz), 122.91, 121.99, 120.18, 115.92 (d, *J* = 21.8 Hz), 111.17, 110.58, 71.11, 59.15, 52.18, 49.97, 41.46, 36.07, 27.71. HRMS (ESI) *m/*z calcd for $C_{26}H_{31}FN_3O_5$ $[M+H]^+$: 484.2169; found: 484.2242.

***N*-((3*S*)-1-((2-amino-2-oxoethyl)amino)-2-hydroxy-4,4-dimethyl-1-oxopentan-3-yl)-1-(4-fluorobenzyl)-1*H*-indole-3-carboxamide (143).** Purified by column chromatography (DCM/MeOH 97:3-94:6). Yield: 66%. Mp: 211 – 212 ºC. $^{1}$H NMR (300 MHz, $CDCl_3$) $\delta$ (ppm): 8.17 – 8.09 (m, 2H), 7.89 (s, 1H), 7.29 – 7.22 (m, 5H), 7.15 – 7.07 (m, 2H), 6.97 (t, *J* = 8.5 Hz, 2H), 6.21 (bs, 1H), 5.77 (s, 1H), 5.30 (s, 2H), 5.28 (s, 1H), 4.27 – 4.11 (m, 1H), 3.50 (d, *J* = 17.7 Hz, 1H), 3.15 (s, 1H), 0.98 (s, 9H). LRMS (CI) *m/*z calcd for $C_{25}H_{30}FN_4O_4$ $[M+H]^+$: 469.2; found: 469.2.

USC UNIVERSIDADE DE SANTIAGO DE COMPOSTELA

***N*-((3*S*)-1-(benzylamino)-2-hydroxy-4,4-dimethyl-1-oxopentan-3-yl)-1-(4-fluorobenzyl)-1*H*-indole-3-carboxamide (144).** Purified by column chromatography (DCM/MeOH 97:3-94:6). Yield: 58%. Mp: 281 – 282 ºC. $^{1}$H NMR (300 MHz, $CDCl_3$) $\delta$ (ppm): 8.09 – 8.02 (m, 1H), 7.72 (s, 1H), 7.45 (t, *J* = 6.0 Hz, 1H), 7.32 – 7.22 (m, 3H), 7.13 – 6.92 (m, 9H), 5.72 (bs, 1H), 5.21 (s, 2H), 4.53 (s, 1H), 4.46 (dd, *J* = 15.0, 6.6 Hz, 1H), 4.28 – 4.18 (m, 2H), 1.10 (s, 9H). $^{13}$C NMR (75 MHz, $CDCl_3$) $\delta$ (ppm): 173.69, 165.70, 164.08, 160.80, 137.77, 136.72, 131.77, 128.71 (d, *J* = 8.2 Hz), 128.39, 127.37, 127.10, 125.85, 122.96, 121.99, 120.60, 115.90 (d, *J* = 21.7 Hz), 111.05, 110.50, 71.58, 65.84, 59.67, 49.93, 43.54, 36.22, 27.83. HRMS (ESI) *m/*z calcd for $C_{30}H_{33}FN_3O_3$ $[M+H]^+$: 502.2428; found: 502.2500.

**1-(4-fluorobenzyl)-*N*-((3*S*)-2-hydroxy-4,4-dimethyl-1-((2-morpholinoethyl)amino)-1-oxopentan-3-yl)-1*H*-indole-3-carboxamide (145).** Purified by column chromatography (DCM/MeOH 99:1-97:3). Yield: 57%. Mp: 106 – 107 ºC. $^{1}$H NMR (300 MHz, $CDCl_3$) $\delta$ (ppm): 8.23 – 8.15 (m, 1H), 7.98 (s, 1H), 7.37 – 7.27 (m, 3H), 7.19 – 7.12 (m, 2H), 7.03 (t, *J* = 8.4 Hz, 2H), 6.99 – 6.93 (m, 1H), 5.82 (s, 1H), 5.35 (s, 2H), 3.62 (t, *J* = 4.8 Hz, 1H), 3.42 – 3.27 (m, 1H), 3.24 – 3.19 (m, 1H), 3.14 – 3.02 (m, 4H), 2.50 – 2.34 (m, 3H), 2.28 – 2.17 (m, 4H), 0.99 (s, 9H). LRMS (CI) *m/*z calcd for $C_{29}H_{38}FN_4O_4$ $[M+H]^+$: 525.3; found: 525.3.

***N*-((3*S*)-1-amino-2-hydroxy-1-oxopentan-3-yl)-1-(cyclohexylmethyl)-1*H*-indole-3-carboxamide (146).** Purified by column chromatography (DCM/MeOH 97:3-94:6). Yield: 26%. Mp: 137 – 138 ºC. $^{1}$H NMR (300 MHz, $CDCl_3$) $\delta$ (ppm): 7.99 – 7.91 (m, 1H), 7.65 (s, 1H), 7.40 – 7.33 (m, 1H), 7.29 – 7.27 (m, 3H), 7.00 (s, 1H), 6.74 – 6.64 (m, 1H), 5.48 (s, 1H), 4.29 (d, *J* = 3.2 Hz, 1H), 4.19 – 4.06 (m, 1H), 3.93 (d, *J* = 7.1 Hz, 2H), 2.10 – 1.92 (m, 2H), 1.91 – 1.78 (m, 1H), 1.76 – 1.56 (m, 9H), 1.22 – 1.12 (m, 2H), 1.05 (t, *J* = 7.4 Hz, 3H). LRMS (CI) *m/*z calcd for $C_{21}H_{30}N_3O_3$ $[M+H]^+$: 372.2; found: 372.2.

***N*-((3*S*)-1-(*tert*-butylamino)-2-hydroxy-1-oxopentan-3-yl)-1-(cyclohexylmethyl)-1*H*-indole-3-carboxamide (147).** Purified by column chromatography (DCM/MeOH 99:1-97:3). Yield: 26%. Oil at room temperature. $^{1}$H NMR (300 MHz, $CDCl_3$) $\delta$ (ppm): 8.09 – 8.01 (m, 1H), 7.71 (s, 1H), 7.38 – 7.32 (m, 1H), 7.26 – 7.22 (m, 2H), 7.09 (d, *J* = 8.0 Hz, 1H), 6.95 (s, 1H), 6.48 (s, 1H), 4.17 (s, 1H), 4.15 – 4.09 (m, 1H), 3.91 (d, *J* = 7.2 Hz, 2H), 1.92 (p, *J* = 7.3 Hz, 2H), 1.86 – 1.78 (m, 1H), 1.73 – 1.52 (m, 5H), 1.28 (s, 9H), 1.21 – 1.08 (m, 3H), 1.02 (t, *J* = 7.3 Hz, 3H), 1.00 – 0.86 (m, 2H). LRMS (CI) *m/*z calcd for $C_{25}H_{38}N_3O_3$ $[M+H]^+$: 428.3; found: 428.3.

USC DE SANTIAGO DE COMPOSTELA

**methyl ((3*S*)-3-(1-(cyclohexylmethyl)-1*H*-indole-3-carboxamido)-2-hydroxypentanoyl)glycinate (148).** Purified by column chromatography (DCM/MeOH 99:1-97:3). Yield: 39%. Mp: 144 – 145 ºC. $^{1}$H NMR (300 MHz, $CDCl_3$) $\delta$ (ppm): 8.05 – 7.99 (m, 1H), 7.68 (s, 1H), 7.67 – 7.60 (m, 1H), 7.39 – 7.32 (m, 1H), 7.26 – 7.22 (m, 1H), 7.16 (s, 1H), 6.97 (d, *J* = 8.3 Hz, 1H), 4.34 (d, *J* = 3.2 Hz, 1H), 4.21 – 4.10 (m, 1H), 4.01 (d, *J* = 5.5 Hz, 2H), 3.92 (d, *J* = 7.1 Hz, 2H), 3.78 – 3.73 (m, 1H), 3.61 (s, 3H), 1.94 (p, *J* = 7.5 Hz, 2H), 1.88 – 1.78 (m, 1H), 1.75 – 1.57 (m, 5H), 1.25 (s, 1H), 1.20 – 1.11 (m, 2H), 1.03 (t, *J* = 7.3 Hz, 3H), 0.99 – 0.90 (m, 2H). $^{13}$C NMR (75 MHz, $CDCl_3$) $\delta$ (ppm): 173.9, 169.7, 167.0, 137.0, 132.3, 125.6, 122.5, 121.6, 120.5, 110.4, 109.6, 74.2, 56.2, 53.4, 52.1, 40.9, 38.5, 31.0, 26.1, 25.6, 22.8, 11.2. LRMS (CI) *m/*z calcd for $C_{24}H_{34}N_3O_5$ $[M+H]^+$: 444.2; found: 444.2.

***N*-((3*S*)-1-(benzylamino)-2-hydroxy-1-oxopentan-3-yl)-1-(cyclohexylmethyl)-1*H*-indole-3-carboxamide (149).** Purified by column chromatography (DCM/MeOH 99:1-97:3). Yield: 37%. Mp: 187 – 189 ºC. $^{1}$H NMR (300 MHz, $CDCl_3$) $\delta$ (ppm): 8.11 (t, *J* = 6.8 Hz, 1H), 7.85 (d, *J* = 8.3 Hz, 1H), 7.38 (d, *J* = 7.7 Hz, 1H), 7.33 – 7.22 (m, 6H), 7.10 (d, *J* = 7.1 Hz, 1H), 6.97 – 6.87 (m, 1H), 6.82 – 6.74 (m, 1H), 5.60 (d, *J* = 2.6 Hz, 1H), 5.46 (d, *J* = 5.0 Hz, 1H), 4.60 – 4.41 (m, 2H), 3.96 (d, *J* = 7.4 Hz, 2H), 3.45 – 3.31 (m, 1H), 1.93 – 1.78 (m, 1H), 1.77 – 1.55 (m, 6H), 1.54 – 1.37 (m, 1H), 1.23 – 1.12 (m, 3H), 1.09 – 0.97 (m, 5H). $^{13}$C NMR (75 MHz, $CDCl_3$) $\delta$ (ppm): 175.12, 172.54, 137.03, 132.56, 132.30, 128.37, 127.25 (d, *J* = 5.6 Hz), 127.11 (d, *J* = 3.4 Hz), 122.67 (d, *J* = 5.0 Hz), 121.77 (d, *J* = 7.3 Hz), 120.64, 120.32, 110.58, 110.42, 76.10, 74.70, 58.36, 56.78, 53.47, 42.92 (d, *J* = 7.5 Hz), 38.51, 30.99, 26.15, 25.61, 24.12, 22.73, 11.57, 11.25. HRMS (ESI) *m/*z calcd for $C_{28}H_{36}N_3O_3$ $[M+H]^+$: 462.2678; found: 462.2751.

**1-(cyclohexylmethyl)-*N*-((3*S*)-2-hydroxy-1-((2-morpholinoethyl)amino)-1-oxopentan-3-yl)-1*H*-indole-3-carboxamide (150).** Purified by column chromatography (DCM/MeOH 99:1-97:3). Yield: 40%. Mp: 115 – 117 ºC. $^{1}$H NMR (300 MHz, DMSO-*d6*) $\delta$ (ppm): 8.31 (s, 1H), 8.23 (s, 0H), 8.08 – 7.99 (m, 1H), 7.88 – 7.67 (m, 1H), 7.65 – 7.60 (m, 1H), 7.53 (d, *J* = 7.9 Hz, 1H), 7.30 – 7.10 (m, 2H), 6.05 (d, *J* = 5.9 Hz, 1H), 5.03 (d, *J* = 3.7 Hz, 1H), 4.13 (d, *J* = 7.2 Hz, 2H), 4.04 (d, *J* = 7.3 Hz, 1H), 3.50 – 3.36 (m, 4H), 3.25 – 2.98 (m, 2H), 2.40 – 2.14 (m, 6H), 1.89 – 1.77 (m, 1H), 1.73 – 1.46 (m, 6H), 1.45 – 1.29 (m, 1H), 1.27 – 0.84 (m, 8H). LRMS (CI) *m/*z calcd for $C_{27}H_{41}N_4O_4$ $[M+H]^+$: 485.3; found: 485.3.

USC UNIVERSIDADE DE SANTIAGO DE COMPOSTELA

***N*-((3*S*)-1-amino-2-hydroxy-4-methyl-1-oxopentan-3-yl)-1-(cyclohexylmethyl)-1*H*-indole-3-carboxamide (151).** Purified by column chromatography (DCM/MeOH 97:3-94:6). Yield: 38%. Mp: 110 – 111 ºC. $^{1}$H NMR (300 MHz, $CDCl_3$) $\delta$ (ppm): 7.99 – 7.93 (m, 1H), 7.66 (s, 1H), 7.39 – 7.33 (m, 1H), 7.30 – 7.23 (m, 2H), 7.13 (s, 1H), 6.83 (d, *J* = 7.9 Hz, 1H), 6.61 (s, 1H), 5.60 (s, 1H), 4.42 (s, 1H), 3.90 (d, *J* = 7.1 Hz, 2H), 3.81 – 3.71 (m, 1H), 2.64 – 2.50 (m, 1H), 1.89 – 1.76 (m, 1H), 1.74 – 1.54 (m, 7H), 1.28 – 1.12 (m, 2H), 1.10 (d, *J* = 6.7 Hz, 3H), 1.04 (d, *J* = 6.5 Hz, 3H), 1.01 – 0.87 (m, 1H). LRMS (CI) *m/*z calcd for $C_{22}H_{32}N_3O_3$ $[M+H]^+$: 386.2; found: 386.2.

***N*-((3*S*)-1-(*tert*-butylamino)-2-hydroxy-4-methyl-1-oxopentan-3-yl)-1-(cyclohexylmethyl)-1*H*-indole-3-carboxamide (152).** Purified by column chromatography (DCM/MeOH 99:1-97:3). Yield: 50%. Mp: 264 – 265 ºC. $^{1}$H NMR (300 MHz, $CDCl_3$) $\delta$ (ppm): 8.05 – 7.98 (m, 1H), 7.70 (s, 1H), 7.40 – 7.32 (m, 1H), 7.30 – 7.19 (m, 2H), 7.06 (d, *J* = 7.9 Hz, 1H), 6.95 (s, 1H), 4.29 (d, *J* = 3.3 Hz, 1H), 3.98 (d, *J* = 7.0 Hz, 1H), 3.94 – 3.87 (m, 2H), 3.77 – 3.67 (m, 1H), 2.62 – 2.48 (m, 1H), 1.90 – 1.76 (m, 1H), 1.73 – 1.51 (m, 6H), 1.39 – 1.31 (m, 1H), 1.24 (s, 9H), 1.15 (d, *J* = 10.9 Hz, 2H), 1.09 (d, *J* = 6.7 Hz, 3H), 1.04 (d, *J* = 6.6 Hz, 3H), 1.01 – 0.86 (m, 1H). LRMS (CI) *m/*z calcd for $C_{26}H_{40}N_3O_3$ $[M+H]^+$: 442.3; found: 442.3.

**methyl ((3*S*)-3-(1-(cyclohexylmethyl)-1*H*-indole-3-carboxamido)-2-hydroxy-4-methylpentanoyl)glycinate (153).** Purified by column chromatography (DCM/MeOH 99:1-97:3). Yield: 54%. Mp: 184 – 186 ºC. $^{1}$H NMR (300 MHz, $CDCl_3$) $\delta$ (ppm): 8.01 – 7.93 (m, 1H), 7.73 – 7.61 (m, 2H), 7.40 – 7.32 (m, 1H), 7.31 – 7.21 (m, 2H), 6.87 (d, *J* = 7.8 Hz, 1H), 4.47 (s, 1H), 3.98 (d, *J* = 5.7 Hz, 2H), 3.91 (d, *J* = 7.2 Hz, 2H), 3.79 – 3.66 (m, 2H), 3.53 (s, 3H), 2.70 – 2.52 (m, 1H), 1.83 (s, 1H), 1.76 – 1.55 (m, 6H), 1.26 – 1.12 (m, 1H), 1.10 (d, *J* = 6.7 Hz, 3H), 1.04 (d, *J* = 6.6 Hz, 3H), 1.02 – 0.87 (m, 3H). $^{13}$C NMR (75 MHz, $CDCl_3$) $\delta$ (ppm): 174.4, 169.6, 167.3, 137.0, 132.3, 125.6, 122.6, 121.6, 120.4, 110.5, 109.5, 73.2, 61.6, 53.4, 52.0, 41.0, 38.5, 31.0, 27.3, 26.1, 25.6, 20.4, 20.0. HRMS (ESI) *m/*z calcd for $C_{25}H_{36}N_3O_5$ $[M+H]^+$: 458.2577; found: 458.2649.

USC UNIVERSIDADE DE SANTIAGO DE COMPOSTELA

***N*-((3*S*)-1-(benzylamino)-2-hydroxy-4-methyl-1-oxopentan-3-yl)-1-(cyclohexylmethyl)-1*H*-indole-3-carboxamide (154).** Purified by column chromatography (DCM/MeOH 99:1-97:3). Yield: 53%. Mp: 132 – 133 ºC. $^1$H NMR (300 MHz, $CDCl_3$) $\delta$ (ppm): 8.17 – 8.11 (m, 1H), 7.84 (s, 1H), 7.40 – 7.34 (m, 1H), 7.34 – 7.21 (m, 8H), 7.18 – 7.10 (m, 1H), 5.73 (s, 1H), 5.42 (d, *J* = 6.8 Hz, 1H), 4.50 (d, *J* = 5.9 Hz, 2H), 3.96 (d, *J* = 7.2 Hz, 2H), 3.20 (t, *J* = 6.1 Hz, 1H), 2.16 – 2.03 (m, 1H), 1.92 – 1.83 (m, 1H), 1.82 – 1.56 (m, 6H), 1.28 – 1.12 (m, 2H), 1.09 (d, *J* = 6.9 Hz, 3H), 1.06 – 0.96 (m, 2H), 0.93 (d, *J* = 6.8 Hz, 3H). LRMS (CI) *m/*z calcd for $C_{29}H_{38}N_3O_3$ $[M+H]^+$: 476.3; found: 476.3.

**1-(cyclohexylmethyl)-*N*-((3*S*)-2-hydroxy-4-methyl-1-((2-morpholinoethyl)amino)-1-oxopentan-3-yl)-1*H*-indole-3-carboxamide (155).** Purified by column chromatography (DCM/MeOH 99:1-97:3). Yield: 40%. Oil at room temperature. $^1$H NMR (300 MHz, DMSO-*d6*) $\delta$ (ppm): 8.32 (s, 0.5H), 8.18 (s, 0.5H), 8.07 – 7.92 (m, 1H), 7.74 – 7.67 (m, 1H), 7.66 – 7.50 (m, 1H), 7.30 – 7.10 (m, 2H), 6.09 (d, *J* = 6.6 Hz, 1H), 5.16 (d, *J* = 3.1 Hz, 1H), 4.99 (d, *J* = 7.4 Hz, 1H), 4.12 (d, *J* = 7.1 Hz, 2H), 3.47 (t, *J* = 4.4 Hz, 1H), 3.40 (t, *J* = 4.6 Hz, 2H), 3.26 – 3.17 (m, 2H), 2.98 – 2.71 (m, 1H), 2.41 – 2.25 (m, 6H), 2.18 – 1.99 (m, 1H), 1.91 – 1.76 (m, 1H), 1.74 – 1.44 (m, 6H), 1.21 – 1.07 (m, 4H), 0.99 (t, *J* = 6.7 Hz, 3H), 0.94 – 0.84 (m, 3H). LRMS (CI) *m/*z calcd for $C_{28}H_{43}N_4O_4$ $[M+H]^+$: 499.3; found: 499.3.

***N*-((3*S*)-1-amino-2-hydroxy-4,4-dimethyl-1-oxopentan-3-yl)-1-(cyclohexylmethyl)-1*H*-indole-3-carboxamide (156).** Purified by column chromatography (DCM/MeOH 97:3-94:6). Yield: 55%. Mp: 270 – 271 ºC. $^1$H NMR (300 MHz, $CDCl_3$) $\delta$ (ppm): 7.92 – 7.85 (m, 1H), 7.66 (s, 1H), 7.43 – 7.35 (m, 2H), 7.29 (d, *J* = 6.4 Hz, 2H), 6.78 – 6.67 (m, 1H), 6.58 (d, *J* = 9.5 Hz, 1H), 4.53 (s, 1H), 4.30 (d, *J* = 9.6 Hz, 1H), 3.94 (d, *J* = 7.2 Hz, 2H), 3.64 (s, 1H), 1.92 – 1.79 (m, 1H), 1.65 (s, 6H), 1.25 (s, 2H), 1.15 (s, 9H), 1.08 – 0.85 (m, 2H). LRMS (CI) *m/*z calcd for $C_{23}H_{34}N_3O_3$ $[M+H]^+$: 400.3; found: 400.3.

***N*-((3*S*)-1-(*tert*-butylamino)-2-hydroxy-4,4-dimethyl-1-oxopentan-3-yl)-1-(cyclohexylmethyl)-1*H*-indole-3-carboxamide (157).** Purified by column chromatography (DCM/MeOH 99:1-97:3). Yield: 50%. Mp: 242 – 243 ºC. $^1$H NMR (300 MHz, DMSO-*d6*) $\delta$ (ppm): 8.12 (s, 1H), 7.99 (d, *J* = 7.7 Hz, 1H), 7.51 (d, *J* = 8.0 Hz, 1H), 7.13 (dt, *J* = 15.9, 7.0 Hz, 2H), 6.98 (s, 1H), 6.83 (d, *J* = 9.9 Hz, 1H), 5.78 (d, *J* = 6.0 Hz, 1H), 4.19 – 3.95 (m, 3H), 3.15 (d, *J* = 5.3 Hz, 1H), 1.88 – 1.73 (m, 1H), 1.70 – 1.41 (m, 8H), 1.27 – 1.07 (m, 2H), 1.04 (s, 9H), 0.99 (s, 9H). LRMS (CI) *m/*z calcd for $C_{27}H_{42}N_3O_3$ $[M+H]^+$: 456.3; found: 456.3.

USC UNIVERSIDADE DE SANTIAGO DE COMPOSTELA

**methyl ((3*S*)-3-(1-(cyclohexylmethyl)-1*H*-indole-3-carboxamido)-2-hydroxy-4,4-dimethylpentanoyl)glycinate (158).** Purified by column chromatography (DCM/MeOH 99:1-97:3). Yield: 57%. Oil at room temperature. $^{1}$H NMR (300 MHz, $CDCl_3$) $\delta$ (ppm): 7.97 – 7.90 (m, 1H), 7.69 (d, *J* = 1.2 Hz, 1H), 7.38 (dd, *J* = 8.4, 3.8 Hz, 2H), 7.33 – 7.23 (m, 2H), 6.66 (d, *J* = 9.3 Hz, 1H), 5.31 (s, 1H), 4.61 (d, *J* = 1.8 Hz, 1H), 4.30 (dt, *J* = 9.3, 1.6 Hz, 1H), 4.00 (t, *J* = 5.2 Hz, 2H), 3.95 (d, *J* = 7.1 Hz, 2H), 3.61 (s, 3H), 1.92 – 1.82 (m, 1H), 1.79 – 1.55 (m, 8H), 1.30 – 1.19 (m, 1H), 1.17 (s, 9H), 1.09 – 0.96 (m, 1H). LRMS (CI) *m/*z calcd for $C_{26}H_{38}N_3O_5$ $[M+H]^+$: 472.3; found: 472.3.

***N*-((3*S*)-1-(benzylamino)-2-hydroxy-4,4-dimethyl-1-oxopentan-3-yl)-1-(cyclohexylmethyl)-1*H*-indole-3-carboxamide (159).** Purified by column chromatography (DCM/MeOH 99:1-97:3). Yield: 28%. Mp: 98 – 99 ºC. $^{1}$H NMR (300 MHz, $CDCl_3$) $\delta$ (ppm): 8.07 – 8.01 (m, 1H), 7.71 (dd, *J* = 5.7, 3.4 Hz, 1H), 7.67 (s, 1H), 7.55 (dt, *J* = 9.1, 4.6 Hz, 1H), 7.37 (d, *J* = 7.5 Hz, 1H), 7.27 (q, *J* = 6.8 Hz, 2H), 7.09 (t, *J* = 7.6 Hz, 2H), 7.00 (q, *J* = 6.8 Hz, 2H), 5.90 (bs, 1H), 4.59 – 4.53 (m, 1H), 4.46 (dd, *J* = 15.1, 6.5 Hz, 1H), 4.33 – 4.17 (m, 3H), 3.88 (d, *J* = 7.0 Hz, 2H), 1.82 (d, *J* = 10.0 Hz, 1H), 1.75 – 1.53 (m, 6H), 1.47 – 1.25 (m, 2H), 1.11 (s, 9H), 0.97 – 0.88 (m, 2H). $^{13}$C NMR (75 MHz, $CDCl_3$) $\delta$ (ppm): 173.8, 167.8, 165.9, 137.8, 137.0, 132.3, 128.4, 127.4, 127.3, 127.0, 125.6, 122.5, 121.6, 120.4, 110.5, 110.1, 71.6, 59.6, 53.4, 43.5, 38.6, 36.2, 31.0, 27.8, 26.2, 25.6. HRMS (ESI) *m/*z calcd for $C_{30}H_{40}N_3O_3$ $[M+H]^+$: 490.2991; found: 490.3064.

**1-(cyclohexylmethyl)-*N*-((3*S*)-2-hydroxy-4,4-dimethyl-1-((2-morpholinoethyl)amino)-1-oxopentan-3-yl)-1*H*-indole-3-carboxamide (160).** Purified by column chromatography (DCM/MeOH 99:1-97:3). Yield: 67%. Mp: 158 – 159 ºC. $^{1}$H NMR (300 MHz, $CDCl_3$) $\delta$ (ppm): 8.21 – 8.11 (m, 1H), 7.92 (s, 1H), 7.45 – 7.30 (m, 2H), 7.32 – 7.27 (m, 2H), 6.97 (s, 1H), 5.81 (s, 1H), 4.03 – 3.91 (m, 2H), 3.74 – 3.65 (m, 1H), 3.62 – 3.56 (m, 1H), 3.43 – 3.27 (m, 2H), 3.22 (s, 1H), 3.14 – 3.05 (m, 3H), 2.55 – 2.15 (m, 6H), 1.95 – 1.80 (m, 1H), 1.78 – 1.56 (m, 5H), 1.23 – 1.10 (m, 5H), 1.05 – 0.97 (m, 9H). LRMS (CI) *m/*z calcd for $C_{29}H_{45}N_4O_4$ $[M+H]^+$: 513.3; found: 513.3.

USC UNIVERSIDADE DE SANTIAGO DE COMPOSTELA

***N*-((3*S*)-1-(*tert*-butylamino)-2-hydroxy-4,4-dimethyl-1-oxopentan-3-yl)-1-(5-fluoropentyl)-1*H*-indole-3-carboxamide (161).** Purified by column chromatography (DCM/MeOH 99:1-97:3). Yield: 56%. Mp: 221 – 222 ºC. $^{1}$H NMR (300 MHz, $CDCl_3$) $\delta$ (ppm): 8.17 (s, 1H), 8.05 – 7.99 (m, 1H), 7.54 (dt, *J* = 8.2, 0.9 Hz, 1H), 7.20 (ddd, *J* = 8.3, 7.0, 1.3 Hz, 1H), 7.14 (ddd, *J* = 8.0, 7.0, 1.1 Hz, 1H), 7.01 (s, 1H), 6.84 (d, *J* = 9.9 Hz, 1H), 5.76 (d, *J* = 6.1 Hz, 1H), 4.45 (t, *J* = 6.0 Hz, 1H), 4.36 (t, *J* = 6.0 Hz, 1H), 4.27 – 4.21 (m, 2H), 4.19 (dd, *J* = 9.9, 1.5 Hz, 1H), 4.16 (dd, *J* = 6.2, 1.5 Hz, 1H), 1.88 – 1.80 (m, 2H), 1.73 – 1.61 (m, 2H), 1.37 – 1.30 (m, 2H), 1.08 (s, 9H), 1.01 (s, 9H). $^{13}$C NMR (75 MHz, $CDCl_3$) $\delta$ (ppm): 172.45, 165.41, 136.59, 131.29, 125.53, 122.53, 121.58, 120.33, 110.77, 110.19, 83.60 (d, *J* = 165.2 Hz), 71.43, 58.70, 51.45, 46.70, 35.93, 29.93 (d, *J* = 19.8 Hz), 28.48, 27.75, 22.81 (d, *J* = 5.0 Hz). LRMS (CI) *m/*z calcd for $C_{25}H_{39}FN_3O_3$ $[M+H]^+$: 448.3; found: 448.3.

***N*-((3*S*)-1-(benzylamino)-2-hydroxy-4,4-dimethyl-1-oxopentan-3-yl)-1-(5-fluoropentyl)-1*H*-indole-3-carboxamide (162).** Purified by column chromatography (DCM/MeOH 99:1-97:3). Yield: 62%. Mp: 116 – 117 ºC. $^{1}$H NMR (300 MHz, $CDCl_3$) $\delta$ (ppm): 8.21 – 8.14 (m, 1H), 7.97 (d, *J* = 7.3 Hz, 1H), 7.92 – 7.86 (m, 1H), 7.65 (s, 1H), 7.42 – 7.21 (m, 5H), 7.15 (d, *J* = 7.3 Hz, 1H), 7.11 – 7.02 (m, 1H), 6.76 – 6.65 (m, 1H), 5.88 (s, 1H), 4.59 – 4.40 (m, 3H), 4.33 (t, *J* = 5.7 Hz, 1H), 4.27 – 4.08 (m, 3H), 3.24 (s, 1H), 1.99 – 1.85 (m, 2H), 1.81 – 1.61 (m, 2H), 1.53 – 1.39 (m, 2H), 1.14 (s, 2H), 1.02 (d, *J* = 13.2 Hz, 7H). $^{13}$C NMR (75 MHz, $CDCl_3$) $\delta$ (ppm): 173.62, 165.87, 137.79, 136.63, 131.47, 128.40, 127.45, 127.11, 125.62, 122.64, 121.74, 120.47, 110.36, 110.15, 83.60 (d, *J* = 165.2 Hz), 71.64, 59.68, 46.73, 43.62, 36.24, 29.92 (d, *J* = 19.9 Hz), 29.67, 27.83, 22.85 (d, *J* = 5.0 Hz). HRMS (ESI) *m/*z calcd for $C_{28}H_{37}FN_3O_3$ $[M+H]^+$: 482.2741; found: 482.2813.

***N*-((3*S*)-1-(*tert*-butylamino)-2-hydroxy-4,4-dimethyl-1-oxopentan-3-yl)-1-pentyl-1*H*-indole-3-carboxamide (163).** Purified by column chromatography (DCM/MeOH 99:1-97:3). Yield: 56%. Mp: 121 – 122 ºC. $^{1}$H NMR (300 MHz, $CDCl_3$) $\delta$ (ppm): 7.98 – 7.89 (m, 1H), 7.66 (s, 1H), 7.36 (s, 1H), 7.32 – 7.22 (m, 2H), 6.48 (d, *J* = 9.9 Hz, 1H), 6.39 – 6.28 (m, 1H), 4.92 (s, 1H), 4.38 (s, 1H), 4.21 (d, *J* = 9.7 Hz, 1H), 4.12 (t, *J* = 7.2 Hz, 2H), 1.85 (dd, *J* = 10.7, 4.3 Hz, 2H), 1.72 (s, 1H), 1.39 – 1.30 (m, 3H), 1.26 (s, 9H), 1.14 (s, 9H), 0.88 (t, *J* = 6.7 Hz, 3H). $^{13}$C NMR (75 MHz, $CDCl_3$) $\delta$ (ppm): 172.2, 165.5, 136.6, 131.3, 125.4, 122.5, 121.6, 120.2, 110.5, 110.3, 71.4, 58.5, 51.7, 46.9, 36.0, 29.6, 29.0, 28.5, 27.7, 22.2, 13.9. LRMS (CI) *m/*z calcd for $C_{25}H_{40}N_3O_3$ $[M+H]^+$: 430.3; found: 430.3.

USC UNIVERSIDADE DE SANTIAGO DE COMPOSTELA

***N*-((3*S*)-1-(benzylamino)-2-hydroxy-4,4-dimethyl-1-oxopentan-3-yl)-1-pentyl-1*H*-indole-3-carboxamide (164).** Purified by column chromatography (DCM/MeOH 99:1-97:3). Yield: 68%. Mp: 230 – 231 ºC. $^1$H NMR (300 MHz, $CDCl_3$) $\delta$ (ppm): 8.19 – 8.13 (m, 1H), 7.99 – 7.92 (m, 1H), 7.88 (s, 1H), 7.64 (s, 1H), 7.44 – 7.35 (m, 2H), 7.35 – 7.20 (m, 3H), 7.16 (d, *J* = 7.5 Hz, 1H), 7.10 – 7.02 (m, 1H), 6.67 (d, *J* = 8.3 Hz, 1H), 5.89 (s, 1H), 4.62 – 4.40 (m, 2H), 4.27 (dd, *J* = 25.4, 7.5 Hz, 1H), 4.12 (q, *J* = 7.2 Hz, 2H), 3.24 (s, 1H), 1.92 – 1.81 (m, 2H), 1.33 (s, 4H), 1.15 (s, 3H), 1.00 (s, 6H), 0.93 – 0.85 (m, 3H). LRMS (CI) *m/*z calcd for $C_{28}H_{38}N_3O_3$ $[M+H]^+$: 464.3; found: 464.3.

***N*-((3*S*)-1-amino-2-hydroxy-1-oxopentan-3-yl)-1-(4-fluorobenzyl)-1*H*-indazole-3-carboxamide (165).** Purified by column chromatography (DCM/MeOH 97:3-94:6). Yield: 30%. Mp: 163 – 164 ºC. $^1$H NMR (300 MHz, $CDCl_3$) $\delta$ (ppm): 8.28 (d, *J* = 8.0 Hz, 1H), 7.68 (d, *J* = 8.5 Hz, 1H), 7.43 – 7.22 (m, 3H), 7.21 – 7.13 (m, 2H), 7.05 (bs, 1H), 6.98 (t, *J* = 8.5 Hz, 2H), 5.90 (bs, 1H), 5.78 (bs, 1H), 5.54 (s, 2H), 4.42 – 4.20 (m, 2H), 1.96 (p, *J* = 7.3 Hz, 2H), 1.04 (t, *J* = 7.4 Hz, 3H). LRMS (CI) *m/*z calcd for $C_{20}H_{22}FN_4O_3$ $[M+H]^+$: 385.2; found: 385.2.

***N*-((3*S*)-1-(*tert*-butylamino)-2-hydroxy-1-oxopentan-3-yl)-1-(4-fluorobenzyl)-1*H*-indazole-3-carboxamide (166).** Purified by column chromatography (DCM/MeOH 99:1-97:3). Yield: 23%. Mp: 160 – 161 ºC. $^1$H NMR (300 MHz, $CDCl_3$) $\delta$ (ppm): 8.31 (d, *J* = 8.2 Hz, 1H), 7.56 (d, *J* = 8.3 Hz, 1H), 7.44 – 7.28 (m, 2H), 7.16 (t, *J* = 7.0 Hz, 2H), 6.98 (t, *J* = 8.5 Hz, 2H), 6.70 (s, 1H), 5.75 (d, *J* = 6.6 Hz, 1H), 5.55 (s, 2H), 4.22 – 4.05 (m, 2H), 1.99 (q, *J* = 7.1 Hz, 2H), 1.22 (s, 9H), 1.05 (t, *J* = 7.5 Hz, 3H). LRMS (CI) *m/*z calcd for $C_{24}H_{30}FN_4O_3$ $[M+H]^+$: 441.2; found: 441.2.

**methyl ((3*S*)-3-(1-(4-fluorobenzyl)-1*H*-indazole-3-carboxamido)-2-hydroxypentanoyl)glycinate (167).** Purified by column chromatography (DCM/MeOH 99:1-97:3). Yield: 25%. Mp: 154 – 155 ºC. $^1$H NMR (300 MHz, $CDCl_3$) $\delta$ (ppm): 8.30 (d, *J* = 7.9 Hz, 1H), 7.74 (d, *J* = 8.4 Hz, 1H), 7.59 – 7.50 (m, 1H), 7.40 – 7.22 (m, 3H), 7.22 – 7.13 (m, 2H), 7.03 – 6.92 (m, 2H), 6.04 (d, *J* = 6.5 Hz, 1H), 5.53 (s, 2H), 4.38 (s, 1H), 4.24 (d, *J* = 7.8 Hz, 1H), 4.01 (d, *J* = 5.6 Hz, 2H), 3.59 – 3.54 (m, 3H), 2.05 – 1.86 (m, 2H), 1.14 – 0.98 (m, 3H). LRMS (CI) *m/*z calcd for $C_{23}H_{26}FN_4O_5$ $[M+H]^+$: 457.2; found: 457.2.

USC UNIVERSIDADE DE SANTIAGO DE COMPOSTELA

***N*-((3*S*)-1-(benzylamino)-2-hydroxy-1-oxopentan-3-yl)-1-(4-fluorobenzyl)-1*H*-indazole-3-carboxamide (168).** Purified by column chromatography (DCM/MeOH 99:1-97:3). Yield: 23%. Mp: 69 – 70 ºC. $^{1}$H NMR (300 MHz, $CDCl_3$) $\delta$ (ppm): 8.28 (d, *J* = 8.4 Hz, 1H), 7.66 (d, *J* = 7.8 Hz, 1H), 7.44 – 7.29 (m, 3H), 7.19 (d, *J* = 8.7 Hz, 1H), 7.10 – 6.90 (m, 5H), 6.83 (t, *J* = 7.6 Hz, 2H), 6.33 (d, *J* = 7.7 Hz, 1H), 5.56 (s, 2H), 4.57 (dd, *J* = 15.2, 7.2 Hz, 1H), 4.40 – 4.33 (m, 1H), 4.27 (dd, *J* = 15.1, 5.4 Hz, 1H), 4.16 – 4.07 (m, 1H), 2.16 – 1.95 (m, 2H), 1.07 (t, *J* = 7.3 Hz, 3H). $^{13}$C NMR (75 MHz, $CDCl_3$) $\delta$ (ppm): 172.89, 164.43, 162.51 (d, *J* = 247.0 Hz), 140.83, 137.90, 136.86, 131.51, 129.07 (d, *J* = 8.2 Hz), 128.30, 127.20 (d, *J* = 3.5 Hz), 127.04, 115.83 (d, *J* = 21.6 Hz), 109.56, 74.35, 56.34, 53.00, 42.96, 23.10, 11.16. HRMS (ESI) *m/*z calcd for $C_{27}H_{28}FN_4O_3$ $[M+H]^+$: 475.2067; found: 475.2148.

***N*-((2*S*,3*S*)-1-(benzylamino)-2-hydroxy-1-oxopentan-3-yl)-1-(4-fluorobenzyl)-1*H*-indazole-3-carboxamide ((*S*)-168).** Purified by column chromatography (DCM/MeOH 99:1-97:3). Yield: 12%. Mp: 173 – 175 ºC. $^{1}$H NMR (300 MHz, $CDCl_3$) $\delta$ (ppm): 8.30 (d, *J* = 8.4 Hz, 1H), 7.45 – 7.28 (m, 6H), 7.21 – 7.14 (m, 2H), 7.11 (d, *J* = 7.5 Hz, 2H), 7.07 – 6.94 (m, 4H), 5.57 (s, 2H), 4.56 – 4.44 (m, 2H), 4.41 (s, 1H), 4.33 (dd, *J* = 15.0, 5.1 Hz, 1H), 4.21 – 4.10 (m, 1H), 2.15 – 2.02 (m, 1H), 2.02 – 1.87 (m, 1H), 1.08 (t, *J* = 7.4 Hz, 3H). $^{13}$C NMR (75 MHz, $CDCl_3$) $\delta$ (ppm): 171.77, 165.11, 162.54 (d, *J* = 245.6 Hz), 140.87, 137.95, 136.70, 131.46 (d, *J* = 2.8 Hz), 129.03 (d, *J* = 8.3 Hz), 128.41, 127.33, 127.28, 127.17, 123.21, 123.17, 122.73, 115.86 (d, *J* = 21.7 Hz), 109.58, 75.81, 58.11, 53.00, 42.88, 23.40, 11.40. LRMS (CI) *m/*z calcd for $C_{27}H_{28}FN_4O_3$ $[M+H]^+$: 475.2; found: 475.3.

***N*-((2*R*,3*S*)-1-(benzylamino)-2-hydroxy-1-oxopentan-3-yl)-1-(4-fluorobenzyl)-1*H*-indazole-3-carboxamide ((*R*)-168).** Purified by column chromatography (DCM/MeOH 99:1-97:3). Yield: 23%. Mp: 69 – 70 ºC. $^{1}$H NMR (300 MHz, $CDCl_3$) $\delta$ (ppm): 8.28 (d, *J* = 8.2 Hz, 1H), 7.65 (d, *J* = 7.4 Hz, 1H), 7.45 – 7.26 (m, 5H), 7.22 – 7.14 (m, 2H), 7.06 (d, *J* = 7.4 Hz, 2H), 7.02 – 6.90 (m, 2H), 6.82 (t, *J* = 7.4 Hz, 2H), 5.55 (s, 2H), 4.57 (dd, *J* = 15.0, 6.7 Hz, 1H), 4.39 – 4.33 (m, 1H), 4.26 (dd, *J* = 15.0, 4.6 Hz, 1H), 4.17 – 4.05 (m, 1H), 2.15 – 1.93 (m, 2H), 1.06 (t, *J* = 7.3 Hz, 3H). $^{13}$C NMR (75 MHz, $CDCl_3$) $\delta$ (ppm): 172.97, 164.17, 162.45 (d, *J* = 247.1 Hz), 140.77, 137.88, 136.91, 131.52 (d, *J* = 2.9 Hz), 129.05 (d, *J* = 8.6 Hz), 128.32, 127.23, 127.12, 127.07, 123.25, 123.00, 122.72, 115.78 (d, *J* = 21.9 Hz), 109.57, 74.00, 55.86, 52.95, 42.93, 23.16, 11.14. HRMS (ESI) *m/*z calcd for $C_{27}H_{28}FN_4O_3$ $[M+H]^+$: 475.2067; found: 475.2148.

USC UNIVERSIDADE DE SANTIAGO DE COMPOSTELA

**1-(4-fluorobenzyl)-*N*-((3*S*)-2-hydroxy-1-((2-morpholinoethyl)amino)-1-oxopentan-3-yl)-1*H*-indazole-3-carboxamide (169).** Purified by column chromatography (DCM/MeOH 99:1-97:3). Yield: 40%. Oil at room temperature. $^{1}$H NMR (300 MHz, $CDCl_3$) $\delta$ (ppm): 8.28 (d, *J* = 8.1 Hz, 1H), 7.70 (d, *J* = 8.4 Hz, 1H), 7.42 – 7.22 (m, 4H), 7.21 – 7.13 (m, 2H), 7.03 – 6.93 (m, 2H), 5.53 (s, 2H), 4.35 – 4.27 (m, 1H), 4.27 – 4.13 (m, 1H), 3.60 – 3.45 (m, 4H), 3.32 (p, *J* = 6.4, 6.0 Hz, 2H), 2.44 – 2.15 (m, 6H), 1.96 (p, *J* = 7.6 Hz, 2H), 1.04 (t, *J* = 7.4 Hz, 3H). LRMS (CI) *m/*z calcd for $C_{26}H_{33}FN_5O_4$ $[M+H]^+$: 498.2; found: 498.2.

***N*-((3*S*)-1-amino-2-hydroxy-4-methyl-1-oxopentan-3-yl)-1-(4-fluorobenzyl)-1*H*-indazole-3-carboxamide (170).** Purified by column chromatography (DCM/MeOH 97:3-94:6). Yield: 47%. Mp: 223 – 225 ºC. $^{1}$H NMR (300 MHz, $CDCl_3$) $\delta$ (ppm): 8.27 (d, *J* = 8.1 Hz, 1H), 7.66 (d, *J* = 8.2 Hz, 1H), 7.41 – 7.22 (m, 3H), 7.22 – 7.13 (m, 3H), 6.99 (t, *J* = 8.5 Hz, 2H), 6.32 (s, 1H), 5.63 (s, 1H), 5.54 (s, 2H), 4.47 (s, 1H), 3.90 – 3.79 (m, 1H), 2.56 – 2.42 (m, 1H), 1.11 (d, *J* = 6.6 Hz, 3H), 1.03 (d, *J* = 6.7 Hz, 3H). $^{13}$C NMR (75 MHz, $CDCl_3$) $\delta$ (ppm): 173.63, 164.49, 162.53 (d, *J* = 247.8 Hz), 140.87, 136.58, 131.38, 129.05 (d, *J* = 8.3 Hz), 127.23, 123.14, 122.60, 115.84 (d, *J* = 21.7 Hz), 109.63, 72.40, 60.53, 53.02, 28.02, 20.17, 19.73. LRMS (CI) *m/*z calcd for $C_{21}H_{24}FN_4O_3$ $[M+H]^+$: 399.2; found: 399.2.

***N*-((3*S*)-1-(*tert*-butylamino)-2-hydroxy-4-methyl-1-oxopentan-3-yl)-1-(4-fluorobenzyl)-1*H*-indazole-3-carboxamide (171).** Purified by column chromatography (DCM/MeOH 99:1-97:3). Yield: 60%. Mp: 176 – 177 ºC. $^{1}$H NMR (300 MHz, $CDCl_3$) $\delta$ (ppm): 8.31 (d, *J* = 8.1 Hz, 1H), 7.56 (d, *J* = 8.4 Hz, 1H), 7.45 – 7.28 (m, 2H), 7.20 – 7.12 (m, 2H), 6.98 (t, *J* = 7.5 Hz, 2H), 6.68 (s, 1H), 5.98 (d, *J* = 7.1 Hz, 1H), 5.55 (s, 2H), 4.35 – 4.28 (m, 1H), 3.80 – 3.68 (m, 1H), 2.59 – 2.45 (m, 1H), 1.19 (s, 9H), 1.13 (d, *J* = 6.6 Hz, 3H), 1.05 (d, *J* = 6.6 Hz, 3H). LRMS (CI) *m/*z calcd for $C_{25}H_{32}FN_4O_3$ $[M+H]^+$: 455.2; found: 455.2.

**methyl ((3*S*)-3-(1-(4-fluorobenzyl)-1*H*-indazole-3-carboxamido)-2-hydroxy-4-methylpentanoyl)glycinate (172).** Purified by column chromatography (DCM/MeOH 99:1-97:3). Yield: 51%. Mp: 258 – 260 ºC. $^{1}$H NMR (300 MHz, $CDCl_3$) $\delta$ (ppm): 8.30 (d, *J* = 8.0 Hz, 1H), 7.66 (d, *J* = 7.9 Hz, 1H), 7.55 – 7.47 (m, 1H), 7.40 – 7.32 (m, 1H), 7.32 – 7.23 (m, 2H), 7.17 (t, *J* = 6.4 Hz, 2H), 7.03 – 6.92 (m, 2H), 6.39 (d, *J* = 7.6 Hz, 1H), 5.52 (s, 2H), 4.49 (d, *J* = 7.4 Hz, 1H), 4.06 – 3.87 (m, 2H), 3.86 – 3.75 (m, 1H), 3.51 – 3.45 (m, 3H), 2.63 – 2.49 (m, 1H), 1.12 (d, *J* = 6.5 Hz, 3H), 1.05 (d, *J* = 6.6 Hz, 3H). LRMS (CI) *m/*z calcd for $C_{24}H_{28}FN_4O_5$ $[M+H]^+$: 471.2; found: 471.2.

USC UNIVERSIDADE DE SANTIAGO DE COMPOSTELA

***N*-((3*S*)-1-(benzylamino)-2-hydroxy-4-methyl-1-oxopentan-3-yl)-1-(4-fluorobenzyl)-1*H*-indazole-3-carboxamide (173).** Purified by column chromatography (DCM/MeOH 99:1-97:3). Yield: 53%. Mp: 87 – 88 ºC. $^{1}$H NMR (300 MHz, DMSO-*d6*) $\delta$ (ppm): 8.36 (t, *J* = 6.3 Hz, 1H), 8.19 (d, *J* = 8.1 Hz, 1H), 7.75 (d, *J* = 8.5 Hz, 1H), 7.55 (d, *J* = 9.8 Hz, 1H), 7.46 (t, *J* = 7.7 Hz, 1H), 7.30 (d, *J* = 7.6 Hz, 1H), 7.27 – 7.19 (m, 2H), 7.06 (t, *J* = 8.8 Hz, 2H), 7.00 (d, *J* = 7.5 Hz, 2H), 6.84 (t, *J* = 7.3 Hz, 1H), 6.71 (t, *J* = 7.5 Hz, 2H), 6.17 (d, *J* = 6.2 Hz, 1H), 5.79 – 5.64 (m, 2H), 4.34 (dd, *J* = 15.3, 7.0 Hz, 1H), 4.27 – 4.15 (m, 2H), 4.06 (dd, *J* = 15.3, 5.5 Hz, 1H), 2.03 – 1.85 (m, 1H), 1.01 (d, *J* = 6.6 Hz, 3H), 0.91 (d, *J* = 6.7 Hz, 3H). $^{13}$C NMR (75 MHz, $CDCl_3$) $\delta$ (ppm): 172.87, 162.03 (d, *J* = 243.1 Hz), 161.57, 141.09, 139.81, 137.76, 133.41, 129.78 (d, *J* = 8.2 Hz), 128.07, 127.42, 127.07, 126.56, 123.05, 122.91, 122.49, 115.88 (d, *J* = 21.5 Hz), 110.94, 71.10, 56.56, 52.06, 42.14, 30.51, 20.33, 20.02. HRMS (ESI) *m/*z calcd for $C_{28}H_{30}FN_4O_3$ $[M+H]^+$: 489.2224; found: 489.2296.

***N*-((2*S*,3*S*)-1-(benzylamino)-2-hydroxy-4-methyl-1-oxopentan-3-yl)-1-(4-fluorobenzyl)-1*H*-indazole-3-carboxamide ((*S*)-173).** Purified by column chromatography (DCM/MeOH 99:1-97:3). Yield: 21%. Mp: 87 – 88 ºC. $^{1}$H NMR (300 MHz, $CDCl_3$) $\delta$ (ppm): 8.30 (d, *J* = 8.2 Hz, 1H), 7.45 – 7.33 (m, 5H), 7.33 – 7.27 (m, 1H), 7.17 (dd, *J* = 8.5, 5.3 Hz, 2H), 7.10 – 7.04 (m, 2H), 7.03 – 6.88 (m, 4H), 5.56 (s, 2H), 4.56 (s, 1H), 4.49 (dd, *J* = 15.0, 6.7 Hz, 1H), 4.30 (dd, *J* = 15.0, 5.4 Hz, 1H), 4.02 – 3.92 (m, 1H), 2.58 – 2.43 (m, 1H), 1.17 (d, *J* = 6.6 Hz, 3H), 1.09 (d, *J* = 6.7 Hz, 3H). $^{13}$C NMR (75 MHz, $CDCl_3$) $\delta$ (ppm): 172.04, 165.21, 162.53 (d, *J* = 247.1 Hz), 140.88, 137.92, 136.67, 131.44 (d, *J* = 3.3 Hz), 129.07 (d, *J* = 8.1 Hz), 128.35, 127.30, 127.29, 127.10, 123.23, 123.17, 122.73, 115.85 (d, *J* = 21.6 Hz), 109.59, 74.51, 62.32, 53.03, 42.80, 29.25, 20.58 (d, *J* = 2.8 Hz). LRMS (CI) *m/*z calcd for $C_{28}H_{30}FN_4O_3$ $[M+H]^+$: 489.2; found: 489.2.

USC UNIVERSIDADE DE SANTIAGO DE COMPOSTELA

***N*-((2*R*,3*S*)-1-(benzylamino)-2-hydroxy-4-methyl-1-oxopentan-3-yl)-1-(4-fluorobenzyl)-1*H*-indazole-3-carboxamide ((*R*)-173).** Purified by column chromatography (DCM/MeOH 99:1-97:3). Yield: 53%. Mp: 87 – 88 ºC. $^{1}$H NMR (300 MHz, $CDCl_3$) $\delta$ (ppm): 8.27 (d, *J* = 8.5 Hz, 1H), 7.72 (d, *J* = 7.9 Hz, 1H), 7.49 – 7.24 (m, 5H), 7.16 (dd, *J* = 8.5, 5.4 Hz, 2H), 7.05 – 6.85 (m, 4H), 6.76 (t, *J* = 7.5 Hz, 2H), 5.53 (s, 2H), 4.55 (dd, *J* = 15.1, 7.1 Hz, 1H), 4.52 – 4.36 (m, 2H), 4.21 (dd, *J* = 15.0, 5.0 Hz, 1H), 3.79 (ddd, *J* = 10.9, 7.9, 3.2 Hz, 1H), 2.65 – 2.49 (m, 1H), 1.13 (d, *J* = 6.6 Hz, 3H), 1.05 (d, *J* = 6.6 Hz, 3H). $^{13}$C NMR (75 MHz, $CDCl_3$) $\delta$ (ppm): 173.40, 164.36, 162.48 (d, *J* = 246.9 Hz), 140.85, 137.92, 136.83, 131.51 (d, *J* = 3.2 Hz), 129.07 (d, *J* = 8.2 Hz), 128.22, 127.20, 127.14, 126.94, 123.28, 123.05, 122.81, 115.81 (d, *J* = 21.8 Hz), 109.60, 72.96, 60.92, 52.96, 42.98, 27.93, 20.33, 19.85. HRMS (ESI) *m/*z calcd for $C_{28}H_{30}FN_4O_3$ $[M+H]^+$: 489.2224; found: 489.2296.

**1-(4-fluorobenzyl)-*N*-((3*S*)-2-hydroxy-4-methyl-1-((2-morpholinoethyl)amino)-1-oxopentan-3-yl)-1*H*-indazole-3-carboxamide (174).** Purified by column chromatography (DCM/MeOH 99:1-97:3). Yield: 44%. Mp: 208 – 209 ºC. $^{1}$H NMR (300 MHz, $CDCl_3$) $\delta$ (ppm): 8.40 (d, *J* = 8.1 Hz, 1H), 8.21 (d, *J* = 8.2 Hz, 1H), 7.72 (d, *J* = 10.1 Hz, 1H), 7.46 – 7.28 (m, 3H), 7.25 – 7.15 (m, 2H), 7.04 – 6.91 (m, 2H), 5.83 (d, *J* = 4.3 Hz, 1H), 5.64 (s, 1H), 5.58 (s, 2H), 4.74 – 4.63 (m, 1H), 3.42 – 3.19 (m, 6H), 2.43 – 2.16 (m, 7H), 1.25 (d, *J* = 6.6 Hz, 3H), 1.14 (d, *J* = 6.7 Hz, 3H). LRMS (CI) *m/*z calcd for $C_{27}H_{35}FN_5O_4$ $[M+H]^+$: 512.3; found: 512.3.

***N*-((3*S*)-1-amino-2-hydroxy-4,4-dimethyl-1-oxopentan-3-yl)-1-(4-fluorobenzyl)-1*H*-indazole-3-carboxamide (175).** Purified by column chromatography (DCM/MeOH 97:3-94:6). Yield: 50%. Mp: 169 – 171 ºC. $^{1}$H NMR (300 MHz, $CDCl_3$) $\delta$ (ppm): 8.33 (d, *J* = 8.1 Hz, 1H), 7.61 (d, *J* = 9.8 Hz, 1H), 7.42 – 7.30 (m, 3H), 7.26 – 7.19 (m, 2H), 7.07 – 6.99 (m, 2H), 6.60 (bs, 1H), 5.59 (s, 2H), 5.54 (bs, 1H), 4.76 (d, *J* = 4.8 Hz, 1H), 4.57 (dd, *J* = 4.8, 1.9 Hz, 1H), 4.28 (d, *J* = 1.9 Hz, 0.5H), 4.24 (d, *J* = 1.9 Hz, 0.5H), 1.18 (s, 9H). LRMS (CI) *m/*z calcd for $C_{22}H_{26}FN_4O_3$ $[M+H]^+$: 413.2; found: 413.2.

USC UNIVERSIDADE DE SANTIAGO DE COMPOSTELA

***N*-((3*S*)-1-(*tert*-butylamino)-2-hydroxy-4,4-dimethyl-1-oxopentan-3-yl)-1-(4-fluorobenzyl)-1*H*-indazole-3-carboxamide (176).** Purified by column chromatography (DCM/MeOH 99:1-97:3). Yield: 60%. Mp: 213 – 214 ºC. $^{1}$H NMR (300 MHz, $CDCl_3$) $\delta$ (ppm): 8.32 (d, $J$ = 8.0 Hz, 1H), 7.54 – 7.48 (m, 1H), 7.40 – 7.28 (m, 3H), 7.25 – 7.14 (m, 2H), 7.05 – 6.95 (m, 2H), 6.21 (s, 1H), 5.57 (s, 2H), 4.78 (d, $J$ = 4.5 Hz, 1H), 4.43 – 4.37 (m, 1H), 4.16 (d, $J$ = 9.8 Hz, 1H), 1.22 (s, 9H), 1.15 (s, 9H). $^{13}$C NMR (75 MHz, $CDCl_3$) $\delta$ (ppm): 171.95, 163.08, 162.49 (d, $J$ = 247.0 Hz), 140.81, 137.21, 131.67 (d, $J$ = 3.2 Hz), 128.97 (d, $J$ = 8.3 Hz), 127.01, 123.29, 122.81 (d, $J$ = 3.2 Hz), 115.78 (d, $J$ = 21.7 Hz), 109.52, 71.45, 58.82, 52.94, 51.65, 35.98, 28.40, 27.64. LRMS (CI) *m/*z calcd for $C_{26}H_{34}FN_4O_3$ $[M+H]^+$: 469.3; found: 469.3.

**methyl ((3*S*)-3-(1-(4-fluorobenzyl)-1*H*-indazole-3-carboxamido)-2-hydroxy-4,4-dimethylpentanoyl)glycinate (177).** Purified by column chromatography (DCM/MeOH 99:1-97:3). Yield: 50%. Mp: 124 – 125 ºC. $^{1}$H NMR (300 MHz, $CDCl_3$) $\delta$ (ppm): 8.31 (d, $J$ = 8.1 Hz, 1H), 7.61 (d, $J$ = 9.7 Hz, 1H), 7.43 – 7.15 (m, 6H), 6.98 (t, $J$ = 8.4 Hz, 2H), 5.55 (s, 2H), 4.62 (s, 1H), 4.29 (d, $J$ = 9.8 Hz, 1H), 4.06 – 3.86 (m, 2H), 3.51 (s, 3H), 1.14 (s, 9H). $^{13}$C NMR (75 MHz, $CDCl_3$) $\delta$ (ppm): 173.56, 169.83, 164.54 (d, $J$ = 245.0 Hz), 163.16, 140.82, 137.25, 131.63 (d, $J$ = 3.3 Hz), 129.04 (d, $J$ = 8.3 Hz), 127.06, 123.27, 122.87 (d, $J$ = 6.6 Hz), 115.81 (d, $J$ = 21.5 Hz), 109.47, 71.28, 59.52, 52.97, 52.16, 41.40, 36.18, 27.64. LRMS (CI) *m/*z calcd for $C_{25}H_{30}FN_4O_5$ $[M+H]^+$: 485.2; found: 485.2.

**methyl ((2*S*,3*S*)-3-(1-(4-fluorobenzyl)-1*H*-indazole-3-carboxamido)-2-hydroxy-4,4-dimethylpentanoyl)glycinate ((*S*)-177).** Purified by column chromatography (DCM/MeOH 99:1-97:3). Yield: 5%. Mp: 124 – 125 ºC. $^{1}$H NMR (300 MHz, $CDCl_3$) $\delta$ (ppm): 8.33 (d, $J$ = 8.1 Hz, 1H), 7.61 (d, $J$ = 8.5 Hz, 1H), 7.47 – 7.27 (m, 4H), 7.24 – 7.16 (m, 2H), 7.00 (t, $J$ = 8.4 Hz, 2H), 5.57 (s, 2H), 5.16 (bs, 1H), 4.59 (s, 1H), 4.17 (d, $J$ = 8.5 Hz, 1H), 4.06 – 3.88 (m, 2H), 3.60 (s, 3H), 1.16 (s, 9H). LRMS (CI) *m/*z calcd for $C_{25}H_{30}FN_4O_5$ $[M+H]^+$: 485.2; found: 485.2.

USC UNIVERSIDADE DE SANTIAGO DE COMPOSTELA

**methyl ((2*R*,3*S*)-3-(1-(4-fluorobenzyl)-1*H*-indazole-3-carboxamido)-2-hydroxy-4,4-dimethylpentanoyl)glycinate ((*R*)-177).** Purified by column chromatography (DCM/MeOH 99:1-97:3). Yield: 50%. Mp: 124 – 125 ºC. $^{1}$H NMR (300 MHz, $CDCl_3$) $\delta$ (ppm): 8.31 (d, *J* = 8.1 Hz, 1H), 7.56 (d, *J* = 9.7 Hz, 1H), 7.38 – 7.25 (m, 4H), 7.24 – 7.17 (m, 2H), 7.04 – 6.97 (m, 2H), 5.57 (s, 2H), 4.60 (s, 1H), 4.19 (d, *J* = 9.3 Hz, 1H), 4.08 – 3.89 (m, 2H), 3.56 (s, 3H), 1.16 (s, 9H). $^{13}$C NMR (75 MHz, $CDCl_3$) $\delta$ (ppm): 173.74, 170.00, 163.02, 162.48 (d, *J* = 246.9 Hz), 140.81, 137.35, 131.67 (d, *J* = 3.3 Hz), 129.02 (d, *J* = 8.2 Hz), 127.05, 123.26, 122.94, 122.80, 115.79 (d, *J* = 21.8 Hz), 109.47, 71.17, 59.19, 52.94, 52.14, 41.36, 36.09, 27.61. LRMS (CI) *m/*z calcd for $C_{25}H_{30}FN_4O_5$ $[M+H]^+$: 485.2; found: 485.2.

***N*-((3*S*)-1-(benzylamino)-2-hydroxy-4,4-dimethyl-1-oxopentan-3-yl)-1-(4-fluorobenzyl)-1*H*-indazole-3-carboxamide (178).** Purified by column chromatography (DCM/MeOH 99:1-97:3). Yield: 67%. Mp: 54 – 56 ºC. $^{1}$H NMR (300 MHz, DMSO-*d6*) $\delta$ (ppm): 8.28 (t, *J* = 6.3 Hz, 1H), 8.21 (d, *J* = 8.1 Hz, 1H), 7.74 (d, *J* = 8.4 Hz, 1H), 7.54 (d, *J* = 10.2 Hz, 1H), 7.46 (t, *J* = 7.6 Hz, 1H), 7.33 – 7.26 (m, 1H), 7.27 – 7.18 (m, 2H), 7.05 (t, *J* = 8.8 Hz, 2H), 6.96 (d, *J* = 7.5 Hz, 2H), 6.83 (t, *J* = 7.4 Hz, 1H), 6.70 (t, *J* = 7.4 Hz, 2H), 6.18 (d, *J* = 6.2 Hz, 1H), 5.81 – 5.64 (m, 2H), 4.40 – 4.26 (m, 3H), 4.02 (dd, *J* = 15.6, 5.2 Hz, 1H), 1.00 (s, 8H), 0.95 (s, 1H). $^{13}$C NMR (75 MHz, DMSO-*d6*) $\delta$ (ppm): 173.38, 162.02 (d, *J* = 244.1 Hz), 161.48, 141.09, 139.74, 137.77, 133.35, 129.77 (d, *J* = 8.2 Hz), 128.06, 127.43, 126.99, 126.54, 123.06, 122.90, 122.52, 115.86 (d, *J* = 21.4 Hz), 110.97, 70.12, 57.38, 52.07, 42.19, 35.92, 27.76. HRMS (ESI) *m/*z calcd for $C_{29}H_{32}FN_4O_3$ $[M+H]^+$: 503.2380; found: 503.2459.

***N*-((2*S*,3*S*)-1-(benzylamino)-2-hydroxy-4,4-dimethyl-1-oxopentan-3-yl)-1-(4-fluorobenzyl)-1*H*-indazole-3-carboxamide ((*S*)-178).** Purified by column chromatography (DCM/MeOH 99:1-97:3). Yield: 7%. Mp: 54 – 56 ºC. $^{1}$H NMR (300 MHz, $CDCl_3$) $\delta$ (ppm): 8.30 (d, *J* = 8.1 Hz, 1H), 7.61 (d, *J* = 8.4 Hz, 1H), 7.44 – 7.24 (m, 5H), 7.20 – 7.13 (m, 2H), 7.10 – 7.02 (m, 2H), 7.02 – 6.91 (m, 4H), 5.56 (s, 2H), 5.26 (d, *J* = 6.7 Hz, 1H), 4.56 (d, *J* = 5.7 Hz, 1H), 4.46 (dd, *J* = 14.9, 6.6 Hz, 1H), 4.26 (dd, *J* = 14.8, 5.3 Hz, 1H), 4.16 (d, *J* = 8.4 Hz, 1H), 1.17 (s, 9H). $^{13}$C NMR (75 MHz, $CDCl_3$) $\delta$ (ppm): 172.03, 164.42, 162.50 (d, *J* = 247.4 Hz), 140.86, 137.85, 136.94, 131.51 (d, *J* = 3.1 Hz), 129.03 (d, *J* = 8.2 Hz), 128.35, 127.44, 127.18, 127.12, 123.25, 123.05, 122.77, 115.81 (d, *J* = 21.7 Hz), 109.59, 74.65, 63.98, 53.01, 43.06, 35.00, 27.73. LRMS (CI) *m/*z calcd for $C_{29}H_{32}FN_4O_3$ $[M+H]^+$: 503.2; found: 503.3.

USC DE SANTIAGO DE COMPOSTELA

***N*-((2*R*,3*S*)-1-(benzylamino)-2-hydroxy-4,4-dimethyl-1-oxopentan-3-yl)-1-(4-fluorobenzyl)-1*H*-indazole-3-carboxamide ((*R*)-178).** Purified by column chromatography (DCM/MeOH 99:1-97:3). Yield: 67%. Mp: 54 – 56 ºC. $^{1}$H NMR (300 MHz, $CDCl_3$) $\delta$ (ppm): 8.32 (d, *J* = 8.0 Hz, 1H), 7.67 (d, *J* = 9.6 Hz, 1H), 7.42 – 7.22 (m, 5H), 7.14 (dd, *J* = 8.3, 5.3 Hz, 2H), 7.05 (d, *J* = 7.4 Hz, 2H), 7.00 – 6.79 (m, 4H), 5.52 (s, 2H), 4.60 (s, 1H), 4.49 (dd, *J* = 16.2, 6.4 Hz, 2H), 4.39 – 4.26 (m, 1H), 4.17 (dd, *J* = 14.8, 4.9 Hz, 1H), 1.14 (s, 9H). $^{13}$C NMR (75 MHz, $CDCl_3$) $\delta$ (ppm): 173.80, 162.90, 162.41 (d, *J* = 246.8 Hz), 140.82, 137.95, 137.37, 131.69 (d, *J* = 3.2 Hz), 128.99 (d, *J* = 8.2 Hz), 128.16, 127.35, 127.04, 126.88, 123.35, 123.04, 122.80, 115.73 (d, *J* = 21.6 Hz), 109.51, 71.12, 58.84, 52.88, 43.33, 35.97, 27.63. LRMS (CI) *m/*z calcd for $C_{29}H_{32}FN_4O_3$ $[M+H]^+$: 503.2; found: 503.3.

**1-(4-fluorobenzyl)-*N*-((3*S*)-2-hydroxy-4,4-dimethyl-1-((2-morpholinoethyl)amino)-1-oxopentan-3-yl)-1*H*-indazole-3-carboxamide (179).** Purified by column chromatography (DCM/MeOH 99:1-97:3). Yield: 55%. Mp: 258 – 259 ºC. $^{1}$H NMR (300 MHz, $CDCl_3$) $\delta$ (ppm): 8.28 (d, *J* = 8.1 Hz, 1H), 7.55 (d, *J* = 9.6 Hz, 1H), 7.39 – 7.27 (m, 3H), 7.24 – 7.16 (m, 2H), 7.13 – 7.06 (m, 1H), 7.00 (t, *J* = 8.4 Hz, 2H), 5.56 (s, 2H), 4.52 (s, 1H), 4.21 (d, *J* = 9.6 Hz, 1H), 3.60 (t, *J* = 4.6 Hz, 4H), 3.41 – 3.21 (m, 2H), 2.49 – 2.23 (m, 6H), 1.14 (s, 9H). LRMS (CI) *m/*z calcd for $C_{28}H_{37}FN_5O_4$ $[M+H]^+$: 526.3; found: 526.3.

***N*-((3*S*)-1-amino-2-hydroxy-1-oxopentan-3-yl)-1-(cyclohexylmethyl)-1*H*-indazole-3-carboxamide (180).** Purified by column chromatography (DCM/MeOH 97:3-94:6). Yield: 21%. Mp: 91 – 93 ºC. $^{1}$H NMR (300 MHz, $CDCl_3$) $\delta$ (ppm): 8.26 (d, *J* = 8.2 Hz, 1H), 7.64 (d, *J* = 8.4 Hz, 1H), 7.39 (d, *J* = 4.0 Hz, 2H), 7.30 – 7.20 (m, 1H), 7.09 (s, 1H), 6.03 (d, *J* = 6.3 Hz, 1H), 5.79 (s, 1H), 4.35 – 4.28 (m, 1H), 4.27 – 4.19 (m, 1H), 4.17 (d, *J* = 7.1 Hz, 2H), 2.06 – 1.89 (m, 3H), 1.75 – 1.52 (m, 7H), 1.28 – 1.09 (m, 2H), 1.04 (t, *J* = 7.4 Hz, 3H), 1.03 – 0.91 (m, 1H). $^{13}$C NMR (75 MHz, $CDCl_3$) $\delta$ (ppm): 175.8, 164.5, 141.4, 136.1, 126.6, 122.7, 122.4, 109.6, 73.9, 55.8, 55.6, 38.7, 30.9, 26.2, 25.6, 23.5, 11.1. LRMS (CI) *m/*z calcd for $C_{20}H_{29}N_4O_3$ $[M+H]^+$: 373.2; found: 373.2.

USC UNIVERSIDADE DE SANTIAGO DE COMPOSTELA

***N*-((3*S*)-1-(*tert*-butylamino)-2-hydroxy-1-oxopentan-3-yl)-1-(cyclohexylmethyl)-1*H*-indazole-3-carboxamide (181).** Purified by column chromatography (DCM/MeOH 99:1-97:3). Yield: 29%. Mp: 228 – 229 ºC. $^1$H NMR (300 MHz, $CDCl_3$) $\delta$ (ppm): 8.29 (d, $J$ = 8.2 Hz, 1H), 7.54 (d, $J$ = 8.3 Hz, 1H), 7.45 – 7.37 (m, 2H), 7.29 (d, $J$ = 3.7 Hz, 1H), 6.74 (s, 1H), 6.00 (d, $J$ = 7.0 Hz, 1H), 4.19 (d, $J$ = 7.4 Hz, 2H), 4.16 – 4.12 (m, 1H), 4.12 – 4.01 (m, 1H), 2.10 – 1.90 (m, 2H), 1.76 – 1.62 (m, 1H), 1.56 – 1.47 (m, 7H), 1.21 (s, 9H), 1.20 – 1.13 (m, 3H), 1.05 (t, $J$ = 7.4 Hz, 3H). LRMS (CI) *m/*z calcd for $C_{24}H_{37}N_4O_3$ $[M+H]^+$: 429.3; found: 429.3.

**methyl ((3*S*)-3-(1-(cyclohexylmethyl)-1*H*-indazole-3-carboxamido)-2-hydroxypentanoyl)glycinate (182).** Purified by column chromatography (DCM/MeOH 99:1-97:3). Yield: 27%. Mp: 57 – 58 ºC. $^1$H NMR (300 MHz, $CDCl_3$) $\delta$ (ppm): 8.28 (d, $J$ = 8.2 Hz, 1H), 7.65 (d, $J$ = 8.2 Hz, 1H), 7.54 (t, $J$ = 5.8 Hz, 1H), 7.43 – 7.35 (m, 2H), 7.29 – 7.22 (m, 1H), 6.19 (d, $J$ = 6.7 Hz, 1H), 4.40 – 4.33 (m, 1H), 4.18 (d, $J$ = 7.2 Hz, 3H), 4.04 – 3.98 (m, 2H), 3.57 (d, $J$ = 1.7 Hz, 3H), 2.06 – 1.88 (m, 3H), 1.76 – 1.52 (m, 6H), 1.29 – 1.12 (m, 4H), 1.04 (t, $J$ = 7.5 Hz, 3H). LRMS (CI) *m/*z calcd for $C_{23}H_{33}N_4O_5$ $[M+H]^+$: 445.2; found: 445.2.

**methyl ((2*S*,3*S*)-3-(1-(cyclohexylmethyl)-1*H*-indazole-3-carboxamido)-2-hydroxypentanoyl)glycinate ((*S*)-182).** Purified by column chromatography (DCM/MeOH 99:1-97:3). Yield: 13%. Mp: 171 – 172 ºC. $^1$H NMR (300 MHz, $CDCl_3$) $\delta$ (ppm): 8.32 (dt, $J$ = 8.1, 1.1 Hz, 1H), 7.52 (t, $J$ = 5.8 Hz, 1H), 7.46 – 7.38 (m, 3H), 7.34 – 7.26 (m, 1H), 4.47 (d, $J$ = 1.8 Hz, 1H), 4.22 (d, $J$ = 7.2 Hz, 2H), 4.20 – 4.13 (m, 1H), 4.05 (dd, $J$ = 5.8, 2.5 Hz, 2H), 3.67 (s, 3H), 2.11 – 1.96 (m, 2H), 1.94 – 1.81 (m, 1H), 1.78 – 1.56 (m, 6H), 1.31 – 1.15 (m, 3H), 1.13 – 0.99 (m, 4H). $^{13}$C NMR (75 MHz, $CDCl_3$) $\delta$ (ppm): 172.3, 169.8, 165.3, 141.4, 136.1, 126.7, 122.8, 122.7, 122.5, 109.6, 75.7, 57.7, 55.8, 52.2, 40.8, 38.7, 30.9, 26.2, 25.6, 22.5, 11.3. LRMS (CI) *m/*z calcd for $C_{23}H_{33}N_4O_5$ $[M+H]^+$: 445.2; found: 445.3.

USC UNIVERSIDADE DE SANTIAGO DE COMPOSTELA

**methyl ((2*R*,3*S*)-3-(1-(cyclohexylmethyl)-1*H*-indazole-3-carboxamido)-2-hydroxypentanoyl)glycinate ((*R*)-182).** Purified by column chromatography (DCM/MeOH 99:1-97:3). Yield: 27%. Mp: 57 – 58 ºC. $^{1}$H NMR (300 MHz, $CDCl_3$) $\delta$ (ppm): 8.30 (dt, *J* = 8.1, 1.1 Hz, 1H), 7.64 (d, *J* = 8.1 Hz, 1H), 7.53 (t, *J* = 5.7 Hz, 1H), 7.44 – 7.37 (m, 2H), 7.31 – 7.24 (m, 1H), 4.38 (d, *J* = 3.3 Hz, 1H), 4.25 – 4.13 (m, 3H), 4.03 (dd, *J* = 5.7, 2.4 Hz, 2H), 3.59 (s, 3H), 2.08 – 1.94 (m, 3H), 1.77 – 1.54 (m, 6H), 1.30 – 1.14 (m, 3H), 1.13 – 0.97 (m, 4H). $^{13}$C NMR (75 MHz, $CDCl_3$) $\delta$ (ppm): 173.5, 169.8, 164.4, 141.4, 136.3, 126.6, 122.6, 122.6, 122.5, 109.6, 74.0, 55.7, 55.6, 52.1, 40.9, 38.6, 30.9, 26.2, 25.6, 23.1, 11.1. LRMS (CI) *m/*z calcd for $C_{23}H_{33}N_4O_5$ $[M+H]^+$: 445.2; found: 445.2.

***N*-((3*S*)-1-(benzylamino)-2-hydroxy-1-oxopentan-3-yl)-1-(cyclohexylmethyl)-1*H*-indazole-3-carboxamide (183).** Purified by column chromatography (DCM/MeOH 99:1-97:3). Yield: 26%. Mp: 169 – 170 ºC. $^{1}$H NMR (300 MHz, $CDCl_3$) $\delta$ (ppm): 8.26 (d, *J* = 8.1 Hz, 1H), 7.77 (d, *J* = 8.3 Hz, 1H), 7.52 (t, *J* = 6.2 Hz, 1H), 7.46 – 7.37 (m, 2H), 7.32 – 7.21 (m, 1H), 7.08 (d, *J* = 7.5 Hz, 2H), 7.04 – 6.96 (m, 1H), 6.90 (t, *J* = 7.3 Hz, 2H), 6.43 (d, *J* = 7.1 Hz, 1H), 4.53 (dd, *J* = 15.0, 6.8 Hz, 1H), 4.39 – 4.25 (m, 2H), 4.21 – 4.14 (m, 3H), 2.06 – 1.92 (m, 3H), 1.74 – 1.51 (m, 6H), 1.28 – 1.09 (m, 3H), 1.04 (t, *J* = 7.4 Hz, 3H), 1.01 – 0.93 (m, 1H). LRMS (CI) *m/*z calcd for $C_{27}H_{35}N_4O_3$ $[M+H]^+$: 463.3; found: 463.3.

***N*-((2*S*,3*S*)-1-(benzylamino)-2-hydroxy-1-oxopentan-3-yl)-1-(cyclohexylmethyl)-1*H*-indazole-3-carboxamide ((*S*)-183).** Purified by column chromatography (DCM/MeOH 99:1-97:3). Yield: 13%. Mp: 175 – 176 ºC. $^{1}$H NMR (300 MHz, $CDCl_3$) $\delta$ (ppm): 8.27 (d, *J* = 8.1 Hz, 1H), 7.47 – 7.40 (m, 3H), 7.37 (d, *J* = 7.4 Hz, 1H), 7.31 – 7.23 (m, 1H), 7.11 (d, *J* = 7.3 Hz, 2H), 7.02 (q, *J* = 7.4 Hz, 3H), 6.13 (bs, 1H), 4.50 (dd, *J* = 14.9, 6.5 Hz, 1H), 4.42 (s, 1H), 4.34 (dd, *J* = 15.0, 5.5 Hz, 1H), 4.19 (d, *J* = 7.2 Hz, 2H), 4.16 – 4.13 (m, 1H), 2.17 – 1.82 (m, 3H), 1.77 – 1.52 (m, 6H), 1.28 – 1.11 (m, 3H), 1.06 (t, *J* = 7.3 Hz, 3H), 0.99 (d, *J* = 13.3 Hz, 1H). $^{13}$C NMR (75 MHz, $CDCl_3$) $\delta$ (ppm): 171.9, 165.4, 141.4, 137.9, 135.9, 128.4, 127.4, 127.1, 126.8, 122.8, 122.7, 122.4, 109.6, 75.8, 58.0, 55.8, 42.9, 38.7, 30.9, 26.2, 25.6, 23.3, 11.4. LRMS (CI) *m/*z calcd for $C_{27}H_{35}N_4O_3$ $[M+H]^+$: 463.3; found: 463.5.

USC UNIVERSIDADE DE SANTIAGO DE COMPOSTELA

***N*-((2*R*,3*S*)-1-(benzylamino)-2-hydroxy-1-oxopentan-3-yl)-1-(cyclohexylmethyl)-1*H*-indazole-3-carboxamide ((*R*)-183).** Purified by column chromatography (DCM/MeOH 99:1-97:3). Yield: 26%. Mp: 169 – 170 ºC. $^{1}$H NMR (300 MHz, $CDCl_3$) $\delta$ (ppm): 8.26 (d, *J* = 8.1 Hz, 1H), 7.72 (d, *J* = 8.0 Hz, 1H), 7.48 (t, *J* = 6.3 Hz, 1H), 7.45 – 7.37 (m, 2H), 7.34 – 7.22 (m, 1H), 7.07 (d, *J* = 6.9 Hz, 2H), 7.02 – 6.95 (m, 1H), 6.88 (t, *J* = 7.4 Hz, 2H), 4.53 (dd, *J* = 15.1, 6.8 Hz, 1H), 4.35 (d, *J* = 3.2 Hz, 1H), 4.28 (dd, *J* = 15.0, 5.2 Hz, 1H), 4.18 (d, *J* = 7.1 Hz, 2H), 4.15 – 4.10 (m, 1H), 2.08 – 1.92 (m, 3H), 1.76 – 1.51 (m, 6H), 1.28 – 1.11 (m, 3H), 1.05 (t, *J* = 7.4 Hz, 3H), 1.01 – 0.94 (m, 1H). $^{13}$C NMR (75 MHz, $CDCl_3$) $\delta$ (ppm): 173.0, 164.5, 141.4, 137.9, 136.2, 128.3, 127.3, 127.0, 126.6, 122.7, 122.6, 122.5, 109.6, 74.1, 55.9, 55.8, 42.9, 38.6, 30.9, 26.2, 25.6, 23.2, 11.1. LRMS (CI) *m/*z calcd for $C_{27}H_{35}N_4O_3$ $[M+H]^+$: 463.3; found: 463.3.

**1-(cyclohexylmethyl)-*N*-((3*S*)-2-hydroxy-1-((2-morpholinoethyl)amino)-1-oxopentan-3-yl)-1*H*-indazole-3-carboxamide (184).** Purified by column chromatography (DCM/MeOH 99:1-97:3). Yield: 34%. Mp: 179 – 180 ºC. $^{1}$H NMR (300 MHz, $CDCl_3$) $\delta$ (ppm): 8.26 (d, *J* = 8.3 Hz, 1H), 7.54 (d, *J* = 7.4 Hz, 1H), 7.41 (d, *J* = 3.6 Hz, 2H), 7.38 – 7.31 (m, 2H), 4.32 – 4.26 (m, 1H), 4.19 (d, *J* = 7.2 Hz, 2H), 4.13 – 4.03 (m, 2H), 3.61 – 3.43 (m, 6H), 3.38 – 3.23 (m, 2H), 2.43 – 1.91 (m, 7H), 1.83 – 1.50 (m, 7H), 1.35 – 1.12 (m, 3H), 1.05 (t, *J* = 7.4 Hz, 3H). LRMS (CI) *m/*z calcd for $C_{26}H_{40}N_5O_4$ $[M+H]^+$: 486.3; found: 486.3.

***N*-((3*S*)-1-amino-2-hydroxy-4-methyl-1-oxopentan-3-yl)-1-(cyclohexylmethyl)-1*H*-indazole-3-carboxamide (185).** Purified by column chromatography (DCM/MeOH 97:3-94:6). Yield: 41%. Mp: 135 – 137 ºC. $^{1}$H NMR (300 MHz, $CDCl_3$) $\delta$ (ppm): 8.25 (d, *J* = 8.2 Hz, 1H), 7.62 (d, *J* = 8.4 Hz, 1H), 7.45 – 7.34 (m, 2H), 7.29 – 7.19 (m, 1H), 7.15 (s, 1H), 5.89 (s, 1H), 4.45 (d, *J* = 2.9 Hz, 1H), 4.17 (d, *J* = 7.1 Hz, 2H), 3.95 – 3.84 (m, 1H), 2.56 – 2.38 (m, 1H), 2.07 – 1.89 (m, 1H), 1.77 – 1.50 (m, 6H), 1.28 – 1.11 (m, 3H), 1.11 (d, *J* = 6.5 Hz, 3H), 1.03 (d, *J* = 6.6 Hz, 3H), 1.00 – 0.92 (m, 1H). $^{13}$C NMR (75 MHz, $CDCl_3$) $\delta$ (ppm): 176.3, 164.6, 141.4, 136.0, 126.7, 122.7, 122.4, 109.6, 72.5, 60.4, 55.8, 38.6, 30.9, 28.2, 26.2, 25.6, 20.2, 19.8. LRMS (CI) *m/*z calcd for $C_{21}H_{31}N_4O_3$ $[M+H]^+$: 387.2; found: 387.2.

USC UNIVERSIDADE DE SANTIAGO DE COMPOSTELA

***N*-((3*S*)-1-(*tert*-butylamino)-2-hydroxy-4-methyl-1-oxopentan-3-yl)-1-(cyclohexylmethyl)-1*H*-indazole-3-carboxamide (186).** Purified by column chromatography (DCM/MeOH 99:1-97:3). Yield: 60%. Mp: 112 – 114 ºC. $^{1}$H NMR (300 MHz, $CDCl_3$) $\delta$ (ppm): 8.28 (d, *J* = 8.2 Hz, 1H), 7.58 (d, *J* = 8.2 Hz, 1H), 7.40 (d, *J* = 3.1 Hz, 2H), 7.26 (td, *J* = 6.2, 5.7, 2.6 Hz, 1H), 6.76 (s, 1H), 6.17 (d, *J* = 7.2 Hz, 1H), 4.34 – 4.27 (m, 1H), 4.17 (d, *J* = 7.1 Hz, 2H), 3.80 – 3.68 (m, 1H), 2.54 (dd, *J* = 11.6, 6.2 Hz, 1H), 2.06 – 1.90 (m, 1H), 1.75 – 1.46 (m, 6H), 1.40 – 1.20 (m, 3H), 1.17 (s, 9H), 1.11 (d, *J* = 6.9 Hz, 3H), 1.03 (d, *J* = 6.6 Hz, 3H), 1.00 – 0.78 (m, 1H). HRMS (ESI) *m/*z calcd for $C_{25}H_{39}N_4O_3$ $[M+H]^+$: 443.2944; found: 443.3030.

**methyl ((3*S*)-3-(1-(cyclohexylmethyl)-1*H*-indazole-3-carboxamido)-2-hydroxy-4-methylpentanoyl)glycinate (187).** Purified by column chromatography (DCM/MeOH 99:1-97:3). Yield: 50%. Mp: 254 – 255 ºC. $^{1}$H NMR (300 MHz, $CDCl_3$) $\delta$ (ppm): 8.27 (d, *J* = 8.2 Hz, 1H), 7.60 (d, *J* = 7.9 Hz, 1H), 7.57 – 7.49 (m, 1H), 7.44 – 7.35 (m, 2H), 7.30 – 7.20 (m, 1H), 6.51 (d, *J* = 7.4 Hz, 1H), 4.53 – 4.45 (m, 1H), 4.18 (d, *J* = 7.1 Hz, 2H), 4.07 – 3.89 (m, 2H), 3.81 – 3.71 (m, 1H), 3.50 (s, 3H), 2.65 – 2.49 (m, 1H), 2.06 – 1.89 (m, 1H), 1.60 (dd, *J* = 27.3, 14.7 Hz, 6H), 1.28 – 1.14 (m, 3H), 1.12 (d, *J* = 6.6 Hz, 3H), 1.04 (d, *J* = 6.6 Hz, 3H), 1.01 – 0.93 (m, 1H). LRMS (CI) *m/*z calcd for $C_{24}H_{35}N_4O_5$ $[M+H]^+$: 459.3; found: 459.3.

***N*-((3*S*)-1-(benzylamino)-2-hydroxy-4-methyl-1-oxopentan-3-yl)-1-(cyclohexylmethyl)-1*H*-indazole-3-carboxamide (188).** Purified by column chromatography (DCM/MeOH 99:1-97:3). Yield: 43%. Mp: 68 – 70 ºC. $^{1}$H NMR (300 MHz, $CDCl_3$) $\delta$ (ppm): 8.25 (d, *J* = 8.5 Hz, 1H), 7.67 (d, *J* = 7.7 Hz, 1H), 7.48 – 7.39 (m, 2H), 7.37 – 7.24 (m, 1H), 7.02 (d, *J* = 7.6 Hz, 2H), 6.92 (t, *J* = 7.3 Hz, 1H), 6.79 (t, *J* = 7.4 Hz, 2H), 6.72 (d, *J* = 8.2 Hz, 1H), 4.60 – 4.46 (m, 2H), 4.25 (d, *J* = 4.9 Hz, 1H), 4.19 (d, *J* = 7.1 Hz, 2H), 3.78 – 3.69 (m, 1H), 2.69 – 2.55 (m, 1H), 2.06 – 1.91 (m, 1H), 1.81 – 1.52 (m, 6H), 1.19 (d, *J* = 10.7 Hz, 3H), 1.16 – 1.10 (m, 3H), 1.05 (d, *J* = 6.6 Hz, 3H), 1.02 – 0.94 (m, 1H). $^{13}$C NMR (75 MHz, $CDCl_3$) $\delta$ (ppm): 173.4, 164.8, 141.5, 137.9, 136.0, 128.2, 127.2, 126.9, 126.7, 122.7, 122.7, 122.6, 109.6, 73.1, 61.4, 61.4, 55.8, 43.0, 38.7, 30.9, 30.9, 27.7, 26.2, 25.6, 25.6, 20.4, 19.8. LRMS (CI) *m/*z calcd for $C_{28}H_{37}N_4O_3$ $[M+H]^+$: 477.3; found: 477.3.

USC UNIVERSIDADE DE SANTIAGO DE COMPOSTELA

***N*-((2*S*,3*S*)-1-(benzylamino)-2-hydroxy-4-methyl-1-oxopentan-3-yl)-1-(cyclohexylmethyl)-1*H*-indazole-3-carboxamide ((*S*)-188).** Purified by column chromatography (DCM/MeOH 99:1-97:3). Yield: 14%. Mp: 148 – 149 ºC. $^{1}$H NMR (300 MHz, $CDCl_3$) $\delta$ (ppm): 8.28 (d, $J$ = 8.2 Hz, 1H), 7.46 – 7.42 (m, 3H), 7.38 (d, $J$ = 7.1 Hz, 1H), 7.32 – 7.25 (m, 1H), 7.11 – 7.01 (m, 3H), 6.95 (t, $J$ = 7.4 Hz, 2H), 6.02 (s, 1H), 4.56 (s, 1H), 4.47 (dd, $J$ = 15.0, 6.6 Hz, 1H), 4.31 (dd, $J$ = 14.9, 5.5 Hz, 1H), 4.23 – 4.18 (m, 2H), 4.00 – 3.91 (m, 1H), 2.59 – 2.42 (m, 1H), 2.07 – 1.91 (m, 1H), 1.76 – 1.53 (m, 6H), 1.23 (d, $J$ = 15.9 Hz, 3H), 1.17 (d, $J$ = 6.5 Hz, 3H), 1.09 (d, $J$ = 6.6 Hz, 3H), 1.01 (s, 1H). $^{13}$C NMR (75 MHz, $CDCl_3$) $\delta$ (ppm): 172.1, 165.6, 141.5, 137.9, 135.8, 128.3, 127.3, 127.1, 126.8, 122.8, 122.7, 122.5, 109.7, 74.6, 62.5, 55.8, 42.8, 38.7, 30.9, 29.2, 26.2, 25.6, 20.7, 20.6. LRMS (CI) *m/*z calcd for $C_{28}H_{37}N_4O_3$ $[M+H]^+$: 477.3; found: 477.4.

***N*-((2*R*,3*S*)-1-(benzylamino)-2-hydroxy-4-methyl-1-oxopentan-3-yl)-1-(cyclohexylmethyl)-1*H*-indazole-3-carboxamide ((*R*)-188).** Purified by column chromatography (DCM/MeOH 99:1-97:3). Yield: 43%. Mp: 68 – 70 ºC. $^{1}$H NMR (300 MHz, $CDCl_3$) $\delta$ (ppm): 8.25 (d, $J$ = 8.2 Hz, 1H), 7.70 (d, $J$ = 7.8 Hz, 1H), 7.51 – 7.41 (m, 3H), 7.33 – 7.22 (m, 1H), 7.02 (d, $J$ = 7.6 Hz, 2H), 6.92 (t, $J$ = 7.4 Hz, 1H), 6.79 (t, $J$ = 7.5 Hz, 2H), 6.68 (d, $J$ = 8.0 Hz, 1H), 4.60 – 4.45 (m, 2H), 4.26 – 4.16 (m, 3H), 3.82 – 3.71 (m, 1H), 2.67 – 2.52 (m, 1H), 2.02 – 1.90 (m, 1H), 1.76 – 1.50 (m, 6H), 1.30 – 1.14 (m, 3H), 1.12 (d, $J$ = 6.8 Hz, 3H), 1.05 (d, $J$ = 6.7 Hz, 3H), 1.01 – 0.93 (m, 1H). $^{13}$C NMR (75 MHz, $CDCl_3$) $\delta$ (ppm): 173.4, 164.8, 141.5, 137.9, 136.0, 128.2, 127.2, 126.9, 126.7, 122.7, 122.7, 122.6, 109.6, 73.1, 61.4, 55.8, 43.0, 38.7, 30.9, 30.9, 27.7, 26.2, 25.6, 20.4, 19.8. LRMS (CI) *m/*z calcd for $C_{28}H_{37}N_4O_3$ $[M+H]^+$: 477.3; found: 477.3.

USC UNIVERSIDADE DE SANTIAGO DE COMPOSTELA

**1-(cyclohexylmethyl)-*N*-((3*S*)-2-hydroxy-4-methyl-1-((2-morpholinoethyl)amino)-1-oxopentan-3-yl)-1*H*-indazole-3-carboxamide (189).** Purified by column chromatography (DCM/MeOH 99:1-97:3). Yield: 42%. Mp: 273 – 275 ºC. $^{1}$H NMR (300 MHz, $CDCl_3$) $\delta$ (ppm): 8.24 (d, *J* = 8.2 Hz, 1H), 7.57 (d, *J* = 7.8 Hz, 1H), 7.45 – 7.36 (m, 2H), 7.32 – 7.20 (m, 1H), 6.42 (s, 1H), 4.49 – 4.37 (m, 1H), 4.18 (d, *J* = 7.1 Hz, 2H), 3.78 – 3.65 (m, 1H), 3.60 – 3.42 (m, 4H), 3.39 – 3.20 (m, 2H), 2.68 – 2.51 (m, 1H), 2.40 – 2.08 (m, 6H), 2.07 – 1.90 (m, 1H), 1.77 – 1.50 (m, 6H), 1.29 – 1.16 (m, 3H), 1.13 (d, *J* = 6.6 Hz, 3H), 1.04 (d, *J* = 6.6 Hz, 3H), 0.97 (d, *J* = 9.4 Hz, 1H). $^{13}$C NMR (75 MHz, $CDCl_3$) $\delta$ (ppm): 173.4, 164.8, 141.4, 135.9, 126.8, 122.8, 122.6, 122.4, 109.7, 73.2, 66.7, 61.7, 57.2, 55.8, 53.2, 38.7, 35.6, 30.9, 27.5, 26.2, 25.6, 20.4, 19.8. LRMS (CI) *m/*z calcd for $C_{27}H_{42}N_5O_4$ $[M+H]^+$: 500.3; found: 500.3.

***N*-((3*S*)-1-amino-2-hydroxy-4,4-dimethyl-1-oxopentan-3-yl)-1-(cyclohexylmethyl)-1*H*-indazole-3-carboxamide (190).** Purified by column chromatography (DCM/MeOH 97:3-94:6). Yield: 44%. Mp: 214 – 215 ºC. $^{1}$H NMR (300 MHz, $CDCl_3$) $\delta$ (ppm): 8.28 – 8.22 (m, 1H), 7.61 (d, *J* = 9.8 Hz, 1H), 7.44 – 7.32 (m, 2H), 7.25 – 7.17 (m, 1H), 7.07 (bs, 1H), 6.04 (bs, 1H), 4.88 (s, 1H), 4.55 (s, 1H), 4.31 (dd, *J* = 16.2, 9.9 Hz, 1H), 4.19 (d, *J* = 7.2 Hz, 2H), 2.08 – 1.91 (m, 1H), 1.64 (dt, *J* = 29.2, 7.7 Hz, 6H), 1.19 (t, *J* = 10.4 Hz, 3H), 1.10 (s, 9H), 1.08 – 0.94 (m, 1H). $^{13}$C NMR (75 MHz, $CDCl_3$) $\delta$ (ppm): 176.0, 163.3, 141.4, 136.4, 126.5, 122.7, 122.5, 122.5, 109.5, 70.7, 58.6, 55.7, 38.7, 36.1, 30.9, 27.5, 26.2, 25.6. LRMS (CI) *m/*z calcd for $C_{22}H_{33}N_4O_3$ $[M+H]^+$: 401.3; found: 401.3.

***N*-((3*S*)-1-(*tert*-butylamino)-2-hydroxy-4,4-dimethyl-1-oxopentan-3-yl)-1-(cyclohexylmethyl)-1*H*-indazole-3-carboxamide (191).** Purified by column chromatography (DCM/MeOH 99:1-97:3). Yield: 65%. Mp: 192 – 193 ºC. $^{1}$H NMR (300 MHz, $CDCl_3$) $\delta$ (ppm): 8.30 (d, *J* = 8.1 Hz, 1H), 7.52 (d, *J* = 9.8 Hz, 1H), 7.43 – 7.35 (m, 2H), 7.29 – 7.20 (m, 1H), 6.37 (s, 1H), 5.03 – 4.95 (m, 1H), 4.44 – 4.38 (m, 1H), 4.20 (d, *J* = 7.2 Hz, 3H), 2.06 – 1.92 (m, 1H), 1.76 – 1.52 (m, 6H), 1.43 – 1.24 (m, 3H), 1.22 – 1.19 (m, 9H), 1.15 (s, 9H), 1.10 – 0.93 (m, 1H). LRMS (CI) *m/*z calcd for $C_{26}H_{41}N_4O_3$ $[M+H]^+$: 457.3; found: 457.3.

USC UNIVERSIDADE DE SANTIAGO DE COMPOSTELA

***N*-((2*S*,3*S*)-1-(*tert*-butylamino)-2-hydroxy-4,4-dimethyl-1-oxopentan-3-yl)-1-(cyclohexylmethyl)-1*H*-indazole-3-carboxamide ((*S*)-191).** Purified by column chromatography (DCM/MeOH 99:1-97:3). Yield: 4%. Oil at room temperature. $^{1}$H NMR (300 MHz, $CDCl_3$) $\delta$ (ppm): 8.31 (d, $J$ = 8.2 Hz, 1H), 7.55 (d, $J$ = 8.7 Hz, 1H), 7.47 – 7.35 (m, 2H), 7.30 – 7.27 (m, 1H), 6.77 (bs, 1H), 5.00 (s, 1H), 4.38 (s, 1H), 4.20 (d, $J$ = 7.2 Hz, 2H), 4.15 – 4.08 (m, 1H), 2.08 – 1.92 (m, 1H), 1.78 – 1.47 (m, 6H), 1.41 – 1.24 (m, 3H), 1.21 (s, 9H), 1.16 (s, 9H), 1.08 – 0.98 (m, 1H). $^{13}$C NMR (75 MHz, $CDCl_3$) $\delta$ (ppm): 171.2, 164.5, 141.4, 136.3, 126.6, 122.7, 122.6, 122.5, 109.6, 74.9, 63.7, 55.7, 50.8, 38.7, 35.0, 30.9, 28.5, 27.7, 26.2, 25.6. LRMS (CI) *m/*z calcd for $C_{26}H_{41}N_4O_3$ $[M+H]^+$: 457.3; found: 457.

***N*-((2*R*,3*S*)-1-(*tert*-butylamino)-2-hydroxy-4,4-dimethyl-1-oxopentan-3-yl)-1-(cyclohexylmethyl)-1*H*-indazole-3-carboxamide ((*R*)-191).** Purified by column chromatography (DCM/MeOH 99:1-97:3). Yield: 65%. Oil at room temperature. $^{1}$H NMR (300 MHz, $CDCl_3$) $\delta$ (ppm): 8.30 (d, $J$ = 8.1 Hz, 1H), 7.51 (d, $J$ = 9.8 Hz, 1H), 7.45 – 7.33 (m, 2H), 7.30 – 7.21 (m, 1H), 6.33 (bs, 1H), 4.41 (s, 1H), 4.20 (d, $J$ = 7.2 Hz, 2H), 4.15 (d, $J$ = 10.1 Hz, 1H), 2.08 – 1.92 (m, 1H), 1.78 – 1.51 (m, 6H), 1.43 – 1.28 (m, 1H), 1.21 (s, 9H), 1.15 (s, 9H), 1.05 (t, $J$ = 12.6 Hz, 2H), 0.91 – 0.79 (m, 1H). $^{13}$C NMR (75 MHz, $CDCl_3$) $\delta$ (ppm): 172.2, 163.3, 141.4, 136.5, 126.5, 122.7, 122.6, 122.4, 109.5, 71.6, 58.9, 55.6, 51.4, 38.7, 36.0, 30.9, 28.4, 27.7, 26.2, 25.6. LRMS (CI) *m/*z calcd for $C_{26}H_{41}N_4O_3$ $[M+H]^+$: 457.3; found: 457.3.

**methyl ((3*S*)-3-(1-(cyclohexylmethyl)-1*H*-indazole-3-carboxamido)-2-hydroxy-4,4-dimethylpentanoyl)glycinate (192).** Purified by column chromatography (DCM/MeOH 99:1-97:3). Yield: 57%. Mp: 181 – 182 ºC. $^{1}$H NMR (300 MHz, $CDCl_3$) $\delta$ (ppm): 8.29 (d, $J$ = 8.2 Hz, 1H), 7.58 (d, $J$ = 9.5 Hz, 1H), 7.47 – 7.34 (m, 2H), 7.33 – 7.19 (m, 2H), 5.18 (bs, 1H), 4.61 (s, 1H), 4.32 – 4.24 (m, 1H), 4.20 (d, $J$ = 7.3 Hz, 2H), 3.98 (d, $J$ = 5.5 Hz, 2H), 3.55 (s, 3H), 2.07 – 1.93 (m, 1H), 1.78 – 1.53 (m, 6H), 1.37 – 1.17 (m, 3H), 1.15 (s, 9H), 1.11 – 0.95 (m, 1H). LRMS (CI) *m/*z calcd for $C_{25}H_{37}N_4O_5$ $[M+H]^+$: 473.3; found: 473.3.

USC UNIVERSIDADE DE SANTIAGO DE COMPOSTELA

***N*-((3*S*)-1-(benzylamino)-2-hydroxy-4,4-dimethyl-1-oxopentan-3-yl)-1-(cyclohexylmethyl)-1*H*-indazole-3-carboxamide (193).** Purified by column chromatography (DCM/MeOH 99:1-97:3). Yield: 63%. Mp: 92 – 94 ºC. $^{1}$H NMR (300 MHz, $CDCl_3$) $\delta$ (ppm): 8.29 (d, *J* = 8.3 Hz, 1H), 7.64 (d, *J* = 9.1 Hz, 1H), 7.46 – 7.37 (m, 2H), 7.31 – 7.16 (m, 2H), 7.11 (d, *J* = 7.3 Hz, 2H), 7.02 – 6.86 (m, 3H), 5.61 (d, *J* = 6.3 Hz, 1H), 4.61 – 4.56 (m, 1H), 4.50 (dd, *J* = 15.0, 6.6 Hz, 1H), 4.29 – 4.15 (m, 4H), 2.07 – 1.88 (m, 1H), 1.78 – 1.51 (m, 6H), 1.19 (s, 3H), 1.18 – 1.14 (m, 9H), 1.10 – 0.93 (m, 1H). $^{13}$C NMR (75 MHz, $CDCl_3$) $\delta$ (ppm): 173.3, 163.7, 141.5, 137.8, 136.3, 128.3, 127.5, 127.1, 126.6, 122.7, 122.5, 109.5, 71.8, 60.0, 55.7, 43.6, 38.7, 36.4, 30.9, 27.7, 26.2, 25.6. LRMS (CI) *m/*z calcd for $C_{29}H_{39}N_4O_3$ $[M+H]^+$: 491.3; found: 491.3.

***N*-((2*S*,3*S*)-1-(benzylamino)-2-hydroxy-4,4-dimethyl-1-oxopentan-3-yl)-1-(cyclohexylmethyl)-1*H*-indazole-3-carboxamide ((*S*)-193).** Purified by column chromatography (DCM/MeOH 99:1-97:3). Yield: 8%. Mp: 66 – 68 ºC. $^{1}$H NMR (300 MHz, $CDCl_3$) $\delta$ (ppm): 8.28 (d, *J* = 8.2 Hz, 1H), 7.59 (d, *J* = 8.3 Hz, 1H), 7.42 (d, *J* = 3.9 Hz, 2H), 7.38 – 7.27 (m, 1H), 7.10 – 6.94 (m, 6H), 4.56 (s, 1H), 4.45 (dd, *J* = 14.9, 6.5 Hz, 1H), 4.28 (dd, *J* = 14.9, 5.4 Hz, 1H), 4.20 (d, *J* = 7.2 Hz, 2H), 4.16 (d, *J* = 10.1 Hz, 1H), 2.02 – 1.91 (m, 1H), 1.75 – 1.51 (m, 6H), 1.29 – 1.19 (m, 3H), 1.17 (s, 9H), 1.06 – 0.98 (m, 1H). $^{13}$C NMR (75 MHz, $CDCl_3$) $\delta$ (ppm): 172.1, 164.7, 141.5, 137.9, 136.2, 128.3, 127.5, 127.1, 126.7, 122.7, 122.5, 109.6, 74.8, 64.0, 55.7, 43.1, 38.7, 35.0, 30.9, 27.7, 26.2, 25.6. LRMS (CI) *m/*z calcd for $C_{29}H_{39}N_4O_3$ $[M+H]^+$: 491.3; found: 491.3.

***N*-((2*R*,3*S*)-1-(benzylamino)-2-hydroxy-4,4-dimethyl-1-oxopentan-3-yl)-1-(cyclohexylmethyl)-1*H*-indazole-3-carboxamide ((*R*)-193).** Purified by column chromatography (DCM/MeOH 99:1-97:3). Yield: 63%. Mp: 92 – 94 ºC. $^{1}$H NMR (300 MHz, $CDCl_3$) $\delta$ (ppm): 8.28 (d, *J* = 8.2 Hz, 1H), 7.62 (d, *J* = 9.2 Hz, 1H), 7.46 – 7.38 (m, 2H), 7.31 – 7.23 (m, 1H), 7.21 – 7.14 (m, 1H), 7.11 (d, *J* = 7.3 Hz, 2H), 7.02 – 6.87 (m, 3H), 4.58 (s, 1H), 4.50 (dd, *J* = 14.7, 6.4 Hz, 1H), 4.31 – 4.19 (m, 1H), 4.21 – 4.13 (m, 3H), 2.06 – 1.91 (m, 1H), 1.76 – 1.53 (m, 6H), 1.18 (s, 3H), 1.15 (s, 9H), 1.07 – 0.93 (m, 1H). $^{13}$C NMR (75 MHz, $CDCl_3$) $\delta$ (ppm): 173.3, 163.7, 141.5, 137.8, 136.3, 128.3, 127.5, 127.1, 126.6, 122.7, 122.5, 109.5, 71.8, 60.0, 55.7, 43.6, 38.7, 36.4, 30.9, 27.7, 26.2, 25.6. LRMS (CI) *m/*z calcd for $C_{29}H_{39}N_4O_3$ $[M+H]^+$: 491.3; found: 491.3.

USC UNIVERSIDADE DE SANTIAGO DE COMPOSTELA

**1-(cyclohexylmethyl)-*N*-((3*S*)-2-hydroxy-4,4-dimethyl-1-((2-morpholinoethyl)amino)-1-oxopentan-3-yl)-1*H*-indazole-3-carboxamide (194).** Purified by column chromatography (DCM/MeOH 99:1-97:3). Yield: 60%. Mp: 222 – 223 ºC. $^{1}$H NMR (300 MHz, $CDCl_3$) $\delta$ (ppm): 8.25 (d, *J* = 8.2 Hz, 1H), 7.54 (d, *J* = 9.5 Hz, 1H), 7.44 – 7.35 (m, 2H), 7.24 – 7.19 (m, 1H), 7.04 – 6.95 (m, 1H), 5.25 – 4.97 (m, 1H), 4.55 – 4.48 (m, 1H), 4.20 (d, *J* = 7.1 Hz, 2H), 4.17 – 4.12 (m, 1H), 3.60 (t, *J* = 4.7 Hz, 4H), 3.30 (q, *J* = 6.0 Hz, 2H), 2.53 – 2.23 (m, 6H), 2.08 – 1.94 (m, 1H), 1.78 – 1.55 (m, 6H), 1.41 – 1.19 (m, 3H), 1.15 (s, 9H), 1.12 – 0.93 (m, 1H). $^{13}$C NMR (75 MHz, $CDCl_3$) $\delta$ (ppm): 173.1, 163.3, 141.4, 136.4, 126.6, 122.7, 122.5, 122.5, 109.6, 71.3, 66.9, 59.7, 56.9, 55.7, 53.2, 38.7, 36.2, 36.1, 30.9, 27.7, 26.2, 25.6. LRMS (CI) *m/*z calcd for $C_{28}H_{44}N_5O_4$ $[M+H]^+$: 514.3; found: 514.3.

***N*-((3*R*)-1-amino-2-hydroxy-4,4-dimethyl-1-oxopentan-3-yl)-1-(4-fluorobenzyl)-1*H*-indole-3-carboxamide (195).** Purified by column chromatography (DCM/MeOH 97:3-94:6). Yield: 50%. Mp: 240 – 242 ºC. $^{1}$H NMR (300 MHz, $CDCl_3$) $\delta$ (ppm): 8.26 – 8.15 (m, 0.5H), 8.00 – 7.86 (m, 1H), 7.72 (s, 0.5H), 7.37 – 7.21 (m, 4H), 7.19 – 7.09 (m, 2H), 7.08 – 6.96 (m, 2H), 6.60 (d, *J* = 10.2 Hz, 1H), 5.84 (s, 1H), 5.54 (bs, 1H), 5.32 (d, *J* = 14.2 Hz, 2H), 4.53 (s, 0.5H), 4.31 (d, *J* = 9.7 Hz, 0.5H), 3.49 (d, *J* = 6.4 Hz, 1H), 1.17 (s, 7H), 1.01 (s, 2H). $^{13}$C NMR (75 MHz, $CDCl_3$) $\delta$ (ppm): 177.30, 165.39, 162.39 (d, *J* = 246.7 Hz), 136.73, 132.31, 132.08, 128.71 (d, *J* = 8.3 Hz), 125.37, 122.73, 121.78, 119.75, 115.67 (d, *J* = 21.7 Hz), 110.72, 69.79, 58.07, 49.79, 35.55, 27.10. HRMS (ESI) *m/*z calcd for $C_{23}H_{27}FN_3O_3$ $[M+H]^+$: 412.1958; found: 412.2031.

***N*-((3*R*)-1-amino-2-hydroxy-4,4-dimethyl-1-oxopentan-3-yl)-1-(4-fluorobenzyl)-1*H*-indazole-3-carboxamide (196).** Purified by column chromatography (DCM/MeOH 97:3-94:6). Yield: 40%. Mp: 169 – 171 ºC. $^{1}$H NMR (300 MHz, $CDCl_3$) $\delta$ (ppm): 8.28 (d, *J* = 8.1 Hz, 1H), 7.61 (d, *J* = 9.9 Hz, 1H), 7.39 – 7.27 (m, 2H), 7.24 – 7.14 (m, 2H), 6.99 (t, *J* = 8.5 Hz, 2H), 6.87 (s, 1H), 5.85 (s, 1H), 5.56 (s, 2H), 4.75 (s, 1H), 4.55 (s, 1H), 4.32 (d, *J* = 10.0 Hz, 1H), 1.13 (s, 9H). $^{13}$C NMR (75 MHz, $CDCl_3$) $\delta$ (ppm): 180.54, 163.25, 162.49 (d, *J* = 247.0 Hz), 140.86 (d, *J* = 4.0 Hz), 136.87 (d, *J* = 3.5 Hz), 131.52, 129.05 (d, *J* = 8.1 Hz), 127.10, 123.08 (d, *J* = 10.1 Hz), 122.55, 115.80 (d, *J* = 21.8 Hz), 109.63, 73.71, 58.30, 53.04, 35.64, 27.25. LRMS (CI) *m/*z calcd for $C_{22}H_{26}FN_4O_3$ $[M+H]^+$: 413.2; found: 413.2.

USC UNIVERSIDADE DE SANTIAGO DE COMPOSTELA

***N*-((3*R*)-1-amino-2-hydroxy-4,4-dimethyl-1-oxopentan-3-yl)-1-(cyclohexylmethyl)-1*H*-indole-3-carboxamide (197).** Purified by column chromatography (DCM/MeOH 97:3-94:6). Yield: 50%. Mp: 270 – 271 ºC. $^1$H NMR (300 MHz, $CDCl_3$) $\delta$ (ppm): 7.92 – 7.85 (m, 1H), 7.66 (s, 1H), 7.43 – 7.35 (m, 2H), 7.29 (d, *J* = 6.4 Hz, 2H), 6.78 – 6.67 (m, 1H), 6.58 (d, *J* = 9.5 Hz, 1H), 4.53 (s, 1H), 4.30 (d, *J* = 9.6 Hz, 1H), 3.94 (d, *J* = 7.2 Hz, 2H), 3.64 (s, 1H), 1.92 – 1.79 (m, 1H), 1.65 (s, 6H), 1.25 (s, 2H), 1.15 (s, 9H), 1.08 – 0.85 (m, 2H). HRMS (ESI) *m/*z calcd for $C_{23}H_{34}N_3O_3$ $[M+H]^+$: 400.2522; found: 400.2595.

***N*-((3*R*)-1-amino-2-hydroxy-4,4-dimethyl-1-oxopentan-3-yl)-1-(cyclohexylmethyl)-1*H*-indazole-3-carboxamide (198).** Purified by column chromatography (DCM/MeOH 97:3-94:6). Yield: 53%. Mp: 214 – 215 ºC. $^1$H NMR (300 MHz, $CDCl_3$) $\delta$ (ppm): 8.28 – 8.22 (m, 1H), 7.61 (d, *J* = 9.8 Hz, 1H), 7.44 – 7.32 (m, 2H), 7.25 – 7.17 (m, 1H), 7.07 (bs, 1H), 6.04 (bs, 1H), 4.88 (s, 1H), 4.55 (s, 1H), 4.31 (dd, *J* = 16.2, 9.9 Hz, 1H), 4.19 (d, *J* = 7.2 Hz, 2H), 2.08 – 1.91 (m, 1H), 1.64 (dt, *J* = 29.2, 7.7 Hz, 6H), 1.19 (t, *J* = 10.4 Hz, 3H), 1.10 (s, 9H), 1.08 – 0.94 (m, 1H). $^{13}$C NMR (75 MHz, $CDCl_3$) $\delta$ (ppm): 176.0, 163.3, 141.4, 136.4, 126.5, 122.7, 122.5, 122.5, 109.5, 70.7, 58.6, 55.7, 38.7, 36.1, 30.9, 27.5, 26.2, 25.6. LRMS (CI) *m/*z calcd for $C_{22}H_{33}N_4O_3$ $[M+H]^+$: 401.3; found: 401.3.

***N*-((3*R*)-1-(*tert*-butylamino)-2-hydroxy-4,4-dimethyl-1-oxopentan-3-yl)-1-(4-fluorobenzyl)-1*H*-indole-3-carboxamide (199).** Purified by column chromatography (DCM/MeOH 99:1-97:3). Yield: 65%. Mp: 189 – 190 ºC. $^1$H NMR (300 MHz, $CDCl_3$) $\delta$ (ppm): 8.27 (s, 1H), 8.03 – 7.97 (m, 1H), 7.54 – 7.47 (m, 1H), 7.34 – 7.26 (m, 2H), 7.18 – 7.08 (m, 4H), 6.98 (s, 1H), 6.88 (d, *J* = 9.8 Hz, 1H), 5.75 (d, *J* = 6.0 Hz, 1H), 5.44 (s, 2H), 4.20 – 4.10 (m, 2H), 1.03 (s, 9H), 0.99 (s, 9H). HRMS (ESI) *m/*z calcd for $C_{27}H_{35}FN_3O_3$ $[M+H]^+$: 468.2584; found: 468.2657.

USC UNIVERSIDADE DE SANTIAGO DE COMPOSTELA

***N*-((3*R*)-1-(*tert*-butylamino)-2-hydroxy-4,4-dimethyl-1-oxopentan-3-yl)-1-(4-fluorobenzyl)-1*H*-indazole-3-carboxamide (200).** Purified by column chromatography (DCM/MeOH 99:1-97:3). Yield: 63%. Mp: 213 – 214 ºC. $^{1}$H NMR (300 MHz, $CDCl_3$) $\delta$ (ppm): 8.32 (d, *J* = 8.0 Hz, 1H), 7.54 – 7.48 (m, 1H), 7.40 – 7.28 (m, 3H), 7.25 – 7.14 (m, 2H), 7.05 – 6.95 (m, 2H), 6.21 (s, 1H), 5.57 (s, 2H), 4.78 (d, *J* = 4.5 Hz, 1H), 4.43 – 4.37 (m, 1H), 4.16 (d, *J* = 9.8 Hz, 1H), 1.22 (s, 9H), 1.15 (s, 9H). $^{13}$C NMR (75 MHz, $CDCl_3$) $\delta$ (ppm): 171.95, 163.08, 162.49 (d, *J* = 247.0 Hz), 140.81, 137.21, 131.67 (d, *J* = 3.2 Hz), 128.97 (d, *J* = 8.3 Hz), 127.01, 123.29, 122.81 (d, *J* = 3.2 Hz), 115.78 (d, *J* = 21.7 Hz), 109.52, 71.45, 58.82, 52.94, 51.65, 35.98, 28.40, 27.64. LRMS (CI) *m/*z calcd for $C_{26}H_{34}FN_4O_3$ $[M+H]^+$: 469.3; found: 469.3.

***N*-((3*R*)-1-(*tert*-butylamino)-2-hydroxy-4,4-dimethyl-1-oxopentan-3-yl)-1-(cyclohexylmethyl)-1*H*-indole-3-carboxamide (201).** Purified by column chromatography (DCM/MeOH 99:1-97:3). Yield: 51%. Mp: 242 – 243 ºC. $^{1}$H NMR (300 MHz, $CDCl_3$) $\delta$ (ppm): 7.96 – 7.88 (m, 1H), 7.61 (s, 1H), 7.41 – 7.34 (m, 1H), 7.30 – 7.27 (m, 2H), 6.45 (d, *J* = 9.6 Hz, 1H), 6.32 (s, 1H), 4.88 (d, *J* = 3.9 Hz, 1H), 4.38 (s, 1H), 4.26 – 4.14 (m, 1H), 3.95 (d, *J* = 7.2 Hz, 2H), 1.95 – 1.79 (m, 1H), 1.78 – 1.54 (m, 9H), 1.26 (s, 9H), 1.15 (s, 9H), 1.08 – 0.78 (m, 1H). LRMS (CI) *m/*z calcd for $C_{27}H_{42}N_3O_3$ $[M+H]^+$: 456.2; found: 456.3.

***N*-((3*R*)-1-(*tert*-butylamino)-2-hydroxy-4,4-dimethyl-1-oxopentan-3-yl)-1-(cyclohexylmethyl)-1*H*-indazole-3-carboxamide (202).** Purified by column chromatography (DCM/MeOH 99:1-97:3). Yield: 61%. Mp: 192 – 193 ºC. $^{1}$H NMR (300 MHz, $CDCl_3$) $\delta$ (ppm): 8.30 (d, *J* = 8.1 Hz, 1H), 7.52 (d, *J* = 9.8 Hz, 1H), 7.43 – 7.35 (m, 2H), 7.29 – 7.20 (m, 1H), 6.37 (s, 1H), 5.03 – 4.95 (m, 1H), 4.44 – 4.38 (m, 1H), 4.20 (d, *J* = 7.2 Hz, 3H), 2.06 – 1.92 (m, 1H), 1.76 – 1.52 (m, 6H), 1.43 – 1.24 (m, 3H), 1.22 – 1.19 (m, 9H), 1.15 (s, 9H), 1.10 – 0.93 (m, 1H). LRMS (CI) *m/*z calcd for $C_{26}H_{41}N_4O_3$ $[M+H]^+$: 457.3; found: 457.3.

USC UNIVERSIDADE DE SANTIAGO DE COMPOSTELA

### 5.3.3 X-ray crystallography of (2*S*)-188

The crystal was grown by slow evaporation from an isopropanol solution. For the crystal structure determination, the data were collected by applying the omega and phi scans method on a Bruker D8 VENTURE PHOTON III-14 diffractometer using Incoatec multilayer mirror monochromated with Cu-Kα radiation (λ = 1.54178 Å) from a microfocus sealed tube source at 100 K with detector resolution of 7.3910 pixels $mm^{-1}$. Computing data were made with the APEX3 v2022.1-1 (BRUKER AXS, 2021), and computing data reduction were made with the SAINT V8.40B (Bruker AXS LLC, 2019). The structure was solved using SHELXT2018/2 and finally refined by full-matrix least-squares based on $F^2$ by SHELXL2019/1. An empirical absorption correction was applied using the SADABS2016/2 program. Software used to molecular graphics: ORTEP for Windows. Software used to prepare material for publication: WinGX publication routines.

Detailed crystallographic data for ligand **(2*S*)-188** has been deposited at the Cambridge Crystallographic Data Centre (deposition number CCDC: 2311279) and are available on request. Hydrogen atoms were treated by a mixture of independent and constrained refinement, and the absolute structure was refined as an inversion twin. Details of the experiment are shown in Table 5.11.

USC UNIVERSIDADE DE SANTIAGO DE COMPOSTELA

Table 5.11. Experimental and computational details of the **(2*S*)-188** X-ray experiment.

| **Crystal data** | **(2*S*)-188** |
|---|---|
| **CCDC** | 2311279 |
| Chemical formula | $C_{28}H_{36}N_4O_3$ |
| $M_r$ | 476.61 |
| Crystal system | Trigonal |
| Space group | $P3_2$ |
| Temperature (K) | 100 |
| *a* (Å) | 13.4763 (9) |
| *c* (Å) | 12.5676 (15) |
| *V* (Å$^3$) | 1976.6 (3) |
| *Z* | 3 |
| *F(000)* | 768 |
| $D_x$ (Mg m$^{-3}$) | 1.201 |
| Radiation type | Cu-Kα |
| $\mu$ (mm$^{-1}$) | 0.63 |
| Crystal size (mm) | 0.13 × 0.02 × 0.02 |
| Tmin, Tmax | 0.729, 0.971 |
| Measured/Independent/ observed [I>2σ(I)] reflection | 10386/2079/1578 |
| $R_{int}$ | 0.121 |
| $\theta_{max}$ (°) | 44.5 |
| $(\sin\theta/\lambda)_{max}$ (Å$^{-1}$) | 0.455 |
| $R[F^2>2\sigma(F^2)]$, $wR(F^2)$, *S* | 0.067, 0.168, 1.08 |
| $\Delta\rho_{max}/\Delta\rho_{min}$ (eÅ$^{-3}$) | 0.29, −0.21 |
| Absolute structure (Flack) | 0.7(12) |

USC UNIVERSIDADE DE SANTIAGO DE COMPOSTELA

# 6 REFERENCES


(1) Sriram, K.; Insel, P. A. G Protein-Coupled Receptors as Targets for Approved Drugs: How Many Targets and How Many Drugs? *Mol Pharmacol* **2018**, *93*, 251–258.

(2) Laeremans, T.; Sands, Z. A.; Claes, P.; De Blieck, A.; De Cesco, S.; Triest, S.; Busch, A.; Felix, D.; Kumar, A.; Jaakola, V.-P.; Menet, C. Accelerating GPCR Drug Discovery With Conformation-Stabilizing VHHs. *Front. Mol. Biosci.* **2022**, *9*, 863099.

(3) Kaczor, A. A.; Wróbel, T. M.; Bartuzi, D. Allosteric Modulators of Dopamine D2 Receptors for Fine-Tuning of Dopaminergic Neurotransmission in CNS Diseases: Overview, Pharmacology, Structural Aspects and Synthesis. *Molecules* **2022**, *28*, 178.

(4) Hilger, D.; Masureel, M.; Kobilka, B. K. Structure and Dynamics of GPCR Signaling Complexes. *Nat Struct Mol Biol* **2018**, *25*, 4–12.

(5) Lagerström, M. C.; Schiöth, H. B. Structural Diversity of G Protein-Coupled Receptors and Significance for Drug Discovery. *Nat Rev Drug Discov* **2008**, *7*, 339–357.

(6) Katritch, V.; Cherezov, V.; Stevens, R. C. Structure-Function of the G Protein–Coupled Receptor Superfamily. *Annu. Rev. Pharmacol. Toxicol.* **2013**, *53*, 531–556.

(7) Hargrave, P. A.; McDowell, J. H.; Curtis, D. R.; Wang, J. K.; Juszczak, E.; Fong, S.-L.; Mohana Rao, J. K.; Argos, P. The Structure of Bovine Rhodopsin. *Biophys. Struct. Mechanism* **1983**, *9*, 235–244.

(8) Lefkowitz, R. J. Historical Review: A Brief History and Personal Retrospective of Seven-Transmembrane Receptors. *Trends in Pharmacological Sciences* **2004**, *25*, 413–422.

(9) Odoemelam, C. S.; Percival, B.; Wallis, H.; Chang, M.-W.; Ahmad, Z.; Scholey, D.; Burton, E.; Williams, I. H.; Kamerlin, C. L.; Wilson, P. B. G-Protein Coupled Receptors: Structure and Function in Drug Discovery. *RSC Adv.* **2020**, *10*, 36337–36348.

(10) Attwood, T. K.; Findlay, J. B. C. Fingerprinting G-Protein-Coupled Receptors. *Protein Eng Des Sel* **1994**, *7*, 195–203.

(11) Hauser, A. S.; Kooistra, A. J.; Munk, C.; Heydenreich, F. M.; Veprintsev, D. B.; Bouvier, M.; Babu, M. M.; Gloriam, D. E. GPCR Activation Mechanisms across Classes and Macro/Microscales. *Nat Struct Mol Biol* **2021**, *28*, 879–888.

(12) Fredriksson, R.; Lagerström, M. C.; Lundin, L.-G.; Schiöth, H. B. The G-Protein-Coupled Receptors in the Human Genome Form Five Main Families. Phylogenetic Analysis, Paralogon Groups, and Fingerprints. *Mol Pharmacol* **2003**, *63*, 1256–1272.

(13) Culhane, K.; Liu, Y.; Yingying, C.; Yan, E. Transmembrane Signal Transduction by Peptide Hormones via Family B G Protein-Coupled Receptors. *Frontiers in Pharmacology* **2015**, *6*.

(14) Reggio, P. H. Cannabinoid Receptors and Their Ligands: Ligand-Ligand and Ligand-Receptor Modeling Approaches. *Handb Exp Pharmacol* **2005**, No. 168, 247–281.


USC UNIVERSIDADE DE SANTIAGO DE COMPOSTELA

(15) Missale, C.; Nash, S. R.; Robinson, S. W.; Jaber, M.; Caron, M. G. Dopamine Receptors: From Structure to Function. *Physiological Reviews* **1998**, *78*, 189–225.
(16) Rondou, P.; Haegeman, G.; Van Craenenbroeck, K. The Dopamine D4 Receptor: Biochemical and Signalling Properties. *Cell. Mol. Life Sci.* **2010**, *67*, 1971–1986.
(17) Buck, S. A.; Quincy Erickson-Oberg, M.; Logan, R. W.; Freyberg, Z. Relevance of Interactions between Dopamine and Glutamate Neurotransmission in Schizophrenia. *Mol Psychiatry* **2022**, *27*, 3583–3591.
(18) Beaulieu, J.-M.; Gainetdinov, R. R. The Physiology, Signaling, and Pharmacology of Dopamine Receptors. *Pharmacol Rev* **2011**, *63*, 182–217.
(19) PubMed https://pubmed.ncbi.nlm.nih.gov/ (accessed 2023 -01 -23).
(20) Beaulieu, J.-M.; Espinoza, S.; Gainetdinov, R. R. Dopamine Receptors - IUPHAR Review 13: Dopamine Receptors. *Br J Pharmacol* **2015**, *172*, 1–23.
(21) Basu, D. Characterization of the Mechanism of Action for Novel Dopamine D2 Receptor Allosteric Modulators.
(22) Im, D.; Inoue, A.; Fujiwara, T.; Nakane, T.; Yamanaka, Y.; Uemura, T.; Mori, C.; Shiimura, Y.; Kimura, K. T.; Asada, H.; Nomura, N.; Tanaka, T.; Yamashita, A.; Nango, E.; Tono, K.; Kadji, F. M. N.; Aoki, J.; Iwata, S.; Shimamura, T. Structure of the Dopamine D2 Receptor in Complex with the Antipsychotic Drug Spiperone. *Nat Commun* **2020**, *11*, 6442.
(23) Wang, S.; Che, T.; Levit, A.; Shoichet, B. K.; Wacker, D.; Roth, B. L. Structure of the D2 Dopamine Receptor Bound to the Atypical Antipsychotic Drug Risperidone. *Nature* **2018**, *555*, 269–273.
(24) Fan, L.; Tan, L.; Chen, Z.; Qi, J.; Nie, F.; Luo, Z.; Cheng, J.; Wang, S. Haloperidol Bound D2 Dopamine Receptor Structure Inspired the Discovery of Subtype Selective Ligands. *Nat Commun* **2020**, *11*, 1074.
(25) Martel, J. C.; Gatti McArthur, S. Dopamine Receptor Subtypes, Physiology and Pharmacology: New Ligands and Concepts in Schizophrenia. *Front. Pharmacol.* **2020**, *11*, 1003.
(26) Hyman, S. E.; Malenka, R. C.; Nestler, E. J. Neural Mechanisms of Addiction: The Role of Reward-Related Learning and Memory. *Annu Rev Neurosci* **2006**, *29*, 565–598.
(27) Neve, K. A.; Seamans, J. K.; Trantham-Davidson, H. Dopamine Receptor Signaling. *Journal of Receptors and Signal Transduction* **2004**, *24*, 165–205.
(28) Popova, E. Role of Dopamine in Retinal Function. In *Webvision: The Organization of the Retina and Visual System [Internet]*; University of Utah Health Sciences Center, 2020.
(29) Albizu, L.; Holloway, T.; González-Maeso, J.; Sealfon, S. C. Functional Crosstalk and Heteromerization of Serotonin 5-HT2A and Dopamine D2 Receptors. *Neuropharmacology* **2011**, *61*, 770–777.
(30) Łukasiewicz, S.; Błasiak, E.; Szafran-Pilch, K.; Dziedzicka-Wasylewska, M. Dopamine D2 and Serotonin 5-HT1A Receptor Interaction in the Context of the Effects of Antipsychotics - in Vitro Studies. *J Neurochem* **2016**, *137*, 549–560.
(31) Cacabelos, R. Parkinson's Disease: From Pathogenesis to Pharmacogenomics. *International Journal of Molecular Sciences* **2017**, *18*, 551.
(32) Homepage | Parkinson's Foundation https://www.parkinson.org/node/79 (accessed 2023 -01 -23).
(33) Bloem, B. R.; Okun, M. S.; Klein, C. Parkinson's Disease. *The Lancet* **2021**, *397*, 2284–2303.

(34) Moustafa, A. A.; Chakravarthy, S.; Phillips, J. R.; Gupta, A.; Keri, S.; Polner, B.; Frank, M. J.; Jahanshahi, M. Motor Symptoms in Parkinson's Disease: A Unified Framework. *Neurosci Biobehav Rev* **2016**, *68*, 727–740.

(35) Zhu, B.; Yin, D.; Zhao, H.; Zhang, L. The Immunology of Parkinson's Disease. *Semin Immunopathol* **2022**, *44*, 659–672.

(36) Kopinathan, A.; Scammells, P. J.; Lane, J. R.; Capuano, B. Multivalent Approaches and beyond: Novel Tools for the Investigation of Dopamine D $_2$ Receptor Pharmacology. *Future Medicinal Chemistry* **2016**, *8*, 1349–1372.

(37) Mehra, S.; Sahay, S.; Maji, S. K. α-Synuclein Misfolding and Aggregation: Implications in Parkinson's Disease Pathogenesis. *Biochim Biophys Acta Proteins Proteom* **2019**, *1867*, 890–908.

(38) Braak, H.; Del Tredici, K.; Rüb, U.; de Vos, R. A. I.; Jansen Steur, E. N. H.; Braak, E. Staging of Brain Pathology Related to Sporadic Parkinson's Disease. *Neurobiol Aging* **2003**, *24*, 197–211.

(39) Borovac, J. A. Side Effects of a Dopamine Agonist Therapy for Parkinson's Disease: A Mini-Review of Clinical Pharmacology. **2006**.

(40) Colamartino, M.; Padua, L.; Meneghini, C.; Leone, S.; Cornetta, T.; Testa, A.; Cozzi, R. Protective Effects of L-Dopa and Carbidopa Combined Treatments on Human Catecholaminergic Cells. *DNA Cell Biol* **2012**, *31*, 1572–1579.

(41) Mao, Q.; Qin, W.; Zhang, A.; Ye, N. Recent Advances in Dopaminergic Strategies for the Treatment of Parkinson's Disease. *Acta Pharmacol Sin* **2020**, *41*, 471–482.

(42) Zhong, Z.; He, X.; Ge, J.; Zhu, J.; Yao, C.; Cai, H.; Ye, X.-Y.; Xie, T.; Bai, R. Discovery of Small-Molecule Compounds and Natural Products against Parkinson's Disease: Pathological Mechanism and Structural Modification. *European Journal of Medicinal Chemistry* **2022**, *237*, 114378.

(43) Kahn, R. S.; Sommer, I. E.; Murray, R. M.; Meyer-Lindenberg, A.; Weinberger, D. R.; Cannon, T. D.; O'Donovan, M.; Correll, C. U.; Kane, J. M.; van Os, J.; Insel, T. R. Schizophrenia. *Nat Rev Dis Primers* **2015**, *1*, 15067.

(44) Seeman, P.; Kapur, S. Schizophrenia: More Dopamine, More D $_2$ Receptors. *Proc. Natl. Acad. Sci. U.S.A.* **2000**, *97*, 7673–7675.

(45) McCutcheon, R. A.; Reis Marques, T.; Howes, O. D. Schizophrenia—An Overview. *JAMA Psychiatry* **2020**, *77*, 201.

(46) Abreu, A. M. NEW LIGANDS AND PHARMACOLOGICAL TOOLS FOR THE STUDY OF G PROTEIN- COUPLED RECEPTORS USING MULTICOMPONENT REACTIONS.

(47) *The Dopamine Receptors*; Neve, K. A., Ed.; The Receptors; Humana Press: Totowa, NJ, 2010.

(48) Li, P.; L. Snyder, G.; E. Vanover, K. Dopamine Targeting Drugs for the Treatment of Schizophrenia: Past, Present and Future. *CTMC* **2016**, *16*, 3385–3403.

(49) Xu, M.; Wang, Y.; Yang, F.; Wu, C.; Wang, Z.; Ye, B.; Jiang, X.; Zhao, Q.; Li, J.; Liu, Y.; Zhang, J.; Tian, G.; He, Y.; Shen, J.; Jiang, H. Synthesis and Biological Evaluation of a Series of Novel Pyridinecarboxamides as Potential Multi-Receptor Antipsychotic Drugs. *Bioorganic & Medicinal Chemistry Letters* **2018**, *28*, 606–611.

(50) Schmidt, A. W.; Lebel, L. A.; Howard, H. R.; Zorn, S. H. Ziprasidone: A Novel Antipsychotic Agent with a Unique Human Receptor Binding Profile. *European Journal of Pharmacology* **2001**, *425*, 197–201.

(51) Tyler, M. W.; Zaldivar-Diez, J.; Haggarty, S. J. Classics in Chemical Neuroscience: Haloperidol. *ACS Chem. Neurosci.* **2017**, *8*, 444–453.

USC UNIVERSIDADE DE SANTIAGO DE COMPOSTELA

(52) Nickols, H. H.; Conn, P. J. Development of Allosteric Modulators of GPCRs for Treatment of CNS Disorders. *Neurobiology of Disease* **2014**, *61*, 55–71.
(53) Fasciani, I.; Petragnano, F.; Aloisi, G.; Marampon, F.; Carli, M.; Scarselli, M.; Maggio, R.; Rossi, M. Allosteric Modulators of G Protein-Coupled Dopamine and Serotonin Receptors: A New Class of Atypical Antipsychotics. *Pharmaceuticals* **2020**, *13*, 388.
(54) Jakubík, J.; Randáková, A.; Chetverikov, N.; El-Fakahany, E. E.; Doležal, V. The Operational Model of Allosteric Modulation of Pharmacological Agonism. *Sci Rep* **2020**, *10*, 14421.
(55) Yartsev, A. Potency and efficacy | Deranged Physiology https://derangedphysiology.com/main/cicm-primary-exam/required-reading/pharmacodynamics/Chapter 415/potency-and-efficacy (accessed 2023 -12 -15).
(56) Kenakin, T. P. Allosteric Drug Effects. In *Pharmacology in Drug Discovery and Development*; Elsevier, 2017; pp 101–129.
(57) Singh, K.; Sona, C.; Ojha, V.; Singh, M.; Mishra, A.; Kumar, A.; Siddiqi, M. I.; Tripathi, R. P.; Yadav, P. N. Identification of Dual Role of Piperazine-Linked Phenyl Cyclopropyl Methanone as Positive Allosteric Modulator of 5-HT2C and Negative Allosteric Modulator of 5-HT2B Receptors. *European Journal of Medicinal Chemistry* **2019**, *164*, 499–516.
(58) Lindberg, J. S.; Culleton, B.; Wong, G.; Borah, M. F.; Clark, R. V.; Shapiro, W. B.; Roger, S. D.; Husserl, F. E.; Klassen, P. S.; Guo, M. D.; Albizem, M. B.; Coburn, J. W. Cinacalcet HCl, an Oral Calcimimetic Agent for the Treatment of Secondary Hyperparathyroidism in Hemodialysis and Peritoneal Dialysis: A Randomized, Double-Blind, Multicenter Study. *Journal of the American Society of Nephrology* **2005**, *16*, 800–807.
(59) Ray, N. Maraviroc in the Treatment of HIV Infection. *Drug Design*.
(60) DiPersio, J. F.; Stadtmauer, E. A.; Nademanee, A.; Micallef, I. N. M.; Stiff, P. J.; Kaufman, J. L.; Maziarz, R. T.; Hosing, C.; Früehauf, S.; Horwitz, M.; Cooper, D.; Bridger, G.; Calandra, G.; for the 3102 Investigators. Plerixafor and G-CSF versus Placebo and G-CSF to Mobilize Hematopoietic Stem Cells for Autologous Stem Cell Transplantation in Patients with Multiple Myeloma. *Blood* **2009**, *113*, 5720–5726.
(61) Schetz, J. Allosteric Modulation of Dopamine Receptors. *MRMC* **2005**, *5*, 555–561.
(62) Sampaio-Dias, I. E.; Rodríguez-Borges, J. E.; Yáñez-Pérez, V.; Arrasate, S.; Llorente, J.; Brea, J. M.; Bediaga, H.; Viña, D.; Loza, M. I.; Caamaño, O.; García-Mera, X.; González-Díaz, H. Synthesis, Pharmacological, and Biological Evaluation of 2-Furoyl-Based MIF-1 Peptidomimetics and the Development of a General-Purpose Model for Allosteric Modulators (ALLOPTML). *ACS Chem. Neurosci.* **2021**, *12*, 203–215.
(63) Sampaio-Dias, I. E.; Silva-Reis, S. C.; García-Mera, X.; Brea, J.; Loza, M. I.; Alves, C. S.; Algarra, M.; Rodríguez-Borges, J. E. Synthesis, Pharmacological, and Biological Evaluation of MIF-1 Picolinoyl Peptidomimetics as Positive Allosteric Modulators of $D_2$ R. *ACS Chem. Neurosci.* **2019**, *10*, 3690–3702.
(64) Sampaio-Dias, I. E.; Reis-Mendes, A.; Costa, V. M.; García-Mera, X.; Brea, J.; Loza, M. I.; Pires-Lima, B. L.; Alcoholado, C.; Algarra, M.; Rodríguez-Borges, J. E. Discovery of New Potent Positive Allosteric Modulators of Dopamine $D_2$ Receptors: Insights into the Bioisosteric Replacement of Proline to 3-Furoic Acid in the Melanostatin Neuropeptide. *J. Med. Chem.* **2021**, *64*, 6209–6220.

USC UNIVERSIDADE DE SANTIAGO DE COMPOSTELA

(65) Silva-Reis, S. C.; Correia, X. C.; Costa-Almeida, H. F.; Pires-Lima, B. L.; Maronde, D.; Costa, V. M.; García-Mera, X.; Cruz, L.; Brea, J.; Loza, M. I.; Rodríguez-Borges, J. E.; Sampaio-Dias, I. E. Stapling Amantadine to Melanostatin Neuropeptide: Discovery of Potent Positive Allosteric Modulators of the D $_2$ Receptors. *ACS Med. Chem. Lett.* **2023**, acsmedchemlett.3c00264.

(66) Sampaio-Dias, I. E.; Sousa, C. A. D.; García-Mera, X.; Ferreira Da Costa, J.; Caamaño, O.; Rodríguez-Borges, J. E. Novel L -Prolyl- L -Leucylglycinamide (PLG) Tripeptidomimetics Based on a 2-Azanorbornane Scaffold as Positive Allosteric Modulators of the D $_2$ R. *Org. Biomol. Chem.* **2016**, *14*, 11065–11069.

(67) Huffman, J. CB2 Receptor Ligands. *MRMC* **2005**, *5*, 641–649.

(68) Zou, S.; Kumar, U. Cannabinoid Receptors and the Endocannabinoid System: Signaling and Function in the Central Nervous System. *IJMS* **2018**, *19*, 833.

(69) Howlett, A. C.; Abood, M. E. CB 1 and CB 2 Receptor Pharmacology. In *Advances in Pharmacology*; Elsevier, 2017; Vol. 80, pp 169–206.

(70) Mackie, K. CANNABINOID RECEPTORS AS THERAPEUTIC TARGETS. *Annu. Rev. Pharmacol. Toxicol.* **2006**, *46*, 101–122.

(71) Gioé-Gallo, C. Discovery and Optimization of Selective CB2 Receptor Agonists. PhD diss., University of Santiago de Compostela, Santiago de Compostela, 2023.

(72) An, D.; Peigneur, S.; Hendrickx, L. A.; Tytgat, J. Targeting Cannabinoid Receptors: Current Status and Prospects of Natural Products. *IJMS* **2020**, *21*, 5064.

(73) Dhopeshwarkar, A.; Mackie, K. CB $_2$ Cannabinoid Receptors as a Therapeutic Target—What Does the Future Hold? *Mol Pharmacol* **2014**, *86*, 430–437.

(74) Rosenbaum, D. M.; Rasmussen, S. G. F.; Kobilka, B. K. The Structure and Function of G-Protein-Coupled Receptors. *Nature* **2009**, *459*, 356–363.

(75) Li, X.; Hua, T.; Vemuri, K.; Ho, J.-H.; Wu, Y.; Wu, L.; Popov, P.; Benchama, O.; Zvonok, N.; Locke, K.; Qu, L.; Han, G. W.; Iyer, M. R.; Cinar, R.; Coffey, N. J.; Wang, J.; Wu, M.; Katritch, V.; Zhao, S.; Kunos, G.; Bohn, L. M.; Makriyannis, A.; Stevens, R. C.; Liu, Z.-J. Crystal Structure of the Human Cannabinoid Receptor CB2. *Cell* **2019**, *176*, 459-467.e13.

(76) Atwood, B. K.; Mackie, K. CB2: A Cannabinoid Receptor with an Identity Crisis: CB2 Expression in Neurons. *British Journal of Pharmacology* **2010**, *160*, 467–479.

(77) Turcotte, C.; Blanchet, M.-R.; Laviolette, M.; Flamand, N. The CB2 Receptor and Its Role as a Regulator of Inflammation. *Cell. Mol. Life Sci.* **2016**, *73*, 4449–4470.

(78) Maccarrone, M.; Bab, I.; Bíró, T.; Cabral, G. A.; Dey, S. K.; Di Marzo, V.; Konje, J. C.; Kunos, G.; Mechoulam, R.; Pacher, P.; Sharkey, K. A.; Zimmer, A. Endocannabinoid Signaling at the Periphery: 50 Years after THC. *Trends in Pharmacological Sciences* **2015**, *36*, 277–296.

(79) Whiting, Z. M.; Yin, J.; de la Harpe, S. M.; Vernall, A. J.; Grimsey, N. L. Developing the Cannabinoid Receptor 2 (CB2) Pharmacopoeia: Past, Present, and Future. *Trends in Pharmacological Sciences* **2022**, *43*, 754–771.

(80) Ofek, O.; Karsak, M.; Leclerc, N.; Fogel, M.; Frenkel, B.; Wright, K.; Tam, J.; Attar-Namdar, M.; Kram, V.; Shohami, E.; Mechoulam, R.; Zimmer, A.; Bab, I. Peripheral Cannabinoid Receptor, CB2, Regulates Bone Mass. *Proc. Natl. Acad. Sci. U.S.A.* **2006**, *103*, 696–701.

(81) Kibret, B. G.; Ishiguro, H.; Horiuchi, Y.; Onaivi, E. S. New Insights and Potential Therapeutic Targeting of CB2 Cannabinoid Receptors in CNS Disorders. *IJMS* **2022**, *23*, 975.

USC UNIVERSIDADE DE SANTIAGO DE COMPOSTELA

(82) Atwood, B. K.; Straiker, A.; Mackie, K. CB2 Cannabinoid Receptors Inhibit Synaptic Transmission When Expressed in Cultured Autaptic Neurons. *Neuropharmacology* **2012**, *63*, 514–523.

(83) Mcguinness, D.; Malikzay, A.; Visconti, R.; Lin, K.; Bayne, M.; Monsma, F.; Lunn, C. A. Characterizing Cannabinoid CB 2 Receptor Ligands Using DiscoveRx PathHunter™ β-Arrestin Assay. *J Biomol Screen* **2009**, *14*, 49–58.

(84) Hashiesh, H. M.; Sharma, C.; Goyal, S. N.; Sadek, B.; Jha, N. K.; Kaabi, J. A.; Ojha, S. A Focused Review on CB2 Receptor-Selective Pharmacological Properties and Therapeutic Potential of β-Caryophyllene, a Dietary Cannabinoid. *Biomedicine & Pharmacotherapy* **2021**, *140*, 111639.

(85) Bie, B.; Wu, J.; Foss, J. F.; Naguib, M. An Overview of the Cannabinoid Type 2 Receptor System and Its Therapeutic Potential. *Current Opinion in Anaesthesiology* **2018**, *31*, 407–414.

(86) CB2 Agonism https://cannakeys.com/cb2-agonism/ (accessed 2023 -12 -17).

(87) Hashiesh, H. M.; Sharma, C.; Goyal, S. N.; Jha, N. K.; Ojha, S. Pharmacological Properties, Therapeutic Potential and Molecular Mechanisms of JWH133, a CB2 Receptor-Selective Agonist. *Front. Pharmacol.* **2021**, *12*, 702675.

(88) Henriquez, J. E.; Crawford, R. B.; Kaminski, N. E. Suppression of CpG-ODN-Mediated IFNα and TNFα Response in Human Plasmacytoid Dendritic Cells (pDC) by Cannabinoid Receptor 2 (CB2)-Specific Agonists. *Toxicology and Applied Pharmacology* **2019**, *369*, 82–89.

(89) Steffens, S.; Veillard, N. R.; Arnaud, C.; Pelli, G.; Burger, F.; Staub, C.; Karsak, M.; Zimmer, A.; Frossard, J.-L.; Mach, F. Low Dose Oral Cannabinoid Therapy Reduces Progression of Atherosclerosis in Mice. *Nature* **2005**, *434*, 782–786.

(90) Vuic, B.; Milos, T.; Tudor, L.; Konjevod, M.; Nikolac Perkovic, M.; Jazvinscak Jembrek, M.; Nedic Erjavec, G.; Svob Strac, D. Cannabinoid CB2 Receptors in Neurodegenerative Proteinopathies: New Insights and Therapeutic Potential. *Biomedicines* **2022**, *10*, 3000.

(91) Xin, Q.; Xu, F.; Taylor, D. H.; Zhao, J.; Wu, J. The Impact of Cannabinoid Type 2 Receptors (CB2Rs) in Neuroprotection against Neurological Disorders. *Acta Pharmacol Sin* **2020**, *41*, 1507–1518.

(92) Munson, A. E.; Harris, L. S.; Friedman, M. A.; Dewey, W. L.; Carchman, R. A. Antineoplastic Activity of Cannabinoids2. *JNCI: Journal of the National Cancer Institute* **1975**, *55*, 597–602.

(93) Fraguas-Sánchez, A. I.; Fernández-Carballido, A.; Torres-Suárez, A. I. Phyto-, Endo- and Synthetic Cannabinoids: Promising Chemotherapeutic Agents in the Treatment of Breast and Prostate Carcinomas. *Expert Opinion on Investigational Drugs* **2016**, *25*, 1311–1323.

(94) Fraguas-Sánchez, A. I.; Martín-Sabroso, C.; Torres-Suárez, A. I. Insights into the Effects of the Endocannabinoid System in Cancer: A Review. *Br J Pharmacol* **2018**, *175*, 2566–2580.

(95) Contino, M.; McCormick, P. J. Editorial: The Canonical and Non-Canonical Endocannabinoid System as a Target in Cancer and Acute and Chronic Pain. *Frontiers in Pharmacology* **2020**, *11*.

(96) Theocharis, S.; Giaginis, C.; Alexandrou, P.; Rodriguez, J.; Tasoulas, J.; Danas, E.; Patsouris, E.; Klijanienko, J. Evaluation of Cannabinoid CB1 and CB2 Receptors Expression in Mobile Tongue Squamous Cell Carcinoma: Associations with

USC UNIVERSIDADE DE SANTIAGO DE COMPOSTELA

Clinicopathological Parameters and Patients' Survival. *Tumour Biol* **2016**, *37*, 3647–3656.

(97) Moreno, E.; Andradas, C.; Medrano, M.; Caffarel, M. M.; Pérez-Gómez, E.; Blasco-Benito, S.; Gómez-Cañas, M.; Pazos, M. R.; Irving, A. J.; Lluís, C.; Canela, E. I.; Fernández-Ruiz, J.; Guzmán, M.; McCormick, P. J.; Sánchez, C. Targeting CB2-GPR55 Receptor Heteromers Modulates Cancer Cell Signaling. *Journal of Biological Chemistry* **2014**, *289*, 21960–21972.

(98) Blasco-Benito, S.; Moreno, E.; Seijo-Vila, M.; Tundidor, I.; Andradas, C.; Caffarel, M. M.; Caro-Villalobos, M.; Urigüen, L.; Diez-Alarcia, R.; Moreno-Bueno, G.; Hernández, L.; Manso, L.; Homar-Ruano, P.; McCormick, P. J.; Bibic, L.; Bernadó-Morales, C.; Arribas, J.; Canals, M.; Casadó, V.; Canela, E. I.; Guzmán, M.; Pérez-Gómez, E.; Sánchez, C. Therapeutic Targeting of HER2–CB $_2$ R Heteromers in HER2-Positive Breast Cancer. *Proc. Natl. Acad. Sci. U.S.A.* **2019**, *116*, 3863–3872.

(99) Gado, F.; Ferrisi, R.; Di Somma, S.; Napolitano, F.; Mohamed, K. A.; Stevenson, L. A.; Rapposelli, S.; Saccomanni, G.; Portella, G.; Pertwee, R. G.; Laprairie, R. B.; Malfitano, A. M.; Manera, C. Synthesis and In Vitro Characterization of Selective Cannabinoid CB2 Receptor Agonists: Biological Evaluation against Neuroblastoma Cancer Cells. *Molecules* **2022**, *27*, 3019.

(100) Qamri, Z.; Preet, A.; Nasser, M. W.; Bass, C. E.; Leone, G.; Barsky, S. H.; Ganju, R. K. Synthetic Cannabinoid Receptor Agonists Inhibit Tumor Growth and Metastasis of Breast Cancer. *Molecular Cancer Therapeutics* **2009**, *8*, 3117–3129.

(101) Alenabi, A.; Malekinejad, H. Cannabinoids Pharmacological Effects Are beyond the Palliative Effects: CB2 Cannabinoid Receptor Agonist Induced Cytotoxicity and Apoptosis in Human Colorectal Cancer Cells (HT-29). *Mol Cell Biochem* **2021**, *476*, 3285–3301.

(102) Arora, A.; Somasundaram, K. Glioblastoma vs Temozolomide: Can the Red Queen Race Be Won? *Cancer Biology & Therapy* **2019**, *20*, 1083–1090.

(103) Schley, M.; Ständer, S.; Kerner, J.; Vajkoczy, P.; Schüpfer, G.; Dusch, M.; Schmelz, M.; Konrad, C. Predominant CB2 Receptor Expression in Endothelial Cells of Glioblastoma in Humans. *Brain Research Bulletin* **2009**, *79*, 333–337.

(104) Singer, E.; Judkins, J.; Salomonis, N.; Matlaf, L.; Soteropoulos, P.; McAllister, S.; Soroceanu, L. Reactive Oxygen Species-Mediated Therapeutic Response and Resistance in Glioblastoma. *Cell Death Dis* **2015**, *6*, e1601–e1601.

(105) Irrera, N.; D'Ascola, A.; Pallio, G.; Bitto, A.; Mannino, F.; Arcoraci, V.; Rottura, M.; Ieni, A.; Minutoli, L.; Metro, D.; Vaccaro, M.; Altavilla, D.; Squadrito, F. β-Caryophyllene Inhibits Cell Proliferation through a Direct Modulation of CB2 Receptors in Glioblastoma Cells. *Cancers* **2020**, *12*, 1038.

(106) Minniti, G.; De Sanctis, V.; Muni, R.; Filippone, F.; Bozzao, A.; Valeriani, M.; Osti, M. F.; De Paula, U.; Lanzetta, G.; Tombolini, V.; Maurizi Enrici, R. Radiotherapy plus Concomitant and Adjuvant Temozolomide for Glioblastoma in Elderly Patients. *J Neurooncol* **2008**, *88*, 97–103.

(107) Morales, P.; Hernandez-Folgado, L.; Goya, P.; Jagerovic, N. Cannabinoid Receptor 2 (CB $_2$ ) Agonists and Antagonists: A Patent Update. *Expert Opinion on Therapeutic Patents* **2016**, *26*, 843–856.

(108) Home | ClinicalTrials.gov https://clinicaltrials.gov/ (accessed 2023 -10 -23).

(109) Banister, S. D.; Longworth, M.; Kevin, R.; Sachdev, S.; Santiago, M.; Stuart, J.; Mack, J. B. C.; Glass, M.; McGregor, I. S.; Connor, M.; Kassiou, M. Pharmacology of Valinate and *Tert* -Leucinate Synthetic Cannabinoids 5F-AMBICA, 5F-AMB, 5F-

USC UNIVERSIDADE DE SANTIAGO DE COMPOSTELA

ADB, AMB-FUBINACA, MDMB-FUBINACA, MDMB-CHMICA, and Their Analogues. *ACS Chem. Neurosci.* **2016**, *7*, 1241–1254.

(110) Banister, S. D.; Connor, M. The Chemistry and Pharmacology of Synthetic Cannabinoid Receptor Agonist New Psychoactive Substances: Evolution. In *New Psychoactive Substances*; Maurer, H. H., Brandt, S. D., Eds.; Handbook of Experimental Pharmacology; Springer International Publishing: Cham, 2018; Vol. 252, pp 191–226.

(111) Gioé-Gallo, C.; Ortigueira, S.; Brea, J.; Raïch, I.; Azuaje, J.; Paleo, M. R.; Majellaro, M.; Loza, M. I.; Salas, C. O.; García-Mera, X.; Navarro, G.; Sotelo, E. Pharmacological Insights Emerging from the Characterization of a Large Collection of Synthetic Cannabinoid Receptor Agonists Designer Drugs. *Biomedicine & Pharmacotherapy* **2023**, *164*, 114934.

(112) Sparkes, E.; Boyd, R.; Chen, S.; Markham, J. W.; Luo, J. L.; Foyzun, T.; Zaman, H.; Fletcher, C.; Ellison, R.; McGregor, I. S.; Santiago, M. J.; Lai, F.; Gerona, R. R.; Connor, M.; Hibbs, D. E.; Cairns, E. A.; Glass, M.; Ametovski, A.; Banister, S. D. Synthesis and Pharmacological Evaluation of Newly Detected Synthetic Cannabinoid Receptor Agonists AB-4CN-BUTICA, MMB-4CN-BUTINACA, MDMB-4F-BUTICA, MDMB-4F-BUTINACA and Their Analogs. *Front. Psychiatry* **2022**, *13*, 1010501.

(113) Ruijter, E.; Scheffelaar, R.; Orru, R. V. A. Multicomponent Reaction Design in the Quest for Molecular Complexity and Diversity. *Angew. Chem. Int. Ed.* **2011**, *50*, 6234–6246.

(114) Zarganes-Tzitzikas, T.; Chandgude, A. L.; Dömling, A. Multicomponent Reactions, Union of MCRs and Beyond. *The Chemical Record* **2015**, *15*, 981–996.

(115) Insuasty, D.; Castillo, J.; Becerra, D.; Rojas, H.; Abonia, R. Synthesis of Biologically Active Molecules through Multicomponent Reactions. *Molecules* **2020**, *25*, 505.

(116) Cimarelli, C. Multicomponent Reactions. *Molecules* **2019**, *24*, 2372.

(117) Cores, Á.; Clerigué, J.; Orocio-Rodríguez, E.; Menéndez, J. C. Multicomponent Reactions for the Synthesis of Active Pharmaceutical Ingredients. *Pharmaceuticals* **2022**, *15*.

(118) Dömling, A.; Ugi, I. Multicomponent Reactions with Isocyanides. *Angew. Chem. Int. Ed.* **2000**, *39*, 3168–3210.

(119) Massarotti, A.; Brunelli, F.; Aprile, S.; Giustiniano, M.; Tron, G. C. Medicinal Chemistry of Isocyanides. *Chem. Rev.* **2021**, *121*, 10742–10788.

(120) Front Matter. In *Multicomponent Reactions*; Zhu, J., Bienaymé, H., Eds.; Wiley, 2005.

(121) Azuaje, J.; Pérez-Rubio, J. M.; Yaziji, V.; El Maatougui, A.; González-Gomez, J. C.; Sánchez-Pedregal, V. M.; Navarro-Vázquez, A.; Masaguer, C. F.; Teijeira, M.; Sotelo, E. Integrated Ugi-Based Assembly of Functionally, Skeletally, and Stereochemically Diverse 1,4-Benzodiazepin-2-Ones. *J. Org. Chem.* **2015**, *80*, 1533–1549.

(122) Azuaje, J.; El Maatougui, A.; Pérez-Rubio, J. M.; Coelho, A.; Fernández, F.; Sotelo, E. Multicomponent Assembly of Diverse Pyrazin-2(1 *H* )-One Chemotypes. *J. Org. Chem.* **2013**, *78*, 4402–4409.

(123) Azuaje, J.; Maatougui, A. E.; Garc, X. Ugi-Based Approaches to Quinoxaline Libraries. *ACS Combinatorial Science*.

(124) Giovenzana, G. B.; Tron, G. C.; Di Paola, S.; Menegotto, I. G.; Pirali, T. A Mimicry of Primary Amines by Bis-Secondary Diamines as Components in the Ugi Four-Component Reaction. *Angew Chem Int Ed* **2006**, *45*, 1099–1102.

USC UNIVERSIDADE DE SANTIAGO DE COMPOSTELA

(125) Banfi, L.; Basso, A.; Lambruschini, C.; Moni, L.; Riva, R. The 100 Facets of the Passerini Reaction. *Chem. Sci.* **2021**, *12*, 15445–15472.
(126) Banfi, L.; Guanti, G.; Riva, R. Passerini Multicomponent Reaction of Protected α-Aminoaldehydes as a Tool for Combinatorial Synthesis of Enzyme Inhibitors. *Chem. Commun.* **2000**, No. 11, 985–986.
(127) Banfi, L.; Basso, A.; Guanti, G.; Riva, R. Passerini Reaction – Amine Deprotection – Acyl Migration (PADAM): A Convenient Strategy for the Solid-Phase Preparation of Peptidomimetic Compounds. *Mol Divers* **2000**, *6*, 227–235.
(128) Owens, T. D.; Araldi, G.-L.; Nutt, R. F.; Semple, J. E. Concise Total Synthesis of the Prolyl Endopeptidase Inhibitor Eurystatin A via a Novel Passerini Reaction–Deprotection–Acyl Migration Strategy. *Tetrahedron Letters* **2001**, *42*, 6271–6274.
(129) Umezawa, H.; Aoyagi, T.; Suda, H.; Hamada, M.; Takeuchi, T. Bestatin, an Inhibitor of Aminopeptidase B, Produced by Actinomycetes. *J. Antibiot.* **1976**, *29*, 97–99.
(130) He, S.; Stankowska, D. L.; Ellis, D. Z.; Krishnamoorthy, R. R.; Yorio, T. Targets of Neuroprotection in Glaucoma. *Journal of Ocular Pharmacology and Therapeutics* **2018**, *34*, 85–106.
(131) Sebastiani, G.; Ceccarelli, E.; Castagna, M. G.; Dotta, F. G-Protein-Coupled Receptors (GPCRs) in the Treatment of Diabetes: Current View and Future Perspectives. *Best Practice & Research Clinical Endocrinology & Metabolism* **2018**, *32*, 201–213.
(132) Bhagwanth, S.; Mishra, R. K.; Johnson, R. L. Development of Peptidomimetic Ligands of Pro-Leu-Gly-$NH_2$ as Allosteric Modulators of the Dopamine $D_2$ Receptor. *Beilstein J. Org. Chem.* **2013**, *9*, 204–214.
(133) Ferreira Da Costa, J.; Caamaño, O.; Fernández, F.; García-Mera, X.; Sampaio-Dias, I. E.; Brea, J. M.; Cadavid, M. I. Synthesis and Allosteric Modulation of the Dopamine Receptor by Peptide Analogs of L-Prolyl-l-Leucyl-Glycinamide (PLG) Modified in the l-Proline or l-Proline and l-Leucine Scaffolds. *European Journal of Medicinal Chemistry* **2013**, *69*, 146–158.
(134) Ghonim, A. E.; Ligresti, A.; Rabbito, A.; Mahmoud, A. M.; Di Marzo, V.; Osman, N. A.; Abadi, A. H. Structure-Activity Relationships of Thiazole and Benzothiazole Derivatives as Selective Cannabinoid CB2 Agonists with in Vivo Anti-Inflammatory Properties. *European Journal of Medicinal Chemistry* **2019**, *180*, 154–170.
(135) Nanda, K. K.; Henze, D. A.; Della Penna, K.; Desai, R.; Leitl, M.; Lemaire, W.; White, R. B.; Yeh, S.; Brouillette, J. N.; Hartman, G. D.; Bilodeau, M. T.; Trotter, B. W. Benzimidazole CB2 Agonists: Design, Synthesis and SAR. *Bioorganic & Medicinal Chemistry Letters* **2014**, *24*, 1218–1221.
(136) Qian, H.-Y.; Wang, Z.-L.; Xie, X.-Y.; Pan, Y.-L.; Li, G.-J.; Xie, X.; Chen, J.-Z. Developing Pyridazine-3-Carboxamides to Be CB2 Agonists: The Design, Synthesis, Structure-Activity Relationships and Docking Studies. *European Journal of Medicinal Chemistry* **2017**, *137*, 598–611.
(137) Guidetti, R.; Astles, P. C.; Sanderson, A. J.; Hollinshead, S. P.; Johnson, M. P.; Chambers, M. G. The SAR Development of Substituted Purine Derivatives as Selective CB2 Agonists for the Treatment of Chronic Pain. *Bioorganic & Medicinal Chemistry Letters* **2014**, *24*, 5572–5575.
(138) Zimuwandeyi, M.; Kola, F.; Lemmerer, A.; Brady, D.; Rousseau, A. L.; Bode, M. L. PADAM Reactions of α-Aminoaldehydes: Identity of Major and Minor Diastereomers from the Passerini Reaction. *Tetrahedron* **2018**, *74*, 2925–2941.

USC UNIVERSIDADE DE SANTIAGO DE COMPOSTELA

(139) Semple, J. E.; Owens, T. D.; Nguyen, K.; Levy, O. E. New Synthetic Technology for Efficient Construction of α-Hydroxy-β-Amino Amides via the Passerini Reaction [1]. *Org. Lett.* **2000**, *2*, 2769–2772.
(140) Basso, A.; Banfi, L.; Guanti, G.; Riva, R.; Tosatti, P. Elaboration of Peptidomimetics Derived from a PADAM Approach: Synthesis of Polyfunctionalised 2(1H)-Pyrazinones via an Unexpected Aromatisation. *Synlett* **2011**, *2011*, 2009–2012.
(141) Shaw, A. Y.; Medda, F.; Hulme, C. Facile and Rapid Route for the Synthesis of Novel Norstatine Analogs via PADAM-Cyclization Methodology. *Tetrahedron Letters* **2012**, *53*, 1313–1315.
(142) Moni, L.; Banfi, L.; Basso, A.; Bozzano, A.; Spallarossa, M.; Wessjohann, L.; Riva, R. Passerini Reactions on Biocatalytically Derived Chiral Azetidines. *Molecules* **2016**, *21*, 1153.
(143) Rotstein, B. H. Unprotected Aziridine Aldehydes in Isocyanide-Based Multicomponent Reactions.
(144) Banister, S. D.; Moir, M.; Stuart, J.; Kevin, R. C.; Wood, K. E.; Longworth, M.; Wilkinson, S. M.; Beinat, C.; Buchanan, A. S.; Glass, M.; Connor, M.; McGregor, I. S.; Kassiou, M. Pharmacology of Indole and Indazole Synthetic Cannabinoid Designer Drugs AB-FUBINACA, ADB-FUBINACA, AB-PINACA, ADB-PINACA, 5F-AB-PINACA, 5F-ADB-PINACA, ADBICA, and 5F-ADBICA. *ACS Chem. Neurosci.* **2015**, *6*, 1546–1559.
(145) Schoeder, C. T.; Hess, C.; Madea, B.; Meiler, J.; Müller, C. E. Pharmacological Evaluation of New Constituents of "Spice": Synthetic Cannabinoids Based on Indole, Indazole, Benzimidazole and Carbazole Scaffolds. *Forensic Toxicol* **2018**, *36*, 385–403.
(146) Hua, T.; Vemuri, K.; Pu, M.; Qu, L.; Han, G. W.; Wu, Y.; Zhao, S.; Shui, W.; Li, S.; Korde, A.; Laprairie, R. B.; Stahl, E. L.; Ho, J.-H.; Zvonok, N.; Zhou, H.; Kufareva, I.; Wu, B.; Zhao, Q.; Hanson, M. A.; Bohn, L. M.; Makriyannis, A.; Stevens, R. C.; Liu, Z.-J. Crystal Structure of the Human Cannabinoid Receptor CB1. *Cell* **2016**, *167*, 750-762.e14.
(147) Lu, C.; Wu, C.; Ghoreishi, D.; Chen, W.; Wang, L.; Damm, W.; Ross, G. A.; Dahlgren, M. K.; Russell, E.; Von Bargen, C. D.; Abel, R.; Friesner, R. A.; Harder, E. D. OPLS4: Improving Force Field Accuracy on Challenging Regimes of Chemical Space. *J. Chem. Theory Comput.* **2021**, *17*, 4291–4300.
(148) Raïch, I.; Rivas-Santisteban, R.; Lillo, A.; Lillo, J.; Reyes-Resina, I.; Nadal, X.; Ferreiro-Vera, C.; de Medina, V. S.; Majellaro, M.; Sotelo, E.; Navarro, G.; Franco, R. Similarities and Differences upon Binding of Naturally Occurring Δ9-Tetrahydrocannabinol-Derivatives to Cannabinoid CB1 and CB2 Receptors. *Pharmacological Research* **2021**, *174*, 105970.
(149) Kenakin, T. Biased Receptor Signaling in Drug Discovery. *Pharmacol Rev* **2019**, *71*, 267–315.
(150) Shchepinova, M. M.; Hanyaloglu, A. C.; Frost, G. S.; Tate, E. W. Chemical Biology of Noncanonical G Protein-Coupled Receptor Signaling: Toward Advanced Therapeutics. *Curr Opin Chem Biol* **2020**, *56*, 98–110.
(151) Glogauer, J.; Blay, J. Cannabinoids, Their Cellular Receptors, and Effects on the Invasive Phenotype of Carcinoma and Metastasis. *Cancer Reports* **2022**, *5*.
(152) Delgado-Peraza, F.; Ahn, K. H.; Nogueras-Ortiz, C.; Mungrue, I. N.; Mackie, K.; Kendall, D. A.; Yudowski, G. A. Mechanisms of Biased β-Arrestin-Mediated

USC UNIVERSIDADE DE SANTIAGO DE COMPOSTELA

Signaling Downstream from the Cannabinoid 1 Receptor. *Mol Pharmacol* **2016**, *89*, 618–629.

(153) Alexander, S. P.; Christopoulos, A.; Davenport, A. P.; Kelly, E.; Mathie, A.; Peters, J. A.; Veale, E. L.; Armstrong, J. F.; Faccenda, E.; Harding, S. D.; Pawson, A. J.; Southan, C.; Davies, J. A.; Abbracchio, M. P.; Alexander, W.; Al-Hosaini, K.; Bäck, M.; Barnes, N. M.; Bathgate, R.; Beaulieu, J.-M.; Bernstein, K. E.; Bettler, B.; Birdsall, N. J. M.; Blaho, V.; Boulay, F.; Bousquet, C.; Bräuner-Osborne, H.; Burnstock, G.; Caló, G.; Castaño, J. P.; Catt, K. J.; Ceruti, S.; Chazot, P.; Chiang, N.; Chini, B.; Chun, J.; Cianciulli, A.; Civelli, O.; Clapp, L. H.; Couture, R.; Csaba, Z.; Dahlgren, C.; Dent, G.; Singh, K. D.; Douglas, S. D.; Dournaud, P.; Eguchi, S.; Escher, E.; Filardo, E. J.; Fong, T.; Fumagalli, M.; Gainetdinov, R. R.; Gasparo, M. de; Gerard, C.; Gershengorn, M.; Gobeil, F.; Goodfriend, T. L.; Goudet, C.; Gregory, K. J.; Gundlach, A. L.; Hamann, J.; Hanson, J.; Hauger, R. L.; Hay, D. L.; Heinemann, A.; Hollenberg, M. D.; Holliday, N. D.; Horiuchi, M.; Hoyer, D.; Hunyady, L.; Husain, A.; IJzerman, A. P.; Inagami, T.; Jacobson, K. A.; Jensen, R. T.; Jockers, R.; Jonnalagadda, D.; Karnik, S.; Kaupmann, K.; Kemp, J.; Kennedy, C.; Kihara, Y.; Kitazawa, T.; Kozielewicz, P.; Kreienkamp, H.-J.; Kukkonen, J. P.; Langenhan, T.; Leach, K.; Lecca, D.; Lee, J. D.; Leeman, S. E.; Leprince, J.; Li, X. X.; Williams, T. L.; Lolait, S. J.; Lupp, A.; Macrae, R.; Maguire, J.; Mazella, J.; McArdle, C. A.; Melmed, S.; Michel, M. C.; Miller, L. J.; Mitolo, V.; Mouillac, B.; Müller, C. E.; Murphy, P.; Nahon, J.-L.; Ngo, T.; Norel, X.; Nyimanu, D.; O'Carroll, A.-M.; Offermanns, S.; Panaro, M. A.; Parmentier, M.; Pertwee, R. G.; Pin, J.-P.; Prossnitz, E. R.; Quinn, M.; Ramachandran, R.; Ray, M.; Reinscheid, R. K.; Rondard, P.; Rovati, G. E.; Ruzza, C.; Sanger, G. J.; Schöneberg, T.; Schulte, G.; Schulz, S.; Segaloff, D. L.; Serhan, C. N.; Stoddart, L. A.; Sugimoto, Y.; Summers, R.; Tan, V. P.; Thal, D.; Thomas, W. W.; Timmermans, P. B. M. W. M.; Tirupula, K.; Tulipano, G.; Unal, H.; Unger, T.; Valant, C.; Vanderheyden, P.; Vaudry, D.; Vaudry, H.; Vilardaga, J.-P.; Walker, C. S.; Wang, J. M.; Ward, D. T.; Wester, H.-J.; Willars, G. B.; Woodruff, T. M.; Yao, C.; Ye, R. D. THE CONCISE GUIDE TO PHARMACOLOGY 2021/22: G Protein-Coupled Receptors. *Br J Pharmacol* **2021**, *178 Suppl 1*, S27–S156.

(154) Kolb, P.; Kenakin, T.; Alexander, S. P. H.; Bermudez, M.; Bohn, L. M.; Breinholt, C. S.; Bouvier, M.; Hill, S. J.; Kostenis, E.; Martemyanov, K. A.; Neubig, R. R.; Onaran, H. O.; Rajagopal, S.; Roth, B. L.; Selent, J.; Shukla, A. K.; Sommer, M. E.; Gloriam, D. E. Community Guidelines for GPCR Ligand Bias: IUPHAR Review 32. *Br J Pharmacol* **2022**, *179*, 3651–3674.

(155) Smith, J. S.; Lefkowitz, R. J.; Rajagopal, S. Biased Signalling: From Simple Switches to Allosteric Microprocessors. *Nat Rev Drug Discov* **2018**, *17*, 243–260.

(156) Wouters, E.; Walraed, J.; Robertson, M. J.; Meyrath, M.; Szpakowska, M.; Chevigné, A.; Skiniotis, G.; Stove, C. Assessment of Biased Agonism among Distinct Synthetic Cannabinoid Receptor Agonist Scaffolds. *ACS Pharmacol Transl Sci* **2019**, *3*, 285–295.

(157) Wouters, E.; Walraed, J.; Banister, S. D.; Stove, C. P. Insights into Biased Signaling at Cannabinoid Receptors: Synthetic Cannabinoid Receptor Agonists. *Biochem Pharmacol* **2019**, *169*, 113623.

(158) Navarro, G.; Reyes-Resina, I.; Rivas-Santisteban, R.; Sánchez de Medina, V.; Morales, P.; Casano, S.; Ferreiro-Vera, C.; Lillo, A.; Aguinaga, D.; Jagerovic, N.; Nadal, X.; Franco, R. Cannabidiol Skews Biased Agonism at Cannabinoid CB1 and

USC UNIVERSIDADE DE SANTIAGO DE COMPOSTELA

CB2 Receptors with Smaller Effect in CB1-CB2 Heteroreceptor Complexes. *Biochem Pharmacol* **2018**, *157*, 148–158.

(159) Aghazadeh Tabrizi, M.; Baraldi, P. G.; Borea, P. A.; Varani, K. Medicinal Chemistry, Pharmacology, and Potential Therapeutic Benefits of Cannabinoid CB2 Receptor Agonists. *Chem Rev* **2016**, *116*, 519–560.

(160) Sun, Y.; Liu, W.-Z.; Liu, T.; Feng, X.; Yang, N.; Zhou, H.-F. Signaling Pathway of MAPK/ERK in Cell Proliferation, Differentiation, Migration, Senescence and Apoptosis. *J Recept Signal Transduct Res* **2015**, *35*, 600–604.

(161) Phillips, H. S.; Kharbanda, S.; Chen, R.; Forrest, W. F.; Soriano, R. H.; Wu, T. D.; Misra, A.; Nigro, J. M.; Colman, H.; Soroceanu, L.; Williams, P. M.; Modrusan, Z.; Feuerstein, B. G.; Aldape, K. Molecular Subclasses of High-Grade Glioma Predict Prognosis, Delineate a Pattern of Disease Progression, and Resemble Stages in Neurogenesis. *Cancer Cell* **2006**, *9*, 157–173.

(162) Solinas, M.; Massi, P.; Cinquina, V.; Valenti, M.; Bolognini, D.; Gariboldi, M.; Monti, E.; Rubino, T.; Parolaro, D. Cannabidiol, a Non-Psychoactive Cannabinoid Compound, Inhibits Proliferation and Invasion in U87-MG and T98G Glioma Cells through a Multitarget Effect. *PLoS ONE* **2013**, *8*, e76918.

(163) Torres, S.; Lorente, M.; Rodríguez-Fornés, F.; Hernández-Tiedra, S.; Salazar, M.; García-Taboada, E.; Barcia, J.; Guzmán, M.; Velasco, G. A Combined Preclinical Therapy of Cannabinoids and Temozolomide against Glioma. *Molecular Cancer Therapeutics* **2011**, *10*, 90–103.

(164) Ferretti, M.; Fabbiano, C.; Bari, M. D.; Conte, C.; Castigli, E.; Sciaccaluga, M.; Ponti, D.; Ruggieri, P.; Raco, A.; Ricordy, R.; Calogero, A.; Tata, A. M. M2 Receptor Activation Inhibits Cell Cycle Progression and Survival in Human Glioblastoma Cells. *Journal of Cellular and Molecular Medicine* **2013**, *17*, 552–566.

(165) Navarro, G.; Ferré, S.; Cordomi, A.; Moreno, E.; Mallol, J.; Casadó, V.; Cortés, A.; Hoffmann, H.; Ortiz, J.; Canela, E. I.; Lluís, C.; Pardo, L.; Franco, R.; Woods, A. S. Interactions between Intracellular Domains as Key Determinants of the Quaternary Structure and Function of Receptor Heteromers*. *Journal of Biological Chemistry* **2010**, *285*, 27346–27359.

USC
UNIVERSIDADE DE SANTIAGO DE COMPOSTELA

# 7 APPENDICES

## 7.1 APPENDIX 1. CONFLICT OF INTEREST

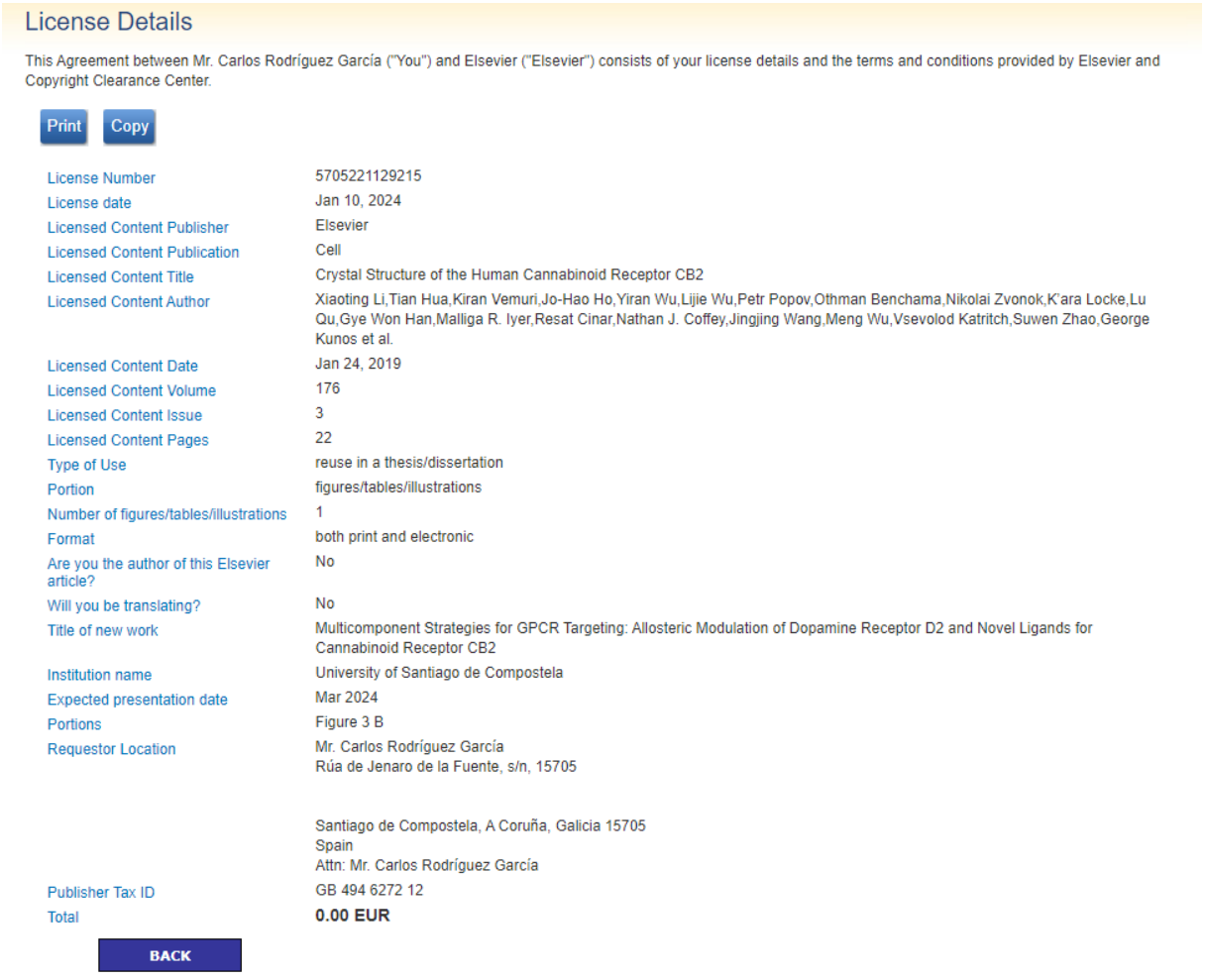
Carlos Rodríguez García, the doctoral candidate, affirms that there is no conflict of interest associated with his Doctoral Thesis.

Santiago de Compostela, February 21, 2024

USC
UNIVERSIDADE DE SANTIAGO DE COMPOSTELA

## 7.2 APPENDIX 2. PERMISSION TO PUBLISH IMAGES AND FIGURES

Figure 1.22. Structure of AM10257 and its binding to CB2R (Adapted from Li, X.; Hua, T.; Vemuri, K.; Ho, J.-H.; Wu, Y.; Wu, L.; Popov, P.; Benchama, O.; Zvonok, N.; Locke, K.; Qu, L.; Han, G. W.; Iyer, M. R.; Cinar, R.; Coffey, N. J.; Wang, J.; Wu, M.; Katritch, V.; Zhao, S.; Kunos, G.; Bohn, L. M.; Makriyannis, A.; Stevens, R. C.; Liu, Z.-J. Crystal Structure of the Human Cannabinoid Receptor CB2. Cell 2019, 176, 459-467.e13. https://doi.org/10.1016/j.cell.2018.12.011).



License Details

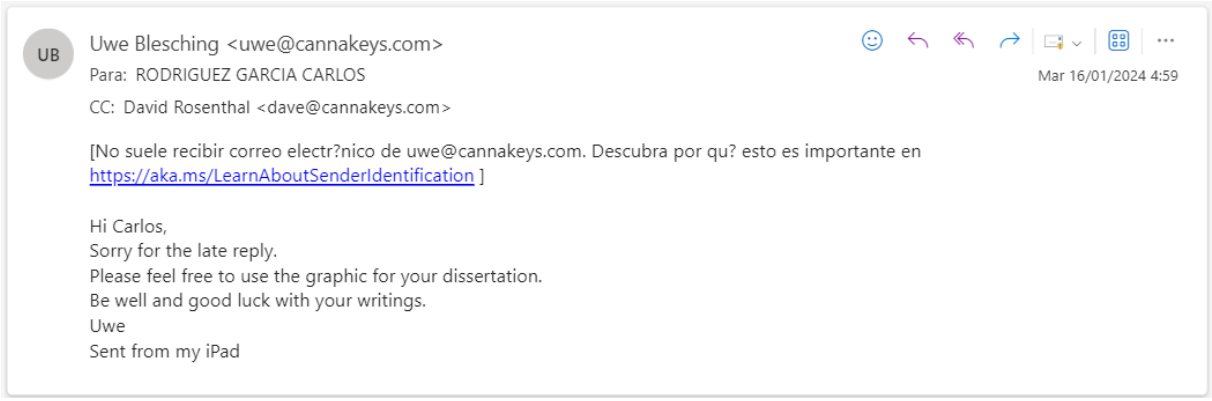
This Agreement between Mr. Carlos Rodríguez García ("You") and Elsevier ("Elsevier") consists of your license details and the terms and conditions provided by Elsevier and Copyright Clearance Center.

Print Copy

| | |
|---|---|
| License Number | 5705221129215 |
| License date | Jan 10, 2024 |
| Licensed Content Publisher | Elsevier |
| Licensed Content Publication | Cell |
| Licensed Content Title | Crystal Structure of the Human Cannabinoid Receptor CB2 |
| Licensed Content Author | Xiaoting Li,Tian Hua,Kiran Vemuri,Jo-Hao Ho,Yiran Wu,Lijie Wu,Petr Popov,Othman Benchama,Nikolai Zvonok,K'ara Locke,Lu Qu,Gye Won Han,Malliga R. Iyer,Resat Cinar,Nathan J. Coffey,Jingjing Wang,Meng Wu,Vsevolod Katritch,Suwen Zhao,George Kunos et al. |
| Licensed Content Date | Jan 24, 2019 |
| Licensed Content Volume | 176 |
| Licensed Content Issue | 3 |
| Licensed Content Pages | 22 |
| Type of Use | reuse in a thesis/dissertation |
| Portion | figures/tables/illustrations |
| Number of figures/tables/illustrations | 1 |
| Format | both print and electronic |
| Are you the author of this Elsevier article? | No |
| Will you be translating? | No |
| Title of new work | Multicomponent Strategies for GPCR Targeting: Allosteric Modulation of Dopamine Receptor D2 and Novel Ligands for Cannabinoid Receptor CB2 |
| Institution name | University of Santiago de Compostela |
| Expected presentation date | Mar 2024 |
| Portions | Figure 3 B |
| Requestor Location | Mr. Carlos Rodríguez García<br>Rúa de Jenaro de la Fuente, s/n, 15705<br><br>Santiago de Compostela, A Coruña, Galicia 15705<br>Spain<br>Attn: Mr. Carlos Rodríguez García |
| Publisher Tax ID | GB 494 6272 12 |
| Total | **0.00 EUR** |

BACK

Figure 1.24. Pharmacological effects of $CB_2R$ activation (Figure from https://cannakeys.com/cb2-agonism/).



UB

Uwe Blesching <uwe@cannakeys.com>

Para: RODRIGUEZ GARCIA CARLOS

Mar 16/01/2024 4:59

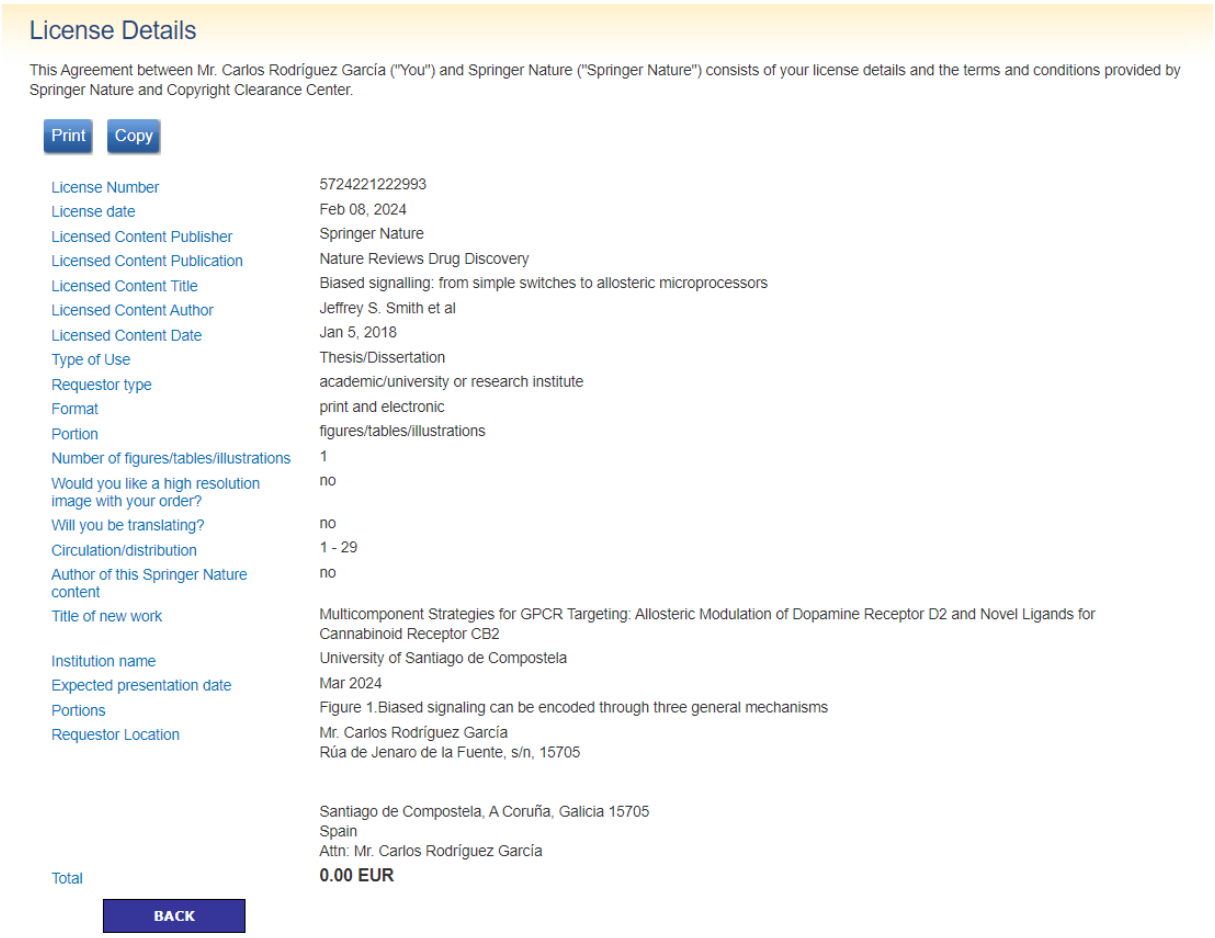
CC: David Rosenthal <dave@cannakeys.com>

[No suele recibir correo electr?nico de uwe@cannakeys.com. Descubra por qu? esto es importante en https://aka.ms/LearnAboutSenderIdentification ]

Hi Carlos,
Sorry for the late reply.
Please feel free to use the graphic for your dissertation.
Be well and good luck with your writings.
Uwe
Sent from my iPad

USC UNIVERSIDADE DE SANTIAGO DE COMPOSTELA

Figure 3.111. Graphical representation of the different facets of the biased signaling phenomena (Figure from Smith, J., Lefkowitz, R. & Rajagopal, S. Biased signaling: from simple switches to allosteric microprocessors. Nat Rev Drug Discov 17, 243–260 (2018). https://doi.org/10.1038/nrd.2017.229).



License Details

This Agreement between Mr. Carlos Rodríguez García ("You") and Springer Nature ("Springer Nature") consists of your license details and the terms and conditions provided by Springer Nature and Copyright Clearance Center.

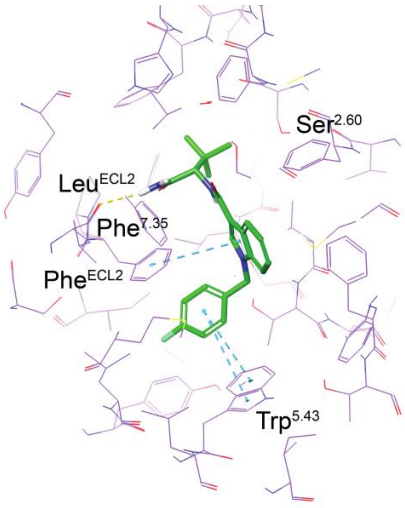
Print Copy

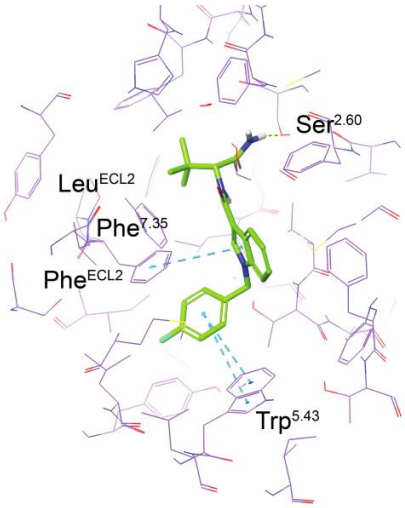
| | |
|---|---|
| License Number | 5724221222993 |
| License date | Feb 08, 2024 |
| Licensed Content Publisher | Springer Nature |
| Licensed Content Publication | Nature Reviews Drug Discovery |
| Licensed Content Title | Biased signalling: from simple switches to allosteric microprocessors |
| Licensed Content Author | Jeffrey S. Smith et al |
| Licensed Content Date | Jan 5, 2018 |
| Type of Use | Thesis/Dissertation |
| Requestor type | academic/university or research institute |
| Format | print and electronic |
| Portion | figures/tables/illustrations |
| Number of figures/tables/illustrations | 1 |
| Would you like a high resolution image with your order? | no |
| Will you be translating? | no |
| Circulation/distribution | 1 - 29 |
| Author of this Springer Nature content | no |
| Title of new work | Multicomponent Strategies for GPCR Targeting: Allosteric Modulation of Dopamine Receptor D2 and Novel Ligands for Cannabinoid Receptor CB2 |
| Institution name | University of Santiago de Compostela |
| Expected presentation date | Mar 2024 |
| Portions | Figure 1.Biased signaling can be encoded through three general mechanisms |
| Requestor Location | Mr. Carlos Rodríguez García<br>Rúa de Jenaro de la Fuente, s/n, 15705<br><br>Santiago de Compostela, A Coruña, Galicia 15705<br>Spain<br>Attn: Mr. Carlos Rodríguez García |
| Total | **0.00 EUR** |

BACK

All the other images shown in this Doctoral Thesis have been personally elaborated or no special permission is required to reuse all or part of their articles.

USC UNIVERSIDADE DE SANTIAGO DE COMPOSTELA




This PhD thesis focuses on the development of novel, potent, and selective ligands for two therapeutically relevant GPCR targets: the dopamine receptor $D_2$ and the cannabinoid receptor $CB_2$. Different isocyanide-based multicomponent strategies were designed to generate focused small molecule collections that enabled the interrogation of the selected targets, the identification of new lead compounds and the evaluation of the most salient features of the SAR within these series. The first chapter deals with the optimization of novel Melanostatin-inspired allosteric modulators of the $D_2R$. Chapter two documents a systematic MCR-assisted pharmacomodulation process that enabled the dissociation of the promiscuous cannabinomimetic profile of model designer drugs to identify potent, selective, and biased $CB_2R$ agonists. The research encompasses molecular design strategies, synthesis, biological evaluation, and structure-activity relationships. Preliminary evidence supporting the attractive antiproliferative activity of selected $CB_2R$ agonists in glioblastoma cell lines is also provided.